AJR

American
Journal of
Roentgenology

January 1993

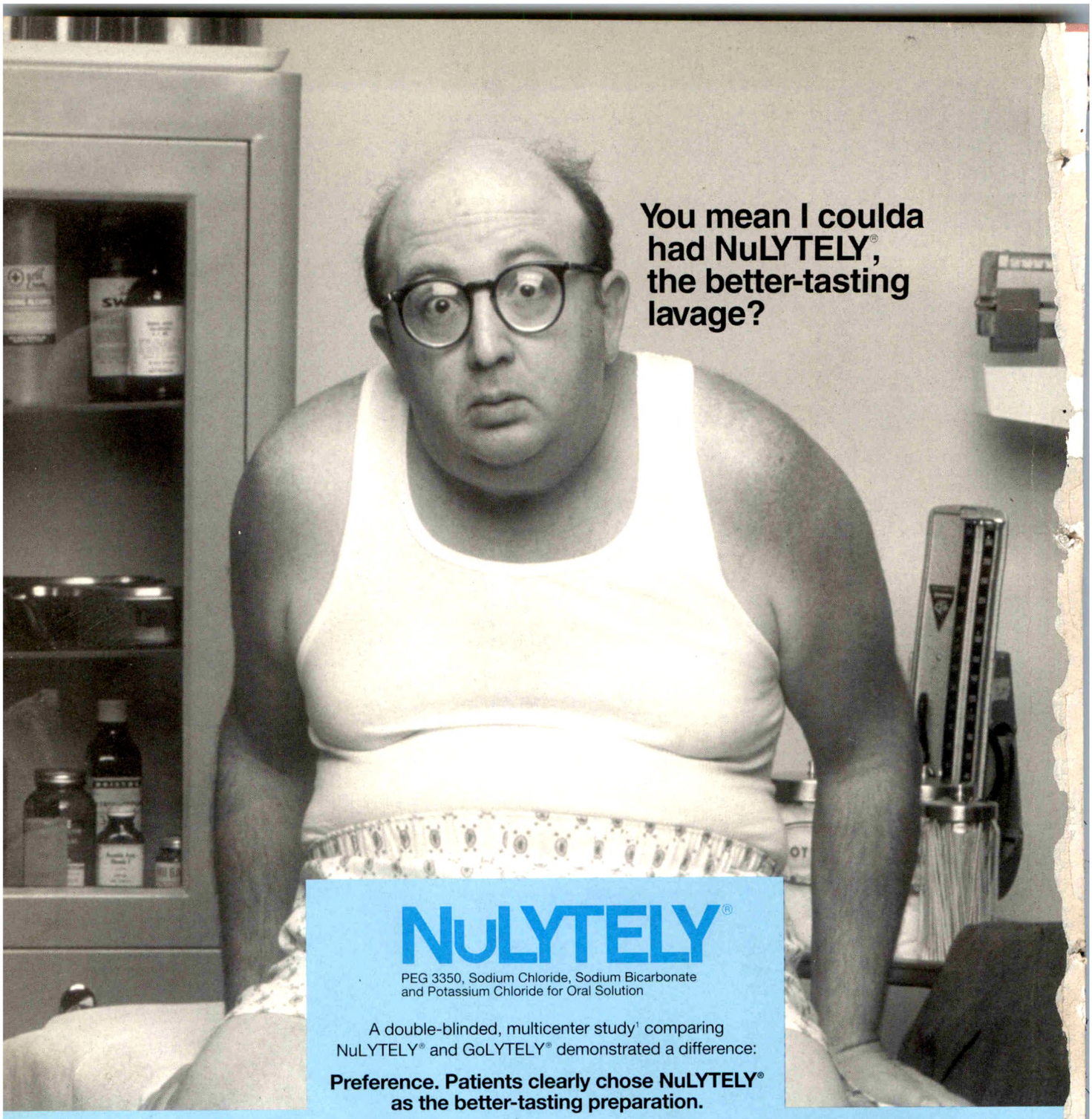

NuLYTELY®

PEG 3350, Sodium Chloride, Sodium Bicarbonate and Potassium Chloride for Oral Solution

A double-blinded, multicenter study[1] comparing NuLYTELY® and GoLYTELY® demonstrated a difference:

Preference. Patients clearly chose NuLYTELY® as the better-tasting preparation.

BRIEF SUMMARY: Before prescribing, see complete prescribing information.

INDICATIONS AND USAGE: NuLYTELY is indicated for bowel cleansing prior to colonoscopy.

CONTRAINDICATIONS: NuLYTELY is contraindicated in patients with gastrointestinal obstruction, gastric retention, bowel perforation, toxic colitis or toxic megacolon.

WARNINGS: No additional ingredients, e.g. flavorings, should be added to the solution. NuLYTELY should be used with caution in patients with severe ulcerative colitis.

PRECAUTIONS: General: Patients with impaired gag reflex, unconscious, or semiconscious patients, and patients prone to regurgitation or aspiration should be observed during the administration of NuLYTELY, especially if it is administered via nasogastric tube. If a patient experiences severe bloating, distention or abdominal pain, administration should be slowed or temporarily discontinued until the symptoms abate. If gastrointestinal obstruction or perforation is suspected, appropriate studies should be performed to rule out these conditions before administration of NuLYTELY.

ADVERSE REACTIONS: Nausea, abdominal fullness and bloating are the most common adverse reactions (occurring in up to 50% of patients) to administration of NuLYTELY. Abdominal cramps, vomiting, and anal irritation occur less frequently. These adverse reactions are transient and subside rapidly. Isolated cases of urticaria, rhinorrhea and dermatitis have been reported with a related drug (GoLYTELY®) which may represent allergic reactions.

CAUTION: Federal law prohibits dispensing without prescription.

STORAGE: Store in sealed container at 25° C. When reconstituted, keep solution refrigerated. Use within 48 hours. Discard unused portion. NDC 52268-0300-01

Manufactured for Braintree Laboratories, Inc. Braintree MA 02184 by Lyne Laboratories, Inc., Stoughton MA 02072.

Reference: 1. Data on file, Braintree Laboratories.

LABORATORIES · INC Braintree

AJR

American Journal of Roentgenology

Diagnostic Imaging and Related Sciences

Official Journal of the American Roentgen Ray Society

Volume 160, No. 1 January 1993

AJR, AMERICAN JOURNAL OF ROENTGENOLOGY (ISSN 0361 803X) is published monthly by the American Roentgen Ray Society, 1891 Preston White Dr., Reston, VA 22091. Annual dues include $50 for journal subscription. Second-class postage paid at Herndon, VA, and at additional mailing offices. **POSTMASTER**, send address changes (Form 3579) to Subscription Fulfillment, AJR, American Journal of Roentgenology, 1891 Preston White Dr., Reston, VA 22091. Subscription rates $125 ($180 foreign); institutions $135 ($190 foreign); in training $25 ($80 foreign); single copy $18 ($22 foreign). The GST number for Canadian subscribers is 123394371. Airmail rates furnished on request. Indexed by *Current Contents* and *Index Medicus*.

0361–803X/92$3.00

X-RAY ACCESSORIES

The Difference is Clear

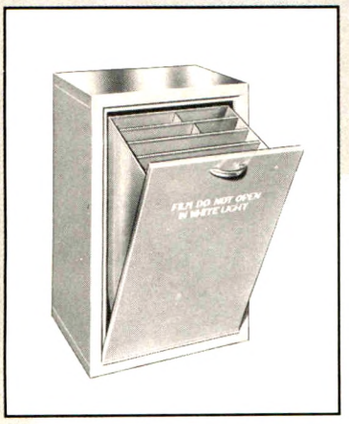

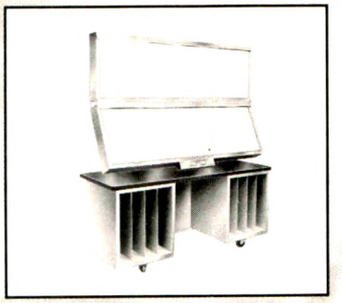

Tried, tested and trusted for over 40 years, S & S x-ray products deliver maximum proficiency and economy -- backed by quality, dependability and innovation.

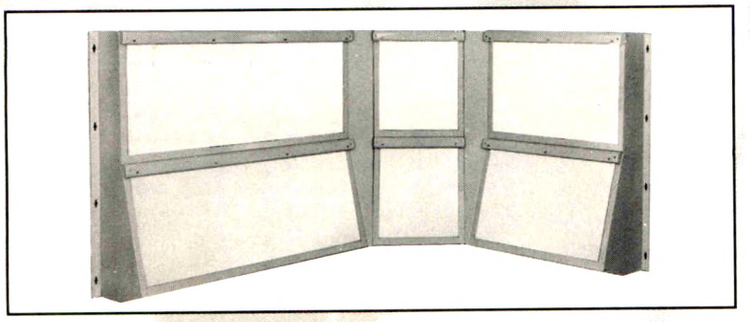

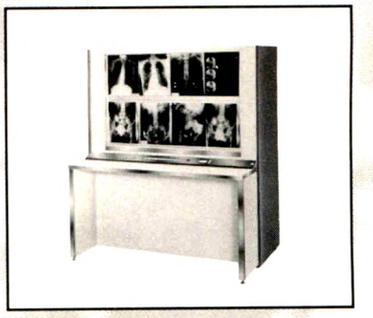

- **X-RAY** Film Viewers
- **X-RAY** Protection
- **X-RAY** Files
- **X-RAY** Darkroom Equipment
- **X-RAY** Cabinets
- **X-RAY** Accessories

For a FREE copy of our fully illustrated, 100+ page catalog, contact S & S directly or your local x-ray dealer.

1101 Linwood Street
Brooklyn, N.Y. 11208

Phone: 718/649-8500
FAX: 718/257-0219
Toll Free: 800/347-XRAY

S&S X-RAY PRODUCTS
Factories in NY, NC, PA, TX

American Journal of Roentgenology

Diagnostic Imaging and Related Sciences

Official Journal of the American Roentgen Ray Society — Volume 160, No. 1 January 1993

Is it time to upgrade your image?

If so, the LORAD M-III is the most advanced, low dose/high resolution product available with a proven record of effectiveness, dependability, ease of use, and upgradeability.

Designed for today's practice, **the LORAD M-III is guaranteed to meet ACR accreditation guidelines** and provide superior images time after time. The M-III also **makes everyone's job easier** with these unique features:

- The built-in **DATAPORT**™ with flexible software and simple screens for setup and optimal exposure control. You select either **Auto-kV or Auto-Time mode** and the M-III does the rest. M-III automatically senses system status, accessories in place, and field size – then sets operating parameters accordingly. With less to remember and fewer opportunities for error, more time can be spent with patients.
- **AutoFilm ID**™, to capture and flash critical data (patient, operator, and technique) directly from the computer to film. The AutoFilm ID™ option ends mixups and guarantees recall of original exposure parameters in future mammograms.

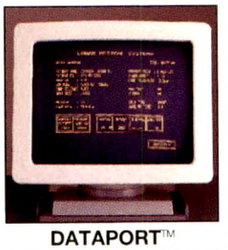

DATAPORT™

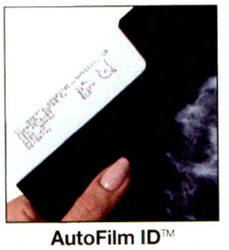

AutoFilm ID™

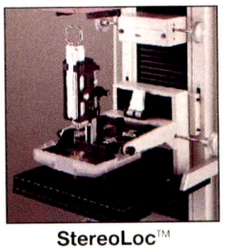

StereoLoc™

- **StereoLoc**™ upright biopsy attachment, proven in years of clinical use, transforms your M-III into an advanced diagnostic system for fine needle aspiration and large core needle biopsy (optional).

Finally, the system you buy today becomes even better tomorrow when you add the **LORAD DSM**™ near real-time **digital imaging for spot mammography.** You will reduce patient dosage, shorten procedure time, and adjust contrast for optimal viewing – all without film handling and processing.

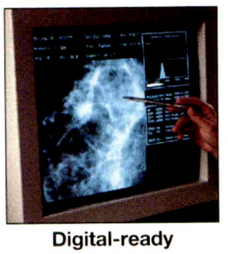

Digital-ready

Your LORAD M-III will keep you at the forefront of breast imaging today and tomorrow. Contact your LORAD representative, or call **1-800-447-1856** and ask **Operator 28** for our new brochures.

LORAD®

Pioneering for better breast health.

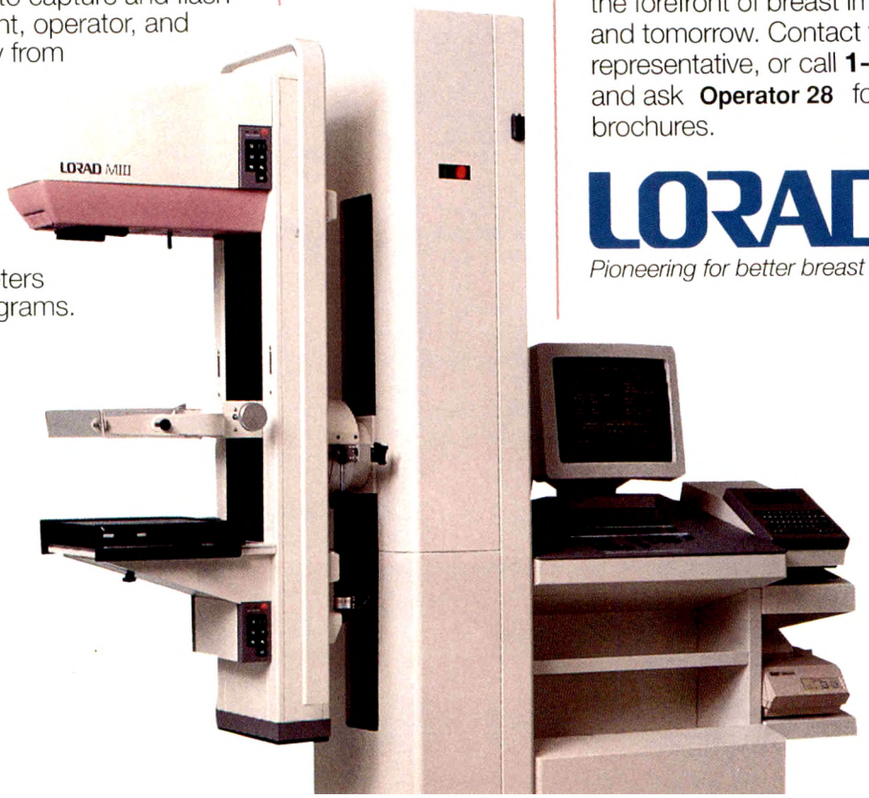

WE'D COMPARE EDGE™ TO THE COMPETITION. IF IT HAD ANY.

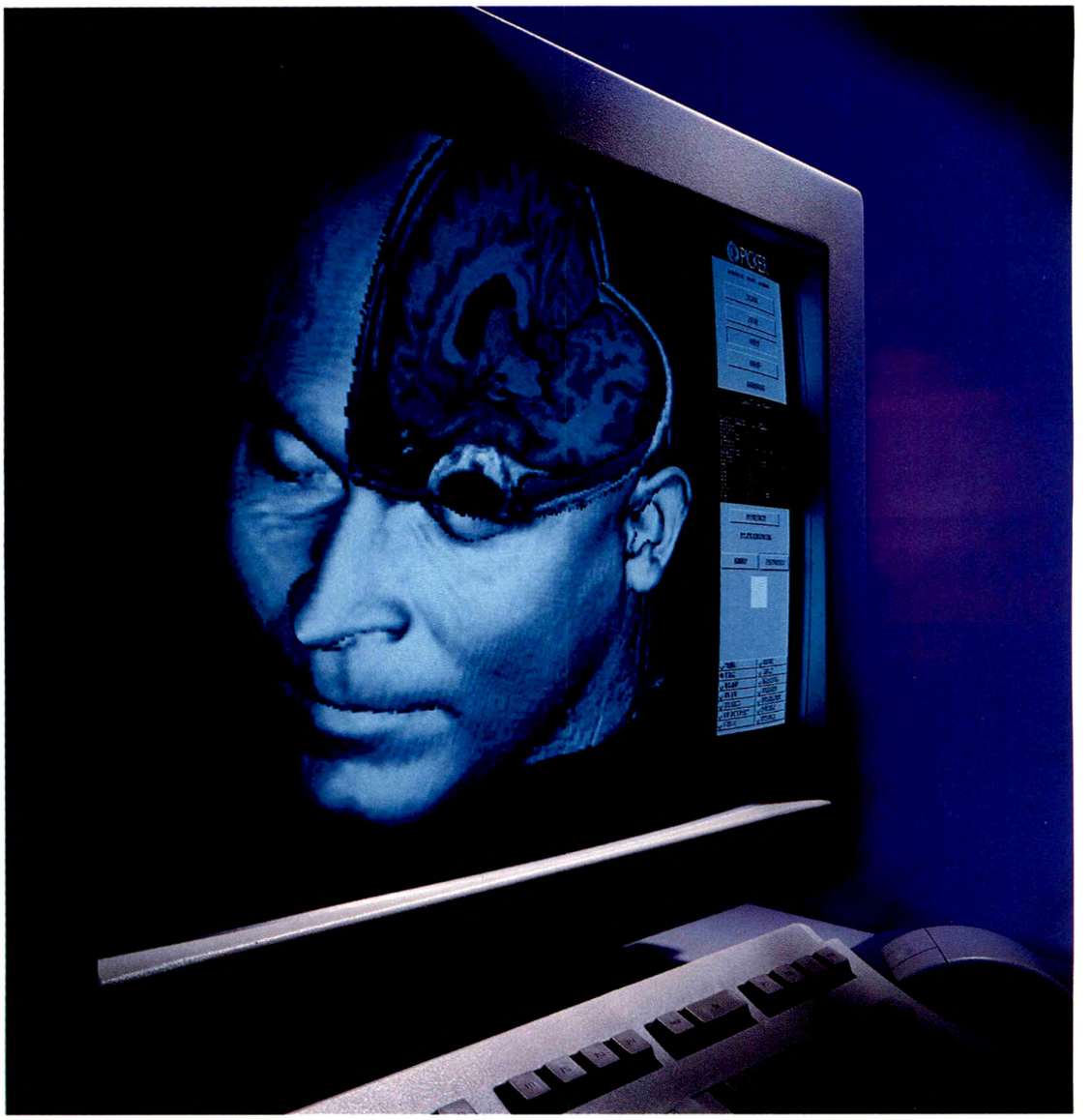

The new 1.5T Edge from Picker defies comparison with any other high-field MR system. It is unmatched in its category: • Volume imaging with real-time reconstruction. • Fastest display and imaging computer. • Innovative single cryogen active shield magnet.
• Exclusive multichannel fully digital RF system.
• High-performance gradient system.

Edge takes high-field MR to real-time volume imaging.

PICKER

MORE THAN IMAGES. INSIGHT.

Time to Renew?

To ensure uninterrupted service, please renew your AJR subscription two months prior to the expiration of your current subscription. To avoid renewal notices and price increases, consider a multiyear subscription. Current prices are available for up to three years.

For assistance with your renewal, call TOLL-FREE

1-800-438-2777

(from anywhere in the U.S. or Canada)

Or write

AJR Subscription
Fulfillment Department
1891 Preston White Drive
Reston, Virginia 22091

CHANGE OF ADDRESS

Please notify us eight weeks in advance. Send us your mailing label or your account number, along with your new address and the date the change of address is to take effect.

AJR

at your service

For customer assistance call TOLL-FREE:

1-800-438-2777

(from anywhere in the U.S. or Canada)

Or write:
AJR Subscription Fulfillment Dept.
1891 Preston White Drive
Reston, Virginia 22091

Keep It All Together

Easily and Conveniently With Bound Volumes of the *American Journal of Roentgenology*

Keeping up with scientific and technological advances in radiology is more important than ever, and that's why each issue of the *American Journal of Roentgenology* is packed with up-to-the-minute information crucial to you and your practice. **Keep this important resource together for easy reference in convenient and attractive bound volumes.**

Bound volumes offer the timely coverage only a journal can provide—penetrating discussions of the topics that interest you most by the brightest names in the field—with all the durability and convenience of a hardcover edition. You'll have a year's worth of vital information all arranged and indexed in one sturdy source. And each carefully crafted volume will make a handsome addition to your permanent library.

To help you keep your reference library up to date, once a year we'll send a reminder so you can order the latest bound volumes. When you send in your paid order, a set will be reserved for you, to be sent as soon as available on 30-day approval. If you do not want the volumes for any reason, simply return them within 30 days for a courteous refund. It's that easy.

For ordering information, contact *AJR* Subscription Fulfillment Department, P.O. Box 17266 Baltimore, MD 21297-0419 or call toll-free

1-800-438-2777

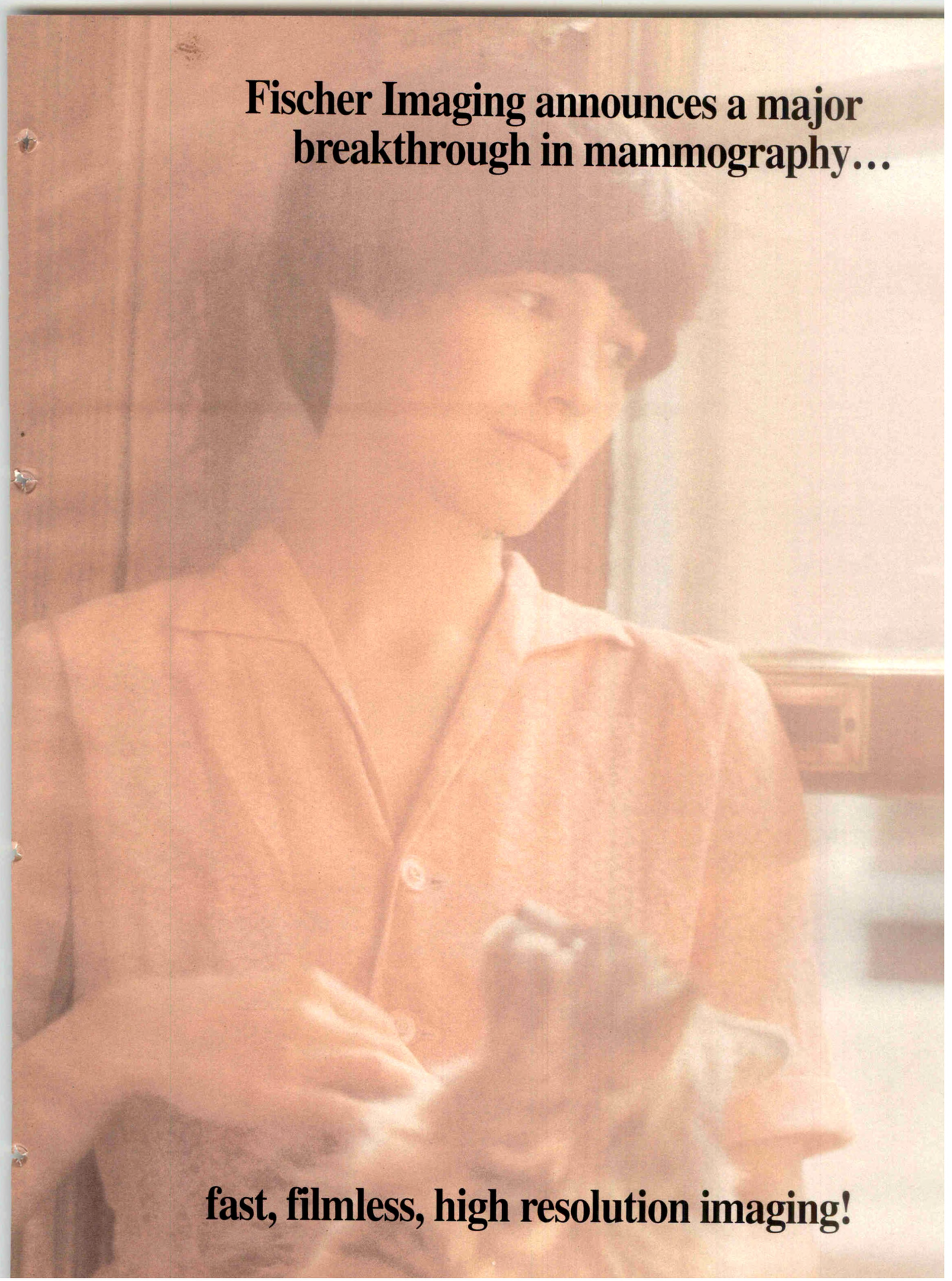
Fischer Imaging announces a major breakthrough in mammography...
fast, filmless, high resolution imaging!

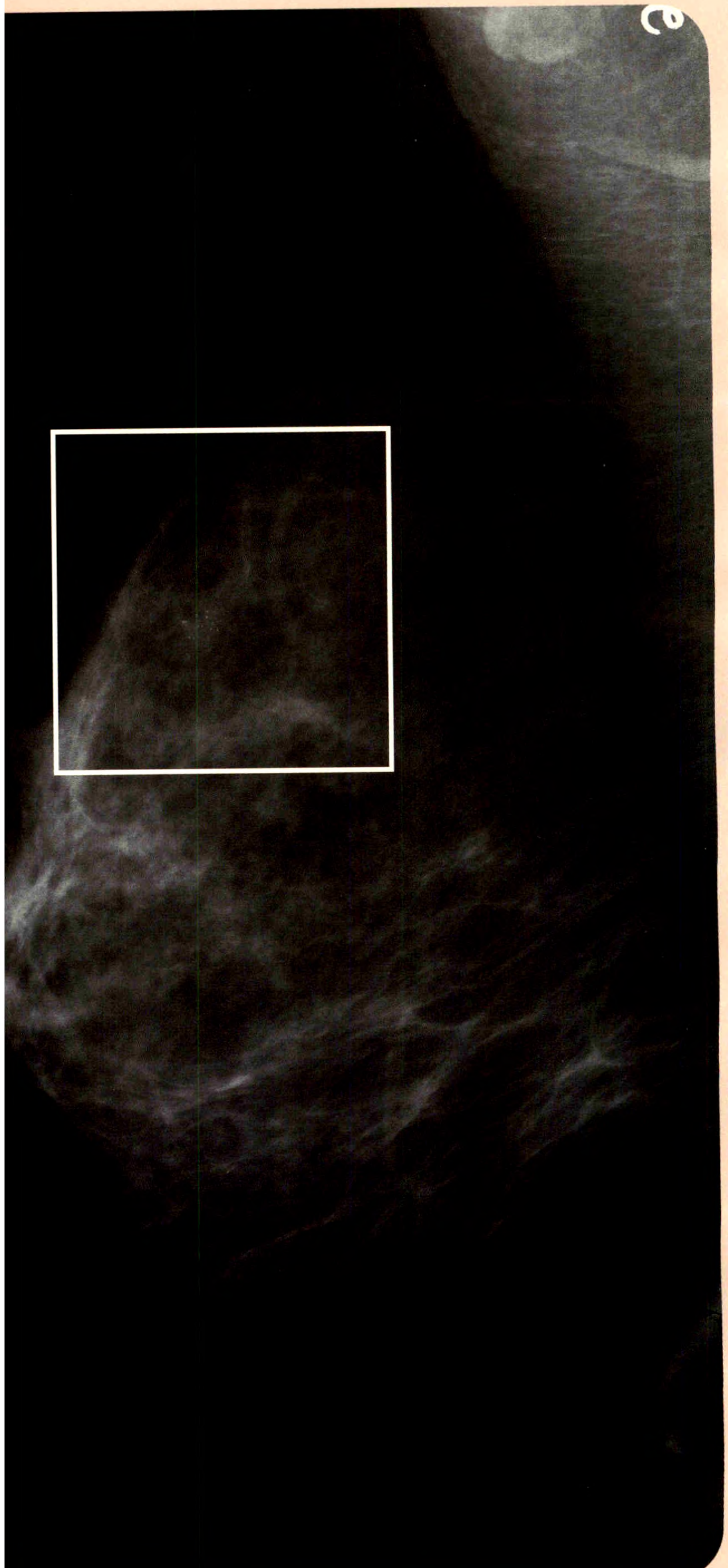

Introducing the MammoVision™ Digital Imaging System

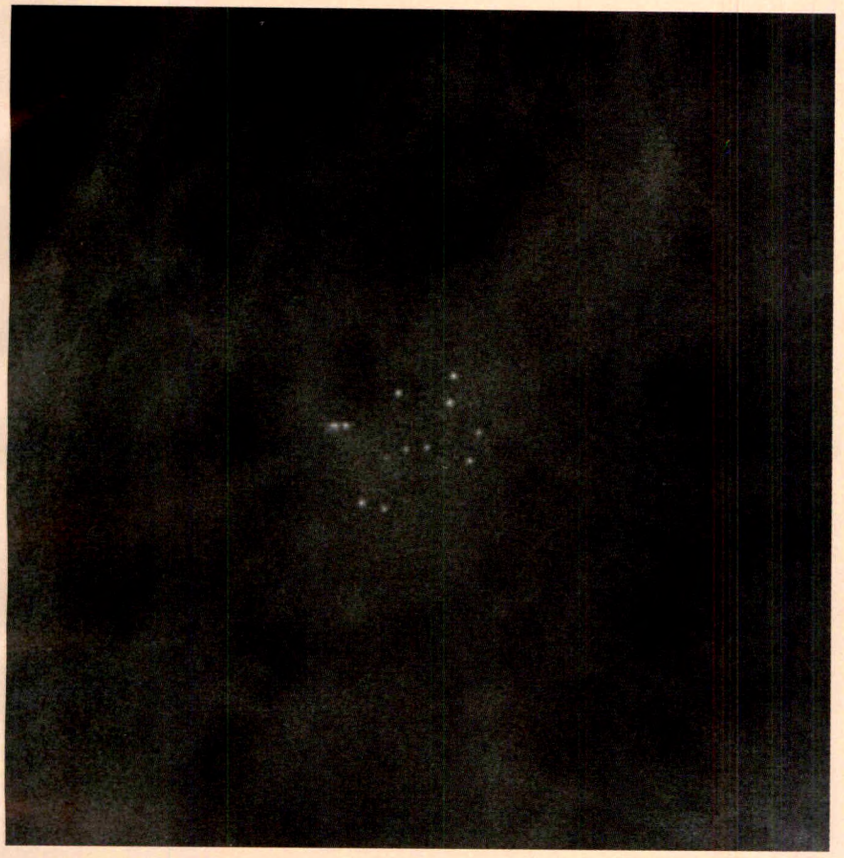

Far left shows a medio-lateral oblique view of the right breast. The region of interest within the 50mm x 50mm window shows evidence of microcalcifications. This patient was recommended for a Mammotest® stereotactic core biopsy procedure.

Near left above shows the enlarged 50mm x 50mm biopsy area from the original film screen mammogram.

Near left below shows the same 50mm x 50mm image digitally acquired during a stereotactic core biopsy procedure. This image is displayed on the MammoVision™ work station using the zoom feature.

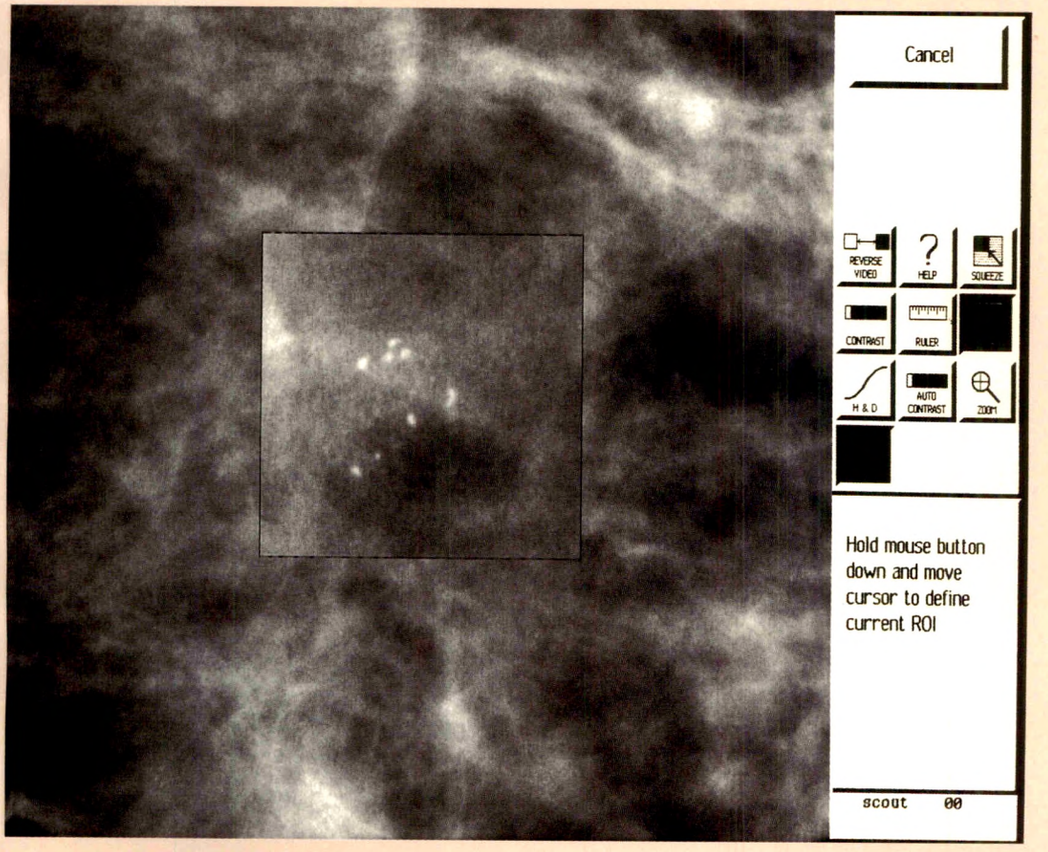

Mammotest® and MammoVision™... mammography for the 21st century.

Fischer Imaging, the pioneer and acknowledged leader in prone-positioning stereotactic core breast biopsies, with over 200 Mammotest® systems installed, now brings digital imaging to the most demanding radiographic application -- mammography.

Experience exceptional resolution and contrast enhancement capabilities not available with conventional film screen... in a fraction of the time.

Only the MammoVision™ Digital Imaging System offers:

- highest resolution and contrast...10 lp/mm, 50mm x 50mm imaging with window and level capability
- fast, filmless image display for reduced biopsy procedure time
- low patient dose (fiberoptically coupled CCD)

Fischer, bringing a history of new developments to imaging...

- First to introduce prone position stereotactic needle core biopsy
- First to provide a system that accommodates automated biopsy guns
- First to offer a digitized method for coordinates placement
- First to offer 1024 x 1024 fiberoptic based digital imaging
- First to incorporate automated needle positioning using polar coordinates

For more information call 1-800-825-8257.

FISCHERIMAGING CORPORATION

12300 North Grant Street
Denver, Colorado 80241
(303) 452-6800
Telex: 3720448 FICXRAY
FAX: (303) 450-4335

AJR Business and Subscriber Information

The American Roentgen Ray Society

AJR, American Journal of Roentgenology, is published monthly to disseminate research on current developments in the radiologic sciences and commentary on topics related to radiology. It is published by the American Roentgen Ray Society (ARRS), 1891 Preston White Dr., Reston, VA 22091; (703) 648-8992. Address inquiries regarding Society business, the annual ARRS meeting, and membership in the Society to the above address.

Correspondence regarding editorial matters should be addressed to Editorial Office, AJR, 2223 Avenida de la Playa, Ste.103, La Jolla, CA 92037-3218; telephone 1-800-348-4257 or (619) 459-2229; FAX (619) 459-8814. For information on manuscript submission, see Guidelines for Authors.

Subscriber Information

ARRS annual dues include $50 for journal subscription. Nonmember subscription rates are as follows: $125/year ($180 foreign); institutions, $135 ($190 foreign); in-training, $25 ($80 foreign). Single copies of the Journal may be purchased for $18 ($22 foreign). Airmail rates will be furnished on request. The GST number for Canadian subscribers is 123394371.

Call toll-free, 1-800-438-2777, with subscription inquiries or problems. Please have the mailing label from your latest issue available when you call.

Report changes of address to Subscription Fulfillment, AJR, 1891 Preston White Dr., Reston, VA 22091. Damaged or unreceived issues must be reported within 60 days of publication (90 days for foreign subscribers) for replacement.

Advertising Information

All advertising is subject to approval by the publisher. Acceptance of advertising does not indicate endorsement of the products or services advertised or the claims made. For display advertising information, contact Gary Walchli, National Sales Representative, AJR, 428 E. Preston St., Baltimore, MD 21202, (410) 528-4291.

For classified advertising information, contact the Publications Department, ARRS, Attn: Terry Fitterer, 1891 Preston White Dr., Reston, VA 22091; telephone (703) 648-8992; FAX (703) 264-8863.

Copyrights, Permissions, and Reprints

 For reprints of a particular article, please contact the author designated in the footnotes for that article.

Indexes

The *AJR* provides volume and yearly indexes (subject and author) in the June and December issues. *AJR* articles are also indexed in *Current Contents*, *Index Medicus*, and the cumulative index published by *Radiology*.

LOTS OF COMPANIES SELL X-RAY SHIELDING PRODUCTS... BUT NUCLEAR ASSOCIATES WROTE THE BOOK!

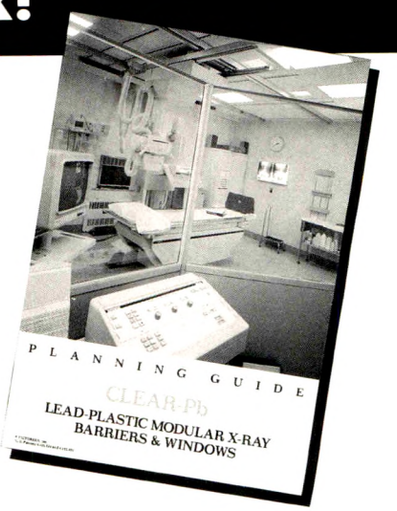

Hot off the press and now available...a best seller in the medical imaging industry...it's the Nuclear Associates Planning Guide for **CLEAR-Pb** Lead-plastic Modular X-Ray Barriers and Windows.

The good news? It's free! Better news? It's chock full of information about **CLEAR-Pb** ...the number one choice for radiation shielding, how it's being used in prestigious medical facilities around the country, and how it can work for your facility and your personnel.

When we're asked to describe the benefits of CLEAR-Pb, we need only three words:

- **SPACE-SAVING** – can be installed into virtually any space easily and economically.
- **VERSATILE** – conforms to the design of your facility; ideal for the planning architect.
- **SAFE** – choose from 6 lead equivalencies from 0.3mm to 2.0mm.

CLEAR-Pb Lead Plastic Modular X-Ray Barriers and Windows are available in over 200 stock sizes. (Larger sizes are available on special order.)

If you're looking for the most extensive line of products to deliver total body protection from secondary radiation, look no further. Call, fax or write today for the Nuclear Associates Planning Guide on **CLEAR-Pb**.

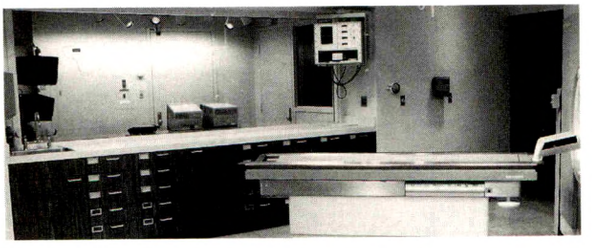

Model 56-604
Jumbo Barrier

Model 56-603
Regular Barrier

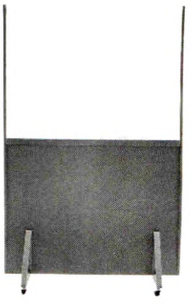

Model 56-616
Deluxe Barrier

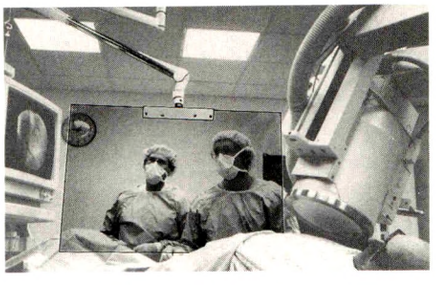

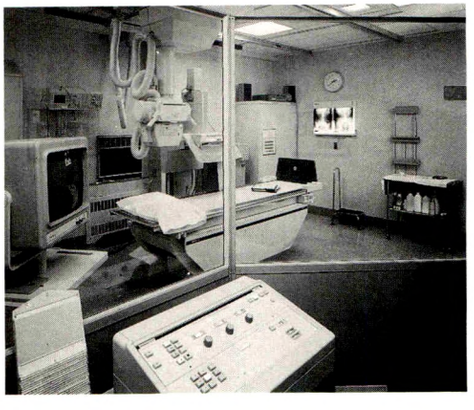

For total body shielding, the CLEAR choice is Nuclear Associates.

For more details, request
Bulletin 3187-44 (Free Planning Guide)
Bulletin 3226-44 (Mobile X-Ray Barriers)

NUCLEAR ASSOCIATES

VICTOREEN

Division of VICTOREEN, INC.
100 VOICE ROAD • P.O. BOX 349
CARLE PLACE, NY 11514-0349 U.S.A.
(516) 741-6360
FAX (516) 741-5414

AJR Guidelines for Authors

Address new and revised manuscripts and correspondence to the Editor:

AJR Editorial Office
2223 Avenida de la Playa, Suite 103
La Jolla, CA 92037-3218
Telephone: (619) 459-2229; FAX: (619) 459-8814

Inquiries regarding classified ads, or permission to republish *AJR* material should be addressed to the publisher:

ARRS
Publications Department
Attention: Terry Fitterer
1891 Preston White Dr.
Reston, VA 22091

The *AJR* publishes original contributions to the advancement of medical diagnosis and treatment. Submitted manuscripts should not contain previously published material and should not be under consideration for publication elsewhere.

Manuscript decisions are based on peer review. Reviewers receive manuscripts without title pages to ensure an unbiased review. Statements made in the article, including changes made by the Editor or manuscript editor, are the responsibility of the author and not of the *AJR* or its publisher. Authors will be sent the edited manuscript, page proof, and proofs of illustrations. If the corresponding author will be unavailable to review page proofs, arrangements should be made for a coauthor or colleague to read and return the proof.

The following guidelines are based on instructions set forth in the **Uniform Requirements for Manuscripts Submitted to Biomedical Journals** (*Ann Intern Med* **1988**;108:258-265). Articles will be edited, however, to conform to the individual style of *AJR*.

General Guidelines for Major Papers

Abstract. Clearly state (in 250 words or fewer) the purpose, methods, results, and conclusions of the study. Include actual data.

Introduction. Briefly describe the purpose of the investigation and explain why it is important.

Methods. Describe the research plan, the materials (or subjects), and the methods used, in that order. Explain in detail how disease was confirmed and how subjectivity in observations was controlled.

Results. Present results in a clear, logical sequence. If tables are used, do not duplicate tabular data in text, but do describe important trends and points.

Discussion. Describe the limitations of the research plan, materials (or subjects), and methods, considering both the purpose and the outcome of the study. When results differ from those of previous investigators, explain the discrepancy.

AUTHOR'S CHECKLIST

For priority handling, complete the following checklist, sign the copyright form on the reverse side of this page, and include both with the manuscript.

___ Two copies of the manuscript (the original and a photocopy) and two complete sets of figures are submitted. One copy has been retained by the author.

___ If appropriate, *AJR* Guidelines for case reports, technical notes, pictorial essays, or letters to the Editor have been followed.

___ The manuscript, including references, figure legends, and tables, is typed double-spaced on 8 1/2 x 11 in. (21.6 x 27.9 cm) *nonerasable* paper. Right-hand margins are not justified.

___ All manuscript pages are numbered consecutively beginning with the abstract. Authors' names do not appear on the manuscript pages.

___ The manuscript is organized as follows: title page, blind title page (title only), abstract, introduction, methods, results, discussion, acknowledgments, references, tables, figure legends, and figures.

___ Informed consent has been obtained from patients who participated in clinical investigations. If experiments were performed on animals, authors complied with NIH guidelines for use of laboratory animals.

___ Use of unfamiliar acronyms and abbreviations is kept to a minimum. When abbreviations are used they are defined at first mention, followed by the abbreviation in parentheses.

___ Metric measurements are used throughout, or the metric equivalent is given in parentheses.

___ Names and locations (city and state only) of manufacturers are given for equipment and nongeneric drugs.

___ Upon acceptance, final version is submitted on either a 5 1/4-in. or 3 1/2-in. DOS-compatible diskette in Wordperfect or ASCII format.

Title Page

___ The following information is given: title of article; names and complete addresses (including zip code) of all authors; current addresses of authors who have moved since study; acknowledgment of grant or other assistance. The corresponding author is clearly identified, and a current address, phone number, and FAX number are given.

___ A blind title page is included in each copy of the manuscript, giving only the title (without the authors' names) for use in the review process.

Abstract

___ An abstract of approximately one and one-half typewritten pages is organized into the following paragraphs.

Objective. In one or two sentences, indicate the specific goal or purpose of the article, and indicate why it is worthy of attention. Explain the hypothesis to be tested, the dilemma to be resolved, or the deficiency to be remedied. The objective stated here must be identical to the one given in the title and introduction of the paper.

Subjects (or materials) and methods. Describe succinctly the methods used to achieve the objective explained in the first paragraph, stating what was done, how it was done, how bias was controlled, what data were collected, and how the data were analyzed.

Results. The findings of the procedures described in the preceding paragraph are presented here. All results should flow logically from the methods described and not stray from the specific objective of the paper. Include as many specific data as possible within the overall length limitation of one typewritten page.

Conclusion. In one or two sentences, present the take-home message to be remembered when all else is forgotten. Describe the conclusion of the study, based solely on the

data provided in the body of the abstract. Conclusions must relate directly to the objective of the paper as defined in the title and first paragraph of the abstract.

___ No abbreviations or reference citations are used.

References

___ References (not to exceed 35) are typed double-spaced starting on a separate page and are **numbered consecutively in the order in which they appear in the text.**

___ All references are cited in the text and are enclosed in brackets and typed on line with the text (not superscript).

___ Unpublished data are not cited in the reference list, but are cited parenthetically in the text, for example, (Smith DJ, personal communication), (Smith DJ, unpublished data). This includes papers submitted, but not yet accepted, for publication.

___ Papers presented at a meeting are not cited in the reference list, but are cited parenthetically in the text (e.g., Smith DJ et al., presented at the American Roentgen Ray Society meeting, May 1990). After first mention, use (Smith DJ et al., ARRS meeting, May 1990).

___ Inclusive page numbers (e.g., 333-335) are given for all references.

___ Journal names are abbreviated according to *Index Medicus*.

___ Style and punctuation of references follow the format illustrated in the following examples (all authors are listed when six or fewer; when seven or more authors, the first three are listed, followed by "et al."):

Journal Article

1. Long RS, Roe EW, Wu EU, et al. Membrane oxygenation: radiographic appearance, *AJR* **1986**;146:1257-1260

Book

2. Smith LW, Cohen AR. *Pathology of tumors*, 6th ed. Baltimore; Williams & Wilkins, **1977**:100-109

Chapter in a book

3. Breon AJ. Serum monitors of bone metastasis. In: Clark SA, ed. *Bone metastases*. Baltimore; Williams & Wilkins, **1983**:165-180

Tables

___ Each table is typed double-spaced on a separate page without vertical or horizontal rules; each has a short, descriptive title. Tables do not exceed two pages in length and contain at least four lines of data.

___ Tables are numbered in the order in which they are cited in the text.

___ Abbreviations are defined in an explanatory note below each table.

___ Tables are self-explanatory and do not duplicate data given in the text or figures.

___ All arithmetic (percentages, totals, differences) has been double checked for accuracy, and tabular data agree with data given in the text.

Figures and Legends

___ Two complete sets of original figures are submitted unmounted in labeled envelopes.

___ Figures are clean, unscratched, glossy prints, uniform in size and magnification, with **white borders**. A separate print (not larger than 5 x 7 in.) is submitted for each figure *part*.

___ All figure parts relating to one patient have the same figure number.

___ Each figure is labeled on the back with the figure number and an arrow indicating "top." For black-and-white figures, labeling is done on a gummed label, which is then affixed to the back of the print. **Never** use labels on **color** figures, but write figure number on the back lightly in pencil. *Never* use ink on front or back of any figures.

___ Authors' names are *not* written on the backs of figures.

___ Only removable (rub-on) arrows and letters are used on the figures. Symbols are uniform in size and style and are not broken or cracked.

___ Line drawings are done in black ink on a white background. They are professional in quality, and all use the same size type. (Only glossy prints are acceptable.)

___ Written permission has been obtained for use of all previously published illustrations (and copies of permission letters are included), and an appropriate credit line is given in the legends.

___ Legends are typed double-spaced, and figure numbers correspond with the order in which the figures are cited in the text.

___ Legends are written in accordance with *AJR* style (refer to any issue and follow format).

Transfer of Copyright Agreement, Conflict of Interest Acknowledgment, Certification of Coauthors, and Exclusive Publication Statement

Complete copyright to the article entitled: _____

_____

is hereby transferred to the American Roentgen Ray Society (for United States government employees to the extent transferable), effective if and when the article is accepted for publication in the *American Journal of Roentgenology*. In the case of the authors who are officers or employees of the United States government, the American Roentgen Ray Society recognizes that works prepared by officers or employees of the United States government as part of their official government duties are in the public domain.

Authors reserve all proprietary rights other than copyright, such as patent rights and the right to use all or part of this article in future works of their own. The authors retain the right of replication, subject only to crediting the original source of publication and receiving written permission from the publisher.

Authors guarantee that this manuscript contains no matter that is libelous or otherwise unlawful, invades individual privacy, or infringes any proprietary rights.

Authors understand that they will receive no royalty or other compensation from the American Roentgen Ray Society.

Authors guarantee that the editor has been or will be informed of any proprietary or commercial interest or conflicts of interest the authors may have that relate directly or indirectly to the subject of this article.

All authors certify that they have made substantive and specific intellectual contributions to the article and assume public responsibility for its content.

Finally, the authors certify that none of the material in this manuscript has been published previously or is currently under consideration for publication elsewhere

First author/date	Second author	Third author
Fourth author	Fifth author	Sixth author

This agreement must be signed by all authors in order for the manuscript to be published.

Case Reports

A case report is a brief description of a special case that provides a message that transcends the individual patient.

Format. There is no abstract. The introduction should be a short paragraph giving the general background and the specific interest of the case. No more than one case should be described in detail (similar ones can be mentioned briefly in the discussion). Emphasis should be on the radiologic aspects; clinical information must be limited to that necessary to provide a background for the radiology. The discussion should be succinct and should focus on the specific message and relevance of radiologic methods. A review of the literature is not appropriate.

Length. Maximum of five double-spaced, typewritten pages, including the references but not the title page or figure legends.

References. Maximum of eight.

Figures. Maximum of four, unless the text is shortened accordingly. Legends must not repeat the text.

Tables and Acknowledgments. Not appropriate in case reports.

Pictorial Essays

A pictorial essay is an article that conveys its message through illustrations and their legends. Unlike other *AJR* articles, which are based on original research, pictorial essays serve primarily as teaching tools, like exhibits at a scientific meeting. They are not encyclopedic book chapters. The introduction should serve as an abstract: define the scope of the paper and explain its importance on one half of a double-spaced typewritten page.

Length. Maximum of four double-spaced, typewritten pages, including the references but not the title page or figure legends.

References. Maximum of four.

Figures. Maximum of 30 figure parts. Number should be as few as necessary to convey the message of the paper.

Tables and Acknowledgments. Not appropriate in pictorial essays.

Opinions, Commentaries, and Perspectives

Opinions, commentaries, and perspectives are special articles dealing with controversial topics or issues of special concern to radiologists.

Format. Include a title page but no abstract. Headings may be used to break up the text.

Length. Maximum of five double-spaced, typewritten pages.

References. Maximum of five.

Tables and Figures. Maximum of four.

Technical Notes

A technical note is a brief description of a specific technique or procedure, modification of a technique, or equipment of interest to radiologists.

Format. No abstracts, headings or subheadings are required. If headings are used, they should be a combination of "Case Report," "Materials and Methods," "Results," and "Discussion." A brief one-paragraph introduction should be included to give the general background. Discussion should be limited to the specific message, including the uses of the technique or equipment. Literature reviews and lengthy case reports are not appropriate.

Length. Maximum of five double-spaced, typewritten pages, including the references but not the title page or figure legends.

References. Maximum of eight.

Figures. Maximum of two, unless the text is shortened accordingly.

Tables and Acknowledgments. Not appropriate in technical notes.

Letters to the Editor and Replies

Letters to the Editor and Replies should offer objective and constructive criticism of published articles. Letters may also discuss matters of general interest to radiologists. Material being submitted or published elsewhere should not be duplicated in letters, and authors must disclose financial associations or other possible conflicts of interest.

Format. All letters should be typed double-spaced on nonletterhead paper, with no greeting or salutation. Titles for letters should be short and pertinent. The title for a reply is simply "Reply." Do not use abbreviations in the title or the text. Authors' names and affiliations should appear at the end of the letter. Do not end a letter with a handwritten signature.

Number of authors. Maximum of four.

Length. Maximum of two double-spaced, typewritten pages, including references.

references. Maximum of four.

Figures. Maximum of two figures *or* one figure with two parts.

Tables and Acknowledgments. Not appropriate in Letters to the Editor and Replies.

Computer Page Articles

Articles published on the computer page deal with practical computer applications to radiology.

Format. Include a title page and an abstract.

Length. Maximum of eight double-spaced, typewritten pages.

References. Maximum of five.

Figures and Tables. Maximum of five. Computer printouts are not acceptable. Figures must be submitted as 5x7 in. glossy prints.

All submissions to the AJR must be accompanied by a completed copy of the Author's Checklist and the signed copyright agreement.

"IS IT TRUE THAT NUCLEAR ASSOCIATES MAKES THE ONLY HAND-HELD SCANNING DENSITOMETER WITH BUILT-IN SINGLE-POINT MEASUREMENT CAPABILITY?"

YES! AND IT'S CALLED MINISCAN.

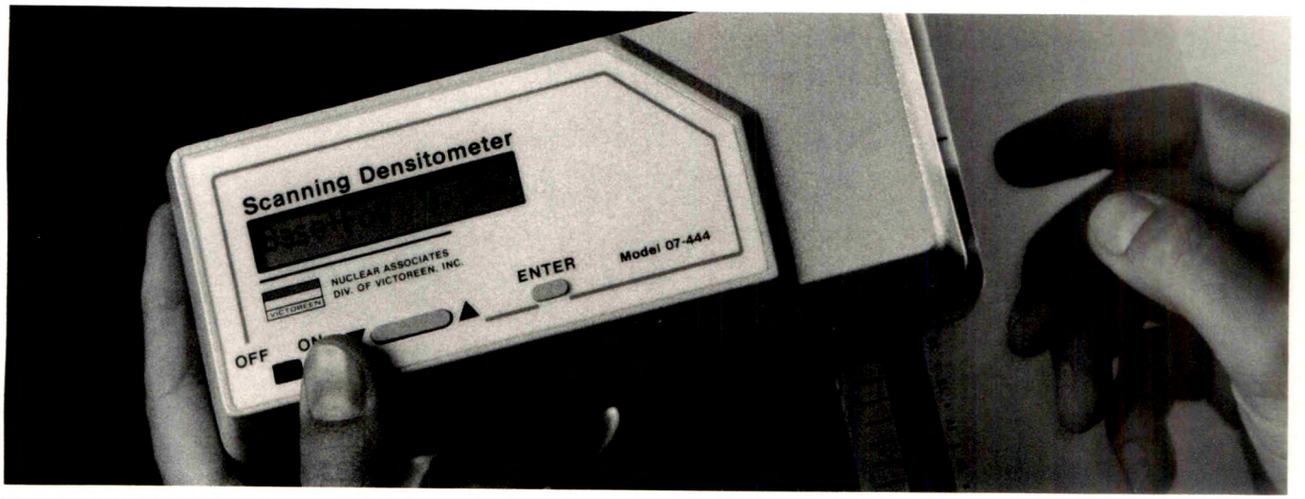

It's a fact. MINISCAN is exactly what you've been looking for to ensure optimum image characteristics for your x-ray film processors.

Lightweight and compact, MINISCAN can be used to make single-point measurements – essential in mammography and cardiology procedures where the most stringent quality control is required. Operating as a transmission densitometer in the single-point mode, MINISCAN lets you spot-check single-point densities; a big help where non-21-step wedges are used or where spot measurements are required.

In addition to its single-point measurement capability, MINISCAN can also measure, analyze and store data for as many as 20 sets of independent strips, allowing you to read the 21 density steps as well as average gradient, relative speed, base plus fog, contrast index, speed index and maximum optical density – all by step number. This data can be converted to hard copy using an IBM™ compatible PC running on Nuclear Associates' FILM-PRO software package.

MINISCAN can be calibrated in-house, using a standard step table, eliminating a lot of down time and the possibility of erroneous calibrations by an outside service. And because MINISCAN is battery-operated, you can take your measurements at the processor site ...another time-saving plus.

When you use MINISCAN in your x-ray processor quality control program, you assure yourself of:

- getting all of the necessary data to show you that your x-ray film processor is delivering optimum image quality.
- detecting - at an early stage - changes that affect image quality, and taking the proper steps to resolve the problem.
- maintaining the highest standards of quality control, resulting in a significant reduction in repeat x-ray examinations.

Whether your format is sheet, spot or cine film, whether your requirements are for single-point measurements or scanning, the MINISCAN Densitometer can play a key role in helping maintain the high quality control standards you strive for.

For more information, request Bulletin 5013-44

IBM ™, International Business Machines, Inc.

NUCLEAR ASSOCIATES

VICTOREEN

Division of VICTOREEN, INC.
100 VOICE ROAD • P.O. BOX 349
CARLE PLACE, NY 11514-0349 U.S.A.
(516) 741-6360
FAX (516) 741-5414


OMNIPRESENT


BECAUSE
S UNIQUE
PROFILE

In the littlest patients, safety is the biggest concern.

So it's reassuring to know that the contrast medium OMNIPAQUE® (iohexol) has been specifically tested and approved for eight pediatric indications. Our years of experience are documented in extensive trials of adults and children, in 35 indications, at a wide variety of dosage levels.[1] OMNIPAQUE gives you the confidence that comes from a time-tested record of safety, and a depth of experience few can match. OMNIPAQUE... for pediatric excretory urography, myelography, CT (head, body, oral GI marker), angiocardiography, voiding cystourethrography, and aortography.

It's omnipresent because it's proven pediatric safe.

OMNIPAQUE®

(IOHEXOL) Injection

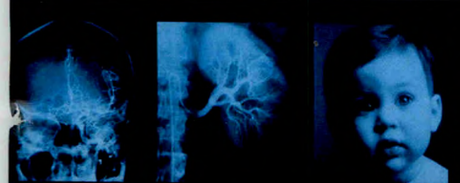

CONFIDENCE, EVERYWHERE YOU LOOK.

All nonionic iodinated contrast media currently available inhibit blood coagulation, in vitro, less than ionic contrast media. Clotting has been reported when blood remains in contact with syringes containing nonionic contrast media. Therefore, meticulous intravascular administration technique is necessary to minimize thromboembolic events. Please see next page for a brief summary of prescribing information.

OMNIPAQUE® 140 [redacted]

(IOHEXOL) INJECTION INTRAVASCULAR

PLEASE CONSULT FULL PRODUCT INFORMATION BEFORE USING. A SUMMARY FOLLOWS:

DESCRIPTION: OMNIPAQUE is a sterile, pyrogen-free and preservative-free, nonionic, water-soluble radiographic contrast medium for intravascular administration in concentrations of 140, 240, 300, and 350 mgI/mL. OMNIPAQUE 140 contains 302 mg of iohexol equivalent to 140 mg of organic iodine per mL; OMNIPAQUE 240 contains 518 mg of iohexol equivalent to 240 mg of organic iodine per mL; OMNIPAQUE 300 contains 647 mg of iohexol equivalent to 300 mg of organic iodine per mL; and OMNIPAQUE 350 contains 755 mg of iohexol equivalent to 350 mg of organic iodine per mL. Each milliliter of iohexol solution contains 1.21 mg tromethamine and 0.1 mg edetate calcium disodium with the pH adjusted between 6.8 and 7.7 with hydrochloric acid or sodium hydroxide. Unused portions must be discarded. Iohexol solution is sensitive to light and should be protected from exposure.

CONTRAINDICATIONS: OMNIPAQUE should not be administered to patients with a known hypersensitivity to iohexol.

WARNINGS—General: Nonionic iodinated contrast media inhibit blood coagulation, in vitro, less than ionic contrast media. Clotting has been reported when blood remains in contact with syringes containing nonionic contrast media.

Serious, rarely fatal, thromboembolic events causing myocardial infarction and stroke have been reported during angiographic procedures with both ionic and nonionic contrast media. Therefore, meticulous intravascular administration technique is necessary, particularly during angiographic procedures, to minimize thromboembolic events. Numerous factors, including length of procedure, catheter and syringe material, underlying disease state, and concomitant medications, may contribute to the development of thromboembolic events. For these reasons, meticulous angiographic techniques are recommended including close attention to guidewire and catheter manipulation, use of manifold systems and/or three-way stopcocks, frequent catheter flushing with heparinized saline solutions and minimizing the length of the procedure. The use of plastic syringes in place of glass syringes has been reported to decrease but not eliminate the likelihood of in vitro clotting.

OMNIPAQUE should be used with extreme care in patients with severe functional disturbances of the liver and kidneys, severe thyrotoxicosis, or myelomatosis. Diabetics with a serum creatinine level above 3 mg/dL should not be examined unless the possible benefits of the examination clearly outweigh the additional risk. OMNIPAQUE is not recommended for use in patients with anuria.

Radiopaque contrast agents are potentially hazardous in patients with multiple myeloma or other paraproteinemia, particularly in those with therapeutically resistant anuria. Although neither the contrast agent nor dehydration has separately proven to be the cause of anuria in myeloma, it has been speculated that the combination of both may be causative factors. The risk in myelomatous patients is not a contraindication; however, special precautions are necessary. Partial dehydration in the preparation of these patients prior to injection is not recommended since this may predispose the patient to precipitation of the myeloma protein in the renal tubules. No form of therapy, including dialysis, has been successful in reversing the effect. Myeloma, which occurs most commonly in persons over age 40, should be considered before instituting intravascular administration of contrast agents.

Ionic contrast media, when injected intravenously or intra-arterially, may promote sickling in individuals who are homozygous for sickle cell disease.

Administration of radiopaque materials to patients known or suspected of having pheochromocytoma should be performed with extreme caution. If, in the opinion of the physician, the possible benefits of such procedures outweigh the considered risks, the procedures may be performed, however, the amount of radiopaque medium injected should be kept to an absolute minimum. The patient's blood pressure should be assessed throughout the procedure and measures for the treatment of hypertensive crisis should be readily available.

Reports of thyroid storm following the use of iodinated, ionic radiopaque contrast media in patients with hyperthyroidism or with an autonomously functioning thyroid nodule suggest that this additional risk be evaluated in such patients before use of any contrast medium.

Urography should be performed with caution in patients with severely impaired renal function and patients with combined renal and hepatic disease.

PRECAUTIONS—General: Diagnostic procedures which involve the use of radiopaque diagnostic agents should be carried out under the direction of personnel with the prerequisite training and with a thorough knowledge of the particular procedure to be performed. Appropriate facilities should be available for coping with any complication of the procedure, as well as for emergency treatment of severe reactions to the contrast agent itself. After parenteral administration of a radiopaque agent, competent personnel and emergency facilities should be available for at least 30 to 60 minutes, since severe delayed reactions have occurred (see ADVERSE REACTIONS: Intravascular—General).

Preparatory dehydration is dangerous and may contribute to acute renal failure in patients with advanced vascular disease, in diabetic patients, and in susceptible nondiabetic patients (often elderly with preexisting renal disease), infants, and small children. Dehydration in these patients seems to be enhanced by the osmotic diuretic action of urographic agents. It is believed that overnight fluid restriction prior to excretory urography generally does not provide better visualization in normal patients. *Patients should be well hydrated prior to and following administration of any contrast medium, including iohexol.*

Acute renal failure has been reported in diabetic patients with diabetic nephropathy and in susceptible nondiabetic patients (often elderly with preexisting renal disease) following excretory urography. Therefore, careful consideration of the potential risks should be given before performing this radiographic procedure in these patients.

Immediately following surgery, excretory urography should be used with caution in renal transplant recipients.

The possibility of a reaction, including serious, life-threatening, fatal, anaphylactoid or cardiovascular reactions should always be considered (see ADVERSE REACTIONS: Intravascular—General). It is of utmost importance that a course of action be carefully planned in advance for immediate treatment of serious reactions, and that adequate and appropriate personnel be readily available in case of any reaction.

The possibility of an idiosyncratic reaction in susceptible patients should always be considered (see ADVERSE REACTIONS: Intravascular—General). The susceptible population includes, but is not limited to, patients with a history of a previous reaction to contrast media, patients with a known sensitivity to iodine per se, and patients with a known clinical hypersensitivity: bronchial asthma, hay fever, and food allergies.

The occurrence of severe idiosyncratic reactions has prompted the use of several pretesting methods. However, pretesting cannot be relied upon to predict severe reactions and may itself be hazardous for the patient. It is suggested that a thorough medical history with emphasis on allergy and hypersensitivity, prior to the injection of any contrast media, may be more accurate than pretesting in predicting potential adverse reactions.

A positive history of allergies or hypersensitivity does not arbitrarily contraindicate the use of a contrast agent where a diagnostic procedure is thought essential, but caution should be exercised (see ADVERSE REACTIONS: Intravascular—General). Premedication with antihistamines or corticosteroids to avoid or minimize possible allergic reactions in such patients should be considered and administered using separate syringes. Recent reports indicate that such pretreatment does not prevent serious, life-threatening reactions, but may reduce both their incidence and severity.

Even though the osmolality of OMNIPAQUE is low compared to diatrizoate- or iothalamate-based ionic agents of comparable iodine concentration, the potential transitory increase in the circulatory osmotic load in patients with congestive heart failure requires caution during injection. These patients should be observed for several hours following the procedure to detect delayed hemodynamic disturbances.

General anesthesia may be indicated in the performance of some procedures in selected adult patients; however, a higher incidence of adverse reactions has been reported in these patients and may be attributable to the inability of the patient to identify untoward symptoms, or to the hypotensive effect of anesthesia, which can reduce cardiac output and increase the duration of exposure to the contrast agent.

Angiography should be avoided whenever possible in patients with homocystinuria, because of the risk of inducing thrombosis and embolism.

In angiographic procedures, the possibility of dislodging plaques or damaging or perforating the vessel wall should be borne in mind during the catheter manipulations and contrast medium injection. Test injections to ensure proper catheter placement are recommended.

Selective coronary arteriography should be performed only in those patients in whom the expected benefits outweigh the potential risk. The inherent risks of angiocardiography in patients with chronic pulmonary emphysema must be weighed against the necessity for performing this procedure.

When OMNIPAQUE is to be injected using plastic disposable syringes, the contrast medium should be drawn into the syringe and used immediately.

If nondisposable equipment is used, scrupulous care should be taken to prevent residual contamination with traces of cleansing agents.

Parenteral products should be inspected visually for particulate matter and discoloration prior to administration. If particulate matter or discoloration is present, do not use.

Information for Patients: Patients receiving injectable radiopaque diagnostic agents should be instructed to:

1. Inform your physician if you are pregnant.
2. Inform your physician if you are diabetic or if you have multiple myeloma, pheochromocytoma, homozygous sickle cell disease, or known thyroid disorder (see WARNINGS—General).
3. Inform your physician if you are allergic to any drugs, food, or if you had any reactions to previous injections of dyes used for x-ray procedures (see PRECAUTIONS—General).
4. Inform your physician about any other medications you are currently taking, including nonprescription drugs, before you are administered this drug.

Drug/Laboratory Test Interaction: If iodine-containing isotopes are to be administered for the diagnosis of thyroid disease, the iodine-binding capacity of thyroid tissue may be reduced for up to 2 weeks after contrast medium administration. Thyroid function tests which do not depend on iodine estimation, eg, T_3 resin uptake or direct thyroxine assays, are not affected. Many radiopaque contrast agents are incompatible in vitro with some antihistamines and many other drugs; therefore, no other pharmaceuticals should be admixed with contrast agents.

Carcinogenesis, Mutagenesis, Impairment of Fertility: No long-term animal studies have been performed to evaluate carcinogenic potential, mutagenesis, or whether OMNIPAQUE can affect fertility in men or women.

Pregnancy Category B: Reproduction studies have been performed in rats and rabbits with up to 100 times the recommended human dose. No evidence of impaired fertility or harm to the fetus has been demonstrated due to OMNIPAQUE. There are, however, no studies in pregnant women. Because animal reproduction studies are not always predictive of human response, this drug should be used during pregnancy only if clearly needed.

Nursing Mothers: It is not known to what extent iohexol is excreted in human milk. However, many injectable contrast agents are excreted unchanged in human milk. Although it has not been established that serious adverse reactions occur in nursing infants, caution should be exercised when intravascular contrast media are administered to nursing women. Bottle feedings may be substituted for breast feedings for 24 hours following administration of OMNIPAQUE.

Pediatric Use: Pediatric patients at higher risk of experiencing adverse events during contrast medium administration may include those having asthma, a sensitivity to medication and/or allergens, congestive heart failure, a serum creatinine > 1.5 mg/dL, or those less than 12 months of age.

ADVERSE REACTIONS

Intravascular—General: Adverse reactions following the use of OMNIPAQUE are usually mild to moderate in severity. However, serious, life-threatening, and fatal reactions, mostly of cardiovascular origin, have been associated with the administration of iodine-containing contrast media, including OMNIPAQUE. The injection of contrast media is frequently associated with the sensation of warmth and pain, especially in peripheral angiography; pain and warmth are less frequent and less severe with OMNIPAQUE than with many contrast media.

Cardiovascular System: Arrhythmias including PVCs and PACs (2%), angina/chest pain (1%), and hypotension (0.7%). Others including cardiac failure, asystole, bradycardia, tachycardia, and vasovagal reaction were reported with an individual incidence of 0.3% or less. In controlled clinical trials involving 1,485 patients, one fatality occurred. A cause and effect relationship between this death and iohexol has not been established.

Nervous System: Vertigo [including dizziness and lightheadedness] (0.5%), pain (3%), vision abnormalities [including blurred vision and photomas] (2%), headache (2%), and taste perversion (1%). Others including anxiety, fever, motor and speech dysfunction, convulsion, paresthesia, somnolence, stiff neck, hemiparesis, syncope, shivering, transient ischemic attack, cerebral infarction, and nystagmus were reported, with an individual incidence of 0.3% or less.

Respiratory System: Dyspnea, rhinitis, coughing, and laryngitis, with an individual incidence of 0.2% or less.

Gastrointestinal System: Nausea (2%) and vomiting (0.7%). Others including diarrhea, dyspepsia, cramp, and dry mouth were reported, with an individual incidence of less than 0.1%.

Skin and Appendages: Urticaria (0.3%), purpura (0.1%), abscess (0.1%), and pruritus (0.1%).

Individual adverse reactions which occurred to a significantly greater extent for a specific procedure are listed under that indication in full prescribing information.

Pediatrics: In controlled clinical trials involving 391 patients for pediatric angiocardiography, urography, and contrast-enhanced computed tomographic head imaging, adverse reactions following the use of OMNIPAQUE 240, OMNIPAQUE 300 and OMNIPAQUE 350 were generally less frequent than with adults.

Cardiovascular System: Ventricular tachycardia (0.5%), 2:1 heart block (0.5%), hypertension (0.3%), and enemia (0.3%).

Nervous System: Pain (0.8%), fever (0.5%), taste abnormality (0.5%), and convulsion (0.3%).

Respiratory System: Congestion (0.3%) and apnea (0.3%).

Gastrointestinal System: Nausea (1%), hypoglycemia (0.3%), and vomiting (2%).

Skin and Appendages: Rash (0.3%).

General Adverse Reactions to Contrast Media: Physicians should remain alert for the occurrence of adverse effects in addition to those discussed above. The following reactions have been reported after administration of other intravascular iodinated contrast media, and rarely with iohexol. *Reactions due to technique:* hematomas and ecchymoses. *Hemodynamic reactions:* vein cramp and thrombophlebitis following intravenous injection. *Cardiovascular reactions:* rare cases of cardiac arrhythmias, reflex tachycardia, chest pain, cyanosis, hypertension, hypotension, peripheral vasodilatation, shock, and cardiac arrest. *Renal reactions:* occasionally, transient proteinuria, and rarely, oliguria or anuria. *Allergic reactions:* asthmatic attacks, nasal and conjunctival symptoms, dermal reactions such as urticaria with or without pruritus, as well as pleomorphic rashes, sneezing, and lacrimation; and rarely, anaphylactic reactions. Rare fatalities have occurred due to this or unknown causes. *Signs and symptoms related to the respiratory system:* pulmonary or laryngeal edema, bronchospasm, dyspnea; or *to the nervous system:* restlessness, tremors, convulsions. *Other reactions:* flushing, pain, warmth, metallic taste, nausea, vomiting, anxiety, headache, confusion, pallor, weakness, sweating, localized areas of edema (especially facial cramps), neutropenia, and dizziness. Rarely, immediate or delayed rigors can occur, sometimes accompanied by hyperpyrexia. Infrequently, "iodism" (salivary gland swelling) from organic iodinated compounds appears 2 days after exposure and subsides by the sixth day.

In general, the reactions which are known to occur upon parenteral administration of iodinated contrast agents are possible with any nonionic agent. Approximately 95% of adverse reactions accompanying the use of water-soluble intravascularly administered contrast agents are mild to moderate in degree. However, severe, life-threatening anaphylactoid reactions, mostly of cardiovascular origin, have occurred. Reported incidences of death range from 6.6 per 1 million (0.00066%) to 1 in 10,000 (0.01%). Most deaths occur during injection or 5 to 10 minutes later, the main feature being cardiac arrest, with cardiovascular disease as the main aggravating factor. Isolated reports of hypotensive collapse and shock are found in the literature. The incidence of shock is estimated to be 1 out of 20,000 (0.005%) patients.

Adverse reactions to injectable contrast media fall into two categories: chemotoxic reactions and idiosyncratic reactions.

Chemotoxic reactions result from the physicochemical properties of the contrast media, the dose, and the speed of injection. All hemodynamic disturbances and injuries to organs or vessels perfused by the contrast medium are included in this category.

Idiosyncratic reactions include all other reactions. They occur more frequently in patients 20 to 40 years old. Idiosyncratic reactions may or may not be dependent on the amount of dose injected, the speed of injection, and the radiographic procedure. Idiosyncratic reactions are subdivided into minor, intermediate, and severe. The minor reactions are self-limited and of short duration; the severe reactions are life-threatening and treatment is urgent and mandatory.

The reported incidence of adverse reactions to contrast media in patients with a history of allergy is twice that in the general population. Patients with a history of previous reactions to a contrast medium are three times more susceptible than other patients. However, sensitivity to contrast media does not appear to increase with repeated examinations.

Most adverse reactions to injectable contrast media appear within 1 to 3 minutes after the start of injection, but delayed reactions may occur.

Regardless of the contrast agent employed, the overall estimated incidence of serious adverse reactions is higher with angiocardiography than with other procedures. Cardiac decompensation, serious arrhythmias, angina pectoris, or myocardial ischemia or infarction may occur during angiocardiography and left ventriculography. Electrocardiographic and hemodynamic abnormalities occur less frequently with OMNIPAQUE than with diatrizoate meglumine and diatrizoate sodium injection.

CONSULT PACKAGE INSERT FOR A MORE DETAILED DISCUSSION OF ADVERSE REACTIONS FOR INTRAVASCULAR USE OF OMNIPAQUE.

OVERDOSAGE: Overdosage may occur. The adverse effects of overdosage are life-threatening and affect mainly the pulmonary and cardiovascular systems. The symptoms include cyanosis, bradycardia, acidosis, pulmonary hemorrhage, convulsions, coma, and cardiac arrest. Treatment of an overdosage is directed toward the support of all vital functions and prompt institution of symptomatic therapy.

The intravenous LD_{50} values of OMNIPAQUE (in grams of iodine per kilogram body weight) are 24.2 in mice and 15.0 in rats.

DOSAGE AND ADMINISTRATION: Details are provided in the package insert.

Distributed by Sanofi Winthrop Pharmaceuticals
New York, NY 10016
Manufactured by Sterling Pharmaceuticals Inc.
Barceloneta, Puerto Rico 00617

Reference:
1. Data on file, Sanofi Winthrop Pharmaceuticals.

sanofi WINTHROP

Hospital Products Division
Sanofi Winthrop Pharmaceuticals
New York, NY 10016

64-210830C OSW-1

ARRS Presidential Address

Ethics in Current Medical Imaging

A. Everette James, Jr.[1]

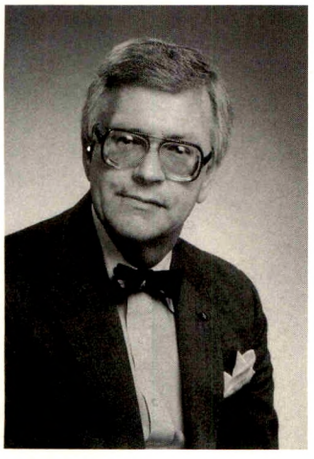

The complexities of modern health care delivery have restructured the relationships of both providers and recipients. These have affected the service disciplines especially, as well as the interrelationships among many providers of medical service themselves [1–4]. These departures from the historical modes of initiation and response in medicine provide radiologists with unprecedented challenges regarding daily judgments of what constitutes appropriate and ethical behavior [5–7].

This address will examine some of these complexities in the context of our historical traditions, offer some observations regarding the effects of the present societal environment, and suggest analysis and attitudes that appear to have future promise.

Traditionally, medicine involved almost exclusively the fundamental relationship of patient and physician—the physician with an all-encompassing fiduciary capacity and the patient in a dependent and accepting role. Most of the principles embodied in the Hippocratic oath and other guidelines for practice conduct reflected this private and quite personal arrangement.

The concepts of ethical behavior in medicine evolved over a rather lengthy period; these codes of conduct were primarily based on personal human relationships, an ordered morality, and religious fundamentals. They were relatively uncluttered by concurrent economic considerations or by initiatives from other disciplines.

The rate constant for the development of ethical medical standards has changed from the historically slow evolutionary process. By midcentury, medical ethics came to occupy an intermediate temporal position in their evolution. As advances in science entered daily practice, the rapid promulgation of medical standards became the norm. The law, however, continued to develop its own behavioral guidelines in the characteristically ponderous method of litigation and precedent decisions that would eventually influence public policy.

The deliberate and almost leisurely pace of the traditional development of ethical norms enjoyed by the medical profession also was characterized by self-analysis, self-determination, and self-regulation. Those changes in professional behavior that did occur among physicians went largely unchallenged, either by other practitioners of the discipline or by the patients as consumers. While the ministry of medicine was indeed a service, patients traditionally viewed (and, to a large extent, still do) the physician as someone who has undergone considerable personal sacrifice in order to become and remain competent to perform this service. The advantaged position of the medical profession was accepted as a natural consequence of the rigorous requirements of

Presented at the annual meeting of the American Roentgen Ray Society, Orlando, FL, May 1992.

[1]Department of Radiology and Radiological Sciences, Vanderbilt University Medical Center, 21st and Garland, Nashville, TN 37232-2675. Address reprint requests to A. E. James, Jr.

AJR 1993;160:1–4 0361–803X/93/1601–0001

entry to practice and the importance of this activity to society. Historically, only a few professions were recognized, and these were regarded with considerable respect by those they served.

Characterization of Medical Practice

Until the mid-20th century, medicine also was characterized by its lack of definitive methods to diagnose and treat human diseases. Much of the care extended to patients was in the form of nurture and the provision of physical comfort, with little use made of complicated and expensive technology. The process of healing depended largely on the powers of the human body and spirit, with the physician supporting patients and their families while this process occurred. The physician was a recognized part of the cure but was not equated with or considered the cure itself [1, 8, 9].

In the decades after midcentury, the character of medicine and especially our discipline changed dramatically [10, 11]. Scientific discoveries were applied to the diagnosis and treatment of disease. Medical technologies were developed that required large sums of public resources. In response to practice opportunities, physicians began to specialize and subspecialize, finding themselves engaged in activities that were quite different and unique. This changed both their conduct and their relations with patients and with their fellow physicians. Confidence in relief and cure of disease shifted from the fundamental nurturing relationship between personal physician and patient to the more impersonal one, with the physician acting as purveyor of this new and powerful technology. Trust and hope on the part of the consumer-patient became confidence and expectation. The physician often became remote from the patient, and little, if any, personal relationship could be established in this environment.

The technological phenomenon, as well as the pioneers in its development and the early users of this instrumentation, was initially greeted with enthusiasm and almost awe. Public programs were developed to foster health care institutions such as hospitals that provided the appropriate locations for these biomedical advances, and methods of compensation were enacted to support their growth. After the Second World War, the groundswell of national pride made Americans confident that our industry, energy, and spirit would make all things possible in the decades to follow. Many of the technical advances developed for other purposes during the war could be and were applied to medicine. The delivery of health care moved from what was, at most, a cottage industry to a major business enterprise involving and consuming a significant portion of public resources.

In this enterprise, the role of physicians became that of a participant in a growth industry over which they came to realize they had much less influence and control than they had enjoyed under previous arrangements. Physicians were often the designated advocates in procuring these technologies. As such, they had no traditional medical guidelines as to what represented proper and ethical behavior [12–14]. Understandably, as they—and their patients—became aware of these advances, the desire for access was often the prime determinant of their actions.

Regulation by Public Policy

Restraints such as certificates of need were used by policymakers to limit acquisitions and regulate the distribution of technology [15, 16]. In response, physicians entered into various financial arrangements in which an unstated intent was to circumvent the regulations. These entrepreneurial schemes would often involve physicians in ownership of the same technology they used on their patients. Their coinvestors might well be businessmen whose primary or sole agenda was to make a profit. The ethics of these arrangements sometimes became a consideration of legality and not just of proper professional conduct. Considerations of bias and conflicts of interest became complicated and difficult to define clearly [1, 17–19].

Another initiative to regulate the use of technology was the enactment of diagnostic related groups (DRGs) [2, 12]. This arrangement allowed a specified amount of financial resources to be used in the evaluation and treatment of a particular constellation of symptoms and presumed diagnoses. Many health analysts thought that DRGs were a prospective pricing system that would determine the type of medical practice physicians could be compensated for rendering. This valued medical services in economic terms. In order to circumvent these regulations, physicians soon learned which presumptive diagnoses would allow them the most latitude in the evaluation and treatment process.

Physicians in this circumstance often found themselves in the role of "gatekeeper," distributing care according to guidelines set by others, rather than practicing without constraint all the medicine they felt necessary in order to diagnose diseases and treat their patients optimally. They were also frustrated because they were sometimes unable to meet the perceived expectations of patients regarding the access to and use of this expensive medical technology. This produced an ethical dilemma for physicians, and the response was sometimes manifested by circumventing the DRG guidelines under the rationale that only they knew what was best for their patients, and their activities were an expression of this fundamental mandate.

More recently, Congress and the Department of Health and Human Services have embarked on programs to restructure the practice of medicine, using guidelines of practice and compensation that could significantly regulate the behavior of physicians [20–23]. Since it is believed that we have entered into an era in which the technological and procedural practice of medicine is too highly rewarded and the "cognitive" (hands-on) practice of medicine is undercompensated, a system of valuation of activity and payment has been proposed to address this issue [24, 25]. A group of economists and policymakers, with the consultation of physicians, have developed a resource-based relative value scale to compensate physicians for their activities.

Primary care involving patient and physician interaction is to be more highly compensated on a relative basis, and technological procedures will presumably become less rewarded. Physicians will now be forced to evaluate their intended course of medical action with a much greater emphasis placed on the direct effect on their personal income. This economic decision process is one in which

physicians feel increasingly uncomfortable, and their behavior will often reflect an attempt to abrogate this responsibility for cost containment that has been thrust on them. Ethical standards in this new practice environment may need to be recast [1, 12].

Development of Standards

Another profound change in health policy that will greatly affect radiology is the development of practice guidelines. Currently in medical imaging there is a concerted effort to address the issue of standard of practice codification in a discipline that is characterized by a continuum of developments [26]. These will provide ethical and legal issues for our specialty practice that are unprecedented [1, 9]. The common law of most states allows introduction of practice guidelines as evidence of the standard of care in malpractice litigation, provided that the data are relevant to the clinical issues involved and meet certain indicia of reliability. Although admitted into evidence, a practice guideline will not constitute a predetermined standard of care that a court is obligated to apply [27, 28].

It is too early in the development of practice guidelines to state conclusively whether they can be usefully applied as the standard of care in malpractice litigation, especially in the dynamics of a discipline such as medical imaging [29]. Numerous technical problems and policy questions are associated with the development of practice guidelines that may make their use as a current prescriptive standard of care in medical imaging problematic, and it remains to be seen whether these issues can be satisfactorily resolved in the near term [23].

Many analysts believe that practice guidelines will enable physicians to provide high-quality medical care more effectively and efficiently, without significantly sacrificing the quality of care. Practice guidelines may assist physicians in reducing the amount of unnecessary or inappropriate diagnostic testing and care for patients, thereby decreasing the costs associated with unneeded diagnostic inquiries and services. Presumably, the number of unwarranted or ill-advised imaging studies would be reduced. Practice guidelines also could reduce the frequency of avoidable injuries caused by substandard care and defensive medicine [30].

The rationale for making practice guidelines the standard of care in malpractice claims has some logic. If practice guidelines are meant to change clinical practice in ways that will yield substantial benefits in improved quality and reduced costs, they could then be applied as judicial standards of care. Since practice guidelines are meant to describe the most appropriate ways to deal with clinical problems, it follows that they may well be the standard that radiologists will be held to when caring for patients. The development of common understandings will be complicated by the wide diversity of medical practices and the infeasibility of developing a single method of guidance for highly complex areas of endeavor, such as radiology.

A number of different applications are expected for practice guidelines, even for the same medical problem [23, 30]. Some users plan to apply them as guides for the treatment of patients and for utilization review procedures in quality assurance to evaluate the competence of individual physicians. These guidelines also might be applied in risk management procedures meant to prevent avoidable injuries of patients. Thus, a single method for development and a single format for presentation of practice guidelines to adequately meet all of these needs should not be anticipated. A practice guideline designed to control costs by describing when it is appropriate or inappropriate to use an expensive medical technology, for example, could presumably be developed and presented in a different manner than a practice guideline that is designed to improve quality by describing optimal strategies for the management of patients with a given medical problem [23].

Uncertainty makes medicine an art as well as a science, and it is not feasible to expect practice guidelines to capture and express the art of medicine or to encompass all of ethical medical behavior. Uncertainty will result in differences of opinion among physicians about the ethical issues surrounding a medical problem and how to address them. Practice guidelines that address disputed areas of medicine will hopefully be less prescriptive and will allow physicians and patients to decide which guideline should be appropriately applied. Practice guidelines that address areas of uncertainty should not be applied as absolute standards of care, or the art of medicine may eventually be lost.

A practice guideline in medical imaging might soon become out-of-date as a result of the development and availability of new technological innovations, but its status as a legal standard could delay implementation of the technology. Recall the fate of nuclear medicine brain scans, pneumoencephalograms, and myelograms with the advent of CT, radionuclide placentography with the introduction of sonography, and certain CT procedures with the introduction and availability of MR imaging. In this structured environment, the flexibility and spontaneity that medicine depends on for advancement might be significantly diminished.

Outcomes Evaluation

Medicine has traditionally been allowed to both value and evaluate the effectiveness and appropriateness of its services. Largely, this analysis has been cast in technical and medical terms. More recently, the phenomenon of increased societal accountability has given emphasis to a new valuation of medical endeavors, outcomes research [8, 25]. Often called "effectiveness research," this method of inquiry or evaluative clinical science addresses the treatment of clinical conditions rather than individual procedures [9]. Outcomes research is a systematic assessment that is often conducted by multidisciplinary teams using judgments encompassing endpoints that reflect the values of patients.

Outcome, defined as the effect on patients' health and well-being, is a major societal concern as well as a substantial investment [8, 25, 31]. While the medical profession has largely assumed that interest in patients' welfare is the primary determinant of their activity, a Congress-mandated study by the Office of Technology Assessment estimated that only 10-20% of physicians' activity resulted in improved welfare of patients. In the past decade, a number of inquiries have shown that the data supplied by traditional research

about medical appropriateness and effectiveness have been either incomplete or misleading. In response, we have seen the recent development of a specialized form of diagnostic inquiry, health services research. Congress has directed substantial resources to the Agency for Health Care Policy and Research for activities in this area of investigation. Their activities will certainly involve sophisticated and expensive technology. The effects on our discipline could be profound. Ethical canons for radiology may have to be restructured again.

Ethics are values. Values depend on individual and personal convictions often buffered and shaped by the environment in which they are developed. As noted in this communication, the complexity of one discipline, as well as its inherently changing nature, will challenge both our character and creativity in responding to ethical challenges and in developing appropriate new guidelines and standards. This will, in the future, more properly emphasize the desired outcomes of the users rather than the providers. Outcomes research will become an increasingly important investigative and evaluative endeavor.

Control and responsibility in the entire health care field will undergo significant realignment in ensuing decades. Physicians are now at a juncture in the evolution of health care where they are being challenged in their fiduciary capacity and are subject to an ever-increasing public accountability. Practice outcomes are now being judged in response to patients' values and quantified whenever possible in public perceptions. Medical ethics are now acquiring a closer fit to general human ethics and not to specialized standards historically accorded to the healing arts. Physicians and health care workers should make every effort to be an active and effective part of this process.

ACKNOWLEDGMENTS

I appreciate the advice of my colleagues at the Institute of Medicine; Clark Havighurst, Duke University; Sy Perry, Georgetown University; John Thornbury, University of Wisconsin; Dick Zaner, Vanderbilt University School of Medicine; John E. Chapman, Vanderbilt University School of Medicine; Harold Jacobson; Gerald Freedman; Henry P. Pendergrass; and members of my staff at Vanderbilt University Medical Center.

REFERENCES

1. James AE Jr, Greeson T, Price RR, Pendergrass HP, et al. Legal and ethical issues in a technologic discipline: new times, new choices. *Invest Radiol* **1986**;21:673–677
2. James AE Jr, Curran WJ, Pendergrass HP, Chapman JE. Academic radiology, turf conflict and antitrust laws. *Invest Radiol* **1990**;25:200–202
3. Hillman AL, Pauly MV, Kerstein JJ. How do financial incentives affect physicians' clinical decisions and the financial performance of health maintenance organizations? *N Engl J Med* **1989**;321:86–92
4. James AE Jr, Chapman JE, Carroll F, et al. Ethical choices in high technology medicine: current dilemmas in diagnostic imaging. *Health Care Instrumentation* **1986**;1:158–167
5. James AE Jr, Partain CL, Hamilton RJ, et al. A critique of the concept of MRI centers. *Magn Reson Imaging* **1987**;5:71–75
6. McNeil BJ, Pauker SG. Decision analysis for public health: principles and illustrations. *Ann Rev Public Health* **1984**;5:135–161
7. James AE Jr, Sloan FA, Pendergrass HP, et al. Hospital cost regulation: some cumulative effects from certificate of need and diagnostic related groups. *Noninvasive Med Imaging* **1984**;1:259–263
8. Wennberg JE. Outcomes research, cost containment, and the fear of health care rationing. *N Engl J Med* **1990**;323:1202–1204
9. Engler RL, Covell JW, Friedman PJ, Kitcher PS, Peters RM. Misrepresentation and responsibility in medical research. *N Engl J Med* **1987**;317:1383–1389
10. James AE Jr, ed. *Medical/legal issues for radiologists*. Chicago: Precept Press, **1987**
11. James AE Jr, Price RR, Sloan F, Zaner R, Chapman J. Certain social considerations in abandoning high technology medical imaging. *Health Matrix* **1987**;5:31–34
12. James AE Jr, Perry S, Zaner RM, Chapman JE, Calvani T. The changing concept of standard of care and the development of medical imaging technology. *Humane Med* **1991**;7:265–271
13. Lohr KN, Yordy KD, Thier SO. Current issues in quality of care. *Health Aff* **1988**;7:518
14. Greer A. The state of the art versus the state of the science. *Int J Technol Assess Health Care* **1988**;4:526
15. James AE Jr, Perry S, Warner SE, Chapman JE, Zaner RM. The diffusion of medical technology: free enterprise and regulatory models in the USA. *J Med Ethics* **1991**;17:150–155
16. James AE Jr, Sloan F, Blumstein J, Winfield AC, Pendergrass HP. Certificate of need in an antitrust context. *J Health Polit Policy Law* **1983**;8: 314–319
17. Kanouse DE, Brook RH, Winkler JD, et al. *Changing medical practice through technology assessment: an evaluation of the NIH consensus development program*. Santa Monica, CA: RAND Corp., **1989**
18. Perry S. The NIH consensus development a decade later. *N Engl J Med* **1987**;317:485–488
19. James AE Jr, Linton O, James AE III, et al. Some legal issues of turf: relation to magnetic resonance. *Magn Reson Imaging* **1990**;8:13
20. Leape L. Practice guidelines and standards: an overview. *Qual Rev Bull* **1990**;16:42–49
21. Chassin MR, Kosecoff J, Park RE, et al. Does inappropriate use explain geographic variation in the use of health care services? A study of three procedures. *JAMA* **1987**;258:2533–2537
22. Hillman BJ, Fajardo LL, Witzke DB, et al. Influences affecting radiologists' choices of academic or private practice careers. *Radiology* **1990**;174: 561–564
23. Havighurst C. Practice guidelines for medical care: the policy rationale. *St. Louis Univ Law Rev* **1990**;34:777–819
24. Eddy D. Resolving conflicts in practice policies. *JAMA* **1990**;264:389–391
25. Roper W, Winkenwerder W, Hackbarth G, Krakauer H. Effectiveness in health care: an initiative to evaluate and improve medical practice. *N Engl J Med* **1988**;319:1179–1202
26. Gabor A. *The man who discovered quality: how W. Edwards Deming brought the quality revolution to America—the stories of Ford, Xerox, and GM*. New York: Random House, **1990**
27. Havighurst CC. Practice guidelines as legal standards governing physician liability. *Law Contemp Prob* **1991**;54:87–117
28. Brennan T. Practice guidelines and malpractice litigation: collision or cohesion? *J Health Polit Policy Law* **1991**;16:67–85
29. Hirshfeld E. Practice parameters and the malpractice liability of physicians. *JAMA* **1990**;263:1556–1562
30. Garnick D, Hendricks A, Brelinan T. Can practice guidelines reduce the number and costs of malpractice claims? *JAMA* **1991**;266:2856–2860
31. Ellwood PM. The Shattuck Lecture. Outcome management: a technology of patient experience. *N Engl J Med* **1988**;318: 1549–1556

Edward B. D. Neuhauser Lecture

Pediatric Neuroradiology: Its Evolution as a Subspecialty

Derek C. Harwood-Nash[1]

Pediatric neuroradiology emerged as the first formal subspecialty of pediatric radiology during the late 1960s. The history of its development as an unusual and effective combination of an age-related and a specific organ-directed clinical subspecialty, and the considerable technical adaptation and innovation within the diagnostic imaging so required, merits its inclusion within the history of the modern matrix of radiology. This Neuhauser Lecture outlines the odyssey of this subspecialty until the present: the adaptation of techniques and equipment to accommodate imaging of patients of all sizes—from 1-kg infants to young adults—and the understanding of the wide spectrum of CNS diseases, many often extremely complex. The evolution of this special body of knowledge and experience, the established and productive fellowship programs, and the significant part pediatric neuroradiology now plays in major scientific and professional associations and societies have led to this subspecialty becoming a lifelong persuasion for a growing number of radiologists.

What is all knowledge too but recorded experience, and a product of history; of which, therefore, reasoning and belief, no less than action and passion, are essential materials?

Thomas Carlyle
Critical and Miscellaneous Essays

Pediatric neuroradiology has evolved to become a specific and objective science. It is a special diagnostic art form, tempered by the radiologist's own clinical experience, often tinged by imagination, yet blended with a delicate touch—all because the margin for error is small. The complexity of developmental neurologic disease, the prevalence of unusual and often congenital neoplasms, the plasticity of the skull base and sutures, and the often difficult techniques are few of the many instances that make pediatric neuroradiology different. It is necessary to be aware of the history of its genesis and development in order to better understand its present significance, and more so to chart its future. The challenges of modern imaging techniques, their adaptation toward effective diagnosis and management of pediatric CNS diseases, and the innovations so required are no different in principle from those required in the past. The rewards, however, are surely now much greater.

Received June 3, 1992; accepted after revision July 13, 1992.
Presented at the conjoint meeting of the Society for Pediatric Radiology and the European Society of Pediatric Radiology, IPR '91, Stockholm, May 1991.
[1]Department of Radiology, University of Toronto, Hospital For Sick Children, 555 University Ave., Toronto, Ontario, Canada M5G IX8. Address reprint requests to D. C. Harwood-Nash.

AJR **1993;160:5–14** 0361–803X/93/1601–0005

To be the Neuhauser Lecturer of the Society for Pediatric Radiology (SPR) is a treasured honor given by one's peers. To have known the late E. B. D. Neuhauser, and his still remarkable wife Gernda, is a privilege. Dr. Neuhauser started pediatric radiology in North America; he greatly assisted and supported those involved in the birth of one of its offsprings, pediatric neuroradiology.

The 1991 Neuhauser Lecture has further significance. The inaugural conjoint meeting in 1987 of the SPR and the European Society of Pediatric Radiology (ESPR)—International Pediatric Radiology (IPR '87)—was held in Toronto, Canada. Its Neuhauser Lecturer, the first by a non–North American, was given by one of Dr. Neuhauser's pupils and by my invitation: Professor Andres Giedion from Switzerland. Dr. and Mrs. Neuhauser were there, and it was Dr. Neuhauser's last meeting. It is fitting therefore that the second conjoint meeting of the SPR and ESPR, IPR '91 in Stockholm, the first meeting of the SPR outside North America, have as its Neuhauser Lecturer a North American, a Canadian, by invitation of its president, Donald R. Kirks of Cincinnati, himself a past pediatric neuroradiology fellow. John A. Kirkpatrick, Dr. Neuhauser's successor at Boston Children's Hospital (who in turn is now succeeded by Dr. Kirks), and Bernard J. Reilly, one of Dr. Neuhauser's earliest fellows and my own predecessor, were also honored at IPR '91 with the SPR's gold medal. Just as Dr. Neuhauser melded and adapted radiologic techniques designed for imaging adults to the clinical problems of pediatrics, whence pediatric radiology evolved, so did pediatric neuroradiology emerge from the practice of neuroradiologic imaging of adults to meet the clinical demands of pediatric neurosurgery and neurology. Both pediatric persuasions form a suitable paradigm of the familiar adage: a child is not a small adult.

Early in the 1960s a small and determined group of neurosurgeons in North America were becoming specialized full-time in pediatrics. This group, by their own actions and demands, formed the catalyst, indeed the challenge, for pediatric neuroradiology to evolve. Neuroradiology as a whole had by then already become formalized, and its early practitioners in North America, Scandinavia, England, and elsewhere in Europe started to develop a secondary interest in children. Notwithstanding, at that time most pediatric neuroradiologic techniques were being performed by neurosurgeons and neurologists. Thus, in 1968 there first arose, within the clinical pediatric neurologic sciences, a few young radiologists, some self-taught, but devoted full-time to a new and defined discipline: pediatric neuroradiology. Formal and defined fellowship training programs soon after evolved at the Hospital for Sick Children in Toronto with myself and Charles Fitz and then with Roy Strand at the Children's Hospital in Boston. Initially, great difficulty was experienced, to be expected, in rightly claiming neuroradiologic procedures from neurosurgeons and neurologists. Quality, safety, and service had to be assured. The demands of these clinicians together with those of orthopedic surgeons were then, and have always been, considerable—now even more so.

Notwithstanding the ease and safety of the new and refined modern techniques of imaging—CT, MR, and the many techniques of sonography well suited to infants and children—a recurring caveat was, and still is, however, that ease in itself is not an excuse or an indication. Definition and accuracy are the paramount principles.

The art of pediatric neuroradiology subsequently flourished worldwide in scope and in the number of practitioners, many prominent within general and pediatric hospital departments and radiologic and neuroscience societies. Many initially so trained by the first few are now themselves training third generations of pediatric neuroradiologists. Scholarly books [1–5] and a crescendo of scientific publications form a significant part of the radiologic literature, more so now with the advent of sophisticated sonography and MR imaging. As in North America, pediatric neuroradiology now flourishes in England, Scandinavia, elsewhere in Europe, Australia, New Zealand, and, lately, in Japan, Israel, and South America, for example. Pediatric neuroradiology has, to many, become a full-time, and even life-long, profession, a now mature subspecialty within clinical diagnostic imaging.

The Evolution of Pediatric Neuroradiologic Techniques

Before and during the 1960s, pediatric radiologists were extraordinarily adept in interpreting standard radiographs of the skull and spine. What few angiograms, myelograms, ventriculograms, and pneumoencephalograms then obtained were also interpreted by neurologists and neurosurgeons and by a few interested and experienced "adult" neuroradiologists [6]. This changed in 1968 [1]. Although detailed descriptions of every nuance of these early techniques exist [1, 6, 7], it is appropriate to outline their past and present uses from the perspective of modern-day practice.

Ventriculography

Historically, the first air ventriculogram was obtained in 1918. This then evolved into pneumoencephalography, performed when clinically permissible by the lumbar route rather than direct transcerebral needle insertion into the ventricles (Fig. 1). Many oil-based contrast media followed and disappeared: iodized poppy seed oil, Lipiodol, Thorotrast, and Pantopaque (ethyl iophenylundecylate). In 1966, a water-soluble contrast agent, methylglucamine iothalamate 60%, was used, but it was extremely neurotoxic if it moved from the ventricular system into the subarachnoid space, causing severe seizures. Metrizamide, introduced in 1973, was much safer, and both plain film and CT contrast-enhanced ventriculography were performed to great effect, often together with air ventriculography (Fig. 2). Safe and nonionic water-soluble contrast agents rapidly followed. The use of such agents with CT continues even today in myelography, providing accurate evaluation of CSF flow from one CSF compartment to another within the intracranial cavity and often showing the degree of aqueduct patency with certainty.

Micropulverized barium was placed in large cerebral abscesses often found serendipitously during ventriculography and after drainage by direct needle puncture, particularly in abscesses occurring in infants (Fig. 3). The walls of the abscesses took up the barium and allowed easy plain film follow-up of their size and shape. Leakage into the ventricular and CSF spaces seemed to have no untoward effects.

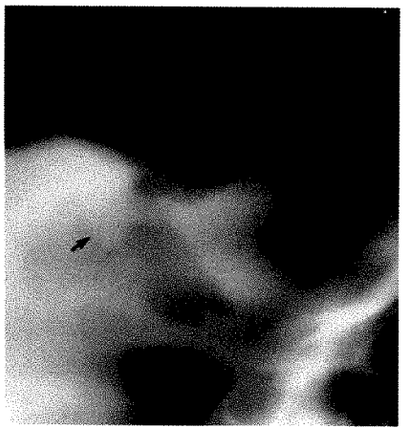

Fig. 1.—Ventriculography. Brow-up ventriculogram of infant with hydrocephalus shows astrocytoma (*arrow*) in roof of third ventricle blocking each foramen of Monro.

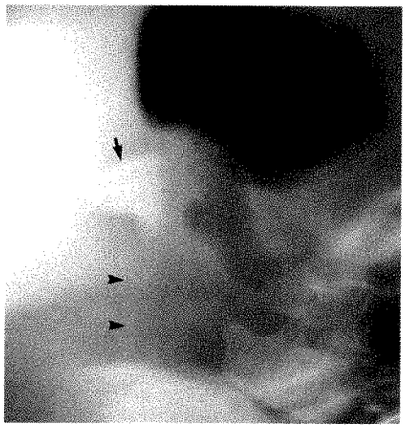

Fig. 2.—Positive-contrast ventriculography. Ventriculogram obtained with a combination of air and water-soluble contrast media (*arrow*) in an infant with hydrocephalus shows contrast material in distorted aqueduct (*arrowheads*) of a Chiari malformation, which could not be filled with air.

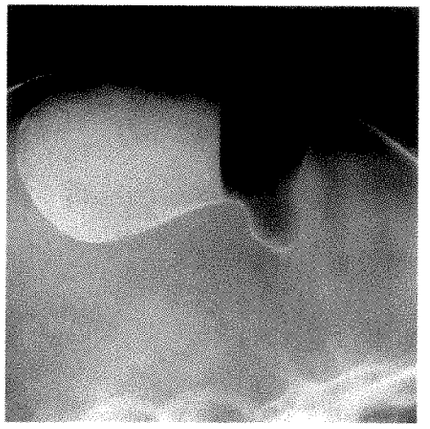

Fig. 3.—Micropaque barium cerebral cystography. Cystogram of infant shows contrast material in huge cerebral abscess that was discovered when ventriculogram was attempted. Abscess subsequently shrank to form a small opacified nidus, which was followed up with skull radiographs only.

Pneumoencephalography

Pneumoencephalography was performed in children suspected of having intracranial abnormalities, in whom no evidence of increased intracranial pressure was present. Infrequently and disturbingly was an unsuspected mass identified, the procedure aborted, and angiography resorted to forthwith.

The paramount principles were safety, accuracy, adequate fixation, and immobilization of the child. Anesthesia was necessary in all but cooperative teenagers. A most necessary homemade primitive "scaffold" (Fig. 4) first had to be constructed to accommodate all ages. This contraption was placed on a wooden stretcher together with a mobile portable C-arm image intensifier and an overhead tube—thus was pneumoencephalography performed. In total, pneumoencephalography was performed, safely, in 1000 infants and children of all ages by this method [1].

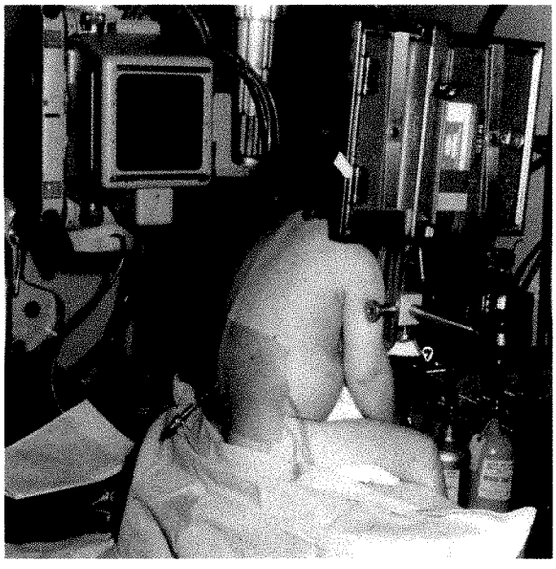

Fig. 4.—Primitive air encephalographic equipment. A homemade patient stand and film holder were placed on a stretcher together with a ceiling-mounted tube, enabling satisfactory air encephalogram to be obtained in an anesthetized child.

This in-house manufacturing started a continuing and often frustrating practice of innovations and also adaptations of equipment, catheters, and needles often initially designed for adults and not for infants and children weighing from 1 kg to 80 kg.

Short-beveled needles, correct head and chin positions, and relatively large volumes of air injected in fractionated amounts provided superb images of the surface anatomy of the brain and ventricles (Fig. 5). All the nuances of the variations of normal anatomy were fully appreciated, more so than with CT and equivalent even to that with MR. Subsequent supine polytomography (available in 1964) supplied superb anatomic detail of the optic nerves, infundibulum, floor of the third ventricle, temporal horns, and anterior ventricular borders to a degree nearly equivalent to that seen on MR images 20 years later.

The acquisition in early 1970 of the remarkable universal system Mimer III (Elema-Schonander) altered this crude method, but this machine was constructed for adults and children (Fig. 6), not for infants. This deficiency led to our design of The Hospital for Sick Children infant cradle (Fig. 7) (subsequently refined by Torgny Greitz of Stockholm), which was then used within the Mimer III system for infants and young children weighing from 800 g to 10 kg. Safe and controlled vertical 360° rotation and side-to-side movement with optimal patient fixation (Fig. 7) enabled ventriculography and pneumoencephalography to be performed while the patient was under anesthesia. An associated special attachment for a leukotome needle (Fig. 8) was made for Harold Hoffman,

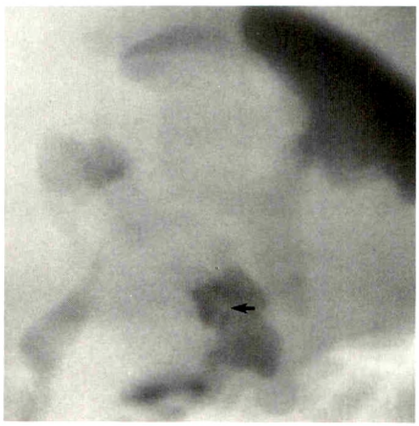

Fig. 5.—Pneumoencephalography. Brow-up pneumoencephalogram shows exquisite surface detail of upper pons, fourth ventricle, aqueduct, quadrigeminal bodies, anterior third ventricle, cavum velum interpositum, and ventricles. Tip of basilar artery (*arrow*) is clearly seen in interpeduncular cistern; air is held by anteriorly placed membrane of Liliequist.

our neurosurgical colleague, and us, whereby the cradle could be used for percutaneous third ventriculostomies (Fig. 8). Furthermore, linear tomography at any angle was also possible. The duration of each of these studies was up to 2 hr. In all, 4000 infants and children at our hospital, and many more elsewhere, were satisfactorily and safely examined in this way by using ventriculography and pneumoencephalography.

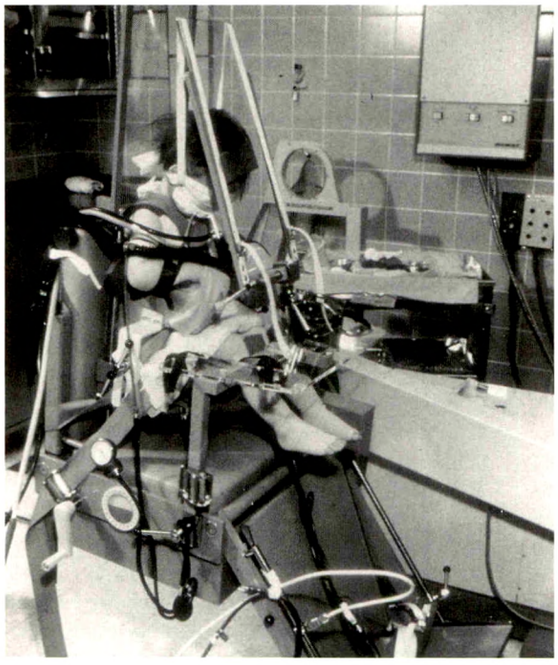

Fig. 6.—Mimer chair with standard child's chair attached shows complex but safe immobilization of anesthetized child. This chair enabled safe 360° rotation.

Myelography

Contrast agents used in myelography paralleled their advent and use in ventriculography; Pantopaque was in vogue in the late 1960s. Myelographic techniques in infants and children were similar to those in adults, with the exception that anesthesia was routinely used. This procedure was initially performed in a dark fluoroscopy room. Image intensification then emerged. It was soon found that the conus and cauda equina, especially in children, were posteriorly positioned in the dural sac, and thus anteroposterior imaging with the patient supine was essential in order to best visualize these areas, areas often having significant abnormalities in children. It was also considered, by us, that removal of the Pantopaque was essential. Hence, for these reasons, supine imaging was performed with the child supine and supported by U-shaped cushions of various heights, with the needle thus in situ during imaging and therefore available at the end of the procedure for removal of contrast material.

Deliberate off-line puncture in the lumbar region was safely performed even in the presence of a low spinal cord. Rarely did the needle tip pierce a hydromyelia, with dramatic images and temporary treatment of the cyst (Fig. 9). Contrast material often entered the fourth ventricle, whereupon, and as in positive-contrast ventriculography, a normal thin central spinal cord canal filled with contrast material.

Air myelography was first performed with great success together with polytomography, but only with patients in the supine, prone, and lateral positions. This soon changed with the advent of the Mimer III system, and total air myelography could be performed with the patient in any position. This usually showed congenital abnormalities of the spinal cord and canal, especially the collapsing cord of hydromyelia, collapsing because of a patent obex permitting egress of the CSF from the hydromyelia after the injection of air. Safe water-soluble contrast agents used together with CT enormously refined myelography [8].

Notwithstanding anesthesia and the complex abnormalities being studied, such myelography usually took only 40 min.

Angiography

Before 1968, pediatric cerebral angiography was usually performed, with various success, by neurologists and neurosurgeons who used direct carotid puncture or retrograde brachial artery techniques. Most of these were also associated with simple hand-injection of contrast material. In Boston and Toronto, the practice was established in 1968 that a few practitioners (radiologists) did all the studies; thus, special expertise and learning centers developed, stimulating the birth of pediatric neuroangiography. The political connotations were obvious.

Direct carotid and vertebral punctures in children were difficult and different. The arteries of the young are relatively tough and extremely mobile and obviously small. Autoclaved reusable and manually sharpened needles were used again and again, and a short bevel was essential (the arterial lumen is often very tiny). Small 6-in. (15-cm) guidewires were often used to thread the needle cannula up the carotid artery for better fixation before injection. Vertebral puncture

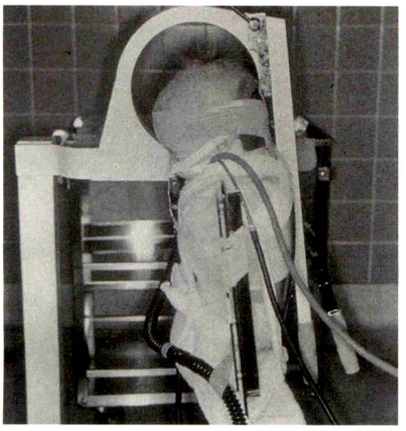

Fig. 7.—Custom-made Hospital for Sick Children infant cradle, used with Mimer III system enabled safe and quick pneumoencephalography, ventriculography, and anesthesia.

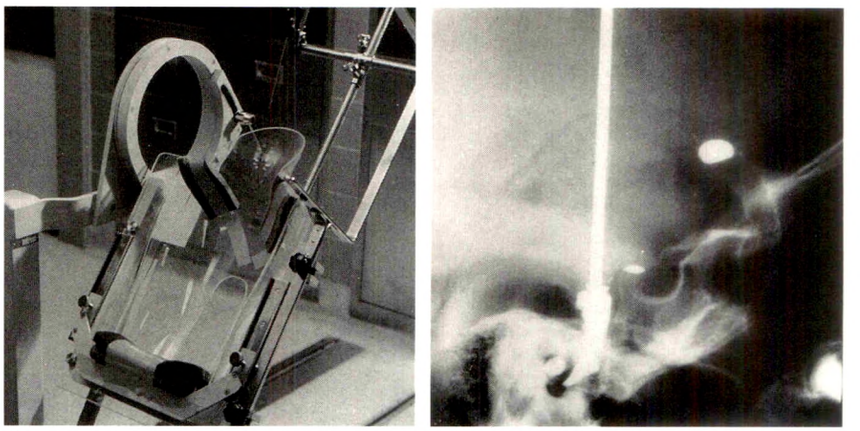

A B

Fig. 8.—Percutaneous third ventriculostomy.
A, Adaptation to cradle made it possible to insert a leukotome needle under direct vision into third ventricle through its floor, which is outlined by contrast material in *B*.
B, Ventriculogram shows contrast material flowing through defect, enabling satisfactory cure by ventriculostomy of hydrocephalus due to aqueduct stenosis.

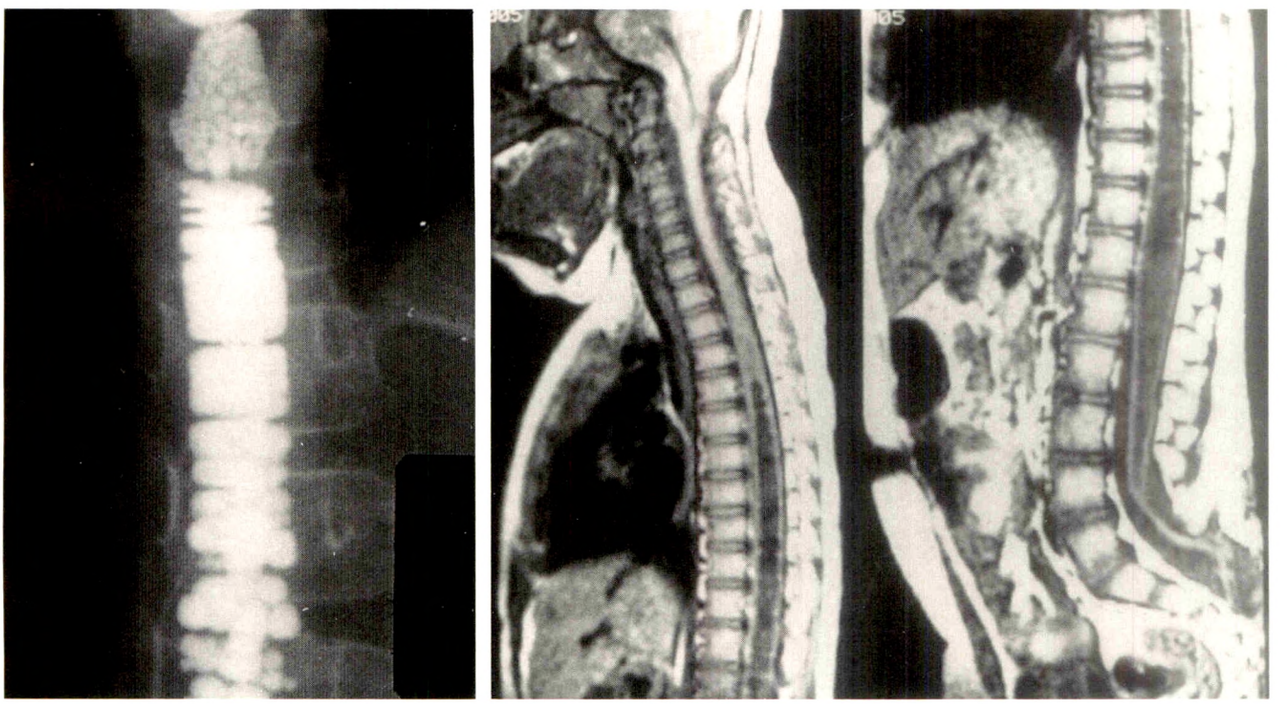

A B

Fig. 9.—Hydromyelia.
A, Pantopaque cystogram obtained inadvertently by puncture of hydromyelia shows classical irregular septa of this condition for the first time.
B, Modern MR images (20 years after *A*) show hydromyelia with septa and Chiari malformation in an infant.

was difficult because of the small size of the artery. Blunt cannulas around a sharp trocar were then developed.

Suboptimal needle positioning and indeed medial and adventitial injections of considerable extent and concern occurred, particularly in inexperienced hands (Fig. 10). With experience, however, these mishaps soon became few and far between. Primitive mechanical injectors helped, particularly in retrograde brachial injections, similar to those performed in adults. A cut-down brachial approach, injection and closure, even in the smallest infant, could be performed in 30 min.

General anesthesia was used from the beginning, and to this date enables perfect cooperation, accuracy of puncture, and the highest quality filming, which initially often was

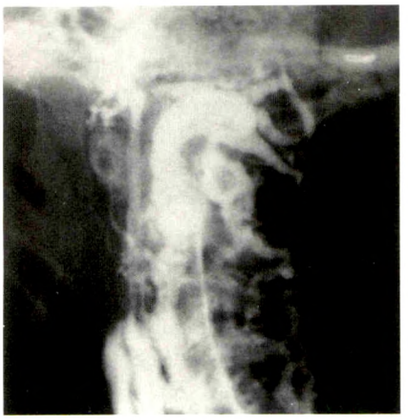

Fig. 10.—Complications of direct-puncture arteriography. Attempted direct percutaneous insertion of needle by inexperienced nonradiologist, unsure position of needle tip, and unwise hand injection of contrast material led to subintimal injection and direct filling of cervical veins, into fascial planes and extradural spinal compartment.

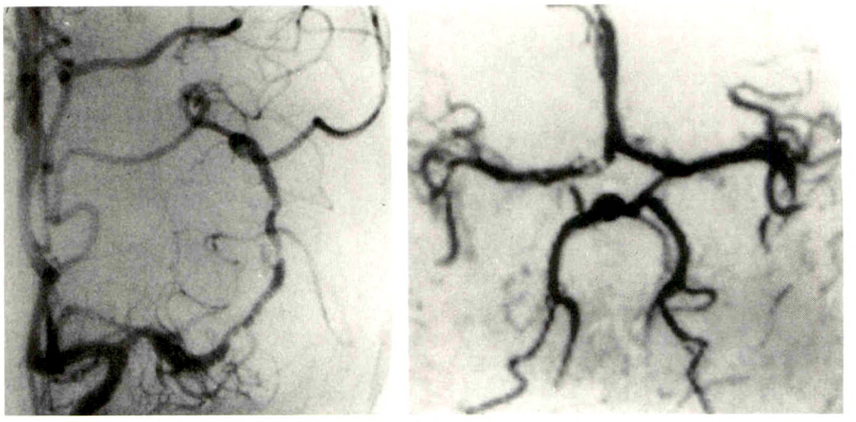

A B

Fig. 11.—Childhood cerebral arterial disease.

A, Angiogram shows classical beaded appearance of cerebral arteriopathy of unknown origin in a child who had a stroke.

B, Basal projection of MR angiogram shows thrombosis of right internal carotid artery, proximal segments of right anterior cerebral artery, and part of right middle cerebral artery, illustrating good visualization of major vessels by this technique. (Courtesy of W. G. Bradley, Jr., Long Beach, CA.)

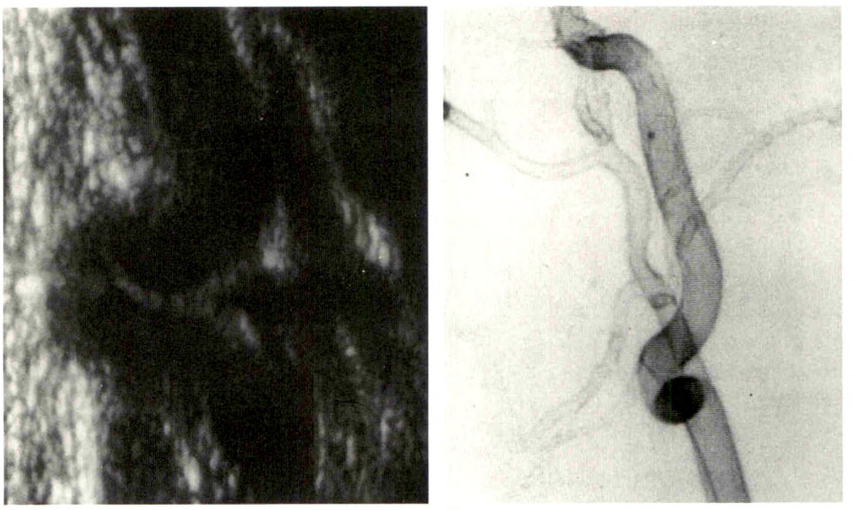

A B

Fig. 12.—Normal kinks of carotid artery in children.

A, Sagittal sonogram shows unusual dilated segment of internal carotid artery, possibly an arterial venous malformation or an unusual aneurysm.

B, Digital angiogram shows normal, commonly seen kink of this internal carotid artery.

bedeviled by primitive rapid film changers and primitive radiographic equipment.

Within anesthesiology, the techniques of hyperventilation were instituted and performed, and still are to this day; our unit has a present experience of more than 3000 angiograms, some obtained in infants weighing as little as 1 kg. This hyperventilation technique produces a carbon dioxide tension of 25–30 mm Hg and thus enables better visualization of smaller, deeper vessels and abnormal vessels, both refractory to the effects of low carbon dioxide tension; with subtraction and magnification, small vessels 100 μm in diameter were well visualized even in the tiniest brain.

Selective cranial angiography via a percutaneous femoral catheter started in 1969 with hand-made and hand-shaped catheters, with special tight S-shaped ends made each day, by using special 3- to 5-French soft catheters. No cut-down insertions were ever necessary. Only infrequently was the end of a small catheter inadvertently placed at the supraclinoid portion of the internal carotid artery or even at the origin of the posterior cerebral artery. These early superselective catheterizations fortunately caused no sequelae. Digital angiographic subtraction images now in use are of a quality nearly equivalent to those obtained with the original cut-film techniques. These have made our tasks easier, but the basic

technique remains unchanged. The full spectrum of the extraordinary vascular disease in children (Fig. 11) soon became apparent, as well as normal variations peculiar to children (Fig. 12). These latter are not now being identified as frequently because of the regrettable reluctance to do angiography and the diminishing number of radiologists with expertise in angiography in the era of modern CT and MR. MR angiography is not sufficiently developed to show small-vessel disease.

The advent of cerebral interventional angiographic techniques has resulted in their successful adaptation for infants and children, particularly with newer, smaller directed catheters, coils, glues, and balloons. The size of the parent vessels in infants and the physiologic fragility and often complex diseases of the infant make it essential for this angiographic art to be practiced only by the most expert and experienced pediatric angiographers.

CT

Initially, the so-called computerized axial tomogram, the CAT scan, revolutionized pediatric neuroradiology as early as 1974—with the use by ourselves and others of a first generation of EMI scanners. The then remarkable polyglot of pixels, originally in 80 × 80 matrix studies and often taking as much as 90 min, provided 13-mm slices and relatively crude (Fig. 13), but "safe," anatomic images [1].

Initially, again, a special cradle had to be built by us to support an infant's head, this thrust into a water bag while the infant was anesthetized. Then, in 1976, we and others acquired the first of a succession of "body" CT scanners that provided dramatic detail enhancement and had wide orifices. Adaptations to the support systems for infants, even today, still have to be made in-house.

This initial imaging evolution in pediatrics thus satisfied at last the basic tenets of neuroimaging of all clinical entities: the diagnostic evaluation of normal and abnormal geography (surface) and character (substance) of the brain and spinal cord and their coverings; previous techniques showed surface geography only. CT and sonography, for example, revolutionized the assessment of brain hypoxia and hemorrhage in the neonate.

A singular problem of CT was the inability to provide accurate sagittal images, which was solved recently, however, with exquisite three-dimensional imaging techniques. The original advantage of CT was that it was safer and showed most abnormalities of the brain substance of the CNS, together with surface anatomic aberrations; thus, the rapid decline of expertise in performing the older studies led to wholesale use of CT regardless of its shortcomings. This in many ways also led to a regrettable decrease in, or indeed neglect of, angiography.

The diagnostic advantages of the anteroposterior view of pneumoencephalography and ventriculography were transferred to the development of the coronal CT views of the head, obtained by having the patient's neck hyperextended with the body supine. Direct sideways-placed sagittal CT scans of the head and spine are possible in small children weighing up to 10 kg. The combination of safe water-soluble myelographic and ventriculographic agents with CT evolved into CT contrast-enhanced ventriculography and CT myelography; the last quickly replaced standard myelography, especially in the assessment of congenital abnormalities of the spine and cord and of the cauda equina, and often is still the gold standard.

No more was anesthesia necessary for CT, and the increasing speed and degree of anatomic definition provided by CT slowly, but not completely, diminished the need for heavy sedation, now mostly given by the IV route.

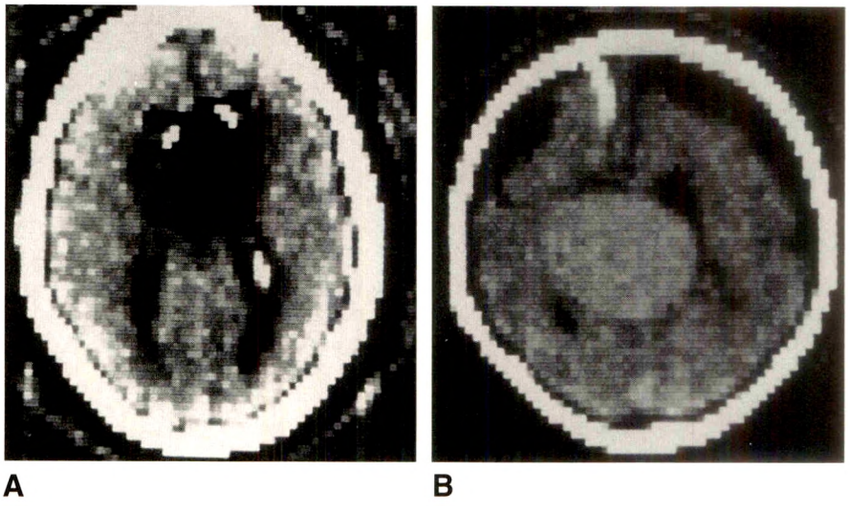

Fig. 13.—Early CT scans of head in children.
***A*, One of earliest EMI scans shows a lipoma of corpus callosum containing calcification.**
***B*, Scan shows essentially an enhancing cyst, which angiograms (*not shown*) indicated was a congenital vein of Galen varix and bilateral chronic subdural hematomas.**

Sonography

A workhorse in pediatric neuroimaging of the infant is sonography. With the relatively recent evolution of extremely high-resolution real-time sonography, and now standard and color Doppler sonography, which is performed more quickly and easily, sonography is a technique that has made its mark in neuroimaging, often as the first imaging procedure of choice for the brain and spinal cord of infants. Germinal matrix hemorrhage in premature neonates, periventricular leukomalacia, complex midline congenital abnormalities in the neonate, ventricular size, craniocervical cord anomalies, the spinal cord, and spinal dysraphism are among the entities wherein sonography has had an enormous impact.

There is a present need, however, for those expert in pediatric sonography and those experienced in pediatric neuroradiology to become more familiar with each others' expertise and knowledge.

Nuclear Medicine

Since 1972, pediatric neuro–nuclear medicine has slowly and steadily evolved with neuroradiology, especially now with the advent of single-photon emission computed tomography (SPECT). For example, the initial use of nuclear medicine studies for the detection of where and how many suspected acquired lesions are in the spine and for the evaluation of blood perfusion or often subtle tissue changes of inflammation and neoplasia in the brain or its coverings is still an important part in the diagnostic protocol of pediatric neuroradiology.

Standard Radiographs

It may whimsically be said that conventional skull and spine radiographs are the newest special procedure. Needless to say, it is still appropriate to recommend posteroanterior and lateral skull radiographs and anteroposterior and lateral spinal radiographs as the first study in the imaging assessment of CNS disease in a child. The exquisite bony detail obtained in any plane by polytomography, particularly of the base of skull, petrous bones, and spine, has been matched in all but the sagittal plane by CT. Only with accurate three-dimensional CT reconstructions is the full topography of bone seen, avoiding common artifacts produced by image slice averaging or by significant bony distortions (e.g., scoliosis and distortions of the craniocervical junction).

MR Imaging and the Challenge of the Future

During the mid and late 1980s the remarkable advent of MR began to reveal many of the nuances of the pathology of childhood CNS diseases indicated clinically but previously hidden, or often, frustratingly, imperfectly seen on or suggested by CT scans.

A new lexicon of disease syndromes and eponyms was thus thrust upon us, now being exquisitely shown in geography and character and often only needing histologic elucidation or affirmation (Fig. 14). Typical of these were unusual aberrations of embryology (Fig. 15), especially within brain

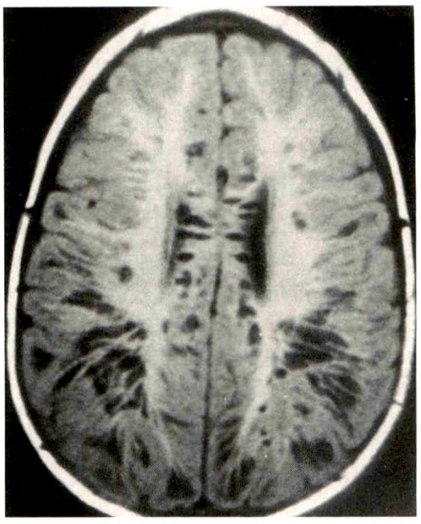

Fig. 14.—Dilated Virchow-Robin spaces. T1-weighted axial MR image of child with Hurler's disease shows multiple and characteristic dilatations of Virchow-Robin spaces.

migrations and sulcations; the precise pattern, development, and alterations of myelin (about which whole textbooks have been written [9]); most subtle alterations of gray and white matter in childhood abnormalities caused by defects in neurochemistry and cerebral enzymes; and especially spinal cord diseases—changes that in many are found by MR to be characteristic.

It is not only the ease of obtaining MR images, and not necessarily the surface depiction of anatomy by MR relative

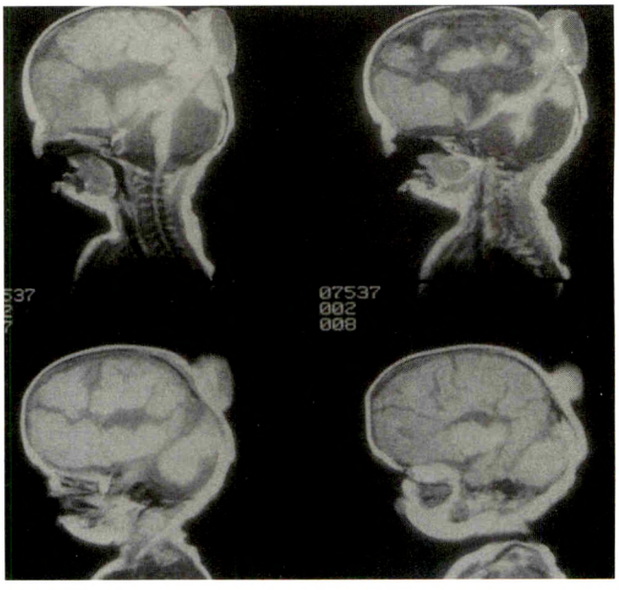

Fig. 15.—Multiple congenital anomalies. Sagittal MR images obtained at multiple levels show, from top left clockwise, a posteriorly placed brainstem and a Dandy-Walker cyst (*top left*); meningoencephalolipocystocele posteriorly (*top right*); and schizencephaly, pachygyri, and central cleft face (*bottom left* and *right*).

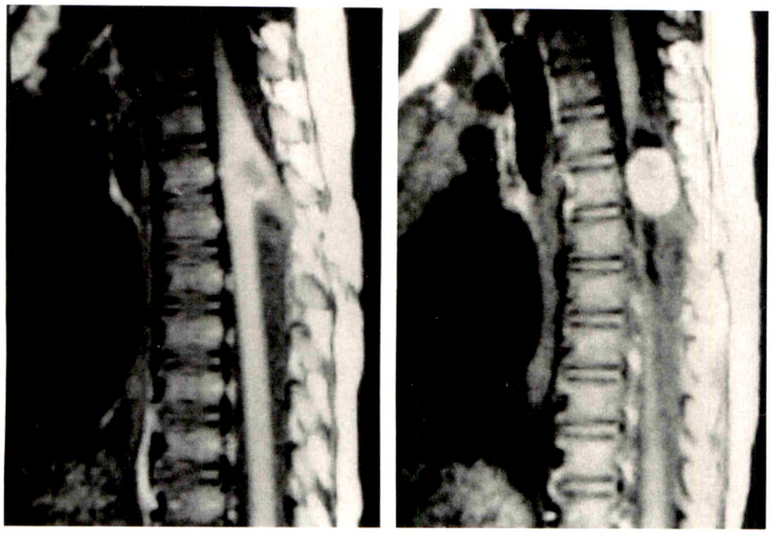

Fig. 16.—Sagittal MR imaging of spine. T1-weighted MR images at contiguous levels show entire tract and intradural location of intradural extramedullary dermoid.

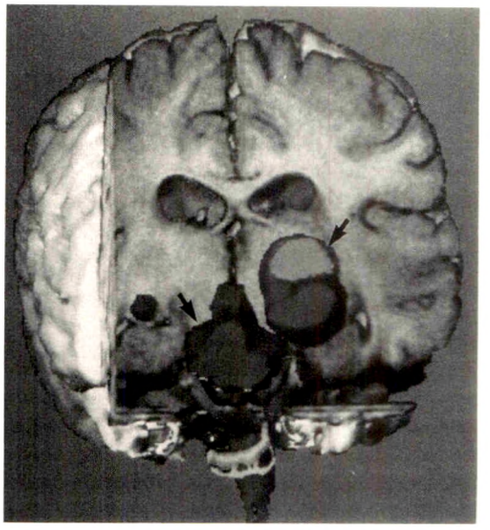

Fig. 17.—Three-dimensional MR image, with computed sectioning viewed from in front, shows extensive hypothalamic glioma (*arrows*) extending to left into basal ganglia.

to CT, that makes MR imaging so attractive, but also often the beauty of the sagittally displayed image of the head and spine (Fig. 16), an art lost with the demise of pneumoencephalography and myelographic tomography.

Perhaps MR angiography eventually will match the anatomic depiction provided by contrast angiography. Certainly all the technologic capabilities of MR—MR spectroscopy, MR sequences, and algorithms applied to the normal and altered functions and evaluation of fluid flow and enzyme abnormalities—will enable us better to understand and diagnose many of the complex diseases that alter these fluid and tissue characteristics in the childhood brain. Pediatric neuroradiology demands a solid basic understanding and knowledge of normal embryology, physiology, and the developing anatomy of the child's CNS, and of the alterations caused by diseases and deformity together with their clinical and pathologic characteristics. A full early and continuing experience with these technologies toward imaging of such abnormalities, be they directed toward the skull, spine, brain, and cord and their vessels and coverings in concert or singularly, is possible only by concentration of patient referrals to major full-time practitioners of pediatric neuroradiology. A significant present and future need exists therefore for continued growth and encouragement of present centers of such experience and expertise in pediatric hospitals or units and for pediatric neuroradiology as part of a total clinical and laboratory neuroscience unit. Standard radiographs and even angiography often appear to defer to more sophisticated CT and MR studies. The regrettable neglect in obtaining both unenhanced and enhanced CT scans, and the reluctance to use direct coronal CT (in complex midline abnormalities), often leads to an underuse of the full diagnostic capabilities of CT. Depiction of surface anatomy of the cord with MR often cannot match that possible with CT contrast myelography, except in the sagittal view, as long as the CT study is performed with care and expertise; however, CT contrast myelography is undeniably associated with more morbidity.

There is still an urgent need for continued expert and safe selective catheter angiography in infants and children. Many consider MR angiography still unable, at least in the near future, to replace all such studies. Pediatric therapeutic neuroangiography is, in select centers worldwide, now an established, safe, and effective procedure for even the smallest infant and can show the most complex vascular abnormalities.

MR techniques for studying the flow of CSF and diffusion/perfusion parameters and the emerging echoplanar techniques, be they directed to speed, anatomic detail, interstitial fluid flow, and the hydrology of hydrocephalus, for example, will have a profound impact on the evaluation of childhood CNS diseases. MR and precise three-dimensional MR imaging (Fig. 17) make anatomy and spatial representation of abnormalities worth the proverbial 1000 words. Emerging new techniques of magnetic source imaging associated with MR promise considerable advancement in the understanding of physiology and anatomic mapping of the developing brain and seizures. Their effectiveness, together with techniques applied to function—MR spectroscopy, magnetic source imaging, SPECT, and positron emission tomography—all have their basis in a clear understanding and imaging of the anatomy and disease processes of the brain in children, that is pediatric neuroradiology.

Epilogue

What of the present and the future? The growing strength and significance of pediatric neurosurgery demands a concomitant expertise and dedication by pediatric neuroradiol-

ogy in all its facets. Pediatric neuroradiology is a major part of a pediatric diagnostic imaging department in a hospital, and is a part of a section of neuroradiology in a general hospital that has specialists in pediatric neurosciences and that treats neonates. It must continue as such a significant component, yet as a particular persuasion. Such concentration of manpower, experience, and teaching is essential to maintain its excellence. The present explosion of knowledge and the sophistication of detection of genetic and biochemical diseases relative to the child's CNS are often overwhelming. Diagnostic imaging must keep pace and, when necessary, take a leadership role.

A pediatric neuroradiology specialist needs to establish a continuing major commitment therein to accommodate the enlarging body of knowledge and increasing technical expertise required. Pediatric neuroradiology, in its formal training, publications (e.g., see the March/April 1992 issue of *AJNR*), and acknowledgment of and participation in major professional societies worldwide and within pediatric radiology and neuroradiology, is now significant. The body of knowledge now accumulated and the relatively large number of its practitioners have now led to the formation of formal scientific groups and professional associations within pediatric radiology and neuroradiology.

In pediatric neuroradiology it is the artistry of images and the clinical theater of the mind that are paramount. To an increasing number of our younger colleagues, it is becoming a fascinating profession, if not a lifelong persuasion.

ACKNOWLEDGMENTS

I thank the many technologists, nurses, and secretaries; pediatric neurosurgeons and neurologists; more than 60 fellows; and colleagues, administrators, and friends at the Hospital for Sick Children who have had an important and much appreciated part in this odyssey.

REFERENCES

1. Harwood-Nash DC, Fitz CR. *Neuroradiology in infants and children.* St. Louis: Mosby, **1976**
2. Barkovich AJ. *Pediatric neuroimaging.* New York: Raven, **1990**
3. Wolpert SM, Barnes PD. *MRI in pediatric neuroradiology.* St. Louis: Mosby–Year Book, **1992**
4. Cohen MI, Edwards MK. *Magnetic resonance imaging of children.* Philadelphia: Decker, **1990**
5. Dibler C, Tulac O. *Pediatric neurology and neuroradiology.* Heidelberg: Springer-Verlag, **1987**
6. Taveras JM, Wood EH. *Diagnostic neuroradiology,* 2nd ed. Baltimore: Williams & Wilkins, **1977**
7. Raimondi AJ. *Pediatric neuroradiology.* Philadelphia: Saunders, **1972**
8. Pettersson H, Harwood-Nash DC. *CT and myelography of the spine and cord: techniques, anatomy and pathology in children.* Heidelberg: Springer-Verlag, **1982**
9. Valk J, van der Knaap MS. *Magnetic resonance imaging of myelin, myelination and myelin disorders.* Heidelberg, Germany: Springer-Verlag, **1989**

Disseminated Histoplasmosis in AIDS: Findings on Chest Radiographs

Dewey J. Conces, Jr.[1]
Stephan M. Stockberger[1]
Robert D. Tarver[1]
L. Joseph Wheat[2]

OBJECTIVE. Our objective was to determine the findings of disseminated histoplasmosis on chest radiographs of patients with AIDS.

MATERIALS AND METHODS. Chest radiographs of 50 AIDS patients with documented extrapulmonary histoplasmosis were analyzed retrospectively. The radiographs were evaluated for the presence of parenchymal opacities, pleural effusions, adenopathy, cavitation, and calcified granulomas and lymph nodes. A modification of the International Labour Office scheme was used to classify parenchymal abnormalities as nodular, linear or irregular, reticulonodular, or air-space opacities.

RESULTS. Abnormalities were present on radiographs in 23 patients. Nodular opacities were present in 10 patients and were diffusely distributed in nine patients. Linear or irregular opacities were present in seven patients, with diffuse distribution in four and limited involvement in three. Air-space opacities were present in seven patients; the distribution varied from segmental to diffuse involvement of the lung. Small pleural effusions were present in five patients. Adenopathy and Kerley's B lines were each present in three patients. In 27 patients, the chest radiographs were normal. Four of these patients had clinical or microbiological evidence of lung involvement.

CONCLUSION. The chest radiographic findings of disseminated histoplasmosis in AIDS patients are varied and nonspecific. The presence of diffuse nodular or linear/irregular opacities in an AIDS patient, especially one who resides in or has resided in an endemic area, should suggest the possibility of disseminated histoplasmosis. Normal findings on chest radiographs do not exclude disseminated infection or lung involvement.

***AJR* 1993;160:15–19**

Patients with AIDS have a severe defect in cell-mediated immunity that predisposes them to fungal infections. In regions endemic for *Histoplasma capsulatum*, these patients are at risk for histoplasmosis [1].

Histoplasmosis in AIDS patients was first reported in 1983 [2]. Since then it has become an important infection in patients with AIDS. Although most cases are encountered in areas endemic for the organism, sporadic cases outside endemic regions have been reported [3, 4]. Because of the profound defect in cell-mediated immunity, most patients have disseminated disease [1, 5]. In 1985, the Centers for Disease Control revised the case definition of AIDS to include persons with extrapulmonary histoplasmosis and serologic evidence of infection with HIV [6]. Previous reports of histoplasmosis in patients with AIDS have concentrated on the clinical presentation, microbiologic and serologic diagnosis, and therapy. We describe the findings on chest radiographs of a series of AIDS patients with disseminated histoplasmosis.

Received March 6, 1992; accepted after revision July 27, 1992.

[1]Department of Radiology, Room 0279, Indiana University School of Medicine and Indianapolis Veterans Affairs Hospital, 550 N. University Blvd., Indianapolis, IN 46202-5253. Address reprint requests to D. J. Conces, Jr.

[2]Department of Medicine, Indiana University School of Medicine and Indianapolis Veterans Affairs Hospital, Indianapolis, IN 46202-5253.

0361–803X/93/1601–0015

Materials and Methods

Eighty-five patients with AIDS and histoplasmosis were seen at our institution between January 1983 and January 1992. The diagnosis of histoplasmosis was based on the culture of *H. capsulatum* from tissue or bodily fluid or the detection of *H. capsulatum* polysaccharide antigen in blood, urine, or other bodily fluid. The records of these patients were retrospectively reviewed. Thirty-five patients were excluded from the study. Nine patients had incomplete clinical or radiographic records. Two patients were infants (<1 year old) and differed greatly in age from the remainder of the group. In 10 patients, the diagnosis was based only on a positive *Histoplasma* antigen test. Because the extent of the infection was difficult to determine in this group, these patients were excluded. Eleven patients had concurrent pulmonary infection by *Pneumocystis carinii*, and their records were not reviewed further. Three patients with pulmonary histoplasmosis were excluded because dissemination could not be documented. The remaining 50 cases with disseminated histoplasmosis made up the study group.

The group consisted of 48 men and two women 22–60 years old (mean, 35 years). All 50 had disseminated histoplasmosis as indicated by culture of *H. capsulatum* from extrapulmonary tissue or bodily fluid. The organism was detected in blood in 44 patients, bone marrow in 25 patients, extrathoracic lymph node in six patients, urine in three patients, rectal mucosa in three patients, liver in one patient, and brain in one patient. The patients were divided into two groups as determined by the presence (27 patients) or absence (23 patients) of lung involvement. Patients were classified as having lung involvement if they met any of the following criteria: culture of *H. capsulatum* from the lung (24 patients), presence of clinically significant pulmonary signs and symptoms such as cough or dyspnea (19 patients), presence of hypoxia (11 patients), or presence of parenchymal disease on chest radiographs (24 patients). Calcified granulomas or lymph nodes were not considered to represent evidence of lung involvement.

AIDS had been previously diagnosed in 11 patients in the study group. HIV infection had been previously established in 26 patients and was first diagnosed at the time of presentation in 13. In 39 patients (78%), disseminated histoplasmosis was the defining illness for AIDS. Risk factors for AIDS included homosexuality in 30 patients, IV drug abuse in three patients, homosexuality and IV drug abuse in four patients, hemophilia in one patient, previous blood transfusions in one patient, heterosexual partner with AIDS in one patient, and unknown in 10 patients.

Posteroanterior and lateral (46) and portable (four) chest radiographs obtained at presentation were reviewed. Subsequent radiographs obtained during therapy were also examined to assess clearing of abnormalities and to detect the development of additional findings. The chest radiographs were reviewed by two observers, and a conclusion was reached by consensus. The radiographs were reviewed to determine the anatomic distribution and pattern of parenchymal disease as well as the presence of other findings, such as calcified granulomas and lymph nodes, adenopathy, pleural effusion, and cavitation.

Parenchymal abnormalities were characterized according to a scheme described by McLoud et al. [7]. This scheme is a modification of the International Labour Office (ILO) system in which the parenchymal opacities are classified as nodular, linear or irregular, reticulonodular, or "ground glass." The ILO classification of small nodular (p, q, r) and small linear or irregular (s, t, u) opacities was retained in this scheme. The modified scheme includes the designation of reticulonodular opacities, which are defined as small rounded opacities with linear markings emanating from them. Another category, ground glass, refers to air-space opacities visible on chest radiographs. These opacities range from a fine hazy pattern that does not obscure normal markings to dense consolidation with associated air bronchograms. Nodular opacities were classified according to their diameters: p = ≤1.5 mm, q = 1.5–3.0 mm, r = 3.0–10 mm. Linear or irregular opacities were classified according to thickness: s = fine, t = medium, u = coarse. When nodular, linear, or irregular opacities were present, the study radiographs were compared directly with ILO standard radiographs. The reticulonodular opacities were classified as x, y, and z and corresponded to the nodular sizes used in the p, q, and r categories. The air-space opacities were characterized as diffuse, lobar, segmental, perihilar, peripheral, diffuse patchy, and other. The distribution of the opacities was assessed for each of six zones (right upper, right middle, right lower, left upper, left middle, left lower). The severity or profusion of the opacities was assessed according to four categories: 0 = normal, 1 = slight, 2 = moderate, and 3 = advanced.

Results

The chest radiographs of the 23 patients with documented extrapulmonary dissemination and no evidence of lung involvement were normal. Abnormalities were present in 23 of 27 patients who had evidence of lung involvement.

Nodular opacities were present in 10 patients and were the most commonly encountered parenchymal abnormality (Fig. 1). The nodular opacities varied in diameter: five were 1.5 mm or smaller, four were 1.5–3.0 mm, and one was larger than 3.0 mm. The nodular opacities were diffusely distributed in all six zones in nine patients and were confined to two zones in one patient. The severity of the changes was classified as slight in three patients, moderate in four, and advanced in three.

Small linear or irregular opacities were found in seven patients (Fig. 2). They were graded as fine to medium in four, medium in one, and coarse in two. The opacities were diffusely distributed in all six zones in four patients. In three patients, the distribution was more limited: to two, three, and four zones each. The patient with medium-thickness irregular opacities involving the right three lung zones also had ipsilateral perihilar air-space opacities. The severity of the changes was rated slight in five patients and moderate in two.

Seven patients had air-space opacities (Fig. 3). In three patients, the opacities were confined to one zone, with either segmental (two) or lobar (one) involvement. One patient had right-sided perihilar air-space opacities as well as ipsilateral medium-thickness irregular opacities. Multiple areas of patchy air-space opacities were seen in one patient. Two patients had diffuse air-space opacities involving all zones of the lungs. In the two cases with diffuse air-space opacities, the opacities took on a nodular appearance as the patients' conditions improved during antifungal therapy. The severity of the opacities was rated as slight in one patient, moderate in three, and advanced in three.

Small pleural effusions were present in five patients. The largest was associated with air-space opacity in the right lower lobe. The remainder were very small and were associated with nodular opacities in one patient and irregular opacities in three patients. Kerley's B lines were present in three patients (Fig. 4). They were associated with nodular opacities in two patients and with irregular opacities in one. These

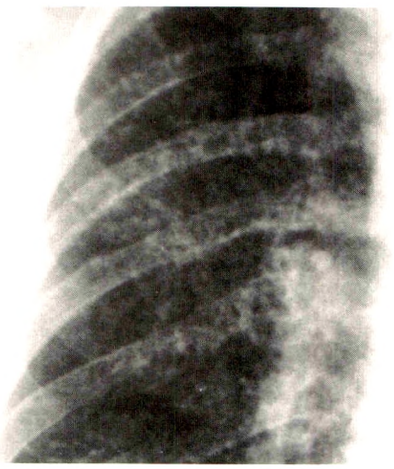

1

Fig. 1.—Previously healthy 39-year-old man with fever and dyspnea was found to be infected with HIV. AIDS was diagnosed after *Histoplasma* was cultured from lung and blood. Collimated chest radiograph of the right upper lobe shows multiple 1–2 mm nodules that were distributed diffusely throughout both lungs.

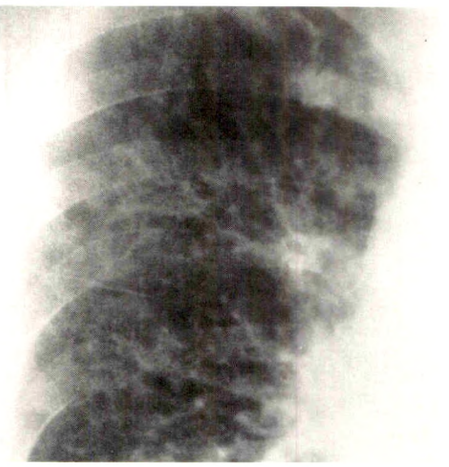

2

Fig. 2.—Patient known to have AIDS had fever and dyspnea. *Histoplasma capsulatum* was identified on transbronchial biopsy. Collimated chest radiograph of right upper lobe shows moderately severe coarse linear/irregular opacities, which were present in all six lung zones.

lines were associated with a pleural effusion in one case, but not in the other two. Clinical indications of congestive heart failure or fluid overload were not present.

Adenopathy was present in three cases: left hilar in one patient and right paratracheal in two. The lymph nodes were mildly enlarged. In one case, the adenopathy predated the histoplasmosis and was thought to be unrelated. In the other two cases, the lymph nodes became smaller after antifungal therapy. Two cases were associated with nodular opacities and one with irregular opacities.

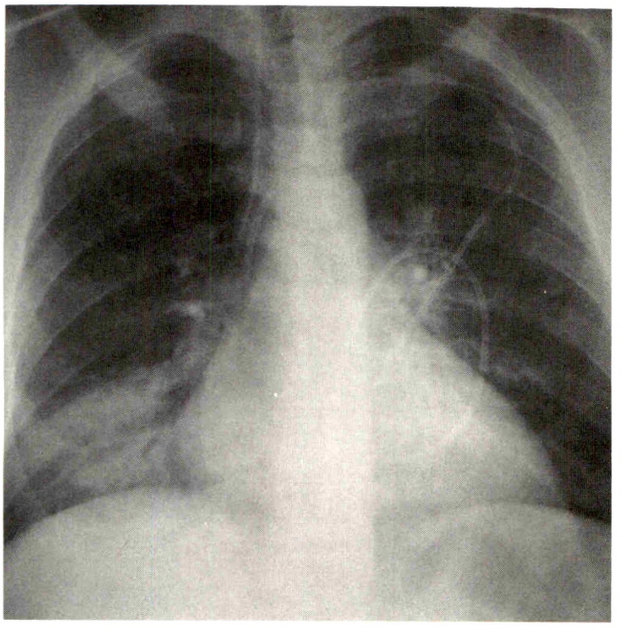

Fig. 3.—Patient known to have HIV infection had fever, cough, and dyspnea. Posteroanterior chest radiograph shows air-space consolidation involving right middle lobe and cardiac enlargement due to left ventricular hypertrophy. Lavage fluid from right middle lobe of lung and blood were positive for *Histoplasma*.

Four patients with pulmonary involvement had normal chest radiographs. Two patients had normal chest radiographs and arterial blood gas measurements, but because they were dyspneic, bronchoscopy was performed; examination of transbronchial biopsy specimens showed *Histoplasma*. Another hypoxic patient with cough and dyspnea had *Histoplasma* organisms in transbronchial biopsy specimens obtained by bronchoscopy. The fourth patient had cough and dyspnea and was hypoxic. Infectious organisms were not identified in bronchoscopic biopsy specimens, but blood cultures were positive for *Histoplasma*. The cough, dyspnea, and hypoxia resolved with antifungal therapy.

The clinical presentation did not differ among patients with the various types of parenchymal abnormalities. Of patients with nodular opacities, three were asymptomatic, four had pulmonary symptoms but were not hypoxic, and three had symptoms and hypoxia. One patient with linear or irregular opacities was asymptomatic; two had only pulmonary signs or symptoms, one had hypoxia alone, and two had both pulmonary signs and symptoms and hypoxia. Air-space opacities were present in one asymptomatic patient, in two patients with only pulmonary signs and symptoms, in one patient with only hypoxia, and in two patients with hypoxia and pulmonary signs and symptoms. The patient with right-sided medium-thickness irregular opacities and ipsilateral perihilar air-space disease was hypoxic. In three patients, radiographic findings progressed after diagnosis and institution of antifungal therapy. In two, nodular opacities progressed to a diffuse pattern of air-space opacities (Fig. 5). These patients died despite appropriate antifungal therapy. In another patient, diffuse irregular opacities progressed to a pattern of diffuse air-space opacities. This patient, however, recovered, with resolution of the parenchymal opacities after therapy. All of the other patients in the study recovered from their infections.

Of the 27 patients with lung involvement, follow-up chest radiographs were available in 21. Of the 19 that survived their illness, the parenchymal opacities resolved; no residual findings remained after therapy.

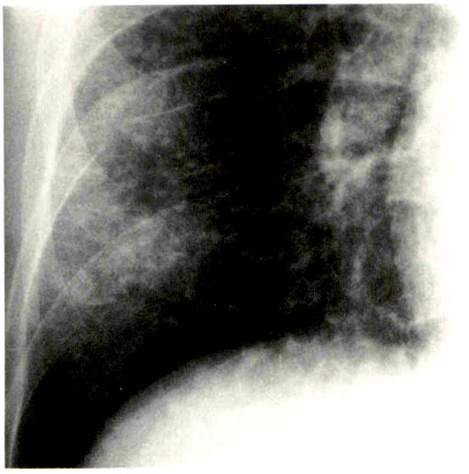

Fig. 4.—39-year-old man with disseminated histoplasmosis and newly diagnosed AIDS. Clinically, no evidence of fluid overload or heart failure was found. Collimated chest radiograph view of base of right lung shows nodular opacities with associated Kerley's B lines.

Calcified lymph nodes or granulomas or both were present in 18 of the 50 patients. Calcified granulomas were noted in six patients with lung involvement and in seven patients without lung involvement. Calcified lymph nodes were detected in six patients with lung involvement and in nine patients without lung involvement.

Discussion

In our series, evidence of parenchymal disease was present on chest radiographs in 23 (46%) of 50 AIDS patients with disseminated histoplasmosis. This is similar to that reported in other series [1, 5, 8], in which "infiltrates" were seen in 48–56% of patients. In previously reported cases [1, 3–5], the description of the parenchymal changes seen has varied; the wide range of terms used to describe the findings includes diffuse, interstitial, and reticulonodular infiltrates. Nightingale et al. [8] classified the pulmonary opacities as nodular, reticulonodular, and apical. In our series, we evaluated the radiographic findings by using a standard scheme that allowed a well-defined characterization of the findings.

Nodular opacities were the most common type of parenchymal abnormality; they were found in 10 (20%) of 50 patients. The size of the nodules varied, but in all but one case they were 3.0 mm or smaller. In all but one patient the nodules were diffusely distributed throughout the lung. This pattern is seen in approximately 35% of non-AIDS patients with disseminated histoplasmosis [2]. A similar pattern has been reported in AIDS patients who are infected with *Cryptococcus* and *Mycobacterium tuberculosis* [9, 10]. This pattern, however, is not usually seen in infections caused by *P. carinii*, *Mycobacterium avium–intracellulare*, or cytomegalovirus [9–11]. Opacities with a linear or irregular appearance were the second most common type of parenchymal abnormality. This pattern was diffuse in its distribution in four of seven cases in which it was present. In our series, none of the patients had reticulonodular opacities.

The nodular and linear or irregular opacities that had a diffuse distribution most likely correspond to the diffuse, interstitial, and reticulonodular infiltrates described in earlier reports [1, 3–5, 8]. In our series, these opacities were present in 34% of cases. In previous reports [1, 5, 8], the corresponding infiltrates were seen in 33–53% of cases.

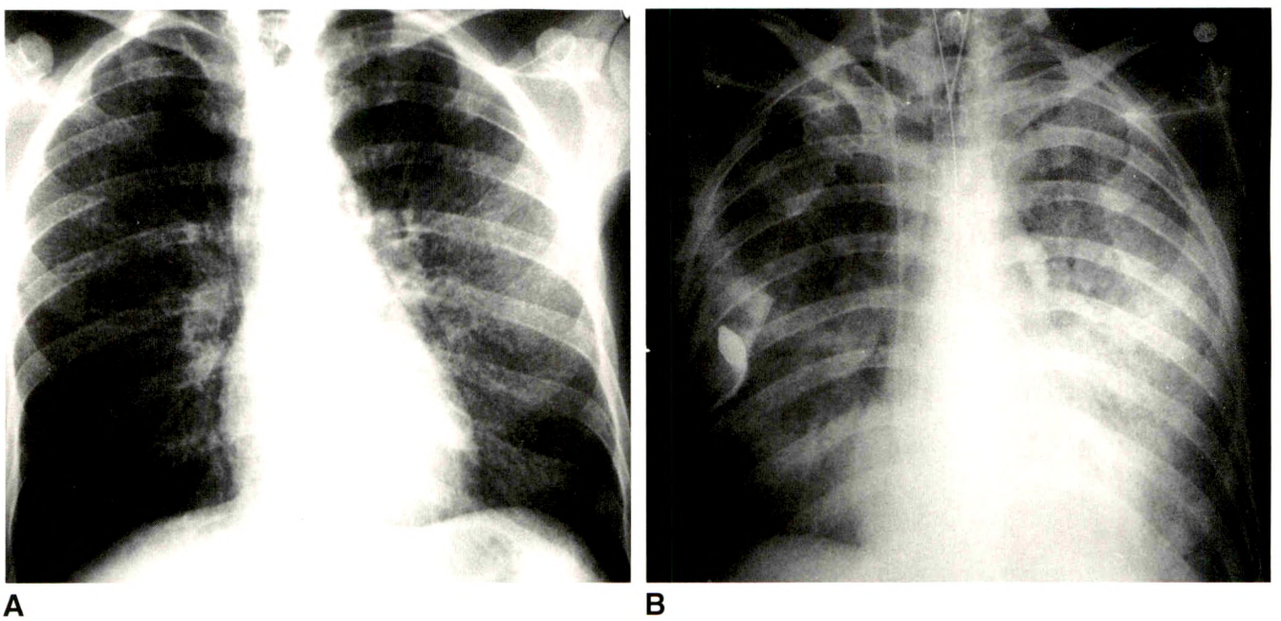

A **B**

Fig. 5.—34-year-old man known to have HIV infection had cough and dyspnea, which had gradually worsened over previous 2 months. *A*, Initial chest radiograph shows diffuse nodular opacities. Disseminated histoplasmosis was diagnosed and antifungal therapy was begun. *B*, Radiograph obtained 2 days after *A* shows progression to diffuse air-space opacities.

We found focal air-space opacities in five (10%) of 50 patients, and these were the only type of opacity in four cases. In previous studies [1, 5, 8] of disseminated histoplasmosis in AIDS patients, localized air-space disease occurred in 0–15% of cases. This contrasts with acute pulmonary histoplasmosis in immunocompetent hosts, in which focal air-space opacity is seen in approximately 75% of cases [2]. The two cases with diffuse air-space opacities took on a nodular appearance as the patients' conditions improved during antifungal therapy. This pattern of clearing raises the possibility that these cases actually represented advanced cases of the nodular pattern of lung opacity. An alternative explanation is that the development of the nodular pattern merely is due to the manner in which the air-space opacities responded to therapy.

The three patterns of parenchymal opacities had similar clinical presentations. None of the patterns appear to have a worse prognosis than the others. Progression of the parenchymal disease after institution of antifungal therapy does, however, appear to be an adverse prognostic finding. Two of the three patients that had radiographic progression of parenchymal opacities died. All patients who did not have worsening of radiographic findings recovered.

The different parenchymal patterns seen with disseminated histoplasmosis may be explained by the pathologic findings that have been reported for non-AIDS immunocompromised patients with disseminated histoplasmosis [12]. In these cases, the primary abnormality in the lung was infiltration of the interstitial tissues with infected macrophages. The interstitial tissues were thickened by the macrophages, which may be the cause of the linear/irregular opacities that were seen in this study. In other cases, macrophages were seen to extend into the alveolus, which may account for the nodular opacities that we encountered in our cases. The nodular densities are not due to granuloma formation, as these were rarely encountered. The cases of focal air-space disease in our series probably represent progressive pneumonitis at the site of the primary infection.

Pleural effusions were uncommon, occurring in only five patients (10%). Pleural effusions were infrequent in earlier series; in the study by Nightingale et al. [8], only one (3%) of 33 patients had a small pleural effusion. Two other series [1, 5] with a total of 120 patients did not report any cases of pleural effusion. The infrequent occurrence of this finding is similar to that seen in immunocompetent hosts with acute histoplasmosis and in non-AIDS cases of disseminated histoplasmosis [2].

Adenopathy was uncommon, occurring in only three cases (6%). In one case it was probably unrelated to the fungal infection; the adenopathy predated the diagnosis of histoplasmosis and did not resolve with therapy. Earlier series [1, 5, 8] also found that adenopathy was uncommon; it occurred in less than 5% of patients. This infrequent occurrence is similar to that seen in non-AIDS cases of disseminated histoplasmosis, but it contrasts with that seen in acute pulmonary histoplasmosis, in which adenopathy is present in 80% of cases [2].

Kerley's B lines were detected in three patients in our series. This type of parenchymal opacity has not been described in earlier reports. Although Kerley's B lines may indicate interstitial edema, the patients with this finding did not have any signs or symptoms of congestive heart failure or fluid overload. The lines probably reflect the interstitial nature of the infection, which is due to the hematogenous dissemination of the organism.

Calcified lymph nodes or granulomas were found in 18 (36%) of 50 patients. This exceeds the 2.8–3.2% reported in earlier series [1, 5]. The rate may have been higher in our study because all our patients lived in an area endemic for histoplasmosis. Most residents in this region eventually have histoplasmosis, which often leaves them with residual calcified lymph nodes and granulomas.

In our series, the chest radiographs were normal in 27 patients, four with lung involvement and 23 without. Our observed frequency of 54% normal chest radiographs in cases of disseminated histoplasmosis is similar to the 43–48% reported in earlier series [1, 5, 8]. Thus, a normal chest radiograph does not exclude the presence of disseminated histoplasmosis. Additionally, lung involvement may be present despite normal chest radiographs, as was seen in four patients in our series.

REFERENCES

1. Wheat LJ, Connolly-Stringfield PA, Baker RL, et al. Disseminated histoplasmosis in the acquired immune deficiency syndrome: clinical findings, diagnosis and treatment, and review of the literature. *Medicine* (Baltimore) **1990**;69:361–374
2. Sathapatayavongs B, Batteiger BE, Wheat J, Slama TG, Wass JL. Clinical and laboratory features of disseminated histoplasmosis during two large urban outbreaks. *Medicine* (Baltimore) **1983**;62:263–270
3. Ankobiah WA, Vaidya K, Powell S, et al. Disseminated histoplasmosis in AIDS: clinicopathologic features in seven patients from a non-endemic area. *N Y State J Med* **1990**;90:234–238
4. Huang CT, McGarry T, Cooper S, Saunders R, Andavolu R. Disseminated histoplasmosis in the acquired immunodeficiency syndrome: report of five cases from a nonendemic area. *Arch Intern Med* **1987**;147:1181–1184
5. Johnson PC, Hamill RJ, Sarosi GA. Clinical review: progressive disseminated histoplasmosis in the AIDS patient. *Semin Respir Infect* **1989**;4:139–146
6. Centers for Disease Control. Revision of the case definition of acquired immunodeficiency syndrome for national reporting United States. *MMWR Morb Mortal Wkly Rep* **1985**;34:373–375
7. McLoud TC, Carrington CB, Gaensler EA. Diffuse infiltrative lung disease: a new scheme for description. *Radiology* **1983**;149:353–363
8. Nightingale SD, Parks JM, Pounders SM, Burns DK, Reynolds J, Hernandez JA. Disseminated histoplasmosis in patients with AIDS. *South Med J* **1990**;83:624–630
9. Suster B, Akerman M, Orenstein M, Wax MR. Pulmonary manifestations of AIDS: review of 106 episodes. *Radiology* **1986**;161:87–93
10. Miller WT Jr, Edelman JM, Miller WT. Cryptococcal pulmonary infection in patients with AIDS: radiographic appearance. *Radiology* **1990**;175:725–728
11. Marinelli DL, Albelda SM, Williams TM, Kern JA, Iozzo RV, Miller WT. Nontuberculous mycobacterial infection in AIDS: clinical, pathologic and radiographic features. *Radiology* **1986**:160:77–82
12. Goodwin RA, Shapiro JL, Thurman GH, Thurman SS, Des Prez RM. Disseminated histoplasmosis: clinical and pathologic correlations. *Medicine* (Baltimore) **1980**:59;133

Book Review

Clinical Imaging. An Atlas of Differential Diagnosis, 2nd ed. By Ronald L. Eisenberg. Gaithersburg, MD: Aspen, 1152 pp., 1992. $165

The aim of this book, as stated in the preface, is to provide "a handy reference for practicing radiologists and residents faced with the increasingly complex daily challenge of interpreting radiographic examinations." The book focuses on pattern recognition, presenting lists of differential diagnoses with descriptions of imaging findings, differential points, and radiologic illustrations.

Like the first edition of *Clinical Imaging* published in 1988, the second edition contains chapters on chest, cardiovascular, gastrointestinal, genitourinary, skeletal, spine, and skull patterns. Additions include chapters on breast disease and mammography and on fetal sonography. The first six chapters, particularly the ones on the gastrointestinal system and the spine, are almost identical to those in the first edition. Two new patterns have been added to the chapter on the genitourinary system, and three new patterns have been added to the chapter on the chest. The chapter on the skeletal system contains one new pattern and a new list titled "Eponyms of Fractures." A separate brief section on echocardiography has been added to the chapter on the cardiovascular system. In the chapter on the skull, 11 new lists discuss brain abnormalities shown on MR imaging. In addition, four other lists have been expanded to include findings on both CT and MR imaging. The new chapter on breast disease and mammography includes four lists and contains 21 pages. The new chapter on fetal sonography includes four lists and contains 17 pages.

The book presents a wide range of radiologic patterns and an extensive table of differential diagnoses for each pattern. Diagnoses are listed in order of likelihood rather than alphabetically or randomly. The text is clear, concise, and well organized. The printing and paper are of high quality, and the numerous illustrations are uniformly excellent.

Clinical Imaging, according to the preface to the first edition, can assist "both the practicing radiologist faced with the reality of daily film reading and the senior resident taking the oral board examination." For those who do not own the first edition of this useful reference, the second edition would be a wise purchase. However, for those who do own the first edition, the second edition offers only limited new information, which may not be worth the $165 cover price.

Similar books offering tables of differential diagnoses and critical bits of information include *Radiology Review Manual*, by Wolfgang Dähnert (Baltimore, Williams & Wilkins, 1990), and *Aids to Radiological Differential Diagnosis*, 2nd ed., by Stephen Chapman and Richard Nakielny (Philadelphia, Bailliere Tindall, 1990). *Radiology Review Manual* contains 583 pages and costs $62. *Aids to Radiological Differential Diagnosis* is a pocket-sized book of approximately 566 pages at a price of $27.95. Although both these books contain line drawings, neither includes radiologic illustrations.

Philip Goodman
University of Texas Medical Branch
Galveston, TX 77555-0709

Diagnostic Success of Bronchoscopic Biopsy in Immunocompromised Patients with Acute Pulmonary Disease:

Predictive Value of Disease Distribution as Shown on CT

Dennis L. Janzen[1]
Brendan D. Adler
Simon P. G. Padley
Nestor L. Müller

OBJECTIVE. The purpose of the study was to determine if the distribution of pulmonary opacities on CT scans could be used to predict the outcome of bronchoscopic biopsy procedures in immunocompromised non-AIDS patients with acute pulmonary complications.

MATERIALS AND METHODS. Thirty-three consecutive immunocompromised patients without AIDS who had acute pulmonary complications and who had had CT, bronchoscopic biopsy procedures, and proved diagnoses were included in the study. The distribution and dominant pattern of pulmonary opacities on CT were assessed independently by two observers. The pathologic diagnoses were invasive aspergillosis (eight), *Candida* pneumonia (six), bronchiolitis obliterans with or without organizing pneumonia (six), drug-induced lung disease (four), *Pneumocystis carinii* pneumonia (four), cytomegalovirus pneumonia (three), pulmonary hemorrhage (one), and recurrent lymphoma (one).

RESULTS. The results of bronchoscopic techniques established a specific diagnosis in 17 patients (52%). In the remaining 16 patients, results of bronchoscopic biopsy could not be used to establish a specific diagnosis; open lung biopsy (15 patients) or transthoracic needle biopsy (one patient) were required for diagnosis. The results of bronchoscopic procedures were diagnostic more often in patients in whom pulmonary opacities involved the central third of the lung than in patients in whom the central third was spared (70% vs 23%, $p = .02$). Results were diagnostic more often in cases in which the causes of acute pulmonary complications were infectious than in cases in which the causes were noninfectious (71% vs 17%, $p < .005$).

CONCLUSION. We conclude that the presence or absence of central disease as shown by CT can be used to suggest whether results of bronchoscopic procedures in immunocompromised non-AIDS patients will be diagnostic.

***AJR* 1993;160:21–24**

Acute pulmonary complications are the leading cause of morbidity and mortality in immunocompromised patients [1-4]. These complications are a difficult clinical problem because the various infectious and noninfectious diseases or abnormalities often have nonspecific clinical, laboratory, and chest radiographic features. Prompt investigation and diagnosis are essential, as early therapy improves survival [5].

The common pulmonary complications and diagnostic approaches are significantly different in AIDS patients than in immunocompromised patients without AIDS. In most clinical protocols, immunocompromised non-AIDS patients suspected of having acute pulmonary complications are treated empirically for bacterial infections. If a patient does not respond, invasive procedures such as bronchoalveolar lavage, bronchoscopic biopsy, open lung biopsy, and transthoracic needle aspiration biopsy are used to establish a specific diagnosis. Transthoracic needle aspiration biopsy is most appropriate for focal cavitating or nodular lesions; diffuse disease usually requires bronchoscopic or open lung biopsy [6]. Bronchoscopic biopsy is safer than open lung biopsy, but the results

Received June 4, 1992; accepted after revision July 14, 1992.

[1]All authors: Department of Radiology, University of British Columbia and Vancouver General Hospital, 855 W. 12th Ave., Vancouver, BC, Canada V5Z 1M9.

0361–803X/93/1601–0021

are diagnostic in fewer cases, ranging from 8% to 68% [6–11]. If the results of bronchoscopic biopsy do not indicate the diagnosis, patients often have open lung biopsy. If we could predict when the results of bronchoscopic biopsy would not be diagnostic, the time, risk, complications, and cost of this procedure could be avoided.

The aim of this study was to determine if the distribution of disease seen on CT scans could be used to predict when the results of bronchoscopic biopsy procedures would be diagnostic in immunocompromised non-AIDS patients with acute pulmonary disease.

Materials and Methods

The records of 33 consecutive immunocompromised patients without AIDS who had acute pulmonary complications and who had CT scans obtained before bronchoscopic procedures were retrospectively reviewed. The eligibility criteria were (1) the occurrence of an acute pulmonary complication, (2) CT examination within 7 days of bronchoscopic biopsy procedure, (3) bronchoscopic biopsy performed according to a standardized routine, and (4) establishment of a specific pathologic diagnosis based on findings from bronchoscopic biopsy. At our institution, a CT examination is performed routinely before biopsy procedures, regardless of findings on chest radiographs in immunocompromised non-AIDS patients, in order to localize the most representative region of abnormal lung. Acute pulmonary complications were defined as the recent onset (<10 days' duration) of pulmonary symptoms and clinical signs.

The study group consisted of 20 men and 13 women 17–62 years old (mean, 34 years). The causes of the immunocompromise were bone marrow transplantation less than 1 year previously (14), bone marrow transplantation with graft-vs-host disease (six), chemotherapy for hematologic malignancy (10), and renal transplant rejection requiring immunosuppressant therapy (three). All bronchoscopic procedures were performed in a standardized fashion by experienced bronchoscopists. The types of procedures were bronchoalveolar lavage only in 22 patients and bronchoalveolar lavage and transbronchial biopsy in 11. Transbronchial biopsies were not performed in patients with thrombocytopenia or in those on mechanical ventilation.

The results of bronchoscopic biopsy procedures indicated a specific diagnosis (i.e., were diagnostic) in 17 (52%) of 33 patients. In the remainder, the diagnosis was subsequently established by open lung biopsy in 15 and by transthoracic needle aspiration biopsy in one. The final diagnoses were invasive aspergillosis (eight), *Candida* pneumonia (six), bronchiolitis obliterans with or without organizing pneumonia (six), *Pneumocystis carinii* pneumonia (four), drug-induced lung disease (four), cytomegalovirus infection (three), pulmonary hemorrhage (one), and recurrent lymphoma (one). In all cases, the clinical features and response to therapy were consistent with the final diagnosis.

CT scans were obtained with a GE 9800 system (GE Medical Systems, Milwaukee, WI). A 10-mm collimation at 10-mm intervals was used for nine patients, and 1.5-mm collimation at 10-mm intervals for 24 patients. A high-spatial-frequency reconstruction algorithm was used in 29 patients. Retrospective targeting of the 1.5-mm collimation scans with a 20- to 25-cm field of view was done in 10 patients. The CT scans were photographed at mediastinal (level, 30–50 H; width, 350–500 H) and lung parenchymal (level, -600 to -800 H; width, 1000–2000 H) settings.

The median interval between CT and the bronchoscopic procedure was 2 days (range, 0–7 days). The information from the CT scans was used to select a representative area of abnormal lung for the bronchoscopic procedure.

The CT scans were reviewed independently by two observers who were unaware of the clinical and pathologic data. The CT scans were assessed for the presence and distribution of air-space consolidation, ground-glass opacity, nodular opacities, and irregular linear opacities. Ground-glass opacity was defined as an area of abnormal lung opacity that did not obscure visualization of the pulmonary vascular structures. The distribution of disease was classified as involving or sparing the medial third of the lung in both the transverse and cephalocaudal planes. Pulmonary opacities that involved this region were classified as having a central distribution whether they were focal or diffuse. Pulmonary opacities located entirely outside of the medial third of the lung or with only minimal involvement of the medial third (10% or less of the pulmonary opacities within the central third) were classified as peripheral.

The diagnostic success rates of bronchoscopic biopsy procedures in patients with and without CT evidence of central pulmonary opacities were compared by using the χ^2-test of significance, with Yates' correction for continuity.

Results

Twenty of 33 patients had central distribution of opacities, and 13 of 33 had peripheral opacities (Table 1). All patients had bilateral pulmonary disease. In assessments of central (Fig. 1) vs peripheral (Fig. 2) opacities, the two independent observers agreed in 32 (97%) of 33 cases. In the one case

TABLE 1: Diagnostic Success of Bronchoscopic Procedures by Disease and Distribution in Immunocompromised Patients Without AIDS with Pulmonary Complications

Disease	Distribution of Pulmonary Findings[a]			
	Central		Peripheral	
	No. of Patients	Success Rate (%)	No. of Patients	Success Rate (%)
Invasive aspergillosis	4	100	4	25
Candida pneumonia	4	100	2	50
Pneumocystis carinii pneumonia	3	67	1	0
Drug-induced lung disease	3	0	1	0
Cytomegalovirus pneumonia	3	100	0	0
Bronchiolitis obliterans	0	0	3	0
Bronchiolitis obliterans organizing pneumonia	1	0	2	50
Pulmonary hemorrhage	1	100	0	0
Recurrent lymphoma	1	0	0	0
Total	20	70	13	23

[a] Pulmonary opacities involving the medial one third of the lung, whether focal or diffuse, were classified as central. Pulmonary opacities located entirely outside the medial third or with only minimal involvement of the medial third (10% or less of the abnormalities within this region) were classified as peripheral.

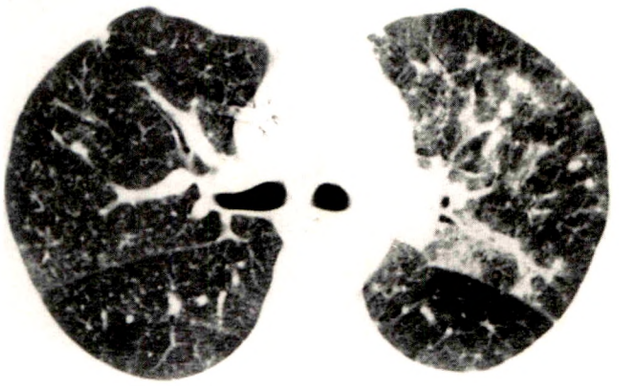

Fig. 1.—CT scan at level of carina in a 27-year-old bone marrow transplant recipient shows air-space consolidation, most severe in left upper lobe, involving central third of lung. Results of bronchoalveolar lavage indicated *Candida albicans* infection.

Fig. 2.—CT scan at level of left atrium in a 41-year-old patient receiving chemotherapy for acute myelogenous leukemia shows bilateral air-space consolidation mainly in peripheral lung regions. Only minimal ground-glass opacities are present in medial aspect of right middle lobe. Results of bronchoalveolar lavage and transbronchial biopsy did not indicate a diagnosis. Open lung biopsy showed invasive aspergillosis.

of disagreement, a consensus opinion was reached after discussion of the CT findings.

A dominant CT pattern of ground-glass opacity was observed in 11 patients; bronchoscopic procedures were diagnostic in four (50%) of eight patients with a central distribution and in none of three patients with a peripheral distribution. Twelve patients had a dominant nodular CT pattern; bronchoscopic biopsy procedures were diagnostic in six (75%) of eight patients with a central distribution and in one (25%) of four patients with a peripheral distribution. A dominant CT pattern of consolidation was observed in seven patients; bronchoscopic procedures were diagnostic in all (100%) of four patients with a central distribution and in one (33%) of three patients with a peripheral distribution of opacities. Three patients had a dominant CT pattern of irregular linear opacities in a peripheral distribution; bronchoscopic procedures were diagnostic in one patient. The descriptions of the dominant pattern of pulmonary opacity by the two observers agreed in all cases.

The results of bronchoscopic biopsy were diagnostic more often in patients with central opacities than in those with peripheral opacities (70% vs 23%, $p = .02$). Central opacities were associated with diagnostic bronchoscopic procedures in the subgroups of patients with dominant CT patterns of ground-glass opacities, nodular opacities, and consolidation, although the small number of observations in these subgroups precluded statistical significance.

The prevalences of infectious diseases were similar in the groups with central and peripheral opacities (70% vs 54%, $p > .10$). Among patients with infectious causes ($n = 21$), results of bronchoscopic procedures were diagnostic more often in those with central opacities than in those with peripheral opacities (93% vs 29%, $p < .0001$). Among patients with noninfectious causes ($n = 12$), no differences were found between those with central opacities and those with peripheral opacities; results were diagnostic in 17% of cases in both groups. The results of bronchoscopic procedures were diagnostic more often in patients with complications caused by infection than in those with complications caused by noninfectious pulmonary diseases (71% vs 17%, $p < .005$).

Discussion

Overall, the results of bronchoscopic procedures were diagnostic in 52% of cases, which is similar to that of previously published series [5–12]. The diagnostic success of bronchoscopic biopsy depends on a variety of factors, including type and number of biopsies, amount of biopsy tissue obtained, and the specific lung disease being assessed. Results are generally diagnostic in patients with bacterial and viral infections [6, 10]. Bronchoscopic biopsy is moderately sensitive and specific in the diagnosis of *Pneumocystis carinii* pneumonia and cryptococcal, fungal, and nocardial infections [11]. We found a strong association between the cause of the pulmonary complication (infectious vs noninfectious) and whether the results of bronchoscopic biopsy were diagnostic. In patients with central pulmonary opacities, the results were diagnostic only in the subgroup with infectious causes; in the subgroup with noninfectious causes, the results were not often diagnostic regardless of the distribution of pulmonary opacities on CT. Among the causes of noninfectious pulmonary complications, drug reactions, graft-vs-host disease, and radiation pneumonitis can rarely be specifically diagnosed on the basis of bronchoscopic findings. The cause is not known before biopsy and therefore cannot be used to guide the selection of biopsy procedure.

Technical factors such as number of biopsies and type of biopsy (bronchoalveolar lavage, brush biopsy, transbronchial forceps biopsy) also influence whether the results are diagnostic [6–8]. Bronchoalveolar lavage is the least invasive form of biopsy and is safer than transbronchial biopsy in patients with thrombocytopenia or who are on mechanical ventilation. Bronchoalveolar lavage is most useful for detecting organisms in the bronchoalveolar air spaces; however it may be difficult to distinguish infection from colonization [9].

Transbronchial biopsy provides small tissue samples suitable for histologic examination, but is associated with higher risks of pneumothorax (7–11%) and hemorrhage (8–17%) than lavage is [12, 13]. The type and number of biopsies are determined by clinical judgment; three to six biopsies from at least two lung segments are usually recommended [6, 7].

The association between disease distribution as shown by CT and the diagnostic success of bronchoscopic procedures in immunocompromised non-AIDS patients has not been previously evaluated. Feldman et al. [14] reported that the results of transbronchial lung biopsy were diagnostic in 84% of patients with diffuse infiltrates and in 43% of patients with localized disease as shown by chest radiography. CT is superior to chest radiography in depicting the location of pulmonary disease because of decreased superimposition of structures. This advantage of CT over chest radiography allows more accurate localization of disease and more accurate prediction of the success of bronchoscopic biopsy in chronic diffuse lung disease [15].

In our series, the results of bronchoscopic biopsies were most often diagnostic in patients in whom CT scans showed central opacities. This association was not due to any known confounding variable, as no significant difference was detected in the prevalences of infectious complications between those with central opacities and those with peripheral opacities.

Our results are most applicable to the subgroup of immunocompromised patients without AIDS who have acute pulmonary complications that are refractory to empiric therapy and require invasive biopsy procedures. This subgroup represents a biased selection from the larger population of immunocompromised non-AIDS patients, as the diseases that can be empirically managed, such as pulmonary edema and bacterial infections, are underrepresented. It is not appropriate to generalize our results to the entire spectrum of immunocompromised non-AIDS patients with acute pulmonary complications, as our study addresses the clinically relevant subgroup for whom the decision regarding type of biopsy procedure needs to be made.

CT is being used increasingly in immunocompromised patients with acute pulmonary complications to characterize pulmonary infiltrates and to guide biopsy procedures [3, 16]. Our results indicate that the location of disease as shown by CT can be used to predict if the results of bronchoscopic procedures will be diagnostic. This information, integrated with the clinical information, is relevant to the selection of biopsy procedure. CT examination of immunocompromised patients with acute pulmonary complications may result in more rapid and efficient investigation, which is especially significant in those patients whose condition is rapidly deteriorating.

REFERENCES

1. Rosenow EC III, Wilson WR, Cockerill FR III. Pulmonary disease in the immunocompromised host (first of two parts). *Mayo Clin Proc* **1985**;60:473–487
2. Krowka MJ, Rosenow EC III, Hoagland HC. Pulmonary complications of bone marrow transplantation. *Chest* **1985**;87:237–246
3. Graham NJ, Müller NL, Miller RR, Shepherd JD. Intrathoracic complications following allogeneic bone marrow transplantation: CT findings. *Radiology* **1991**;181:153–156
4. Pearson ADJ. Bone marrow transplantation and the lung (editorial). *Thorax* **1986**;41:497–502
5. Ramsey PG, Rubin RH, Tolkoff-Rubin NE, Cosimi AB, Russell PS, Greene R. The renal transplant patient with fever and pulmonary infiltrates: etiology, clinical manifestations, and management. *Medicine* (Baltimore) **1980**;59:206–222
6. Stover DE, Zaman MB, Hajdu SI, Lange M, Gold J, Armstrong D. Bronchoalveolar lavage in the diagnosis of diffuse pulmonary infiltrates in the immunosuppressed host. *Ann Intern Med* **1984**;101:1–7
7. Hedemark LL, Kronenberg RS, Rasp FL, Simmons RL, Peterson PK. The value of bronchoscopy in establishing the etiology of pneumonia in renal transplant recipients. *Am Rev Respir Dis* **1982**;126:981–985
8. Springmeyer SC, Silvestri RC, Sale GE, et al. The role of transbronchial biopsy for the diagnosis of diffuse pneumonias in immunocompromised marrow transplant recipients. *Am Rev Respir Dis* **1982**;126:763–765
9. Saito H, Anaissie EJ, Morice RC, Dekmezian R, Bodey GP. Bronchoalveolar lavage in the diagnosis of pulmonary infiltrates in patients with acute leukemia. *Chest* **1988**;94:745–749
10. Williams D, Yungbluth M, Adams G, Glassroth J. The role of fiberoptic bronchoscopy in the evaluation of immunocompromised hosts with diffuse pulmonary infiltrates. *Am Rev Respir Dis* **1985**;131:880–885
11. Thurlbeck WM, Miller RR, Müller NL, Rosenow EC, eds. Acute infiltrative lung disease in the immunocompromised host. In: *Diffuse diseases of the lung: a team approach*. Philadelphia: Decker, **1991**:66–91
12. Wilson WR, Cockerill FR III, Rosenow EC III. Pulmonary disease in the immunocompromised host (second of two parts). *Mayo Clin Proc* **1985**;60:610–631
13. Ognibene FP, Pass HI, Roth JA, Shelhamer JH. The diagnosis and therapy of respiratory disease. In: Parillo JE, Masur H, eds. *The critically ill immunosuppressed patient*. Rockville, MD: Aspen, **1987**:39–80
14. Feldman NT, Pennington JE, Ehrie MG. Transbronchial lung biopsy in the compromised host. *JAMA* **1977**;238:1377–1379
15. Mathieson JR, Mayo JR, Staples CA, Müller NL. Chronic diffuse infiltrative lung disease: comparison of diagnostic accuracy of CT and chest radiography. *Radiology* **1989**;171:111–116
16. Müller NL, Miller RR. Acute diffuse lung disease. In: Putman CE, ed. *Diagnostic imaging of the lung*, vol. 46. *Lung biology in health and disease*. New York: Marcel Dekker, **1990**:337–441

Left Paracardiac Mass Caused by Dilated Pericardiacophrenic Vein: Report of Four Cases

Jin Wook Chung[1]
Jung-Gi Im
Jae Hyung Park
Joon Koo Han
Choong Gon Choi
Man Chung Han

OBJECTIVE. The pericardiacophrenic vein is a possible route of collateral circulation when either the superior or the inferior vena cava is obstructed. When the vein is dilated, it can cause an abnormal appearance on chest radiographs. We describe four such patients.

MATERIALS AND METHODS. We studied four patients who had abnormalities on conventional chest radiographs due to a grossly dilated pericardiacophrenic vein, confirmed by means of venacavography, CT, or MR imaging. We analyzed the cause of the dilatation and the radiologic findings associated with the dilated pericardiacophrenic vein.

RESULTS. The cause of the dilated pericardiacophrenic vein was the membranous obstruction of the inferior vena cava in all four patients. Chest radiographs revealed an undulating vascular shadow (in two cases) or a shadow of several masses (in one case) along the left border of the heart or a poorly defined haziness mimicking a pulmonary parenchymal infiltrate (in one case). A direct communication between the left hepatic vein and the left inferior phrenic vein was seen near their insertion into the inferior vena cava in three cases. Hepatic venous outflow and some of the systemic venous return were directed to this left inferior phrenic–pericardiacophrenic route.

CONCLUSION. When obstruction of the inferior vena cava is clinically suspected and the chest radiograph shows abnormalities at the left paracardiac area, a dilated pericardiacophrenic vein due to obstruction in the suprahepatic portion of the inferior vena cava, most likely a membrane, should be considered in the differential diagnosis.

AJR 1993;160:25–28

The pericardiacophrenic vein, a tributary of the left brachiocephalic vein, has diaphragmatic branches that anastomose with the inferior phrenic vein. Therefore, it can serve as a collateral pathway when either the superior or the inferior vena cava is obstructed [1, 2]. We report four patients in whom a dilated pericardiacophrenic vein caused a paracardiac mass on chest radiographs. All four were proved to have membranous obstruction in the suprahepatic portion of the inferior vena cava.

Materials and Methods

Review of the past 10 years' radiology files at Seoul National University Hospital revealed four patients with a dilated pericardiacophrenic vein shown on a chest radiograph. The diagnosis was confirmed by means of venacavography, CT, or MR imaging in all four patients.

Venacavography was performed in two of the four patients. CT images were obtained in all four patients on CT/T 9800 or 8800 scanners (GE Medical Systems, Milwaukee, WI) with bolus injection of contrast medium. MR imaging was performed in one patient with a 2.0-T superconducting system (Spectro-20000; Gold Star, Seoul, Korea).

We analyzed the cause of the dilatation and the radiologic findings associated with the dilated pericardiacophrenic vein.

Received May 21, 1992; accepted after revision July 28, 1992.

[1]All authors: Department of Radiology, Seoul National University College of Medicine, 28 Yongon-dong Chongno-gu, Seoul 110-744, Korea. Address reprint requests to J. W. Chung.

0361–803X/93/1601–0025

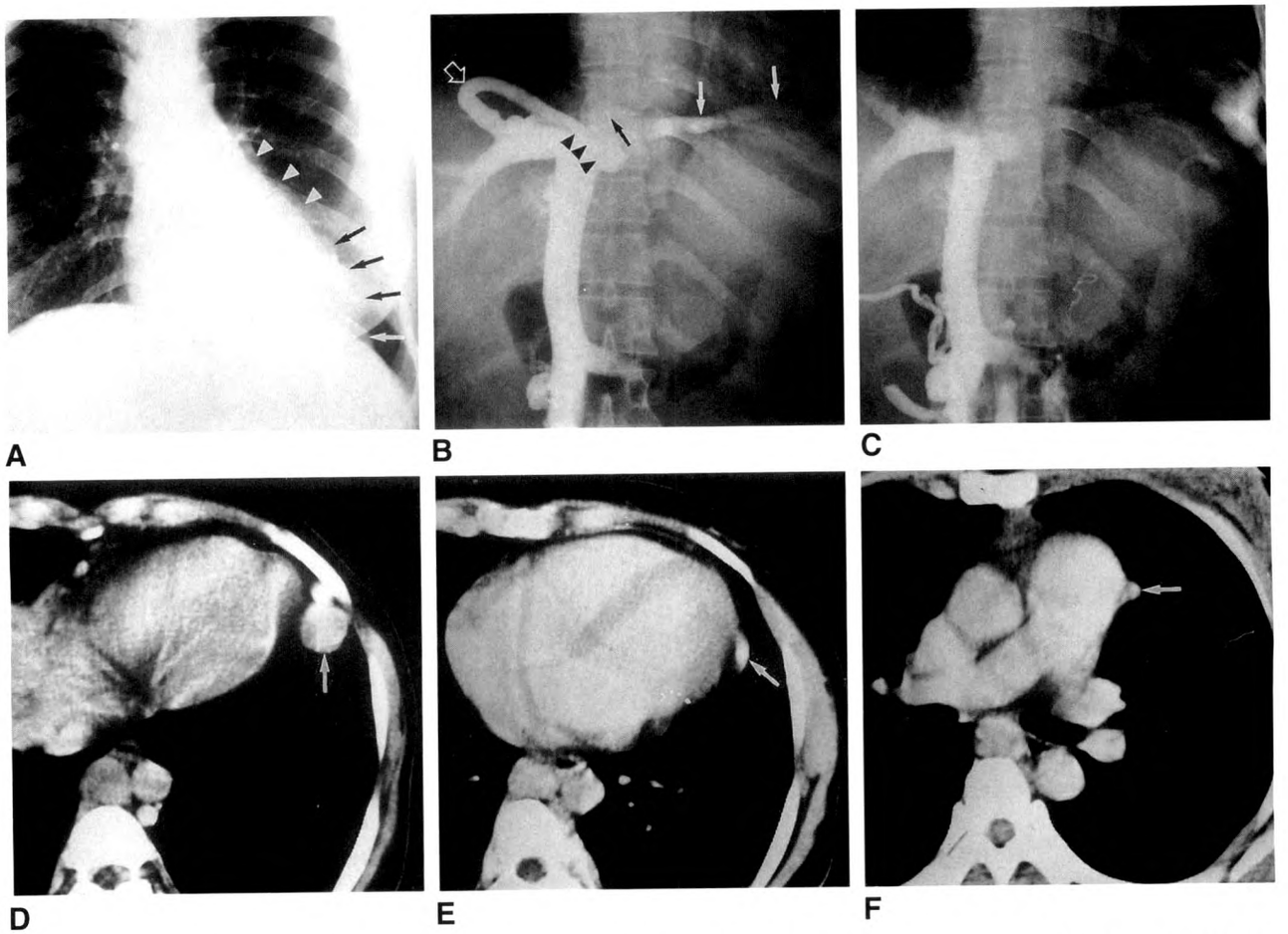

Fig. 1.—Typical radiographic findings and collateral pathway of dilated pericardiacophrenic vein in 41-year-old woman with membranous obstruction of inferior vena cava.

***A*, Chest radiograph shows an undulating vascular shadow at left lower border of heart (*arrows*) and two parallel contours of left upper border of heart (*arrowheads*). Azygos vein also is distended.**

***B*, Venacavogram shows complete obstruction of inferior vena cava by membrane (*arrowheads*). Right hepatic outflow is directed to left hepatic vein via an intrahepatic collateral (*open arrow*). Direct communication (*black arrow*) of left hepatic vein and left inferior phrenic vein (*solid white arrows*) is visible near insertion site into inferior vena cava.**

***C*, On delayed venacavogram, an entangled vascular mass at left cardiophrenic angle is well visualized.**

***D–F*, Sequential CT scans show intrathoracic course of left pericardiacophrenic vein (*arrow*). It originates from left cardiophrenic angle (*D*), ascends along left border of heart (*E* and *F*), and finally drains into left innominate vein.**

Results

The cause of the dilated pericardiacophrenic vein was the membranous obstruction of the inferior vena cava, with blocking of the hepatic venous outflow in all four cases.

An undulating vascular shadow along the left border of the heart was seen on chest radiographs in two patients (Fig. 1A). When the vein was markedly dilated, it simulated a pleural effusion or mediastinal masses (Fig. 2A). In one patient, the vein mimicked a pulmonary parenchymal infiltrate (Fig. 3A). A dilated azygos vein was seen in three patients (Figs. 1A and 3A).

CT and MR images revealed a vascular mass in the left cardiophrenic angle, the anastomotic site between the pericardiacophrenic vein and the inferior phrenic vein (Figs. 1–3). When traced upward, the vein passed along the lateral border of the left ventricle, the conus arteriosus, the aorticopulmonary window, and the aortic arch before draining into the left innominate vein (Fig. 1).

The collateral pathway was shown in three patients by venacavography or MR imaging (Figs. 1 and 3). A direct communication between the left hepatic vein and the left inferior phrenic vein was seen near their insertion into the inferior vena cava. The hepatic venous outflow was directed to the dilated left inferior phrenic vein, which anastomosed with the left pericardiacophrenic vein (Fig. 1). In the remaining patient, CT showed the obstruction of the hepatic segment of the inferior vena cava and the markedly dilated inferior phrenic vein. Despite the obstruction of the inferior vena cava, the azygos vein was relatively small in diameter, and other collaterals were not evident. Some of the systemic venous return seemed to be directed to the inferior phrenic–pericardiacophrenic route via transhepatic collaterals (Fig. 2).

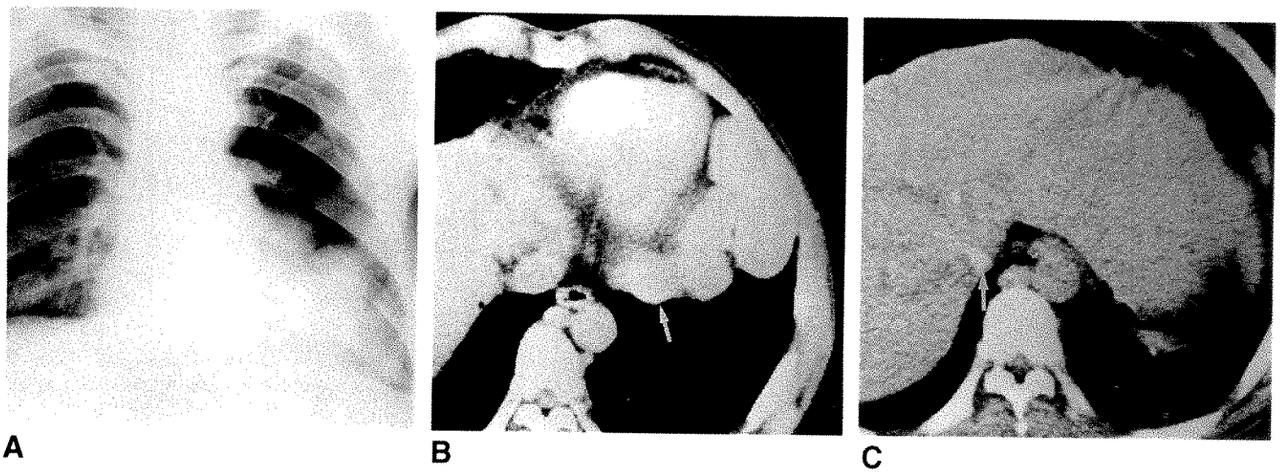

Fig. 2.—Manifestation of markedly dilated pericardiacophrenic vein as left paracardiac masses in 58-year-old man with membranous obstruction of inferior vena cava.

A, Chest radiograph shows round extrapulmonary masses along left border of heart and upper mediastinum.

B, CT scan reveals markedly dilated inferior phrenic vein (*arrow*) and a tortuous vascular mass at cardiophrenic angle. Azygos vein is relatively small in diameter compared with that in other patients with dilated pericardiacophrenic vein.

C, More caudal CT scan shows luminal obliteration and calcification of inferior vena cava (*arrow*). Hepatic veins are not visualized because of poor contrast enhancement.

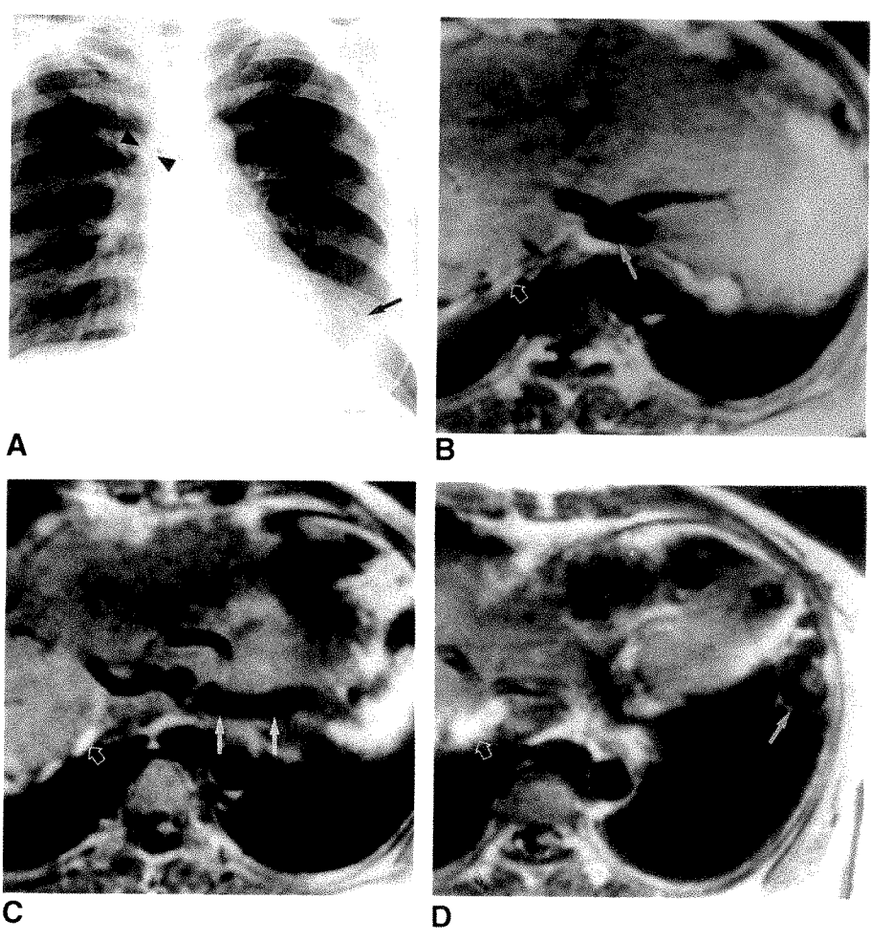

Fig. 3.—Varix at left cardiophrenic angle mimicking pulmonary parenchymal infiltrate in 50-year-old woman with membranous obstruction of inferior vena cava.

A, Chest radiograph reveals poorly defined haziness at left cardiophrenic angle (*arrow*) and distended azygos vein (*arrowheads*).

B–D, Sequential axial MR images (750/30, ECG-gated) at level of diaphragm show confluence of hepatic veins (*solid arrow* in *B*), direct communication with inferior phrenic vein (*solid arrows* in *C*), and formation of entangled vascular mass around cardiac apex (*solid arrow* in *D*). Azygos vein also is grossly dilated. Intrahepatic segment of inferior vena cava is not identified, and only a focal fat collection is shown at that site (*open arrows*).

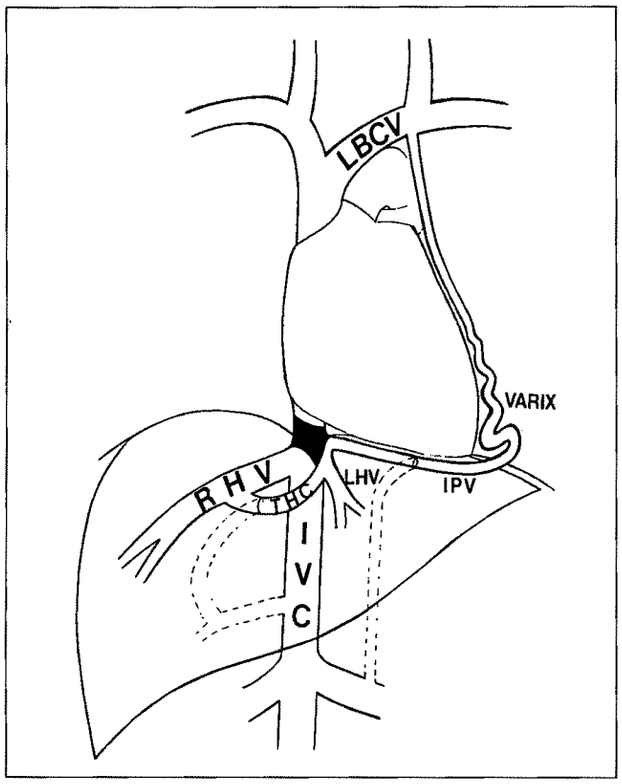

Fig. 4.—Schematic drawing of collateral pathway via a pericardiacophrenic vein in our cases of membranous obstruction of inferior vena cava. LBCV = left brachiocephalic vein, RHV = right hepatic vein, THC = transhepatic collateral, LHV = left hepatic vein, IPV = inferior phrenic vein, IVC = inferior vena cava, dotted lines = potential collateral pathways via inferior hepatic vein or IPV draining into left renal vein.

Discussion

The pericardiacophrenic vein drains the pericardium, pleura, and diaphragm and ascends along the left border of the heart with the accompanying phrenic nerve between the mediastinal pleura and the pericardium [3]. It drains into either the internal mammary vein or the left superior intercostal vein, or directly into the left brachiocephalic vein [4]. It could be the collateral pathway when either the superior or the inferior vena cava is obstructed. However, it has seldom been reported as a major route of collateral circulation in vena caval obstruction except in membranous obstruction of the inferior vena cava [2]. All four of our patients with a dilated pericardiacophrenic vein had membranous obstruction of the inferior vena cava.

In cases of vena caval obstruction, many routes of collateral circulation exist, such as the azygos or hemiazygos system, internal mammary chain, portosystemic collaterals, and superficial collaterals of the abdominal wall. The site of obstruction appears to determine the collateral pathway. Simson [2] described a few patients with membranous obstruction of the inferior vena cava in whom the inferior phrenic vein was patent below the obstruction and the pericardiacophrenic veins were tortuous and varicose. In our patients, the ostia of the inferior phrenic vein were obstructed. According to Bennette et al. [5], the left inferior phrenic vein has its origin above the diaphragm near the apex of the heart and terminates in the left side of the left hepatic vein in 74% of cases. That is, the ostia of the inferior phrenic vein and the left hepatic vein are near each other. Persistent communication of the two veins at the insertion site could occur during the process of vena cava and hepatic outflow obstruction. Direct communication of the left hepatic vein and the left inferior phrenic vein near where they insert into the inferior vena cava was clearly shown in three of our patients by venacavography or MR imaging. The flow in the left inferior phrenic vein is reversed, and systemic venous return also can be directed to the inferior phrenic vein via transhepatic collaterals (Fig. 4).

The radiologic importance of the pericardiacophrenic vein has been mentioned only with respect to the risk of inadvertent catheterization and possible perforation [1]. However, a grossly dilated pericardiacophrenic vein can cause various abnormal findings on chest radiographs. A correct diagnosis of membranous obstruction of the inferior vena cava can lead to curative treatment with surgery or percutaneous transluminal angioplasty [6, 7]. The undulating vascular shadow along the left border of the heart, accompanied by the distended azygos vein, suggests the diagnosis of obstruction in the suprahepatic portion of the inferior vena cava, most likely by a membrane. In one of our cases, we suggested the correct diagnosis after reviewing a chest radiograph without any clinical information. The patient was treated successfully with percutaneous transluminal angioplasty. When obstruction of the inferior vena cava is clinically suspected and the chest radiograph shows abnormalities at the left border of the heart or at the cardiophrenic angle, a dilated pericardiacophrenic vein should be considered in the differential diagnosis.

REFERENCES

1. Ovenfors C-O, Ounjian ZJ. Aberrant position of central venous catheter introduced via internal jugular vein. *AJR* **1977**;128:483–484
2. Simson IW. Membranous obstruction of the inferior vena cava and hepatocellular carcinoma in South Africa. *Gastroenterology* **1982**;82:171–178
3. Godwin JD, Chen JTT. Thoracic venous anatomy. *AJR* **1986**;147:674–684
4. Yune HY, Klatte EC. Mediastinal venography. *Radiology* **1972**;105: 285–291
5. Bennette P, Hannoun L, Menegaux F, Calmat A, Cabrol C. Anatomic study of the left inferior diaphragmatic vein. *Bull Assoc Anat* **1983**;67:69–77
6. Espana P, Figuera D, Miguel JF, Anaya A, Menendez J, Durantez A. Membranous obstruction of the inferior vena cava and hepatic veins. *Am J Gastroenterol* **1980**;73:28–32
7. Sato M, Yamada R, Tsuji K, et al. Percutaneous transluminal angioplasty in segmental obstruction of the hepatic inferior vena cava: long-term results. *Cardiovasc Intervent Radiol* **1990**;13:189–192

Perspective

Value of Fluoroscopy in Patients with Suspected Bilateral Hemidiaphragmatic Paralysis

Ian Y. Ch'en[1] and John D. Armstrong II

Bilateral hemidiaphragmatic paralysis (BHP) is an important clinical problem in hospitals where cardiac surgery is commonly performed. Often overlooked as a cause of hypercapnic respiratory failure, BHP can lead to substantial difficulty in patients' treatment and morbidity. In addition to hypothermic phrenic nerve injury associated with "ice chip" cardioplegia, causes of BHP include malignant mediastinal tumors and numerous neurologic disorders (e.g., Chiari malformation, multiple sclerosis, and paraneoplastic neuritis) [1, 2]. The radiographic appearance of BHP typically consists of diaphragmatic elevation, volume loss, and bibasilar linear opacities probably caused by platelike atelectasis [2]. Currently, nonimaging procedures (spirometry, transdiaphragmatic pressure measurement, and phrenic nerve stimulation) are regarded as diagnostically important, while fluoroscopic examination is condemned for diagnostic inaccuracy in both the radiologic and general medicine literature [1–3]. This article discusses normal and BHP-related respiratory mechanics and advocates a systematic fluoroscopic approach for evaluation of BHP. In so doing, it challenges the traditional bias against the use of fluoroscopy for assessment of this disorder.

Mechanics of Respiration

Normally during quiet breathing, the dome-shaped diaphragm (and to a lesser extent the external intercostal muscles) contracts to lift the rib cage and push down the abnormal viscera; this action produces the negative intrathoracic pressure gradient required for inspiration. Quiet expiration occurs after passive elastic recoil of the lung and thoracic wall with relaxation of the diaphragm. In normal deep, or voluntary, inspiration, the accessory muscles of inspiration (e.g., sternocleidomastoid, scalene) actively contract to augment maximal diaphragmatic contraction to further expand the chest cage. Similarly, forced expiration is augmented by active contraction of expiratory muscles (predominantly the anterior abdominal wall musculature including rectus abdominis, internal and external oblique, and transversus abdominis) to force the relaxing diaphragm upward into the chest owing to elevation of intraabdominal pressure. An important observation throughout these processes is that the direction of diaphragmatic and anterior abdominal wall movement is always linked to the transdiaphragmatic pressure gradient. Thus, any cephalic movement of abdominal contents (e.g., during normal exhalation) will be associated with an upward movement of the diaphragm and inward abdominal wall movement, while descent of abdominal contents (e.g., during normal inhalation) will lead to reciprocal downward movement of the diaphragm and outward abdominal wall movement.

In the setting of BHP, the diaphragm behaves passively like an elastic membrane between the thoracic and abdominal compartments. During inspiration, negative intrathoracic pressure is generated solely by the active contraction of external intercostal and accessory inspiratory musculature. Such thoracoabdominal pressure difference leads to upward excursion of the paralyzed diaphragm accompanied by

Received May 21, 1992; accepted after revision July 8, 1992.

[1]Both authors: Department of Radiology, Box A 030, University Hospital, University of Colorado Health Sciences Center, 4200 E. Ninth Ave., Denver, CO 80262-0030. Address reprint requests to I. Y. Ch'en.

AJR **1993;160:29–31** 0361–803X/93/1601–0029

upward movement of the abdominal viscera and inward movement of the anterior abdominal wall. This phenomenon, the so-called thoracoabdominal paradox, characterized by outward chest wall and inward abdominal wall motion during inspiration, is the most important clinical sign of BHP. It is accentuated when the patient is recumbent because of the more cephalic resting position of abdominal viscera and hemidiaphragms, as well as less mechanical support for outward abdominal wall movement, particularly if the patient is supine. Paradoxical diaphragmatic excursion can be shown unequivocally on fluoroscopic examination.

Besides thoracoabdominal paradox, some patients compensate for BHP by adopting an unusual breathing pattern in the upright position. This is characterized by active exhalation to a lung gas volume below the usual resting volume with subsequent passive inspiration. By actively increasing intraabdominal pressure with expiratory muscle contraction, abdominal contents and the flaccid hemidiaphragms are elevated into the thorax during the expiratory phase of breathing. Then, abdominal wall relaxation with passive inspiration causes concomitant descent of both the diaphragm and the abdominal viscera toward the abdomen. This compensatory mechanism presents a confusing fluoroscopic picture because passive diaphragmatic descent during inspiration mimics normal diaphragmatic contraction. Fortunately, fluoroscopic examination with the patient recumbent can overcome this interpretative pitfall.

Fluoroscopic Evaluation

A systematic and thorough fluoroscopic evaluation for BHP should be made with the patient in both the supine and lateral decubitus (or oblique) positions. Fluoroscopy with the patient in the lateral decubitus (or oblique) position allows simultaneous visualization of both hemidiaphragms, each in its entirety. Further, the increase in muscular tension on the dependent hemidiaphragm (owing to cephalic displacement of the abdominal viscera) improves muscle length-tension properties so that dependent hemidiaphragmatic motion, normal or abnormal, will be identified more easily [4]. Supine positioning accentuates paradoxical diaphragmatic and thoracoabdominal motion, and more importantly, minimizes the aforementioned compensatory breathing pattern in BHP, which may otherwise lead to false-negative diagnosis.

The comfort and cooperation of patients can be substantially improved during fluoroscopy by verbal reassurance, expeditious examination, and the use of supplemental oxygen (nasal cannula or mask). Initially, quiet breathing is assessed to determine the timing of potential diaphragmatic motion. The fluoroscopist gently palpates the patient's abdomen to detect abdominal muscle contraction, define the phase of respiration, and detect thoracoabdominal paradox. In ventilator-dependent patients, fluoroscopic observation is focused on each hemidiaphragm during quiet breathing and during deep breathing attempts, after disconnection from the *ventilator* for defined brief periods (e.g., 15-sec periods of observation of each hemidiaphragm repeated one or more times as necessary). The potential for rapid lowering of intrathoracic pressure with "sniffing" improves the detection of subtle paradoxical excursion or restriction of diaphragmatic movement during unassisted respiration.

Contrary to a widely held notion, sniff-induced paradoxical diaphragmatic excursion during fluoroscopy is not equivalent to functional abnormality. Of 776 healthy subjects examined by Alexander [5], 6% had paradoxical excursion of either hemidiaphragm when the "sniff test" was performed in the anteroposterior position. The majority of these subjects exhibited paradoxical motion involving only the anterior hemidiaphragm (owing to partial eventration), with normal excursion of the posterior portion. Fluoroscopic examination in the lateral (or oblique) projection can thus avoid a false-positive outcome.

The two forms of demonstrable diaphragmatic excursion in BHP are paradoxical movement of both hemidiaphragms and apparent "normal" bilateral downward inspiratory and upward expiratory hemidiaphragmatic excursions. As stated earlier, paradoxical movement of the diaphragm appears as upward inspiratory excursion and is appreciated more readily when recumbent. Downward expiratory diaphragmatic movement occurs during relaxation of intercostal and accessory inspiratory muscles.

A potential fluoroscopic misinterpretation is the illusion of normal downward inspiratory diaphragmatic motion despite the presence of paradoxical excursion. This appearance is due to upward inspiratory movement of the chest wall, which overshadows paradoxical diaphragmatic movement and closely resembles normal active diaphragmatic contraction. The observer notes that the anterior ribs move cephalad and the hemidiaphragms appear to move downward. Significant interpretative error is avoided by comparison of diaphragmatic motion with some fixed extrathoracic object. If the fluoroscope is vertically locked in a position where the hemidiaphragm being examined projects just above the lower horizontal cone at the end of the patient's exhalation, then one may concentrate on hemidiaphragmatic excursion as related to the edge of the cone (and not on upward rib movement). In this way, true diaphragmatic paradox in BHP is detected.

On fluoroscopy, compensatory active exhalation and passive inspiration in BHP can mislead the observer because the direction of diaphragmatic movement is congruent with the normal breathing cycle. This adaptive mechanism tends to occur when the patient is in the upright position and is minimized if the patient is recumbent (e.g., supine). With supine positioning, the anterior abdominal wall flattens, abdominal contents and hemidiaphragms move passively into the thorax, and resting lung gas volumes decrease significantly. This breathing pattern thus becomes ineffective with the patient recumbent owing to further reduction in (already decreased) vital capacity; the patient may become acutely uncomfortable and perhaps panicky. Consequently, fluoroscopic confirmation that each hemidiaphragm exhibits paradoxical or no motion on attempted inspiration supports the diagnosis of BHP.

Conclusions

Contrary to popular belief, diaphragmatic fluoroscopy can be effectively used to evaluate BHP. Unfortunately, its

usefulness for this purpose is disregarded by many radiologists and clinicians because it traditionally has been performed inadequately. With fundamental knowledge of respiratory mechanics, the proposed systematic fluoroscopic evaluation of each hemidiaphragm with the patient recumbent will minimize interpretative pitfalls in BHP. Consequently, the simplicity and accuracy of fluoroscopy may establish this widely available technique as a diagnostically important procedure for assessment of BHP. A prospective study designed to systematically evaluate the use of fluoroscopy in suspected cases of BHP would contribute to our understanding.

REFERENCES

1. Chandler KW, Rozas CJ, Kory RC, Goldman AL. Bilateral diaphragmatic paralysis complicating local cardiac hypothermia during open heart surgery. *Am J Med* **1984**;77:243–249
2. Fraser RG, Paré JAP, Fraser RS, Genereux GP. *Diagnosis of diseases of the chest*, vol. 4, 3rd ed. Philadelphia: Saunders, **1991**:2921–2931
3. Loh L, Goldman M, Davis JN. The assessment of diaphragm function. *Medicine* (Baltimore) **1977**;56:165–169
4. Tarver RD, Conces DJ, Cory DA, Vix VA. Imaging the diaphragm and its disorders. *J Thorac Imaging* **1989**;4:1–18
5. Alexander C. Diaphragmatic movements and the diagnosis of diaphragmatic paralysis. *Clin Radiol* **1966**;17:79–83

Blistered Feet

Stefan C. Schatzki [1]

George Catlin's paintings constituted the first in-depth pictorial record of the American Plains Indians. Catlin, a self-taught artist, traveled extensively among the Native American tribes west of the Mississippi in the years 1830–1837. A previous article in this series [*AJR* 1991;157:110] discussed Catlin's early career.

In 1837, Catlin started the second part of his extraordinary career and began to show and tell others about what he alone had seen. He gathered his paintings and his multiple artifacts, including costumes, pipes, weapons, baskets, and so on, and inaugurated the era of Catlin's Indian Gallery. Catlin was a showman and his exhibition, which began in Albany, NY, and subsequently traveled to New York City, Washington, Philadelphia, and Boston, excited the public. At each location, huge numbers crowded in to see and hear about a wild west that they dimly knew. Two years later, as audiences began to dwindle, Catlin sailed to England with his Indian Gallery. He would not return to the United States for 31 years.

At first, his exhibition was a huge success in Europe. Starting in London and other cities in England, he later moved to Paris. His Indian Gallery amazed and delighted spectators and he became a celebrity. He met Queen Victoria and King Louis Philippe of France, who invited him to exhibit his paintings at the Louvre. In 1840, Catlin added visiting members of the Iowa and Ogibwa tribes to his show, enabling Europeans to see live reenactments of parts of the various Native American cultures. Catlin also began to paint again, producing over 100 additional works, including portraits of the visiting Native Americans as well as scenes of their life, produced from his earlier sketches done in the West.

It was during this period, in England, not in the American West, that Catlin painted the striking portrait reproduced here. This painting of Blistered Feet, in which the medicine man wears a medallion of George III, is one of Catlin's finest and most powerful portraits, and it attracted the attention of the French critic Charles Baudelaire.

While in London, Catlin published a book based on field notes from his earlier travels in the West. The book, which has been reprinted many times, is still used by anthropologists to study the early Native American cultures. Nonetheless, Catlin's audiences began to diminish, and he fell heavily in debt. His gallery, since renamed Catlin's Indian Collection, was in danger of being seized by European creditors. In 1852, a wealthy American, Joseph Harrison, paid off Catlin's debts and took possession of the collection, shipping it back to Philadelphia for storage.

Catlin was now 56, penniless, and deaf. His life's work was gone. However, "with no other means on earth than my hands and my brush," Catlin's resourcefulness returned. Before leaving Europe, utilizing his sketches and primarily from memory, he re-created much of his Indian Gallery. He traveled to the West Coast of North America and again began to paint Native Americans in their own surroundings. When he finally returned to New York in 1870, he had a new collection of paintings, which he called Catlin's Cartoon Collection.

Joseph Henry, the first secretary of the Smithsonian Institution, invited Catlin to exhibit the Cartoon Collection at the Smithsonian. He gave Catlin a room in one of the towers of the building, where he lived and continued to paint until he contracted his final illness in 1872. He died in Jersey City, NJ, on December 23, 1872. Although he had produced hundreds of new paintings, he continued to be concerned to the end about the original collection that had been taken from him in Europe in 1852. Almost the last words he spoke were "What will happen to my gallery?"

Catlin's original Indian Gallery was donated to the Smithsonian in 1879. Many of the ethnological specimens had been ruined and many of the paintings damaged. They were first exhibited at the Smithsonian in 1883. Soon after the turn of the century, most of the paintings were again put in storage.

Interest in Catlin's work revived after World War II. In 1953, some of his paintings again toured Western Europe. In 1965, a greater part of the collection was exhibited at the National Collection of Fine Arts in Washington, DC, where many of Catlin's pictures can now be seen regularly.

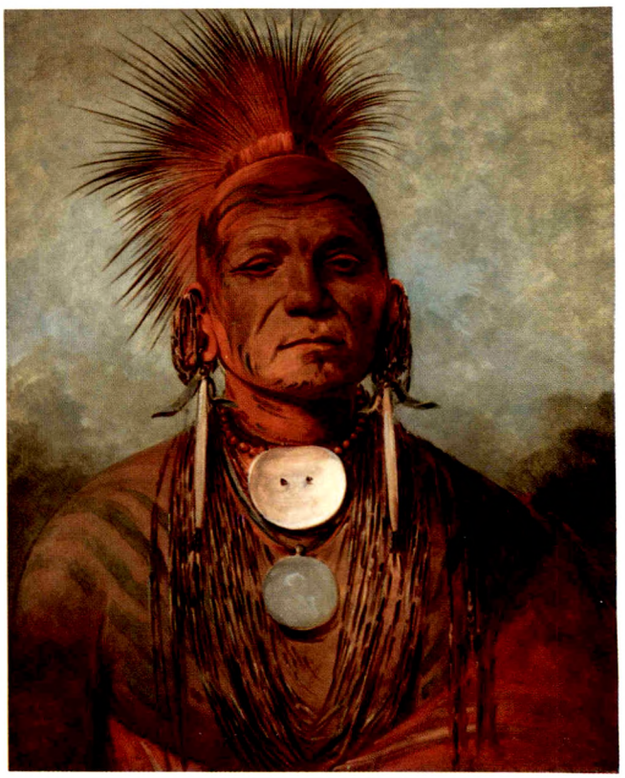

George Catlin (1794–1872), *Se-Ton-Ti-Yah, Blistered Feet, a Medicine Man of the Iowa Tribe*, 1844. Oil on canvas, 28 × 23 in. National Gallery of Art, Washington, DC. Paul Mellon collection.

[1] Department of Radiology, Mount Auburn Hospital, 330 Mount Auburn St., Cambridge, MA 02238.

***AJR* 1993;160:32** 0361–803X/93/1601–0032

Case Report

Subclavian Vein Thrombosis Detected with Spiral CT and Three-dimensional Reconstruction

Richard Tello,[1] Elizabeth Scholz, J. Paul Finn, and Philip Costello

Volumetric CT [1], or spiral CT, has been successfully used to examine thoracic blood vessels such as the pulmonary arteries for emboli [2], to image the heart after bypass graft surgery [3], and to assess for aortic vascular disease [4]. The use of spiral CT to examine venous structures in the thorax and upper limbs has not, to our knowledge, been previously described.

Full assessment for potential thrombus in the superior vena cava or a major tributary in a patient in whom malignant tumors are of primary concern would normally require not only contrast-enhanced thoracic CT but bilateral upper extremity phlebography. Such an approach would entail the use of large amounts of iodinated contrast media and multiple departmental resources. We report a case in which we used spiral CT with three-dimensional reconstruction to generate phlebographic images of subclavian vein thrombosis.

Case Report

A 54-year-old woman with a 45 pack-year smoking history had progressive pain in the left shoulder and edema in the left arm and face for 2 weeks. Posteroanterior and lateral radiographs showed hilar fullness. A request was made for upper extremity phlebographic and thoracic CT assessment. To avoid the need for two examinations, the spiral CT technique was modified to gain information regarding the venous structures of interest.

The patient was positioned on a fourth-generation CT scanner (Somatom Plus-S; Siemens Medical Systems, Erlangen, Germany) with the arms lying along the body, rather than extending above the head, in order to maintain the upper extremities within the imaging volume. In addition, IV access was established into both arms, the left at the forearm and the right at the wrist, with a 20-gauge angiocatheter. Initial assessment was performed with simultaneous injection of Renografin-60 (diatrizoate meglumine; Squibb, Princeton, NJ) from a Mark IV injector (Medrad, Pittsburgh, PA) into both arms via a Y adapter at 3 ml/sec for 6 sec (18 ml). After a 10-sec delay, single-level dynamic multiscanning was performed at the level of the pulmonary arterial root by using an 8-mm-thick image and standard thoracic algorithms, with data acquisition for 32 sec. Images were reconstructed at 1-sec intervals, and indicator dilution curve analysis with the vendor-supplied gamma variate analysis software showed arrival of contrast material at the pulmonary root 16 sec after initiation of the test injection. A second study used the spiral technique from the apex to the base of the lungs. An 8 mm/sec table feed was used, and 8-mm-thick image slices were obtained for 32 sec with the standard acquisition and standard reconstruction algorithms. Renografin-60 was administered via the power injector and Y adapter after a 16-sec delay at 1.7 ml/sec for 50 sec (82 ml).

Images were then reconstructed at 2-mm intervals; thresholding to visualize the opacified veins was chosen at 150 H, and three-dimensional reconstruction was performed. Three-dimensional viewing software provided by the manufacturer was used, and the best images were selected for clinical analysis.

An axial image of the upper thorax (Fig. 1A) showed the right subclavian vein with contrast material in it, whereas the left subclavian vein terminated in a soft-tissue mass with additional collateral vessels seen around the left humerus and along the anterior chest wall. Closer inspection of the area of the left subclavian vein showed that the contrast material terminated in a meniscal filling defect, which subsequent MR angiography showed to be a thrombus with a mass encasing the vessel. This was later proved to be adenocarcinoma.

Received June 8, 1992; accepted after revision July 8, 1992.

[1]All authors: Department of Radiology, Harvard Medical School, New England Deaconess Hospital, 185 Pilgrim Rd., Boston, MA 02215. Address reprint requests to R. Tello.

AJR 1993;160:33–34 0361–803X/93/1601–0033

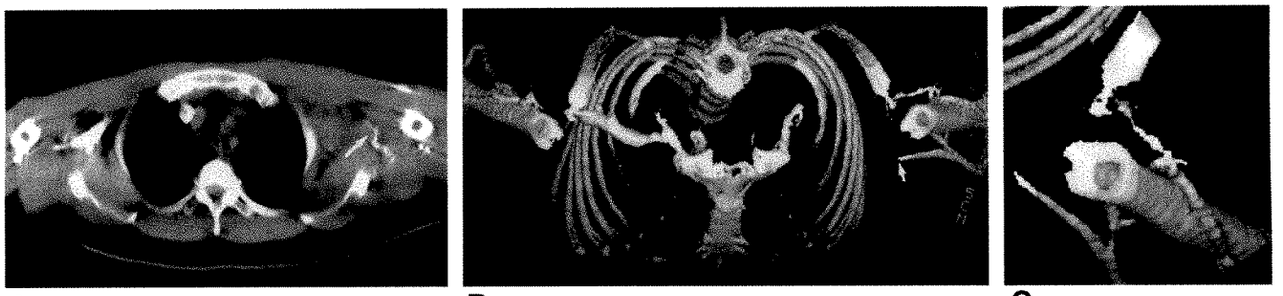

Fig. 1.—*A*, Axial spiral CT scan of upper lung shows opacified right subclavian vein and no opacification of left subclavian vein with thrombus (*arrow*) and surrounding mass.
***B*, Three-dimensional phlebogram from a right cephalic viewing position shows tapering of left brachial vein with collaterals (*arrow*).**
***C*, Three-dimensional phlebogram from a left posterior cephalic viewing position shows tapering of left brachial vein with collaterals.**

Figures 1B and 1C show three-dimensional reconstructions of the opacified venous structures in this patient, or the equivalent of three-dimensional phlebograms. These images show that flow from the right brachial vein continues into the right subclavian vein and then into the superior vena cava; on the left side, the brachial vein tapers with a beaded appearance, and anterior chest wall collaterals are seen anterior to the left humerus without flow in the left subclavian vein or beyond.

Discussion

This case highlights the use of volumetric or spiral CT to facilitate the solution of a complex problem that would normally require multiple examinations, or for patients who might not be eligible for MR angiographic examination. By the integration of dynamic CT techniques and rapid three-dimensional display of vascular structures, volumetric angiography and phlebography may become practical. Thus, volumetric CT when coupled with dynamic CT and three-dimensional reconstruction allows for rapid three-dimensional examination of vascular anatomy with angiogramlike images, and when axial images are evaluated, the surrounding soft tissues also can be assessed to elucidate the cause of venous obstruction.

Of note, by selectively controlling the time delay, either arterial or venous structures may be selectively demonstated. By using a 16-sec delay, the venous structures are visualized before arterial enhancement; thus, three-dimensional reconstruction elucidates venous structures selectively. If a longer time delay is used before spiral acquisition, then preferential arterial enhancement and arterial structures can be shown on three-dimensional reconstruction.

REFERENCES

1. Kalender WA, Seissler W, Klotz E, Vock P. Spiral volumetric CT with single-breath-hold technique, continuous transport, and continuous scanner rotation. *Radiology* **1990**;176:181–183
2. Remy-Jardin M, Deffontaines C. Chest evaluation with use of spiral volumetric CT with the single-breath-hold technique (abstr). *Radiology* **1991**;181(P):273
3. Costello P, Ecker CP, Tello RJ, Hartnell GG. Spiral CT assessment of coronary artery bypass grafts (abstr). *Radiology* **1991**;181(P):150
4. Costello P, Dupuy DE, Ecker CP. Spiral CT of the thorax with small volumes of contrast material: a comparative study (abstr). *Radiology* **1991**;181(P):274

MR Angiography of the Portal and Hepatic Venous Systems: Preliminary Experience with Echoplanar Imaging

Mark A. Goldberg[1]
E. Kent Yucel
Sanjay Saini
Peter F. Hahn
John A. Kaufman
Mark S. Cohen

OBJECTIVE. The purpose of this study was to evaluate the ability of echoplanar MR angiography to depict the major hepatic and portal venous structures.

SUBJECTS AND METHODS. Echoplanar and conventional MR angiographic examinations were performed in 10 subjects (seven healthy volunteers, three patients with focal hepatic lesions). A gradient-recalled echo (GRE) time-of-flight technique (125/10 [TR/TE], 90° flip angle) was used for echoplanar angiography. Eight complete single-excitation images were acquired at each level in 1.5 sec and then collapsed into a single maximal intensity projection. Conventional time-of-flight MR angiography (34/13, 30° flip angle) also was performed. The vascular anatomy from the right atrium to the splenic vein was imaged (6-mm contiguous levels) in three 10.5-sec breath-holds with echoplanar imaging, as compared with seven 11.5-sec breath-holds with conventional MR angiography. Echoplanar and conventional images were compared quantitatively and qualitatively.

RESULTS. Echoplanar imaging was 61% faster than conventional MR angiography. Vessel-to-liver signal-intensity ratios were significantly higher for echoplanar imaging ($p < .0001$), signal-to-noise ratios were significantly higher for conventional MR angiography ($p < .0001$), and contrast-to-noise ratios were comparable. Qualitatively, echoplanar imaging and conventional MR angiography provided similar anatomic information about the hepatic and portal veins.

CONCLUSION. Angiograms of the hepatic and portal venous systems that are of diagnostic quality can be acquired much more quickly with echoplanar imaging than with conventional MR angiography.

***AJR* 1993;160:35–40**

Diagnostic imaging of the hepatic vascular anatomy is essential to verify vessel patency, to show the relationship of masses to vessels (and therefore hepatic segments), and to distinguish small lesions from vessels. Successful evaluation of the patency of the major portal veins with MR angiography has been reported in several series [1–5]. Conventional MR angiography of the liver is generally performed using gradient-recalled echo (GRE) time-of-flight techniques [1–4, 6–9]. Such GRE, "bright blood" techniques have been shown to augment significantly the information gained from spin-echo (SE) imaging in evaluation of the portal venous anatomy [1, 3].

Echoplanar imaging using the Instascan technique, as described elsewhere [10–12], is a single-excitation method that can acquire data for an entire image in approximately 40 msec. Echoplanar imaging can be used to depict T1- or T2-weighted contrast using SE, inversion-recovery, or GRE pulse sequences. For MR angiography, the need for optimal recovery of vascular signal dictated our use of GRE echoplanar imaging. In this study, we used a newly developed GRE time-of-flight technique [6] to perform echoplanar MR angiography. We qualitatively and quantitatively compared echoplanar MR angiograms with conventional GRE time-of-flight MR angiograms of the portal and hepatic venous anatomy.

Received April 22, 1992; accepted after revision June 26, 1992.

[1]All authors: Department of Radiology, Massachusetts General Hospital, 32 Fruit St., Boston, MA 02114. Address reprint requests to M. A. Goldberg.

0361–803X/93/1601–0035

Materials and Methods

MR Imaging

We studied 10 subjects, including seven healthy volunteers and three patients. Informed consent was obtained from all subjects in accordance with the institution's Committee on Human Studies. Of the three patients, one had a hemangioma and two had metastatic disease. All subjects were studied using a modified 1.5-T Signa scanner (GE Medical Systems, Milwaukee, WI). This system can be used for both conventional and echoplanar imaging using the Instascan technique (Advanced NMR Systems, Wilmington, MA) [10–12].

The principles of the echoplanar time-of-flight MR angiography technique are described elsewhere [6]. At a given anatomic level, stationary spins were first saturated with four 90° preparation pulses. Eight complete GRE echoplanar images were then sequentially acquired at this anatomic level by using the following experimentally optimized imaging parameters: TR = 125 msec (i.e., time between successive single-excitation images), TE = 10 msec, 6-mm slice thickness, and 90° flip angle, resulting in a total imaging time per level of 1.5 sec. This imaging period enabled sampling over the entire course of an average cardiac cycle (i.e., heart rate of 60 beats per minute). Each echoplanar image was acquired with a matrix size of 128×128, a 20×40 cm field of view (FOV), and a tracking superior saturation pulse. We used 56.25% k-space coverage to reduce TE to its minimum value. Gradient-moment nulling [13–15] was not used, as the motion-related signal losses were small and did not justify the required increase in TE [6]. We combined the eight individual images into a single maximal intensity projection for each level to minimize the effects of temporal variation in the vascular signal. Seven 6-mm-thick contiguous levels (no gap) were acquired in a single 10.5-sec breath-hold. Three such acquisitions, for a total of 21 levels, were obtained in each subject, covering the venous anatomy from the level of the right atrium to that of the splenic vein.

For conventional time-of-flight MR angiography, we used a 256×128 matrix and a 36-cm FOV, resulting in a pixel size comparable to that of the echoplanar image. Imaging parameters were TR = 34 msec, minimum TE = 13 msec, one excitation, and a 30° flip angle. Flow compensation and a superior saturation pulse were used. Three 6-mm contiguous slices were acquired during each 11.5-sec breath-hold. Seven breath-holds were necessary to cover the same 21 anatomic levels imaged with the echoplanar technique. Both conventional and echoplanar images were acquired at end-expiration after coaching the patient to ensure reproducible anatomic localization from one breath-hold to the next.

Image Analysis

Signal intensity measurements covering operator-defined regions of interest were made in each of the following vessels: inferior vena cava; right, middle, and left hepatic veins; main, right, and left portal veins; splenic vein; and superior mesenteric vein. The inferior vena cava and hepatic veins were measured as close to their confluence as possible, and the right and left portal veins were measured as close to the bifurcation of the main portal vein as possible. Noise was measured as the standard deviation of the signal intensity in the corner of each image over a rectangular region of interest including 200–300 pixels. We calculated signal-to-noise ratios, vessel-to-liver signal-intensity ratios, and vessel-to-liver contrast-to-noise ratios for each vessel. Average signal-to-noise, signal-intensity, and contrast-to-noise ratios for each vessel, measured on the conventional and echoplanar images, were compared by using a paired two-tailed t-test.

For qualitative comparison, four reviewers experienced in abdominal MR imaging independently rated the visualization of each of the vessels measured previously and of the following vessels: the anterior and posterior divisions of the right portal vein and the medial and lateral divisions of the left portal vein. Each vessel was rated according to the following scale: 1 = vessel not identified; 2 = vessel equivocally identified; 3 = vessel identified, but poorly defined; 4 = vessel identified and moderately well defined; and 5 = vessel clearly defined, allowing definite evaluation of patency. We used the Wilcoxon signed rank test to compare the average qualitative ratings of the four reviewers for the two imaging techniques.

Results

Table 1 summarizes the quantitative comparison of the echoplanar maximal intensity projections and the conventional MR angiograms. Signal-to-noise ratios were significantly higher for the conventional images ($p < .0001$); signal-intensity ratios were significantly higher for the echoplanar

TABLE 1: Echoplanar vs Conventional MR Angiography

Vessel	Contrast-to-Noise Ratio		Signal-Intensity Ratio[a]		Signal-to-Noise Ratio[a]	
	EP	Conv.	EP	Conv.	EP	Conv.
Inferior vena cava	26.1	28.0	3.2	1.3	37.8	113.6
Right hepatic vein	22.4	25.2	2.9	1.3	34.0	110.8
Middle hepatic vein	20.8	26.0	2.8	1.3	32.0	110.2
Left hepatic vein	17.5	16.7	2.6	1.2	28.6	102.6
Main portal vein	23.6	30.7[b]	3.0	1.4	35.1	119.6
Right portal vein	21.5	29.0[c]	2.9	1.4	32.9	118.0
Left portal vein	19.6	25.1	2.8	1.3	30.7	113.4
Splenic vein	14.2	27.2[d]	2.4	1.3	25.1	116.8
Superior mesenteric vein	16.6	27.2[e]	2.6	1.3	27.0	118.1

Note.—EP = echoplanar imaging, Conv. = conventional time-of-flight MR angiography.

[a] Values for echoplanar and conventional MR angiography were significantly different ($p < .001$) for all vessels examined.

[b] $p < .02$.

[c] $p < .01$..

[d] $p < .0005$.

[e] $p < .001$.

images ($p < .0001$); and contrast-to-noise ratios were generally comparable, although slightly higher for the conventional images. The most pronounced differences in the contrast-to-noise ratio were noted in the splenic vein ($p < .0005$) and the superior mesenteric vein ($p < .001$), where conventional MR angiography was superior. Statistically significant differences also were present in the main portal vein ($p < .02$) and the right portal vein ($p < .01$). The contrast-to-noise ratio per unit imaging time averaged for all vessels was 49% higher for echoplanar imaging than for conventional MR angiography.

Table 2 summarizes results of the qualitative evaluation of echoplanar and conventional MR angiography. For echoplanar imaging, an average rating of 4.0 or greater was reported for the inferior vena cava; the main, right, and left portal veins; the right and middle hepatic veins; and the superior mesenteric vein (Figs. 1 and 2). With conventional MR angiography, average ratings of 4.0 or greater were reported for all of those vessels plus the anterior and posterior divisions of the right portal vein and the splenic vein. The difference in average ratings for the splenic vein (3.4 for echoplanar imaging vs 4.2 for conventional MR angiography) was statistically significant ($p < .01$; Fig. 3). Although the higher rating for visualization of the left hepatic vein with echoplanar imaging was statistically significant ($p < .05$), this vein and the medial and lateral divisions of the left portal vein were relatively poorly imaged by both techniques.

Of the three patients imaged, one had a large metastatic lesion in the dome of the liver, displacing and compressing the hepatic veins. The vascular anatomy in relation to the mass was shown to advantage by both techniques (Fig. 4), and the findings were confirmed surgically. The other two patients had focal hepatic lesions (one metastatic disease, one hemangioma), which were small and showed no appreciable effect on the hepatic vasculature on conventional or echoplanar MR angiograms.

TABLE 2: Qualitative Assessment of Vessel Visualization

Vessel	Echoplanar MR Angiography	Conventional MR Angiography
Inferior vena cava	4.2 (±0.9)	4.5 (±0.6)
Main portal vein	4.5 (±0.6)	4.5 (±0.5)
Right portal vein	4.6 (±0.6)	4.8 (±0.8)
Anterior division	3.9 (±0.9)	4.3 (±0.8)
Posterior division	3.7 (±1.1)	4.0 (±1.0)
Left portal vein	4.2 (±0.9)	4.2 (±1.0)
Medial division	2.5 (±1.3)	2.5 (±1.1)
Lateral division	2.2 (±1.1)	2.4 (±1.1)
Right hepatic vein	4.4 (±0.7)	4.5 (±0.7)
Middle hepatic vein	4.1 (±1.0)	4.0 (±1.0)
Left hepatic vein	3.6 (±1.3)	3.2 (±1.2)[a]
Splenic vein	3.4 (±0.9)	4.2 (±0.7)[b]
Superior mesenteric vein	4.0 (±1.1)	4.5 (±0.8)

Note.—Vessel visualization was rated on a scale of 1–5, where 1 = vessel not identified and 5 = vessel clearly defined. All values are mean ratings (±SD) for four observers.

[a] $p < .05$.

[b] $p < .01$.

Discussion

Angiograms of the hepatic and portal venous systems that are of diagnostic quality can be acquired by using echoplanar imaging. In our study, echoplanar images were acquired in three breath-holds of 10.5 sec each. Seven breath-holds of comparable duration were required to image the same levels with conventional time-of-flight MR angiography. When the echoplanar imaging technique was used, a single level could be imaged in 1.5 sec, as compared with 3.8 sec for conventional MR angiography. The reduced number of breath-holds significantly increases patients' comfort and tolerance of the MR examination, particularly critically ill patients. The 10.5-sec breath-hold duration was arbitrarily selected to accommodate ill or less cooperative patients. Longer or shorter breath-holds could be tailored for each patient, covering a larger or smaller number of levels, respectively.

Noise is predicted to be higher with the echoplanar imaging technique [6, 10], and this is accentuated by the use of maximal intensity projections, which maximize noise as well as vascular signal.

The higher vessel-to-liver signal-intensity ratios with echoplanar imaging, reflecting higher vascular signal, com-

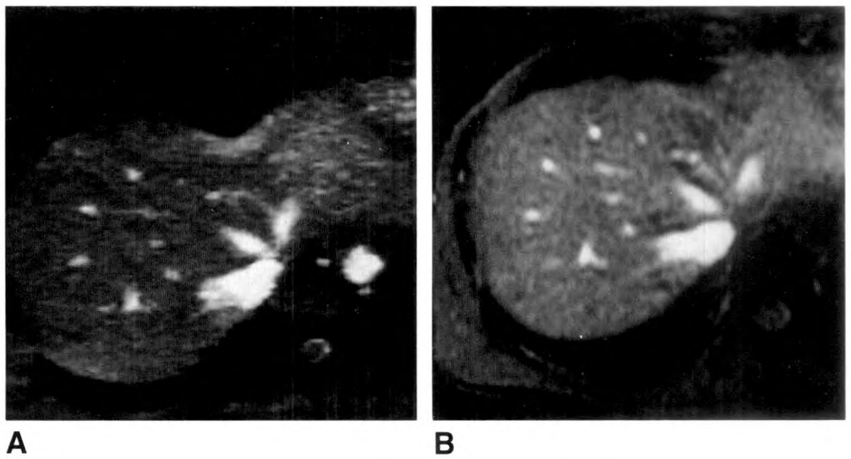

Fig. 1.—MR angiograms at level of hepatic venous confluence.

***A*, Echoplanar MR angiogram shows hepatic veins and inferior vena cava to advantage.**

***B*, Conventional MR angiogram shows similar findings.**

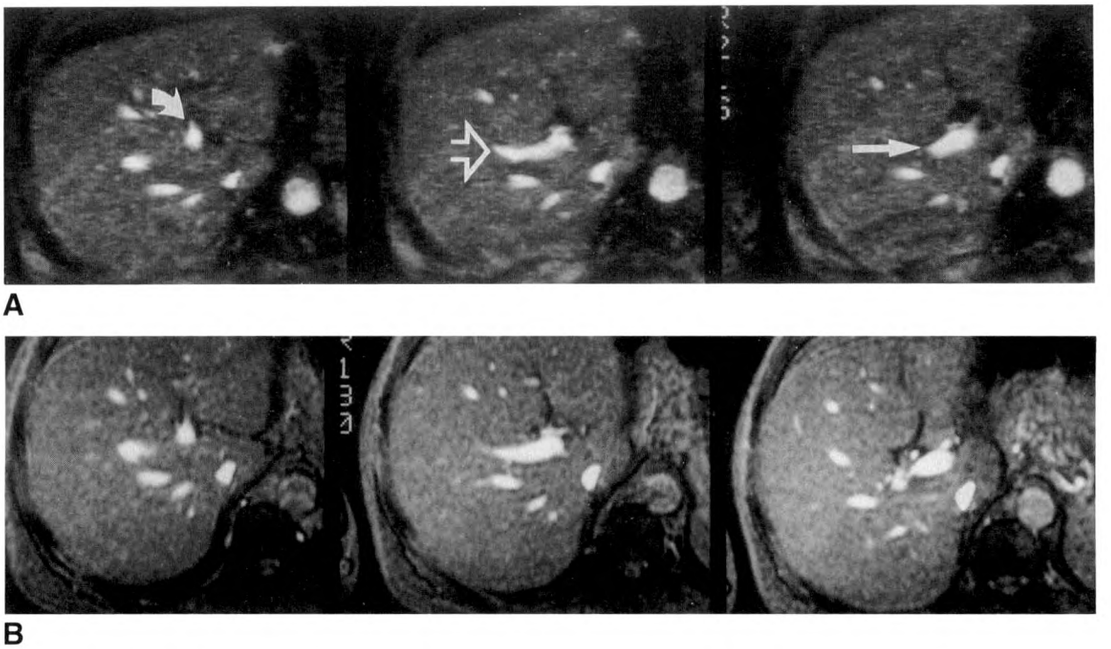

A

B

Fig. 2.—MR angiograms at level of portal vein.
A, Echoplanar MR angiograms clearly show main portal vein (*straight solid arrow*) bifurcating into right (*open arrow*) and left (*curved arrow*) portal veins.
B, Conventional MR angiograms also show vascular anatomy to advantage.

pensate for the increased noise and result in generally comparable contrast-to-noise ratios. The average vessel-to-liver contrast-to-noise ratio per unit imaging time is 49% higher for echoplanar imaging than for conventional MR angiography. Although the differences between the contrast-to-noise ratios for echoplanar and conventional MR angiograms were statistically significant in the splenic vein, superior mesenteric vein, main portal vein, and right portal vein, the vessel-to-liver contrast-to-noise ratios for echoplanar imaging were still extremely high (14.2, 16.6, 23.6, and 21.5, respectively). Of these four vessels, only the splenic vein received significantly lower qualitative ratings ($p < .01$) with echoplanar imaging. The tracking superior saturation pulse included in the echoplanar imaging sequence most likely contributed to this effect because of the slight superior-inferior orientation typical of the splenic vein.

The echoplanar imaging technique appears somewhat less sensitive to in-plane flow, resulting in poorer visualization of the right portal vein divisions and splenic vein as judged by the reviewers (Fig. 3). The parameters used were experimentally optimized for imaging through-plane flow in the main portal vein and inferior vena cava. Potential modifications to improve visualization of in-plane flow might include the use of flow compensation, thinner slices,

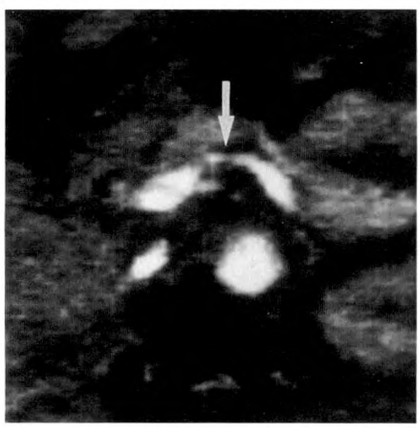

A

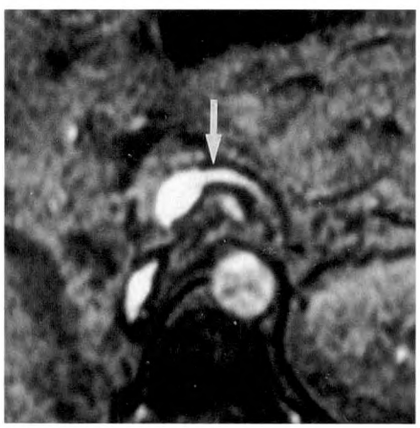

B

Fig. 3.—MR angiograms of splenic vein.
A, On echoplanar MR angiogram, splenic vein (*arrow*) is not clearly defined at its confluence with superior mesenteric vein.
B, Conventional MR angiogram shows splenic vein (*arrow*) to slightly better advantage.

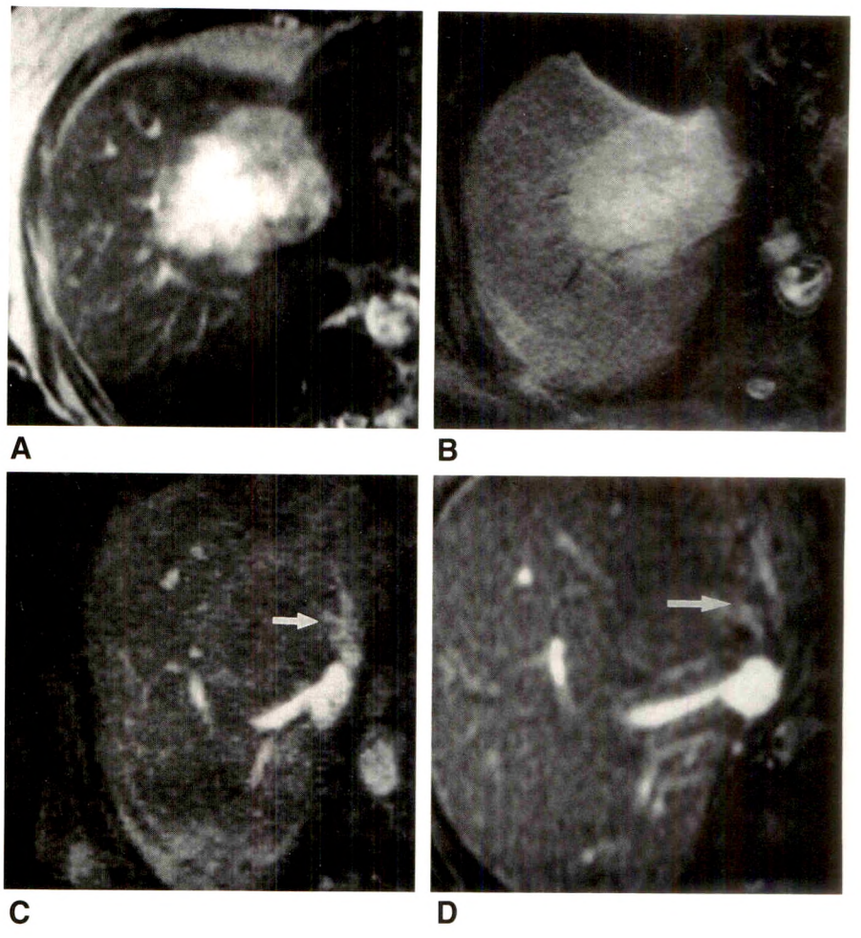

Fig. 4.—Metastatic colonic carcinoma involving dome of liver near hepatic venous confluence.

***A*, Conventional T2-weighted (3000/80) SE MR image shows metastatic lesion.**

***B*, T2-weighted (TR = infinite, TE = 25 msec) echoplanar SE MR image shows same lesion. Entire liver was imaged with 10-mm contiguous sections in a single 12-sec breath-hold. Note absence of motion-induced phase artifacts.**

***C*, Echoplanar MR angiogram shows displacement of the hepatic veins *(arrow)* by space-occupying lesion. Signal from lesion and other stationary protons is suppressed on MR angiograms.**

***D*, Conventional MR angiogram shows similar changes involving middle and left hepatic veins (*arrow*).**

decreased flip angles, or longer TRs. Further work in this area will be necessary. This report has addressed only time-of-flight echoplanar angiography. Other groups have investigated flow-velocity mapping by using phase-based echoplanar techniques [16-18], which are less dependent on through-plane flow. Phase-contrast angiography can be performed with echoplanar imaging and is the subject of an ongoing investigation.

A unique feature of echoplanar MR angiography is the temporal resolution that is achieved. Eight complete images are acquired at each anatomic level in 1.5 sec. Therefore these images typically span a complete cardiac cycle, and when combined into a maximal intensity projection, compensate for pulsatility effects. Whereas the normal portal venous system shows little pulsatility, the hepatic venous system shows transmitted cardiac pulsations [3, 19].

Hypertensive portal venous systems may have temporally altered flow patterns [20, 21] for which echoplanar MR angiography has theoretical advantages. If desired, temporal changes at a given anatomic level could be shown by displaying each image in a cine loop instead of using a maximal intensity projection.

At least two reports have suggested that time-of-flight MR angiography alone is insufficient to evaluate portal venous anatomy. Silverman et al. [1] suggested that conventional time-of-flight MR angiography is a useful adjunct but cannot be used alone because of "poor contrast with surrounding tissues, difficulty in identifying vascular margins, and flow artifacts." Using receiver-operating-characteristic analysis, Arrivé et al. [3] found no significant difference between the abilities of conventional SE and GRE MR angiography to show the patency of the portal venous system when used alone. However, they achieved a statistically significant improvement in diagnostic accuracy by combining the techniques. "Bright blood" GRE methods may show signal loss that could be mistaken for clot, caused by turbulence, streaming effects [1, 3], or slow flow [3, 22] as may occur in portal hypertension. On the other hand, "black blood" SE images may show intraluminal signal due to flow-related enhancement or motion artifact that could result in false-positive interpretations [1, 3, 23–28].

A key advantage, therefore, of echoplanar over conventional MR angiography is that it can be combined with rapidly acquired T1- and T2-weighted images. With echoplanar MR imaging, T1- or T2-weighted contiguous images of the entire liver can be obtained in a single 12-sec breath-hold. If conventional time-of-flight MR angiography must be combined with SE acquisitions to achieve satisfactory sensitivity and

specificity, the total imaging time exceeds that of echoplanar imaging by orders of magnitude (e.g., approximately 10 min vs 12 sec to acquire a T2-weighted image). Thus a major focus of the research at our institution is evaluation of the potential advantages of echoplanar imaging in the detection and characterization of hepatic masses. Echoplanar T1-weighted, T2-weighted, and angiographic images could then be combined to develop an efficient integrated liver imaging protocol.

ACKNOWLEDGMENTS

We thank Terry A. Campbell for technical assistance in performing the MR examinations.

REFERENCES

1. Silverman PM, Patt RH, Garra BS, et al. MR imaging of the portal venous system: value of gradient-echo imaging as an adjunct to spin-echo imaging. *AJR* **1991**;157:297–302
2. Edelman RR, Zhao B, Liu C, et al. MR angiography and dynamic flow evaluation of the portal venous system. *AJR* **1989**;153:755–760
3. Arrivé L, Menu Y, Dessarts I, et al. Diagnosis of abdominal venous thrombosis by means of spin-echo and gradient-echo MR imaging: analysis with receiver operating characteristic curves. *Radiology* **1991**;18:661–668
4. Finn JP, Edelman RR, Jenkins RL, et al. Liver transplantation: MR angiography with surgical validation. *Radiology* **1991**;179:265–269
5. Zirinsky K, Markisz JA, Rubenstein WA, et al. MR imaging of portal venous thrombosis: correlation with CT and sonography. *AJR* **1988**;150:283–288
6. Crawley AM, Cohen MS, Yucel EK, Poncelet B, Brady TJ. Single-shot magnetic resonance imaging: applications to angiography. *Cardiovasc Intervent Radiol* **1992**;15:32–42
7. Edelman RR, Mattle HP, Atkinson DJ, Hoogewoud HM. MR angiography. *AJR* **1990**;154:937–946
8. Edelman RR, Wentz KU, Mattle H, et al. Projection arteriography and venography: initial clinical results with MR. *Radiology* **1989**;172:351–357
9. Winkler ML, Ortendahl DA, Mills TC, et al. Characteristics of partial flip angle and gradient reversal MR imaging. *Radiology* **1988**;166:17–26
10. Cohen MS, Weisskoff RM. Ultra-fast imaging. *Magn Reson Imaging* **1991**;9:1–37
11. Rzedzian RR, Pykett IL. Instant images of the human heart using a new, whole-body MR imaging system. *AJR* **1987**;149:245–250
12. Pykett IL, Rzedzian RR. Instant images of the body by magnetic resonance. *Magn Reson Med* **1987**;5:563–571
13. Laub GA, Kaiser WA. MR angiography with gradient motion rephasing. *J Comput Assist Tomogr* **1988**;12:377–382
14. Weiskoff RM, Crawley AM, Wedeen VJ. Flow sensitivity and flow compensation in instant imaging (abstr). In: *Book of abstracts: Society of Magnetic Resonance in Medicine 1990*, vol. 1. Berkeley, CA: Society of Magnetic Resonance in Medicine, **1990**:398
15. Mitchell DG, Vinitski S, Burk DL, Levy DW, Rifkin MD. Motion artifact reduction in MR imaging of the abdomen: gradient moment nulling versus respiratory-sorted phase encoding. *Radiology* **1988**;169:155–160
16. Firmin D, Klipstein R, Hounsfield G, Paley M, Longmore D. Echo planar high resolution flow velocity mapping. *Magn Reson Med* **1989**;12:316–327
17. Feinberg D, Jakab P. Tissue perfusion in humans studied by Fourier velocity distribution, line scan, and echo planar imaging. *Magn Reson Med* **1990**;16:280–293
18. Poncelet B, Wedeen VJ, Mikulis D, McKinistry RC, Brady TJ. Visualization of brain motion with echo planar imaging phase mapping (abstr). *J Magn Reson Imaging* **1991**;1:149–150
19. Strandness DE, Sumner DS. Venous hemodynamics and control of venous capacity. In: *Hemodynamics for surgeons*. New York: Grune & Stratton, **1975**:120–160
20. Williams DM, Cho KJ, Aisen AM, Eckhauser FE. Portal hypertension evaluated by MR imaging. *Radiology* **1985**;157:703–706
21. Ralls PW. Color Doppler sonography of the hepatic artery and portal venous system. *AJR* **1990**;155:517–525
22. Atlas SW, Mark AS, Fram EK, Grossman RI. Vascular intracranial lesions: applications of gradient-echo MR imaging. *Radiology* **1988**;169:455–461
23. Waluch V, Bradley WG. NMR even echo rephasing in slow laminar flow. *J Comput Assist Tomogr* **1984**;8:594–598
24. Axel L. Blood flow effects in magnetic resonance imaging. *AJR* **1984**;143:1157–1166
25. Bradley WG, Waluch V. Blood flow: magnetic resonance imaging. *Radiology* **1985**;154:443–450
26. Ehman RL, McNamara MT, Brasch RC, Felmlee JP, Gray JE, Higgins CB. Influence of physiologic motion on the appearance of MR images. *Radiology* **1986**;159:777–782
27. Bradley WG. Flow phenomena in MR imaging. *AJR* **1988**;150:983–994
28. Bradley WG, Waluch V, Lai KS, Fernandez EJ, Spalter C. The appearance of rapidly flowing blood on magnetic resonance images. *AJR* **1984**;143:1167–1174

Recurrent Bleeding After Variceal Hemorrhage: Predictive Value of Portal Venous Duplex Sonography

A. Schmassmann[1,2]
M. Zuber[3]
M. Livers[4]
K. Jäger[5]
H. R. Jenzer[3]
H. F. Fehr[1]

OBJECTIVE. Risk assessment of recurrent variceal bleeding is essential for therapeutic decisions and is usually performed by endoscopy of the upper gastrointestinal tract. We studied the value of portal venous duplex sonography in predicting subsequent variceal bleeding in patients with cirrhosis.

SUBJECTS AND METHODS. Thirty patients with cirrhosis who received sclerotherapy because of acute variceal hemorrhage for the first time (hemorrhage group), 30 patients with cirrhosis who had no previous hemorrhage (nonhemorrhage group), and 30 control subjects were examined prospectively. With the use of portal duplex and color Doppler sonography, flow direction, flow velocity, vein diameter, and response to respiration of portal vein vessels were measured and portosystemic collaterals and thrombosis of portal vessels were visualized. The results of these measurements and imaging findings were combined into a Doppler sonoscore. At entry into the study, all patients were classified on the basis of a sonoscore as having a low (sonoscore, <4) or a high (sonoscore, ≥4) risk for subsequent hemorrhage. During a mean follow-up period of 2 years (range, 15–36 months), the predictive value of this Doppler sonoscore was studied.

RESULTS. In the hemorrhage group, the prevalence of recurrent hemorrhage was 40%, despite sclerotherapy, and the mortality rate was 60%. In patients with a Doppler sonoscore of 4 or more, the prevalence of recurrent hemorrhage was 67%, whereas in patients with a score less than 4, the prevalence was only 22% ($p < .02$). After sclerotherapy, endoscopic criteria showed no significant correlation with the prevalence of bleeding. In the nonhemorrhage group, the prevalence of variceal hemorrhage occurring was 13%, and Doppler sonographic criteria showed no significant correlation with the prevalence of subsequent hemorrhage.

CONCLUSION. We conclude that Doppler sonography, performed after the first occurrence of variceal hemorrhage, provides useful prognostic information regarding the risk of recurrent hemorrhage. If these results are confirmed, Doppler sonography may be used to select the best method of treatment.

***AJR* 1993;160:41–47**

Received April 24, 1992; accepted after revision July 7, 1992.

Presented in part at the Congress of SGHG, Basel, Switzerland, September 1991.

[1]Department of Gastroenterology, Kantonsspital Aarau, 5001 Aarau, Switzerland.

[2]Present address: Gastrointestinal Unit, Inselspital, University Hospital Bern, 3010 Bern, Switzerland. Address reprint requests to A. Schmassmann.

[3]Department of Cardiology, Kantonsspital Aarau, 5001 Aarau, Switzerland.

[4]Department of Radiology, Kantonsspital Aarau, 5001 Aarau, Switzerland.

[5]Department of Angiology, Kantonsspital Basel, Petersgraben 4, 4031 Basel, Switzerland.

0361–803X/93/1601–0041

Hemorrhage from esophageal varices is the major life-threatening consequence of chronic liver disease. Among patients admitted because of an initial variceal hemorrhage, about 40% will have recurrent hemorrhages and about two thirds will die within 1 year after the first hemorrhagic episode [1]. To estimate the risk of variceal hemorrhage, varix size and color, assessed by endoscopy, has shown a good correlation with the risk of subsequent variceal hemorrhage [2–4]. In contrast, portal vein pressure does not show a close correlation with the risk of variceal hemorrhage [5]. Repeated sclerotherapy is the most widely used treatment for variceal hemorrhage, and most studies show a reduction in recurrent bleeding after sclerotherapy and at least comparable results with shunt surgery [6, 7]. Eradication of esophageal varices by endoscopic sclerotherapy, however, eliminates most of the endoscopic prognostic features, and after sclerotherapy a reliable risk assessment of recurrent hemorrhage is difficult. A proper risk assessment in these patients, however, is essential as they are not likely to sur-

vive another severe hemorrhagic episode. Surgical or transcatheter shunt placement or liver transplantation should be considered before hemorrhage recurs.

Duplex and color Doppler sonographic studies allow noninvasive visualization of the portal venous system [8–11]. Flow direction, flow velocity, vein diameter, and response to respiration of portal vein vessels can be measured, and portosystemic collaterals and thrombosis of portal vessels can be visualized. However, the prognostic significance of these parameters is unknown. The goal of this study was to assess the value of portal venous duplex sonography in predicting subsequent variceal hemorrhage in a group of patients undergoing initial treatment with sclerotherapy and in a group of patients with cirrhosis who had no previous hemorrhage.

Subjects and Methods

Selection of Patients for Variceal Hemorrhage Group

From January 1989 to December 1990, all patients admitted to the Department of Gastroenterology, Kantonsspital Aarau, because of upper gastrointestinal tract hemorrhage who required blood transfusion were eligible for this study if they met all 10 entry criteria: (1) emergency endoscopy showed esophageal varices; (2) varices were considered the most likely source of the hemorrhage; (3) the patient had no known previous hemorrhage from varices; (4) the patient had not previously been treated for esophageal varices (sclerotherapy, shunt surgery, β-blockers); (5) the patient had biopsy-proved liver cirrhosis, or in case of severe coagulopathy, clinical, biochemical, and sonographic signs and symptoms suggestive of liver cirrhosis; (6) the patient had no other disease (e.g., hepatocellular carcinoma) that reduced life expectancy to less than 1 year; (7) the patient agreed to participate in the study; (8) the patient had not been included in an earlier stage of the study; (9) the patient survived the first 2 weeks after hemorrhage and was not comatose 2 weeks after hemorrhage; and (10) it was possible to perform Doppler sonography.

Forty-two consecutive patients had had an initial significant variceal hemorrhage and fulfilled the first five entry criteria. Twelve of these were excluded: two patients had hepatocellular carcinoma, two refused to participate, and eight died within 2 weeks or had severe liver failure with coma 2 weeks after the initial hemorrhage. The remaining 30 patients met all 10 criteria and made up the hemorrhage group. Liver cirrhosis was proved by liver biopsy in 25 patients. In the remaining five, biopsy was contraindicated because of coagulopathy. However, these five had clear-cut clinical, biochemical, and sonographic signs and symptoms of cirrhosis. The patients received sclerotherapy (1% of intravariceal polidocanol, 10–40 ml per treatment session) every week until the esophageal varices disappeared. Endoscopy was performed at 3-month intervals. If varices were found, they were treated again.

Selection of Subjects for Nonhemorrhage and Control Group

From January 1989 to December 1990, all patients admitted to the Department of Gastroenterology, Kantonsspital Aarau, for liver biopsy were eligible for the study if they met all five entry criteria: (1) biopsy showed liver cirrhosis; (2) the patient had no known previous hemorrhage from varices and had not previously been treated for esophageal varices (sclerotherapy, shunt surgery, β-blockers); (3) the patient had no other disease (e.g., hepatocellular carcinoma) that reduced life expectancy to less than 1 year; (4) the patients agreed to participate in the study; and (5) it was possible to perform Doppler sonography. Thirty-five patients fulfilled the first three entry criteria; however, five refused to participate. The remaining 30 patients met all five criteria and made up the nonhemorrhage group.

Thirty age- and sex-matched volunteers without any liver disease made up the control group.

Initial Investigations

Endoscopic examination of the upper gastrointestinal tract was performed in all patients with liver cirrhosis. Esophageal varices were assessed according to the endoscopic criteria proposed by the Japanese Research Society for Portal Hypertension [2]. Variceal size (F1–F3) and the presence of red signs (presence of red wale markings, cherry red or hematocystic spots) were recorded and Beppu's score was calculated [2]. Upon entry into the study, all patients in both groups were classified as being at low (≥0) or high (<0) risk for subsequent hemorrhage according to this endoscopic score. All patients in the hemorrhage group had emergency endoscopy within 12 hr after hospitalization. All results were based on the findings of the first endoscopic examination and were not changed, even if additional information was provided by subsequent examinations.

At the beginning of the study, the following information was recorded for all patients with liver cirrhosis: average daily consumption of alcoholic beverages; degree of encephalopathy and ascites; number of platelets; prothrombin time; serum concentrations of bilirubin, albumin, aspartate aminotransferase, alkaline phosphatase, albumin, and creatinine; and levels of serologic markers (antibodies to hepatitis B and C, mitochondria, and DNA). Patients were classified according to the Child-Turcotte classification as modified by Pugh et al. [12]. Both continuous-scale (from 5 to 15) and ordinal-scale (grading: A = 5–6, B = 7–9, C = 10–15) scores were used.

Duplex and Color Doppler Sonography

In all three groups, the subjects fasted overnight, and Doppler sonography was performed while they were supine. Real-time sonographic equipment with a 3.75-MHz sector-array transducer with pulsed duplex and color Doppler capability (Toshiba SSH-160) was used. With this system, vessels were first detected by using real-time sonography and longitudinal scans; the sample volume was then positioned in the center of the vessel itself, and the gate was adjusted from 5 to 10 mm to obtain optimal Doppler waveforms. The Doppler waveforms were obtained in the portal vein at about the midpoint between the confluence of the splenic vein and superior mesenteric vein and the portal bifurcation; in the ascending part of the splenic vein in front of the tail of the pancreas; and in the superior mesenteric vein at a distance of about 2 cm from the confluence with the splenic vein. The patients intermittently held their breath for 5 sec during gentle inspiration while the waveforms were recorded. Maximal velocity was measured. No correction was performed to calculate the mean velocity. If portal or splenic vein thrombosis was present, velocity measurements were excluded. The Doppler waveforms were also recorded after deep inspiration and during expiration, to determine the response of the vein diameter (D) to respiration ([100 × D at inspiration/D at expiration] − 100 in %). The following variables were evaluated by two observers: velocity; diameter; response to respiration; and patency of the portal vein, splenic vein, and superior mesenteric vein; the presence and number of portosystemic collaterals; and the maximal longitudinal diameter of the spleen. The flow measurements were made at the smallest possible angle to minimize the error caused by large Doppler angles. This angle was always less than 60°. For measurement of velocity in the superior mesenteric vein, the Doppler angle was more than 60° in many patients; thus, we excluded these results from analysis.

The diameter of the vessels was measured at the same location as the Doppler waveforms. The left gastric (coronary) vein, and gastroesophageal, gastrorenal, splenorenal, and paraumbilical collaterals were visualized, if present [13]. The left gastric vein was considered abnormal if the diameter was 5 mm or more and the flow was hepatofugal. Gastroesophageal varices were considered to be present if a continuous low-velocity flow in the region of the gastroesophageal junction was found [14]. The presence or absence of complete or partial portal/splenic vein thrombosis (cutoff or sudden amputation of the portal vein branches inside the hepatic parenchyma) was carefully assessed [15, 16]. Visualization of collaterals and venous thrombosis was clearly facilitated by the use of color sonography. At the beginning of the study, various sonographic and Doppler parameters were combined into a Doppler sonoscore to assess the risk of subsequent hemorrhage (Table 1). According to this Doppler sonoscore, all patients were divided at the time of study entry into low-risk (sonoscore, <4) and high-risk (sonoscore, ≥4) subgroups. The sonographers and the patients were not aware of the subclassification into low- or high-risk groups.

Before the study began, we tried to minimize interobserver variation. The two observers met several times until a satisfactory degree of agreement in the interpretation was reached. The reproducibility of the individual measurements was assessed. The coefficient of variations for maximal velocity in the portal vein of the same person within 3 days was less than 10%.

Follow-up and Statistical Analysis

All 60 patients were part of a follow-up study (range, 15–36 months; mean, 2 years). Patients in the hemorrhage group had endoscopy every 3 months. Patients in the nonhemorrhage group had clinical follow-up examinations every 6 months. At each episode of hemorrhage, we recorded the date of the start of hemorrhage and the most likely source. Variceal hemorrhage or death were regarded as end points. The patients were followed up until March 1992. The patients did not have any surgical or transcatheter procedures related to the liver disease and did not receive β-blockers.

Patients with liver cirrhosis in both groups were classified upon entry in the study into two subgroups according to their Doppler sonoscore (low-risk subgroup, <4, vs high-risk subgroup, ≥4), the velocity in the portal vein (≥10 cm/sec vs <10 cm/sec), the diameter of the portal vein (<13 vs ≥13 mm), the endoscopic score (≥0 vs <0), and the Child classification (Child A vs Child B or C). The prognostic parameters were compared by univariate analysis (log rank test).

Results are given as mean ± standard deviation and were considered significant at $p < .05$. Groups were compared with Student's unpaired t-test or χ^2-test.

TABLE 1: Doppler Sonoscores for the Risk Assessment of Variceal Hemorrhage in a Patient with Liver Cirrhosis

Parameter	No. of Points
Maximal velocity[a]	
Velocity: 5–10 cm/sec in portal vein or < 5 cm/sec in splenic vein	1
Velocity: 1–4.9 cm/sec in portal vein	2
Reversed (hepatofugal) flow in portal vein	0
Maximal diameter of portal vein	
≥13 mm	1
≥17 mm	2
Response to respiration	
<40% and diameter ≥6 mm in superior mesenteric vein	1
Spleen size	
Maximal longitudinal diameter ≥15 cm	1
Left gastric vein	
Left gastric vein ≥5 mm and hepatofugal flow	1
Gastroesophageal collaterals	
Present	1
Vein thrombosis	
Partial, intrahepatic vein thrombosis	1
Portal or splenic vein thrombosis[a]	2

Note.—The maximal score is 9. A score of 4 or more indicates high risk for variceal bleeding.

[a] Patients with portal or splenic vein thrombosis received two points for thrombosis, but zero points for velocity in the portal vein.

Results

The characteristics of the patients in the hemorrhage and nonhemorrhage groups are summarized in Table 2. We found no significant difference between the groups as regards age, sex, or cause of liver cirrhosis. The percentage of patients with liver cirrhosis caused by alcohol was 63% in the hemorrhage group and 60% in the nonhemorrhage group. Patients with the first variceal hemorrhage (hemorrhage group) had a higher Child classification than patients with newly diagnosed liver cirrhosis (nonhemorrhage group). The percentage of grade 3 varices and the percentage of red color signs were higher, and accordingly, the endoscopic scores of Beppu et al. [2] were lower in the hemorrhage group.

Doppler sonographic findings in cirrhotic patients in the hemorrhage, nonhemorrhage, and control groups at entry

TABLE 2: Characteristics of Patients in the Hemorrhage and Nonhemorrhage Groups

Characteristic	Hemorrhage Group ($n = 30$)	Nonhemorrhage Group ($n = 30$)
Age (mean ± SD)	62 ± 10	58 ± 13
Male (%)	67	70
Female (%)	33	30
Cirrhosis verified by biopsy (%)	84	100
Cause of liver cirrhosis (%)		
Alcohol	63	60
Hepatitis B or C	27	23
Primary biliary cirrhosis	7	7
Cryptogenic cirrhosis	3	10
Child classification (%)		
A	50	80
B	17	20
C	33	0
Ascites (%)		
Moderate	40	10
Severe	13	0
Encephalopathy (%)		
Precoma	50	0
Coma	10	0
Grade of varices (%)		
Grade 3 varices	90	30
Red color signs	53	15
Endoscopic score (mean ± SD)	−0.24 ± 0.42	0.89 ± 0.59

Note.—For patients with cirrhosis caused by alcohol, the average daily alcohol consumption was >60 ml absolute alcohol, and they had no other risk factors for cirrhosis. Endoscopic scores were according to Beppu et al. [2].

TABLE 3: Doppler Sonographic Findings at Study Entry in Cirrhotic Patients in the Hemorrhage Group and the Nonhemorrhage Group and in Control Subjects

Characteristic	Hemorrhage Group ($n = 30$) (Mean ± SD)	Nonhemorrhage Group ($n = 30$) (Mean ± SD)	Control Subjects ($n = 30$) (Mean ± SD)	Hemorrhage vs Nonhemorrhage Group (p Value)[a]
Portal vein				
Velocity (cm/sec)[b]	14.2 ± 7	18.1 ± 5	27.2 ± 6	<.05
Diameter (mm)	14.6 ± 5.0	12.7 ± 1.7	9.2 ± 1.5	NS
Splenic vein				
Velocity (cm/sec)	13.9 ± 5.5	14.6 ± 6.5	19.9 ± 4.6	NS
Diameter (mm)	10.1 ± 2.8	7.5 ± 1.6	4.6 ± 1.7	<.01
Response to respiration[c] in superior mesenteric vein	13 ± 7	18 ±12	89 ± 34	NS
Spleen size (cm)	14.9 ± 3.2	13.0 ± 2.4	10.3 ± 1.1	NS
Portosystemic collaterals (%)[d]				
To inferior vena cava	50	30	0	NS
Gastroesophageal varices	90	33	0	<.001
Left gastric vein ≥ 5 mm and hepatofugal flow	43	15	0	<.05
Partial vein thrombosis (%)	10	3	0	NS
Total vein thrombosis (%)	7	3	0	NS
Mean Doppler sonoscore[e]	3.8 ± 1.6	1.8 ± 0.8	0	<.0001
Doppler sonoscore ≥4(%)	40	7	0	<.01

Note.—NS = not significant.

[a]Results in control subjects were highly significant ($p < .001$) vs hemorrhage and nonhemorrhage groups in all parameters (exception: vein thrombosis).

[b]Maximal velocity was measured; no correction was performed to calculate mean velocity.

[c]Response to respiration = (D at inspiration × 100/D at expiration) − 100; D = diameter.

[d]Collaterals to inferior vena cava: splenorenal, gastrorenal, and paraumbilical veins.

[e]Doppler sonoscore for the risk assessment of variceal bleeding according to Table 1.

into the study are summarized in Table 3. The Doppler sonoscore was more than zero in 95% of cirrhotic patients and was zero in all control subjects. Flow velocity in the portal and splenic veins was clearly lower in patients with cirrhosis than in control subjects ($p < .0001$). The diameters of the portal, splenic, and superior mesenteric veins were enlarged in cirrhotic patients compared with control subjects ($p < .0001$). In addition, the effect of respiration on the diameter of the superior mesenteric vein was decreased in patients with cirrhosis. Portosystemic collaterals and venous thrombosis were found in cirrhotic patients only.

Flow velocity in the portal vein was significantly decreased and the diameter of the splenic vein was significantly increased in the hemorrhage group as compared with the nonhemorrhage group. In addition, the left gastric vein and gastroesophageal collaterals could be visualized more often in the hemorrhage group than in the nonhemorrhage group. The mean Doppler sonoscore was clearly higher in the hemorrhage group.

During the mean follow-up period of 2 years, 12 patients in the hemorrhage group had recurrent hemorrhage (prevalence, 40%) and 18 patients died (mortality rate, 60%). Hemorrhage recurred because of varices in the distal esophagus or at the gastroesophageal junction in 10 patients and from gastric varices in two patients. To assess the predictive value of the Doppler sonoscore, patients had been categorized upon entry in the study into low- (<4) or high- (≥4) risk subgroups. The cumulative percentage of patients in the hemorrhage group without recurrent hemorrhage in relation to the Doppler sonoscores during the follow-up period is shown in Figure 1. In patients with a Doppler sonoscore of 4 or more, the prevalence of recurrent hemorrhage was 67% despite intensive sclerotherapy; in patients with a Doppler sonoscore less than 4, the prevalence was only 22% ($p < .02$, log rank test). If we consider only patients in the hemorrhage group with a sonoscore of 4 or more and if we exclude patients who did not survive 2 years, eight (89%) of nine patients had recurrent hemorrhage.

In contrast, single Doppler sonographic parameters did not show significant predictive results. Patients were subdivided at entry into the study according to the velocity in the portal vein, with a threshold of 10 cm/sec. In the hemorrhage group, bleeding recurred in 56% if the velocity was less than 10 cm/sec; it recurred in 33% if the velocity was 10 cm/sec or greater. The difference was not significant. Similar analyses have been performed with the diameter of the portal vein by using a threshold of 13 mm, but again no significant predictive results were found.

In contrast to the Doppler sonoscore, endoscopic parameters such as form of varices, the presence of red color signs, and the number of treatment sessions needed to eradicate esophageal varices had no significant predictive results according to the log rank test. No significant difference in the prevalence of recurrent hemorrhage was noted between patients in Child class A or in Child class B or C. However, the mortality rate was significantly higher ($p < .01$, log rank test) in patients classified in Child B or C (78%) than in patients classified in Child A (22%).

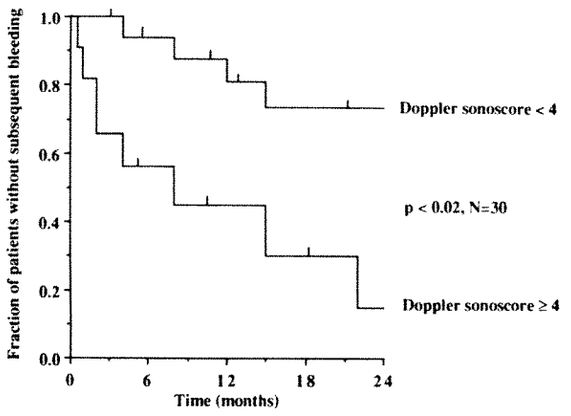

Fig. 1.—Cumulative percentage of patients without subsequent bleeding in relation to Doppler sonoscores (Table 1) during a follow-up period of 24 months. The Doppler sonoscore was assessed at study entry in patients with liver cirrhosis and first variceal hemorrhage. In patients with a Doppler sonoscore of 4 or more (n = 12), the prevalence of recurrent hemorrhage was 67%; in patients with a score less than 4 (n = 18), it was only 22% (p < .02, log rank test). Vertical bars represent patients who died during the follow-up period without recurrent hemorrhage.

In addition to the log rank test, which is the appropriate test to assess the predictive value of the parameters, we used another statistical approach that avoids the problem of determining a threshold value upon entry into the study but that still provides information about the significance of the various parameters. In the original hemorrhage group, we used unpaired t-tests to compare Doppler sonographic, endoscopic, and clinical parameters between patients who had recurrent hemorrhage and patients who did not (Table 4). Again, the mean Doppler sonoscore was significantly (p < .05) higher in patients who had recurrent hemorrhage than in those who did not. The velocity in the portal vein was lower in the patients who had recurrent hemorrhage than in those who did not; however, the difference was not significant. The diameter of the portal vein and visualization of the left gastric vein or gastroesophageal collaterals tended to be increased in patients who had recurrent hemorrhage; however, the differences were not significant.

TABLE 4: Doppler Sonographic, Endoscopic, and Clinical Findings in the Hemorrhage Group at Study Entry in Relation to the Presence of Rehemorrhage During the Follow-up Period

Variable	No Rehemorrhage (n = 18) (mean ± SD)	Rehemorrhage (n = 12) (mean ± SD)	p Value
Doppler sonoscore	3.3 ± 1.5	5.0 ± 1.6	<.05
Velocity (cm/sec) in portal vein	17.2 ± 11	9.5 ± 9	NS
Diameter (mm) in portal vein	13.2 ± 3.9	16.3 ± 6.2	NS
Left gastic vein, ≥5 mm (%)	22	50	NS
Gastroesophageal collaterals (%)	83	100	NS
Endoscopic score	−0.2 ± 0.4	−0.3 ± 0.2	NS
Child classification	8.1 ± 2.3	8.9 ± 1.6	NS

Note.—Endoscopic scores were according to Beppu et al. [2]. Child classification is given as continuous-scale score [12]. NS = not significant.

In the hemorrhage group, endoscopic scores and the Child classification did not show any significant differences with either statistical test, neither with the log rank test nor with the unpaired t-test, between those who had recurrent hemorrhage and those who did not (Table 4). Other endoscopically derived parameters, such as endoscopic score 1 week after the first hemorrhage or the number of treatment sessions needed to eradicate the varices, were also not significantly correlated to the prevalence of recurrent hemorrhage.

In the nonhemorrhage group, four patients (13%) had variceal hemorrhage and six patients (mortality rate, 20%) died during follow-up. The Doppler sonoscores had no significant predictive value in determining variceal hemorrhage. In contrast, the endoscopic score showed a significant (p < .05, log rank test) predictive result despite the rather low prevalence of hemorrhage.

Discussion

For physicians who treat patients with hemorrhage from esophageal varices, risk assessment of recurrent hemorrhage and optimal timing of liver transplantation or shunt placement are essential. Our results suggest that Doppler sonography of the portal vein system can be used to predict recurrent hemorrhage after an initial variceal hemorrhage in patients who survive at least 2 weeks. In patients with a Doppler sonoscore of 4 or more, the prevalence of recurrent hemorrhage was 67% despite intensive sclerotherapy; in patients with a Doppler sonoscore less than 4, the prevalence was only 22%. Thus, it may be possible to use Doppler sonography to determine which patients are likely to have recurrent hemorrhage. However, because of the limited number of patients per group, further studies with larger numbers of patients are necessary. If these results are confirmed, Doppler sonography may be used to select the best treatment method after the first variceal hemorrhage.

Our results are supported by other studies that showed a significant correlation between Doppler sonographic findings and the size of esophageal varices [14, 15, 17]. However, to our knowledge, this is the first prospective study showing that Doppler sonography can be used to predict the risk of recurrent hemorrhage in patients after sclerotherapy of the first variceal hemorrhage. In contrast to measurements of the portohepatic gradient, Doppler sonography allows noninvasive assessment of multiple factors significantly correlated with esophageal varices, portal hypertension, and prevalence of recurrent hemorrhage [5, 15]. In this study, endoscopic and clinical criteria could not be used to predict the risk of recurrent hemorrhage in patients who had sclerotherapy. In this respect, the noninvasive Doppler study may be superior to invasive measurement of the portohepatic gradient and may be as good as angiography [5, 15, 17–19].

In the nonhemorrhage group of patients who had newly diagnosed liver cirrhosis, the prevalence of subsequent hemorrhage was only 13%, and Doppler sonographic parameters showed no significant correlation with prevalence. The lack of significance can be explained either by a statistical type II error caused by the low prevalence or by the inability with Doppler sonography to distinguish between submucosal esophageal varices, which represent a potential

bleeding site, and paraesophageal veins, which do not bleed and are invisible on endoscopy [13, 14].

To assess the individual importance of Doppler sonographic parameters, we compared control, nonhemorrhage, and hemorrhage groups, and subgroups of the hemorrhage group with and without subsequent recurrent hemorrhage. If we consider all sonographic, endoscopic, and clinical parameters, the differences between control subjects and patients with liver cirrhosis were high; the differences between the nonhemorrhage group and the hemorrhage group were medium; and the differences between the subgroups of the hemorrhage group with and without recurrent hemorrhage were rather small and only significant for one parameter, the Doppler sonoscore.

If only one Doppler sonographic parameter, such as vein diameter or velocity, is considered, considerable overlapping was observed between cirrhotic patients and control subjects and between the hemorrhage and nonhemorrhage groups. To improve the sensitivity, specificity, and predictive values of Doppler sonographic parameters, we combined these parameters and created a new Doppler sonoscore for the risk assessment of variceal hemorrhage. Before the study began, we decided to classify patients as being either at low (<4) or high (≥4) risk for subsequent hemorrhages. Similar approaches have been tried by others. Moriyasu et al. [20] proposed a congestion index (area/velocity) and found significant differences between patients with cirrhosis and control subjects [20]. Medhat et al. [15] developed a sonoscore based on real-time sonography and found a significant correlation with esophageal varices and bleeding prevalence. However, as these scores did not combine all available information, we tried to improve this score. We combined all available Doppler and sonographic variables associated with variceal hemorrhage and also included some signs related to portal hypertension (Table 1). Increased diameter of the portal vein, decreased response to respiration in the superior mesenteric vein, intrahepatic partial vein thrombosis, and increased size of the spleen are associated with portal hypertension, but are not clearly correlated with the prevalence of hemorrhage [17, 21]. In most patients, only some of these signs were present, and the patients usually had a score of 1–3 and were classified into the low-risk group. In contrast, clearly decreased velocity in the portal vein, an enlarged left gastric vein with hepatofugal flow, and the presence of gastroesophageal collaterals are clearly associated with esophageal hemorrhage [13, 14, 17, 19]. If one or two of these signs were present in addition to the portal hypertension signs, the patients usually had a score between 4 and 6 and were classified into the high-risk group. Collaterals to the lower vena cava, such as gastrorenal, splenorenal, and paraumbilical collaterals, were disregarded, since they are not associated with the risk of variceal hemorrhage and may even be protective as the blood is shunted away from the gastroesophageal varices [13, 17, 22, 23]. Reversed (hepatofugal) flow in the portal vein, if associated with reversed flow in the superior mesenteric or splenic veins and hepatopetal flow in the left gastric vein, also may be protective, since the blood may be shunted through collaterals to the inferior vena cava [24]. Thus, we heavily weighted the Doppler and sonographic signs correlated with esophageal hemorrhage, slightly weighted signs correlated with portal hypertension, and disregarded protective signs. Further Doppler sonographic signs, such as increase in splenic and superior mesenteric artery blood flow; increase in the resistive index (>0.78) of hepatic artery flow; increase in superior mesenteric, splenic, and portal venous flow; and loss of triphasic flow pattern in the hepatic veins were not included. Because the relative importance of the various variables is unknown, the score system had to be developed arbitrarily. The use of combined criteria, however, showed clear advantages over the use of a single variable. Because the pitfalls, sources of errors, and observer variability in Doppler sonography of the portal system are significant [25–27], we examined patients only in one medical center, and Doppler sonography was performed only by two very experienced operators.

Endoscopic variables have been shown to be a useful tool for determining the risk of the first variceal hemorrhage [2, 3]. This was demonstrated in the nonhemorrhage group despite a rather low prevalence of hemorrhage. These data are in agreement with previous studies that showed a high predictive value for endoscopic findings, especially the red color signs [2, 3]. However, in this study, endoscopy did not show clear prognostic signs for estimating the risk of recurrent hemorrhage in patients treated with sclerotherapy. The lack of significance, however, does not exclude a statistical type II error, especially if we consider that the number of patients per group was only 30. Nevertheless, there are many other reasons for the lack of significance. Endoscopy was performed on an emergency basis within 12 hr after the initial hemorrhage. In this situation, visualization is limited, treatment is urgent, and varices may not be completely distended because of hypovolemia. Thus, in some patients, possibly those with severe hemorrhage, endoscopic findings may have been underestimated because the varices were not dilated or red color signs were obscured by blood. At the second endoscopic examination, scoring of the varices was even more difficult than at the first examination, as many varices were already thrombosed and partially ulcerated. Sclerotherapy obscures many of the endoscopic prognostic features that indicate recurrent bleeding is likely, and after sclerotherapy, a reliable assessment of the risk of recurrent hemorrhage is difficult. Although the Child classifications were clearly correlated with survival time in the hemorrhage group, as reported by other authors [4, 28], this was not found for any of the Doppler sonographic or endoscopic variables.

In conclusion, Doppler sonography of the portal venous system can be used to predict recurrent hemorrhage in patients who have had an initial occurrence of variceal hemorrhage. This risk assessment, however, is far from perfect. In our opinion, Doppler sonography is a useful noninvasive procedure, best performed after the first variceal hemorrhage. In contrast, in patients without previous variceal hemorrhage, most data suggest that endoscopy is superior to Doppler sonography for predicting the risk of variceal hemorrhage. Further prospective studies, performed in larger groups of patients, may determine more precisely the predictive value of individual parameters of Doppler sonography.

REFERENCES

1. Graham DY, Smith JL. The course of patients after variceal hemorrhage. *Gastroenterology* **1981**;80:800–809
2. Beppu K, Inokuchi K, Koyanagi N, et al. Prediction of variceal hemorrhage by esophageal endoscopy. *Gastrointestinal Endosc* **1981**;27:213–218
3. North Italian Endoscopic Club for the Study and Treatment of Esophageal Varices. Prediction of the first variceal hemorrhage in patients with cirrhosis of the liver and esophageal varices. *N Engl J Med* **1988**;319: 983-989
4. Terblanche J, Burroughs AK, Hobbs KEF. Controversies in the management of bleeding esophageal varices. *N Engl J Med* **1989**;320:1393–1398, 1469–1475
5. Lebrec D, de Fleury P, Rueff B, Nahum H, Benhamou JP. Portal hypertension, size of esophageal varices, and risk of gastrointestinal bleeding in alcoholic cirrhosis. *Gastroenterology* **1980**;79:1139–1144
6. Copenhagen Esophageal Varices Sclerotherapy Project. Sclerotherapy after first variceal hemorrhage in cirrhosis. *N Engl J Med* **1984**;311:1594–1600
7. Cello JP, Grendell JH, Crass RA, Trunkey DD, Cobb EE, Heilbron DC. Endoscopic sclerotherapy versus portocaval shunt in patients with severe cirrhosis and variceal hemorrhage. *N Engl J Med* **1984**;311:1589–1594
8. Nelson RC, Lovett KE, Chezmar JL, et al. Comparison of pulsed Doppler sonography and angiography in patients with portal hypertension. *AJR* **1987**;149:77-81
9. Ohnishi K, Saito M, Sato S, Sugita S, Tanaka H, Okuda K. Clinical utility of pulsed Doppler flowmetry in patients with portal hypertension. *Am J Gastroenterol* **1986**;81:1–8
10. Ozaki C, Anderson JC, Liebermann RP, Rikkers LF. Duplex ultrasonography as a noninvasive technique for assessing portal hemodynamics. *Am J Surg* **1988**;155:70–75
11. Patriquin H, Lafortune M, Burns BN, Dauzat M. Duplex doppler examination in portal hypertension. *AJR* **1987**;149:71–76
12. Pugh RNH, Murray-Lyon IM, Dawson JL, Pietroni MC, Williams R. Transection of the esophagus for bleeding esophageal varices. *Br J Surg* **1973**;60:646–649
13. Van Leeuwen MS. Doppler ultrasound in the evaluation of portal hypertension. *Clin Diagn Ultrasound* **1990**;26:53–76
14. Schwaighofer B, Frühwald F, Hay U, Kainberger F, Renner F. Diagnosis of varices in liver cirrhosis: duplex ultrasound versus gastroscopy. *ROFO* **1987**;146:38–41
15. Medhat A, Iber FL, Dunne M, Baum R. Ultrasonographic findings with bleeding and nonbleeding esophageal varices. *Am J Gastroenterol* **1988**;83:58–63
16. Ralls PW. Color Doppler sonography of the hepatic artery and portal venous system. *AJR* **1990**;155:517–525
17. Vilgrain V, Lebrec D, Menu Y, Scherrer A, Nahum H. Comparison between ultrasonographic signs and the degree of portal hypertension in patients with cirrhosis. *Gastrointest Radiol* **1990**;15:218–222
18. Nunez D, Russell E, Yrizarri J, Pereiras R, Viamonte M Jr. Portosystemic communications studied by transhepatic portography. *Radiology* **1978**;127:75–79
19. Takashi M, Igarashi M, Hino S, et al. Esophageal varices: correlation of left gastric venography and endoscopy in patients with portal hypertension. *Radiology* **1985**;155:327–331
20. Moriyasu F, Nishida O, Ban N, et al. Congestion index of the portal vein. *AJR* **1986**;146:735–739
21. Bolondi L, Gandolfi L, Arienti V, et al. Ultrasonography in the diagnosis of portal hypertension: diminished response of portal vessels to respiration. *Radiology* **1982**;142:167–172
22. Ohnishi K, Sato S, Saito M, et al. Clinical and portal hemodynamic features in cirrhotic patients having a large spontaneous splenorenal and/or gastrorenal shunt. *Am J Gastroenterol* **1986**;81:450–455
23. Mostbeck GH, Wittich GR, Herold C, et al. Hemodynamic significance of the paraumbilical vein in portal hypertension: assessment with duplex US. *Radiology* **1989**;170:339–342
24. Gaiani S, Bolondi L, LiBassi S, Zironi G, Siringo S, Barbara L. Prevalence of spontaneous hepatofugal portal flow in liver cirrhosis. *Gastroenterology* **1991**;100:160–167
25. Sabbá C, Weltin GG, Cicchetti DV, et al. Observer variability in echo–Doppler measurements of portal flow in cirrhotic patients and normal volunteers. *Gastroenterology* **1990**;98:1603–1611
26. Parvey HR, Eisenberg RL, Giyanani V, Krebs CA. Duplex sonography of the portal venous system: pitfalls and limitations. *AJR* **1989**;152:765–770
27. Gill RW. Measurement of blood flow by ultrasound: accuracy and sources of error. *Ultrasound Med Biol* **1985**;11:625–641
28. Garden OJ, Motyl H, Gilmour WH, Utley RJ, Carter DC. Prediction of outcome following acute variceal hemorrhage. *Br J Surg* **1985**;72:91–95

Leopard. Serengeti National Park, Tanzania

Henry Wheeler[1]

[1]San Diego, CA.

AJR **1993;160:48** 0361–803X/93/1601–0048

Metastases to the Pancreas and Peripancreatic Lymph Nodes from Carcinoma of the Right Side of the Colon: CT Findings in 12 Patients

Chusilp Charnsangavej[1]
Nancy O. Whitley[2]

OBJECTIVE. Our objective was to describe the CT findings of metastases to the pancreas from carcinoma of the colon and to discuss the pathways of metastasis based on the anatomic relationship between the mesocolon and the pancreas.

MATERIALS AND METHODS. Clinical features and CT scans of 12 patients who had proved metastases to the pancreas from adenocarcinoma of the colon were retrospectively reviewed to define the characteristics of pancreatic lesions. The primary tumors were in the cecum (three patients), ascending colon (five patients), and transverse colon (four patients). Direct extension of the tumor to the pancreas was excluded. Metastases were diagnosed by aspiration or surgical biopsy.

RESULTS. Seven patients (58%) had obstruction of the bile duct and/or pancreatic duct. Four others had symptoms related to the mass, including pain and gastrointestinal obstruction. In eight patients (67%), metastatic tumors involved the pancreas as a focal mass; in the other four (33%), the masses were lobulated and engulfed the pancreas and were indistinguishable from peripancreatic nodal disease. The masses were hypodense in nine patients (75%) and isodense in three patients (25%). Extrapancreatic metastatic disease was seen in nine patients (75%).

CONCLUSION. Clinical features and CT findings in patients with pancreatic metastases from carcinoma of the colon are similar to those of primary pancreatic ductal adenocarcinomas. The diagnosis of metastasis should be considered when a patient has a pancreatic mass and a history of colon carcinoma.

AJR 1993;160:49–52

The imaging appearance of colon cancer metastatic to the pancreas is not well documented in the literature. Primary tumors that commonly metastasize to the pancreas are melanoma; carcinomas of the lung, breast, kidney; and carcinomas in the gastrointestinal tract such as in the stomach and small bowel [1–4]. Only a few reports [3] of cases of pancreatic metastases from carcinoma of the colon have included CT findings. We report CT findings of metastatic disease to the pancreas from primary adenocarcinomas in the cecum, ascending colon, and transverse colon in 12 patients and discuss the pathways of metastasis based on the anatomic relationship between the mesocolon and the pancreas.

Materials and Methods

CT scans collected between 1989 and 1991 from 12 patients with colon cancer metastatic to the pancreas were reviewed retrospectively. Cases of direct extension of the primary tumor to the pancreas were excluded. The medical records of these patients were reviewed with attention to the clinical features, the sites of primary tumors, the staging of primary tumors, and the time between diagnosis of the primary tumor and discovery of metastatic disease. The group consisted of eight men and four women 31–74 years old (mean, 58 years).

All CT scans were obtained with the GE 9800 Quick, the 9800 High-Light HTD, or the 9800 High-Light Advantage system (GE Medical Systems, Milwaukee, WI). In six patients, 10-mm sections with 10-mm intervals were used, and scans were obtained from the dome

Received June 18, 1992; accepted after revision July 28, 1992.

[1]Department of Diagnostic Radiology, Division of Diagnostic Imaging, Box 57, The University of Texas M. D. Anderson Cancer Center, 1515 Holcombe Blvd., Houston, TX 77030. Address reprint requests to C. Charnsangavej.

[2]Department of Diagnostic Radiology, The University of Maryland Medical Systems Hospital, 22 S. Greene St., Baltimore, MD 21201.

0361–803X/93/1601–0049

of the diaphragm down to the iliac crest after IV administration of contrast material at a rate of 1.5 ml/sec. In the other six, 1.5-mm sections and 5-mm scan intervals were used, and scans of the pancreas were obtained after a bolus injection of IV contrast material.

The primary tumors were located in the cecum in three patients, ascending colon in five, and transverse colon in four. In only one patient was the primary tumor still present in the ascending colon when the patient was seen because of obstructive jaundice. This patient was thought to have a primary carcinoma in the pancreatic head. In the other 11 patients, the primary tumors had been removed; the average time between diagnosis of primary tumors in the colon and discovery of metastases in the pancreas was 32 months (range, 6 months to 14 years). In one patient, metastatic disease to the pancreatic head developed 14 years after a right hemicolectomy; biopsy of the mass showed histologic characteristics similar to those of the primary carcinoma of the colon.

Among the 11 patients in whom the primary tumors had been removed, the pathologic stages at the time of resection according to the TNM classification were defined as T3 in nine and T2 in two patients, and as N0 in four, N1 in one, and N2 in six patients. Two patients had hepatic metastases at the time of resection.

Metastatic carcinoma of the colon was confirmed pathologically in 11 of 12 patients—by pancreatic biopsy in three patients, surgery in six, and aspiration biopsy of the peripancreatic nodes in two. The 12th patient had multiple sites of metastasis, and the results of biopsy of the vertebral body of L5 confirmed the diagnosis. Histologic or cytologic diagnosis was made by comparing the biopsy specimens with the original tumors or by observing the characteristic features of columnar epithelium, peripheral palisading, and necrosis that were highly suggestive of adenocarcinoma of the colon.

Results

In eight patients (67%), metastases involved the pancreas (Figs. 1 and 2). Four patients had peripancreatic nodal involvement with invasion of the pancreatic parenchyma, one had a paraduodenal mass inseparable from the pancreas, and three had nodal disease extending up along the hepatoduodenal ligament. The masses were hypodense relative to normal parenchyma in four patients (Fig. 2) and isodense in the other four (Fig. 1). Three (75%) of the four patients with tumor in the head of the pancreas had obstructive jaundice (Fig. 1), and jaundice developed in the fourth during the course of follow-up. Two patients had symptoms of gastrointestinal obstruction, because the mass compressed either the antrum of the stomach or the duodenum.

Four patients (33%) had a metastatic tumor in the body or tail of the pancreas. Three tumors were hypodense and caused obstruction of the pancreatic duct; both characteristics were indistinguishable from those of primary pancreatic carcinoma (Fig. 3). The other mass engulfed the pancreas and could not be separated from peripancreatic nodes (Fig. 4). Two patients in this group had a mass in the left upper quadrant of the abdomen and pain in the upper abdomen, and two patients were asymptomatic.

Nine (75%) of the 12 patients with carcinoma of the colon metastatic to the pancreas had extrapancreatic disease, including hepatic metastases (five patients), peritoneal metastases (three patients), lung metastasis (one patient), and bone metastasis (one patient). Three patients had no other metastases at the time the pancreatic masses were discovered. Three patients had elevated levels of carcinoembryonic antigen.

Discussion

Metastases to the pancreas are uncommon. In large autopsy series [5, 6], secondary tumors of the pancreas accounted for only 3–12% of metastases. Abrams et al. [5] analyzed autopsy findings in 1000 patients who died from malignant tumors and found that only 5.4% of carcinomas of the colon metastasized to the pancreas. Most secondary tumors of the pancreas reported in the radiologic literature [1–4] were from carcinomas of the lung, breast, and kidney

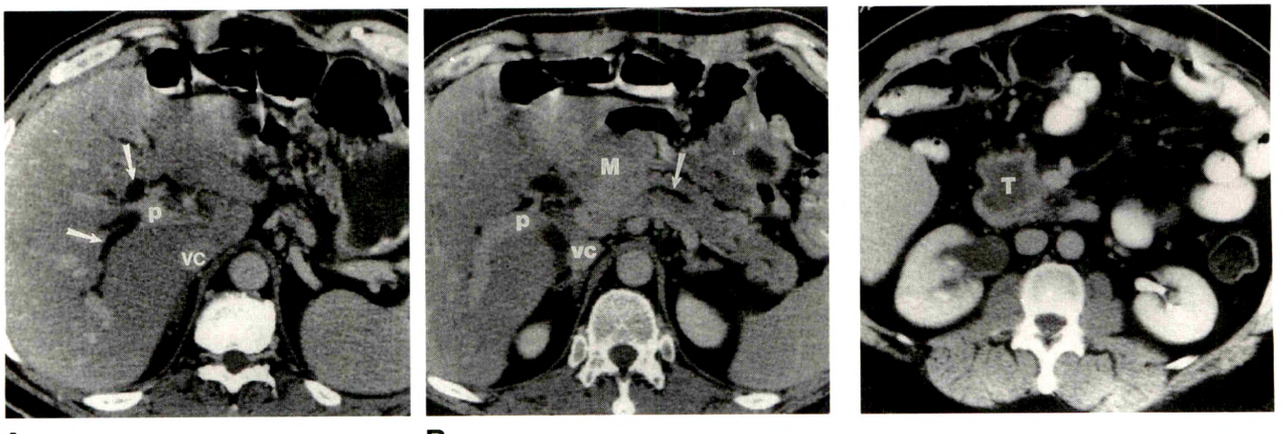

A B

Fig. 1.—Metastasis to head of pancreas from colon carcinoma in a 58-year-old man with obstructive jaundice and gastric outlet obstruction who had a right hemicolectomy for adenocarcinoma 3 years earlier.

***A*, CT scan at hilum of liver shows dilated intrahepatic bile duct (*arrows*).**

***B*, CT scan 1.5 cm caudal to *A* shows mass (M) in head of pancreas that has caused obstruction of pancreatic duct (*arrow*) and antrum of stomach. Aspiration biopsy showed tumor had characteristics consistent with those of primary colonic carcinoma.**

p = portal vein, vc = inferior vena cava.

Fig. 2.—CT scan shows metastasis to head of pancreas from colon carcinoma in a 52-year-old man in whom carcinoma of transverse colon was diagnosed 4 years earlier. Patient also had lung, peritoneal, and hepatic metastases. Tumor (T) in head of pancreas is hypodense. Diagnosis was confirmed by surgical biopsy.

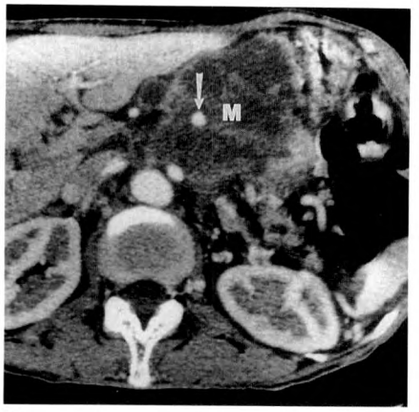

3

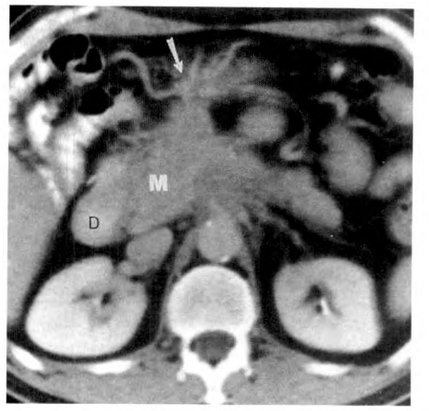

4

Fig. 3.—CT scan shows metastasis to body of pancreas from carcinoma of ascending colon in a 62-year-old woman who had a right hemicolectomy 2 years earlier. Patient had weight loss, pain in left upper quadrant, and elevated serum carcinoembryonic antigen levels. Note large hypodense mass (M) with encasement of splenic artery (*arrow*) and obstruction of splenic vein. Patient also had hepatic and splenic metastases (*not shown*). Mass was indistinguishable from primary tumor of pancreas. Specimens from aspiration biopsy showed cytologic features similar to those of primary tumor.

Fig. 4.—CT scan shows isodense mass (M) at head of pancreas with infiltration and lobulated appearance in an 88-year-old man who had a right hemicolectomy for carcinoma of right transverse colon 3 years earlier. Patient had pain in right upper quadrant of abdomen and no jaundice. Aspiration biopsy confirmed diagnosis of metastatic colon carcinoma. D = duodenum, *arrow* = gastrocolic trunk.

and from melanoma. Only a few examples of carcinoma of the colon with pancreatic metastasis were reported by Murunaka et al. [3] and Wernecke et al. [7]. Our study of 12 patients is the largest one to date that includes the CT findings of pancreatic metastases from carcinoma of the colon.

In our study, clinical features and CT findings in seven patients who had pancreatic metastases from carcinoma of the colon could not be distinguished from those of a primary ductal adenocarcinoma, and in four of the seven, the diagnosis at referral was carcinoma of the pancreas. Among the eight patients who had a focal mass in the pancreas, seven masses (88%) were hypodense and three (37%) of them had a CT density between 20 and 30 H, consistent with an area of tumor necrosis or mucin production. These features of hypodensity (scirrhous area or fibrosis of the tumor) and the area of tumor necrosis had prevalences similar to those observed in primary ductal adenocarcinomas of the pancreas (83% and 12%, respectively) [8].

In four patients who had bulky and lobulated masses engulfing the pancreas, two masses were hypodense and the other two were isodense. Three involved the head of the pancreas and extended up along the hepatoduodenal ligament and one locally infiltrated around the head and body of the pancreas. Distinguishing peripancreatic nodal disease from isolated pancreatic masses can be difficult, particularly when the masses are large and the tissue planes are obliterated [4]. With this CT appearance, one should consider the possibility of metastatic disease from other gastrointestinal or pancreatic primary tumors or from lymphoma.

All patients in this study had primary carcinoma that originated from the right side of the colon and the transverse colon, and the primary tumor was not contiguous with the pancreas. We excluded patients who had primary tumors in the hepatic flexure or splenic flexure, where they can directly invade the duodenum and the pancreatic head, or the tail of the pancreas along the mesocolon [9], so as to clearly limit our study to cases of metastases. The prevalence of pancreatic metastases from carcinoma of the colon among this group of patients is not known because these cases were gathered through a retrospective review of the teaching collections covering a 3-year period. However, from our unpublished data when we reviewed pathways of nodal metastases for carcinoma of the ascending and transverse portions of the colon, we found metastatic disease to the pancreas in four (3%) and direct invasion of the pancreas in another four (3%) of 125 patients evaluated. On the other hand, in a review [10] of 173 cases of carcinoma of the descending colon, sigmoid colon, and rectum, no examples of metastasis to the pancreas were seen, although theoretically, tumors of the left side of the colon can spread via the lymphatic system along the inferior mesenteric vein [11] toward the superior mesenteric vein just caudal to the body of the pancreas and can involve the pancreas.

We think that the most likely mode of spread in most of our cases was via the lymphatic system. The pathways of lymphatic drainage of the colon are well documented [11, 12]. The pathways can be followed along the vessels in the mesocolon toward the root of the mesocolon, which covers the head, body, and tail of the pancreas. For the cecum and ascending colon, the primary lymphatic drainage runs along the ileocolic vessels toward the root of the superior mesenteric artery and vein adjacent to the head and body of the pancreas. For the transverse colon, the lymphatic drainage follows the middle colic vessels in the transverse mesocolon to where they join the superior mesenteric vessels anterior to the head of the pancreas. Because of these drainage pathways, nodal metastases from carcinoma of the cecum, ascending colon, and transverse colon could end up in the nodes around the head and body of the pancreas. Further progression of these nodal metastases is likely to involve the pancreatic parenchyma, and the tumors become inseparable from the pancreas.

In summary, when a patient with a history of carcinoma of the cecum, ascending colon, or transverse colon has a pancreatic mass, with or without obstruction of the pancreatic or the bile duct, and the mass can be focal or infiltrative, metastatic disease should be considered in the differential diagnosis. Aspiration biopsy may be needed to establish the diagnosis.

REFERENCES

1. Rumancik WM, Megibow AJ, Bosniak MA, Hilton S. Metastatic disease to the pancreas: evaluation by computed tomography. *J Comput Assist Tomogr* **1984**;8:829–834
2. Lee JKT, Sagel SS, Stanley RJ. *Computed body tomography with MRI correlation.* New York: Raven, **1989**:564
3. Murunaka T, Teshima K, Honda H, Nanjo T, Hanada K, Oshiumi Y. Computed tomography and histologic appearance of pancreatic metastases from distant sources. *Acta Radiol* **1989**;30:615–619
4. Moss M, Gamsu G, Genant HK. *Computed tomography of the body with magnetic resonance imaging,* vol. 3. Philadelphia: Saunders, **1992**:923–925
5. Abrams HL, Spiro R, Goldstein N. Metastases in carcinoma: analysis of 1000 autopsied cases. *Cancer* **1950**;3:74–85
6. Willis RA. *The spread of tumors on the human body.* London: Butterworths, **1951**:216–219
7. Wernecke K, Peters PE, Galanski M. Pancreatic metastases: US evaluation. *Radiology* **1986**;160:399–402
8. Freeny PC, Marks WM, Ryan JA, Traverso LW. Pancreatic ductal adenocarcinoma: diagnosis and staging with dynamic CT. *Radiology* **1988**; 166:125–133
9. Meyers M. Dynamic radiology of the abdomen. In: *Normal and pathological anatomy,* 3rd ed. New York: Springer-Verlag, **1988**:103–115
10. Granfield CA, Charnsangavej C, Dubrow RA, et al. Regional lymph node metastases in carcinoma of the left side of the colon and rectum: CT demonstration. *AJR* **1992**;159:757–761
11. Rouviere H. *Anatomy of the human lymphatic system.* Ann Arbor, MI: Edwards Brothers, **1938**:188–195
12. Goligher J. *Surgery of the anus, rectum and colon.* London: Bailliere Tindell, **1984**:26

Pictorial Essay

CT of Blunt Trauma to the Bowel and Mesentery

Hanh Vu Nghiem,[1] R. Brooke Jeffrey, Jr., and Robert E. Mindelzun

The high mortality and morbidity rates associated with traumatic rupture of the hollow viscera have been attributed to the clinical difficulty in establishing an early diagnosis. CT has been shown to be accurate for detecting bowel and mesenteric injuries caused by blunt trauma and may be useful in predicting the need for either surgical repair or conservative management. However, many major gastrointestinal injuries have subtle CT findings. In this pictorial essay, we illustrate the broad spectrum of gastrointestinal abnormalities that can be shown by CT in patients with blunt abdominal trauma.

Diagnosis of Bowel and Mesenteric Injuries

Bowel and mesenteric injuries are found in approximately 5% of all patients undergoing laparotomy after blunt abdominal trauma and are most often associated with motor vehicle accidents [1]. Although undiagnosed bowel and mesenteric injuries make up only a small fraction of all injuries due to blunt abdominal trauma, they can cause life-threatening hemorrhage from disruption of mesenteric vessels and fatal peritonitis from bowel perforation. Also, initial clinical examination often reveals no reliable signs or symptoms of gastrointestinal injury. Associated visceral injuries can mask the findings of gastrointestinal perforation. The mortality rate associated with duodenal perforation approaches 65% when diagnosis and repair are delayed [1].

Although diagnostic peritoneal lavage is a valuable and effective means of detecting intraperitoneal hemorrhage after blunt trauma, the lavage findings are nonspecific for the site of origin and extent of the injury. Peritoneal lavage is also insensitive to injuries of retroperitoneal organs, including those of the duodenum and the colon [1]. Retained peritoneal fluid and gas from peritoneal lavage markedly limit the ability to diagnose bowel injury with CT. With meticulous scanning techniques, including the use of water-soluble oral contrast material and careful search for subtle findings of bowel perforation, most significant bowel and mesenteric injuries can be reliably identified with CT preoperatively, and associated injuries to other abdominal viscera can be confirmed. CT may also be useful in selecting patients who can be treated without surgery [1, 2].

CT Technique

Optimal CT technique is essential for the diagnosis of many subtle traumatic gastrointestinal lesions. At our institution, CT for blunt abdominal trauma is performed after oral and IV administration of contrast material. Intravenously, 150 ml of 60% iodinated contrast material is administered IV as a sustained bolus at 2 ml/sec, after which dynamic incremental bolus CT scans (GE 9800) are obtained at 1-cm intervals throughout the abdomen and pelvis. Whenever possible, contrast material (400–700 ml of 1% diatrizoate meglumine) is administered orally, via a nasogastric tube, which is pulled back into the thoracic part of the esophagus immediately before scanning to minimize streak artifacts. It is critical to view the completed scan at the CT console with wide windows (>500 H) to detect subtle pneumoperitoneum before the patient is taken off the table. Regions of interest can be examined with selective scanning.

CT Findings

Pneumoperitoneum

Free air in either the peritoneal cavity or the retroperitoneum after injury of the gastrointestinal tract is a relatively specific sign of perforation. CT can show minute quantities of extraluminal air (Fig. 1). Pneumoperitoneum is usually

Received May 18, 1992; accepted after revision June 19, 1992.

[1] All authors: Department of Radiology, Stanford University Medical Center, Room H-1307, Stanford, CA 94305-5105. Address reprint requests to R. B. Jeffrey, Jr.

AJR 1993;160:53–58 0361–803X/93/1601–0053

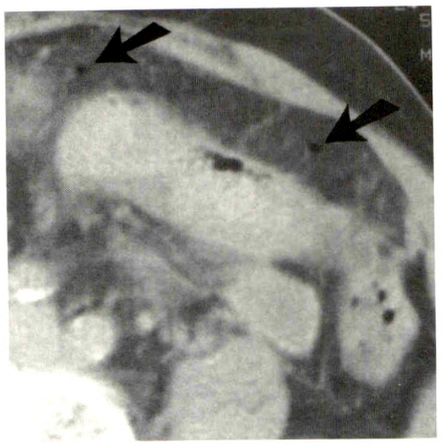

Fig. 1.—Traumatic perforation of jejunum. Contrast-enhanced CT scan obtained with wide window settings shows subtle pneumoperitoneum (*arrows*).

seen outlining the anterior peritoneal surface. Free air is commonly seen in the perihepatic region, in the perisplenic region, or trapped in the leaves of the mesentery or in the interstices of the omentum (Fig. 2). Free air may also be trapped by adhesions or ligaments such as the falciform ligament or the ligament for the ductus venosus.

Free Intraabdominal Fluid

Free intraperitoneal fluid is common in patients with bowel and mesenteric injuries. The fluid may be of low density (<20 H) if it is extravasated from the small bowel (Fig. 3), of intermediate density (>25 H) if it is from hemoperitoneum, or of very high density (>150 H) if it is extravasated oral contrast material (Figs. 4 and 5). Blood or free fluid between bowel loops is a key finding indicating an injury of the bowel or mesentery. Hemoperitoneum from hepatic or splenic lacerations usually accumulates within the subdiaphragmatic spaces, paracolic gutters, or pelvis. It is rarely noted between bowel loops. Low-density fluid between loops of bowel is an ominous finding of small-bowel perforation (Fig. 6). Small-bowel fluid is largely composed of gastric secretions, bile, and pancreatic fluid. Because gas is not routinely found within much of the small bowel, small-bowel perforation can occur without pneumoperitoneum, and its only evidence may be loculated fluid between bowel loops

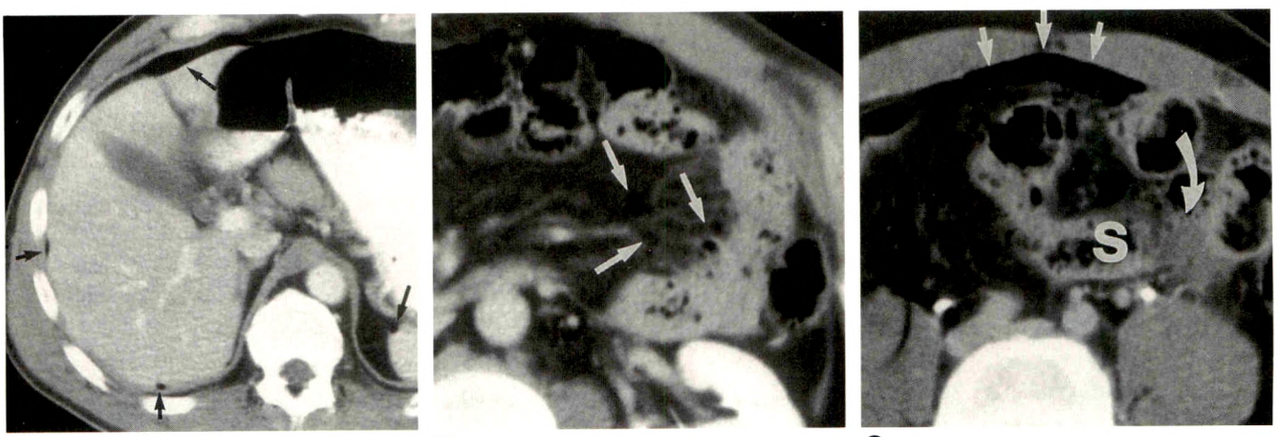

Fig. 2.—Traumatic perforation of sigmoid colon.
A and *B*, Contrast-enhanced CT scans show pneumoperitoneum in anterior part of abdomen, perihepatic and perisplenic space, and between reflections of the mesentery (*arrows*).
C, Contrast-enhanced CT scan at more caudal level shows a high-attenuation hematoma or sentinel clot (*curved arrow*) adjacent to sigmoid colon (S).

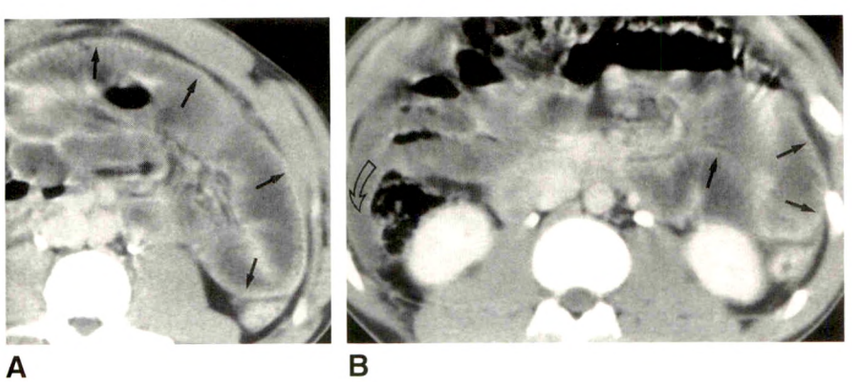

Fig. 3.—Traumatic perforation of jejunum.
A and *B*, Contrast-enhanced CT scans through lower part of abdomen show diffuse enhancement and mild thickening of wall of small bowel (*straight arrows*). Free intraperitoneal fluid with density similar to that of water is seen in right paracolic gutter (*curved arrow*).

(Fig. 7). A rare form of very high density fluid (>120 H) is arterial blood actively hemorrhaging into the abdomen. On contrast-enhanced CT scans, active arterial bleeding is isodense with adjacent major arterial structures (Fig. 8). In the focal form, localized areas of extravasation are often associated with large hematomas. In the diffuse form, extravasated IV contrast material appears as high-density fluid that conforms to the peritoneal cavity or the involved extraperitoneal spaces [3].

Bowel Wall Findings

On CT scans, intramural hematomas result in circumferential or eccentric thickening of the bowel wall (Fig. 9). The presence of an intramural hematoma in an adult with blunt trauma is highly suggestive of bowel laceration. Intense enhancement of the bowel wall also suggests injury of the bowel (Fig. 3), and in one study [4], it was shown that intense enhancement of the bowel wall accompanied by bowel wall thickening and free intraperitoneal fluid strongly suggested bowel perforation and peritonitis.

Mesenteric Injury

Small areas of hemorrhage may result in streaky soft-tissue infiltration of normal mesenteric fat (Fig. 6A). Larger, more confluent hematomas may exert significant mass effect on adjacent bowel loops. The presence of a mesenteric hematoma should prompt a careful search for any evidence of gastrointestinal perforation or laceration of mesenteric vasculature. Furthermore, the "sentinel dot" sign (i.e., the higher attenuation values of blood noted near the

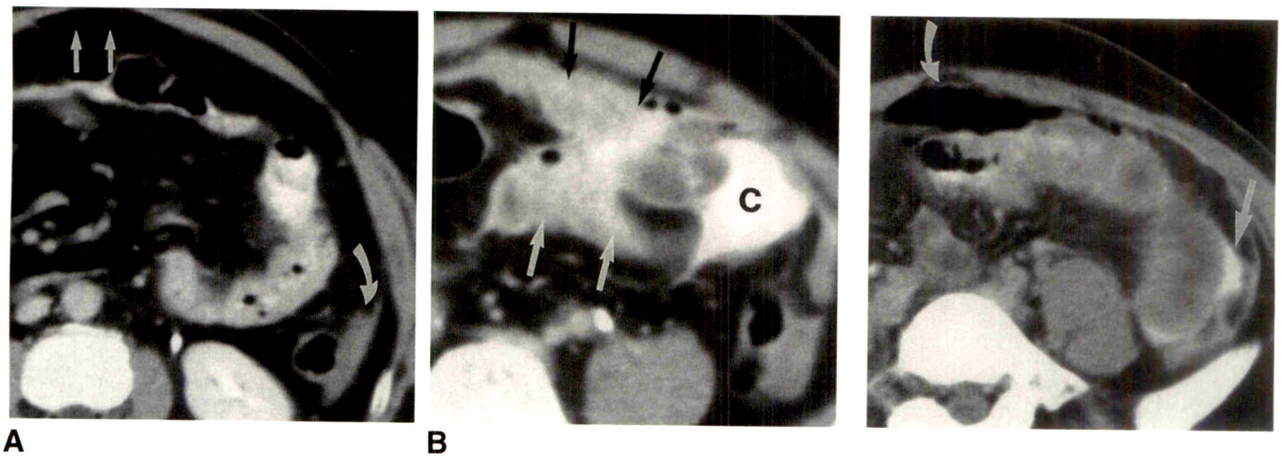

Fig. 4.—Traumatic laceration of proximal part of jejunum.
***A*, Contrast-enhanced CT scan shows free air in anterior part of abdomen (*straight arrows*) and hemoperitoneum (*curved arrow*) in left paracolic gutter.**
***B*, Contrast-enhanced CT scan shows a triangular collection of extravasated oral contrast material (c) that has very high density, adjacent to a distorted contrast-filled loop of jejunum (*arrows*), diagnostic of perforation.**

Fig. 5.—Traumatic perforation of jejunum. CT scan shows extravasation of oral contrast material (*straight arrow*) and pneumoperitoneum (*curved arrow*).

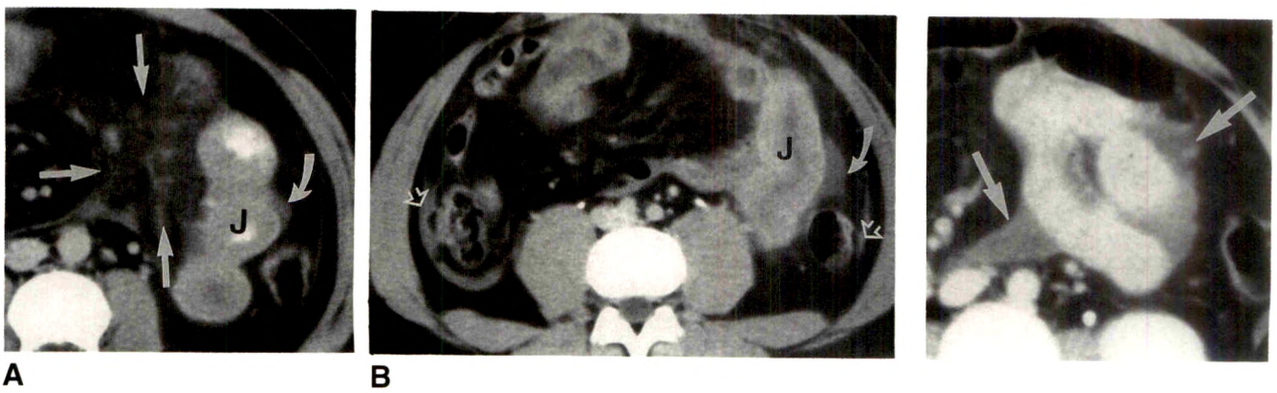

Fig. 6.—Traumatic laceration of jejunum.
***A* and *B*, Contrast-enhanced CT scans show marked thickening of wall of jejunum (J) and fluid adjacent to injured bowel loop (*curved arrows*). Fluid has density similar to that of water. Soft-tissue infiltration of mesentery denotes mesenteric hematoma (*straight arrows*). Hemoperitoneum is noted in paracolic gutters (*open arrows*).**

Fig. 7.—Traumatic perforation of jejunum. Contrast-enhanced CT scan shows triangular fluid collections (*arrows*) between bowel loops. Fluid has a density (18 H) similar to that of water. No pneumoperitoneum was present. Perforation of jejunum was found at exploratory laparotomy.

site of visceral injury) between bowel loops (Figs. 2, 10, and 11) is strong evidence of mesenteric and gastrointestinal injury [5].

Findings of Delayed Perforation

In some patients, perforation of the small bowel may be delayed (Fig. 12). Initial CT findings may be normal in this instance. In patients with developing signs of fever or peritonitis, follow-up CT should be done without hesitation. Other delayed complications may include bowel necrosis (Fig. 13).

Features of Specific Gastrointestinal and Mesenteric Injuries

Gastric Injury

Gastric injury from blunt abdominal trauma is more common in children than in adults (Fig. 14). A common finding in patients with this injury is a distended stomach, which usually occurs after eating. The anterior wall of the stomach is the most common site of rupture, followed by the greater curvature, the lesser curvature, and the posterior wall in order of decreasing frequency. Delay in diagnosis prolongs the period of peritoneal contamination and contributes to sepsis and intraabdominal abscess, which is often extensive, recurrent, and difficult to treat. Trauma to the left side of the body is present in many patients with gastric perforation, and the most common associated injury is rupture of the spleen. Significant left-sided thoracic injury is the second most common associated injury [6].

Duodenal Injury

Hematoma and perforation occur most commonly in the descending and horizontal segment of the duodenum. The horizontal segment of the duodenum crosses the vertebral column and is easily compressed against the spine by a direct blow. Depending on the site of duodenal perforation, ectopic gas or oral contrast material can extravasate into the right anterior pararenal space (Fig. 15) or the peritoneal

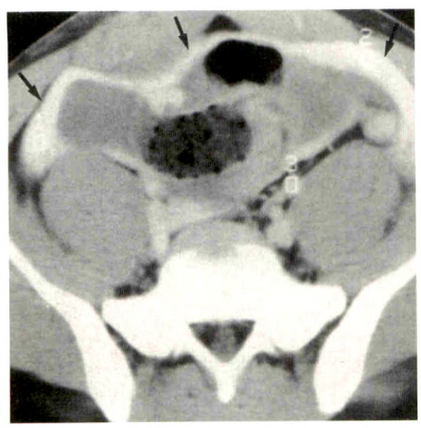

A

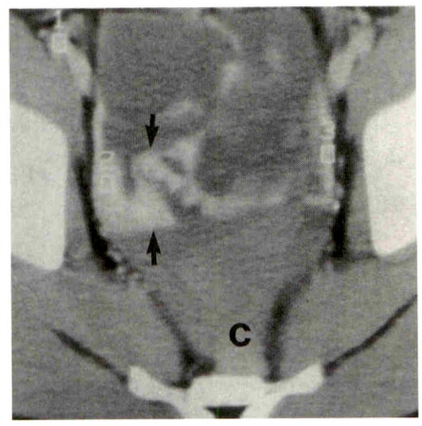

B

Fig. 8.—Traumatic laceration of ileocolic artery. (Reprinted from Jeffrey et al. [3].)
A, Contrast-enhanced CT scan shows diffuse fluid of very high density (*arrows*) throughout peritoneal cavity, representing extravasated IV contrast material.
B, Contrast-enhanced CT scan shows actively hemorrhaging arterial blood (*arrows*) mixed with clotted blood (C) and lysed blood in pelvis.

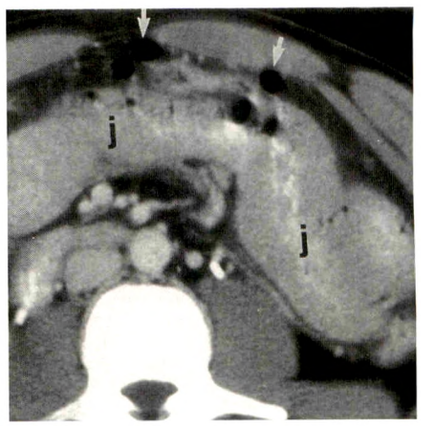

Fig. 9.—Traumatic perforation of jejunum. Contrast-enhanced CT scan shows significant thickening of bowel wall, representing intramural hematoma of jejunum (j) and free intraperitoneal air (*arrows*).

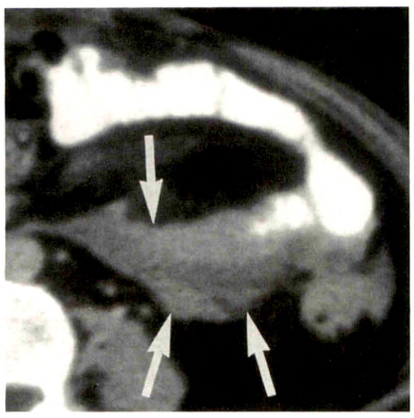

10

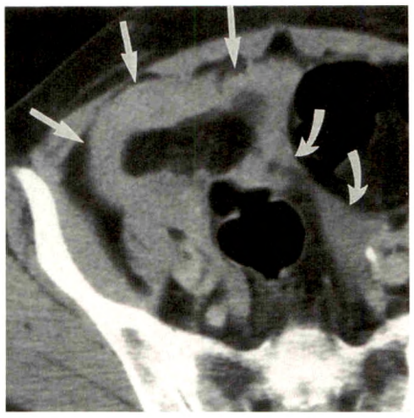

11

Fig. 10.—Traumatic laceration of mesentery. Contrast-enhanced CT scan shows localized high-attenuation hematoma (*arrows*) in small-bowel mesentery.

Fig. 11.—Traumatic avulsion of omentum and laceration of mesentery with sentinel clot sign. CT scan shows high-attenuation hematoma in omentum (*straight arrows*) and between loops of bowel (*curved arrows*). Nearly complete avulsion of lower portion of omentum and laceration of root of mesentery supplying middle part of ileum were found at exploratory laparotomy.

cavity. It is important to search for an associated injury of the head of the pancreas [7].

Jejunal and Ileal Injury

The jejunum and ileum are generally injured at or near a point of fixation such as the ligament of Treitz (Fig. 16) and the ileocecal valve. Rupture of the small bowel occurs most frequently on the antimesenteric border. Abdominal pain and signs of peritoneal irritation develop slowly, because the bowel contents, particularly the jejunal contents, usually have neutral pH, have low bacterial counts, and are not enzymatically active [8].

Colonic Injury

Compression of the upper abdomen caused by a steering wheel or lap-type seat belts appears to predispose patients to colonic injury. The transverse colon, sigmoid colon, and cecum are the most common sites of injury. Injury of the transverse colon most often involves intramural hematomas or serosal tear without fecal spillage. More serious injuries, including avulsion of the mesentery, full-thickness laceration, transection, and devascularization of a segment of the colon are more often seen in injuries of the ascending and descending colon [9]. Rarely, traumatic ventral herniation of the transverse colon through a diastasis of the rectus abdominis muscles may result from abdominal wall injury caused by blunt trauma (Fig. 16).

Mesenteric Injury

Mesenteric hematomas are the most common blunt gastrointestinal injuries shown by CT. Once a mesenteric hematoma has been shown by CT, a careful search should be made for any evidence of gastrointestinal perforation and disruption of mesenteric vasculature [1, 2].

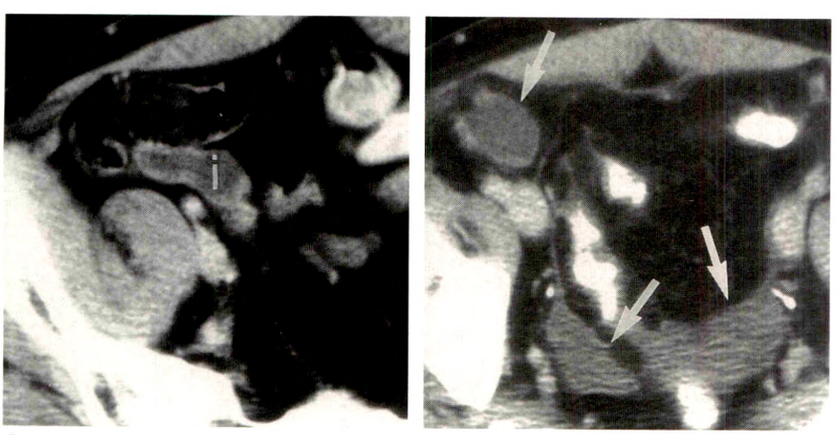

A B

Fig. 12.—Delayed traumatic perforation of distal part of ileum.
***A*, Initial contrast-enhanced CT scan shows normal distal part of ileum (i).**
***B*, Contrast-enhanced CT scan obtained 1 week later shows fluid adjacent to distal part of ileum and in pelvis (*arrows*). Density of fluid was similar to that of water. Perforation of ileum was found at exploratory laparotomy.**

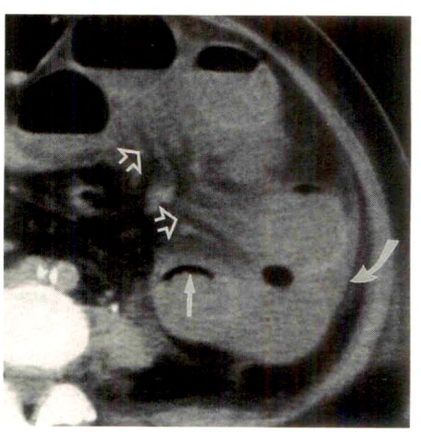

Fig. 13.—Surgically proved bowel necrosis resulting from blunt abdominal trauma. Contrast-enhanced CT scan shows dilated loops of bowel with poor definition of bowel wall and pneumatosis (*straight arrow*). Note associated mesenteric infiltration (*open arrows*) and free fluid in paracolic gutter (*curved arrow*).

Fig. 14.—Traumatic rupture of stomach in a child. Contrast-enhanced CT scan shows pneumoperitoneum (*arrows*) in anterior part of abdomen. Note streak artifacts from nasogastric tube, which was inadvertently not withdrawn before scanning

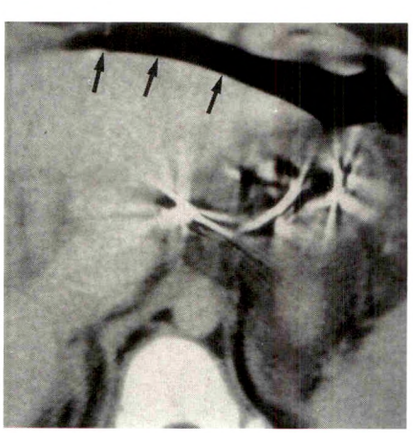

14

Fig. 15.—Traumatic perforation of duodenum. Contrast-enhanced CT scan shows free air in retroperitoneum (*straight arrows*), diagnostic of perforation, and free fluid in right anterior pararenal space (*curved arrow*).

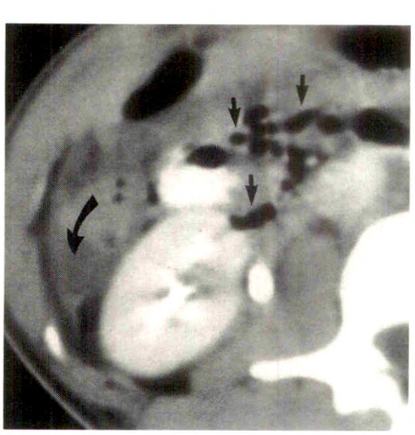

15

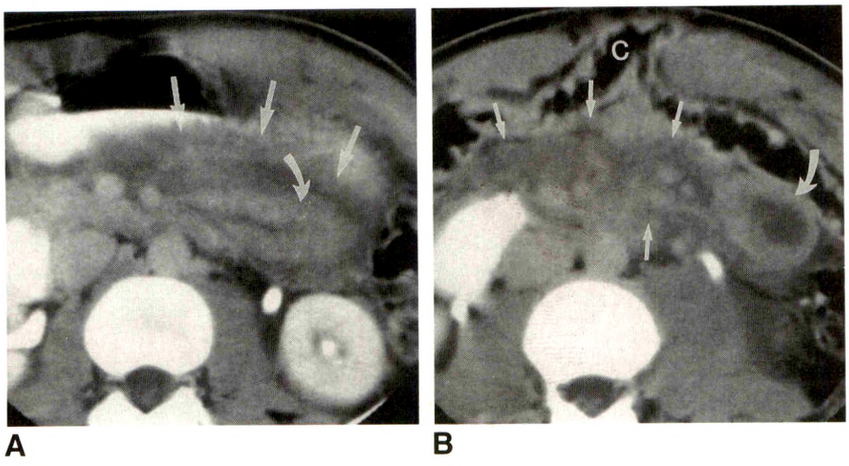

Fig. 16.—Intramural hematoma of jejunum and midline hernia of transverse colon after blunt trauma. (Reprinted with permission from Rizzo et al. [1].)

***A*, Contrast-enhanced CT scan shows thickening of bowel wall due to intramural hematoma of proximal part of jejunum (*curved arrow*) just distal to ligament of Treitz. Note surrounding intraperitoneal hemorrhage (*straight arrows*).**

***B*, At more caudal level, contrast-enhanced CT scan shows traumatic midline herniation of transverse colon (C) through abdominal wall and diastasis of rectus muscles. Again note mural hematoma of jejunum (*curved arrow*) and adjacent hemorrhage (*straight arrows*).**

REFERENCES

1. Rizzo MJ, Federle MP, Griffiths BG. Bowel and mesenteric injury following blunt abdominal trauma: evaluation with CT. *Radiology* **1989**;173: 143–148
2. Donohue JH, Federle MP, Griffiths BG, Trunkey DD. Computed tomography in the diagnosis of blunt intestinal and mesenteric injuries. *J Trauma* **1987**;27:11–17
3. Jeffrey RB Jr, Cardoza JD, Olcott EW. Detection of active intraabdominal arterial hemorrhage: value of dynamic contrast-enhanced CT. *AJR* **1991**;156:725–729
4. Hara H, Babyn PS, Bourgeois D. Significance of bowel wall enhancement on CT following blunt abdominal trauma in childhood. *J Comput Assist Tomogr* **1992**;16:94–98
5. Orwig D, Federle MP. Localized clotted blood as evidence of visceral trauma on CT: the sentinel clot sign. *AJR* **1989**;153:747–749
6. Brunsting LA, Morton JH. Gastric rupture from blunt abdominal trauma. *J Trauma* **1987**;27:887–890
7. Hofer GA, Cohen AJ. CT signs of duodenal perforation secondary to blunt abdominal trauma. *J Comput Assist Tomogr* **1989**;13:430–432
8. Schenk WG III, Lonchyna V, Moylan JA. Perforation of the jejunum from blunt abdominal trauma. *J Trauma* **1983**;23:54–56
9. Strate RG, Grieco JG. Blunt injury to the colon and rectum. *J Trauma* **1983**;23:384–387

Pictorial Essay

Gastric Syphilis: Radiologic Findings

Blaise V. Jones[1] and Joel E. Lichtenstein[1,2]

Syphilis, a venereal infection caused by the spirochetal bacterium *Treponema pallidum*, has long been considered a primary public health concern in the United States. With the onset of the antibiotic era, the prevalence of the disease dramatically plummeted, as did interest in its radiologic manifestations. Rolfs and Nakashima [1] have shown that the prevalence of primary and secondary syphilis increased 34% from 1981 to 1989, to its highest level since 1949. Given this dramatic increase, classic manifestations of syphilis may warrant renewed attention. In its secondary and tertiary stages, syphilis can cause a wide range of gastric lesions that can mimic many other entities, from gastritis or benign ulcer disease to gastric carcinoma. Indeed, the acute gastritis of early secondary syphilis produces the earliest radiologically detectable signs of the disease. Cases of gastric syphilis submitted to the Armed Forces Institute of Pathology and cases drawn from the University of Cincinnati teaching file are used to illustrate the varied findings in this disease.

Early Disease

In the primary phase of the infection, the bacteria enter through the skin or mucous membranes, invading blood and lymphatic vessels and accumulating in regional lymph nodes. Within several weeks, a firm, relatively painless ulcerating nodule, or chancre, forms at the site of initial invasion. Primary syphilis has no radiologic manifestations, and the chancre resolves spontaneously, sometimes without being noticed by the patient [2].

If untreated, the infection progresses to secondary syphilis, which is characterized by rash, fever, lymphadenopathy, and mucocutaneous inflammation. At this stage, a small percentage of patients will have acute gastritis, clinically manifested as pain accompanied by vomiting, but typically with minimal nausea. Radiographs show a nonspecific gastritis, with diffusely thickened folds that may become nodular (Fig.1A), with or without detectable ulcers [3] (Fig. 2). The organisms can be observed in tissue specimens at this time [4] (Fig. 1B). Histologically, the gastritis is manifested by a mucosal and perivascular mononuclear cell infiltrate. Similar radiologic and histologic changes in the small bowel have also been described, although this manifestation is quite rare [5].

Late Disease

A portion of untreated patients progress from secondary syphilis to manifest signs and symptoms of tertiary syphilis. Outside of the gastrointestinal tract, the classic findings are aortitis, parenchymal or skeletal gumma formation, and tabes dorsalis with associated neuropathic joint disease. As the infection continues to this stage, a mass, or gumma, may develop in the gastric wall in some patients [6] (Fig. 3A). This lesion is characterized histologically by layers of fibroblasts and mononuclear cells surrounding rubbery central necrosis [2].

With or without gumma formation, the inflammatory reaction in the stomach tends to evolve into a fibrotic narrowing of the gastric wall. These constrictive lesions may form in the body of the stomach (Fig. 3B). Early investigators thought that this was a characteristic finding of gastric syphilis and termed it the "hourglass" or "dumbbell" shaped stomach. This appearance can also be seen in benign gas-

Received May 11, 1992; accepted after revision July 7, 1992.

[1]Department of Diagnostic Radiology, University of Cincinnati Hospitals, 234 Goodman Ave., M.L. 742, Cincinnati, OH 45267. Address reprint requests to B. V. Jones.

[2]Visiting Professor, Armed Forces Institute of Pathology.

AJR **1993;160:59–61** 0361–803X/93/1601–0059

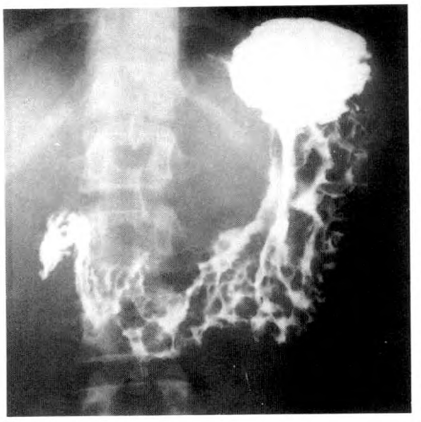

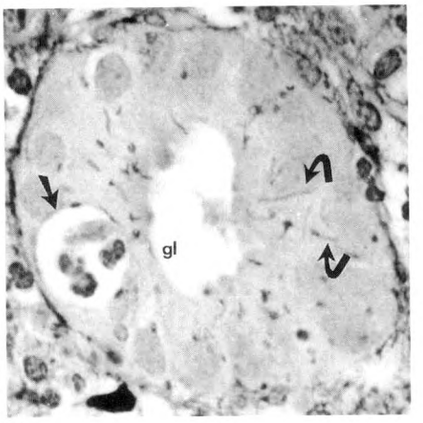

A B

Fig. 1.—Acute syphilitic gastritis in 33-year-old woman with postprandial vomiting.
A, Radiograph shows markedly thickened and irregular folds, typical of early gastric syphilis.
B, Photomicrograph of biopsy specimen from same patient shows spirochetes (*curved arrows*) within the epithelium of a gastric gland. Note intraepithelial abscess (*straight arrow*). gl = gland lumen (silver stain).

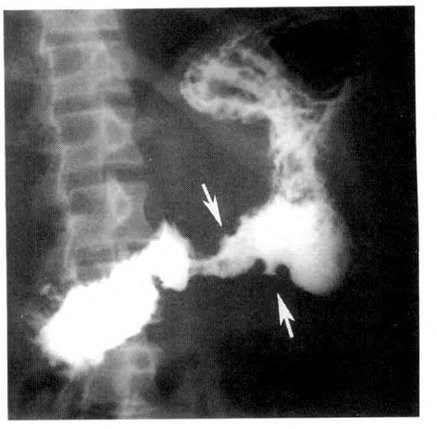

Fig. 2.—Acute syphilitic gastritis in 34-year-old woman with abdominal pain and vomiting. Large ulcers (*arrows*) can be seen in the antrum.

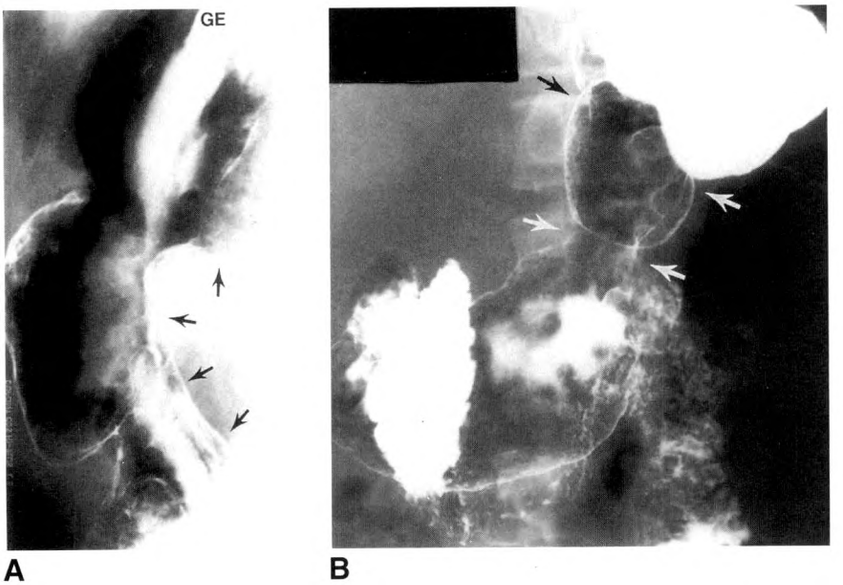

A B

Fig. 3.—Tertiary syphilis in 63-year-old woman with weight loss, epigastric fullness, and vomiting.
A, Nearly lateral radiograph of the stomach shows deformity of the posterior wall by a mass lesion (*arrows*). These findings suggest formation of a gumma, a subacute inflammatory lesion that may be seen in the early stages of tertiary syphilis. GE = gastroesophageal junction.
B, Left posterior oblique radiograph shows two concentric narrowings *(arrowheads)* in body of the stomach. Although considered a classic finding by early authors, such a manifestation is seen in only 20% of patients with late-stage gastric syphilis. The narrowing may progress distally to involve antrum and pylorus, as shown in Fig. 5, or may infiltrate the entire stomach, mimicking scirrhous carcinoma.

tric ulcer disease, gastric carcinoma, caustic ingestion, and tuberculosis. Radiographically, the finding that distinguishes this lesion from carcinoma is that a malignant stricture classically has a sharper "shoulder" at the margins of a short isthmus rather than the more gradual transition from a long isthmus seen in syphilis [3] (Fig. 4).

More commonly, the gastric narrowing associated with the late stages of syphilis is seen in the antrum, causing a funnel-shaped deformity and often extending across the pylorus. Marked abnormality can persist even after appropriate treatment (Fig. 5). The appearance may mimic gastric Crohn's disease, resembling the "shofar" or "ram's horn" configuration described by Farman et al. [7]. Other diseases causing granulomatous inflammation, such as sarcoidosis, amyloidosis, and eosinophilic gastritis, may also cause similar antral lesions. If untreated, the mural infiltration may progress to involve the entire stomach, causing fibrosis and shrinkage (Fig. 6). The resulting *linitis plastica* appearance is difficult to distinguish from scirrhous carcinoma [3]. Once the fibrosis of late-stage gastric syphilis becomes manifest, it is typically difficult to detect organisms in biopsy specimens.

Like tuberculosis, syphilis has long been recognized as a great mimicker of other diseases. It is an entity that has become unfamiliar to an entire generation of physicians, but recent demographic data suggest that it will be an increasingly frequent clinical challenge. Although uncommon, the features of syphilis in the stomach should be recognized, as they can provide a window of opportunity for treatment before the disease progresses and causes permanent disability.

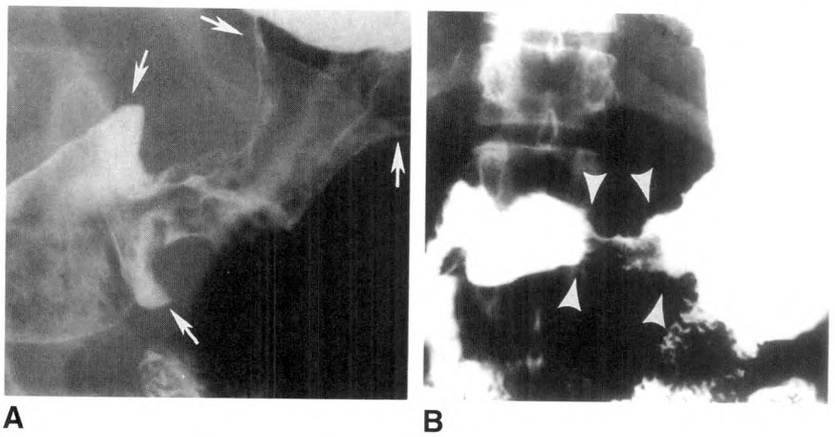

Fig. 4.—*A* and *B*, Concentric antral lesions of gastric carcinoma (*A*) and gastric syphilis (*B*). Radiographs show characteristic abrupt transition at the proximal and distal extent (*arrows*) of lesion in carcinoma (*A*), as opposed to the more smooth narrowing *(arrowheads)* in syphilis (*B*).

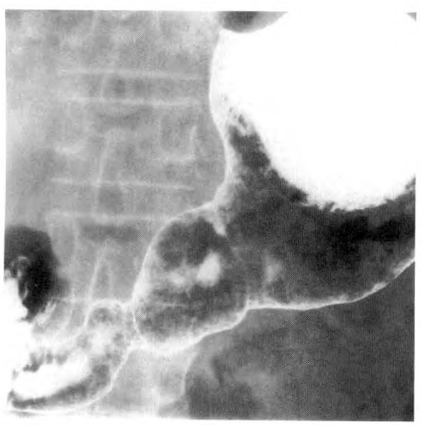

Fig. 5.—Antral deformity after treatment of tertiary syphilis (same patient as Fig. 3, 6 months later). Radiograph shows smooth antral tapering. Inflammation and subsequent deformity extended distally from mid-portion of stomach. In this case, the appearance is suggestive of the "ram's horn" or "shofar" configuration described by Farman et al. [7] in Crohn's disease of stomach.

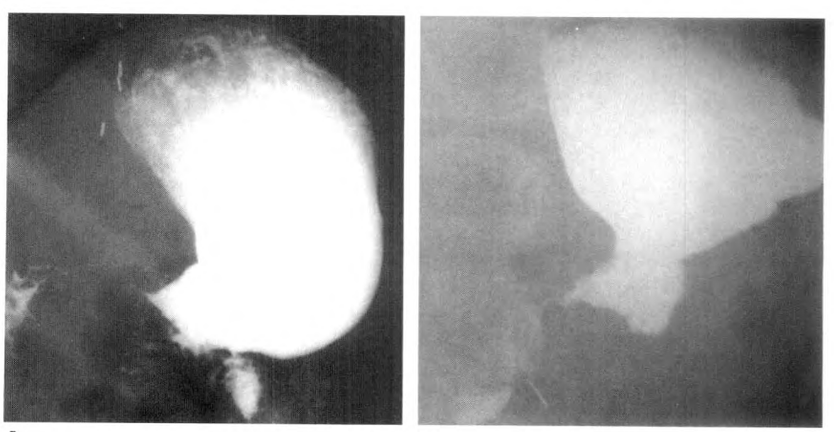

Fig. 6.—*A* and *B*, Antral narrowing of Crohn's disease of the stomach (*A*) vs gastric syphilis (*B*). Radiographs show little distinction between appearance of stomach in adolescent with regional enteritis (*A*) and adult with tertiary syphilis (*B*).

REFERENCES

1. Rolfs RT, Nakashima AK. Epidemiology of primary and secondary syphilis in the United States, 1981 through 1989. *JAMA* **1990**;264:1432–1437
2. Robbins SL, Cotran RS, Kumar V, eds. *Pathologic basis of disease*, 3rd ed. Philadelphia: Saunders, **1984**:335–338
3. Moore AB, Aurelius JR. Roentgenologic manifestations in eighty-seven cases of gastric syphilis. *AJR* **1928**;19:425–432
4. Butz WC, Watts JC, Rosales-Quintana S, Hicklin MD. Erosive gastritis as a manifestation of secondary syphilis. *Am J Clin Pathol* **1975**;63:895–900
5. Schlossberg D, Rudy FR, Jackson FW, Dumalag LB. Syphilitic enteritis. *Arch Intern Med* **1984**;144:811–812
6. Willeford G, Childers JH, Hepner WR. Gumma of the stomach in congenital syphilis. *Pediatrics* **1952**;10:162–167
7. Farman J, Faegenburg D, Dallemand S, Chen CK. Crohn's disease of the stomach: the "ram's horn" sign. *AJR* **1975**;123:242–251

Cathode Rays and Controversy

Ronald L. Eisenberg[1]

One hundred years ago, Heinrich Rudolf Hertz demonstrated that cathode rays could pass through a thin metal foil of gold, silver, or aluminum. His pupil, Philipp Lenard, exploited his teacher's discoveries by constructing a vacuum tube with a thin (0.00265 cm) aluminum window sealed in the glass wall of the bulb at a point where the cathode rays were focused. By using a few particles of fluorescent potassium phosphate, on October 12, 1892, Lenard observed that the cathode rays not only penetrated through the window but also traveled several inches in free air [1]. Although the cathode rays were invisible, their effects could be studied with fluorescent substances and they could darken a photographic plate securely protected by a lightproof holder.

Lenard did not realize that the cathode rays, after passing through the aluminum window, were mixed with an abundance of another kind of ray. At the time, he was unaware that he was making "X-ray pictures."

Years later, however, Lenard became embroiled in a bitter controversy as to whether he, rather than Roentgen, should be honored as the discoverer of X-rays. Lenard initially respected and admired Roentgen and sent him a letter of congratulations on "your great discovery" [2]. In turn, Roentgen acknowledged the work of Lenard and Hertz in his famed Würzburg lecture. Roentgen and Lenard even shared two prestigious physics prizes, in Vienna in 1896 and in Paris a year later.

Lenard's unquenchable animosity began when Roentgen alone was awarded the first Nobel prize in physics in 1901. Feeling himself betrayed, Lenard proclaimed himself the true discoverer of the X-ray. Almost 70 years later, it was revealed that the Advisory Committee of the Swedish Academy of Sciences recommended that the prize be divided equally between Roentgen and Lenard. However, the full Academy disregarded this recommendation, since the late Nobel had specified that it be given only to the *single* most distinguished scientist of the year. The decision was unanimous in favor of Roentgen [3].

Even after being awarded his own Nobel prize in 1905, Lenard's animosity continued unabated. Among his statements downgrading Roentgen's efforts while glorifying his own is the following [2]:

> I am the mother of the x-rays. Just as a midwife is not responsible for the mechanism of birth, so is Roentgen not responsible for the discovery of x-rays, which merely fell into his lap. All Roentgen had to do was push a button, since all the groundwork had been prepared by me.

In effect, Lenard claimed that anybody could have discovered X-rays after *his* (Lenard's) work on cathode rays. However, Lenard never gave a satisfactory explanation as to why he himself had not accomplished this task. In addition, he never mentioned that the so-called Lenard tube was actually based on Hertz's work.

Roentgen's reaction was philosophical. As he wrote to his friend Zehnder, "Well, dear heaven, the envious are never lacking when something occurs as with me. That is always the case" [4].

Philipp Lenard (1862-1947)

Lenard's unbridled hatred of Roentgen climaxed during the time of his (Lenard's) commanding position in the Nazi hierarchy of scientists. In his four-volume work on German physics, there is no mention of Roentgen (or Einstein) in the text, but the foreword is a lengthy diatribe against the Jews. The implication, drawn by many persons in Germany, was that Roentgen was a Jew. When asked about this by American radiologist Lewis Etter, Lenard replied "No, but he was a friend of Jews and acted like one" [2].

The final chapter in the controversy occurred at the time of the 50th anniversary of Roentgen's discovery. The Physical Medical Society of Würzburg applied to the Nazi Minister of Post and Telegraph for a memorial stamp to be made in honor of Roentgen, similar to those issued for other famous scientists. The minister (Ohensorg), a physicist and student of Lenard, rejected the request, saying that the proposal was not in order since such an honor was reserved "only for the illustrious" [2]. The first German stamp honoring Roentgen was not issued until 1952.

REFERENCES

1. Glasser O. The genealogy of the Roentgen rays. II. *AJR* **1934**;30: 349–367
2. Etter LE. Some historical data relating to the discovery of the Roentgen rays. *AJR* **1946**;56:220–231
3. Knutsson F. Roentgen and the Nobel prize: the discussion at the Royal Swedish Academy of Sciences in Stockholm in 1901. *Acta Radiol (Diagn)* **1974**;15:465–473
4. Kraft E. W. C. Roentgen: his friendship with Ludwig Zehnder. *NY State J Med* **1973**;73:1002–1008

This History Page, which originally appeared on page 996 of the November issue of *AJR*, was inadvertently printed without a line identifying the author. It is reprinted here with the author's name in place. *AJR* apologizes for this error.

In preparation of the 1995 centennial celebration of the discovery of the X-ray, the *AJR* will periodically publish History Pages, which deal with events leading up to and occurring around the time of the discovery.

[1]Department of Radiology, Highland General Hospital, 1411 E. 31st St., Oakland, CA 94602.

***AJR* 1993;160:62** 0361–803X/92/1601–0062

Case Report

Leukemic Infiltration of the Gallbladder Wall Mimicking Acute Cholecystitis

David E. Finlay,[1] Steven L. Mitchell, Janis Gissel Letourneau, and Deborah G. Longley

The sonographic findings of gallbladder wall thickening, hypoechoic zones within the gallbladder wall, and pericholecystic fluid are nonspecific for, but are often present in, acute cholecystitis. We report a case of leukemic infiltration of the gallbladder wall that mimicked acute cholecystitis both clinically and on imaging studies.

Case Report

A 35-year-old man had bone marrow transplantation for acute lymphoblastic leukemia. He did well after transplantation, except that graft-vs-host disease of the skin developed. A recent bone marrow aspirate indicated clinical remission. He was admitted 2 months after transplantation with fever and pain in the right upper quadrant. Although blood cultures yielded gram-positive cocci, routine laboratory studies did not localize the source of infection. WBC count was 3.5×10^9/l with a normal differential count. Levels of hepatic enzymes, serum bilirubin, and coagulation parameters were all elevated. Findings on chest and sinus radiographs were normal.

CT 2 days after admission revealed an abnormal, septated area of fluid density around the gallbladder lumen (Fig. 1A). Sonography showed a diffusely thickened gallbladder wall containing hypoechoic zones (Fig. 1B). It was uncertain whether these findings represented pericholecystic fluid in addition to wall thickening. Maximal tenderness was elicited by direct pressure of the transducer over the gallbladder. No biliary dilatation or gallstones were present. Hepatobiliary scintigraphy (not shown) with disofenin (Hepatolite, Du Pont, Billerica, MA) showed no biliary excretion of radiotracer, and the gallbladder was not visualized.

The patient had cholecystectomy on the fourth day after admission for presumptive acalculous cholecystitis. Gross pathologic examination revealed a distended gallbladder with evidence of hemorrhage seen on both the serosal and mucosal surfaces. Cut section of the gallbladder wall demonstrated intramural hemorrhage as well. No gallstones were present. Microscopic sections revealed leukemic infiltration involving the entire thickness of the gallbladder wall.

Postoperatively, a severe coagulopathy developed with subsequent pulmonary and renal failure. The patient died on the eighth day after surgery.

Discussion

Acute lymphoblastic leukemia is a neoplastic disease of unknown origin characterized by the proliferation of lymphoblasts in the bone marrow and in other hematopoietic organs [1]. Although symptoms usually result from bone marrow failure, any organ can be involved by leukemic infiltration, even when the bone marrow aspirate is normal, as in our case [2].

Gallbladder involvement is rare in acute lymphoblastic leukemia [2], and the radiologic appearance of this entity has not been described previously. In our case, leukemic infiltration of the gallbladder wall mimicked acute acalculous cholecystitis both clinically and on imaging studies. Moreover, the morphologic appearance of the gallbladder at surgery was consistent with acute hemorrhagic cholecystitis, with the underlying diagnosis revealed only on microscopic examination. A similar case was seen at this institution 1 year before the current case. Again, clinical signs and symptoms were consistent with cholecystitis. Sonograms and nuclear hepatobiliary scans were virtually identical to those in the current

Received June 2, 1992; accepted after revision July 14, 1992.

[1]All authors: Department of Radiology, University of Minnesota Hospital, 420 Delaware St. S.E., Box 292 UMHC, Minneapolis, MN 55455. Address reprint requests to D. E. Finlay.

AJR 1993;160:63–64 0361–803X/93/1601–0063

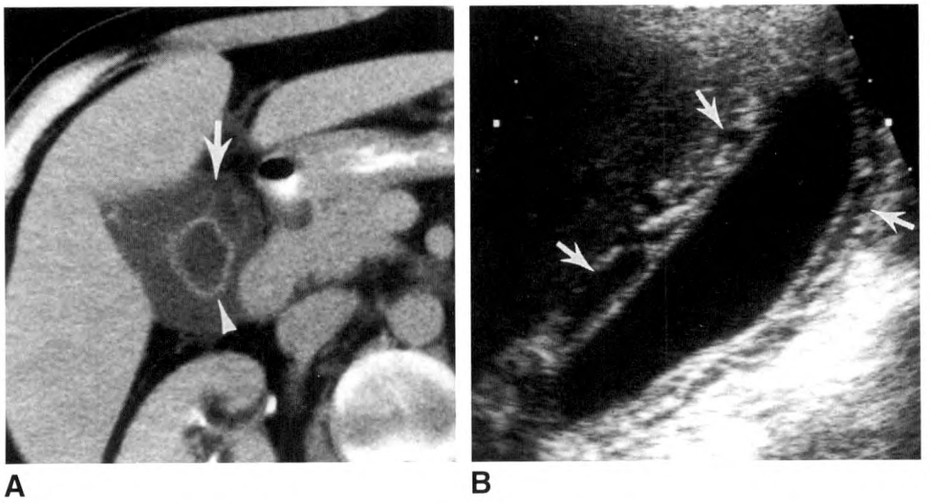

Fig. 1.—*A*, CT scan shows area of fluid density containing septa (*arrow*), which surround gallbladder lumen (*arrowhead*).

***B*, Sonogram shows a diffusely thickened gallbladder wall containing numerous hypoechoic zones (*arrows*). The presence of pericholecystic fluid was thought to be possible.**

case, showing a thickened gallbladder wall containing hypoechoic zones and absence of radionuclide activity in the gallbladder and biliary tree. Diagnosis of leukemic gallbladder infiltration was made only on microscopic examination of the resected specimen.

In patients who have had bone marrow transplantation, the gallbladder frequently appears abnormal on imaging studies, most commonly demonstrating discrete echogenic nonshadowing luminal foci or masses (sludge) and gallbladder wall thickening on sonography [3]. Graft-vs-host disease has also been known to involve the gallbladder and can result in similar findings [3]. Often compounding the clinical picture are the superimposed effects of parenteral hyperalimentation and hepatotoxic medications, which can also be associated with gallbladder wall thickening. Consequently, gallbladder wall abnormalities seen with sonography or CT may result from a variety of pathologic conditions in bone marrow transplant recipients.

A leukemia patient with clinical and imaging evidence of gallbladder inflammation but without gallstones will usually, and appropriately, be thought to have acalculous cholecystitis [4]. However, as this case shows, leukemic infiltration of the gallbladder wall may closely mimic acalculous cholecystitis and should be considered a diagnostic possibility.

REFERENCES

1. Hoffman R, Benz EI, Shattil SJ, Furie B, Cohen HJ. *Hematology: basic principles and practice.* New York: Churchill Livingstone, **1991**:776–783, 793–804
2. Silverstein MN, Bayrd ED. Nonmeningeal extramedullary relapse in leukemia. *Arch Intern Med* **1969**;123:401–404
3. Frick MP, Snover DC, Feinberg SB, Salomonowitz E, Crass JR, Ramsay NK. Sonography of the gallbladder in bone marrow transplant patients. *Am J Gastroenterol* **1984**;79:122–127
4. Pitkaranta P, Haapianinen R, Taavitsainen M, Elonen E. Acalculous cholecystitis after bone marrow transplantation in adults with acute leukemia. *Eur J Surg* **1991**;157:361–364

Diagnosis of Arteriogenic Impotence: Efficacy of Duplex Sonography as a Screening Tool

Karim Valji[1]
Joseph J. Bookstein

OBJECTIVE. The results of duplex sonography of the cavernosal artery were compared with the results of pharmacoarteriography in a series of impotent men in order to assess the validity of sonography as a screening tool for the diagnosis of arteriogenic impotence.

SUBJECTS AND METHODS. Duplex sonography was performed in 30 impotent men after intracavernosal injection of papaverine and phentolamine. Maximal acceleration, peak systolic velocity, and resistive index were determined for the cavernosal artery. All patients had selective pharmacoarteriography and cavernosometry, which were used to diagnose arterial disease (bilateral hemodynamically significant stenoses or occlusions), suspected arteriolar dysfunction (inconspicuous helicine arterioles), or venoocclusive insufficiency (pharmacologic maintenance erectile flow greater than 25 ml/min). Seventeen patients had arterial insufficiency, four had arteriolar dysfunction, and nine had no significant arterial disease.

RESULTS. Significant differences in Doppler measurements were found between patients without significant arterial disease and those with arterial insufficiency, including peak systolic velocity (50 ± 25 cm/sec vs 33 ± 17 cm/sec, $p = .04$), acceleration (524 ± 261 cm/sec^2 vs 199 ± 111 cm/sec^2, $p < .001$), and resistive index (88 ± 12% vs 73 ± 11%, $p = .002$). Differences were also noted between the group without significant arterial disease and the group with arteriolar dysfunction. When peak systolic velocity of less than 25 cm/sec or acceleration less than 400 cm/sec^2 was used as an indication of inadequate arterial patency, the sensitivities were 35% and 100%, the specificities were 61% and 46%, and the negative predictive values were 42% and 100%, respectively, in the diagnosis of arterial insufficiency.

CONCLUSION. Duplex sonography of the cavernosal arteries may be a useful screening tool in patients with suspected arteriogenic impotence only when acceleration is evaluated in addition to peak systolic velocity. The specificity of the method may be partially limited by the inability to distinguish between arterial and arteriolar disease.

AJR 1993;160:65–69

Penile vascular catheterization (pharmacoarteriography and pharmacocavernosometry) is widely regarded as the gold standard in the diagnosis of vasculogenic impotence [1, 2]. However, the expense, small risk, and mild discomfort associated with these procedures have stimulated interest in less invasive methods to detect those patients who would benefit from the procedure. Nocturnal penile tumescence testing [3], the penile brachial index [4], and response to intracavernosal injection of papaverine [5] have been considered as potential screening tools. Duplex sonography of the cavernosal arteries has received considerable attention since its description in 1985 by Lue et al. [6]. Diminished peak systolic velocity (PSV) and elevated end-diastolic velocity (EDV) are currently used as indexes of arteriogenic and venogenic impotence, respectively [7, 8]; at some centers, the decision to perform vascular catheterization is based on the results of such studies [9]. Despite the popularity and appeal of penile sonography, the validity of accepted velocity thresholds, and of the technique in general, has not been thor-

Received June 16, 1992; accepted after revision July 23, 1992.

[1]Both authors: Department of Radiology, 8756, University of California, San Diego, 225 Dickinson St., San Diego, CA 92103. Address reprint requests to K. Valji.

0361–803X/93/1601–0065

oughly appraised. We performed a prospective study comparing duplex sonography of the cavernosal arteries with pharmacoarteriography in order to assess the validity of sonography as a screening tool for arteriogenic impotence.

Subjects and Methods

Between August 1990 and March 1992, 30 consecutive impotent men referred for initial evaluation of erectile dysfunction had penile vascular catheterization and duplex sonography of the cavernosal arteries. All patients had a history of at least 9 months of inability to achieve erections adequate for intercourse. There was no clinical evidence of an isolated neurogenic cause of impotence in any patient. Serum testosterone was normal in the seven patients in whom results were available. The patients were 17–70 years old (mean, 51 years). Risk factors for arterial disease included a history of tobacco use in 11, diabetes in one, and pelvic trauma in three. Erectile dysfunction had been present since puberty in two patients. Noninvasive studies of erectile function had been performed previously in some cases, but were not considered a prerequisite to angiography. Duplex sonographic studies had been obtained by referring physicians in some cases, but to our knowledge, such studies had not been used to screen patients before referral.

Vascular catheterization was performed in a single outpatient session as previously described [1, 10, 11]; local anesthesia and IV sedation were used. Oblique pelvic arteriograms were obtained to detect aortoiliac disease and to guide selective catheterization. Oblique internal pudendal arteriograms were obtained with an ultralong reverse-curve catheter [12] placed in the mid internal pudendal artery with twofold magnification and film-screen technique. An intracavernosal injection of 60 mg of papaverine (Eli Lilly, Indianapolis, IN) and 1 mg of phentolamine (Regitine, CIBA Pharmaceuticals, Summit, NJ) was given 2–3 min before arteriography to enhance opacification of the penile arteries. Venous outflow was reduced by applying a tourniquet around the base of the penis during and for 1 min after injection in order to prevent immediate washout of agents from the corpora. Additional projections were obtained when penile vessels were obscured because of overlap on the initial films. Studies were bilateral unless the initial arteriogram was clearly normal or clearly showed significant bilateral disease. Arteriograms were interpreted by an experienced vascular radiologist who had no knowledge of the sonographic results. Arteriograms were inspected for variant arterial anatomy, multiplicity of cavernosal arteries, and extent and hemodynamic significance of arterial disease. In addition, the number and size of helicine arterioles were assessed.

The venoocclusive mechanism was evaluated by using the pharmacologic maintenance erectile flow method [10]. After intracavernosal injection of 60 mg of papaverine and 1 mg of phentolamine, normal saline was infused into the corpora cavernosa through a 21-gauge needle, and intracavernosal pressure was recorded simultaneously through a second needle. The pharmacologic maintenance erectile flow was defined as the steady-state flow rate at which intracavernosal pressure was maintained at 150 mm Hg.

Duplex sonography of the cavernosal arteries was performed in all patients either immediately after arteriography (15 patients) or as a separate procedure within 2 weeks after arteriography (15 patients). The technique for intracavernosal injection in both groups was as described earlier. Sonography was performed with an Acuson 128 unit (Acuson, Inc., Mountain View, CA) with a 7.5-MHz B-mode imager and pulsed Doppler probe with real-time spectral analysis. Color Doppler imaging enabled rapid detection of cavernosal arteries and was helpful in obtaining a suitable angle of insonation (always <60°) for accurate angle-corrected velocity calculations. Images were recorded on hard-copy film (3-M Image Manager, Minneapolis, MN) for subsequent analysis. PSV, EDV, resistive index (RI), and acceleration ([PSV – EDV]/pulse rise time) were determined for both cavernosal arteries. In the first 15 patients, Doppler analysis was begun 5 min after injection of the vasodilators for arteriography, and several samples were obtained over the next 8–37 min (mean, 15 min). In the remaining 15 patients, dynamic scanning was started within 2 min after injection of the vasodilators and continued for 13–51 min (mean, 37 min). In the latter group, scanning was continued until the spectral waveform remained unchanged. Mean values of the various Doppler measurements for each patient were calculated by averaging the maximal values obtained in the right and left cavernosal arteries during the entire scanning period. Patients were observed after the procedure to ensure that penile detumescence was complete.

Arteriograms and duplex sonograms were obtained and interpreted independently. *Arterial insufficiency* was defined as the presence of bilateral hemodynamically significant stenoses (indicated by >75% reduction in luminal diameter or by opacification of collateral vessels) or occlusions from the internal iliac to cavernosal arteries. *Arteriolar dysfunction* was suspected when helicine arterioles were very narrow or inconspicuous despite well-demonstrated patency of proximal arteries and intracavernosal pressure less then 35 mm Hg at the time of arteriography. *Venoocclusive dysfunction* was defined as a pharmacologic maintenance erectile flow greater than 25 ml/min [1].

Results are expressed as mean ± SD. Mean flow measurements were compared between patients with early and dynamic scanning by using the unpaired t-test. Mean flow measurements were compared among the various diagnostic groups by using one-way analysis of variance with post hoc testing (SYSTAT Statistical Package, Evanston, IL).

Results

Of the 30 patients examined, nine had no significant arterial disease, 17 had arterial insufficiency diagnosed on the basis of arteriographic findings (10 of whom had coexistent venoocclusive insufficiency), and four had arteriolar dysfunction (two of whom had coexistent venoocclusive insufficiency). The sites of arterial disease were the internal iliac (n = 2), internal pudendal (n = 7), common penile (n = 14), and cavernosal (n = 8) arteries. In 11 patients, accessory cavernosal arteries were detected in addition to the main left and right arteries; six of these patients had no significant arterial disease and five had arterial insufficiency.

The results of arteriography and duplex sonography for patients who had early scanning (n = 15) and dynamic scanning (n = 15) are compared in Table 1. No significant differences in mean values were noted between patients scanned immediately after arteriography and those examined with dynamic scanning at another time. The distributions of mean values of Doppler measurements for individual patients in the three diagnostic groups are given in Figure 1. Compared with patients without significant arterial disease, patients with arterial insufficiency had lower mean acceleration (p < .001), mean PSV (p = .04), and mean RI (p = .002). Significant differences were also found between patients without significant arterial disease (Fig. 2) and those with suspected arteriolar dysfunction (Fig. 3) for PSV (p = .01), acceleration (p = .001), and RI (p = .03).

TABLE 1: Correlation of Results of Duplex Sonography and Pharmacoarteriography in Impotent Men

Results of Arteriography	Results of Duplex Sonography		
	Peak Systolic Velocity (cm/sec)	Acceleration (cm/sec^2)	Resistive Index (%)
No significant arterial disease			
Early scanning (n=5)	58 ± 33	497 ± 336	82 ± 12
Dynamic scanning (n=4)	40 ± 6	559 ± 166	96 ± 4
Total (n=9)	50 ± 25	524 ± 261	88 ± 12
Arterial insufficiency			
Early scanning (n=8)	32 ± 14	213 ± 132	70 ± 8
Dynamic scanning (n=9)	33 ± 21	188 ± 95	76 ± 13
Total (n=17)	33 ± 17	199 ± 111	73 ± 11
Arteriolar dysfunction			
Early scanning (n=2)	22 ± 2	184 ± 38	75 ± 5
Dynamic scanning (n=2)	16 ± 6	126 ± 106	72 ± 9
Total (n=4)	19 ± 5	155 ± 73	73 ± 9

Note.—Values are mean ± SD. Early scanning was performed for a limited time immediately after arteriography.

Statistical analysis of these data in which previously defined [6] and newly established thresholds for the various parameters were used is given in Table 2.

Discussion

The results of our study challenge the validity of current standards used in duplex sonography for the diagnosis of arteriogenic impotence. When the widely accepted threshold for normal PSV in the cavernosal artery (>25 cm/sec) was used, the sensitivity and overall accuracy of the technique were surprisingly low in detecting significant arterial disease. In more than half the patients with significant disease by arteriography, the mean PSV was greater than 25 cm/sec. Importantly, PSV could not be used to distinguish patients with arterial disease from those with narrowing of helicine arterioles, who were suspected of having arteriolar dysfunction.

We found that acceleration in the cavernosal artery was a more sensitive predictor of arterial insufficiency than PSV, although the specificity was low. Other investigators also have found that acceleration correlates well with the results

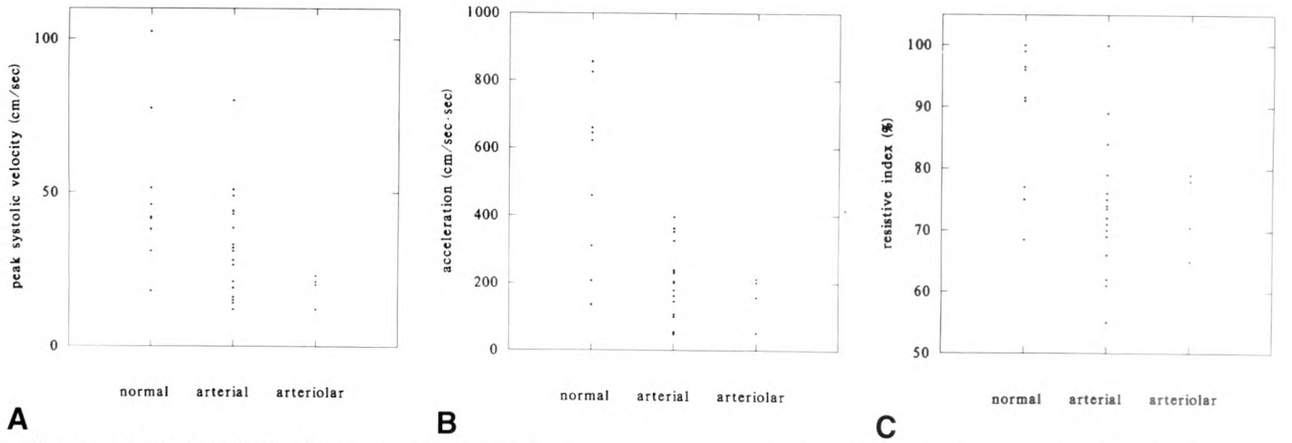

Fig. 1.—*A–C*, Graphs show distribution of mean maximal flow measurements in cavernosal arteries for patients with no significant arterial disease (normal), central arterial insufficiency (arterial), and arteriolar dysfunction (arteriolar). Duplex sonography was used to determine peak systolic velocity (*A*), acceleration (*B*), and resistive index (*C*).

Fig. 2.—Patient with normal supply to penile artery. Selective magnification right internal pudendal arteriogram after intracavernosal injection of vasodilators shows widely patent internal pudendal, common penile, dorsal, and cavernosal arteries. Note prominent opacification of helicine arterioles (*arrow*). Mean Doppler measurements were peak systolic velocity, 52 cm/sec; end-diastolic velocity, 16 cm/sec; acceleration, 459 cm/sec^2; and resistive index, 69%.

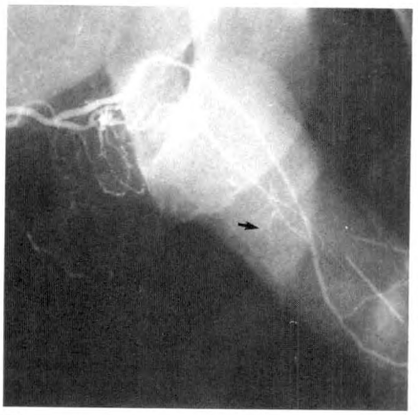

2

Fig. 3.—Patient with arteriolar dysfunction. Selective left internal pudendal arteriogram after intracavernosal injection of vasodilators shows widely patent central arteries but virtually no opacification of helicine arterioles. At duplex sonography, mean Doppler measurements were peak systolic velocity, 20 cm/sec; acceleration, 211 cm/sec^2; and resistive index, 78%.

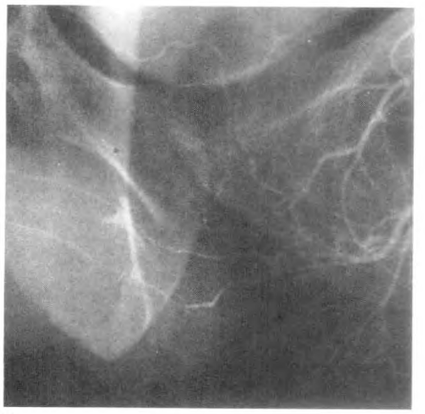

3

TABLE 2: Efficacy of Duplex Sonography in the Diagnosis of Arterial Insufficiency, and of Either Arterial Insufficiency or Arteriolar Dysfunction, in Impotent Men

Threshold Value	Sensitivity (%)	Specificity (%)	Accuracy (%)	Positive Predictive Value (%)	Negative Predictive Value (%)
Arterial insufficiency only					
Peak systolic velocity < 25 cm/sec	35	61	47	55	42
Acceleration < 400 cm/sec^2	100	46	77	71	100
Resistive index < 80%	82	46	67	67	67
Arterial insufficiency or arteriolar dysfunction					
Peak systolic velocity < 25 cm/sec	48	89	60	91	42
Acceleration < 400 cm/sec^2	100	67	90	88	100
Resistive index < 80%	86	67	80	86	67

Note.—All values are percentages.

of arteriography and is a more accurate indicator than PSV of the degree of pharmacologically induced erection [13–15]. Upstream stenoses may cause a slower rate of rise of the transmitted pressure pulse (the "parvus and tardus" pulse), reflected in a lower acceleration. This pattern has been described as a sign of proximal disease in the carotid artery [16]. The hemodynamics of the cavernosal artery are not entirely analagous to the hemodynamics of the carotid arteries, particularly because of the nature of the collateral circulation. Nonetheless, we found measurement of acceleration in the cavernosal artery useful for detecting proximal arterial disease. In our study, a threshold acceleration of 400 cm/sec^2 had a sensitivity of 100%, a specificity of 46%, and an accuracy of 77% in the detection of significant arterial disease. The specificity and accuracy improved if low flow measurements were considered to be diagnostic of either arterial or arteriolar disease.

The RI appeared to be a sensitive predictor of arterial disease in this study. However, we doubt its diagnostic usefulness because we cannot provide a rational explanation for its value in the assessment of the penile vascular system. Because the RI reflects blood flow in the artery and resistance in the distal circulation (helicine arterioles, cavernosal lacunae, and draining venules), both arterial disease and venoocclusive insufficiency will affect the RI. In accord with our previous experience [1], we found that a large fraction of patients with arteriogenic impotence had coexistent venoocclusive disease. Thus, we cannot explain the high sensitivity of the RI for the detection of arterial disease despite large differences in venoocclusive function.

We have recently postulated that disease of the helicine arterioles may contribute to erectile dysfunction in some patients [17]. We suspect arteriolar dysfunction when the helicine branches are poorly seen on magnification arteriograms despite good visualization of the penile arteries. Although the existence of arteriolar disease as a cause of impotence has yet to be proved, we cannot easily dismiss these arteriographic findings, which were clearly present in a small group of patients. Narrowing of the helicine arterioles may have an important functional component in many cases and may result from a number of extrinsic or intrinsic factors (e.g., drug or tobacco use, anxiety, increased sympathetic tone). In such patients, increased resistance from arteriolar disease could reduce flow in the cavernosal artery. PSV and acceleration were diminished in all four patients with suspected arteriolar dysfunction despite normal proximal arteries. Findings in these four patients constituted the majority of false-positive diagnoses of arterial insufficiency based on duplex sonography.

Our results are in conflict with several recently published preliminary studies [6–8] that conclude that duplex sonography may be a sensitive and accurate tool for the diagnosis of arteriogenic impotence. Although a range of PSV values has been observed in volunteers without erectile dysfunction [18], the range of velocities in patients with arterial insufficiency is unknown. Our results show significant variability in PSV for patients with known arteriogenic impotence. Direct correlation between the results of pharmacoarteriography and the results of duplex sonography has been favorable in three studies [8, 19, 20] and unfavorable in one [21]. However, the three series with positive correlations had important limitations. These studies involved direct comparison between sonographic and arteriographic findings in somewhat smaller groups of patients (12 to 25 subjects). Selection bias may have been present because arteriograms were not routinely obtained in patients who had normal PSV values shown by duplex sonography in any study. In addition, it is difficult to be certain that all arteriograms were obtained by using optimal selective magnification techniques. In fact, the lack of optimal techniques for arteriography, cavernosometry, and sonography may limit most studies that compare these techniques.

Several factors may contribute to the inaccuracy of Doppler measurements of the cavernosal artery as predictors of significant arterial disease: (1) The accuracy of flow velocities calculated from Doppler shift frequencies is dependent on an optimal angle of insonation. (2) If Doppler sampling is obtained at a site of cavernosal artery stenosis, velocity measurements may not suggest the presence of disease. For example, one patient in our study with a focal stenosis of the mid cavernosal artery seen at arteriography had a PSV of 28 cm/sec in the proximal cavernosal artery. One minute later, the PSV at the site of the stenosis was 140 cm/sec. (3) Multiple cavernosal arteries are found in many patients.

When sonography is used, the extent of more proximal disease may be overestimated if nondominant arteries with slow flow are sampled. (4) When intracavernosal pressure rises spontaneously above about 35 mm Hg after injection of vasodilators, filling of cavernosal arteries and helicine arterioles may be impeded. Blood flow measurements in this situation may be spuriously diminished. (5) A patient's anxiety may cause marked functional alterations in flow in the cavernosal arteries. Some of these potential pitfalls may be eliminated by meticulous attention to technique, use of color Doppler scanning, and correlation of results with the degree of penile rigidity.

Recent investigations in potent [22] and impotent [23] men have emphasized the dynamic nature of blood flow in the cavernosal artery after pharmacologic relaxation of the corpora cavernosa. Although systolic and diastolic flow is maximal within the first 5 min after injection in most subjects [23], maximal peak velocity occurs later in a small percentage of men. We observed a wide range in the time required to reach maximal systolic velocity and acceleration. Although we did not specifically evaluate the changing spectral patterns in patients, we used the maximal Doppler measurements obtained during the entire scanning period to calculate mean values.

In the first 15 patients in our study, scanning was performed for a short interval immediately after arteriography. In the last 15 patients, prolonged dynamic scanning was performed at a separate sitting. We cannot entirely dismiss the possible effects of arteriography on cavernosal artery flow measurements, especially functional changes that might result from the mild discomfort that some patients experience during contrast injection. However, the absence of significant differences in results between these two groups (Table 1) supports the validity of our findings. In addition, we analyzed the results in patients who had prolonged scanning and found that no errors in diagnosis would have been made if scanning time had been limited to 10 min. Indeed, three errors in diagnosis based on PSV would have been avoided (false-negative cases would have become true-positive cases).

In conclusion, duplex sonography of the cavernosal arteries may not be a reliable screening tool for patients with suspected arteriogenic impotence when PSV alone is evaluated. The technique is more reliable when acceleration in the cavernosal artery is also measured. Thorough assessment of these Doppler parameters may improve the overall value of sonography as a diagnostic tool in these patients. Sonography may also play a role complementary to that of arteriography. For example, when the hemodynamic significance of a stenosis is difficult to establish from an optimal arteriogram, duplex scanning may provide some evidence for the significance of disease. Finally, we postulate that arteriolar dysfunction may be a component of impotence in some patients and may be suspected when acceleration and PSV are diminished on duplex studies and helicine arterioles are inconspicuous at pharmacoarteriography despite patent arteries.

ACKNOWLEDGMENTS

We thank John Forsythe, Holly Lloyd, and Barbara Taylor for assistance in performing sonographic studies.

REFERENCES

1. Bookstein JJ. Penile angiography: the last angiographic frontier. *AJR* **1988**;150:47–54
2. Rosen MP, Schwartz AN, Levine FJ, Greenfield AJ. Radiologic assessment of impotence: angiography, sonography, cavernosography, and scintigraphy. *AJR* **1991**;157:923–931
3. Karacan I, Moore C. Nocturnal penile tumescence: an objective diagnostic aid for erectile dysfunction. In: Bennett AH, ed. *Management of male impotence*. Baltimore: Williams & Wilkins, **1982**:62–72
4. Abelson D. Diagnostic value of the penile pulse and blood pressure: a Doppler study of impotence in diabetics. *J Urol* **1975**;113:636–639
5. Abber JC, Lue TF, Orvis BR, McClure RD, Williams RD. Diagnostic tests for impotence: a comparison of papaverine injection with the penile-brachial index and nocturnal penile tumescence monitoring. *J Urol* **1986**;135:923–925
6. Lue TF, Hricak H, Marich KW, Tanagho EA. Vasculogenic impotence evaluated by high-resolution ultrasonography and pulsed Doppler spectrum analysis. *Radiology* **1985**;155:777–781
7. Benson CB, Vickers MA. Sexual impotence caused by vascular disease: diagnosis with duplex sonography. *AJR* **1989**;153:1149–1153
8. Quam JP, King BF, James EM, et al. Duplex and color Doppler sonographic evaluation of vasculogenic impotence. *AJR* **1989**;153:1141–1147
9. Paushter DM. Role of duplex sonography in the evaluation of sexual impotence. *AJR* **1989**;153:1161–1163
10. Bookstein JJ. Cavernosal venoocclusive insufficiency in male impotence: evaluation of degree and location. *Radiology* **1987**;164:175–178
11. Bookstein JJ, Valji K, Parsons L, Kessler W. Pharmacoarteriography in the evaluation of impotence. *J Urol* **1987**;137:333–337
12. Fellmeth B, Bookstein JJ, Lurie A. Ultralong, reverse-curve angiographic catheter. *Radiology* **1989**;172:872–873
13. Velcek D, Sniderman KW, Vaughan ED, Sos TA, Muecke EC. Penile flow index utilizing a Doppler wave analysis to identify penile vascular insufficiency. *J Urol* **1980**;123:669–672
14. Meuleman EJH, Bemelmans BLH, vanAsten WNJC, Doesburg WH, Skotnicki SH, Debruyne FMJ. The value of combined papaverine testing and duplex scanning in men with erectile dysfunction. *Int J Impotence Res* **1990**;2:87–98
15. Mellinger BC, Fried JJ, Vaughan ED. Papaverine-induced penile blood flow acceleration in impotent men measured by duplex scanning. *J Urol* **1990**;144:897–899
16. Kotval PS. Doppler waveform parvus and tardus: a sign of proximal flow obstruction. *J Ultrasound Med* **1989**;8:435–440
17. Bookstein JJ, Valji K. The arteriolar component of impotence: a possible paradigm shift. *AJR* **1991**;157:932–934
18. Lue TF, Mueller SC, Jow YR, Hwang TI-S. Functional evaluation of penile arteries with duplex ultrasound in vasodilator-induced erection. *Urol Clin North Am* **1989**;16:799–807
19. Schwartz AN, Lowe M, Berger RE, Wang KY, Mack LA, Richardson ML. Assessment of normal and abnormal erectile function: color Doppler flow sonography versus conventional techniques. *Radiology* **1991**;180:105–109
20. Mueller SC, van Wallenberg-Pachaly H, Voges GE, Schild HH. Comparison of selective internal iliac pharmacoarteriography, penile brachial index and duplex sonography with pulsed Doppler analysis for the evaluation of vasculogenic (arteriogenic) impotence. *J Urol* **1990**;143:928–932
21. Rajfer J, Canan V, Dorey FJ, Mehringer CM. Correlation between penile angiography and duplex scanning of cavernous arteries in impotent men. *J Urol* **1990**;143:1128–1130
22. Schwartz AN, Wang KY, Mack LA, et al. Evaluation of normal erectile function with color flow Doppler sonography. *AJR* **1989**;153:1155–1160
23. Fitzgerald SW, Erickson SJ, Foley WD, Lipchik EO, Lawson TL. Color Doppler sonography in the evaluation of erectile dysfunction: patterns of temporal response to papaverine. *AJR* **1991**;157:331–336

Book Review

Diagnostic Imaging in Infertility, 2nd ed. By Alan C. Winfield and Ann Colston Wentz. Baltimore: Williams & Wilkins, 301 pp., 1992. $85

Imagine this television advertisement of the future: A woman is lying on the kitchen floor: "Help, I'm infertile, and I can't get pregnant...." The woman pushes a button on the "key chain of life," and in rushes a radiologist, sonographic probe in one pocket, contrast material in the other. Behind the radiologist is a staff ready to help and with years of experience to offer. Farfetched? Perhaps, but the desperation is genuine, as is the need for imaging specialists to be prepared to offer consultative diagnoses and tests in, at times, truly emergent situations, as biological clocks tick on, further narrowing the pregnancy window.

Pinpointing the cause or causes of "not getting pregnant" is one of the more artful aspects of medical practice. That art is enhanced by the radiologist's palette of tests, with the expanding array of options now approaching the choices in a new crayon box (even color sonography). Where do we start? What test should be used first? Where does a workup begin? What are the risks and benefits of different tests? What can these tests do to help the infertile couple?

The guiding forces in this text are the principal authors: Dr. Winfield from the Department of Radiology and Radiological Sciences, Vanderbilt University Medical Center, and Dr. Wentz from the Department of Obstetrics and Gynecology, Northwestern University School of Medicine. These recognized experts from two different fields give the reader a dual perspective, blending imaging and interpretation with insightful clinical knowledge. As the foreword notes, "teamwork" and "collaboration" in medicine usually result in improved care for patients. The list of contributors to this book reflects this team approach, which likewise benefits the reader, be the reader a radiologist or a gynecologist. Of the nine contributors, four are radiologists.

The book has 14 chapters. The female half of the pregnancy equation gets the most attention in this publication: 12 chapters detailing female "problems" and imaging primarily and one chapter giving an overall view of infertility. Only the last chapter looks at the causes of infertility and the role of imaging in males.

The only criticism I have of this fine text is that it has only 11 pages on imaging males. The expanding urologic literature, especially that on color Doppler sonography and use of papaverine vis-à-vis evaluation of male dysfunction, are not even mentioned, although this is now a hot topic. The technique and expectations of this imaging procedure would be of interest to radiologists who are consulted by colleagues who deal with patients who have sexual problems. Perhaps the next edition could also include more urologic input.

For radiologists who occasionally obtain hysterosalpingograms, the initial chapter reviews the technique, choices of agents, risks, timing, and alternatives—all essential information for improving patient care. For those radiologists who are more experienced in the diagnostic imaging of infertility, the remaining chapters are equally important, as the chapters illustrate, with high-quality radiographs, examples of clinical findings, some common, some not so common. Information difficult to come by in large, less focused radiologic texts is included. The chapter devoted to hysteroscopy is important reading, even for radiologists, because it compares the findings of this "direct" visualization technique with the indirect findings of contrast studies. As the author states, hysteroscopy "complements and adds...accuracy. It does not replace the older (indirect) radiographic technique." Again, the team approach, with radiologists and clinicians interacting, helps guide the art in the therapy. Also, consistently, the illustrations are superb.

The chapter devoted to transvaginal sonography is terrific reading, packing in virtually all anyone needs to know about the application of the technique. This includes invasive transvaginal needle aspiration, clues to subtle uterine abnormalities, and the use of measurements of endometrial thickness to predict the success of a pregnancy. This chapter also touches on using color Doppler sonography to evaluate corpus luteum function and the correlation of this function with pregnancy (although references to a superb body of original work from the United Kingdom would direct readers to more up-to-date information on the use of Doppler studies). The inclusion of the next chapter is a bit curious: it focuses on early pregnancy, a topic too large for this text perhaps. For definitive answers, those most likely involved with patients with infertility would refer questions about imaging to colleagues already expert in obstetric sonography.

In summary, I highly recommend this text. It is a good purchase for libraries, residents, and radiologists in academia or private practice. Buy it. Read it. Share it.

Michael Crade
Long Beach Memorial Medical Center
Long Beach, CA 90801

Correlation of Duplex Sonography with Arteriography in Patients with Erectile Dysfunction

Carol B. Benson[1]
John E. Aruny[1]
Martyn A. Vickers, Jr.[2]

OBJECTIVE. Our objective was to assess the accuracy of using measurements of peak systolic velocity in the cavernosal artery for the diagnosis of arteriogenic impotence.

MATERIALS AND METHODS. Twenty consecutive men with erectile dysfunction had duplex sonography after intracavernosal injection of papaverine to induce an erection. Peak systolic velocities in the right and left cavernosal arteries were measured by using Doppler sonography. Right and left selective penile arteriography was performed with low-osmolality contrast media after intracavernosal injection of papaverine and intraarterial tolazoline. On the basis of the angiographic findings, penile arterial function was classified as normal, moderately insufficient, or severely insufficient. Doppler measurements of peak systolic velocity were correlated with arteriographic results.

RESULTS. All 11 cavernosal arteries with peak velocities less than 25 cm/sec were associated with arterial disease, nine severe and two moderate. Thirteen of 17 cavernosal arteries with peak systolic velocities 25–34 cm/sec were associated with arterial disease, five severe and eight moderate. Only one of the 12 cavernosal arteries with peak velocity at or greater than 35 cm/sec was associated with arterial disease.

CONCLUSION. We conclude that peak systolic velocity in the cavernosal artery as measured on duplex sonography is an accurate predictor of arterial disease in patients with erectile dysfunction. A peak systolic velocity of at least 35 cm/sec indicates normal arterial supply. At peak systolic velocities less than 35 cm/sec, the likelihood and severity of arterial disease increase as the peak systolic velocity decreases, with a peak velocity less than 25 cm/sec indicating a high likelihood of severe arterial disease.

AJR 1993;160:71–73

The hemodynamic function of the penis can be evaluated by performing duplex sonography before and after injection of a vasoactive pharmacologic agent, such as papaverine or prostaglandin E_1, to induce an erection. After injection of one of these pharmacologic agents, the diameter of the cavernosal arteries and peak systolic blood-flow velocity can be used to predict the presence of arterial disease in patients with erectile dysfunction [1–5]. Measurement of the peak systolic velocity in the cavernosal arteries on duplex sonography reportedly correlates well with the presence or absence of arterial disease, but little has been published on the usefulness of duplex sonography for determining the extent or severity of arterial disease. In addition, it is not certain what peak systolic velocity represents the cutoff between normal and abnormal arterial flow. Proposed values include 25, 30, 35, and 40 cm/sec [1–10].

Selective penile arteriography is the gold standard for diagnosing abnormalities of the arterial system [11–14]. The blood supply to the corpus cavernosum is derived from the internal iliac artery, which gives rise to the internal pudendal artery, which in turn supplies the common penile artery and ultimately the cavernosal artery. Intracorporal injection of papaverine followed by selective injection of

Received May 11, 1992; accepted after revision July 28, 1992.

[1]Department of Radiology, Harvard Medical School, Brigham and Women's Hospital, 75 Francis St., Boston, MA 02115. Address reprint requests to C. B. Benson.

[2]Department of Urology, Harvard Medical School, Brigham and Women's Hospital, Boston, MA 02115.

0361–803X/93/1601–0071

the pudendal artery with Priscoline (tolazoline) and then contrast material permits evaluation of the penile, cavernosal, and dorsal arteries on each side [13, 15]. Arterial stenoses and occlusions can be detected [15].

We used selective arteriography to assess prospectively the accuracy of duplex studies of cavernosal arteries for diagnosing the presence and severity of arterial disease in patients with erectile dysfunction. In addition, we determined the peak systolic velocity that most accurately predicted a normal arterial supply to the corpora cavernosa.

Materials and Methods

The study group consisted of 20 consecutive nondiabetic men 19–57 years old (mean, 41 years) who had erectile dysfunction. All patients had normal results on physical examinations, including neurologic examinations, penile biothesiometry (examination to assess sensory neurologic integrity), and endocrine studies.

Each patient was examined as follows. The penis was scanned with Acuson 128 and 128XP units with a 7-MHz linear transducer to look for abnormalities in the cavernosal tissue. A tourniquet was then placed at the base of the penis, and 45–60 mg of papaverine was injected into one corpus cavernosum. The tourniquet was removed 2 min after injection. Several Doppler spectral waveforms were obtained from each of the right and left cavernosal arteries during the 3–7 min after injection. The peak systolic velocity was measured from each spectral waveform; correction was made for the angle of incidence (Fig. 1). The highest peak systolic velocity for each cavernosal artery was used for the study.

Each patient subsequently had arteriography of the distal aorta and pelvic arteries, followed by selective right and left internal pudendal arteriography. Selective angiography was performed after adequate sedation and the intracorporal injection of 60 mg of papaverine. Selective injection of 25 mg of tolazoline into the arterial catheter was followed immediately by injection of 10–15 ml of low-osmolality contrast medium. The 30° ipsilateral anterior oblique projection (Fig. 2) was used for imaging [15].

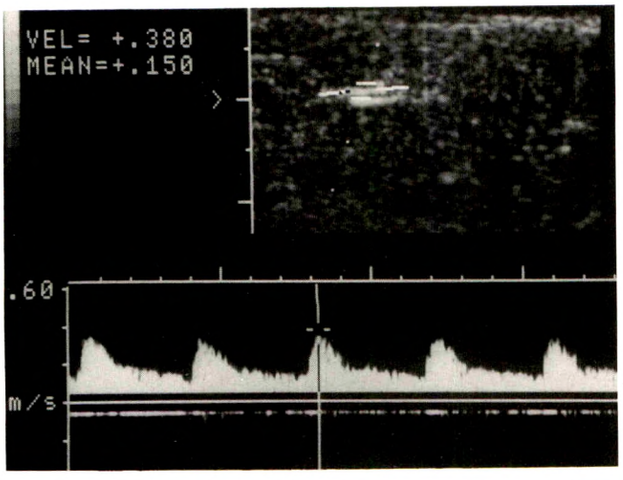

Fig. 1.—Normal cavernosal artery. Duplex sonogram with Doppler gate placed over cavernosal artery *(top)* and spectral waveform *(bottom)*. Caliper indicates peak systolic velocity is 38 cm/sec. Measurement is calculated from Doppler shift, corrected for angle of long axis of cavernosal artery with respect to incident Doppler pulse.

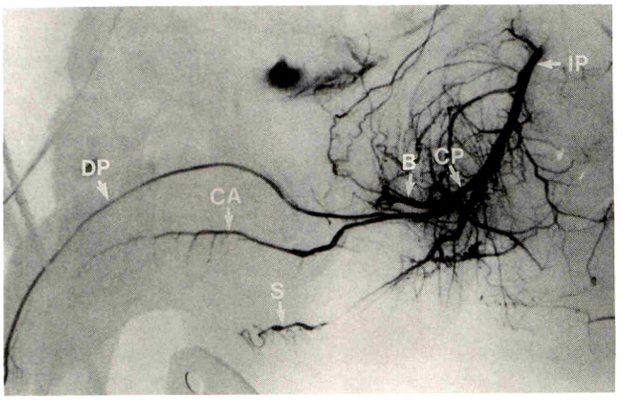

Fig. 2.—Normal selective internal pudendal angiogram. Subtraction angiogram of selective injection of left internal pudendal artery (IP) shows normal common penile (CP), dorsal penile (DP), and cavernosal (CA) arteries. Scrotal branches (S) and artery to bulb (B) are visualized also.

The arterial supply to each side of the penis was classified on the basis of penile arteriography as follows: normal if the internal pudendal, common penile, and cavernosal arteries were normal or normal variants; moderate arterial disease if a single area of greater than 50% stenosis was found in the internal pudendal, common penile, or cavernosal artery; and severe arterial disease if one of the feeding arteries or the cavernosal artery was occluded or multiple stenoses greater than 50% involving both the feeding arteries and the cavernosal artery were found. The peak systolic velocity in the cavernosal artery was correlated with the angiographic classification of arterial patency.

Results

Forty cavernosal arteries were studied in 20 patients. Eleven of these had peak velocities of less than 25 cm/sec. None of the 11 was normal on angiography. Two (18%) of 11 were associated with moderate arterial disease, and the other nine (82%) with severe arterial disease of the proximal feeding arteries, the cavernosal artery, or both.

Ten cavernosal arteries had peak velocities of 25–29 cm/sec. Two (20%) of these were normal on angiography, four (40%) were associated with moderate arterial disease, and four others (40%) with severe disease.

Seven cavernosal arteries had peak velocities of 30–34 cm/sec. Arteriography was normal in two (29%), showed moderate arterial disease in four (57%), and showed severe arterial disease in one (14%).

Twelve cavernosal arteries had peak systolic velocities of 35 cm/sec or greater. Of these, arteriography was normal in 11 (92%) and showed severe arterial disease with compensatory filling from the contralateral side in one (8%).

Overall, as peak systolic velocity increased, the prevalence of angiographically normal cavernosal arteries increased 0% when the peak velocity was less than 25 cm/sec to 92% with peak velocities of 35 cm/sec or greater, and the prevalence of severe arterial disease decreased from 82% with peak velocities of less than 25 cm/sec to 8% with peak velocities greater than 35 cm/sec.

Discussion

Impotence, defined as the inability to generate or maintain an erection adequate for sexual activity, results from organic disease in 50–90% of cases [16, 17]. Most of these cases are the result of hemodynamic dysfunction with arterial insufficiency and/or venous incompetence. Approximately 30% of impotent patients with hemodynamic abnormalities have isolated arterial insufficiency. Another 50% have combined arterial insufficiency and venous incompetence [6]. Thus, arteriogenic factors can be found in approximately 80% of men with impotence resulting from hemodynamic dysfunction [6, 18].

Treatment of arteriogenic impotence depends on the severity of arterial insufficiency. Patients with mild to moderate arterial impairment can be successfully treated with self-injection of vasoactive agents, such as papaverine, phentolamine, or prostaglandin E_1 [4, 18]. Patients with severe arterial disease due to isolated occlusion of one or both feeding arteries to the penis can be treated with angioplasty or bypass surgery [15, 19, 20].

The diagnosis of arterial insufficiency of the penis can be established by using selective penile angiography [10–12, 14]; however, this is an invasive procedure that is expensive and time-consuming, and may be painful. Duplex sonography is a useful technique for diagnosing hemodynamic abnormalities of the penis [1–10]. The consensus in the literature is that the diagnosis of arteriogenic impotence is best determined by measuring the cavernosal arterial peak systolic velocity after intracorporal injection of papaverine [1–10, 16]; however, the cutoff values for peak velocity used to distinguish normal from impaired arterial function vary greatly from 25 cm/sec up to 40 cm/sec [1–10]. A possible explanation for the broad range of proposed cutoff values is that studies evaluating the use of Doppler measurements have used a variety of standards for arterial function. In some studies, the arterial supply was defined as normal if the subject was normally potent [7, 8]. In others, the erectile angle was measured [4–6], and, in others, intracorporal pressure [6, 7]. Furthermore, previous studies did not attempt to determine if peak systolic velocity measurements could be used to predict severity of disease. The goal of our study was to define the best cutoff value of the peak systolic velocity for normal cavernosal arteries and to determine if measurements of peak systolic velocity can be used to assess the severity of disease.

The results of our study, comparing measurements of cavernosal arterial peak systolic velocity with the results of selective penile arteriography, showed a good correlation between the peak systolic velocity and the presence and severity of arterial insufficiency. A peak systolic velocity of 35 cm/sec or greater indicates normal arterial function. Most cavernosal arteries with peak velocities of 25–34 cm/sec have some impairment (76% in our study), and virtually all with peak velocities less than 25 cm/sec have some degree of arterial impairment (100% in our study). The severity of disease also increases as peak velocity decreases: 14% severe disease with peak velocities of 30–34 cm/sec, 40% severe disease with peak velocities of 25–29 cm/sec, and 82% severe disease with peak velocities of less than 25 cm/sec.

In conclusion, our study indicates that the measurement of the cavernosal arterial peak systolic velocity is an accurate method for diagnosing arteriogenic impotence. The measurement can be used to predict the presence or absence of arterial insufficiency; a peak velocity of 35 cm/sec is the best discriminating cutoff value. If arterial disease is present, the severity of disease can be estimated from the peak systolic velocity. Moderate disease is likely if the peak systolic velocity is 25–34 cm/sec, and severe disease is likely if the peak velocity is less than 25 cm/sec.

REFERENCES

1. Lue TF, Hricak H, Marich KW, Tanagho EA. Vasculogenic impotence evaluated by high-resolution ultrasonography and pulsed Doppler spectrum analysis. *Radiology* **1985**;155:777–781
2. Lue TF, Hricak H, Marich KW, Tanagho EA. Evaluation of arteriogenic impotence with intracorporeal injection of papaverine and the duplex ultrasound scanner. *Semin Urol* **1985**;3:43–48
3. Quam JP, King BF, James EM, et al. Duplex and color Doppler sonographic evaluation of vasculogenic impotence. *AJR* **1989**;153:1141–1147
4. Benson CB, Vickers MA. Sexual impotence caused by vascular disease: diagnosis with duplex sonography. *AJR* **1989**;153:1149–1153
5. Hattery RR, King BF, Lewis RW, James EM, McKusick MA. Vasculogenic impotence: duplex and color Doppler imaging. *Radiol Clin North Am* **1991**;29:629–645
6. Lue TF, Mueller SC, Jow YR, Hwang TIS. Functional evaluation of penile arteries with duplex ultrasound in vasodilator-induced erection. *Urol Clin North Am* **1989**;16:799–807
7. Schwartz AN, Wang KY, Mack LA, et al. Evaluation of normal erectile function with color flow Doppler sonography. *AJR* **1989**;153:1155–1160
8. Schwartz AN, Lowe M, Berger RE, Wang KY, Mack LA, Richardson ML. Assessment of normal and abnormal erectile function: color Doppler flow sonography versus conventional techniques. *Radiology* **1991**;180:105–109
9. Shabsigh R, Fishman IJ, Shotland Y, Karacan I, Dunn JK. Comparison of penile duplex ultrasonography with nocturnal penile tumescence monitoring for the evaluation of erectile impotence. *J Urol* **1990**;143:924–927
10. Bassiouny HS, Levine LA. Penile duplex sonography in the diagnosis of venogenic impotence. *J Vasc Surg* **1991**;13:75–83
11. Bookstein JJ, Lang EV. Penile magnification pharmacoarteriography: details of intrapenile arterial anatomy. *AJR* **1987**;148:883–888
12. Schwartz AN, Freidenberg D, Harley JD. Nonselective angiography after intracorporal papaverine injection: an alternative technique for evaluating penile arterial integrity. *Radiology* **1988**;167:249–253
13. Rosen MP, Greenfield AJ, Walker TG, et al. Arteriogenic impotence: findings in 195 impotent men examined with selective internal pudendal angiography. *Radiology* **1990**;174:1043–1048
14. Mueller SC, v. Wallenberg-Pachaly H, Voges GE, Schild HH. Comparison of selective internal iliac pharmaco-angiography, penile brachial index and duplex sonography with pulsed Doppler analysis for the evaluation of vasculogenic (arteriogenic) impotence. *J Urol* **1990**;143:928–932
15. Benson CB, Vickers JR MA, Aruny J. Evaluation of impotence. *Semin Ultrasound CT MR* **1991**;12:176–190
16. Krysiewicz S, Mellinger BC. The role of imaging in the diagnostic evaluation of impotence. *AJR* **1989**;153:1133–1139
17. Paushter DM. Role of duplex sonography in the evaluation of sexual impotence. *AJR* **1989**;153:1161–1163
18. Benson CB, Doubilet PM, Vickers MA Jr. Sonography of the penis. *Ultrasound Q* **1991**;9:89–109
19. Goldstein I. Overview of types and results of vascular surgical procedures for impotence. *Cardiovasc Intervent Radiol* **1988**;11:240–244
20. Virag R, Zwang G, Dermange H, Legman M. Vasculogenic impotence: a review of 92 cases with 54 surgical operations. *Vasc Surg* **1981**;15:9–17

Radiologic-Pathologic Conferences of the Massachusetts General Hospital

Transitional Cell Carcinoma

Michael H. Lev and Felix S. Chew[1]

A 48-year-old man with repeated episodes of gross hematuria and a diagnosis of "stone disease" complained of left flank pain. An excretory urogram revealed a mass in the upper pole of the left kidney and irregular filling defects (Fig. 1A). A contrast-enhanced CT scan showed the mass was within the collecting system (Fig. 1B). The bladder and ureter were normal, and results of cytologic examination of the urine were normal. After nephroureterectomy, a bulky, sessile, papillary tumor arising from the uroepithelium was found in the upper pole. Microscopy revealed focal invasion of the renal parenchyma, and the final pathologic diagnosis was papillary transitional cell carcinoma, grade 2/3.

Papillary transitional cell carcinomas constitute the vast majority of renal pelvocaliceal tumors; only 7–8% of all malignant renal tumors are found in this location. The most remarkable etiologic factor in the occurrence of these uroepithelial tumors is exposure to industrial chemical carcinogens, particularly *o*-aminophenols common in the dyestuff, rubber, cable, plastic, and gas industries. Abuse of phenacetin, which is metabolized to an *o*-aminophenol and excreted in the urine, is also associated with these tumors [1].

The gross appearance of papillary transitional cell carcinomas has been described as soft, bulky, tan-pink, translucent, and glistening, sometimes with an aborescent surface formed by a myriad of delicate filiform projections from the neoplastic epithelium [1, 2] (Figs. 1C and 1D). Because these mucosal tumors usually are sessile and exophytic, their imaging appearance is that of an intraluminal mass that distorts and sometimes obliterates or obstructs the lumen [3]. The filiform surface of the tumor results in an irregular, blurred interface with the administration of contrast material. Less commonly, the tumors are smooth and infiltrating or polypoid. Patients with tumors that obstruct the urinary tract may present when the tumors are small, but patients with tumors that do not obstruct the urinary tract may not present until the tumors are large. The tumors enhance on CT, but most are hypovascular on angiography [3].

Transitional cell carcinoma is more common in males, and the prevalence increases with age (average age at diagnosis is 65 years). The most common signs and symptoms are gross hematuria and pain. Findings on urine cytology are false-negative in about 40% of such tumors in the renal pelvis. Because of the likelihood of metachronous and synchronous lesions, treatment is usually total nephroureterectomy.

REFERENCES

1. Bennington JL, Beckwith JB. *Tumors of the kidney, renal pelvis, and ureter.* Washington, DC: Armed Forces Institute of Pathology, **1975**:243–311
2. Weiss MA, Mills SE. *Atlas of genitourinary tract disorders.* Philadelphia: Lippincott, **1988**:11.46–11.54
3. Leder RA, Dunnick NR. Transitional cell carcinoma of the pelvicalices and ureter. *AJR* **1990**;155:713–722

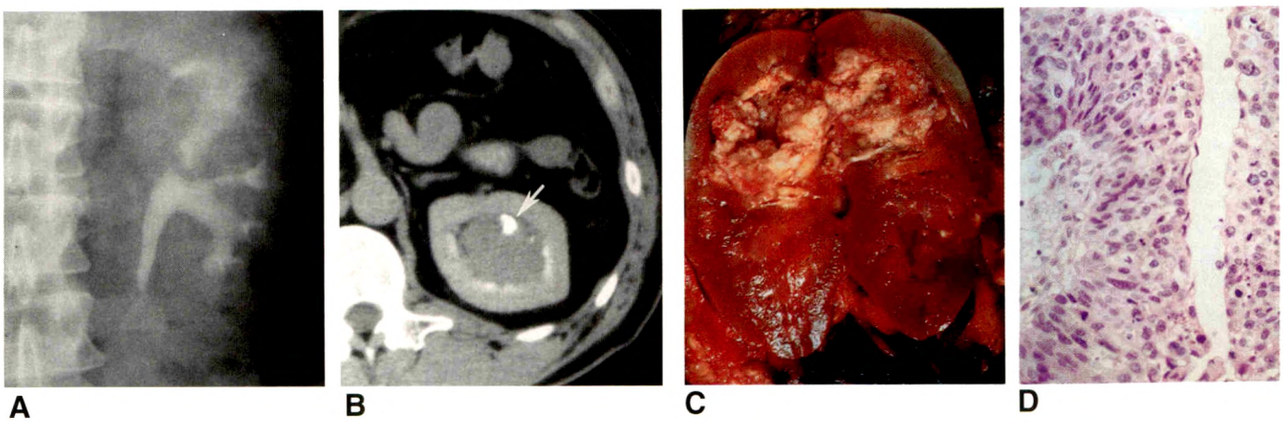

Fig. 1.— Transitional cell carcinoma.
***A*, Excretory urogram shows infundibulum of upper pole distorted by mass with irregular surface.**
***B*, CT scan with IV contrast enhancement shows mass filling collecting system of upper renal pole and displacing the contrast-filled lumen (*arrow*).**
***C*, Coronally sectioned nephroureterectomy specimen shows a bulky lesion with an aboresecent, glistening surface.**
***D*, High-power photomicrograph shows a filiform projection.**

From the weekly radiologic-pathologic correlation conferences conducted by Jack Wittenberg. Pathology editor: Andrew E. Rosenberg. Radiology editors: Felix S. Chew, William E. Palmer, Daniel I. Rosenthal

[1]Both authors: Department of Radiology, Massachusetts General Hospital and Harvard Medical School, 32 Fruit St., Boston, MA 02114. Address reprint requests to F. S. Chew.

Imaging of En Bloc Renal Transplants: Normal and Abnormal Postoperative Findings

David S. Memel[1]
Gerald D. Dodd III[1]
Ajit N. Shah[1]
Albert B. Zajko[1]
Mark L. Jordan[2]
Ron Shapiro[2]
Thomas R. Hakala[2]

OBJECTIVE. Cadaveric kidneys from donors less than 5 years old, previously considered inferior graft material, are now being successfully transplanted en bloc into children and adults. On the basis of our experience with 132 patients, we describe the general principles of the procedure and review the spectrum of normal and abnormal imaging findings in patients who have undergone this promising transplantation procedure.

MATERIALS AND METHODS. Paired cadaveric kidneys obtained from donors less than 5 years old (mean age, 24 months) were transplanted en bloc to 132 patients (mean age, 37 years) at our institution between 1981 and 1991. All available medical, surgical, pathologic, and imaging records were retrospectively reviewed to define the surgical technique, 1-year survival rate of the graft, appearance of the transplant on postoperative imaging studies, and the prevalence of and imaging findings caused by vascular, urinary, infectious, and neoplastic complications after transplantation. Complications were confirmed by a definitive imaging study, surgical exploration, or study of a pathologic specimen.

RESULTS. Paired donor kidneys were transplanted en bloc extraperitoneally into the recipient's right or left iliac fossa, with intact portions of the donor aorta and inferior vena cava anastomosed to the recipient's external iliac artery and vein. One-year graft survival was 70% during the first 8 years of the study and 78% during the last 2 years. Postoperative imaging, particularly sonography and scintigraphy, clearly depicted the normal individual kidneys, urinary collecting systems, and en bloc vasculature. Postoperative complications were vascular (arterial stenoses and thromboses, venous thromboses, and pseudoaneurysms) in 18%, urinary (obstruction and anastomotic leak) in 11%, infectious (caliceal fungal balls) in 1%, and neoplastic (posttransplant lymphoma) in 1%. The complications involved one kidney in 60% of the patients and both kidneys in 40%. The imaging findings caused by these complications were similar to those caused by complications occurring after transplantation of single cadaveric kidneys; however, their detection was more difficult because of the complexity of the en bloc graft.

CONCLUSION. Because of the shortage of available donor organs, en bloc renal transplantation will most likely become increasingly popular. Familiarity with the imaging appearance of the normal transplant and of posttransplantation complications will allow radiologists to perform effective postoperative imaging evaluations.

AJR 1993;160:75–81

Received May 11, 1992; accepted after revision July 7, 1992.

Presented at the annual meeting of the American Roentgen Ray Society, Orlando, FL, May 1992.

[1]Department of Radiology, University of Pittsburgh Medical Center, Presbyterian University Hospital, DeSoto at O'Hara Sts., Pittsburgh, PA 15213. Address reprint requests to G. D. Dodd III.

[2]Department of Surgery, University of Pittsburgh Medical Center, Presbyterian-University Hospital, DeSoto at O'Hara Sts., Pittsburgh, PA 15213.

0361–803X/93/1601–0075

Renal transplantation is the preferred treatment for most patients with end-stage renal disease [1–3]. Although the number of patients requiring renal transplantation increases annually, the number of renal transplantations done each year is limited by a chronic shortage of donor organs [4–8]. Although kidneys from children are considered by many surgeons to be inferior graft material, the increasing demand for donor organs has led to a reevaluation of the use of cadaveric kidneys from young (<5 years old) donors [4, 8–11]. With advances in surgical techniques and the use of new immunosuppressive medications, children and

adults who have en bloc transplantation of paired cadaveric kidneys from young donors have a 1-year graft survival rate similar to that obtained with transplantation of single cadaveric kidneys from adults [4, 9, 10]. On the basis of our experience with 132 patients who received en bloc renal transplants of paired cadaveric kidneys from young donors, we describe the general principles of the procedure and the spectrum of imaging findings seen after transplantation.

Materials and Methods

Between January 1981 and November 1991, paired cadaveric kidneys from young donors were transplanted en bloc to 132 patients at our institution. Of these 132 patients, 125 had complete preoperative and postoperative clinical records available for review. We retrospectively reviewed these records (medical, surgical, pathologic, and imaging) to ascertain the surgical technique used, define the imaging appearance of the graft after transplantation, and determine the prevalences and imaging appearances of vascular, urinary, infectious, and neoplastic complications after transplantation. All complications were confirmed by a definitive imaging study (such as angiography in the case of vascular complications), surgical exploration, or examination of a pathologic specimen. The follow-up period after transplantation ranged from 3 months to 10 years, with at least 1-year follow-up in 72% of patients. Follow-up consisted of clinical examination and indicated imaging studies. We did not evaluate medical complications (rejection, acute tubular necrosis, recurrent disease, or immunosuppressant toxicity) or complications related to transplant biopsies, as these have no characteristics unique to the procedure we describe, occur with a prevalence similar to that reported for transplantation of a single cadaveric kidney from an adult (Jordan ML, personal communication), and have already been extensively reported in the radiologic literature pertaining to transplants from adults.

The recipients consisted of 69 males and 63 females, 6–72 years old (mean, 37 years). All donors were less than 5 years old (mean, 24 months). The immunosuppressive regimen for patients (n = 88) who received transplants between January 1981 and November 1989 consisted of cyclosporine (Sandimmune; Sandoz, East Hanover, NJ) and prednisone (Deltasone; Upjohn, Kalamazoo, MI) with or without azathioprine (Imuran; Burroughs Wellcome, Research Triangle Park, NC). For patients (n = 44) who received transplants after November 1989, the immunosuppressive regimen consisted of FK 506 (Fujisawa Pharmaceutical Company, Osaka, Japan) and prednisone.

The imaging studies reviewed included renal sonograms from 89 patients, ^{99m}Tc-diethylenetriamine pentaacetic acid (^{99m}Tc-DTPA) renal scintigrams from 87, abdominal and pelvic CT scans from 23, excretory urograms from seven, cystograms or voiding cystourethrograms from 15, nephrostograms from two, angiograms from eight, and MR images from two. The imaging equipment used changed during the 10 years studied; however, since 1983, most sonograms were obtained with the Acuson Model 128 Computed Sonography system (Acuson, Mountain View, CA) with a 3.5- or 5-MHz transducer; renal scintigrams were obtained with a Siemens Orbiter 3700 Rotating Gamma Camera (Siemens Medical Systems Inc., Des Plaines, IL); and CT scans and MR images were obtained with a GE 9800 CT and 1.5-T Signa MR system, respectively (GE Medical Systems, Milwaukee, WI).

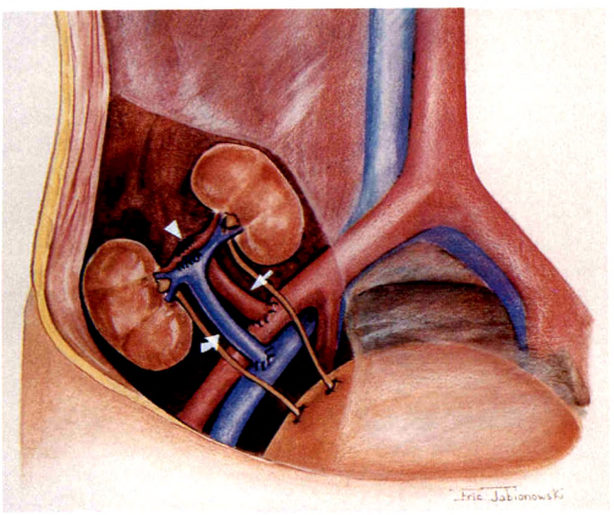

Fig. 1.—Drawing shows extraperitoneal location in right iliac fossa of en bloc transplant of cadaveric kidneys from a young donor. The donor aorta (*straight arrow*) and inferior vena cava (IVC, *curved arrow*) anastomose end-to-side to recipient's external iliac artery and vein. Note oversewn ends of donor aorta and IVC (*arrowhead*) and anterior location of ureters.

Results

Surgical Technique and Normal Postoperative Anatomy

Paired cadaveric kidneys from young donors were harvested en bloc with preservation of the ureters, main renal arteries and veins, and segments of suprarenal and infrarenal abdominal aorta and inferior vena cava (IVC). Before the transplants were placed in the recipient's pelvis, the donor aorta and IVC were oversewn just cephalad to the origin of the renal arteries and veins, and all side branches of the donor aorta and IVC were ligated. The donor kidneys were then preferentially placed extraperitoneally into the recipient's right iliac fossa unless the presence of scarring or a previous graft mandated placement in the left side of the pelvis. The caudal ends of the donor aorta and IVC were anastomosed end-to-side to the recipient's external iliac artery and vein, respectively. If the donor aorta and IVC were too short, arterial and venous cadaveric extension grafts were sewn end-to-end to the caudal ends of the donor aorta and IVC and end-to-side to the recipient's external iliac artery and vein. The donor ureters were implanted into the recipient's bladder through individual or common ureteroneocystostomies (Fig. 1).

The final orientation of the paired donor kidneys in the recipient's pelvis varied from patient to patient. The kidneys' relationship to each other was anterior-posterior, cranial-caudal, or medial-lateral, depending on the constraints imposed by the length of the donor ureters and vessels and the recipient's pelvic anatomy. Regardless of the orientation of the transplanted kidneys, the donor IVC coursed anterior to the donor aorta and the recipient's external iliac artery before anastomosing with the recipient's ipsilateral external iliac vein. The donor ureters arose posterior to the vessels in the renal pelves and coursed anterior to the donor aorta and IVC and the recipient iliac vessels before anastomosing with the recipient's bladder (Fig. 2).

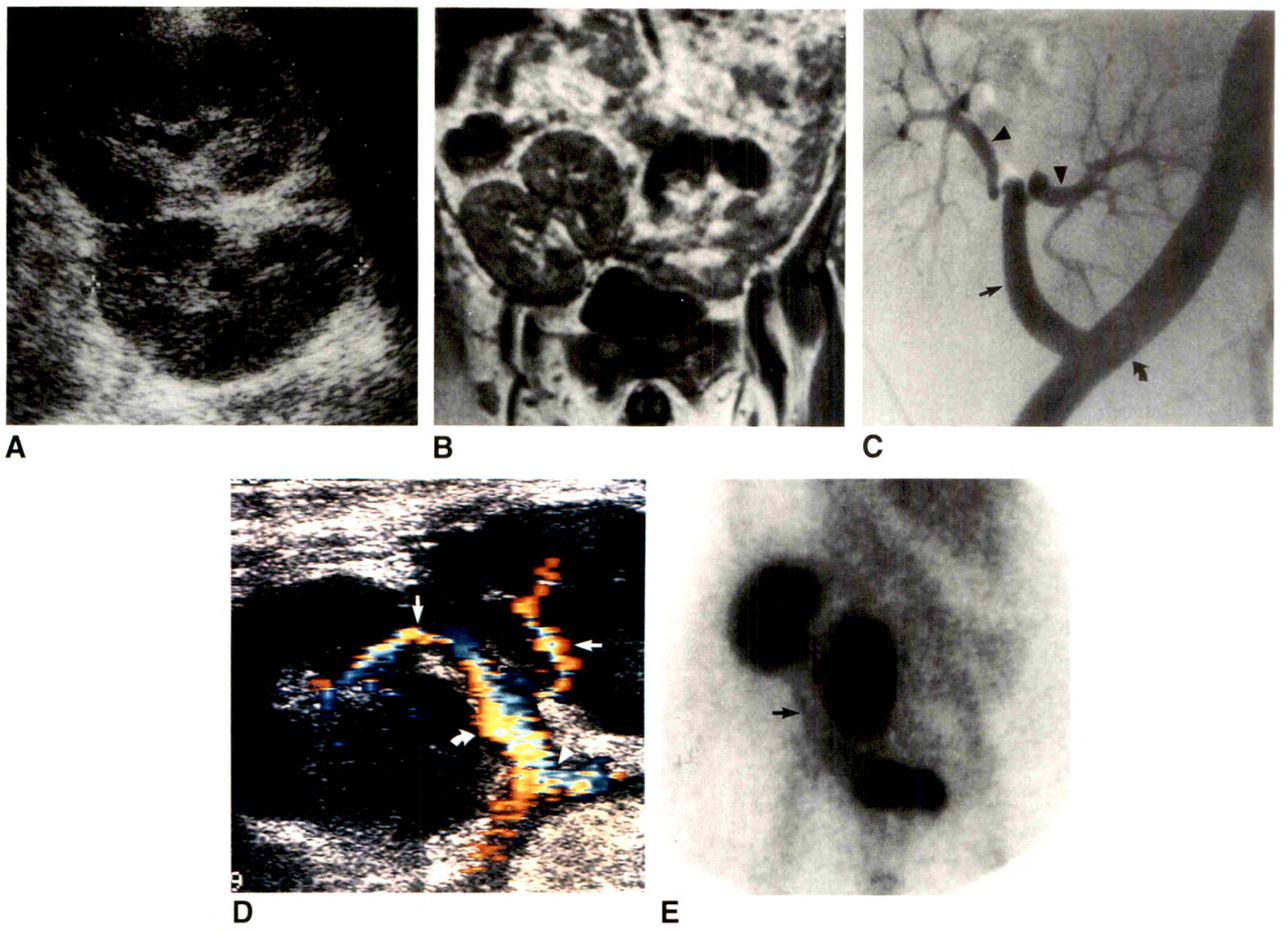

Fig. 2.—Normal imaging findings after en bloc transplantation of paired cadaveric kidneys from a young donor.

***A*, Sagittal sonogram of right side of pelvis shows transplanted kidneys in an anterior-posterior orientation. Note clear depiction of two separate kidneys.**

***B*, T1-weighted (600/20) coronal MR image shows paired kidneys in right iliac fossa in a medial-lateral orientation, with medial kidney positioned cephalad.**

***C*, Arteriogram shows donor aorta (*straight arrow*) anastomosed end-to-side to the recipient external iliac artery (*curved arrow*). Note donor main renal arteries (*arrowheads*).**

***D*, Transverse color Doppler sonogram shows normal donor main renal arteries (*straight arrows*), donor aorta (*curved arrow*), and anastomosis of donor aorta to recipient's external iliac artery (*arrowhead*).**

***E*, Renal scintigram shows normal function in both transplanted kidneys. Note medial-lateral orientation, with lateral kidney positioned cephalad. Ureters (*arrow*) can be detected coursing toward recipient's bladder.**

Graft Survival

The overall 1-year graft survival rate in our study population was 70%. The 1-year graft survival rate in the subgroup of patients who received transplants after November 1989 and received FK 506 was 78%.

Complications After Transplantation

Thirty-eight (30%) of the 125 patients with complete clinical records for the follow-up period after transplantation had a total of 43 complications. The imaging studies of 30 of the 38 patients were available for review and were found to show all (n = 34) complications in these patients.

Vascular complications.—Twenty-two patients (18%) had a total of 26 vascular complications, including arterial stenoses and thromboses, venous thromboses, and pseudoaneurysms. Arterial stenoses occurred in four patients (3%). Three of the patients had unilateral stenosis of a renal artery, and one patient had stenosis at the anastomosis of the donor aorta to the recipient external iliac artery. Imaging studies of three of the four patients were available for review. In all cases, stenosis was initially diagnosed on the basis of sonograms, which showed a focal increase in arterial velocity at the stenotic site. In one of the patients with unilateral stenosis of a renal artery, marked dampening of the intrarenal arterial flow in one kidney led to the search for and discovery of ipsilateral high-velocity flow in the main renal artery, indicative of a significant stenosis. Flow to the contralateral kidney was normal (Fig. 3). Angiography was performed in two of the four patients with renal artery stenosis, and the angiographic findings confirmed the sonographic findings in both cases (Fig. 4).

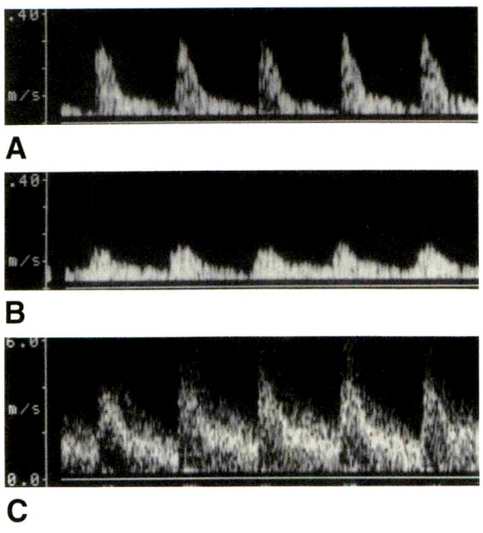

Fig. 3.—*A–C*, Unilateral stenosis of main renal artery of medial en bloc transplanted cadaveric kidney from a young donor.

***A*, Angle-corrected Doppler waveform of interlobar artery in lateral kidney shows rapid systolic upstroke, peak velocity of 0.3 m/sec, and moderate difference between peak systolic and lowest diastolic flow.**

***B*, Angle-corrected Doppler waveform of interlobar artery in medial kidney shows slower systolic upstroke, lower peak velocity (0.15 m/sec), and less difference between peak systolic and lowest diastolic flow than in lateral kidney.**

***C*, Angle-corrected Doppler waveform of main renal artery of medial transplanted kidney shows peak velocities greater than 6.0 m/sec, with spectral broadening highly suggestive of a significant stenosis.**

Arterial thromboses occurred in 12 patients (10%). Four patients (3%) had unilateral renal artery thrombosis and eight (6%) had aortic graft thrombosis or bilateral renal artery thrombosis. Imaging studies of nine of the 12 patients were available for review. The arterial thromboses were detected with sonography in seven patients and scintigraphy in two. Color and duplex Doppler sonography showed arterial and venous flow in only one of the paired transplant kidneys in patients with unilateral renal artery thrombosis. In patients with aortic graft thrombosis or bilateral renal artery thrombosis no arterial or venous flow was shown in either kidney. Renal scintigraphy showed unilateral renal artery thrombosis as a region of decreased uptake of radionuclide ("cold spot"), relative to background radioactivity, in the location of the thrombosed kidney (Fig. 5). In one patient with chronic unilateral renal artery thrombosis, CT showed that the infarcted kidney was markedly atrophic (Fig. 6). Angiographic correlation was obtained in three patients and confirmed the sonographic findings in each case. Surgical confirmation was obtained in all 12 of the patients with arterial thromboses.

Venous thromboses occurred in eight patients (6%). Three (2%) had unilateral renal vein thrombosis, and five (4%) had IVC graft thrombosis or bilateral renal vein thrombosis. Imaging studies of five of the eight patients were available for review. Venous thromboses were detected with color and duplex Doppler sonography in three patients and with renal scintigraphy in two. Sonography in patients with unilateral renal vein thrombosis showed that one of the paired transplanted kidneys, the one without renal vein thrombosis, had a normal imaging appearance. The kidney with renal vein thrombosis was enlarged, had decreased parenchymal echogenicity, no renal venous flow, and prolonged reversed diastolic arterial flow (Fig. 7). Sonography in patients with IVC graft thrombosis or bilateral renal vein thrombosis showed that both kidneys were enlarged, with decreased echogenicity, no venous flow in the IVC graft or both main renal veins, and prolonged reversed diastolic arterial flow in the aortic graft or both main renal arteries. Renal scintigraphy in patients with unilateral renal vein thrombosis showed normal uptake of radionuclide in one kidney and almost total absence of uptake in the kidney with renal vein thrombosis. In patients with IVC graft or bilateral renal vein thrombosis, neither kidney was visualized, and uptake of radionuclide in the transplant bed matched the background radioactivity in

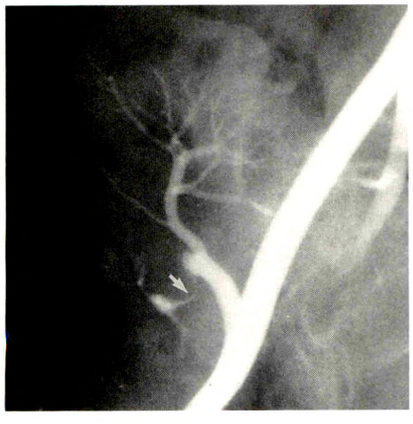

Fig. 4.—Unilateral stenosis of main renal artery of lateral en bloc transplanted cadaveric kidney from a young donor. Arteriogram shows a stenosis (*arrow*) involving most of main renal artery.

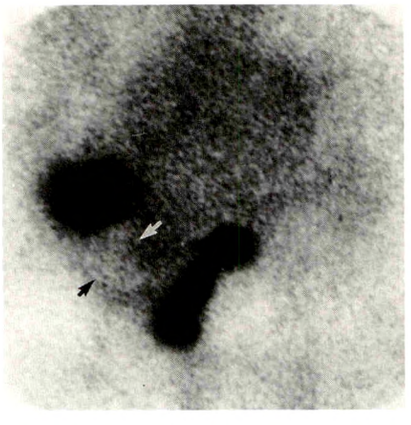

Fig. 5.—Acute unilateral thrombosis of main renal artery in inferomedial en bloc transplanted cadaveric kidney from a young donor. Renal scintigram shows a cold spot (*arrows*) in region of inferomedial kidney situated between nephrogram of superolateral kidney and bladder.

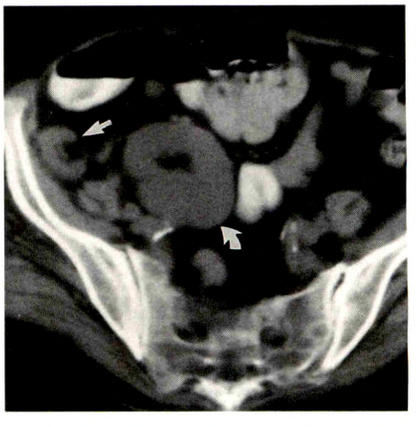

Fig. 6.—Chronic unilateral thrombosis of main renal artery in lateral en bloc transplanted cadaveric kidney from a young donor. Unenhanced axial CT scan of pelvis shows an atrophic lateral kidney (*straight arrow*) and a normal-sized medial kidney (*curved arrow*).

the pelvis. Venous thrombosis was confirmed surgically in all patients.

Extrarenal pseudoaneurysms occurred in two patients (2%). The location of the pseudoaneurysm was the site of the oversewn end of the donor aorta in one patient and the anastomosis of the donor aorta to the external iliac artery in the other. In the latter patient the pseudoaneurysm was mycotic in origin. Both pseudoaneurysms were initially detected on color and duplex Doppler sonograms as anechoic, cystic structures with turbulent pulsatile flow in their lumen (Fig. 8A) and to-and-fro flow at their neck (Fig. 8B). Angiographic confirmation was obtained in both cases (Fig. 8C). In one case, the pseudoaneurysm was seen as a focal area of intermediate signal on T1-weighted spin-echo MR images and as an area of high signal on gradient-echo MR images obtained in the region of the renal hila.

Urinary complications.—Fourteen patients (11%) had a total of 15 urinary complications. The complications included unilateral ureteral obstruction in seven (6%) and unilateral anastomotic urine leaks in eight (6%). Imaging studies were available for review in six of the seven patients with ureteral obstruction. Sonography showed unilateral hydronephrosis, and scintigraphy confirmed the obstructive nature of the hydronephrosis in all six cases available for review. Nephrostograms were used to localize the site of obstruction in two patients. In one patient, unilateral hydronephrosis due to a stricture at the ureteropelvic junction was detected on CT scans (Fig. 9) and confirmed with a nephrostogram.

Imaging studies were available for review in seven of the eight patients with urinary leaks. Sonography showed perinephric fluid collections in all seven cases. The fluid was nonspecific in appearance and randomly located in the transplant bed. Renal scintigraphy confirmed the presence of the leaks by showing extravasation of radionuclide in each of the patients. Contrast cystography was performed in addition to sonography and scintigraphy in four of the seven patients with leaks and showed extravasation of contrast material in all four patients. In one patient, an excretory urogram showed extravasation of contrast material (Fig. 10).

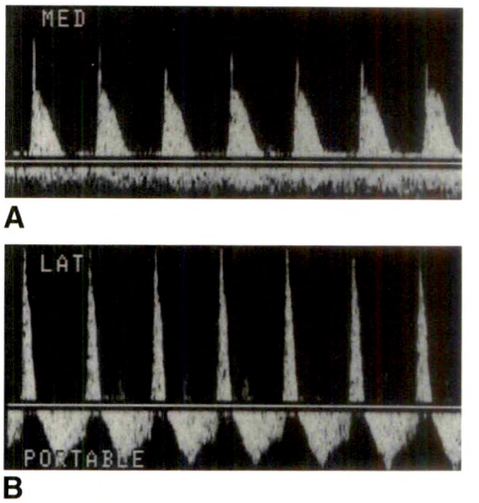

Fig. 7.—*A* and *B*, Unilateral thrombosis of main renal vein in lateral en bloc transplanted cadaveric kidney from a young donor. Angle-corrected Doppler waveforms of interlobar arteries of medial (*A*) and lateral (*B*) kidneys are significantly different. Doppler waveform of lateral kidney shows prolonged reversed diastolic flow; venous flow was not detectable. This combination of findings is highly suggestive of unilateral renal vein thrombosis.

Infectious and neoplastic complications.—Two patients (2%) had one miscellaneous complication each. The complications included unilateral calcified fungus balls in the renal collecting system of one patient (Fig. 11) and bilateral posttransplantation lymphoproliferative disorder in the renal parenchyma of the other. The latter complication initially was seen as a unilateral focal hypoechoic renal mass. After unilateral graft nephrectomy, a new mass associated with posttransplantation lymphoma subsequently developed in the remaining transplanted kidney.

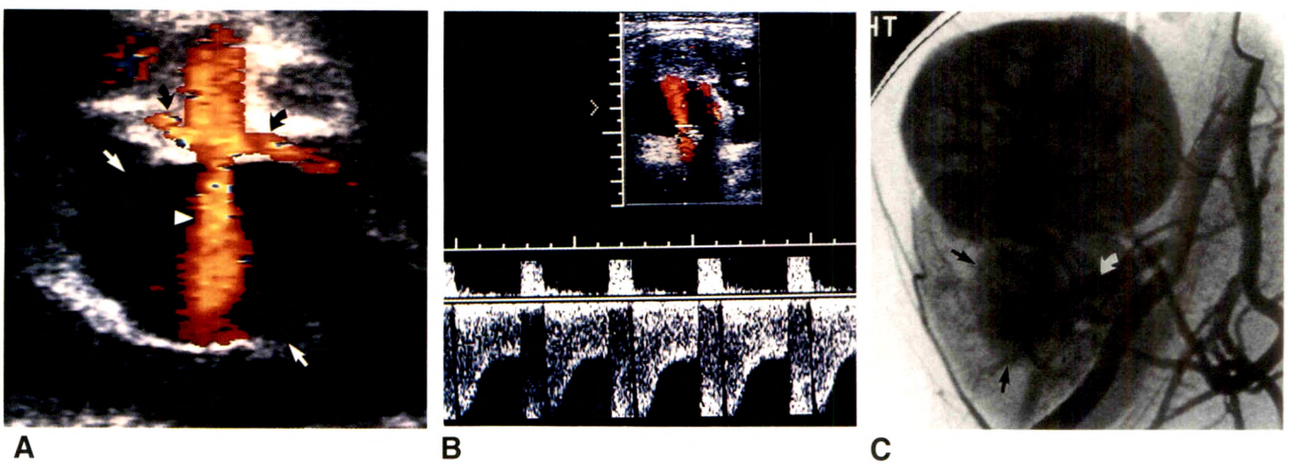

Fig. 8.—Extrarenal pseudoaneurysm of en bloc transplanted paired cadaveric kidneys from a young donor.
***A*, Color Doppler sonogram shows cystic mass (*straight arrows*) arising from oversewn end of donor aorta adjacent to origin of main renal arteries (*curved arrows*). Note color jet (*arrowhead*) from oversewn end of aorta into cyst.**
***B*, Duplex Doppler sonogram at origin of color jet shows to-and-fro flow characteristic of a pseudoaneurysm.**
***C*, Corresponding arteriogram obtained with tip of catheter in recipient common iliac artery shows contrast material opacifying a spherical extravascular structure (*straight arrows*), arising from oversewn end of donor aorta (*curved arrow*), that was surgically confirmed to be a pseudoaneurysm.**

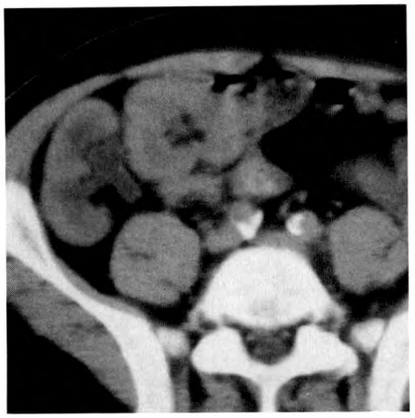

Fig. 9.—Unilateral hydronephrosis in lateral en bloc transplanted cadaveric kidney from a young donor. Unenhanced axial CT scan of pelvis shows dilatation of pelvicaliceal system of lateral kidney. Pelvicaliceal system in medial kidney is normal.

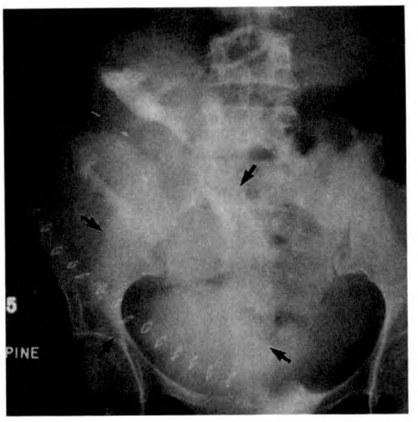

Fig. 10.—Unilateral urine leak from ureteral anastomosis of medial en bloc transplanted cadaveric kidney from a young donor. Anteroposterior excretory urogram shows abundant extravasated contrast material (*arrows*) in right side of pelvis, displacing medial ureter and bladder and causing mild dilatation of pelvicaliceal system and ureter of medial kidney.

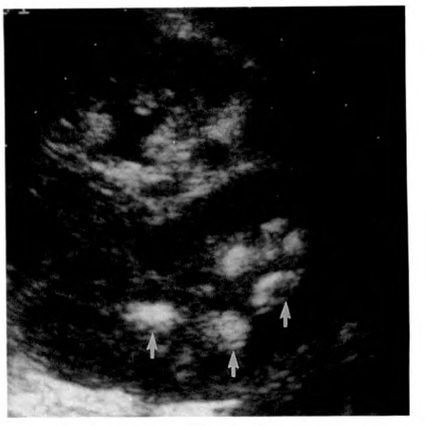

Fig. 11.—Unilateral calcified caliceal fungus balls (*Candida albicans*) in medial en bloc transplanted cadaveric kidney from a young donor. Longitudinal sonogram of pelvis shows echogenic material (*arrows*) in calices of posteromedial kidney. Corresponding CT scan (*not shown*) showed echogenic material had an attenuation value consistent with that of calcium. Urine cultures grew *C. albicans*.

Discussion

Single kidneys from cadaveric donors less than 5 years old are considered by many surgeons to be unacceptable grafts for renal transplantation. Perceived limitations include limited functional renal mass and the small size of the main renal arteries and veins [4, 6, 10, 12]. The limited functional renal mass of single allografts from young donors prevents the grafts from providing complete renal excretory function in adult recipients for at least 2–3 months after transplantation and limits the ability of the grafts to withstand episodes of rejection. The small size of the grafts' main renal arteries and veins significantly increases the technical difficulty of transplantation and the prevalence of vascular complications after transplantation.

En bloc transplantation of paired cadaveric kidneys from young donors was developed in an attempt to overcome these limitations [4, 9–11, 13]. The transplantation of two kidneys into one recipient doubles the amount of functional renal mass present in the immediate postoperative period, thus more closely approximating the renal mass of a single cadaveric kidney transplanted from an adult. The greater renal mass provided by en bloc transplantation of paired cadaveric kidneys from young donors allows earlier assumption of normal excretory function in adult recipients and increases the capacity of the graft to withstand episodes of rejection. The prevalence of rejection, acute tubular necrosis, recurrent disease, and immunosuppressant toxicity in en bloc renal grafts is similar to that reported for single cadaveric renal grafts from adults (Jordan ML, personal communication). When the kidneys are transplanted en bloc with intact segments of abdominal aorta and IVC, the donor aorta and IVC can be used for the vascular anastomoses. The use of these larger vessels overcomes some of the technical difficulties and complications associated with small-vessel surgery. The combination of these inherent advantages, current methods of organ preservation, refined surgical techniques, and new immunosuppressive agents is producing a 1-year graft survival rate that rivals the survival rate for single cadaveric kidneys transplanted from adults [4, 9, 10].

Postoperative vascular complications of en bloc transplantation of paired cadaveric kidneys from young donors are similar to those seen with transplantation of single cadaveric kidneys from adults, but the prevalence differs. Renal artery stenoses occur less frequently and arterial and venous thromboses occur more frequently in en bloc transplants from young donors than has been reported for single transplants from adult donors [1, 14–18]. The lower prevalence of renal artery stenosis probably occurs because the renal arteries are not involved in the vascular anastomosis and thus are less subject to trauma during transplantation [10]. It has been postulated that the greater prevalence of arterial thrombosis is due to the oversewn end of the donor aorta forming a cul-de-sac, which predisposes to thrombosis [10, 19]. The cause of the greater prevalence of venous thrombosis has not been elucidated. The spectrum and prevalence of postoperative urinary, infectious, and neoplastic complications is the same for transplantation of paired cadaveric kidneys from young donors and transplantation of single cadaveric kidneys from adults [20, 21]. The vascular, urinary, infectious, and neoplastic complications associated with en bloc transplantation of paired cadaveric kidneys from young donors are more complex than those associated with transplantation of single cadaveric kidneys from adults, because one or both of the transplanted kidneys or ureters, or any of the multiple donor vessels in the en bloc renal transplants may be involved in the postoperative complications.

Postoperative imaging of transplanted paired cadaveric kidneys from young donors requires individual evaluation of each of the two donor kidneys and ureters, and the complex

en bloc renal vasculature. If each donor kidney and ureter and the entire en bloc vasculature are not evaluated, unilateral complications can be overlooked. If detected early, irreversible unilateral complications can be treated with unilateral graft nephrectomy, thus leaving the patient with one functional kidney [11]. However, if the graft is incompletely evaluated and a unilateral complication, such as renal arterial or venous thrombosis, is overlooked, the complication may later involve the contralateral kidney, necessitating complete graft nephrectomy.

Although multiple imaging techniques can be used to visualize the en bloc transplanted kidneys, the techniques are not equally effective for depicting the complex graft anatomy or showing postoperative complications. We have found gray-scale sonography to be the most effective technique for evaluating the position, parenchyma, and collecting system of each of the paired transplanted kidneys and the urinary bladder. As with transplantation of single cadaveric kidneys from adult donors [1, 14, 16–18, 22–24], color and duplex Doppler sonography are effective for the evaluation of the vascular anatomy and detection of vascular complications in en bloc transplantation of paired cadaveric kidneys from young donors. However, because it is technically difficult and time consuming to examine all the en bloc vasculature, in patients undergoing routine examination after transplantation, we rely on a survey of the intrarenal vasculature, main renal vessels in the renal hila, and proximal portions of the donor aorta and IVC to detect significant vascular abnormalities. If an abnormality is detected during the vascular survey or if clinical findings are strongly suggestive of a vascular complication, the entire vascular tree is examined in detail with both color and duplex Doppler sonography. In addition to the Doppler evaluation of the discrete en bloc vasculature, we also examine all intrarenal cysts and small to moderate-sized perivascular fluid collections related to the transplanted kidneys to exclude the presence of pulsatile flow indicative of a pseudoaneurysm. Angiography is used to confirm many of the vascular complications detected with sonography and to examine patients in whom sonographic examination is suboptimal. Renal scintigraphy is useful for obtaining information about graft parenchymal function and for evaluating the patency and integrity of the renal collecting system in patients thought to have a urinary obstruction or leak. Contrast urography, CT, and MR imaging occasionally provide additional useful information in evaluating complications detected with sonography and scintigraphy; however, they are not used in routine screening of en bloc renal transplants.

The success of en bloc transplantation of paired cadaveric kidneys from young donors provides a practical alternative to transplantation of single cadaveric kidneys from adult donors. With the demand for renal transplantation far exceeding the supply of donor organs, en bloc renal transplantation will most likely become increasingly popular. Familiarity with the surgical technique, the normal imaging appearance of the grafts after transplantation, and the imaging findings of postoperative complications will enable radiologists to perform effective postoperative imaging of patients who receive en bloc renal transplants.

ACKNOWLEDGMENTS

We acknowledge Velma Scantlebury, John J. Fung, and Thomas E. Starzl for the performance of many of the organ transplantations included in this study. We thank Scharmen R. Confer for help in collecting data and LaVonne Buttyan for secretarial support and help in manuscript preparation.

REFERENCES

1. Becker JA. The role of radiology in evaluation of the failing renal transplantation. *Radiol Clin North Am* **1991**;29:511–525
2. Hardie I, Strong R, Wall D, et al. Results of 1000 kidney transplants in Brisbane. *Transplant Proc* **1989**;21:3775–3776
3. Pozniak MA, Kelcz F, Dodd GD III. Renal transplant ultrasound: imaging and Doppler. *Semin Ultrasound CT MR* **1991**;12:319–334
4. Ratner LE, Flye MW. Successful transplantation of cadaveric en-bloc paired pediatric kidneys into adult recipients. *Transplantation* **1991**;51:273–275
5. Chevalier C, Dupuy JM, Busson M, Hors J, Foulon G. A retrospective and prospective study of the number of kidney transplants in 31 countries. *Transplant Int* **1989**;2:187–192
6. Wetzels JFM, Hoitsma AJ, Koene RAP. Influence of cadaver donor age on renal graft survival. *Clin Nephrol* **1986**;25:256–259
7. Hong JH, Shirani K, Arshad A, et al. Influence of cadaver donor age on the success of kidney transplants. *Transplantation* **1981**;32:532–534
8. Dreikorn K, Rohl L, Horsch R. The use of double renal transplants from paediatric cadaver donors. *Br J Urol* **1977**;49:361–364
9. Darras FS, Jordan ML, Shapiro R, et al. Transplantation of pediatric en bloc kidneys under FK 506 immunosuppression. *Transplant Proc* **1991**;23:3089–3090
10. Schneider JR, Sutherland DR, Simmons RL, Fryd DS, Najarian JS. Long-term success with double pediatric cadaver donor renal transplants. *Ann Surg* **1983**;197:439–442
11. Meakins JL, Smith EJ, Alexander JW. En bloc transplantation of both kidneys from pediatric donors into adult patients. *Surgery* **1972**;71:72–75
12. Wengerter K, Matas AJ, Tellis VA, Quinn T, Soberman R, Veith FJ. Transplantation of pediatric donor kidneys to adult recipients: is there a critical donor age? *Ann Surg* **1986**;204:172–175
13. Gruessner RWG, Matas AJ, Lloveras G, et al. A comparison of single and double pediatric cadaver donor kidneys for transplantation. *Clin Transplant* **1989**;3:209–214
14. Dodd GD III, Tublin ME, Shah A, Zajko AB. Imaging of vascular complications associated with renal transplants. *AJR* **1991**;157:449–459
15. Jordan ML, Cook GT, Cardella CJ. Ten years of experience with vascular complications in renal transplantation. *J Urol* **1982**;128:689–692
16. Grenier N, Douws C, Morel D, et al. Detection of vascular complications in renal allografts with color Doppler flow imaging. *Radiology* **1991**;178: 217–223
17. Taylor KJW, Morse SS, Rigsby CM, Bia M, Schiff M. Vascular complications in renal allografts: detection with duplex Doppler ultrasound. *Radiology* **1987**;162:31–38
18. Needleman L, Kurtz AB. Doppler evaluation of the renal transplant. *JCU* **1987**;15:661–673
19. Andersen OS, Jonasson O, Merkel FK. En bloc transplantation of pediatric kidneys into adult patients. *Arch Surg* **1974**;108:35–37
20. Cohen HL, Beck JA. Imaging of renal transplantation and its complications. In: Taveras JM, Ferrucci JT, eds. *Radiology: diagnosis, imaging, intervention*, vol 4. Philadelphia: Lippincott, **1989**:ch.121:1–9
21. Dodd GD III, Greenler DP, Confer SR. Thoracic and abdominal manifestations of lymphoma occurring in the immunocompromised patient. *Radiol Clin North Am* **1992**;30:597–610
22. Tobben PJ, Zajko AB, Sumkin JH, et al. Pseudoaneurysms complicating organ transplantation: roles of CT, duplex sonography, and angiography. *Radiology* **1988**;169:65–70
23. Braun B, Weilemann LS, Weigand W. Ultrasonographic demonstration of renal vein thrombosis. *Radiology* **1989**;138:157–158
24. Reuther G, Wanjura D, Bauer H. Acute renal vein thrombosis in renal allografts: detection with duplex Doppler ultrasound. *Radiology* **1989**;170:557–558

Book Review

Current Opinion in Radiology. Genitourinary Radiology and Ultrasound 1992. Guest editors: Howard M. Pollack and Ruth B. Goldstein. Philadelphia: Current Science, 1992;4(2):1–149. $30; by subscription, 6 issues annually.

This book is one of a series of volumes on various topics in radiology. This issue reviews some of the recent literature, controversial issues, and advances in the broad areas of genitourinary radiology and diagnostic sonography. These sections are edited by Drs. Pollack and Goldstein, respectively, with contributions on individual topics from 23 different authors.

The section on genitourinary radiology begins with an editorial summary by Dr. Pollack. This is followed by six articles dealing with specific areas in the field. Topics covered include contrast material, color Doppler imaging, MR imaging of the genitourinary system, urinary tract stone disease, diagnosis of erectile dysfunction, and staging of gynecologic malignant neoplasms. The section on sonography begins with an overview written by Dr. Goldstein. Subsequently, individual sections deal with a range of topics including vascular, gastrointestinal, gynecologic, endovaginal, and translabial sonography; sonography of first-trimester fetal anomalies; intrauterine growth retardation; and sonography of neonates, infants, and children.

Each review article presents and discusses the major developments that have occurred in the topic area. The reviews then discuss several papers in each area that are considered significant. Relevant previous and current studies are cited. A large number of the articles discussed are from 1991. A selected bibliography, including abstracts in most cases, is printed at the end of each section, and often includes additional references not cited in the summary section. Each reference is graded by the reviewer in terms of its overall interest level.

The reviewers generally do a thorough job in reviewing the major literature in question. The selected topics are covered in a comprehensive fashion. The writing is clear and concise. The summaries and authors' comments often provide additional information and meaningful points of view. The illustrations provided are of high quality and include several excellent color Doppler images; all illustrations are clearly and accurately labeled. The printing and paper stock are of excellent quality.

The volume generally achieves its stated goal: a comprehensive review of the current important literature on specific topics of interest in genitourinary radiology and sonography. As such, it will be useful to practicing radiologists, as it provides an efficient means of quickly reviewing the pertinent literature in the selected areas. The bibliographies provide an ample starting point for a more detailed review, if desired. Senior radiology residents will also find the volume useful before board examinations. For radiologists who regularly read the current literature, the book provides little new information, but it does a nice job of organizing and summarizing the major articles on selected topics.

Michael E. Flisak
Loyola University Medical Center
Maywood, IL 60153

Kidney Dimensions at Sonography: Correlation with Age, Sex, and Habitus in 665 Adult Volunteers

Seyed Alireza Emamian[1,2]
Michael Bachmann Nielsen[1]
Jan Fog Pedersen[1]
Lars Ytte[3]

OBJECTIVE. The purpose of this study was to investigate the normal sonographic measurements of the kidney in adult volunteers.

SUBJECTS AND METHODS. Length, width, and thickness of the kidney and its central echogenic area and the parenchymal thickness of the upper pole were measured in an age- and sex-stratified random sample of 665 volunteers 30, 40, 50, 60, and 70 years old. Measurements were made with the volunteers prone. Volumes of the kidney, the central echogenic area, and the renal parenchyma were calculated. Renal dimensions and renal and parenchymal volume were correlated with age, height, weight, body mass index, and total body area. In 94 subjects, renal length was measured with the volunteers supine also.

RESULTS. Median renal lengths were 11.2 cm on the left side and 10.9 cm on the right side. Median renal volumes were 146 cm^3 in the left kidney and 134 cm^3 in the right kidney. Renal size decreased with age, almost entirely because of parenchymal reduction. Renal volume correlated best with total body area. Renal length correlated best with body height. Measurements of renal length obtained with the subjects supine were not significantly different from those obtained with the subjects prone.

CONCLUSION. The most exact measurement of renal size is renal volume, which showed the strongest correlation with height, weight, and total body area. Clinically, measurement of renal length is most practical and can be done with the subject prone or supine.

AJR 1993;160:83–86

Sonography of the kidneys has replaced standard radiography for evaluation of renal disease. Because abnormalities of kidney size are present in many renal diseases, it is valuable to have a set of standard sonographic measurements to use when these patients are examined [1].

Only a few reports [2–5] have described the use of sonography to obtain renal measurements in adults. We used this imaging technique to measure renal dimensions, stratified by age and sex, in 665 adult volunteers.

Subjects and Methods

An age- and sex-stratified random sample of 2500 men and women 30, 40, 50, 60, and 70 years old who lived in the western part of the county of Copenhagen was drawn from The National Person Register. All subjects received a standardized written invitation to a general health examination. The examinations took place between February and October 1991. The project was approved by the Ethical Committee for Copenhagen County. Of 2500 subjects, 1775 (71%) attended the general health examination. Of these, 686 were selected at random and had sonography of the kidneys. Twenty-one of the 686 subjects were excluded for the following reasons: solitary cysts larger than 4 cm in diameter (eight cases), polycystic kidneys (two cases), bilateral multiple (four or more) cysts (two cases), unilateral kidney (two cases), hydronephrosis (two cases), pregnancy (one case), extreme obesity (one case), partial nephrectomy (one case), renal transplantation (one case), and renal tumor (one case). Sonographic evidence of nephrolithiasis was not considered a reason for exclu-

Received April 6, 1992; accepted after revision July 14, 1992.

This work was supported by The Danish Hospital Foundation for Medical Research, Regions of Copenhagen, The Faeroe Islands, and Greenland (grant no. 90/91).

[1]Department of Radiology and Ultrasound, Glostrup Hospital, University of Copenhagen, DK-2600 Glostrup, Denmark.

[2]The Glostrup Population Studies, Department of Internal Medicine C, Glostrup Hospital, University of Copenhagen, DK-2600 Glostrup, Denmark.

[3]Department of Surgery T, Glostrup Hospital, University of Copenhagen, DK-2600 Glostrup, Denmark.

0361–803X/93/1601–0083

sion. Information on serum levels of creatinine was not available. The remaining 665 participants (358 women, 307 men) form the basis of this study.

For the purpose of the health examinations, the participants fasted overnight. Two to three hours before renal sonography, they were offered a light meal. All participants were asked to empty the bladder just before the examination. Real-time gray-scale sonography was performed with a Picker LSC 7000/7000A (Picker International, Frankfurt M, Germany) system with a 3.5-MHz curved-array transducer with a wide (11-cm) contact surface. The examination began with the subject supine; the preaortic region was examined to exclude the presence of a horseshoe kidney. Renal measurements were obtained with the subject prone. Length, width, and thickness of the kidney and of its central echogenic area (including sinus fat, calices, and vessels) were measured. The longitudinal dimensions of the kidneys were measured in a section visually estimated to represent the largest longitudinal section. The width and thickness were measured in a section perpendicular to the longitudinal axis of the kidney as assessed from the longitudinal image. The probe was thus not necessarily perpendicular to the skin. The level of this transverse section was intended to be placed quite close to the hilum of the kidney but at the same time free of the pelvis. Width and thickness were then measured in two orthogonal directions.

In 94 randomly selected 30-year-old subjects, the renal length in an approximate coronal section was measured with subjects supine and compared with the length measured when the subjects were prone. True supine position was generally sufficient; however, slight elevation of the examined side was necessary in a few cases for optimal visualization.

For calculations, the following formulas were used. Volumes of the kidney (renal volume) and the central echogenic area (central echogenic volume) = length × thickness × width × 0.5. Renal parenchymal volume = renal volume − central echogenic volume. Total body area [6] = weight$^{0.425}$ × height$^{0.725}$ × 71.84. Body mass index = weight/(height)^2. Renal shape index = renal length/(renal width + renal thickness). Relative volume of central echogenic area = central echogenic volume × 100/renal volume.

For statistical analysis, we used the Mann-Whitney test and the Pearson correlation coefficient.

Results

Table 1 gives renal lengths and widths by age, sex, and side. Figure 1 shows the median renal length vs age and sex. Figure 2 shows renal length vs body height.

Median volumes of the central echogenic area were 24 and 21 cm^3 for the left and right kidneys, respectively. Left/right median values for thickness of the kidneys and parenchymal thickness at the upper poles were 46/43 and 16/15 mm, respectively. These measurements differed only slightly between different age groups. Median renal volumes on the left and right sides were 146 and 134 cm^3, respectively. Renal volume was significantly larger in men than in women ($p < .00001$). For all age and sex groups, renal measurements except renal width and parenchymal thickness were smaller for the right kidney than for the left kidney.

Renal length and renal volume showed only slight differences between volunteers 30 to 60 years old and were distinctly decreased in volunteers 70 years old. However, the correlation between renal shape index and age was highly significant; the kidney was relatively wider and thicker in older volunteers ($p < .00001$; Table 2). Reduction in renal volume with age seems to be almost totally due to reduction in parenchymal volume, as the relative volume of the central echogenic area increased slightly but significantly with age ($p<.00001$; Table 2).

Renal measurements were correlated with the subjects' height, weight, total body area, and body mass index. The strongest correlation with renal volume was found for total body area; the correlation coefficients for left and right kidneys were .595 and .600, respectively. Correlations with renal parenchymal volume were slightly poorer. Renal length correlated best with body height; the correlation coefficients for left and right kidney were .461 and .416, respectively.

In all age groups except the 70-year-olds, a significant correlation was found between kidney length and body height, for both kidneys and both sexes.

The mean differences between the renal lengths measured with the subjects prone and supine were 0.5 mm (±10 mm, 2 SD) and 0.7 mm (±10 mm, 2 SD) for the left kidney and the right kidney, respectively.

TABLE 1: Renal Measurements at Sonography in 665 Volunteers

Measurements	Age (yr)					Women	Men	All
	30	40	50	60	70			
No. of subjects								
Women	68	82	95	75	38	358	0	358
Men	53	62	73	87	32	0	307	307
Renal length (mm)								
Left	115 (104, 128)	113 (103, 123)	113 (102,125)	111 (100, 122)	105 (94, 120)	110 (99, 121)	115 (104, 126)	112 (101, 123)
Right	111 (101, 124)	112 (100, 123)	110 (100, 122)	108 (95, 120)	104 (91, 118)	107 (95, 120)	112 (101, 124)	109 (98, 122)
Renal width (mm)								
Left	59 (51, 66)	58 (50, 65)	58 (53, 65)	58 (51, 65)	56 (49, 62)	56 (49, 62)	60 (53, 68)	58 (51, 65)
Right	58 (50, 66)	58 (52, 66)	58 (52, 64)	57 (50, 64)	55 (50, 63)	56 (50, 61)	59 (53, 66)	57 (51, 64)

Note.—Values are medians. Numbers in parentheses are 10th and 90th percentiles.

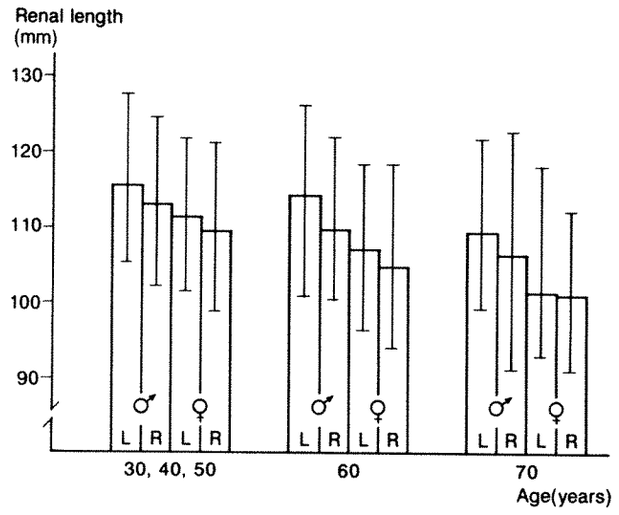

Fig. 1.—Graph shows distribution of lengths of right and left kidneys, measured at sonography, by age and sex in 665 volunteers. Median values are given; error bars indicate 10th and 90th percentiles.

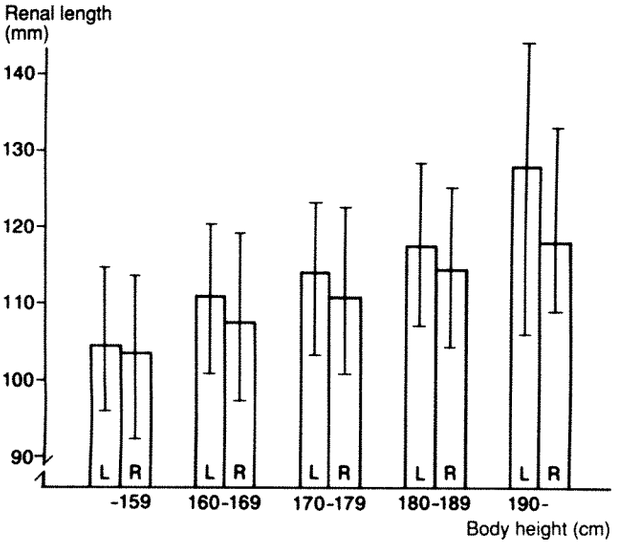

Fig. 2.—Graph shows lengths of left and right kidneys, measured at sonography, in relation to body height in 665 volunteers. Median values are given; error bars indicate 10th and 90th percentiles.

Discussion

Most radiologic studies of renal size have been two-dimensional and have used excretory urograms [7–9]; a few three-dimensional studies of renal volume have used renal angiography [10] or CT [11]. These studies involved patients with no radiologic evidence of renal disease, unlike our study, which used randomly selected volunteers. Measurements can be obtained quickly and easily with sonography.

TABLE 2: Renal Shape Index and Relative Volume of Central Echogenic Area at Sonography in 665 Volunteers

Measurements	Age (yr)					All
	30	40	50	60	70	
No. of subjects	121	144	168	162	70	665
Renal shape index						
Left kidney	1.11	1.10	1.08	1.07	1.04	1.09
Right kidney	1.13	1.12	1.09	1.07	1.05	1.09
Relative volume of central echogenic area						
Left kidney	15.4	16.1	16.3	17.4	18.4	16.5
Right kidney	14.9	15.2	16.1	16.5	17.1	15.8

Note.—Renal shape index = renal length/(renal width + renal thickness), relative volume of central echogenic area = central echogenic volume × 100/renal volume. For renal shape index, differences were significant (for both kidneys) for 30-year-olds vs 50-year-olds ($p < .05$). For relative volume, differences were significant for both kidneys for 30-year-olds vs 50-year-olds and for the left kidney for 50-year-olds vs 70-year-olds ($p < .01$).

Renal dimensions measured by using sonography are smaller than those obtained by using radiography [12], because no geometric magnification and no osmotic diuresis caused by IV contrast medium occur. In a previous study [13] of donor kidneys, the measurements made by using sonography were more accurate than measurements based on plain radiographs, excretory urograms, or renal angiograms.

In contrast to information on renal measurements in children and infants, only a few reports have been published on renal measurements in adults [2–5]. The unique feature of our study is that we had well-defined age groups with a large number of participants for each age group and sex. This allowed us to define differences in renal dimensions on the basis of age, sex, and habitus. The 665 participants claimed to be healthy. However, some of them might have had mild or subclinical renal disease. Serum levels of creatinine were not measured; however, it seems unlikely that a study of randomly selected volunteers would include many subjects with renal disease.

Most studies [14–17] of infants and children showed no difference in renal dimensions between the sexes. Our study showed a sex difference in adults, which is in agreement with previous postmortem [18] and radiologic studies [8].

With sonography, renal cysts are frequently found in asymptomatic patients. Small cysts cause only minor changes in renal and parenchymal volume, whereas large cysts can compress the parenchyma and deform the kidney. For these reasons, we excluded eight subjects who had large cysts and two who had multiple cysts.

As judged from the renal shape index, the kidney becomes relatively wider and thicker with age. This small, but highly significant shift in renal shape is interesting, but of no practical consequence. One possible explanation for this phenomenon could be the relaxation of the abdominal wall with age, so that the kidneys are squeezed less in older per-

sons. This would also explain the broadening that becomes most pronounced for the right kidney, which has been squeezed more because of the liver.

In this and previous radiographic studies [19], only minor changes in the volume of the central echogenic area were observed with increasing age. This contrasts with an earlier radiologic study that suggested that renal parenchyma is replaced with sinus fat with age [20]. Our results suggest that the external measurements, leading to an estimate of total renal volume, are sufficient to represent renal mass and that further attempts to measure the renal parenchymal mass are superfluous.

In all age groups, the parenchymal volume of the right kidney was significantly smaller than that of the left ($p<.00001$ for subjects 30–60 years old; $p = .013$ for subjects 70 years old). One possible explanation is that because the spleen is smaller than the liver, the left kidney has more space for growth. Another explanation is that because the left renal artery is shorter and straighter than the right one, increased blood flow in the left artery may result in relatively increased volume.

The parenchymal thickness at the upper pole showed slight changes with age and between sexes. Measurement of parenchymal thickness is less feasible because the built-in calipers on the sonographic unit allow measurements in increments of 1 mm only and because accurate definition of the border between renal parenchyma and the central echogenic area may be difficult. However, measurements of parenchymal thickness may be useful in pathologic conditions.

The most precise assessment of abnormalities in renal size would require measurement of renal volume or even parenchymal volume in relation to sex, weight, or total body area, but such calculations are not clinically practical. Measurement of renal length is easy, and the obtained values can be compared with the values in the reference figures and tables. For everyday situations, measurement of renal length is therefore recommended. The small difference and acceptable standard deviation indicate that renal length can be measured with the subject either supine or prone.

REFERENCES

1. Edell SL, Kurtz AB, Rifkin MD. Normal renal ultrasound measurements. In: Goldberg BB, Kurtz AB. *Atlas of ultrasound measurements.* Chicago: Year Book Medical, **1990**:146–160
2. Spiegl G, Jeanty P, Kittel F, Struyven J. Ultrasonic measure of the normal kidney. *J Belge Radiol* **1982**;65:513–518
3. Wang F, Cheok SP, Kuan BB. Renal size in healthy Malaysian adults by ultrasonography. *Med J Malaysia* **1989**;44:45–51
4. Brandt TD, Neiman HL, Dragowski MJ, Bulawa W, Claykamp G. Ultrasound assessment of normal renal dimensions. *J Ultrasound Med* **1982**;1:49–52
5. Borre GE, Borre DG, Pereira H, Duval AA, Corona R. New quantified echographic features of normal kidney: hydronephrosis classification. *Roentgenblatter* **1990**;43:519–523
6. *Documenta Geigy: scientific tables*, 7th ed. Basel: Geigy, **1970**:537
7. McLachlan M, Wasserman P. Changes in sizes and distensibility of the aging kidney. *Br J Radiol* **1981**;54:488–491
8. Karn MN. Radiographic measurements of kidney section area. *Ann Hum Genet* **1962**;25:379–385
9. Friedenberg MJ, Walz BJ, McAllister WH, Locksmith JP, Gallagher TL. Roentgen size of normal kidneys: computer analysis of 1286 cases. *Radiology* **1965**;84:1022–1030
10. Hegedüs V. Three-dimensional estimation of renal shape and volume at angiography. *Acta Radiol Diagn* **1972**;12:87–99
11. Gourtsoyiannis N, Prassopoulos P, Cavouras D, Pantelidis N. The thickness of the renal parenchyma decreases with age: a CT study of 360 patients. *AJR* **1990**;155:541–544
12. Moël H. Kidney size and its deviation from normal in acute renal failure. *Acta Radiol* **1961**;206[suppl]:5–74
13. Ninan VT, Koshi KT, Niyamthullah MM, et al. A comparative study of estimating renal size in normal adults. *Nephrol Dial Transplant* **1990**;5:851–854
14. Han BK, Babcock DS. Sonographic measurements and appearance of normal kidneys in children. *AJR* **1985**;145:611–616
15. Christophe C, Cantraine F, Bogaert C, et al. Ultrasound: a method for kidney size monitoring in children. *Eur J Paediatr* **1986**;145:532–538
16. Dinkel E, Ertel M, Peters H, Berres M, Schulte-Wissermenn H. Kidney size in childhood: sonographic growth charts for kidney length and volume. *Pediatr Radiol* **1985**;15:38–43
17. Holloway H, Jones TB, Robinson AE, Harpen MD, Wiseman HJ. Sonographic determination of renal volumes in normal neonates. *Pediatr Radiol* **1983**;13:212–214
18. Wald H. The weight of normal adult human kidneys and its variability. *Arch Pathol* **1937**;23:493–500
19. Griffiths GJ, Cartwright G, McLachlan MSF. Estimation of renal size from radiographs: is the effort worthwhile? *Clin Radiol* **1974**;26:249–256
20. Simon AL. Normal renal size: an absolute criterion. *AJR* **1964**;92:270–272

Pictorial Essay

Nongynecologic Applications of Transvaginal Sonography

Thomas S. Chang,[1,2] Marcela Böhm-Vélez,[1] and Ellen B. Mendelson[1]

Transvaginal sonography has become an invaluable technique for examining the uterus and adnexa, primarily because it provides better spatial resolution than transabdominal sonography does. This characteristic also makes it useful for evaluating the nongynecologic structures in the pelvis. As many of these structures are imaged incidentally during gynecologic transvaginal sonography, familiarity with their normal and abnormal appearances is important. With minor modifications in technique, targeted studies of these structures are easily performed. We illustrate the technique used, normal anatomy seen, and abnormalities commonly encountered in transvaginal sonography of nongynecologic pelvic structures.

During transvaginal sonography of the uterus and adnexa, many nongynecologic structures are imaged incidentally. Because of this, familiarity with their normal and abnormal appearances is important for anyone who obtains or interprets transvaginal sonograms. Optimal imaging of these structures requires modifications of the usual transvaginal technique [1]. The specific modifications needed differ for each structure, but can be grouped according to location relative to the uterus: anterior, posterior, or lateral. Figure 1 depicts the anatomic relationships seen in the two projections obtained transvaginally, namely, sagittal and coronal.

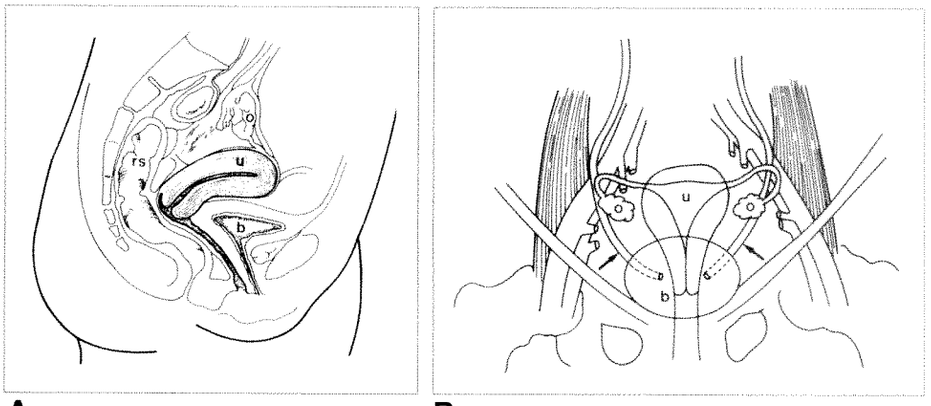

Fig. 1.—*A* and *B*, Sagittal and coronal diagrams show normal relationship of nongynecologic structures to uterus (u) and ovaries (o). rs = rectosigmoid colon, b = urinary bladder, and *arrows* = ureters.

Received April 20, 1992; accepted after revision July 9, 1992.
Presented at the annual meeting of the American Roentgen Ray Society, Orlando, FL, May 1992.
[1]Department of Radiology, The Western Pennsylvania Hospital, 4800 Friendship Ave., Pittsburgh, PA 15224.
[2]Present address: Department of Radiology, Magee-Women's Hospital, 300 Halket St., Pittsburgh, PA 15213. Address reprint requests to Thomas S. Chang.

AJR **1993;160:87–93** 0361–803X/93/1601–0087

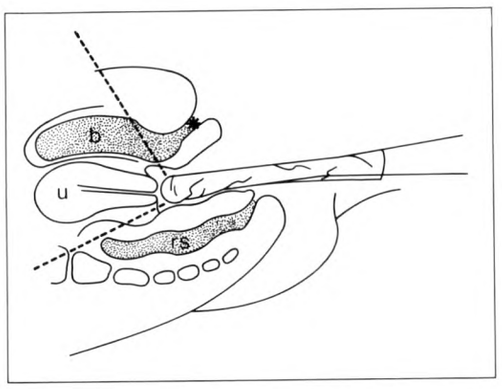

Fig. 2.—Diagram shows transvaginal technique for evaluating structures anterior to uterus (u). When transducer handle is moved posteriorly, bladder (b) is included within ultrasound beam (*dashed lines*). Urethra (*asterisk*) is best visualized with end of transducer pointing anteriorly and positioned more caudally, just inside vaginal introitus. rs = rectosigmoid colon.

Structures Anterior to the Uterus

Technique

For structures anterior to the uterus, the transducer tip is aimed anteriorly by moving the handle posteriorly (Fig. 2). Transducer manipulation is facilitated by elevating the patient's hips with a pillow or placing the patient in the lithotomy position. Examination of the bladder is best performed with mild to moderate bladder distension (Fig. 3) and with the transducer tip positioned in the vaginal fornix. Excessive bladder distension limits the study by placing much of the bladder wall out of the field of view. Visualization of the urethra requires positioning the transducer just inside the vaginal introitus [1].

Urinary Bladder

The normal bladder wall is homogeneous, relatively smooth, and no more than 6 mm thick [2] (Fig. 4). Urine is anechoic, but urine streaming into the bladder from the ureters is sometimes echogenic (the ureteral jet phenomenon) [3].

Neoplasms may appear as polypoid masses or areas of focal wall thickening (Fig. 5A), but these are nonspecific findings also found in benign processes (Fig. 5B). Malignant tumors can cause obstruction of the ureters or bladder neck. With infection, focal or generalized wall thickening, echogenic urine, or a fluid-debris level may be present (Fig. 6). Bladder calculi and fungus balls are less common findings associated with certain infections. Besides neoplasm and cystitis, other causes of wall thickening include previous irradiation and surgery [2]. Fistulas involving the bladder may be inflammatory, neoplastic, or iatrogenic and also can cause the urine to appear echogenic (Fig. 7). When the bladder outlet is obstructed, trabeculae (Fig. 8), diverticula (Fig. 9), and increased residual urine after voiding are often shown; calculi also may be present because of stasis. Stress incontinence can be diagnosed by observing descent of the bladder neck while the patient coughs or performs the Valsalva maneuver [1].

Urethra

The urethra has a homogeneous, smooth wall that is best visualized when the lumen contains urine. Urethral dilatation suggests a stricture (Fig. 10). Urethral diverticula (Fig. 11) usually result from infection and obstruction of paraurethral glands. They are located posterolateral to the mid urethra and may contain calculi [1].

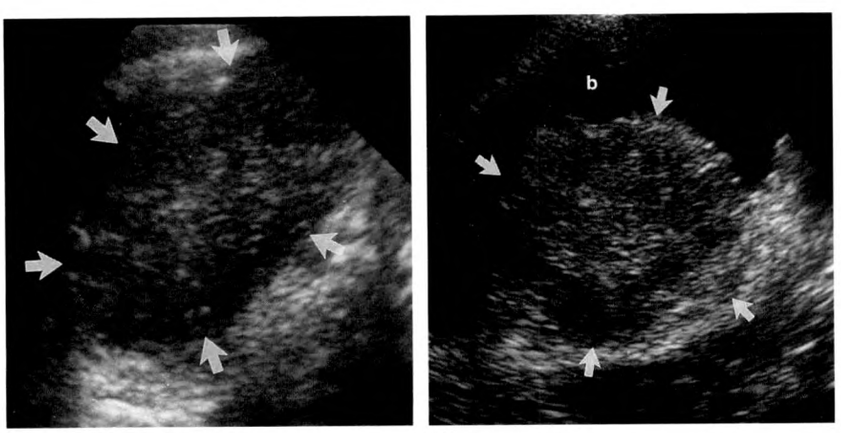

Fig. 3.—Modification of technique for evaluating structures anterior to uterus.

***A*, Routine transvaginal sonogram of a patient with an empty bladder shows a solid mass (*arrows*) anterior to uterus. No distinguishing landmarks are present to aid in determining origin of mass.**

***B*, Sonogram of same patient with moderate bladder distension shows mass (*arrows*) arising from bladder wall and projecting into bladder (b). Urine helps to define extent of mass by separating bladder walls and allowing accurate determination of wall thickness. Mass was histologically proved to be a transitional cell carcinoma.**

(Adapted with permission from Mendelson and Böhm-Vélez [1].)

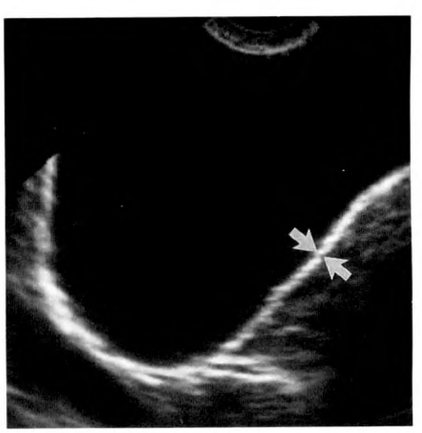

Fig. 4.—Normal bladder. Transvaginal sonogram shows normal bladder wall (*arrows*) as a thin echogenic line less than 6 mm thick. Urine is anechoic. (Adapted with permission from Mendelson and Böhm-Vélez [1].)

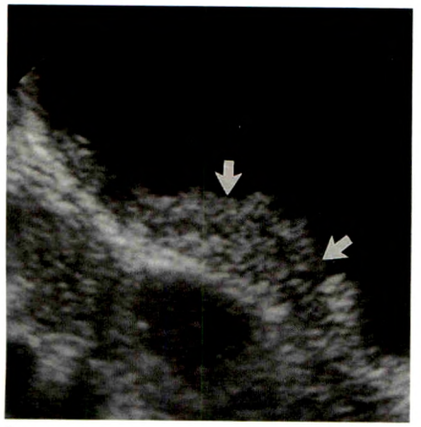

A

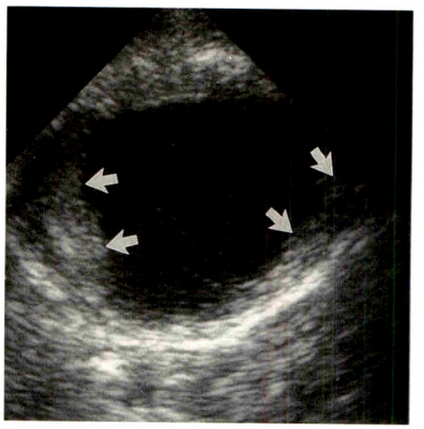

B

Fig. 5.—*A* and *B*, Transvaginal sonograms show focal thickening of bladder wall (*arrows*), a nonspecific finding that can be seen in transitional cell carcinoma (*A*) and cystitis (*B*). The presence of echogenic urine in *B* is consistent with cystitis but does not exclude neoplasm, especially if there is hemorrhage. (*A* adapted with permission from Mendelson and Böhm-Vélez [1].)

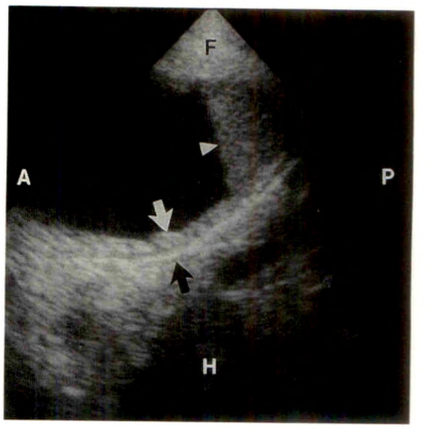

Fig. 6.—Cystitis. Sagittal transvaginal sonogram shows echogenic urine, fluid-debris level (*arrowhead*), and mural thickening (*arrows*), suggesting an inflammatory process. Fluid-debris level is seen vertically because sagittal transvaginal images are oriented with patient's feet (F) at top of image, head (H) at bottom, anterior aspect (A) on left, and posterior aspect (P) on right. (Adapted with permission from Mendelson and Böhm-Vélez [1].)

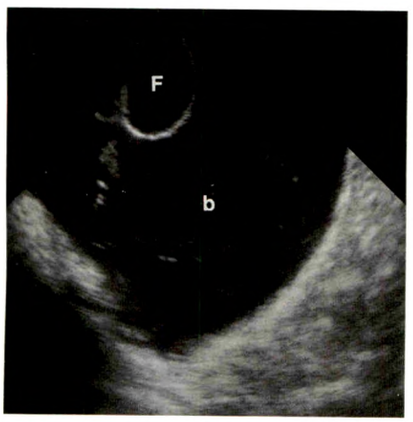

Fig. 7.—Rectovesical fistula. Transvaginal sonogram of bladder (b) shows low-level echoes within urine, representing fecal and inflammatory material. F = Foley catheter balloon. (Adapted with permission from Mendelson and Böhm-Vélez [1].)

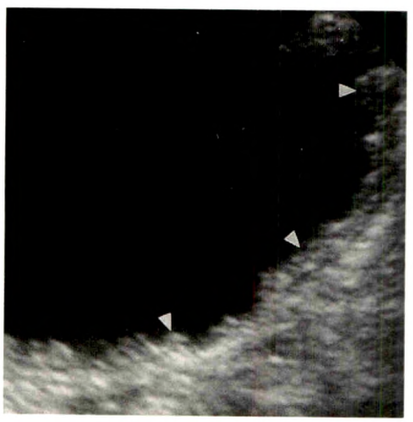

Fig. 8.—Bladder outlet obstruction. Transvaginal sonogram shows bladder trabeculae appearing as generalized wall thickening and irregularity (*arrowheads*). Appearance of wall is similar to that in cystitis, although echogenicity of urine may differ. (Adapted with permission from Mendelson and Böhm-Vélez [1].)

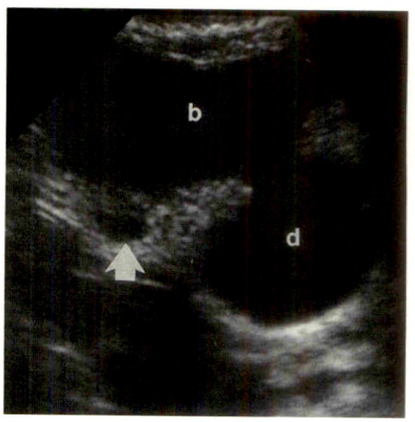

Fig. 9.—Bladder diverticula. Sagittal transvaginal sonogram shows neck of a large diverticulum (d) arising from bladder (b). Anterior to this is a second, smaller diverticulum (*arrow*), but its neck is not imaged in plane of section. (Adapted with permission from Mendelson and Böhm-Vélez [1].)

Structures Posterior to the Uterus

Technique

For structures posterior to the uterus, the examination is performed with the transducer handle moved anteriorly so that its tip is aimed posteriorly (Fig. 12). A water enema is often useful for evaluating masses in this region because it shows whether the abnormality is inside or outside the rectosigmoid colon [2]. A water enema is necessary for visualizing the rectosigmoid mucosa also [1].

Small Intestine

Small-bowel segments are identified during real-time scanning as fluid- or gas-containing tubular structures with peristaltic activity (Fig. 13A). They are usually seen posterior to the uterus, but may be anterior in location if the uterus is retroverted. Their normal diameter is less than 3 cm.

Dilatation of the small bowel is seen in obstruction and paralytic ileus (Fig. 13B), which are distinguishable by the presence or absence, respectively, of peristalsis. In gastroenteritis, the normal-diameter bowel segments are filled with

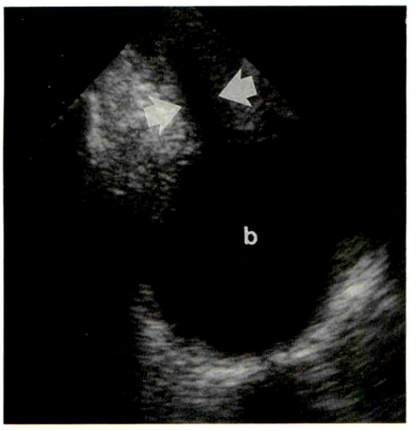

10

11

Fig. 10.—Urethral stricture. Postvoiding transvaginal sonogram shows residual urine in bladder (b) and distended urethra (*arrows*) in this patient with urethral stricture. Bladder volume can be estimated on this midline sagittal projection by this equation from Haylen et al. [4]: Bladder volume (ml) = [5.9 × height (cm) × depth (cm)] − 14.6. (Adapted with permission from Mendelson and Böhm-Vélez [1].)

Fig. 11.—Urethral diverticulum. Transvaginal sonogram shows oval, hypoechoic structure (*arrow*) near indistinctly seen urethra (*arrowheads*), representing an infected paraurethral gland that has become a urethral diverticulum. Neck of diverticulum is not visualized. Large volume of urine in this bladder (b) after voiding suggests associated voiding dysfunction. (Adapted with permission from Mendelson and Böhm-Vélez [1].)

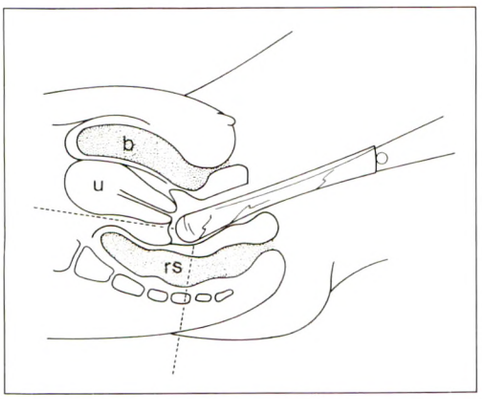

Fig. 12.—Diagram shows transvaginal technique for evaluating structures posterior to uterus (u). Moving probe handle anteriorly permits inclusion of rectosigmoid colon (rs) and other posterior structures within ultrasound beam (*dashed lines*). b = bladder. (Adapted with permission from Mendelson and Böhm-Vélez [1].)

fluid and hyperactive. In regional enteritis, thickening of the bowel wall or matted loops of bowel may be observed [2].

Rectosigmoid Colon

The normal rectosigmoid colon contains stool, gas, or both, which often hinder its evaluation. It can be differentiated from the small bowel because it is located more posteriorly and has less peristaltic activity.

Wall thickening, an intraluminal mass, or obstruction may be signs of neoplasm. Uncomplicated sigmoid diverticula are difficult to detect, but diverticular abscesses can be visualized as complex masses that may contain echogenic foci with posterior acoustic shadowing (Fig. 14). In fecal impaction, a complex intraluminal mass is present, often in conjunction with proximal dilatation of the bowel. A water enema can be helpful in confirming this diagnosis [1].

Appendix

The use of transvaginal sonography for diagnosing acute appendicitis has not been described. An appendiceal abscess, however, may be seen as a pelvic fluid collection or a complex right-sided pelvic mass that is separate from the ovary [1] (Fig. 15).

Structures Lateral to the Uterus

Technique

Imaging of the lateral areas of the pelvis requires angling of the transducer toward the pelvic side walls. For optimal visualization of the most lateral regions, it may be necessary to turn the patient to an oblique position or to compress the abdomen to bring structures closer to the transducer [1].

Blood Vessels

Blood vessels appear as nearly anechoic tubular structures with flow easily shown by color or duplex Doppler

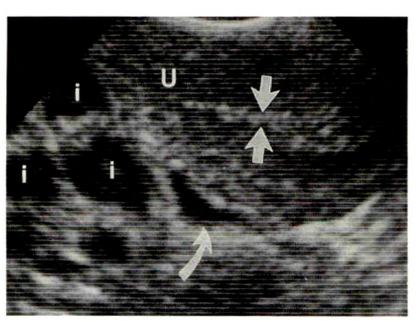

A

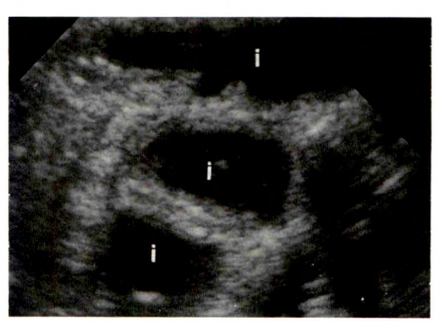

B

Fig. 13.—Transvaginal sonograms of bowel.
***A*, Normal small intestinal segments (i) are often seen on routine transvaginal real-time sonography as peristaltic fluid-filled tubular structures, here identified anterosuperior to a retroverted uterus (u) in sagittal plane. *Curved arrow* = free fluid, *straight arrows* = endometrium.**
***B*, Distended intestine (i) suggests paralytic ileus or mechanical obstruction. Real-time examination is important to assess peristaltic activity. (Adapted with permission from Mendelson and Böhm-Vélez [1].)**

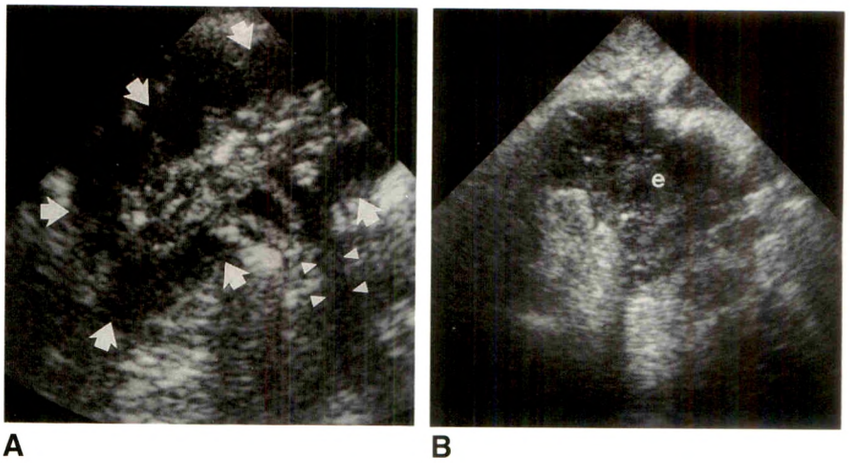

Fig. 14.—Transvaginal sonograms of complex masses associated with colon.

***A*, Sigmoid diverticular abscess is seen as a complex mass (*arrows*) containing echogenic foci representing gas and fecal material. Neck of diverticulum is suggested (*arrowheads*). (Courtesy of Barbara J. Weinstein, Pittsburgh, PA.)**

***B*, Cyclical bleeding of ectopically implanted endometrial tissue resulted in this endometrioma (e) of colon, indistinguishable from abscess and other complex masses. (Adapted with permission from Mendelson and Böhm-Vélez [1].)**

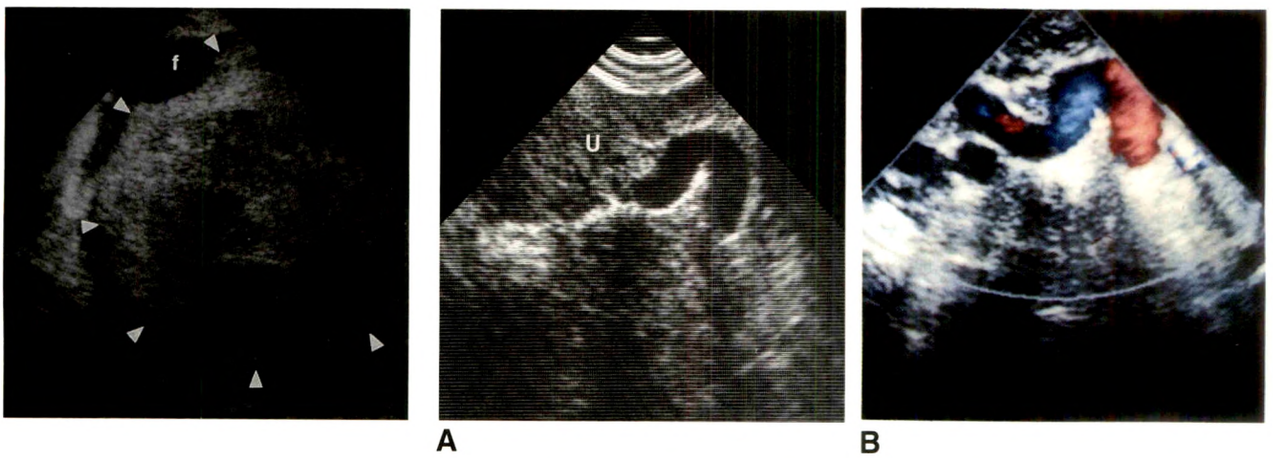

Fig. 15.—Appendiceal abscess. Transvaginal sonogram shows free intraperitoneal fluid (f) demarcating a nonspecific complex mass (*arrowheads*) in right pelvis. Fluid contains echoes, consistent with this inflammatory process. (Adapted with permission from Mendelson and Böhm-Vélez [1].)

Fig. 16.—Color Doppler imaging for differentiation of tubular structures.

***A*, Transvaginal sonogram shows an anechoic, tubular structure adjacent to uterus (u) in this patient with clinically suspected pelvic inflammatory disease.**

***B*, Transvaginal color Doppler image shows vascular flow, definitively excluding hydrosalpinx.**

sonography (Fig. 16). Slow flow is often better detected with real-time sonography as low-level echoes streaming within the lumen. The presence of flow within a vessel distinguishes it from similarly shaped hydrosalpinx, hydroureter, or fluid-filled bowel. The internal iliac vessels are consistently seen lateral to the ovaries, with the artery located anterior to the vein. The ovarian vessels are superolateral to the ovaries, but are usually not visible [1].

When a prominent pelvic vein is seen, a diagnosis of varix might be suggested (Fig. 17). However, because the diameter of normal pelvic veins varies widely, no consistently accepted size criterion exists for making this diagnosis [2].

Ureters

The ureters are located anterior to the internal iliac vessels at the level of the ovaries and are generally not visualized unless the ureteral lumina are distended. The ureters are distinguishable from the internal iliac vessels by their more echogenic walls and by the absence of flow in the ureters on Doppler imaging [1]. Ureteral abnormalities sometimes encountered include hydroureter and ureterocele.

Lymph Nodes

Lymph nodes are hypoechoic and are usually not detected unless they are enlarged. Benign pelvic lymph nodes can be up to 2 cm in diameter [1]. Lymphadenopathy may be due to inflammatory or neoplastic processes.

Free Fluid

Free fluid in the pelvis is often seen with high-resolution transvaginal sonography. In the premenopausal patient, a small amount of anechoic fluid in the cul-de-sac is normal. When the fluid accumulation is larger, it is important to char-

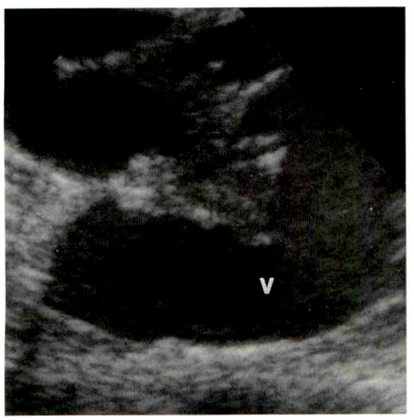

Fig. 17.—Pelvic varix. Transvaginal sonogram shows a dilated pelvic vein (v) with unidirectional movement of internal echoes on real-time examination, consistent with sluggish blood flow. (Adapted with permission from Mendelson and Böhm-Vélez [1].)

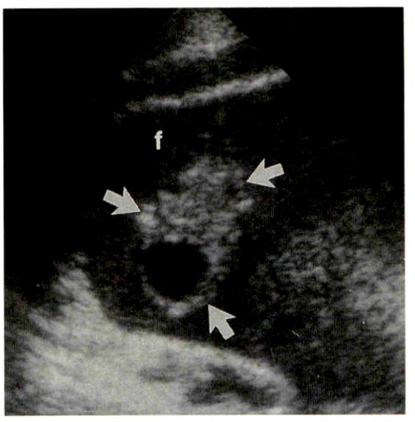

Fig. 18.—Malignant ascites. Transvaginal sonogram of a patient with uterine leiomyosarcoma shows echogenic fluid (f) representing malignant ascites surrounding a follicle-containing ovary (*arrows*).

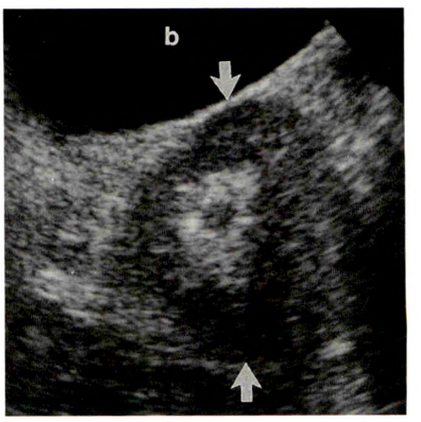

Fig. 19.—Pelvic kidney. Transvaginal sonogram shows reniform structure (*arrows*) superior to bladder (b), representing a pelvic kidney. No kidney was present in ipsilateral renal bed. Bladder is slightly more distended than for transvaginal sonography of uterus and adnexa. (Courtesy of Barbara J. Weinstein, Pittsburgh, PA. Adapted with permission from Mendelson and Böhm-Vélez [1].)

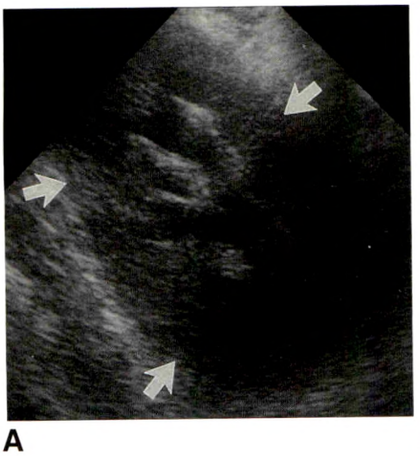

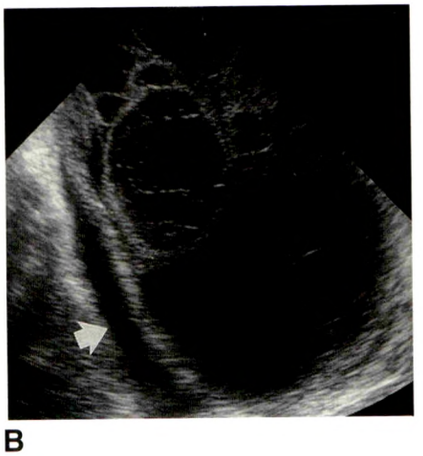

Fig. 20.—Renal transplant.
A, Transvaginal sonogram shows pelvicaliectasis within central portion of this transplanted kidney (*arrows*) in iliac fossa.
B, Transvaginal sonogram shows a complex, predominantly cystic mass adjacent to renal pelvis. This was a complicated urinoma that may have caused hydronephrosis. Free fluid (*arrow*) also is visible. (Adapted with permission from Mendelson and Böhm-Vélez. [1].)

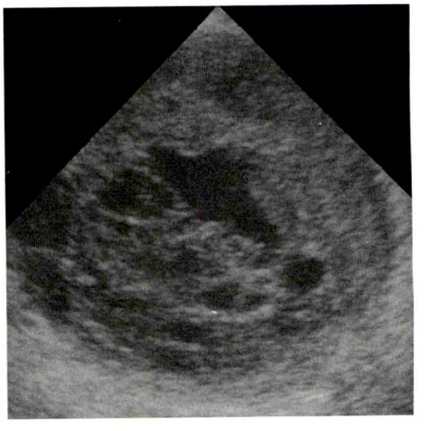

Fig. 21.—Hematoma. Transvaginal sonogram shows an indeterminate complex mass in pelvis. Clinical history of anticoagulant therapy was clue to diagnosis of maturing hematoma. (Reprinted with permission from Mendelson and Böhm-Vélez [1].)

acterize the appearance of the fluid. Anechoic fluid is seen with transudative ascites or rupture of an ovarian cyst or follicle. Echogenic fluid may signify an emergent process such as hemoperitoneum from a ruptured ectopic pregnancy. Other causes of echogenic fluid include pelvic inflammatory disease; diverticular (Fig. 14A), appendiceal (Fig. 15), or postoperative abscesses; and malignant ascites [1] (Fig. 18).

Miscellaneous Masses

Kidneys

If a reniform mass is detected in the superior part of the pelvis, the renal beds should be evaluated. An empty renal fossa suggests the diagnosis of pelvic kidney [3] (Fig. 19). Hydronephrosis may be present because of the increased risk of obstruction at the ureteropelvic junction. Although a pelvic kidney is usually an isolated finding, the uterus should be examined for associated anomalies.

Renal transplants are found in the iliac fossae. Complications of renal transplantation include urinoma (Fig. 20), hematoma, and lymphocele [1].

Hematomas

Hematomas are varied in appearance, ranging from simple to complex fluid collections, depending on the age of the hematoma [3] (Fig. 21). Acute hematomas have mixed

Fig. 22.—Adhesions. Transvaginal sonogram shows an unusual appearing complex mass, which resulted from adhesions between mesentery and surrounding tissues.

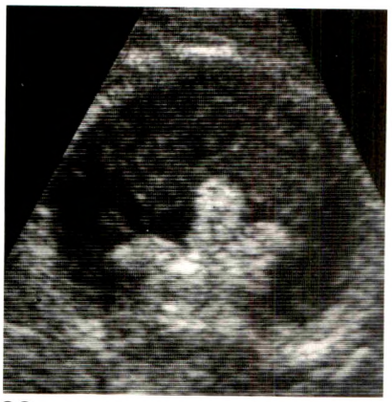

22

Fig. 23.—Parovarian (paratubal) cyst. Transvaginal sonogram shows a large simple cyst that was separate from ovaries and uterus, consistent with a parovarian cyst. These benign cysts are found in the mesosalpinx and arise from the parovarium, a remnant of the mesonephric duct.

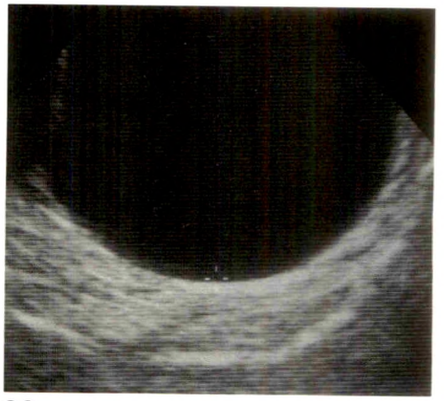

23

echogenicity and become anechoic or develop septa with time. Pelvic hematomas are most commonly seen shortly after pelvic surgery. Rounded echogenic collections associated with the ovary most likely are hemorrhagic cysts or endometriomas.

Abscesses

Abscesses appear as nonspecific complex fluid collections that often contain echogenic foci with posterior acoustic shadowing, representing gas. Possible causes of abscesses, other than pelvic inflammatory disease, include diverticulitis (Fig. 14A), appendicitis (Fig. 15), and postoperative complications [1].

Adhesions

The differential diagnosis of a complex mass in the postoperative patient includes a mass formed by peritoneal adhesions [1] (Fig. 22). Correlation of sonographic findings with clinical history is important in this situation.

Cysts

Nonovarian cystic masses visualized transvaginally include mesenteric and duplication cysts, urachal cysts, lymphoceles, and parovarian cysts [1] (Fig. 23). These can usually be differentiated on the basis of location and clinical history.

Conclusion

Transvaginal sonography can be a useful method for evaluating the nongynecologic structures of the female pelvis. Its value depends on knowledge of the special technical modifications required for imaging the lower urinary tract, rectosigmoid colon, and lower quadrants of the abdomen. Familiarity with the normal and abnormal appearances of these structures is also crucial.

REFERENCES

1. Mendelson EB, Böhm-Vélez M. Nongynecologic applications. In: Nyberg DA, Hill LM, Böhm-Vélez M, Mendelson EB, eds. *Transvaginal ultrasound.* St. Louis: Mosby–Year Book, **1992**:295–308
2. Dodson MG. The fallopian tubes, adnexa, pelvic vessels, bowel, and urinary bladder. In: *Transvaginal ultrasound.* New York: Churchill Livingstone, **1991**:145–164
3. Rifkin MD, Needleman L, Kurtz AB, et al. Sonography of nongynecologic cystic masses of the pelvis. *AJR* **1984**;142:1169–1174
4. Haylen BT, Frazer MI, Sutherst JR, West CR. Transvaginal ultrasound in the assessment of bladder volumes in women: preliminary report. *Br J Urol* **1989**;63:149–151

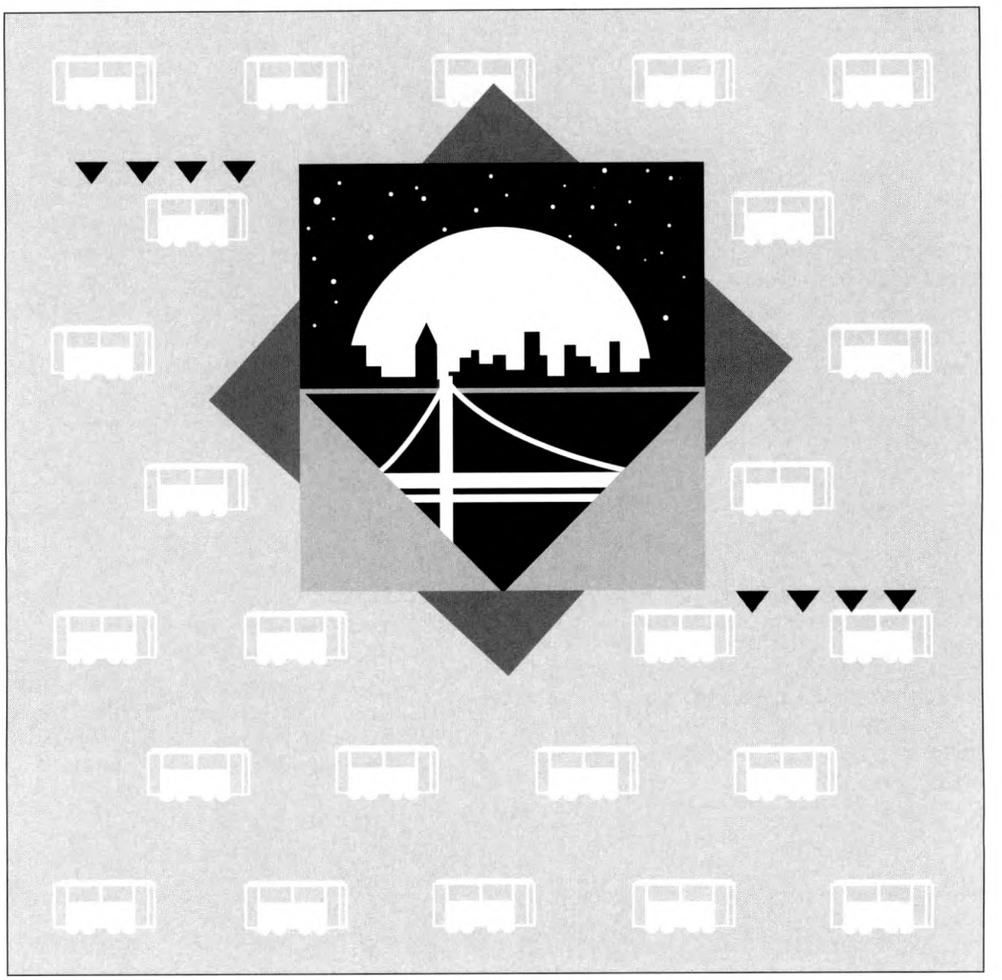

San Francisco

American Roentgen Ray Society

93rd Annual Meeting

April 25–30, 1993

San Francisco Marriott • San Francisco, CA

Review Article

Trauma to the Upper Thoracic Spine: Anatomy, Biomechanics, and Unique Imaging Features

Georges Y. El-Khoury[1] and Camelia G. Whitten

This review summarizes the anatomic and biomechanical features of the thoracic spine, which are different from those of the more mobile segments of the spine, and emphasizes their role in trauma. The distinguishing characteristics of the thoracic spine are the presence of the ribs and their articulations. The rib cage restricts motion and adds stiffness to the spine. During trauma, it provides the thoracic spine with additional strength and energy-absorbing capacity. Above the T10 level, most injuries produce a basic pattern consisting of an anterior fracture-dislocation involving two contiguous vertebrae, often with associated neurologic impairment. The definition of spinal instability remains controversial. CT is the imaging technique of choice for evaluation of spine fractures; however, MR imaging is superior in the evaluation of spinal cord injury and posttraumatic disk herniation. MR imaging also provides prognostic information not obtainable with other imaging methods.

The thoracic spine is the largest segment of the spine, and it is a common site for trauma, especially in its lower portion (T10–T12). The anatomic and biomechanical features of the thoracic spine make its response and tolerance to mechanical stresses different from those of the more mobile portions of the spine. This review considers the anatomy, biomechanics, and unique imaging features of the normal and traumatized upper portion of the thoracic spine.

Anatomy and Biomechanics of the Thoracic Spine

Gross Anatomy

The thoracic spine consists of 12 vertebrae; it has a ventral curve that develops in utero and is maintained, although somewhat modified, throughout life. The vertebral bodies anteriorly are primarily load-bearing. The arches posteriorly act in resisting tension. The anteroposterior diameter of the vertebral bodies gradually increases from T1 to T12, whereas the transverse width decreases from T1 to T3 and then increases progressively down to T12 [1]. Normally, the vertical height of the thoracic vertebral bodies is about 2–3 mm less anteriorly than posteriorly, which partially contributes to thoracic kyphosis. The sides of the bodies are somewhat concave. In the thoracic spine, the laminae are broad and heavily overlapped. The pedicles project posteriorly from the superior aspect of the vertebral body. Extending dorsomedially from the pedicles are the laminae, which fuse in the midline to form the dorsal wall of the spinal canal [1, 2]. The lumen of the spinal canal varies in size throughout its length, but its narrowest segment is in the thoracic spine. Neural elements within the thoracic portion of the spinal canal are, therefore, more frequently affected by conditions that result in even minimal narrowing of the spinal canal [3, 4]. The articular processes arise from both the superior and inferior surfaces of the laminae. The articulating facets are

Received July 1, 1992; accepted after revision July 28, 1992.
[1] Both authors: Department of Radiology, The University of Iowa Hospitals and Clinics, 200 Hawkins Dr., Iowa City, IA 52242. Address reprint requests to G. Y. El-Khoury.

AJR 1993;160:95–102 0361–803X/93/1601–0095

situated on the posterior surface of the superior articular process and ventral surface of the inferior process. Throughout most of the thoracic region (T1–T10), the facets are in the coronal plane, thus providing significant resistance to anterior translation. At T11 and T12, facets begin to change their orientation to simulate the lumbar pattern (oblique sagittal orientation), where they limit rotation and have less effect on anterior translation [4].

The most distinguishing features of the thoracic spine are related to the presence of the ribs and their articulations [1, 2]. Ribs articulate with vertebrae at two sites. Rib heads articulate with the vertebrae at the disk, and the rib tubercle articulates with the transverse process at the costotransverse articulation.

Demifacets above and below the disk articulate with the head of the rib to form the costovertebral joint, which is a synovial joint divided by an intraarticular ligament into two separate compartments. The heads of the first, 11th, and 12th ribs articulate with single vertebral facets of the corresponding vertebrae rather than with two demifacets of adjacent vertebrae [1, 2]. The head of the rib is an important landmark for identifying the intervertebral disk during axial imaging. The rib cage restricts motion and adds stiffness to the spine. This is especially true in extension and to a lesser extent in flexion and lateral rotation. Biomechanically, the rib cage is considered part of the structure of the spine, thus providing additional strength and energy-absorbing capacity during trauma. The rib cage and sternum increase the moment of inertia and therefore stiffen the spine when it is subjected to rotatory forces [5]. Andriacchi et al. [6] predicted that the compression tolerance of the spinal column in the presence of the rib cage is increased by a factor of 4. In clinical situations, when costovertebral disruption is present, the ability of the spine to carry normal physiologic loads should be questioned.

The transverse processes project laterally from the articular pillars between the superior and inferior articular facets. They diminish in length from the top to the bottom of the thoracic spine. The tip of each transverse process from T1 to T10 bears an oval costal facet. Costotransverse joints are formed by the articulation of the rib tubercles and tips of the transverse processes. T11 and T12 transverse processes do not articulate with ribs [1, 2].

Compared with the cervical and lumbar spine, the height of disks in the thoracic spine is decreased, but the annulus fibrosus is thicker. The disks in the thoracic region seem to be effective in limiting rotation [4]. The anterior and posterior longitudinal ligaments, ligamenta flava, and interspinous and supraspinous ligaments in the thoracic spine are not significantly different from these ligaments at other spinal segments.

Radiographic Anatomy

Conventional radiography continues to be the mainstay of any diagnostic investigation of the thoracic spine. Plain radiography should precede any complex imaging procedure, and the interpretation of these complex studies should be undertaken only with the plain radiographs at hand. Anteroposterior and lateral radiographs are always required. Anteroposterior radiographs can be obtained easily; however, diagnostic lateral radiographs may be more difficult to obtain in patients with multisystem trauma because the examination is performed with the patient in the supine position. In cooperative patients, high-quality lateral views of the thoracic spine can be obtained by using a long exposure (3–6 sec, 50 mA, and 70 kVp) and breathing technique. A swimmer's view of the upper thoracic spine is often beneficial when the upper thoracic vertebrae are not adequately visualized.

Anteroposterior radiographs are ideal for the evaluation of the vertebral bodies. The superior and inferior endplates of the vertebral bodies are seen as linear horizontal lines. The lateral margins are concave. Pedicles appear as oval structures projecting over the superior corners of the vertebral bodies. Absence of a pedicle, or asymmetry in the size or density of the pedicles, warrants further investigation to rule out neoplasm. Pedicle thinning, with a slight increase in the interpediculate distance at the level of the thinning, is normally seen at the thoracolumbar junction in 7% of the population. The thinned pedicles may even have concave medial borders [7, 8]. The articular facets and laminae are difficult to evaluate on the anteroposterior view. The transverse processes are visible as lateral extensions of the upper half of the vertebrae, whereas the costotransverse joints can be detected as two oblique lines close to the ends of the transverse processes. Rib heads, which are detected at the level of the intervertebral disks, articulate with the superior and inferior corners of adjacent vertebral bodies. The paraspinal soft tissues of the thoracic spine should be closely applied to the vertebral bodies and only minimally visible. No focal swelling should be identified in the paraspinal soft tissues of the normal thoracic spine.

Lateral radiographs are helpful in assessing vertebral body height, disk height, endplate irregularity, erosions, and alignment. On the lateral projection, vertebral bodies are seen as rectangular structures. The pedicles extend posteriorly from the superior half of the body. Located above and below the pedicles are the articular processes. The spinal canal and neural foramina are clearly delineated on lateral radiographs. The inferior portions of the neural foramina are occluded by the heads of the ribs [1]. The spinous processes are virtually impossible to visualize on the lateral view owing to the superimposition of the ribs.

Trauma to the Upper Thoracic Spine

Fractures in the upper thoracic spine (T1–T10) are not uncommon. Of 2416 patients with acute fractures of the vertebral column admitted to the Northwestern University Acute Spine Injury Center between 1972 and 1986, 16% of the 376 fractures involved the upper thoracic spine [9].

Fractures of the Upper Thoracic Spine

Historically, fractures of the upper thoracic spine (T1–T10) have been grouped with fractures of the thoracolumbar junction and lumbar spine. These regions differ in both their neurologic and osseous aspects [3]. Bohlman [3] drew attention to the unique features of trauma involving the upper thoracic

spine and noted the following: (1) Because of its stiffness, considerable violence is necessary to produce fractures or fracture-dislocations in the upper thoracic spine. (2) Because of the narrow spinal canal in this region, injuries of the spinal cord are frequently associated with injuries of the upper thoracic spine. (3) Most of the osseous injuries occur in flexion and axial loading because very little rotatory motion occurs in the upper thoracic spine.

Anteroposterior and lateral views of the thoracic spine are helpful in assessing alignment. An abrupt change in alignment indicates spinal injury (Figs. 1A and 2B). The presence of abnormal kyphosis, pleural fluid, paraspinal swelling, rib fractures, dislocations at the costovertebral joints, or widening of the interpediculate distance also suggests thoracic spine injury (Figs. 2A and 2B).

Rogers et al. [10] recognized that fractures of the upper thoracic spine do not fit easily into the common fracture classifications and thus should be treated separately. In a review of 35 patients with acute injury to the upper thoracic spine and associated paraplegia, they found the basic pattern of injury, affecting 32 of 35 patients, consisted of an anterior fracture-dislocation involving two contiguous vertebrae (Figs. 2A and 2B). Sharafuddin et al. [11] described similar radiographic findings in three patients with fracture-dislocations of the thoracic spine.

Anteriorly wedged vertebrae are usually considered abnormal in the clinical setting of trauma. However, normal wedging of the lower thoracic vertebral bodies, especially in males, is common [12, 13]. Fletcher [12] and Lauridsen et al. [13] proposed using a wedging ratio that compares heights of the anterior vs the posterior vertebral bodies. Wedging ratios of 0.80 in males and 0.87 in females (95% confidence limits) at the T8 to T12 levels are considered within normal limits [12, 13].

The posterior aspects of the vertebral bodies are visible on lateral radiographs. Disruption, or bulging, of this line into the spinal canal is a reliable indicator of a burst fracture in the spine (Fig. 3). In a study of 114 patients with burst fractures, Daffner et al. [14] found disruption of the posterior vertebral body line in all. This line should be carefully scrutinized in patients with trauma to the thoracic spine.

The spinous processes consistently project over the midline, and each tubercle (tip) of the spinous process extends slightly below the inferior endplate of its respective vertebral body. The "double spinous process sign" seen on the anteroposterior radiograph is a reliable indicator of a fracture of the spinous process [15, 16] (Fig. 4).

CT is a useful adjunct to standard radiography when assessing trauma of the thoracic spine, particularly in the evaluation of vertebral fracture and retropulsed fragments [17–20] (Fig. 3B). Keene et al. [17] and Brant-Zawadzki et al. [18] demonstrated that CT combined with standard radiography is equal or superior to conventional tomography in assessing the extent of spine trauma. Brant-Zawadzki et al. [18] reported that conventional tomography added no clinically significant information in the acute stage.

Spinal Cord Injury

Fractures associated with spinal cord injury most often occur at C4–C7 and the thoracolumbar junction; however, midthoracic spine fractures account for a sizable portion of

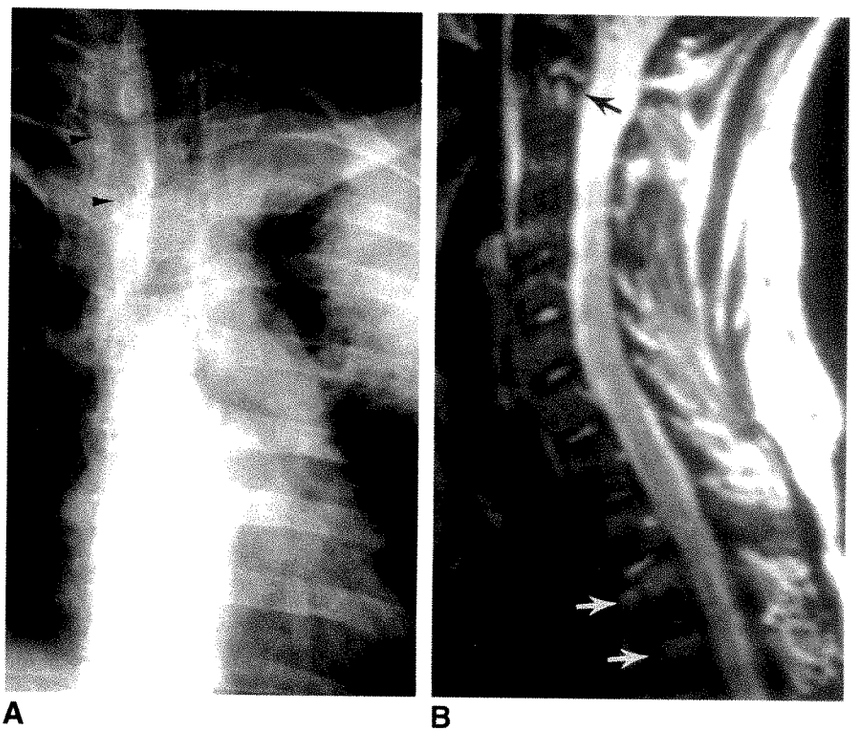

Fig. 1.—Abnormal alignment and noncontiguous fractures.

***A*, Anteroposterior chest radiograph shows fluid in left pleural space and abnormal alignment between T2 and T3 (*arrowheads*), suggesting a fracture-dislocation.**

***B*, Sagittal T2-weighted MR image shows T3 and T4 vertebral body fractures (*white arrows*) and a noncontiguous fracture of odontoid (*black arrow*).**

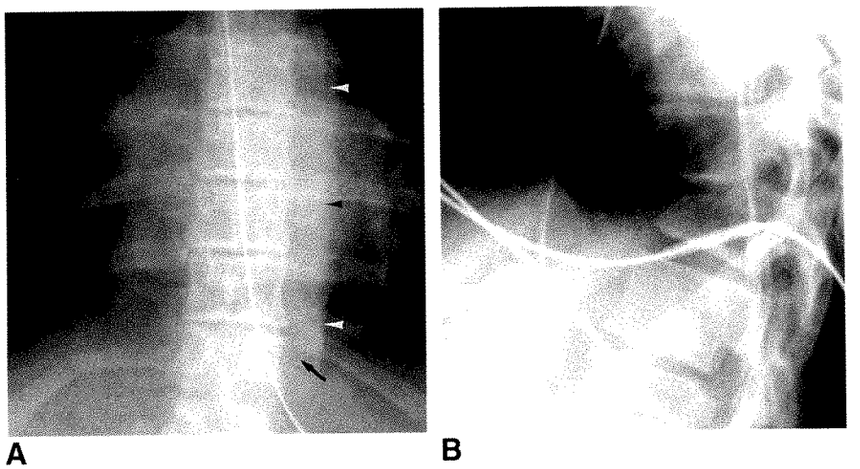

Fig. 2.—Anterior fracture-dislocation of thoracic spine.

A, Anteroposterior radiograph shows interruption in outline of pedicles at T10, left paraspinal swelling (*arrowheads*), and left costovertebral dislocation at T11 (*arrow*).

B, Lateral radiograph of thoracic spine shows anterior fracture-dislocation of T10 on T11, with secondary kyphosis at T10–T11.

C, Sagittal T2-weighted MR images show transection of cord with hemorrhage and edema within spinal cord.

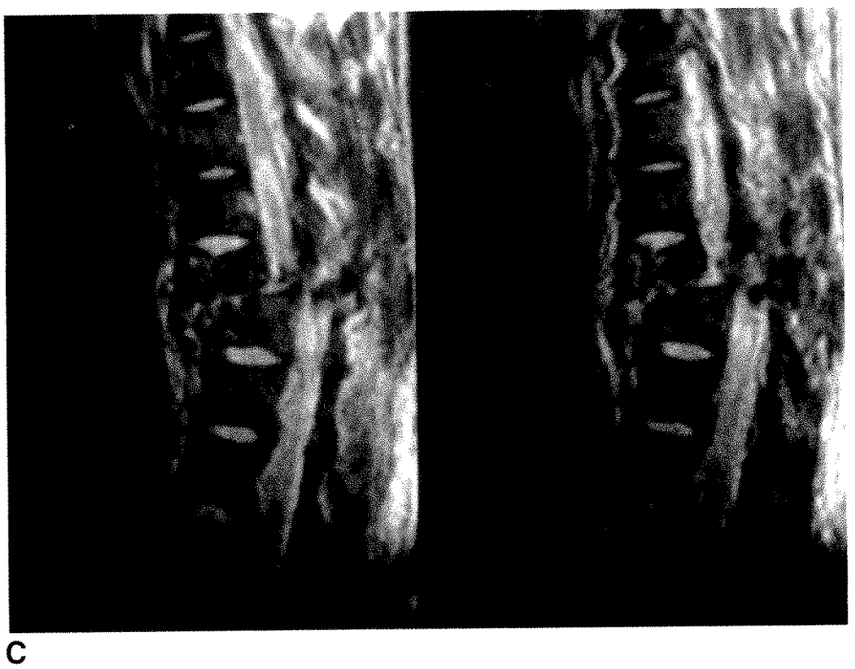

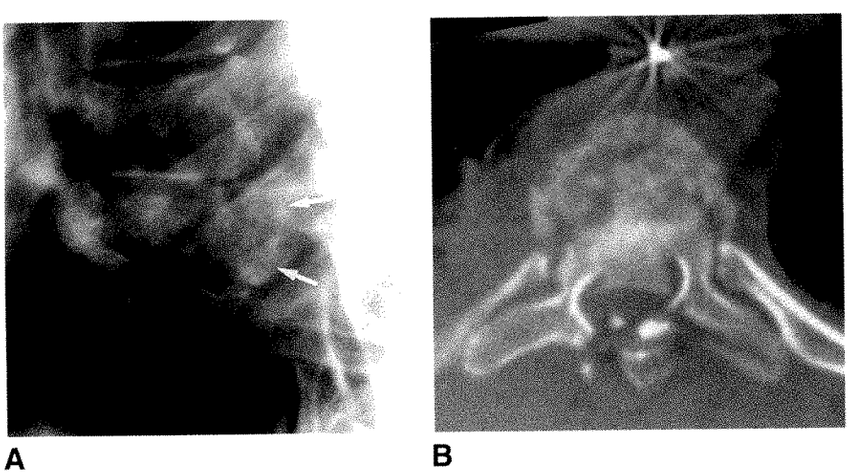

Fig. 3.—Disruption of posterior vertebral body line.

A, Lateral radiograph of thoracic spine shows posterior displacement and bulging of posterior vertebral body line of T10 (*arrows*), indicating retropulsed fragments within spinal canal.

B, Axial CT scan through T10 confirms presence of retropulsed fragment within spinal canal.

fractures with injury to the spinal cord [10]. Owing to the small diameter of the thoracic spinal canal and the sparse vascular supply to the thoracic spinal cord, fractures of the upper thoracic spine are usually associated with neurologic injury [9, 21]. Meyer [9] reported that 63% of the fractures of the upper thoracic spine seen at the Northwestern University Acute Spine Injury Center between 1972 and 1986 resulted in complete neurologic injuries to the spinal cord, while the thoracic spinal cord escaped injury in only 10%. Clinical evaluation has been, until recently, the only method for predicting outcome in patients with spinal cord injury. Clinical assessment, however, cannot distinguish between transection, hemorrhage, and edema of the spinal cord, as indicated by the occasional observation of significant recovery after an apparently complete lesion [22]. MR imaging is capable of showing edema and hemorrhage within the spinal cord. In addition, several authors [22–29] have recognized a distinct correlation between the pattern of spinal cord injury on MR imaging and neurologic recovery. Hemorrhage within the spinal cord suggests that there will be little improvement in neurologic function. Edema within the spinal cord, particularly if it is limited to one spinal segment, implies a more favorable outcome. The optimum time for prognostic imaging is 24–72 hr after the injury. For assessment of spinal injury, MR imaging has recently been advocated as the examination of choice, after conventional radiography, particularly when a neurologic deficit is present or is progressing [27] (Fig. 2C). MR imaging also has the added advantage of showing the cervicothoracic junction in heavy patients [27].

Holdsworth [30] in 1970 and Bohlman [3] in 1985 stated that shearing fractures of the upper thoracic spine are always associated with complete paraplegia; however, some reports [11, 31–33] describe patients with severe fracture dislocations of the thoracic spine in whom the spinal cord was not injured.

The "floating laminae" or "floating arches" mechanism may explain how the spinal cord escapes injury in fracture-dislocations of the thoracic spine. Bilateral pedicular fractures at several levels allow the posterior elements to remain aligned while the vertebral bodies displace forward [31–33]. With the floating arches mechanism, the spinal canal actually enlarges, in a fashion similar to that seen with spondylolisthesis, owing to a defect in the pars interarticularis. Simpson et al. [33] warned that although plain radiographs may suggest transection of the spinal cord, they should never be used to infer the state of the spinal cord in an obtunded or unconscious patient. Careful handling of the unstable spine in these circumstances should continue until the neurologic status of the patient can be thoroughly evaluated.

Multilevel Spinal Injuries

Up to 17% of fractures of the upper thoracic spine are associated with another noncontiguous spinal fracture [10]. Often, the second level of injury is not recognized early enough to prevent clinically significant extension of the neurologic deficit [34]. Common sites for second noncontiguous fractures are the upper cervical spine and thoracolumbar junction [10, 34, 35]. The multiplanar capabilities of MR imaging facilitate early diagnosis of multilevel trauma, occasionally revealing unsuspected injuries (Fig. 1B). It is therefore mandatory to search for other spine fractures whenever a fracture is detected in the upper thoracic spine. The presence of these second-level spinal injuries is further testimony to the severity and complicated nature of the forces involved in injuries of the upper thoracic spine [10].

Fracture of the Upper Thoracic Spine vs Aortic Transection

Traditionally, mediastinal widening, apical cap, and pleural fluid have been attributed to aortic transection [36]. However, these findings are also seen in more than half the patients with an injury to the upper thoracic spine [3, 37–39] (Fig. 4). Dorr et al. [39] found a 36% frequency of hemothorax in patients with injuries to the thoracic spine. In a review of the radiographs of 54 patients with fractures between the C6 and T8 vertebral levels, Dennis and Rogers [38] found that 69% had a wide mediastinum. A spine fracture could be detected on the chest radiograph in half of their patients. These authors concluded that if a fracture of the upper thoracic spine can be detected to account for the mediastinal widening, aortic rupture becomes unlikely in the absence of clinical signs and symptoms to support such a diagnosis [38].

Fractures of the upper thoracic spine and aortic rupture have an important clinical feature in common: both conditions can cause paraparesis or paraplegia [37]. Aortic rupture can cause diminished blood supply to the spinal cord, resulting in ischemia and necrosis [40]. Therefore, in patients in whom both aortic rupture and fracture of the upper thoracic spine are possibilities, the proper sequencing of diagnostic tests and careful handling of the patient are essential. Bolesta and Bohlman [37] recommend first ruling out an aortic injury and then localizing the fracture or dislocation. Such patients should be immobilized and handled judiciously when they are transported to and from the angiography suite.

Sternal Fractures

The sternum is frequently buckled or fractured in patients with trauma to the upper thoracic spine. Radiographically, the appearance of this indirect injury to the sternum differs from that of direct trauma to the sternum and should alert radiologists to severe injury in the thoracic spine [41]. An indirect sternal injury is identified by the pattern of displacement of the bone fragments. Forces transmitted to the sternum through the ribs, as a result of spine fracture or dislocation, posteriorly displace the upper sternal fragment relative to the lower portion of the sternum (Fig. 5). This pattern of displacement is different from that usually seen with direct trauma to the sternum, where forces applied to the front of the chest posteriorly displace the lower sternal fragment [42].

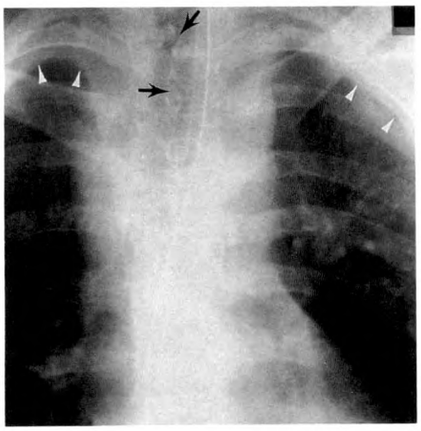

Fig. 4.—Injury to upper thoracic spine vs aortic transection. Anteroposterior chest radiograph obtained with patient supine shows widening of mediastinum and apical pleural capping (*arrowheads*). These findings are seen in both upper thoracic spine injury and aortic transection. Nasogastric tube is not shifted to right, and left main bronchus is not depressed. Spinous processes of T1 and T2 (*arrows*) are duplicated (double spinous process sign), indicating fractures. Findings on aortic angiogram were normal.

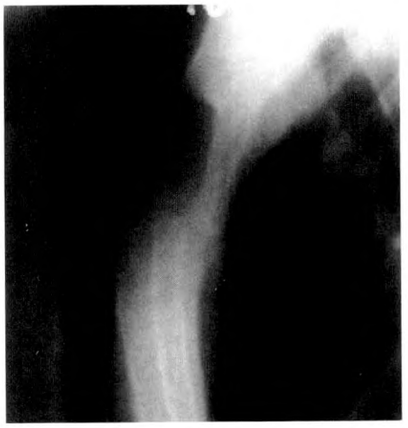

Fig. 5.—Sternal fracture. Lateral radiograph of sternum in a patient with T6–T7 fracture shows characteristic appearance of sternal fractures associated with thoracic spine injury: posterior displacement of upper sternal fragment relative to lower fragment.

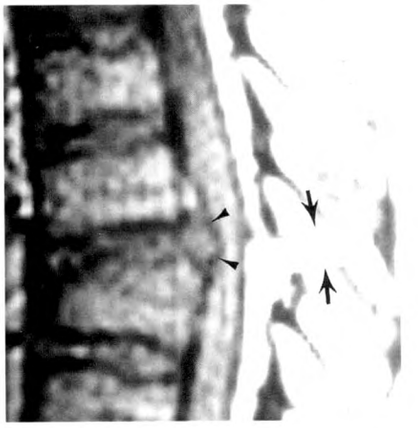

Fig. 6.—Traumatic thoracic disk herniation. Sagittal T1-weighted MR image shows a traumatic herniation of disk at T8–T9 (*arrowheads*). Note also fracture in vertebral arch (*arrows*) and mild anterior subluxation of T8 on T9.

Traumatic Disk Herniation

Intervertebral disk herniation after injury to the cervical spine is well known [28, 43–45]. Posttraumatic disk herniation in the thoracic spine, however, is not uncommon [46] (Fig. 6). Pratt et al. [46] reported that three of their six patients with acute injury to the thoracic spine had disk herniations shown by MR imaging. Because the presence of a herniated disk can significantly alter the surgical management of a spine injury, radiologists may be asked to address this question when evaluating spine trauma [28, 43, 45, 46]. Because MR imaging provides more information than CT regarding the integrity of the spinal cord, disks, and ligaments, it should be the imaging technique of choice in the evaluation of disk herniation or other soft-tissue injury to the spine [45–48].

Spinal Instability

Spinal instability after trauma is an exceedingly important issue for surgeons, because its presence or absence determines how the patient is treated. The definition of instability has been controversial, and no single scheme to determine instability is universally accepted.

White and Panjabi [5] defined clinical instability as "the loss of the ability of the spine under physiologic loads to maintain relationships between vertebrae in such a way that there is neither damage nor subsequent irritation to the spinal cord or nerve roots, and in addition, there is no development of incapacitating deformity or pain due to structural changes."

Holdsworth [30] thinks that the integrity of the posterior column, consisting of the vertebral arch and its ligaments, is the key to spinal stability. In 1983, Denis [49] reported that instability did not result from rupture of the posterior column alone and advanced the clinically based three-column theory. He asserted that, for an injury to be unstable, the middle column, consisting of the posterior portion of the vertebral body, posterior annulus, and posterior longitudinal ligament, should be disrupted [49]. He also separated spinal injuries into four major types: compression fracture, burst fracture, flexion-distraction (seat-belt) fracture, and fracture-dislocation. This three-column concept and fracture classification are widely used in the evaluation of thoracolumbar spine trauma.

Some investigators [4, 10, 50] have observed that these concepts do not seem to apply to the rigid portion of the thoracic spine. As an alternative, Daffner et al. [50] proposed radiographic criteria for instability that would apply to the entire vertebral column. When one or more of the following five radiographic signs are present, the injury is considered unstable: displaced vertebrae, widened interlaminar or interspinous distance, perched or dislocated facet joints, increased interpediculate distance, and disrupted posterior vertebral body line.

Other investigators think that although the three-column theory is clinically attractive, it is not valid biomechanically. Studies of kinematics during spinal loading and fracture have shown significant variability in injuries produced with similar forces [4]. Yoganandan et al. [51] proposed that instability should be considered as a continuum, in which partial injuries to different structures of the spine may allow pathologic amounts of motion, even if gross failure is not evident initially. This continuum of instability may lead to late deformity as well as to neurologic deterioration (Fig. 7).

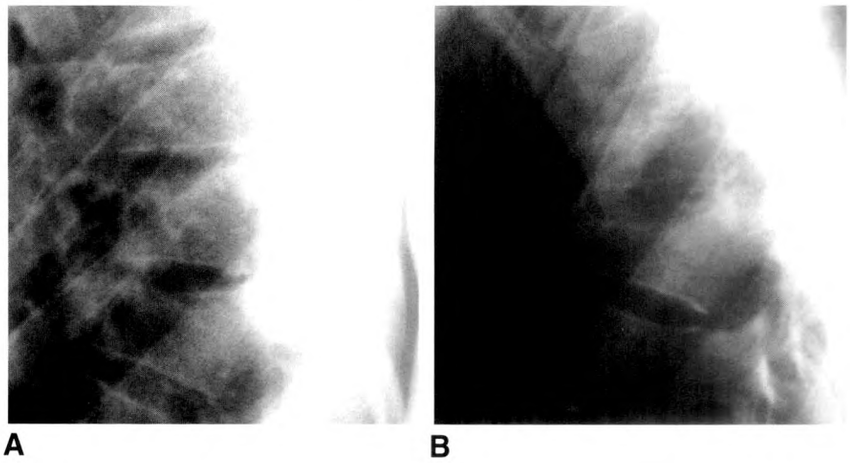

Fig. 7.—Delayed instability.
***A*, Lateral radiograph of thoracic spine obtained at admission in a 22-year-old woman involved in a car accident shows vertebral body compression fractures involving three midthoracic vertebrae. She was neurologically intact at admission. The injury was judged to be stable and was treated with a brace.**
***B*, 8 weeks after *A*, the patient returned with weakness and neurologic deficits in lower extremities. Lateral radiograph shows increased wedging of bodies of T6 and T7 and progressive kyphosis as compared with *A*.**

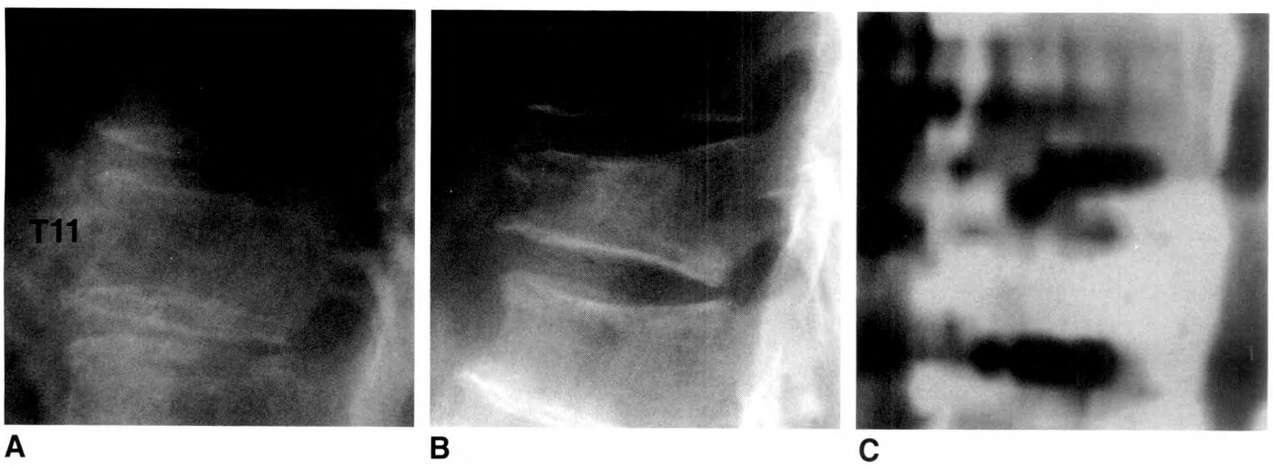

Fig. 8.—Kümmell's disease.
***A*, Lateral radiograph of thoracolumbar junction obtained on day of injury shows normal T11 vertebra.**
***B*, Lateral radiograph obtained 2 months after injury shows collapse of T11 vertebra.**
***C*, Sagittally reconstructed CT scan, obtained at same time as *B*, shows intravertebral and intradiskal vacuum phenomena, characteristically associated with Kümmell's disease.**

Delayed Posttraumatic Vertebral Collapse (Kümmell's Disease)

Delayed posttraumatic vertebral collapse, also known as Kümmell's disease, has been reported in the thoracic and thoracolumbar regions [52]. This is a poorly understood phenomenon, but it is generally accepted that minor trauma without overt fracture can lead to delayed collapse of the involved vertebra. Evidence favors avascular necrosis as the mechanism for the delayed collapse, as the majority of reported patients were on long-term corticosteroid therapy [53]. Spinal angiography and pathologic findings also support avascular necrosis as the mechanism underlying delayed vertebral collapse [52]. Radiographically, Kümmell's disease presents as vertebral body collapse after minor trauma and often is associated with intravertebral and intradiskal vacuum phenomena (Fig. 8).

REFERENCES

1. Louis R. *Surgery of the spine.* Berlin: Springer-Verlag, **1983**:26-34
2. Williams PL, Warwick R, Dyson M, Bannister LH. *Gray's anatomy*, 37th ed. New York: Churchill Livingstone, **1989**:319–322, 496–497
3. Bohlman HH. Treatment of fractures and dislocations of the thoracic and lumbar spine. *J Bone Joint Surg [Am]* **1985**;67-A:165–169
4. Maiman DJ, Pintar FA. Anatomy and clinical biomechanics of the thoracic spine. *Clin Neurosurg* **1992**;38:296–324
5. White AA III, Panjabi MM. *Clinical biomechanics of the spine.* Philadelphia: Lippincott, **1978**:42–47, 191–192
6. Andriacchi T, Schultz A, Belytschko T, Galante J. A model for studies of mechanical interactions between the human spine and rib cage. *J Biomech* **1974**;7:497–507
7. Benzian SR, Mainzer F, Gooding CA. Pediculate thinning: a normal variant at the thoracolumbar junction. *Br J Radiol* **1971**;44:936–939
8. Charlton OP, Martinez S, Gehweiler JA Jr. Pedicle thinning at the thoracolumbar junction: a normal variant. *AJR* **1980**;134:825–826
9. Meyer PR. Fractures of the thoracic spine: T1 to T10. In: Meyer PR, ed. *Surgery of spine trauma.* New York: Churchill Livingstone, **1989**: 525–571

10. Rogers LF, Thayer C, Weinberg PE, Kim KS. Acute injuries of the upper thoracic spine associated with paraplegia. *AJR* **1980**;134:67–73
11. Sharafuddin MJA, Hitchon PW, El-Khoury GY, Dyste GN. Locked facets in the thoracic spine: report of three cases and a review. *Spinal Disord* **1990**;3:255–258
12. Fletcher GH. Anterior vertebral wedging: frequency and significance. *AJR* **1947**;57:232–238
13. Lauridsen KN, De Carvalho A, Andersen AH. Degree of vertebral wedging of the dorso-lumbar spine. *Acta Radiol* **1984**;25:29–32
14. Daffner RH, Deeb ZL, Rothfus WE. The posterior vertebral body line: importance in the detection of burst fractures. *AJR* **1987**;148:93–96
15. Baker BK, Sundaram M, Awwad EE. Case report 688. *Skeletal Radiol* **1991**;20:463–464
16. Zanca P, Lodmell EA. Fracture of the spinous processes: a "new" sign for the recognition of fractures of cervical and upper dorsal spinous processes. *Radiology* **1951**;56:427–428
17. Keene JS, Goletz TH, Lilleas F, Alter AJ, Sackett JF. Diagnosis of vertebral fractures. *J Bone Joint Surg [Am]* **1982**;64-A:586–595
18. Brant-Zawadzki M, Miller EM, Federle MP. CT in the evaluation of spine trauma. *AJR* **1981**;136:369–375
19. Ghoshhajra K, Rao KCVG. CT in spinal trauma. *Clin Imaging* **1980**;4: 309–318
20. McAfee PC, Yuan HA, Fredrickson BE, Lubicky JP. The value of computed tomography in thoracolumbar fractures. *J Bone Joint Surg [Am]* **1983**;65-A:461–473
21. Meyer PR. Vascular anatomy of the spinal cord: T1 to T10. In: Meyer PR, ed. *Surgery of spine trauma.* New York: Churchill Livingstone, **1989**: 85–106
22. Bondurant FJ, Cotler HB, Kulkarni MV, McArdle CB, Harris JH Jr. Acute spinal cord injury: a study using physical examination and magnetic resonance imaging. *Spine* **1990**;15:161–168
23. Yamashita Y, Takahashi M, Matsuno Y, et al. Acute spinal cord injury: magnetic resonance imaging correlated with myelopathy. *Br J Radiol* **1991**;64:201–209
24. Kulkarni MV, McArdle CB, Kopanicky D, et al. Acute spinal cord injury: MR imaging at 1.5 T. *Radiology* **1987**;164:837–843
25. Kulkarni MV, Bondurant FJ, Rose SL, Narayana PA. 1.5 Tesla magnetic resonance imaging of acute spinal trauma. *RadioGraphics* **1988**;8: 1059–1082
26. Hackney DB, Asato R, Joseph PM, et al. Hemorrhage and edema in acute spinal cord compression: demonstration by MR imaging. *Radiology* **1986**;161:387–390
27. Kerslake RW, Jaspan T, Worthington BS. Magnetic resonance imaging of spinal trauma. *Br J Radiol* **1991**;64:386–402
28. Schaefer DM, Flanders A, Northrup BE, Doan HT, Osterholm JL. Magnetic resonance imaging of acute cervical spine trauma: correlation with severity of neurological injury. *Spine* **1989**;14:1090–1095
29. Schaefer DM, Flanders AE, Osterholm JL, Northrup BE. Prognostic significance of magnetic resonance imaging in the acute phase of cervical spine injury. *J Neurosurg* **1992**;76:218–223
30. Holdsworth F. Fractures, dislocations, and fracture-dislocations of the spine. *J Bone Joint Surg [Am]* **1970**;52-A:1534–1551
31. Gertzbein SD, Offierski C. Complete fracture-dislocation of the thoracic spine without spinal cord injury: a case report. *J Bone Joint Surg [Am]* **1979**;61-A:449–451
32. Sasson A, Mozes G. Complete fracture-dislocation of the thoracic spine without neurologic deficit. *Spine* **1987**;12:67–70
33. Simpson AHRW, Williamson DM, Golding SJ, Houghton GR. Thoracic spine translocation without cord injury. *J Bone Joint Surg [Br]* **1990**;72-B:80–83
34. Calenoff L, Chessare JW, Rogers LF, Toerge J, Rosen JS. Multiple level spinal injuries: importance of early recognition. *AJR* **1978**;130:665–669
35. Gupta A, El Masri WS. Multilevel spinal injuries: incidence, distribution and neurological patterns. *J Bone Joint Surg [Br]* **1989**;71-B:692–695
36. Gundry SR, Burney RE, MacKenzie JR, et al. Assessment of mediastinal widening associated with traumatic rupture of the aorta. *J Trauma* **1983**;23:293–299
37. Bolesta MJ, Bohlman HH. Mediastinal widening associated with fractures of the upper thoracic spine. *J Bone Joint Surg [Am]* **1991**;73-A:447–450
38. Dennis LN, Rogers LF. Superior mediastinal widening from spine fractures mimicking aortic rupture on chest radiographs. *AJR* **1989**;152:27–30
39. Dorr LD, Harvey JP Jr, Nickel VL. Clinical review of the early stability of spine injuries. *Spine* **1982**;7:545–550
40. Dommisse GF. The blood supply of the spinal cord: a critical vascular zone in spinal surgery. *J Bone Joint Surg [Br]* **1974**;56-B:225–235
41. Gopalakrishnan KC, El Masri WS. Fractures of the sternum associated with spinal injury. *J Bone Joint Surg [Br]* **1986**;68-B:178–181
42. Fowler AW. Flexion-compression injury of the sternum. *J Bone Joint Surg [Br]* **1957**;39-B:487–496
43. Eismont FJ, Arena MJ, Green BA. Extrusion of an intervertebral disc associated with traumatic subluxation or dislocation of cervical facets: case report. *J Bone Joint Surg [Am]* **1991**;73-A:1555–1560
44. Rizzolo SJ, Piazza MR, Colter JM, Balderston RA, Schaefer D, Flanders A. Intervertebral disc injury complicating cervical spine trauma. *Spine* **1991**;16:S187–S189
45. Robertson PA, Ryan MD. Neurological deterioration after reduction of cervical subluxation: mechanical compression by disc tissue. *J Bone Joint Surg [Br]* **1992**;74-B:224–227
46. Pratt ES, Green DA, Spengler DM. Herniated intervertebral discs associated with unstable spinal injuries. *Spine* **1990**;15:662–665
47. Tracy PT, Wright RM, Hanigan WC. Magnetic resonance imaging of spinal injury. *Spine* **1989**;14:292–301
48. Flanders AE, Schaefer DM, Doan HT, Mishkin MM, Gonzalez CF, Northrup BE. Acute cervical spine trauma: correlation of MR imaging findings with degree of neurological deficit. *Radiology* **1990**;177:25–33
49. Denis F. The three column spine and its significance in the classification of acute thoracolumbar spinal injuries. *Spine* **1983**;8:817–831
50. Daffner RH, Deeb ZL, Goldberg AL, Kandabarow, Rothfus WE. The radiologic assessment of post-traumatic vertebral stability. *Skeletal Radiol* **1990**;19:103–108
51. Yoganandan N, Maiman DJ, Pintar F, et al. Microtrauma in the lumbar spine: a cause of low back pain. *Neurosurgery* **1988**;23:162–168
52. Brower AC, Downey EF Jr. Kümmell disease: report of a case with serial radiographs. *Radiology* **1981**;141:363–364
53. Maldague BE, Noel HM, Malghem JJ. The intravertebral vacuum cleft: a sign of ischemic vertebral collapse. *Radiology* **1978**;129:23–29

Sonography of the Shoulder in Patients with Tears of the Rotator Cuff: Accuracy and Value for Selecting Surgical Options

Stephen N. Wiener[1]
William H. Seitz, Jr.[2]

OBJECTIVE. The management of patients with signs and symptoms referable to the rotator cuff depends on the presence of cuff injury and the size of the tear. Treatment options include conservative nonsurgical management for patients with an intact or partially torn cuff, arthroscopic decompression of the coracoacromial space for those not responding to nonsurgical management, and a range of surgical techniques to repair full-thickness tears. This study was designed to determine whether sonographic evaluation with classification of the extent of cuff injury is accurate for purposes of treatment planning.

SUBJECTS AND METHODS. Preoperative sonography of the rotator cuff was performed on 225 patients, and findings were classified into intact, partial tear, small full-thickness tear, large full-thickness tear, and massive tear groups. Surgical correlation with the predicted sonographic classification was provided by arthroscopic inspection or open surgery.

RESULTS. The sonographic findings were surgically confirmed for 206 (92%) of the 225 patients. More extensive cuff injury was encountered during surgery than had been predicted sonographically in 11 patients (5%); less extensive injury than predicted was found during surgery in eight patients (4%).

CONCLUSION. Our results show a high correlation between the sonographic classification of rotator cuff injury and the surgical findings. The selection of appropriate treatment programs can be reliably based on the sonographic classification.

***AJR* 1993;160:103–107**

Alleviation of disabling signs and symptoms and restoration of function are the goals of therapy for patients with complaints referable to the rotator cuff in the shoulder. Medical treatment and a range of surgical therapeutic options are available, and the choice between them depends on the presence and magnitude of the pathologic changes. Sonography of the shoulder is effective for detecting tears of the rotator cuff. The size of the tear can be classified and the findings used as a basis for management decisions. This report assesses the accuracy of preoperative sonography of the shoulder and the implications of the findings on subsequent surgical management.

Subjects and Methods

From 1985 to 1991, 800 patients with signs and symptoms referable to impingement and suspected tears of the rotator cuff were referred for shoulder sonography. Of these, 106 men and 119 women 21–81 years old (mean, 59 years old) ultimately required surgical management.

Shoulder sonography was performed as described by Crass et al. [1] with either a Diasonics DRF 400 or an Acuson 128 system and with the patient seated. A 7.5-MHz linear-array transducer was used routinely; an additional 5-MHz linear-array transducer was used for patients with large shoulders. The shoulder was examined anteriorly and laterally in both axial and sagittal planes with the patient's arm in neutral and in internally rotated positions; the latter was achieved by placing the patient's wrist against the small of the patient's back.

Received March 30, 1992; accepted after revision July 7, 1992.

[1]Department of Radiology, The Mt. Sinai Medical Center, One Mt. Sinai Dr., Cleveland, OH 44106. Address reprint requests to Stephen N. Wiener.

[2]Department of Orthopaedic Surgery, The Mt. Sinai Medical Center, One Mt. Sinai Dr., Cleveland, OH 44106.

0361–803X/93/1601–0103

Sonographic observations and conclusions were made during real-time imaging by using the imaging monitor. Observations were made on the presence and magnitude of joint fluid, calcifications, the appearance of the long tendon of the biceps muscle and the adjacent bicipital groove, the contour of the humeral head and tuberosities, and the thickness and echogenicity of the subscapularis and supraspinatus portions of the rotator cuff. Criteria used for tears of the rotator cuff (Fig. 1) were as follows: (1) partial-thickness tear: a focal hypoechoic zone within the substance of the rotator cuff, small hypoechoic discontinuities of the internal or external surfaces of the cuff, or the presence of a large dominant linear echogenic focus within the substance of the cuff with or without associated diminution of the cuff thickness; (2) full-thickness tear: a hypoechoic zone extending through the entire substance of the cuff or segmental or complete loss of rotator cuff substance with visualized tear margins; and (3) massive tear: nonvisualization of the rotator cuff with "approximation" of the deltoid muscle to the surface of the humeral head. Cuff arthropathy was indicated by irregular changes in contour involving the humeral head; these usually were associated with a high-riding humeral head. An estimate of the size of a full-thickness tear was made from images recorded in both axial and sagittal planes (Fig. 2). The plane in which the tear was largest was used for classification purposes. In the axial plane, the width of the cuff defect or the hypoechoic zone or the distance between the visualized cuff margins was measured. In the sagittal plane, the distance was measured from the greater tuberosity to the visualized cuff margin or the length of the depressed interface between the supraspinatus and overlying deltoid muscle. If the supraspinatus portion was not visualized, the tear was classified as massive and was assumed to be greater than 3 cm. The sonographic findings were classified as intact normal, partial-thickness tear, small full-thickness tear (<1 cm), large full-thickness tear (1-3 cm), or massive tear with or without cuff arthropathy (Fig. 3).

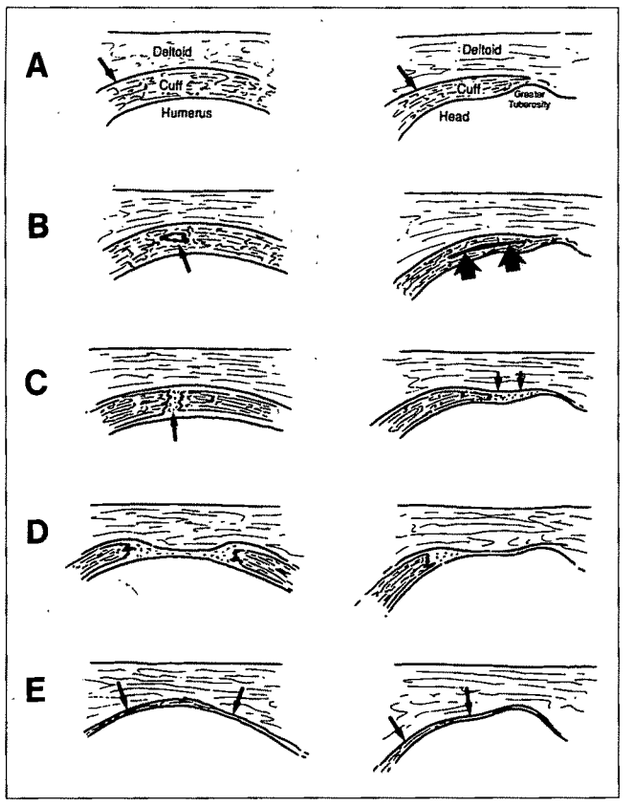

Fig. 1.—*A–E*, Drawings show sonographic appearance of rotator cuff integrity in axial (*left*) and sagittal (*right*) planes.

***A*, Normal rotator cuff with preserved anterior echogenic arc (*arrow*) of subdeltoid fascia and peritendinous fat.**

***B*, Partial-thickness tear appearing as intratendinous hypoechoic (*thin arrow*) or dominant echogenic (*thick arrows*) focus.**

***C*, Small full-thickness tear appearing as hypoechoic area of cuff discontinuity (*long arrow*) and loss of anterior arc and cuff substance at junction of cuff with greater tuberosity (*short arrows*).**

***D*, Large full-thickness tear.**

***E*, Massive tear. Rotator cuff is not visualized. Subdeltoid fascia (*arrows*) "approximates" humeral head.**

Fig. 2.—Drawings show sonographic appearances of full-thickness tear in axial (*left*) and sagittal (*right*) planes. Measurement of tear size (*solid arrows*) defined by width of substance loss and/or length of depressed segment of anterior echogenic arc (*open arrow*).

The surgical treatment was generally based on the sonographic classification. Patients with a classification of intact normal or partial tear who did not respond to medical management within a designated time had arthroscopic decompression of the subacromial space. Before the decompression, the rotator cuff was completely evaluated by means of arthroscopic visualization and palpation through multiple portals of the rotator cuff [2, 3]. In each instance, the subscapularis, supraspinatus, and infraspinatus portions of the rotator cuff were examined from their insertion to their musculotendinous junctions. Patients with small full-thickness tears were treated by arthroscopic decompression combined with a limited anterolateral splitting incision of the deltoid muscle with local reattachment of the focally detached tendon edge. The rotator cuff was examined arthroscopically as described. Patients with large full-thickness or massive tears had formal open surgical exposure for examination and repair of the rotator cuff. The integrity of the cuff and the size of the tear were graded on the basis of surgical findings, and the results were compared with the sonographic classification.

Results

Table 1 lists the results of the sonographic examinations and the corresponding surgical findings. On the basis of sonographic findings, 71 patients had an intact rotator cuff, and 154 had either a partial- or a full-thickness tear. When the surgical findings were used as the gold standard, the sonographic findings correlated with the surgical findings in 206 (92%) of 225 patients. A normal rotator cuff was confirmed surgically in 63 (89%) of the 71 patients; three had partial thickness tears, and five had small full-thickness tears. A partial- or full-thickness tear was confirmed for 143 (93%) of 154 patients. The sonographic finding of a partial-thickness tear was not confirmed surgically for five patients; four had a normal rotator cuff, and one had a small full-thickness tear. The sonographic finding of a full-thickness tear was confirmed surgically in 84 (99%) of 85 patients. One of the 85 had a partial-thickness tear, the size of the tear was classified incorrectly for five patients. The binary decision charts that show the effectiveness of using shoulder sonograms to detect the presence of a tear and to correctly classify the extent of a tear are shown in Figure 4.

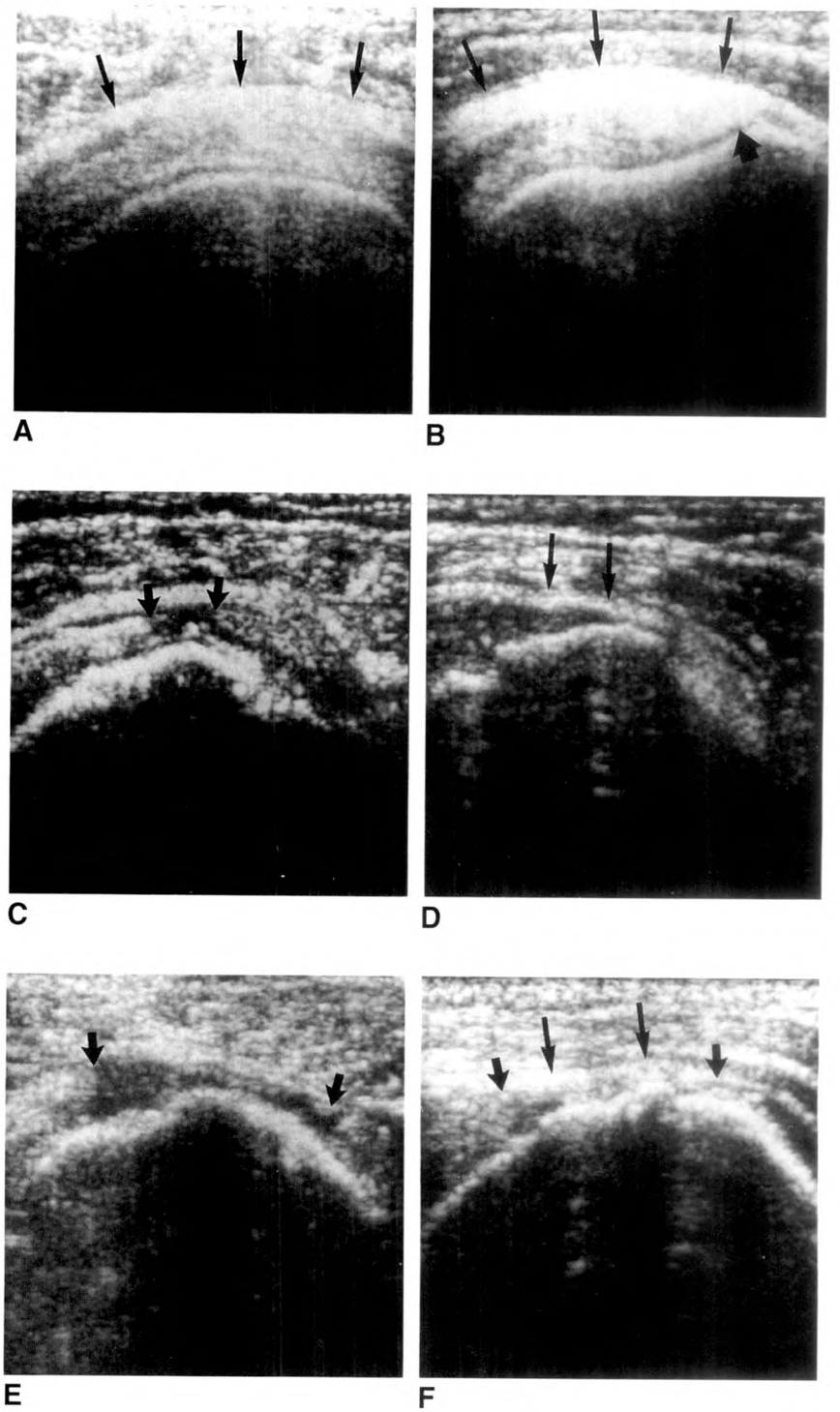

Fig. 3.—Axial (*A*, *C*, and *E*) and sagittal (*B*, *D*, and *F*) sonograms of rotator cuff and tears of rotator cuff.

A and *B*, Normal intact cuff with convex arc of peritendinous fat (*long arrows*) and attachment of supraspinatus tendon to greater tuberosity (*short arrow* in *B*).

C and *D*, Small full-thickness tear. Note edges (*arrows* in *C*) on axial view and decreased thickness of cuff and subtle loss of peritendinous convexity (*arrows* in *D*) on sagittal view.

E and *F*, Large full-thickness tear. *Short arrows* indicate extent of tear. *Long arrows* indicate marked loss of peritendinous convexity.

Discussion

For patients with symptoms of rotator cuff impingement, a range of management options can be used to alleviate symptoms that may be disabling and to restore normal shoulder movement. A spectrum of rotator cuff abnormalities may be encountered, from early inflammation of the subacromial-subdeltoid bursa and rotator cuff tendon through partial-thickness injury to full-thickness tear, detachment, and progressive retraction, and finally, degenerative changes affecting the glenohumeral joint. Knowledge of the extent of damage and of the quality of the remaining rotator cuff tissue is key to management. Patients with an intact rotator cuff or a partial-thickness tear are initially managed nonsurgically. Medical management includes antiinflammatory agents and rehabilitative physiotherapy designed to strengthen the cuff

TABLE 1: Sonographic vs Surgical Findings in Tears of the Rotator Cuff

Songraphic Findings	No. of Patients	Surgical Findings				
		Normal	Partial-Thickness Tear	Full-Thickness Tear		Massive Tear
				Small	Large	
Normal	71	63	3	5	0	0
Partial-thickness tear	69	4	64	1	0	0
Small full-thickness tear	29	0	0	27	2	0
Large full-thickness tear	32	0	1	1	29	1
Massive tear	24	0	0	0	1	23
Total	225	67	68	34	32	24

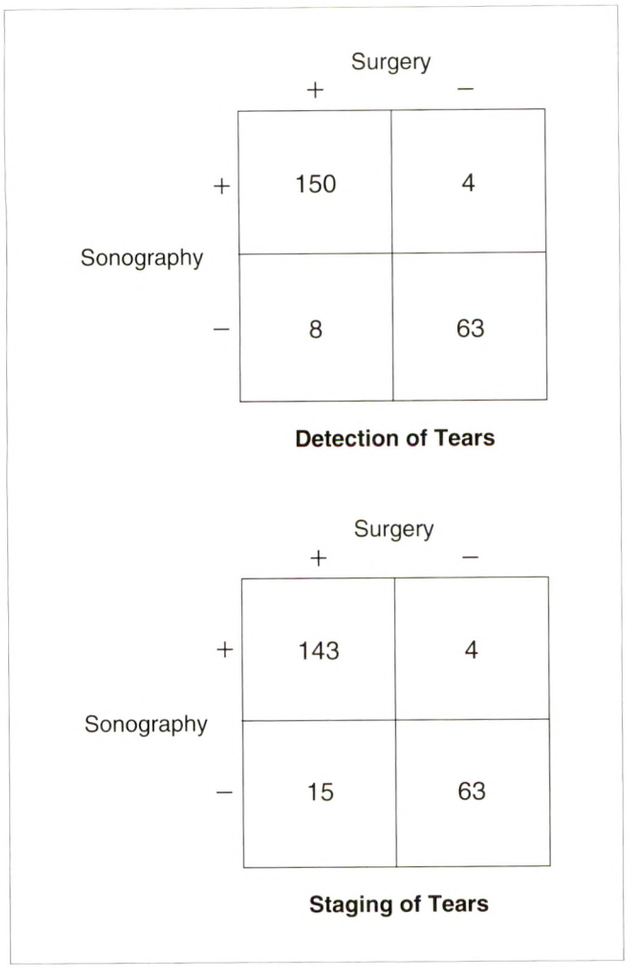

Fig. 4.—Binary decision matrices for sonography vs surgery in tears of the rotator cuff. For detection of tears, sonography has a sensitivity of 95% (150/158), a specificity of 94% (63/67), a positive predictive value of 97% (150/154), and a negative predictive value of 89% (63/71). For staging of tears, sonography has a sensitivity of 91% (143/158), a specificity of 94% (63/67), a positive predictive value of 97% (143/147), and a negative predictive value of 81% (63/78).

and scapula-support musculature and to reduce impingement on the overlying coracoacromial arch. Many of these patients respond well and will not require surgery. For those who do not respond within a designated time, arthroscopic decompression is recommended [4]. Patients with small full-thickness tears and persistent symptoms do not respond favorably when treatment is limited to arthroscopic decompression (Seitz et al., presented at the American Shoulder & Elbow Surgeons [ASES] annual meeting, March 1991). For these patients, arthroscopic decompression is combined with a small anterolateral incision for splitting and retraction of the deltoid muscle and focal reattachment of the detached tendon edge. This minimizes soft-tissue violation, morbidity, and the length of convalescence. For patients with large full-thickness tears, formal open surgical exposure of the rotator cuff is required for mobilization and advancement of the retracted tendon edges. Massive tears may require additional tendon grafting or transfer [5, 6] (Neer et al., presented at ASES annual meeting, February 1988). Finally, joint replacement may be required to relieve pain and promote stability for those patients with associated arthropathy [7].

Several radiologic techniques have been used to detect tears of the rotator cuff. Each has limitations, and no clear consensus on the optimal diagnostic study has emerged. Contrast arthrography is an invasive procedure and does not show tears when no free communication with the subacromial-subdeltoid bursa occurs. MR imaging is currently expensive and time-consuming and MR criteria for diagnosis of a tear are not universally accepted [8–10]. Our results and those from other studies [11–16] emphasize the accuracy of shoulder sonography for determining the integrity of the rotator cuff. Although surgical proof was lacking for 575 patients and the surgical group was biased in favor of those with persistent signs and symptoms or functional limitations of the shoulder joint, the surgical findings confirmed the sonographic findings and grade of rotator cuff injury in most patients (Table 1).

Unfortunately, less favorable results of shoulder sonography have been reported [17–19] and have discouraged the general use of this technique [20]. Insufficient experience is often cited as the cause for poor results [13, 17]. This reason

would appear to be more of an indictment of the operator then an inherent limitation of the technique. The selection of inappropriate criteria also contributes to diagnostic error, especially if hyperechoic foci are considered to be tears [11, 15, 19, 21, 22]. A frank full-thickness tear is seen as a hypoechoic zone. Inferior results have also been reported when partial-thickness tears were included in the assessment of overall results [2]. Many patients with partial-thickness tears are asymptomatic [3]. As described previously, the presence of a partial-thickness tear has minimal impact on the choice of therapeutic option. From a practical point of view, patients with a partial-thickness tear are managed initially just as those with an intact cuff are managed. Finally, although images were obtained in the axial and sagittal planes for record-keeping purposes, active viewing of the texture and thickness of the rotator cuff from the imaging monitor was considered essential for diagnosis. In our experience with more than 2500 shoulder sonograms, judgments based solely on the "hard copy" are frequently in error. Shoulder sonography, performed by the radiologist, can be completed and a diagnosis established within 15 min. The simplicity, rapidity, low cost, and accuracy of the examination make it especially attractive as a screening and presurgical staging study. The benefits include more precise preoperative planning, reduction in surgical morbidity, and better estimates of recovery time.

REFERENCES

1. Crass JR, Craig EV, Feinberg SB. Ultrasonography of rotator cuff tears: a review of 500 diagnostic studies. *JCU J Clin Ultrasound* **1988**;16:313–327
2. Pattee GA, Synder SJ. Sonographic evaluation of the rotator cuff: correlation with arthroscopy. *Arthroscopy* **1988**;4:15–20
3. Ellman H. Diagnosis and treatment of incomplete rotator cuff tears. *Clin Orthop* **1990**;254:64–74
4. Seitz WH, Froimson AI, Shapiro JD. Chronic impingement syndrome: the role of ultrasonography and arthroscopic anterior acromioplasty. *Orthop Rev* **1989**;18:364–375
5. Brown AO, Bigliani LU. The shoulder: impingement and rotator cuff tears. *Contemp Orthop* **1987**;14:53–55
6. Cofield RH, Hoffmeyer P, Lanzer WL. Surgical repair of chronic rotator cuff tears. *Orthop Trans* **1990**;14:251–252
7. Neer CS II, Craig EV, Fukuda H. Cuff tear arthropathy. *J Bone Joint Surg [Am]* **1983**;65-A:1232–1244
8. Crass JR, Craig EV. Noninvasive imaging of the rotator cuff. *Orthopaedics* **1988**;11:57–64
9. Traughber PD, Goodwin TE. Shoulder MRI: arthroscopic correlation with emphasis on partial tears. *J Comput Assist Tomogr* **1992**;16:129–133
10. Farley TE, Neumann CH, Steinbach LS, et al. Full-thickness tears of the rotator cuff of the shoulder. *AJR* **1992**;158:347–351
11. Crass JR, Craig EV, Thompson RC, Feinberg SB. Ultrasonography of the rotator cuff: surgical correlation. *JCU J Clin Ultrasound* **1984**;12:487–492
12. Mack LA, Matsen FA, Kilcoyne RF, et al. Ultrasound evaluation of the rotator cuff. *Radiology* **1985**;157:205–209
13. Mack LA, Nyberg DA, Matsen FA. Sonographic evaluation of the rotator cuff. *Radiol Clin North Am* **1988**;26:161–177
14. Hodler J, Fretz CJ, Terriel F, Gerber C. Rotator cuff tears: correlation of sonographic and surgical findings. *Radiology* **1988**;169:791–794
15. Middleton WD, Edelstein G, Ranus WR, et al. Sonographic detection of rotator cuff tears. *AJR* **1985**;144:349–353
16. Soble MG, Kaye AD, Guay RC. Rotator cuff tear: clinical experience with sonographic detection. *Radiology* **1989**;173:319–321
17. Burk DL, Karasick D, Kurtz AB, et al. Rotator cuff tears: prospective comparison of MR imaging with arthrography sonography and surgery. *AJR* **1989**;153:87–92
18. Vick CW, Bell SA. Rotator cuff tears: diagnosis with sonography. *AJR* **1990**;154:121–123
19. Brandt TD, Cardone BW, Grant TH, et al. Rotator cuff sonography: a reassessment. *Radiology* **1989**;173:323–327
20. Hall FM. Sonography of the shoulder. *Radiology* **1989**;173:310
21. Middleton WD. Status of rotator cuff sonography. *Radiology* **1989**; 173:307–309
22. Middleton WD, Reinus WR, Melson GL, Totty WG, Murphy WA. Pitfalls of rotator cuff sonography. *AJR* **1986**;146:555–560

The reader's attention is directed to the commentary on this article, which appears on pages 109–110.

Book Review

Imaging of Athletic Injuries. A Multimodality Approach. By Joseph R. Martire and E. Mark Levinsohn. New York: McGraw-Hill, 333 pp., 1992. $89

This medium-sized volume covers those aspects of musculoskeletal imaging that the authors consider relevant to athletic injuries. The emphasis is on three-phase bone scintigraphy, MR imaging, and CT. The material reflects the authors' extensive experience with these techniques in their respective capacities as attending radiologist for the Union Memorial Hospital and Sports Medicine Center and professor of musculoskeletal radiology at the State University of New York Health Science Center. Throughout the book, illustrations are favored over text, but the text is sufficient to make this book more than simply an atlas.

The book is organized by anatomic region into seven chapters, starting with the knee then going on to the lower leg, foot, and ankle; pelvis, hip, and thigh; shoulder and humerus; hand; wrist, forearm, and elbow; and finally the spine. Each chapter has a one- to two-page introduction written by an orthopedist that gives a clinical perspective from which to approach the following imaging material. The chapters themselves are divided into acute problems, chronic problems, and diagnostic problems (i.e., disorders mimicking athletic injuries). Each chapter has an extensive reference list, from 85 to 145 references per chapter.

The illustrations throughout the book are of excellent quality and of a size that facilitate perception of the abnormalities being shown. The plain radiographs, cross-sectional images, and bone scintigrams are all well reproduced, clearly labeled, and accompanied by well-written captions. The line drawings by Dan Beisel, which are scattered through the book, are clear and accurate. Tables in each chapter list differential diagnoses, frequency of injuries, and comparative accuracy of various imaging techniques, complementing the text nicely. The index is well set out and useful; for instance, the entry "heel pain" directs the reader to a section showing an anatomic drawing, a table listing causes of heel pain, and a short discussion of appropriate imaging techniques.

The text is well written and appropriately concise for a text/atlas of this type, concentrating on defining the disease process in question; outlining the most appropriate imaging studies for the process; and, when necessary, detailing any relevant clinical, anatomic, or pathologic background necessary for understanding the imaging involved. Numerous subheadings divide the text into easily manageable paragraphs.

Although most of the material presented can be found scattered through numerous other sources, this book brings together a wide spectrum of disease processes and imaging techniques directed at one particular focus, that is, diagnosis of those problems that particularly affect athletes. The book has a slight overemphasis on the use of three-phase bone scans, presumably reflecting the extensive experience of one of the authors. For example, illustrations are provided of the appearance on three-phase scan of a ruptured popliteal cyst and also of some vascular entities, including ulnar artery thrombosis and a digital artery aneurysm. This is, however, a minor quibble, and the text has not only abundant references to but also many excellent illustrations of the use of other techniques.

One of the best features of this book is its treatment of athletic injuries that are not really covered in standard imaging texts. For example, although most radiologists are reasonably familiar with shin splints, not many are accustomed to dealing with thigh splints. A discussion the features of thigh splints, including anatomic and pathologic basis and imaging characteristics, can be found in this text. One or two minor omissions, such as the lack of any reference to the so-called SLAP lesion of the superior glenoid labrum detract only slightly from the usefulness of the book.

Any radiologist who deals with athletes or indeed any group of young active patients will find this text both informative and useful. It is both easy to read and extremely well illustrated and referenced. The focus on athletic injuries is maintained throughout, making this much more than a simple gathering of material that is elsewhere available. I expect it will find favor not only with practicing musculoskeletal radiologists but also with radiologists in general practice, residents, and fellows in training.

Anthony J. Doyle
University of Utah
Salt Lake City, UT 84132

Commentary

Sonographic Detection and Quantification of Rotator Cuff Tears

William D. Middleton[1]

Much has been written about rotator cuff sonography since the original reports appeared in 1985, including a whole book on the subject [1]. The preceding article by Wiener and Seitz [2] reports their experience during the past 6 years. Their analysis includes a meticulous correlation of sonographic and surgical findings in a large number of patients. Like all studies, certain limitations are unavoidable. However, critical review of this paper reveals only minor shortcomings. In most respects, it provides an excellent reflection of the current capabilities of shoulder sonography.

The present study can be broken down into several parts. The first part deals with the accuracy of sonography in detecting full-thickness (complete) rotator cuff tears. This aspect of rotator cuff sonography has been studied extensively in the past, and it is well documented that high sensitivity can be achieved. However, the examination is technically difficult to master, and success depends heavily on the experience and expertise of the operator. While the high accuracy obtained by Wiener and Seitz in detecting complete tears is gratifying to those who have encouraged the use of rotator cuff sonography, it does not add significant new information to the radiologic literature. On the other hand, their use of hypoechoic defects, focal loss of rotator cuff substance, and nonvisualization of the rotator cuff as criteria for detecting complete tears are useful, since they substantiate recommendations made in other recent publications [3, 4].

The second part of the study deals with partial tears and does provide new data on the subject. Ninety-four percent (64/68) of surgically confirmed partial tears were correctly distinguished from normal anatomy and from complete tears. Only five false-positive diagnoses of partial tears (four normal rotator cuffs and one small complete tear) were encountered. It remains to be seen if these excellent results can be reproduced at other institutions.

The third aspect of the study correlates sonographic and surgical measurements of the sizes of complete rotator cuff tears and provides valuable new information. Again, the results were excellent, with 94% (79/84) of the sonographic measurements correctly predicting tears of less than 1 cm, between 1–3 cm, and more than 3 cm in size. The schematic illustrations depicting the technique for quantifying the size of tears (Fig. 2) provide a nice reference for sonographers who are attempting to incorporate these methods into their own practice.

All of these first three aspects of the study deal with a correlation of sonographic and surgical findings. A potential limitation of this approach is the lack of analysis of the 575 patients with normal findings on sonograms and no surgical follow-up. Exclusion of these patients makes it impossible to determine the true-negative and false-negative rate; thus, the sensitivity, specificity, and negative predictive value cannot be reliably calculated. Nonetheless, the study population does include 71 patients with normal sonographic findings in whom surgical correlation was obtained because of persistent symptoms. It is reasonable to assume that these patients were more likely to have rotator cuff tears and thus false-negative sonographic examinations than were the large group of less symptomatic patients in whom surgery was not performed. Therefore, one could argue that the true-

This article is a commentary on the preceding article by Wiener and Seitz.

[1]Mallinckrodt Institute of Radiology, Washington University School of Medicine, 510 S. Kingshighway, St. Louis, MO 63110. Address reprint requests to W. D. Middleton.

AJR 1993;160:109–110 0361–803X/93/1601–0109

negative rate was artificially decreased and the false-negative rate was artificially increased by analyzing only the 225 patients for whom there was surgical correlation. In other words, inclusion of the unproved cases might actually have improved the sonographic results.

Another potential limitation of the study revolves around the surgeon's use of the sonographic results to tailor the surgical approach. Prior knowledge of the sonographic findings could certainly bias the surgical findings in such a way that there would be fewer false-positives and false-negatives. Although this might artificially improve the sonographic results, the end point is the patient's outcome, and it is difficult to justify an alternative study design in which the surgeon is blinded to potentially valuable preoperative information.

Another aspect of this study deals with the value of sonography in determining treatment planning. The authors conclude that sonography allows "more precise preoperative planning, reduction in surgical morbidity, and better estimates of recovery time." Unfortunately, the study provides no hard data that clearly substantiate these statements. The results do not indicate how often the surgical approach, as predicted sonographically, was adequate in treating the patient's problem or how often surgery had to be extended or altered because of unsuspected surgical findings. In addition, the study did not have a control group that was preoperatively assessed by some means other than sonography, so it is not really possible to say that sonography was "more precise" or "better" because there is nothing to compare it with. Nonetheless, the excellent sonographic–surgical correlation described in the first part of the study would seem to substantiate that sonography can provide information that is quite useful in surgical planning; and thus preoperative sonography is likely to reduce surgical morbidity and recovery time.

In summary, the results of Wiener and Seitz's study demonstrate that sonography is clearly capable of providing much more information than just whether or not a complete rotator cuff tear is present. Owing to refinements in equipment and technique, and to a better understanding of normal and abnormal sonographic findings, it is now possible to provide precise quantitative assessment of tear size such that decisions concerning conservative vs surgical management can be made. When surgery is necessary, sonography can help to optimize the surgical approach. These results provide optimism for an expanded role of sonography as an inexpensive, rapid, and noninvasive means of evaluating the rotator cuff.

REFERENCES

1. Katthagen BD. *Ultrasonography of the shoulder*, 1st ed. New York: Thieme, **1990**
2. Wiener SN, Seitz WH Jr. Sonography of the shoulder in patients with tears of the rotator cuff: accuracy and value for selecting surgical options. *AJR* **1993**;160:103–107
3. Mack LA, Rogers JV, Winter TC, Matsen FA. Ultrasound of the rotator cuff. In: Seeger LL, ed. *Diagnostic imaging of the shoulder*. Baltimore: Williams & Wilkins, **1992**:96–118
4. Middleton WD. Status of rotator cuff sonography. *Radiology* **1989**; 173:307–309

Stress Fractures of the Tarsal Navicular Bone:
CT Findings in 55 Cases

Zoltan S. Kiss[1]
Karim M. Khan[2]
Peter J. Fuller[3]

OBJECTIVE. The purpose of this article is to present the CT findings in 55 cases of tarsal navicular stress fracture before and after treatment and to describe the CT protocol used.

MATERIALS AND METHODS. Fifty-five navicular stress fractures in 54 patients whose initial and follow-up CT scans were available for study were retrospectively reviewed. In most cases, contiguous 1.5-mm axial and 3-mm coronal scans of the navicular bone had been obtained. Both feet were scanned for comparison. Follow-up scans were obtained between 4 weeks and 6 years.

RESULTS. On review, fractures were evident in all cases, but six small fractures (11%) were missed at the initial interpretation. All fractures involved the central third of the proximal dorsal margin of the navicular bone. Fifty-three fractures (96%) were partial. Forty-three partial fractures were linear, five were linear with bone fragments, and five were rim defects with ossicles. In 13 cases (24%) the fracture was small, 10% or less of bone height. The earliest sign of healing, slight dorsal cortical bridging, was seen in three of eight cases in which follow-up was done at 6 weeks. Firm cortical union was noted in 10 (32%) of 31 by 4 months. Nonunion occurred in 12 and was indicated by the persistence of the fracture gap and lack of cortical healing. Medullary cysts (five) and cortical notching (two) were noted to persist after complete healing.

CONCLUSION. CT scanning is a suitable method for detecting navicular stress fracture and for performing follow-up examinations. Small fractures may be overlooked owing to lack of familiarity with their appearance.

***AJR* 1993;160:111-115**

Stress fracture of the tarsal navicular bone is an important, though uncommon, cause of foot pain in athletes [1]. CT scanning is increasingly used in the diagnosis of these fractures [2, 3], but to our knowledge the CT appearance of these lesions has not been previously reviewed in the radiologic literature. We present the CT findings in 55 cases of navicular stress fractures before and after treatment and describe the CT protocol we have found most useful for detecting these fractures.

Materials and Methods

The clinical and radiologic findings in 82 patients with 86 radiologically confirmed navicular stress fractures, seen in five major sports medicine clinics in Melbourne, Australia, between June 1981 and September 1991 were retrospectively reviewed. The clinical details and methods of treatment of these patients have been reported by Khan et al. [4]. From this original group, 54 patients with 55 fractures, whose initial and follow-up CT scans were available for study, were selected for review. The patients' initial presentation, clinical course, and treatment outcome were determined from medical charts including surgical reports. The patients in this group participated in a wide variety of sports and included recreational, amateur, and professional athletes. The group included 24 females and 30 males 15–30 years old (mean, 21 years). All had foot pain. The average time between the onset of signs and symptoms and diagnosis was 4 months (range, 3 days to 2 years). Clinical follow-

Received May 11, 1992; accepted after revision June 26, 1992.

[1]Department of Radiology, Mercy Private Hospital, 141 Grey St., East Melbourne, Victoria 3002, Australia. Address reprint requests to Z. S. Kiss.

[2]Olympic Park Sports Medicine Centre, Swan St., Melbourne, Victoria 3004, Australia.

[3]Sports Medicine Centres of Victoria, 330 High St., Ashwood, Victoria 3147, Australia.

0361–803X/93/1601–0111

up was 6–84 months (mean, 24 months). Radiologic studies included plain radiographs (47 cases), ^{99m}Tc-scintigraphy (49 cases), and CT scans at the time of presentation and after treatment (55 cases). The initial CT scans were obtained at various institutions, and several different scanning protocols were used. Most of the follow-up CT scans were obtained with a GE 9800 scanner (GE Medical Systems, Milwaukee). A bone algorithm was used with the following scan protocol: First, with the foot flat, the gantry was angled to the plane of the talonavicular joint, and contiguous 1.5-mm scans were obtained from the proximal margin of the bone distally in the axial plane (Fig. 1A). Then, the foot was placed in the anatomic position, the gantry was angled to the plane of the dorsum of the foot, and contiguous 3-mm scans were obtained in the coronal plane from the dorsal margin of the bone in a plantar direction (Fig. 1B). Scans were recorded on a window setting of 3000 H at a level of 500 H. Both feet were scanned for comparison. All available radiologic images were reviewed by a radiologist and two sports medicine physicians. CT scans were reviewed for the position, appearance, and extent of fracture, which was measured in two planes by using calipers. The sagittal extent of the fracture was measured on the axial scans and the horizontal extent on the coronal scans. Fracture size was expressed as a percentage of the sagittal bone height or horizontal bone length. Follow-up CT scans, obtained between 4 weeks and 6 years, were reviewed for signs of healing or of nonunion.

Results

All fractures involved the central one third of the proximal dorsal articular margin of the navicular bone. Two fractures were complete and 53 were partial. Forty-three partial fractures were linear, five were linear with a bone fragment, and five had rim defects with associated ossicles. Linear fractures were either straight (Fig. 2) or curved laterally in the sagittal plane (Fig. 3). Linear fractures associated with a bone fragment (Fig. 4) appeared Y-shaped on the axial image. Ossicles had a rounded margin and a corresponding shallow cortical defect in the adjacent bone rim, without a linear component (Figs. 5 and 6). On CT scans, all fractures were detectable in both planes, and 37 (67%) extended the same distance in both planes. In three patients, a fracture that was partial in one plane appeared complete in the other plane. In 13 cases (24%), the fracture was 10% or less of bone height and was less than 5 mm deep. In 27 (49%) the fracture was between 10% and 50% of bone height, and in 15 (27%) it was greater than 50% of bone height.

Follow-up scans were obtained in all 55 cases at various intervals between 4 weeks and 6 years (Table 1). Most scans were obtained at 12 weeks (25 cases). Several patients had more than one follow-up scan. The earliest sign of fracture healing was slight dorsal cortical bridging, seen in three cases at 6 weeks. Firm cortical union was noted in 10 (32%) of 31 cases by 4 months. By 12 months, firm cortical bridging was present in three cases and two fractures were healed—one with a residual cyst. Seven patients were scanned more than 1 year after the initial examination. In all seven cases, the fracture had healed, but in two, a small dorsal cortical notch was present at the fracture site. In five, a residual cyst or cleft was noted.

Clinical nonunion was diagnosed in 12 patients. In these cases, follow-up CT scans showed persistence of the fracture gap without cortical bridging. In one case, treated with weight-bearing rest, CT showed sclerosis outlining the fracture margins, indicating nonunion (Fig. 7).

Discussion

The correct diagnosis of tarsal navicular stress fractures is frequently delayed for several months, partly because the clinical onset is insidious, with nonspecific signs and symptoms, and partly because these fractures often are not evident on plain radiographs of the foot [5]. In 1982, Torg et al. [6] reviewed the diagnosis and treatment of 21 cases of navicular stress fracture and suggested a systematic approach to radiologic workup, including plain radiography, bone scintigraphy, and fine-section linear tomography. Since that time, CT scanning has become widely accepted for the detection of bone abnormalities and is now the method of choice for the confirmation of these fractures. CT scanning offers better spatial resolution than linear tomography does and allows scanning in the axial plane. This is an advantage when fractures are oriented in the sagittal plane.

On CT scans, the proximal articular rim of the normal navicular bone appears extremely dense, almost sclerotic, and is ringlike on true axial images (Fig. 3). This apparent bone sclerosis may reflect the great mechanical load normally

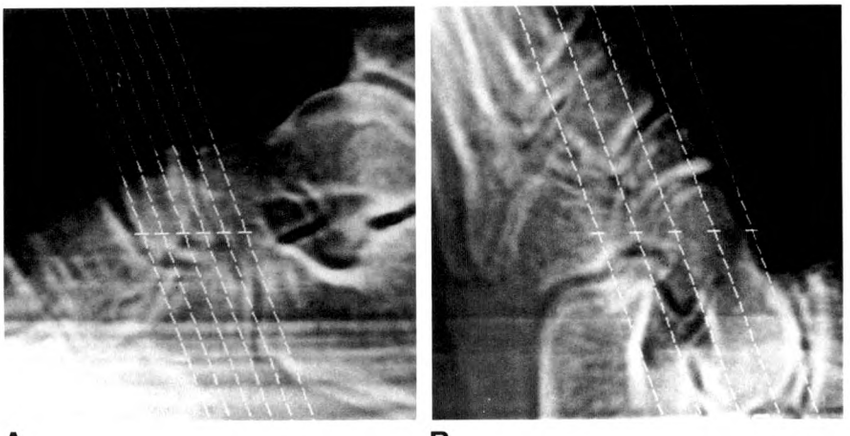

A B

Fig. 1.—Digital scout radiographs of feet. Lines indicate scan planes and region to be scanned.

***A*, Axial scans are obtained with the foot down. Gantry is angled to plane of talonavicular joint. Scans of 1.5-mm sections begin just proximal to navicular articular rim.**

***B*, Coronal scans are obtained with the foot in anatomic position. Gantry is tilted to approximate plane of dorsal surface of bone. Scans of 3-mm sections include proximal dorsal articular margin of bone.**

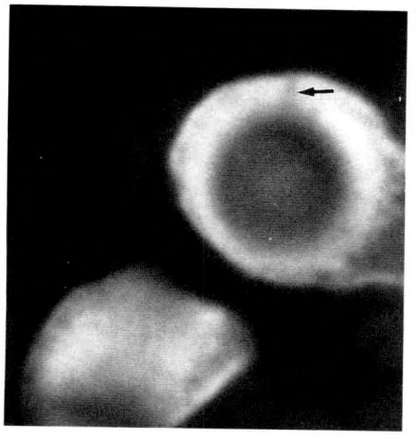

Fig. 2.—Partial linear fracture of right navicular bone in a 21-year-old male middle-distance runner who had signs and symptoms for 2 months. Axial CT scan shows 3-mm sagittal fracture (*arrow*) of middle third of proximal dorsal articular margin of bone.

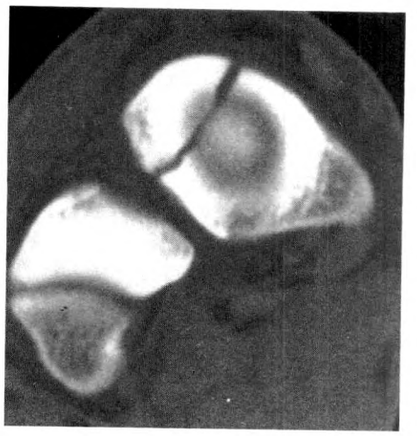

Fig. 3.—Complete fracture of right navicular bone in a 22-year-old female sprinter who had signs and symptoms for 6 weeks. Axial CT scan angled to plane of talonavicular joint shows complete, undisplaced fracture curving slightly laterally from middle third of dorsum of bone. In this plane, normal proximal articular rim of navicular bone appears as a sclerotic ring.

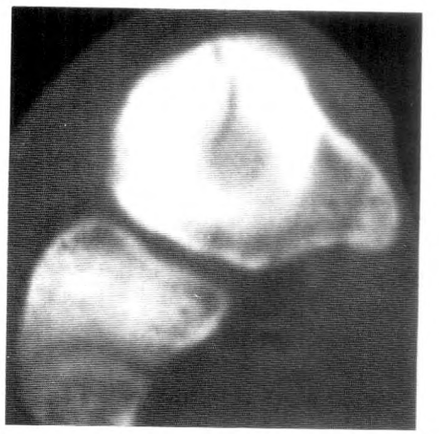

Fig. 4.—Partial linear fracture of right navicular bone in a 22-year-old heptathlete who had signs and symptoms for 1 month. Axial CT scan shows a Y-shaped fracture with an undisplaced small bone fragment in normally sclerotic dorsal rim of navicular bone.

borne by the relatively small, concave articular surface of this bone during weight bearing. In this series, all fractures occurred in the dense rim. Although most stress fractures are linear defects, some have associated bone fragments, and others appear as rim defects without a linear component. A linear fracture with small bone fragments was seen in five cases. On axial scans, such fractures have a Y-shaped appearance, with the fragment contained in the bifurcation of the Y (Fig. 4). These fractures most likely correspond to the transverse fragments on linear tomograms described by Torg et al. [6]. Rim defects, without a linear fracture line but with associated ossicles, were also seen in five cases. In one, a small osteochondral fragment was partially separated from the adjacent bone (Fig. 5); in the other four, rounded ossicles were clearly demarcated from a congruent cortical defect. Such rim fractures with ossicles may represent stress avulsion fractures, as recently described by Orava et al. [7]. Accessory ossicles in this region have a similar appearance, but their margins are beveled and are incongruent with the adjacent cortex [8]. It may be difficult to distinguish avulsion fractures and accessory ossicles on the basis of the CT appearance alone. However, an appropriate clinical history, localized tenderness over the navicular bone, and abnormal findings on a bone scan should suggest a fracture. The demonstration of small bone fragments or ossicles may be significant, because in symptomatic persons, surgical removal of the separated bone results in earlier healing of the fracture [7].

Tarsal navicular stress fractures respond well to conservative treatment [4, 6], and surgery is reserved for the removal of bone fragments and the treatment of nonunited or displaced fractures [4]. The CT appearance of healing stress fractures confirms the previously reported findings of Torg et al. [6], who used linear tomography. Early healing is indi-

Fig. 5.—Partial osteochondral rim fracture of left navicular bone in a 15-year-old female sprinter who had signs and symptoms for 3 months. Axial CT scan not in plane of talonavicular joint shows a saucer-shaped fracture line (*arrow*) in dorsal cortical rim of bone and a small undisplaced fragment. Adjacent bone sclerosis is normal. Location of fracture is typical for stress fracture. No linear fracture line is present.

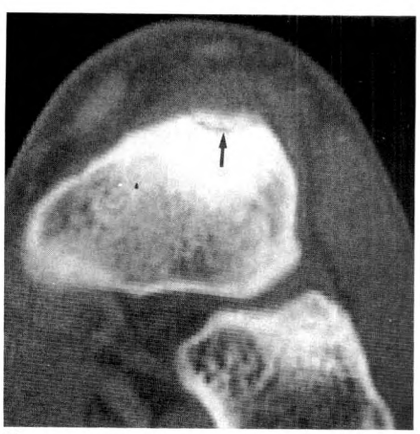

5

Fig. 6.—Partial fracture of left navicular bone with small ossicle in a 16-year-old male sprinter who had signs and symptoms for 3 months. Coronal CT scan shows a clearly defined ossicle (*arrow*) with a corresponding defect in dorsal articular rim of left navicular bone.

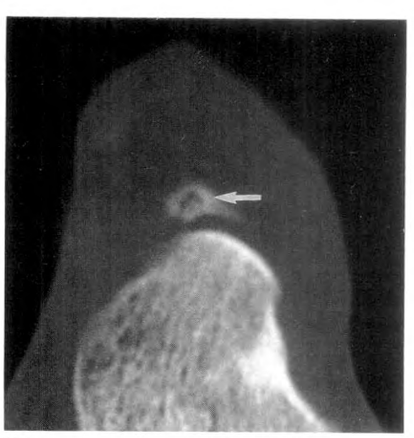

6

TABLE 1: Summary of Follow-up CT Findings in 55 Cases

Follow-up Interval/Major Finding	No.
4–6 Weeks	
No change	2
Widening gap	2
Early cortical bridging	3
Ossicle removed	1
Total	8
2–4 Months	
Fracture extended	2
Widened gap	1
No change	13
Surgery	
Ossicles removed	2
Fixation screw	3
Firm cortical union	10
Total	31
6–12 Months	
No change	2
Surgery (fixation screw)	2
Firm cortical union	3
Healed	1
Healed; residual central cyst	1
Total	9
More than 12 months	
Healed; residual central cyst or cleft	5
Healed; residual cortical notch	2
Total	7

cated by dorsal cortical bridging, which may be seen as early as 6 weeks and which often is followed by firm cortical union by 3–4 months. Radiologic signs of fracture healing, however, lag behind clinical findings, and may vary, depending on the treatment interval and on whether the patient has been bearing weight. However, CT scans obtained 6 weeks after treatment begins may be misleading because they may show apparent fracture widening and loss of fracture line definition because of demineralization. At this stage, absence of navicular pain and tenderness is a better indicator of fracture healing than CT findings, and therefore routine scanning of the foot for follow-up of healing is not recommended. Even at 3 or 4 months, a significant number of cases show little change in the appearance of the fracture although they are clinically uniting. After complete clinical union, with radiologic evidence of solid cortical bridging, central cysts or clefts or a notch in the dorsal cortical margin may persist at the fracture site for months or years (Figs. 8 and 9).

Clinical nonunion is indicated by tenderness over the navicular bone and persistent pain on exercise and was seen in 12 cases in this series. CT scans showed a lack of cortical bridging and persistence of the fracture gap in all 12 cases. In one case (Fig. 7), treated initially by weight-bearing rest, sclerosis was noted along the fracture margin and was assumed to be a sign of nonunion. It must be stressed that the normal sclerosis of the proximal navicular articular margin is not a sign of nonunion, as has been suggested by previous authors [2, 6]. The absolute sensitivity or specificity of CT in the detection of navicular stress fractures cannot be determined from this study. Fractures were seen on all CT scans reviewed but were missed in six cases (11%) at the time of initial presentation. The most likely cause for misdiagnosis is lack of familiarity with the appearance of small fractures confined to the dorsal bone margin. Detection of small fractures depends on careful attention to scan positioning and filming. It is essential that all of the proximal articular surface of the navicular bone is included in the scan plane. Because of the normally high density of this region of the bone, it is also important to view and film the images at appropriately high window and level settings (3000 H/500 H). Fine-section 1.5-mm axial scans, with comparison views

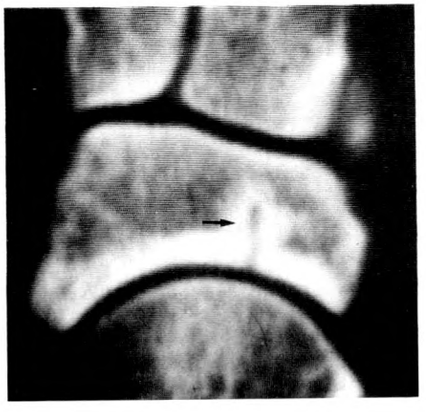

Fig. 7.—Nonunited partial fracture of right navicular bone in a 19-year-old female sprinter whose treatment was weight-bearing rest for 6 months. Coronal CT scan shows blurring of cortical defect and sclerosis (*arrow*) surrounding medullary portion of fracture, indicative of nonunion. Proximal marginal sclerosis is normal.

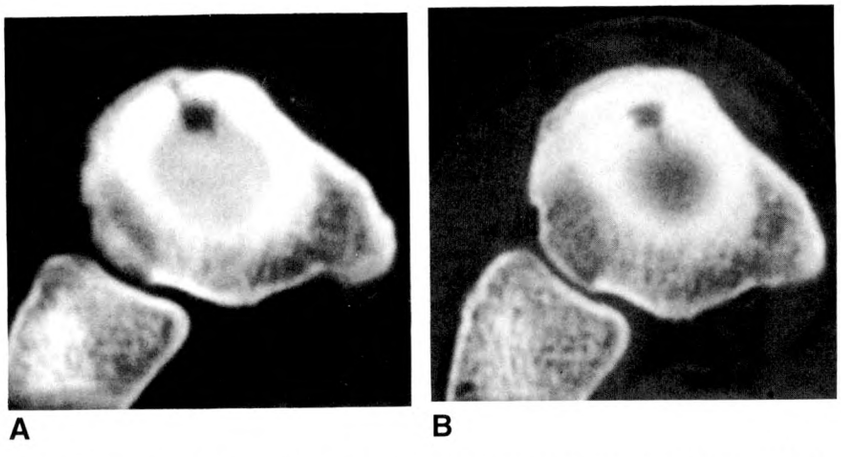

Fig. 8.—Stages in healing of partial fracture of right navicular bone in a 23-year-old female sprinter.

***A*, Axial CT scan obtained 6 weeks after foot was immobilized with non–weight-bearing cast shows cortical bridging with 5-mm residual cyst.**

***B*, Axial CT scan obtained 13 months after *A* shows dense cortical healing with persistent cyst and small cleft. Patient was asymptomatic at this time.**

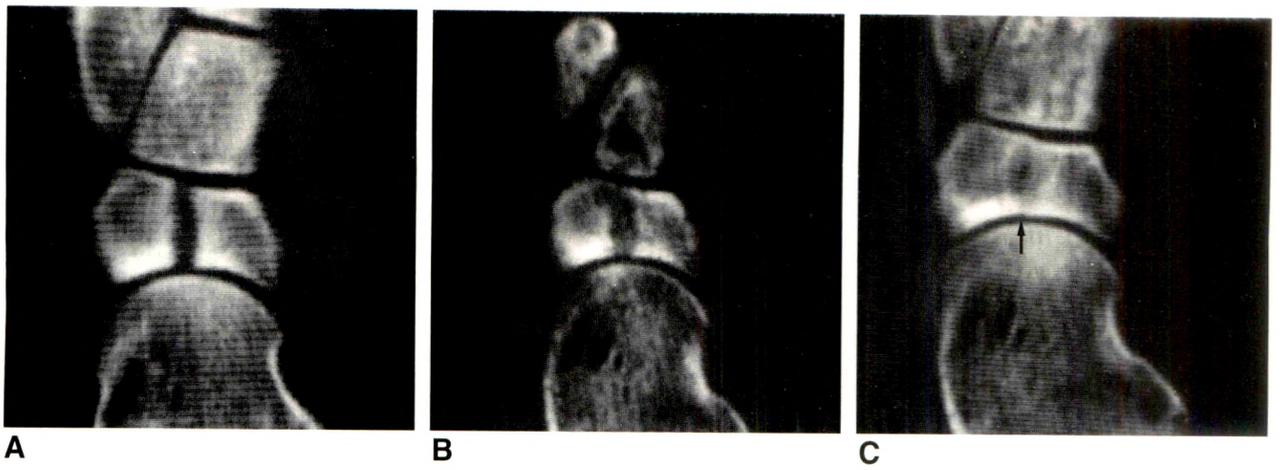

Fig. 9.—Stages in healing of complete tarsal navicular fracture in a 17-year-old female basketball player.
***A*, Coronal CT scan shows a complete sagittal fracture with a 3-mm gap at time of initial diagnosis.**
***B*, Coronal CT scan obtained after patient had 3 months of non–weight-bearing rest shows fracture margins are blurred and callus is forming.**
***C*, Coronal CT scan obtained 3 months after *B* shows complete cortical fusion has occurred, with a small step defect in proximal articular margin of bone (*arrow*). Normal proximal cortical sclerosis is present at all stages (*A*–*C*).**

of both feet, were used in our scan protocol to aid in the detection of small fractures. With experience, however, 3-mm scans of one leg only are sufficient for diagnosis. Scanning in two planes is helpful for accurately measuring fracture depth and length but is not essential for diagnosis, as all fractures were evident in both planes.

REFERENCES

1. Pavlov H, Torg JS, Freiberger RH. Tarsal navicular stress fractures: radiographic evaluation. *Radiology* **1983**;148:641–645
2. Fitch KD, Blackwell JD, Gilmour W. Operation for non-union of stress fracture of the tarsal navicular. *J Bone Joint Surg [Br]* **1989**;71-B:105–110
3. Ting A, King W, Yocum L, et al. Stress fractures of the tarsal navicular in long distance runners. *Clin Sports Med* **1988**;7:89–101
4. Khan KM, Fuller PJ, Brukner PD, Kearney C, Burry H. Outcomes of conservative and surgical management of navicular stress fracture in athletes: 86 cases demonstrated with computerized tomogram (CT). *Am J Sports Med* **1992**;20:657–666
5. Gordon GM, Solar J. Tarsal navicular stress fractures. *J Am Podiatr Med Assoc* **1985**;75:363–366
6. Torg JS, Pavlov H, Cooley LH, et al. Stress fractures of the tarsal navicular: a retrospective review of 21 cases. *J Bone Joint Surg [Am]* **1982**;64-A:700–712
7. Orava S, Karpakka J, Hulkko A, Takala T. Stress avulsion fracture of the tarsal navicular: an uncommon sports-related overuse injury. *Am J Sports Med* **1991**;4:392–395
8. Pavlov H, Torg J. *The running athlete*. Chicago: Year Book Medical, **1987**:40–44

Book Review

MRI Atlas of the Joints. Normal Anatomy and Pathology. By John D. Reeder and Samuel M. Andelman. Baltimore: Williams & Wilkins, 246 pp., 1992. $85

MRI Atlas of the Joints: Normal Anatomy and Pathology is an unusual amalgam of an anatomic atlas and a text/teaching file. The text is divided into six sections according to commonly imaged joints: wrist, elbow, shoulder, hip, knee, and ankle. The section on the knee is 67 pages long, approximately one quarter of the book. Each section begins with a two- to three-page summary of the pertinent anatomy. These summaries are the book's strongest suit, as they are pithy and clear. They do, however, presume a basic general understanding of the anatomy. Each summary is illustrated with several line diagrams of anatomic cutaways of the various joints. Because of their orientation and lack of detailed labeling, the diagrams add little to the corresponding text. After the overview of anatomy, the book provides an extensive series of MR images, in three planes, of the joint being discussed. These images are T1-weighted 3- to 5-mm sections without corresponding specimen photographs. The image quality is mediocre, particularly for images of small parts such as the wrist and ankle. The labeling of normal anatomy is quite accurate; however, the detail of the labeling is inadequate for an atlas.

The teaching-file section is also a strong point of the book. Although the image quality is suboptimal, the cases selected for discussion are by and large appropriate. The major exceptions in terms of case selection are the absence of discussions of chondromalacia in the section on the knee and of medial collateral ligament abnormalities and bursitis in the section on the elbow. Also, too much emphasis is placed on neoplasms and systemic disease for a book of this level. The discussions that follow the case presentations are excellent: clear, accurate, and easy to follow. They are, however, quite brief, and readers with even a modest experience in musculoskeletal MR imaging will find little new information. Additionally, some discussions are too concise for such clinically significant entities as triangular tears of the fibrocartilage, avascular necrosis, and osteomyelitis.

The quality of paper and binding is good. The illustrations, however, are less than state of the art. The cost, $85, seems appropriate for the book's length.

This book has relatively little direct competition. It is not truly an atlas of musculoskeletal MR imaging and pales when compared with the book by Kang and Resnick. As a text of musculoskeletal MR imaging, it is too brief to be compared with those by Berquist, Firooznia et al., and Bloem and Sartoris. As a teaching file, it is most similar to Mink and Deutsh's *MRI of the Musculoskeletal System: A Teaching File.* That text, although more detailed and informative, lacks a consistent discussion of normal anatomy. *MRI Atlas of the Joints* will be most appropriate for beginning residents on their first MR rotation and those who desire an overview of musculoskeletal MR imaging; others, I fear, would soon outgrow it.

Mark E. Schweitzer
Thomas Jefferson University Hospital
Philadelphia, PA 19107

Intrinsic and Extrinsic Carpal Ligaments: Evaluation by Three-dimensional Fourier Transform MR Imaging

Saara M. S. Totterman[1]
Richard Miller[2]
Bruce Wasserman[1]
Judy S. Blebea[1,3]
Deborah J. Rubens[1]

OBJECTIVE. As evaluation of the anatomic and functional integrity of intrinsic and extrinsic carpal ligaments with conventional imaging methods is difficult, we designed a study to evaluate the ability of three-dimensional Fourier transform MR imaging to show the carpal ligaments.

SUBJECTS AND METHODS. We obtained coronal MR images of 15 cadaveric wrists and 15 wrists of patients, using three-dimensional volume acquisition with a gradient-recalled echo sequence and a 1.5-T magnet. The MR findings were compared with the findings on dissection in the 15 cadaveric wrists and with the surgical findings in eight patients.

RESULTS. All the volar ligaments had a striated appearance on MR images, with alternating bands of low and intermediate signal intensity. No tears of the extrinsic ligaments were seen. The intrinsic scapholunate and lunotriquetral ligaments were seen as structures with more homogeneously intermediate intensity attaching to their adjacent bone through high-signal-intensity hyaline cartilage. For the cadaveric wrists, MR indications of a tear of the scapholunate ligament were true-positive in three and false-negative in three; indications of a tear of the lunotriquetral ligament were true-positive in five, false-positive in two, and false-negative in one. For the eight patients with surgical confirmation, the MR findings regarding tears were true-positive in two and true-negative in six. Neither surgery nor MR imaging showed any tears of the scapholunate ligament.

CONCLUSION. Three-dimensional Fourier transform MR imaging with thin slices provides the resolution necessary to visualize the anatomic detail of the extrinsic and intrinsic ligaments of the wrist, but additional clinical experience with this technique will be required to determine its diagnostic capabilities.

***AJR* 1993;160:117–123**

Although the clinical importance of the extrinsic and intrinsic carpal ligaments is emphasized in the literature on hand surgery [1, 2], evaluation of the anatomic and functional integrity of these ligaments can be difficult. With ligamentous injuries and degenerative disease, clinical symptoms and signs are often nonspecific [1], plain radiographic findings are frequently normal, and arthrographic findings can be difficult to correlate with clinical findings [3, 4].

The inherent ability of MR imaging to enable distinction of cartilage from ligament suggests that this technique could be used to evaluate all ligaments, including those of the wrist. Because carpal ligaments are small and intricate [1, 2, 5], detailed MR images of them require use of techniques that provide both thin contiguous slices and a high signal-to-noise ratio. Three-dimensional Fourier transform (3DFT) MR imaging provides thinner slices at a higher signal-to-noise ratio than two-dimensional Fourier transform imaging does [6], and with gradient-recalled echo (GRE) sequences, the imaging time is sufficiently short to permit its use clinically [7–9]. In view of these considerations, we designed a preliminary study to evaluate, first with cadavers and then with patients, the ability of 3DFT GRE MR imaging to show normal anatomy of and pathologic changes in extrinsic and intrinsic carpal ligaments.

Received May 21, 1992; accepted after revision July 17, 1992.

[1]Department of Diagnostic Radiology, University of Rochester School of Medicine and Dentistry, 601 Elmwood Ave., Rochester, NY 14642. Address reprint requests to S. M. S. Totterman.

[2]Department of Orthopaedics, University of Rochester School of Medicine and Dentistry, Rochester, NY 14642.

[3]Present address: Department of Radiology, University of Cincinnati Hospital, 234 Goodman St., Cincinnati, OH 45267-0814.

0361–803X/93/1601–0117

Materials and Methods

Fifteen fresh frozen and thawed cadaveric wrists and 15 wrists of patients were imaged with a 1.5-T MR system (Signa, General Electric, Milwaukee, WI). On the basis of the results of earlier investigations [10], we decided to restrict imaging to the coronal plane. For all studies, a body coil was used as the transmitter. For five cadaveric wrists and two wrists of patients, a two-piece single-loop surface coil [11] was used as the receiver. For all other studies, a two-coil array (a two-piece surface coil combined with a second single-loop coil, both of which are perpendicular to the axis of the primary magnetic field and to each other) was used as the receiver coil (Fig. 1).

The position of the hand and wrist was specific. The hand was placed in a comfortable fisted position across the gantry so that the wrist lay in approximately 15° of extension and neutral radioulnar deviation. The configuration of the surface coils was such that the long axis of the forearm was required to align perpendicularly to the magnetic field. The required alignment was achieved by positioning the patient supine with the wrist overhead, with a soft support under the chest to avoid hyperflexion of the shoulder. The position was well tolerated by patients.

The imaging protocol was established on the basis of pilot studies with five cadaveric wrists and two wrists of volunteers. To determine the optimal imaging parameters, we imaged these wrists by using a TR of 60–90 msec (60 msec was the shortest TR time available for an 8-cm field of view), a TE of 13–30 msec, and a flip angle of 5–90°. The optimal slice thickness was determined by using thicknesses of 0.7, 1.0, 1.5, and 3.0 mm. To evaluate the importance of the matrix size, we imaged wrists by using 256 × 256 and 256 × 128 matrices. All images were acquired by using an 8-cm field of view and one excitation. With a TR/TE/flip angle combination of 69/17/20°, the imaging time was 9 min 30 sec, and the major volar extrinsic and intrinsic ligaments and the articular cartilage were visualized. A slice thickness of 1 mm was thin enough for visualization of all the ligaments and thick enough for acceptable signal-to-noise ratio. A 256 × 256 matrix was required to distinguish the ligaments from the cartilages and to distinguish the adjacent cartilages from each other.

The MR images were read in consensus by two radiologists. On the images, the major volar ligaments, including the radioscaphocapitate, the radiolunotriquetral, the radioscapholunate, and the deltoid ligaments were identified [1, 2] (Fig. 2). Similarly, the interosseous intrinsic ligaments, including the scapholunate and lunotriquetral ligaments, were identified [1, 2] (Fig. 2). The triangular fibrocartilage complex also was identified, but the details of our observations regarding that complex are the subject of a separate report. After the MR study was completed, the intrinsic and major volar ligaments of the cadaveric wrists were evaluated first via a dorsal radiocarpal arthrotomy and subsequently by complete volar and dorsal dissection. These ligaments cannot be distinguished as separate structures by volar gross dissection. They are best seen from their posterior aspect as visualized through dorsal arthrotomy. First, the intrinsic interosseous ligaments were examined, with special attention to the appearance, orientation, and size of the fibers. A search was made for partial and full-thickness tears also. To detect small tears, we injected saline into the intact midcarpal joint and detected leaks by direct visualization through the radiocarpal arthrotomy incision. After that, the major volar ligaments were examined. Normal and pathologic findings on dissection were correlated with the corresponding MR images. The prospective MR findings were correlated with the surgical findings also in the eight patients who subsequently underwent arthrotomy.

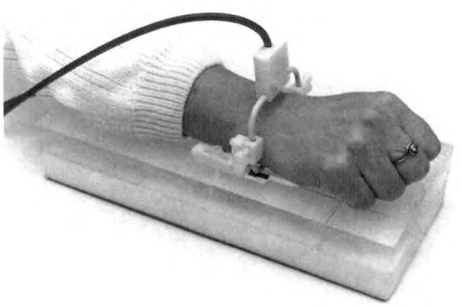

Fig. 1.—Two-piece receiver coil used for MR imaging of ligaments of wrist.

Results

One of the important observations from this investigation was that neither the normal anatomy of nor pathologic changes in the extrinsic and intrinsic wrist ligaments could be fully appreciated without evaluating all the thin contiguous MR images. Therefore, Figure 3 shows most of the sections of a representative normal cadaveric wrist.

Normal Findings

This imaging technique provided particularly good contrast between cartilage, ligament, and bone. All cartilages in the radiocarpal joint, midcarpal joint, and distal radioulnar joint appeared as high-signal-intensity areas with fine low-signal-intensity outer borders (Fig. 3). The articular ridge between the scaphoid and lunate fossae on the articular surface of the radius was covered by a thin layer (1–2 mm thick) of soft tissue (Fig. 4). This tissue had low signal intensity on MR images (Fig. 3). Low-signal-intensity synovial tissue was commonly seen in the more dorsal sections of the midcarpal joints at the level of the triquetral hamate articulation (Figs. 3 and 5).

The appearance of the major volar ligaments was similar in both cadaveric and patients' wrists. The radioscaphocapitate, radiolunotriquetral, and deltoid ligaments were consistently visualized on at least three contiguous slices (Fig. 3). All these ligaments appeared as striated structures with alternating bands of low and intermediate signal intensity.

The radioscaphocapitate ligament is the most radial of the major volar ligaments. It originates at the styloid process of the radius, continues across the waist of the scaphoid bone, and attaches to the head of the capitate bone [2] (Figs. 2 and 3). Because of its relatively large size and obliquity, its configuration and course could usually be followed through four or five contiguous slices.

The radiolunotriquetral ligament originates on the radius just ulnar to the radioscaphocapitate ligament (Figs. 2–4). The deep fibers of the radiolunotriquetral ligament were attached to the volar aspect of the lunate bone, securing the radius to the lunate bone and the lunate bone to the triquetral bone (Fig. 3). The radiolunate and lunotriquetral portions of the ligament were visualized in two to three slices.

The deltoid ligament consists of a fan-shaped array of fibers extending from the capitate bone to the triquetral, scaphoid, and lunate bones (Figs. 2 and 5). The lunate

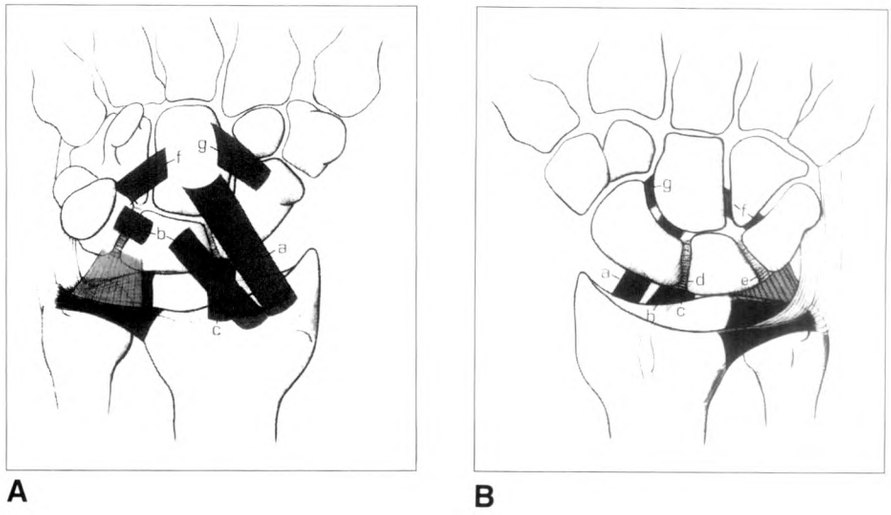

Fig. 2.—*A* and *B*, Diagrams show volar (*A*) and dorsal (*B*) views of intrinsic and major volar ligaments. a = radioscaphocapitate ligament, b = radiolunotriquetral ligament, c = radioscapholunate ligament, d = scapholunate (intrinsic) ligament, e = lunotriquetral (intrinsic) ligament, f = capitotriquetral arm of deltoid ligament, and g = capitoscaphoid arm of deltoid ligament.

fascicle is frequently absent [2]. It was not seen in this series and is not illustrated in Figure 2. With the hand in the fisted imaging position, the most volar portion of the capitate bone is located dorsal to the most volar aspect of the lunate bone. Consequently, the capitotriquetral arm of the deltoid ligament was visualized at the same level as the deeper fibers of the radiolunotriquetral and radioscaphocapitate ligaments (Fig. 3).

For all these ligaments, the striated fascicular structure and orientation of the bundles seen on the MR images could also be detected in the dissected wrists.

The radioscapholunate ligament originates on the radius more dorsally and medially than the radiolunotriquetral ligament does (Figs. 2 and 4). Its origin on the cortical bone in the volar indentation of the radius could be readily seen on the MR images (Fig. 3). On MR images, this ligament had areas of mixed high and intermediate signal intensity, but the striations prominent in the other volar ligaments were not apparent. Both dissections and MR images showed that the volar fibers were attached to the cortex of the corresponding bones. The more dorsal fibers merged with the fibers of the intrinsic scapholunate ligament (Fig. 4).

The intrinsic scapholunate ligament is horseshoe-shaped in the sagittal plane (Fig. 5) and connects the volar, proximal, and dorsal borders of the scaphoid bone to the lunate bone (Figs. 2, 4, and 5). On MR images, it appeared as a structure with low to intermediate signal intensity (Fig. 3). The most volar and dorsal portions of the ligament were directly attached to the scaphoid and lunate bones. The midportion of the ligament showed variable attachment to bone and articular cartilage, with variable signal intensities. The proximal-distal dimension of the midportion of the ligament was termed its "thickness." The thickness of this ligament in the midcoronal plane varied from 2 mm in some specimens to as much as one third the height of the lunate bone in others.

The intrinsic lunotriquetral ligament is also horseshoe-shaped in the sagittal plane (Fig. 6), and like the scapholunate ligament, it connects the volar, proximal, and dorsal borders of the two bones (Figs. 2, 4, and 6). It appeared to be much thinner in proximal-distal dimension than the scapholunate ligament. Its volar and dorsal portions appeared to attach directly to the corresponding cortical bone, with the low signal intensity of the ligament blending with the low signal intensity of the bone (Fig. 3). The midportion of the ligament appeared to attach to the corresponding cartilage of the lunate and triquetral bones (Fig. 3), with the homogeneous low-signal intensity of the ligament blending into the higher signal intensity of the articular cartilage.

Pathologic Findings

The MR images for both surgical cases and cadaveric dissection were interpreted both prospectively and retrospectively. No tears of the radioscaphocapitate, radiolunotriquetral, radioscapholunate, or deltoid ligaments were detected either on MR images or by dissection in these wrists.

On MR images, tears of the scapholunate ligament appeared as a discontinuity in the normal homogeneous low signal intensity of the intact ligament. The tears involved either the middle part of the substance (Fig. 7) of the ligament or its attachment to the lunate or scaphoid bone (Fig. 8). In some cases in which the ligament had detached from the cartilage, the remnant had retracted, making that portion of the ligament appear thicker.

On dissection, five cadaveric wrists showed a full-thickness tear of the scapholunate ligament, and one showed a partial-thickness tear. Prospective interpretation of the MR images of the 15 cadaveric wrists falsely indicated no tear in three wrists. In all three cases, the defects were small, involving only the dorsal third of the ligament. Two of these short-segment small tears could be detected retrospectively. None of the eight patients who had surgery were thought to have tears of the scapholunate ligament on the basis of preoperative MR images, and no tears were detected at surgery.

MR findings with respect to torn lunotriquetral ligaments were similar to those noted for the scapholunate ligament. On MR images of both patients' and cadaveric wrists, tears

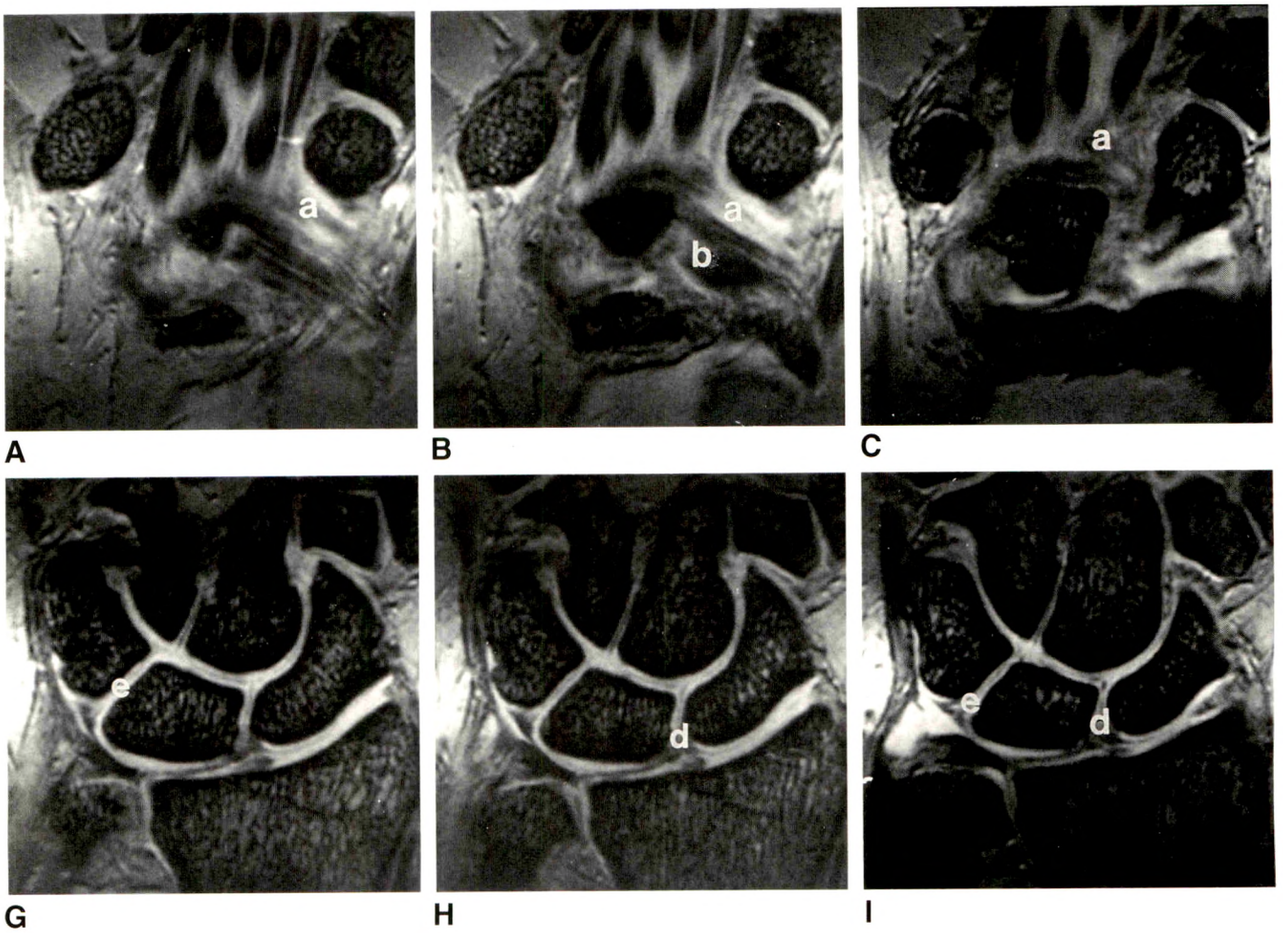

of the lunotriquetral ligament appeared as discontinuities in the normal homogeneous low signal intensity of an intact ligament (Fig. 8). All tears of the lunotriquetral ligament in this study occurred in the midportion (volar to dorsal) of the ligament. Defects were noted both in the middle of the substance and at the cartilaginous junction of the ligament. Dissection showed full-thickness tears of the lunotriquetral ligament in six of the 15 cadaveric wrists. MR findings interpreted as showing a tear were false-negative for one wrist and false-positive for two. In the eight patients who had surgery, two tears of the lunotriquetral ligament were identified prospectively with MR, and both of these were confirmed at surgery. No MR findings were false-positive or false-negative with respect to lunotriquetral ligaments in these eight patients.

Discussion

3DFT GRE MR imaging is useful in the evaluation of large joints [7–9, 12]. The improved signal-to-noise ratio offered by this technique has allowed use of thin slices in the knee, and this has led to improved visualization of meniscal cartilage and cartilage injuries [12]. In the spine, thin-section technique has been shown to provide excellent visualization of the spinal cord and CSF [13, 14].

Thin and contiguous slices are needed for adequate MR imaging of the wrist because even many of the larger ligaments about the wrist are no more than 1–2 mm thick. Although 3DFT GRE imaging in conjunction with a specialized surface coil was used in this study, other imaging sequences might be comparable, or more effective. Regardless of the pulse sequence used, however, both thin (1.0–1.5 mm) and contiguous slices are needed.

This study showed that the extrinsic and intrinsic carpal ligaments can be depicted in detail with 3DFT MR imaging. The MR appearance of the volar ligaments, bands of low signal intensity separated from each other by areas of higher signal intensity, corresponded well with the anatomic findings in dissected cadaveric wrists, which showed these ligaments were composed of strong fascicles separated by loose connective tissue. The orientation and configuration of

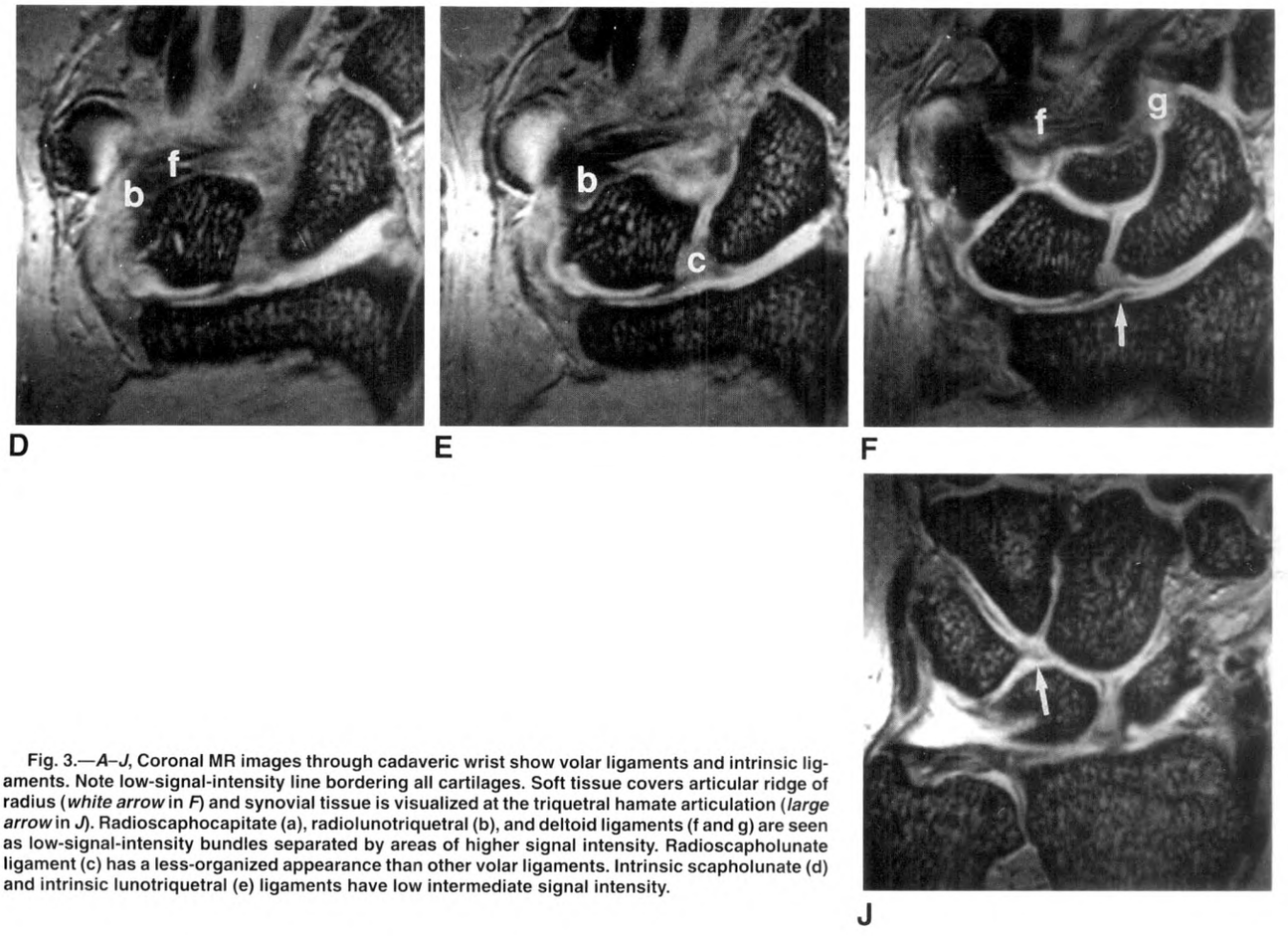

Fig. 3.—*A–J*, Coronal MR images through cadaveric wrist show volar ligaments and intrinsic ligaments. Note low-signal-intensity line bordering all cartilages. Soft tissue covers articular ridge of radius (*white arrow* in *F*) and synovial tissue is visualized at the triquetral hamate articulation (*large arrow* in *J*). Radioscaphocapitate (a), radiolunotriquetral (b), and deltoid ligaments (f and g) are seen as low-signal-intensity bundles separated by areas of higher signal intensity. Radioscapholunate ligament (c) has a less-organized appearance than other volar ligaments. Intrinsic scapholunate (d) and intrinsic lunotriquetral (e) ligaments have low intermediate signal intensity.

the fascicular bands associated with the various ligaments was sufficiently specific that these individual ligaments could be readily distinguished from one another on both MR images and gross dissection. The orientation of the ligaments was optimal for imaging in the coronal plane, as this made it possible to visualize them in several contiguous slices. Use of a 1-mm slice thickness minimized partial volume effects. Although none of the wrists in this series had tears of the major volar ligaments, we think that disruption of any of these ligaments could be readily visualized with this MR technique.

The MR appearance of the radioscapholunate ligament differed from the appearance of both the other extrinsic volar ligaments and the intrinsic ligaments. Histologically, the collagen fibers of the radioscapholunate ligament are loosely organized, and this ligament is more vascular than the neighboring ligaments [15]. As the fibers of the radioscapholunate ligament merge with the fibers of the scapholunate ligament [15], these two structures cannot be distinguished from each other on MR images. An explanation for the variable signal intensity of the attachment of the midportion of the scapholunate ligament to the corresponding structure is being sought. Because of partial volume effects, small tears in the thin dorsal third of the horseshoe-shaped ligament may be difficult to visualize. This problem was thought to be responsible for the three false-negative findings of partial tears of the scapholunate ligament in cadaveric specimens.

One potential cause for false-positive findings indicating tears of the scapholunate ligament is misinterpretation of the low signal intensity associated with the soft tissue covering the ridge between the scaphoid and lunate fossae of the radius. If the low signal associated with this tissue is interpreted as being part of the scapholunate ligament, the normal joint fluid visualized between this tissue and the adjacent scapholunate ligament may be interpreted as a tear of the scapholunate ligament.

Although we had no false-positive or false-negative MR findings indicating presence or absence of tears of the lunotriquetral ligament in the eight wrists of patients who had surgery, this ligament was inconsistently visualized in the cadaveric wrists. The explanation for the two false-positive MR findings in the cadaveric specimens is unclear. Even in

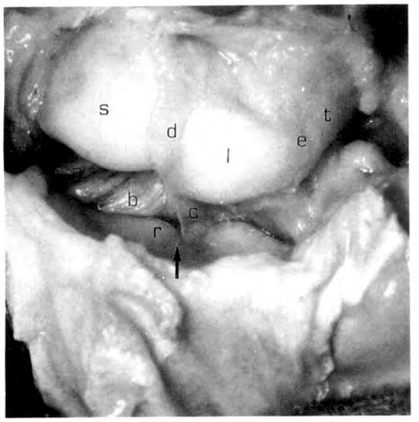

Fig. 4.—Dorsal dissection of radiocarpal joint shows radioscaphocapitate (a), radiolunotriquetral (b), radioscapholunate (c), scapholunate (d), and lunotriquetral (e), ligaments; radius (r); and scaphoid (s), lunate (l), and triquetral (t) bones. Note soft tissue (*arrow*) at radiolunate ridge.

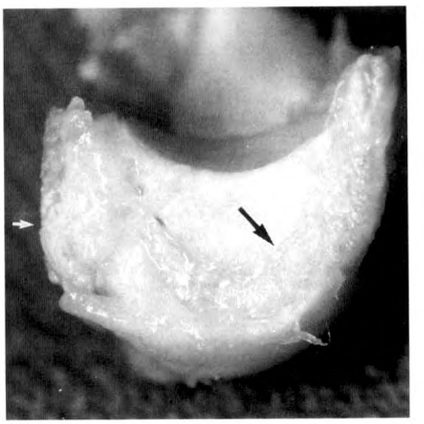

Fig. 5.—Sagittal section through scapholunate joint shows scapholunate ligament viewed from radial aspect (volar aspect is indicated by *small arrow*). Dorsal two thirds of this horseshoe-shaped ligament (*large arrow*) is thinner than volar third.

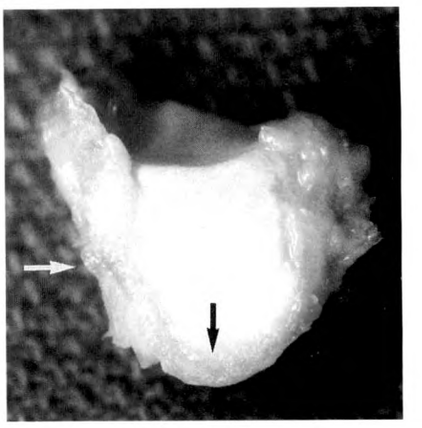

Fig. 6.—Sagittal section through lunotriquetral joint shows lunotriquetral ligament (*black arrow*) viewed from radial aspect (volar aspect is indicated by *white arrow*). Ligament is horseshoe-shaped and thin throughout its extent.

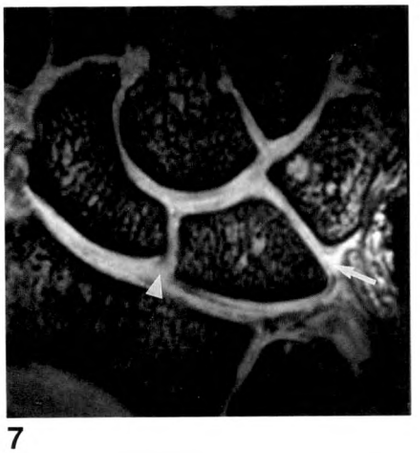

7

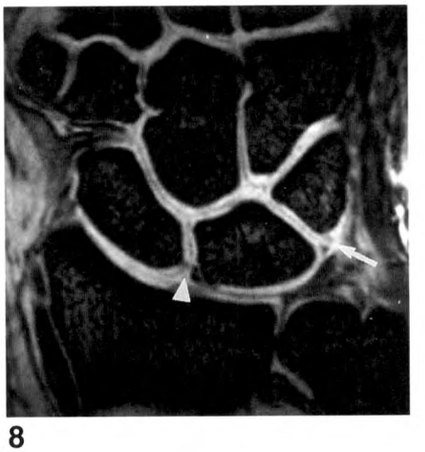

8

Fig. 7.—Coronal MR image of wrist shows tears of scapholunate and lunotriquetral ligaments. Note midsubstance tear in scapholunate ligament (*arrowhead*) and absence of lunotriquetral ligament (*arrow*).

Fig. 8.—Coronal MR image of wrist with tears in scapholunate and lunotriquetral ligaments. Scapholunate ligament is detached from scaphoid bone (*arrowhead*), and lunotriquetral ligament is detached from triquetral bone (*arrow*).

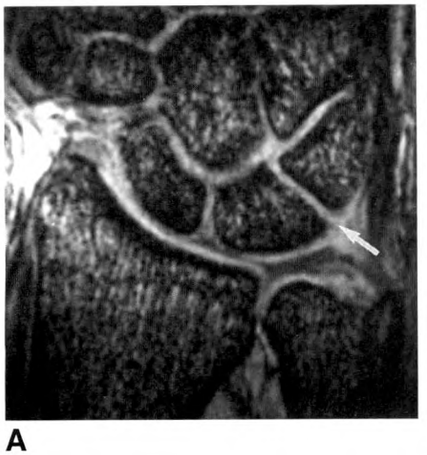

A

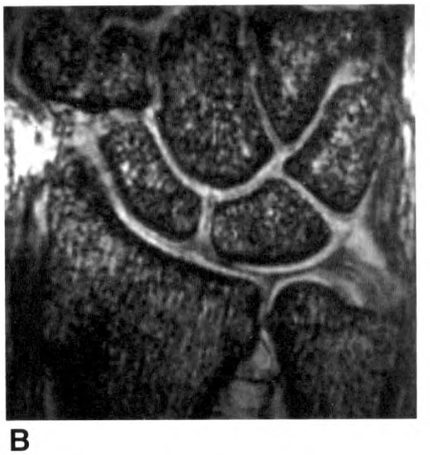

B

Fig. 9.—*A*, Coronal MR image of wrist shows tear in dorsal third of lunotriquetral ligament (*arrow*).

B, More volar section of same wrist shows normal ligament.

retrospect, the ligaments in these wrists could not be visualized. These false-positive findings might be due to postmortem changes within degenerative ligaments that caused increased water content within the ligament and associated increased signal intensity with subsequent misinterpretation. One avoidable potential cause for false-positive MR findings of tears of the lunotriquetral ligament in patients is the lack of familiarity with the normal MR appearance at the ligament-bone interface. Because the ligament inserts through cartilage at both the lunate and triquetral attachments, the high signal associated with the cartilage should be anticipated and interpreted as a normal finding, not as a discontinuity or tear within the ligamentous tissue. The high prevalence of lunotriquetral tears in cadaveric wrists reflects the high prevalence of tears in the wrists of elderly persons.

The contrast inherent in this imaging technique enables clear distinction of hyaline cartilage from the adjacent subchondral bone and collagenous ligamentous tissue. The explanation for the consistent observation of a thin, low-signal-intensity border to the otherwise high signal associated with the articular cartilage is unclear. We think that this border may represent the horizontally oriented collagenous surface layer of normal hyaline cartilage, or perhaps some other architectural or chemical differences in the surface of the cartilage, as opposed to its deeper aspects [16].

One of the potential benefits of using MR imaging to evaluate the ligamentous integrity of the carpus is the possibility of staging or quantifying ligamentous defects. Degenerative changes leading to small perforations of the intrinsic ligaments are common [17]. Inasmuch as many of the small central perforations are asymptomatic, specific knowledge of the exact location and extent of ligamentous tears may be useful.

Although our experience is limited, the results of this study show that 3DFT imaging with very thin slices provides detailed information about the extrinsic and intrinsic ligaments of the wrist. We think that refinements of this technique will further improve our ability to precisely localize and stage the extent of ligamentous and soft-tissue disorders of the wrist.

ACKNOWLEDGMENT

The authors thank Beverly Pollet for her wonderful work in preparing this manuscript.

REFERENCES

1. Mayfield JK, Johnson RP, Kilcoyne RF. The ligaments of the human wrist and their functional significance. *Anat Rec* **1976**;186:417–428
2. Taleisnik J. The ligaments of the wrist. *J Hand Surg* **1976**;2:110–118
3. Zinberg EM, Palmer AK, Coren AB, Levinsohn EM. The triple-injection wrist arthrogram. *J Hand Surg [Am]* **1988**;13-A:803–809
4. North ER, Thomas S. An anatomic guide for arthroscopic visualization of the wrist capsular ligaments. *J Hand Surg [Am]* **1988**;13-A:815–822
5. Zlatkin MB, Chao PC, Osterman AL, Schnall MD, Dalinka MK, Kressel HY. Chronic wrist pain: evaluation with high-resolution MR imaging. *Radiology* **1989**;173:723–729
6. Carlson J, Crooks L, Ortendahl D, Kramer DM, Kaufman L. Signal-to-noise ratio and section thickness in two-dimensional versus three-dimensional Fourier transform MR imaging. *Radiology* **1988**;166:266–270
7. Harms SE, Muschler G. Three-dimensional MR imaging of the knee using surface coils. *J Comput Assist Tomogr* **1986**;10:773–777
8. Spritzer CE, Vogler JB, Martinez S, et al. MR imaging of the knee: preliminary results with a 3DFT GRASS pulse sequence. *AJR* **1988**; 150:597–603
9. Haggar AM, Froelich JW, Hearshen DO, Sadasivan K. Meniscal abnormalities of the knee: 3DFT fast-scan GRASS MR imaging. *AJR* **1988**;150:1341–1344
10. Totterman S, Miller R, Szumowski J, Rubens D, Blebea J. MRI of wrist using ultrathin slices (abstr). In: *Works in progress: Society of Magnetic Resonance Imaging 1990*. Berkeley, CA: Society of Magnetic Resonance Imaging, **1990**:21
11. Totterman SM, Heberger R, Miller R, Rubens D, Blebea JS. Two-piece wrist surface coil. *AJR* **1991**;156:343–344
12. Harms SE, Flamig DP, Fisher CF, Fulmer JM. New method for fast MR imaging of the knee. *Radiology* **1989**;173:743–750
13. Hennig J, Friedburg H, Ott D. Fast three-dimensional imaging of cerebrospinal fluid. *Magn Reson Med* **1987**;5:380–383
14. Tsuruda JS, Norman D, Dillon W, Newton TH, Mills DG. Three-dimensional gradient-recalled MR imaging as a screening tool for the diagnosis of cervical radiculopathy. *AJNR* **1989**;10:1263–1271
15. Berger RA, Blair WF. The radioscapholunate ligament: a gross and histologic description. *Anat Rec* **1984**;210:393–405
16. Lehner KB, Rechl HP, Gmeinwieser JK, Heuck AF, Lukas HP, Kohl HP. Structure, function, and degeneration of bovine hyaline cartilage: assessment with MR imaging in vitro. *Radiology* **1989**;170:495–499
17. Viegas SF, Ballantyne G. Attritional lesions of the wrist joint. *J Hand Surg [Am]* **1987**;12-A:1025–1029

Book Review

Pediatric Skeletal Radiology. Edited by Martin H. Reed. Baltimore: Williams & Wilkins, 677 pp., 1992. $140

This textbook is the combined effort of several North American and Canadian pediatric radiologists. The work covers pediatric skeletal radiology from head to toe.

The book is divided into four main sections. The first, or general, section covers various topics, including dysplasias, metabolic and hematologic abnormalities, soft tissues and joints, and miscellaneous abnormalities. The second section consists of chapters on the axial skeleton and includes ones on the thorax, the skull, and facial bones. The appendicular skeleton is covered in the third section. Included here are chapters on the hand and foot, injuries, infection, and normal and abnormal development patterns and another chapter on miscellaneous disorders. The final section on techniques has chapters on determination of skeletal maturity, metacarpal phalangeal profile analysis, arthrography, and limb length discrepancies. Some of the more commonly used techniques (e.g., scoliosis measurement and foot varus/valgus determination) are mentioned in preceding chapters.

The image quality is excellent throughout the book. The numerous images used are mainly plain radiographs, without many examples of scintigrams, CT scans, or MR images. A design problem detracts from many images: They are separated from the relevant text by pages of information on subsequent subjects. Many of the images would be more instructive if explanatory arrows were used to point out subtleties. The legends for the parts of one figure have been reversed, thereby mislabeling the thanatophoric dysplasia as normal. Another oversight was printing a figure upside down.

The layout of the book would benefit from a different organizational sequence. The first chapter is about dysplasias, whereas the chapter about development is in the middle of the book. I found no objective difference between the short chapter in the first section called "Trauma" and a subsequent chapter titled "Injuries" in the third section. The same applies to the two "Miscellaneous" chapters.

The chapters on the spine and tumors are comprehensive, educational, and concise. As with all books written by more than one author, the writing style varies from chapter to chapter. In addition, the first section contains multiple grammatical errors. Constant referral to topics in other sections has resulted in some areas of cursory coverage. The length of explanations is not always related to the frequency of occurrence of the conditions described. It is unusual to find discussion of the skull and facial bones in a book on skeletal radiology. The two chapters on these areas are superficial and attempt to cover such topics as retinoblastoma, sinusitis, and juvenile angiofibroma, which might be better dealt with in a neuroradiology textbook.

In summary, parts of this book are too superficial for a pediatric radiologist and yet too detailed for a medical student. Although I cannot recommend *Pediatric Skeletal Radiology*, the book may still be of use to general radiology residents who already have a foundation in radiology.

Ronald B. J. Glass
Children's National Medical Center
Washington, DC 20010

Review Article

Viral Infections of the CNS in Children: Imaging Features

D. W. W. Shaw[1] and W. A. Cohen[2]

In this paper, we review the imaging findings associated with the major viral infections of the CNS in infants and children. We approach these infections by grouping them into several categories: congenital infections in neonates, aseptic meningitis and encephalitis, acute disseminated encephalomyelitis and other postviral syndromes in older children, and HIV infection.

Imaging has various functions in children with viral CNS infection. With some agents, such as reactivated latent herpesvirus type 1, imaging may suggest the diagnosis. With others, such as congenital cytomegalovirus (CMV), imaging may suggest the presence of infection and show the extent of involvement, but immunologic and culture methods are needed to suggest the causal agent (Fig. 1). With epidemic encephalitis, such as Western equine encephalitis, imaging findings are used to exclude a bacterial process or complications. In patients with acute disseminated encephalomyelitis, imaging may show the extent of disease and suggest the nature of the process.

The wide range of clinical and imaging findings and the spectrum of agents seen with viral CNS infections in children reflect the immaturity of children's nervous and immune systems. In the fetal nervous system, the severity of the sequelae of infection tends to reflect the gestational age of the fetus at the time of exposure. Other age-related differences are seen with neonates and young children, whose immature immune system renders them susceptible to a different spectrum of viral agents with a wide range of virulence.

Congenital and Perinatal Viral Infections

The principal congenital viral infections, rubella, cytomegalovirus (CMV) infection, and herpes simplex commonly occur in the perinatal period and have been grouped with toxoplasmosis (caused by an obligate intracellular parasite) as the TORCH infections. Infection with HIV type I also occurs perinatally; however, the principal manifestations of HIV infection most often occur outside the perinatal period. Vaccination programs have diminished the prevalence of perinatal infections caused by other agents, such as measles, mumps, and varicella-zoster viruses, and reports of neonatal infection with other viral agents, such as enterovirus, are only sporadic.

In general, sequelae of an intrauterine infection reflect the agent involved and the stage in fetal development at which exposure occurred. Early infections can result in embryonic death with resorption or spontaneous abortion, intrauterine growth retardation, and developmental anomalies. Some congenital viral infections, such as rubella, CMV infection, herpes simplex, herpes zoster, and HIV infection, can persist in the neonate. The clinical features of these infections, such as encephalitis or failure to thrive, can then reflect the persistence of viral infection in addition to the effects of intrauterine exposure.

Perinatal exposure to viral agents occurs via three pathways. In utero, the placenta is generally effective in protecting the fetus; thus, most episodes of maternal viremia are not associated with placental or fetal involvement. Nevertheless, placental transgression does occur and is the usual route by which the fetus is infected. Less commonly, trans-

Received April 8, 1992; accepted after revision August 10, 1992.

[1]Department of Radiology, University of Washington Medical Center, Children's Hospital and Medical Center, 4800 Sandpoint Way NE, Seattle, WA 98105. Address reprint requests to D. W. W. Shaw.

[2]Department of Radiology, University of Washington, Harborview Medical Center, 325 9th Ave., Seattle, WA 98104.

AJR **1993;160:125–133** 0361–803X/93/1601–0125

mission involves ascending infection via the cervix. Exposure also may occur during delivery, either as the infant descends through the vaginal canal or by direct contact with the monitor's electrodes [1].

Radiologic manifestations of this group of infections are similar, with differences stemming from the time of exposure during gestation and the age of the child when the diagnosis is made. In general, the later the diagnosis is made, the more difficult it is to identify the causal agent. Often, antibody titers indicating exposure to a specific agent are the only way to confirm a specific diagnosis. Imaging in the young infant is complicated by incomplete myelination of white matter, with its lower density on CT scans and hyperintensity on T2-weighted MR images, which can obscure abnormalities (or result in overdiagnosis of cerebral edema).

Cytomegalovirus Infection

CMV, a DNA virus of the herpesvirus group, is the most frequent cause of congenital viral infections and is reported to be present in 1% of neonates, although only 10% of infected neonates are symptomatic. Most significant congenital infections (with clinically apparent sequelae) occur by placental transgression during the primary episode of maternal infection; the prevalence may be as high as 58%. Conversely, asymptomatic infection, whether congenital or perinatal, is more common if maternal viremia results from reactivation of a latent infection or if neonatal exposure occurs via cervical secretions or infected breast milk [2].

CNS sequelae associated with congenital CMV infections include seizures, mental retardation, optic atrophy, sensorineural hearing loss, and hydrocephalus. Pathologically, cerebellar hypoplasia, periventricular calcifications, cerebral atrophy, porencephaly and subependymal cysts, polymicrogyria, and delayed myelination have been described [2]. CMV may remain latent and be shed during asymptomatic periods. Reactivation can occur, most commonly in those who become immunocompromised, as has been reported in an infant with human T-cell leukemia virus type 3 [3].

Either MR imaging or CT can be used to assess the extent of disease. Calcifications are better evaluated with CT, whereas the extent of parenchymal disease is more accurately shown with MR imaging [4]. MR findings in one group of 10 children included dilated lateral ventricles in 10, large subarachnoid spaces in eight, oligogyria and pachygyria in eight, delayed myelination in seven, paraventricular cysts in six, and intracranial calcification in one [5]. Intracranial calcification (Figs. 1 and 2), reported in up to 40% of affected children, is typically periventricular but can also be found in basal ganglia and subcortical and cortical regions [2]. Subependymal periventricular cysts, usually in the occipital lobe, are thought to be associated with necrosis and gliosis. Such cysts can also be diagnosed with sonography. Similar cysts have been associated with rubella, bacterial ventriculitis, and intraventricular hemorrhage. Associated microgyria is a frequent neuropathologic finding but may appear on imaging studies as oligogyria or pachygyria [6]. This focal cerebral dysplasia (Fig. 3) is thought by some to result from congenital vascular insufficiency [7]. Cerebral atrophy, indicated by an increase in the size of ventricles and subarachnoid spaces, can be shown with MR imaging, CT, or sonography; however, MR is more sensitive for the detection of delayed or pathologic myelination [5].

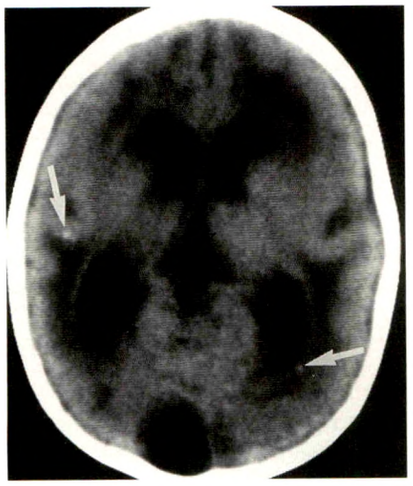

Fig. 1.—10-month-old child with developmental delay and microcephaly. Presumptive diagnosis was cytomegalovirus (CMV) encephalitis. Axial CT scan shows hydrocephalus, hypodensity, volume loss, and punctate calcifications (*arrows*) in a predominantly periventricular distribution. Most likely cause is intrauterine infection by *Toxoplasma*, rubella virus, CMV, or herpesvirus. Serum assays for rubella, toxoplasmosis, and herpes simplex were negative. It was not possible to test a child of this age for infection with CMV.

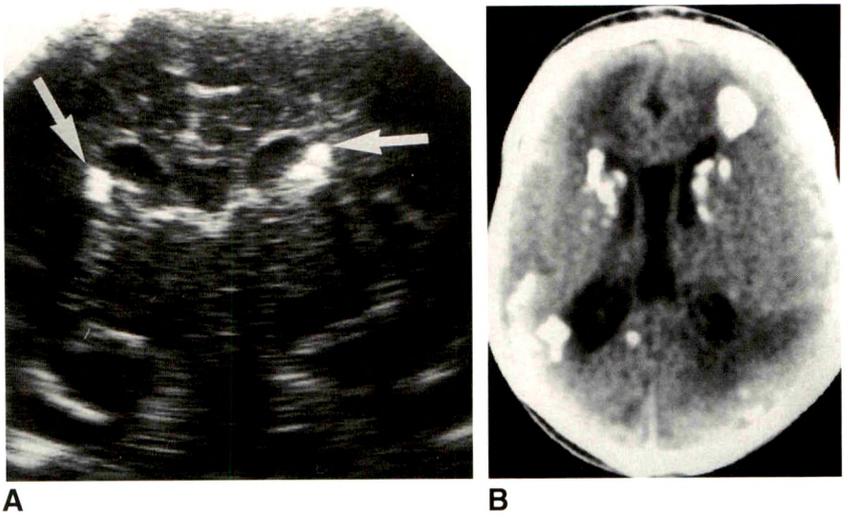

A B

Fig. 2.—1-month-old child whose mother was infected by cytomegalovirus (CMV) during pregnancy. Presumptive diagnosis was CMV encephalitis.

A, Coronal sonogram shows hydrocephalus with bilateral, highly echogenic periventricular foci (*arrows*). This appearance is highly suggestive of an intrauterine infection.

B, Axial CT scan through body of lateral ventricles shows hydrocephalus and prominent periventricular calcifications. This appearance is typical for a neonate who had a severe early intrauterine infection. Calcifications are better shown on unenhanced CT scans than on MR images.

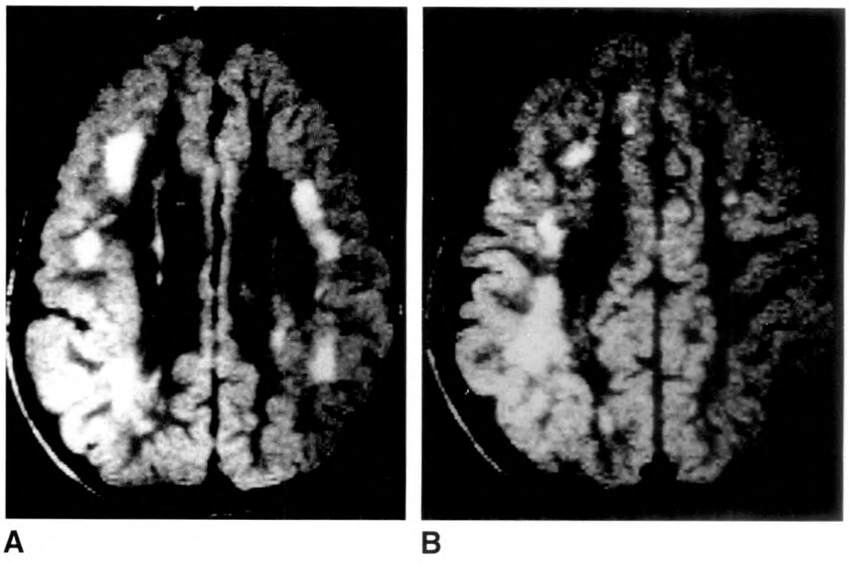

Fig. 3.—Congenital cytomegalovirus (CMV) encephalitis.

***A* and *B*, Axial MR images through bodies of lateral ventricles (*A*) and centrum semiovale (*B*) show dysplastic cortex in right frontal lobe and areas of increased T2 signal scattered through white matter. Calcifications were present in corresponding areas on CT scan. (Courtesy of A. J. Barkovich, San Francisco, CA.)**

Herpes Simplex

Herpes simplex types I and II are also caused by DNA viruses of the herpesvirus group. Either type can be perinatal; however, type 2 accounts for 80–90% of neonatal and almost all congenital herpesvirus infections. Fetal herpes simplex is relatively rare, but CNS sequelae of such infection are generally severe. In one series of 13 infants infected in utero, 12 had skin lesions, seven had microcephaly, five had hydrocephalus, two had microphthalmia, and eight had chorioretinitis [8]. Unlike the case in other perinatal infections, intrapartum transmission via direct contact rather than transplacental transgression is the origin of most neonatal herpesvirus infections; the reported prevalence is between one in 200 and one in 5000 deliveries. Diagnosis is difficult because the mother may not have a history of genital herpes or evidence of active infection. Furthermore, neonatal herpetic skin lesions may be absent (or misdiagnosed) [9].

Classically, neonatal herpetic infections are divided into three clinical categories: (1) skin, eye, and mouth; (2) disseminated; and (3) CNS infections. Cutaneous infections are the most common (43%) and the mildest form; nevertheless, without treatment, the infection will progress to disseminated or CNS disease in 75% of infected children. Disseminated disease tends to manifest by 10–11 days after birth, with signs and symptoms that suggest severe bacterial sepsis. CNS manifestations are present in approximately half of the cases. In disseminated herpes simplex, the mortality rate is almost 80% in untreated infants and usually more than 50% in those who are treated. Isolated CNS herpesvirus infection manifests in neonates 2–4 weeks after birth as fever and lethargy followed by seizures [10]. Pathologically, all cells of the CNS can be infected, yet the predilection is involvement of endothelial cells, which can result in vascular thrombosis and hemorrhage [9].

CT scans and MR images may show focal evidence of cerebral edema, but either can show normal findings during the initial episode of encephalitis. Thus, neither CT nor MR findings should be used to exclude diagnosis. The most frequent initial finding on CT scans is widespread, patchy areas of low attenuation in the cerebral cortex and white matter (Fig. 4), which Noorbehesht et al. [11] found in 12 of 15 infants. The earliest reported diagnosis was in a 1-week-old neonate. On MR images, patchy areas of increased T2 signal are seen in the cerebral hemispheres and the basal ganglia, thalamus, and cerebellum. Neonatal infections do not have the temporal lobe predilection seen in herpesvirus infections in older children and adults [12]. Encephalomalacia, which develops rapidly, may be visible within the first 2–3 weeks. Foci of hemorrhage and dystrophic calcification occur in the basal ganglia and periventricular white matter, although hemorrhage has been seen more often on pathologic examinations than on imaging studies. A linear gyriform pattern of increased attenuation on non–contrast-enhanced CT has been reported and attributed to the presence of calcification [11, 13], to changes in local vascularity, or to prolonged retention of contrast material in regions where the blood-brain barrier is disrupted [14] (Fig. 4). We have also occasionally observed a linear gyriform pattern of hyperintensity on T1-weighted images. Some have speculated the underlying disease relates to cortical laminar necrosis. CT early in the course of infection is not a good predictor of outcome, although findings on later scans are more accurate indicators of prognosis [11]. Sonography in neonates with herpesvirus infection may show linear thalamic echogenicities, thought to reflect vasculopathy [15].

Rubella

Placental transmission of the rubella virus occurs at the time of primary maternal infection. If this occurs during the first trimester, the risk of fetal infection may approach 85%. Gestational age at the time of infection is the most important factor in ultimate outcome. The infection can kill the fetus or have no apparent effect. Infections in the first 2 months of gestation are associated with cataracts and cardiac abnormalities. In 10–20% of affected infants, an acute meningoencephalitis is present at birth, which can be correlated with motor and mental retardation. In the remainder of young

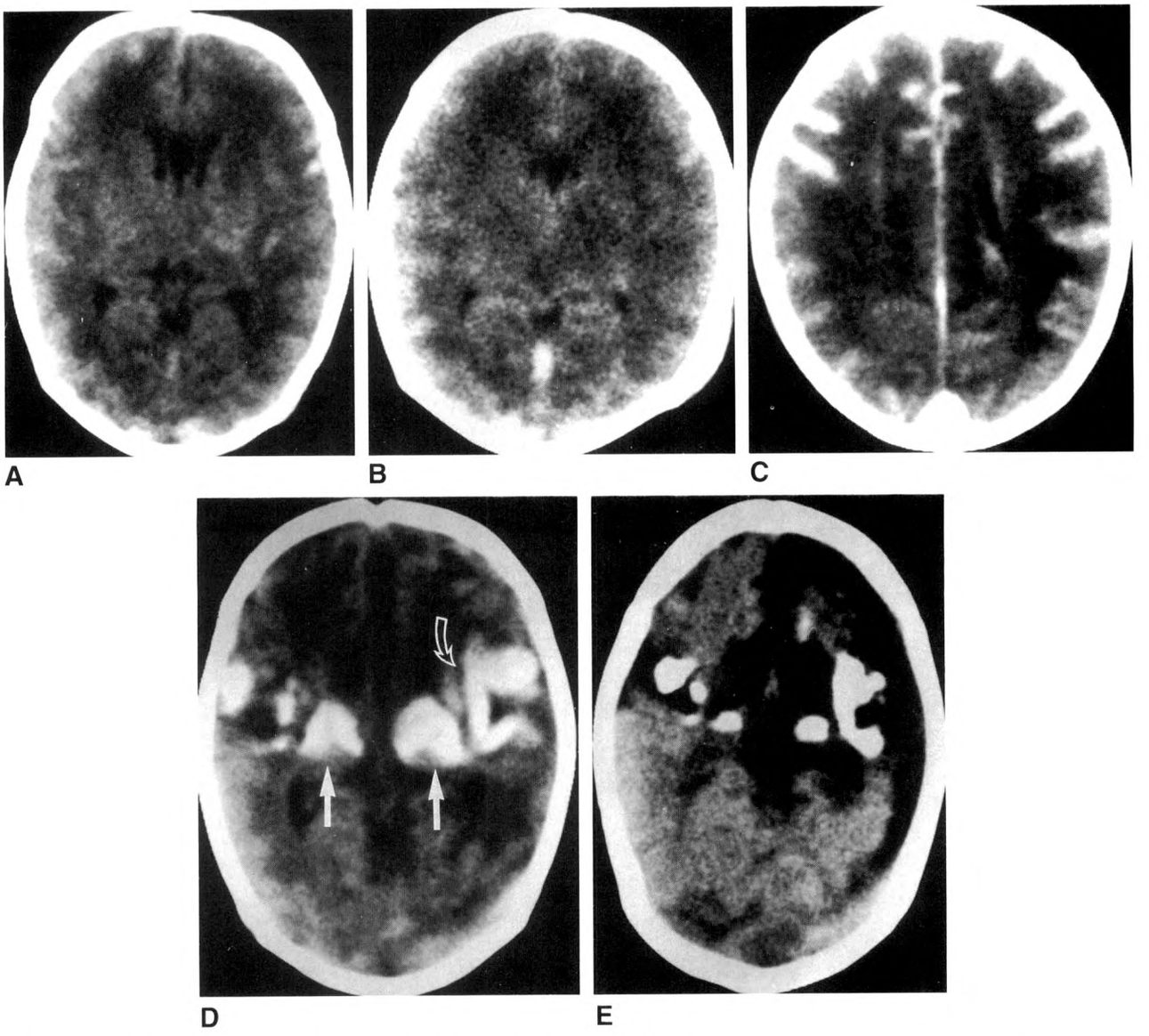

Fig. 4.—2-week-old child who had had a seizure. Presumptive diagnosis was herpes simplex.

A, Initial unenhanced axial CT scan shows patchy areas of low attenuation throughout both hemispheres. Sulcal pattern is difficult to discern.

B and *C*, Axial CT scans, obtained 1 week after *A*, without (*B*) and with (*C*) IV contrast material show patchy areas of low attenuation throughout white matter. Ventricles are somewhat smaller than normal, suggestive of underlying edema. On *C*, note gyral pattern of enhancement in cortex and along edges of ventricles.

D, Axial CT scan obtained when child was 1 month old. IV contrast material had been given 12 hr before this scan. Patchy areas of low attenuation remain scattered throughout white matter, while striking, gyriform pattern of increased density is present in both ganglia (*solid arrows*), right frontal operculum, and left insula (*open arrow*). Areas of high attenuation, which can represent calcification, local hemorrhage, or delayed clearance of IV contrast material, can develop quite rapidly in children.

E, Unenhanced CT scan (obtained 1 month after *D*) shows marked periventricular and parenchymal calcification; marked encephalomalacic change with loss of tissue in both frontal lobes, more so in left one than in right one; and marked dilatation of both lateral ventricles.

infants, rubella may be subclinical [16]. Deafness, often not detected until the infant is older, is the most common feature of congenital rubella. Congenital rubella has been implicated as the cause of a chronic progressive panencephalitis similar to subacute sclerosing panencephalitis associated with measles [17, 18]. The pathologic appearance of rubella is characterized by a generalized vasculitis with relatively little cellular necrosis [19].

Microcephaly and intracranial calcifications are seen with congenital rubella. Of five patients with congenital rubella who had CT, four had areas of low density in the centrum semiovale and periventricular white matter, and two had calcified nodules [20]. The white matter changes may have reflected the delayed myelination described in pathologic studies [19]. Because of the widespread use of vaccination, few descriptions of neonatal rubella have been published.

HIV Infection

A characteristic dysmorphic syndrome associated with congenital HIV infection has been reported [21]. The primary features included growth failure and microcephaly. This has not, however, been consistently observed, and the imaging features of the syndrome have not been described. More commonly, the CNS abnormalities associated with HIV infection become manifest during infancy and early childhood [22].

Acute Meningitis or Encephalitis

Acute viral infection of the CNS commonly causes meningitis or encephalitis, whether in children or adults. Most viruses are pantropic, able to produce either meningitis or encephalitis. Because most viral meningitides are benign and self-limited, exclusion of other, particularly bacterial, infections that may require active medical intervention is often the main clinical issue. Enteroviruses (echoviruses, coxsackieviruses) are thought to be responsible for 50–80% of all cases of viral meningitis. Other viral agents include mumps virus, Epstein-Barr virus, and arbovirus, although in any particular case, the specific organism usually is not identified [23]. Clinically, patients have headache, fever, and signs and symptoms of meningeal irritation.

Encephalitis occurs when the brain parenchyma is invaded by the virus and clinically should be suspected if the patient has seizure, delirium, and focal neurologic signs. Viral encephalitis may occur sporadically (nonepidemic) or in epidemics; the season, timing, and geographical distribution generally reflect the vector mechanism [24].

Imaging findings in patients with viral meningitis are generally normal. Viral meningitis does not produce the meningeal enhancement seen with contrast-enhanced CT or gadolinium-enhanced MR imaging in some cases of severe bacterial meningitis. Unless encephalitis is also present, the brain parenchyma is also normal, and even with some viral encephalitides, such as that caused by enterovirus, the CT or MR appearance remains normal. Other organisms such as herpesvirus may produce a necrotizing or hemorrhagic infection that is visible on CT or MR.

Epidemic Encephalopathies

The most common viral encephalitides are spread by arthropods (ticks and mosquitoes). The causal agents have previously been classified as arboviruses, although more recently this classification has been reorganized. Those commonly encountered in North America include Eastern equine encephalitis, Western equine encephalitis, and Venezuelan equine encephalitis, all of which occur as sporadic epidemics most severely affecting the young and elderly. Mortality in those more than 50 years old who have clinically evident and diagnosed Eastern equine encephalitis may reach 80%, and survivors less than 10 years old have significant sequelae. Yet in patients 15–55 years old, the disease may be mild or inapparent. Western equine encephalitis has a similar clinical picture but is more prevalent in those less than 1 year old. Venezuelan equine encephalitis tends to be a rather mild infectious syndrome; encephalitis symptoms are seen in 4% of young patients and only 0.4% of adults infected. Pathologically, in those dying, both gray and white matter can be involved with perivascular inflammation and formation of inflammatory nodules. Patchy areas of demyelination may be seen in the white matter. In these entities, CT findings generally have not been useful for diagnosis, and little information on MR findings has been reported [24].

Herpes Simplex

Herpesvirus is thought to be the most frequent cause of nonepidemic encephalitis. It is common in children and adults; 33% of patients in the National Institutes of Health trial of acyclovir vs vidarabine treatment of herpes simplex were less than 20 years old [25]. Most cases of herpes simplex that occur outside the neonatal period are due to herpesvirus type I infection. Unlike many viral encephalitides that represent a primary infection, encephalitis caused by herpes virus I occurs as a reactivation of latent virus within the trigeminal ganglion. Encephalitis results from retrograde transport of virus into the CNS. Although the infection rapidly disseminates throughout the brain, characteristically, the temporal lobes are involved first.

The earliest CT findings, which reflect this initial temporal lobe localization (Fig. 5), have low density in the temporal lobes associated with hemorrhage and streaky contrast enhancement [26]. Localized or generalized edematous changes can progress ultimately to atrophy, multicystic encephalomalacia, and gyriform high attenuation (Fig. 5). This gyriform high density is more commonly seen in children (and neonates) than in adults [13]. MR similarly shows edema with mass effect and increased T2 signal within the temporal lobe. Rarely, herpesvirus encephalitis can be manifested as diffuse brainstem encephalitis without alteration of the level of consciousness [25]. In general, the imaging appearance with CT does not accurately reflect the clinical course, which is significant because early treatment with antiviral agents, most recently acyclovir, has improved the otherwise 67% mortality associated with herpesvirus encephalitis [9]. MR is more sensitive than CT for detecting the presence of infection and has been used to show response to antiviral therapy [27].

Mumps

Mumps virus previously was the single most common agent producing aseptic meningitis and mild encephalitis. Immunization has markedly diminished the incidence and subsequent complications of mumps, although the vaccine is successful in only 75–90% of patients. In the CNS, mumps produces meningism in more than half the cases. Associated encephalitis is much rarer but also has a significant mortality and morbidity. Pathologically, mumps produces areas of perivascular inflammation and demyelination scattered throughout the CNS [28]. Not unexpectedly, MR has been reported to be more sensitive than CT in delineating these lesions; however, not many imaging studies have been done [29]. Some think that mumps encephalitis is similar to other postinfectious encephalitides [28].

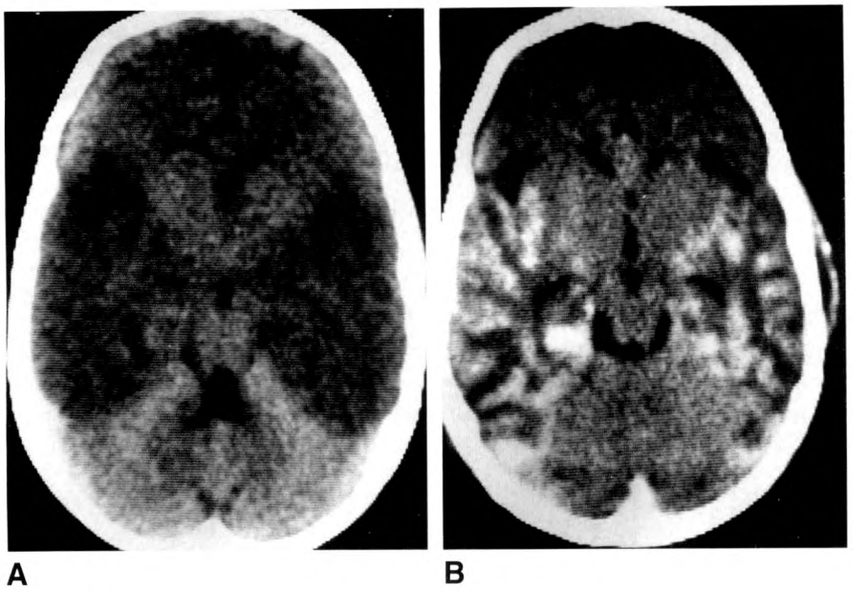

Fig. 5.—18-month-old child with clinical evidence of encephalitis. Presumptive diagnosis was herpes simplex.

***A*, Initial unenhanced CT scan shows areas of low attenuation within both temporal lobes, compression of both temporal horns and both lateral ventricles, and extension of this process into the parietooccipital regions bilaterally. Accompanying scan obtained after injection of contrast material (*not shown*) showed no abnormal enhancement.**

***B*, Axial CT scan obtained 1 week after *A*. IV contrast material has been administered. Mass effect is diminished, basal cisternal and ventricular structures are larger than normal, and gyral pattern of enhancement is present throughout both temporal lobes. This pattern of temporal lobe involvement is classic for herpetic infection outside the perinatal period. Herpes simplex is commonly thought to result from reactivation of virus residing within trigeminal ganglia.**

Rubella, Measles, and Chickenpox

The common viral infections of childhood occasionally can involve the CNS at the time of the acute infection. Chickenpox (varicella) is associated with an acute meningoencephalomyelitis, and encephalitis has been reported with German measles (rubella). Before immunization became widespread, encephalitis as a complication of measles occurred in about one per 1000 cases. It is now seen only rarely in immunologically normal children. Measles encephalitis pathologically resembles subacute sclerosing panencephalitis.

Subacute sclerosing panencephalitis, which can occur years after a primary infection with measles, continues to have an unclear pathogenesis. Some think that it represents reactivation of a latent infection, infection with a variant of the measles virus that is behaving as a "slow virus," or an immunologic response to a previous infection with measles virus. CT findings in a patient with subacute sclerosing panencephalitis may be normal or may show patchy low density, mainly in the white matter. These lesions may enhance with IV contrast material [30]. MR imaging shows patchy areas of increased T2 and decreased T1 signal intensity in the white matter and basal ganglia, which may represent inflammation, demyelination, gliosis, or some combination of these [31].

Acute Disseminated Encephalomyelitis

Acute disseminated encephalomyelitis commonly occurs as a sequela to another process, such as measles, rubella, varicella-zoster, smallpox, mumps, and upper respiratory infections. Considered to have a similar pathogenesis are the encephalitides that occur after vaccination for smallpox, measles, or rabies. With the reduced use of vaccination for smallpox and the development of vaccines for the common childhood exanthems, most episodes of acute disseminated encephalomyelitis are now related to viral infections of the upper respiratory tract.

Acute disseminated encephalomyelitis is thought to be an immunologic reaction to the viral infection, less commonly a reaction to a viral toxin. Virus has not been isolated from patients with this syndrome. The pathologic appearance suggests loss of myelin, sparing of axons, perivascular lymphocytic and mononuclear infiltration, edema, and endothelial proliferations. Lesions can be located throughout the CNS, including cerebrum, cerebellum, brainstem, and spinal cord. Although acute disseminated encephalomyelitis is mainly a white matter process, lesions can be found in the gray matter. Acute hemorrhagic leukoencephalitis is thought to be an aggressive form of acute disseminated encephalomyelitis in which microscopic areas of hemorrhage occur.

MR is more sensitive than CT for the diagnosis. CT findings in patients with the clinical diagnosis of acute disseminated encephalomyelitis may be normal or the scans may show areas of patchy low attenuation in the white matter accompanied by focal or more diffuse cortical enhancement. In general, lesions seen on CT tend not to correspond to the extent or pattern of clinical disease [32]. However, on T2-weighted MR images, multiple areas of increased signal are found throughout the CNS and correspond to the patient's clinical deficits (Fig. 6). As in multiple sclerosis, in acute disseminated encephalomyelitis, T2-weighted images are more sensitive than T1-weighted images for detection of the abnormalities [33]. In three patients, Atlas et al. [34] found clear abnormalities on T2-weighted images and no abnormalities on T1-weighted images (Fig. 7). Others [35] have seen similar abnormalities and found similar insensitivity of CT compared with MR imaging, although the exact imaging sequences used were less well defined. Contrast enhancement has been seen in lesions of acute disseminated encephalomyelitis in animal models [36].

Children with acute disseminated encephalomyelitis can have a subacute process that reflects the areas of the CNS involved. Common signs and symptoms include headache, diplopia, ataxia, hemiparesis, seizures, dysarthria, and coma [35]. Treatment with steroids is used to minimize the residual neurologic deficits [33].

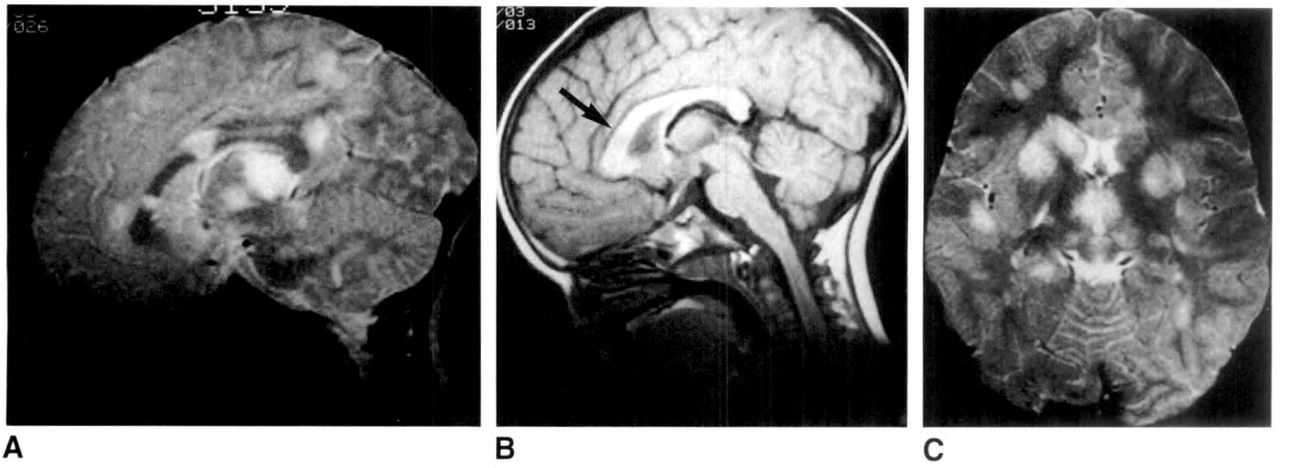

Fig. 6.—2-year-old who was lethargic and had had a viral infection of upper respiratory tract 3 weeks earlier. Presumed diagnosis was acute disseminated encephalomyelitis.

A, Paramedian sagittal T2-weighted MR image shows multiple areas of increased signal throughout both gray and white matter. Lesions are present in all compartments, including posterior fossa and brainstem. Lesions are present in corpus callosum (white matter) and thalamus (gray matter) also.

B, Sagittal T1-weighted MR image shows an area of relatively low signal intensity (*arrow*) in anterior body of corpus callosum, which corresponds to an area of increased signal on T2-weighted images. However, most lesions seen on T2-weighted images are inapparent on T1-weighted images.

C, Axial T2-weighted MR image shows multiple areas of increased signal in both gray and white matter, including right caudate nucleus, bilateral lentiform nuclei, and both thalami. Unlike lesions of multiple sclerosis, those of acute disseminated encephalomyelitis can occur in gray matter or white matter tracts.

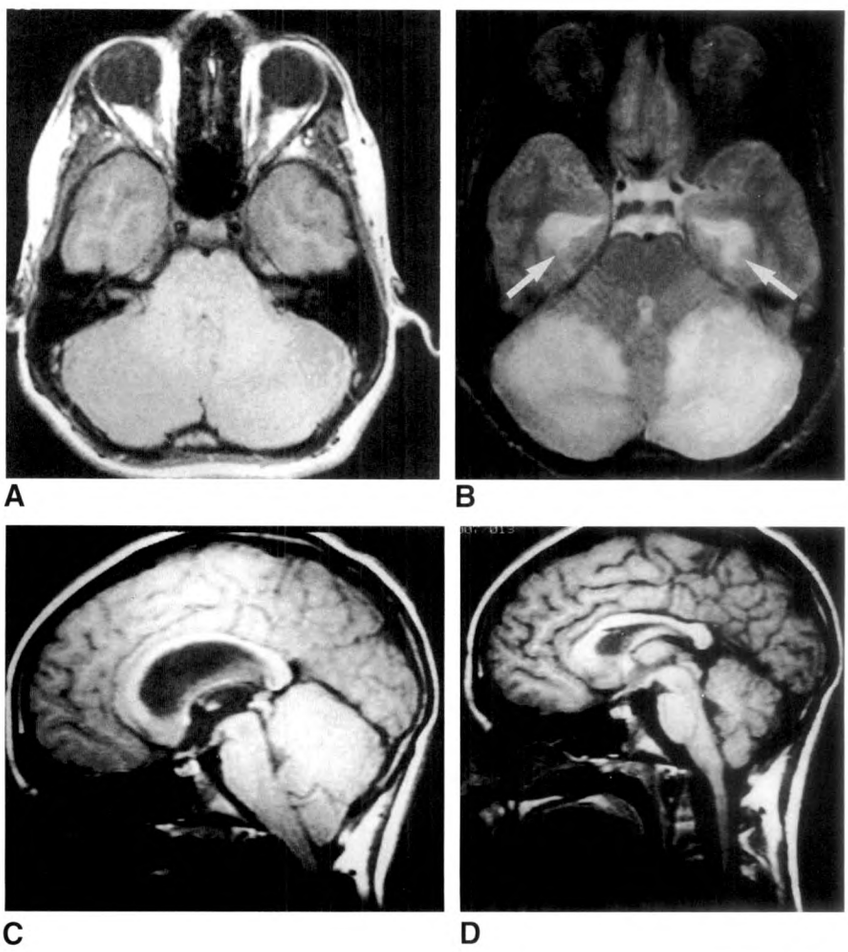

Fig. 7.—9-year-old boy with headache and cerebellar findings 3 weeks after an infection of upper respiratory tract. Presumed diagnosis was acute disseminated encephalomyelitis.

A, Axial T1-weighted MR image shows compression of fourth ventricle, effacement of cerebellar folia bilaterally, and a suggestion of lower signal intensity in both cerebellar hemispheres.

B, Axial T2-weighted MR image at same level as *A* shows large areas of increased signal intensity in both cerebellar hemispheres. Extent of involvement is shown better on T2- than on T1-weighted MR images. Patient has acute hydrocephalus with dilated temporal horns and periventricular transudation of CSF (*arrows*).

C, Sagittal T1-weighted MR image shows swollen cerebellar hemispheres, compression of fourth ventricle, compression of brainstem, and downward displacement of cerebellar tonsils.

D, Sagittal T1-weighted MR image obtained 3 weeks later shows resolution of process within cerebellum. Fourth ventricle is slightly enlarged, cerebellar folia are well seen, and brainstem and cerebellar tonsils have returned to a normal position.

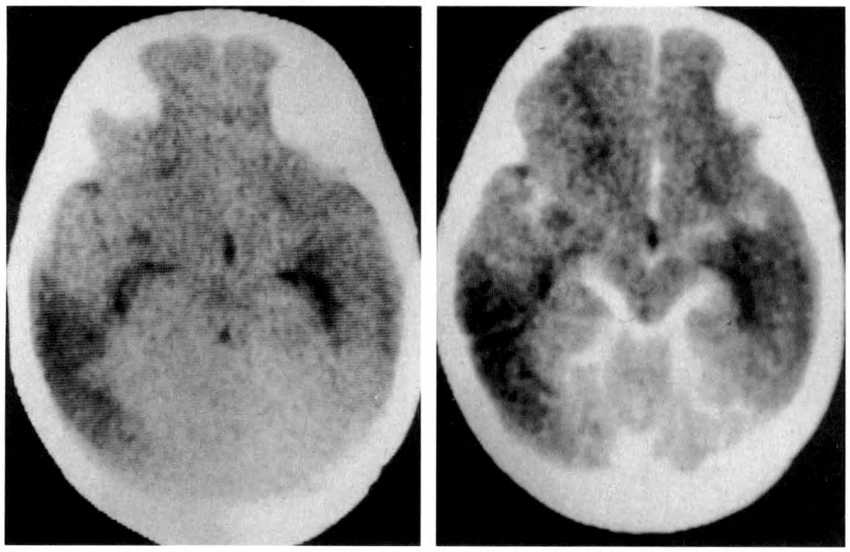

Fig. 8.—1-year-old child who had a fever and lethargy and whose mother was seropositive for HIV. *Pneumococcus* was cultured from CSF. Presumed diagnosis was pneumococcal meningitis.

***A*, Axial CT scan shows obscured cisterns, hydrocephalus, and an area of low attenuation in posterior temporal lobe on right side, suggestive of an area of infarction. Relative obscuring of cisterns suggests either a highly aggressive process or hemorrhage within basal cisterns.**

***B*, Contrast-enhanced axial CT scan shows marked enhancement of all basal cisternal structures. As on *A*, an area of infarction in posterotemporal lobe on right side is not enhanced. This scan epitomizes one of the problems in HIV-positive children: Those children who have CNS infections tend to have severe manifestations of common diseases rather than opportunistic infections.**

HIV Infection in Infants and Children

Infants and children infected with HIV are particularly at risk for neurologic complications. Most childhood exposure to HIV results from transmission from an infected mother (transplacental exposure), exposure to maternal blood during delivery, or ingestion of virus during breast feeding [22]. Diagnosis of HIV may be difficult in infants because passively transmitted maternal antibodies may be present in children up to 15 months after birth. Thus, early diagnosis requires culture of virus, demonstration of viral antigens, evidence of immunodeficiency, or the presence of a characteristic symptom complex. The number of children who have acquired HIV from transfusions or from contaminated blood products is somewhat smaller; however, these children were infected early in the course of the epidemic and do not form a significant proportion of new cases. A separate classification for HIV infection in children less than 13 years old has been established by the Centers for Disease Control [37].

In children, neurologic manifestations of HIV infection tend to have typical clinical features, including failure to reach developmental milestones, apathy, and spastic paraparesis [22]. In a study by Belman et al. [38], 61 of 68 infants and children had CNS dysfunctions as a manifestation of HIV infection. Neurologic signs included microcephaly, developmental delay, cognitive deficits, bilateral pyramidal tract signs, mild-to-moderate spastic diparesis or paraparesis, movement disorders, and ataxia. Seizures were uncommon.

Opportunistic infections are exceedingly unusual in infants and children who have AIDS, although sporadic cases of CNS lymphoma have been reported. Infectious complications include severe manifestations of more common diseases, such as those caused by Epstein-Barr virus, *Streptococcus pneumoniae*, and *Hemophilus influenzae* (Fig. 8). Disseminated CMV encephalitis has been seen at autopsy and *Candida* infections have been reported. Also occurring in children are episodes of intracranial hemorrhage associated with immune thrombocytopenia [38, 39].

Most imaging findings in HIV-positive children have been obtained with CT. In one study [40], 23 of 25 patients with a subacute progressive course had atrophy associated with decreased attenuation in the white matter. Also seen were bilateral symmetric calcification in 10 and calcification in the frontal lobes in two. In patients who had serial studies, progressive atrophy was found in 16 of 17. Of 12 patients with a more static course, five had atrophy, and two had basal ganglia calcification [37]. In another study [41] of 14 patients, both MR and CT showed central volume loss in eight patients and peripheral volume loss in seven, old hemorrhage in one, multifocal abnormal signal in one, and cervical lymphatic hypertrophy in four. CT was better than MR for showing striatal thalamic calcification (one), whereas only MR showed delayed myelination (one). Despite this, and because of the greater ease of obtaining CT scans, CT may be the study of choice.

Summary

Children are susceptible to a wide variety of viral infections that involve the CNS, in greater frequency than adults. Particularly vulnerable is the developing fetus. Imaging of neonates revealing periventricular calcification, cerebral atrophy, or microcephaly should raise the spectrum of congenital or perinatal TORCH infections. Although a specific diagnosis will generally be established by immunologic techniques, some findings in association can suggest a more specific identity; such as pachygyric-appearing brain consistent with the microgyria of CMV, or the linear gyriform cortical pattern of increased attenuation on CT scans (or hyperintensity on T1-weighted MR images) seen with perinatal herpes.

Imaging of uncomplicated viral meningitis will generally be unremarkable. Children, however, are more susceptible to complication than adults. Evidence of focal brain parenchymal edema in this setting suggests concomitant encephalitis.

A hemorrhagic process, especially involving the temporal lobes, is highly suggestive of herpes encephalitis; although CT or MR imaging should not be used to absolutely exclude this entity early in its course.

Areas of hyperintensity on T2-weighted MR images after a systemic viral infection or vaccination raise the spectre of acute disseminated encephalitis, although a definite cause is likely to remain elusive. CT is less sensitive for showing the pathologic changes.

Subacute presentations of CNS dysfunction associated with evidence of atrophy, decreased white matter attenuation, and basal ganglia calcification in this day raise the possibility of HIV infection.

REFERENCES

1. Klein JO, Remington JS. Current concepts of infections of the fetus and newborn infant. In: Remington JS, Klein JO, eds. *Infectious disease of the fetus and newborn infant.* Philadelphia: Saunders, **1990**:1–14
2. Bale JF Jr. Human cytomegalovirus infection and disorders of the nervous system. *Arch Neurol* **1984**;41:310–320
3. Post MJD, Curless RG, Gregorios JB, Scott GB, Sheldon JJ. Reactivation of congenital cytomegalic inclusion disease in an infant with HTLV-III associated immunodeficiency: A CT-pathologic correlation. *J Comput Assist Tomogr* **1986**;10:533–536
4. Holland BA, Kucharcyzk W, Brant-Zawadzki M, Norman D, Haas DK, Harper PS. MR imaging of calcified intracranial lesions. *Radiology* **1985**;157:353–356
5. Boesch Ch, Issakainen J, Kewitz G, Kikinis R, Martin E, Boltshauser E. Magnetic resonance imaging of the brain in congenital cytomegalovirus infection. *Pediatr Radiol* **1989**;19:91–93
6. Bignami A, Appicciutolo L. Micropolygyria and cerebral calcification in cytomegalic inclusion disease. *Acta Neuropathol* **1964**;4:127–137
7. Marques-Dias MJ, Hartmant-van Rijckevorsel G, Landrieu P, Lyon G. Prenatal cytomegalovirus disease and cerebral microgyria: Evidence for perfusion failure, not disturbance of histogenesis, as the major cause of fetal cytomegalovirus encephalopathy. *Hippokrates* **1984**;15:18–24
8. Hutto C, Arvin A, Jacobs R, et al. Intrauterine herpes simplex virus infections. *J Pediatr* **1987**;110:97–101
9. Whitley RJ. Herpes simplex virus infections. In: Remington JS, Klein JO, eds. *Infectious disease of the fetus and newborn infant.* Philadelphia: Saunders, **1990**:282–301
10. Herman TE, Cleveland RH, Kushner DC, Taveras JM. CT of neonatal herpes encephalitis. *AJNR* **1985**;6:773–775
11. Noorbehesht B, Enzmann DR, Sullender W, Bradley JS, Arvin AM. Neonatal herpes simplex encephalitis: correlation of clinical and CT findings. *Radiology* **1987**;162:813–819
12. Benator RM, Magill HL, Gerald B, Igarashi M, Fitch SJ. Herpes simplex encephalitis: CT findings in the neonate and young infant. *AJNR* **1985**;6:539–543
13. Taccone A, Gambaro G, Chiorzi M. Computed tomography (CT) in children with herpes simplex encephalitis. *Pediatr Radiol* **1988**;19:9–12
14. Junck L, Enzmann DR, DeArmond SJ, Okerlund M. Prolonged brain retention of contrast agent in neonatal herpes simplex encephalitis. *Radiology* **1981**;140:123–126
15. Ben-Ami T, Yousefzadeh D, Backus M, Reichman B, Kessler A, Hammerman-Rozenberg C. Lenticulostriate vasculopathy in infants with infections of the central nervous system sonographic and Doppler findings. *Pediatr Radiol* **1990**;20:575–579
16. Preblud SR, Alford CA Jr. Rubella. In: Remington JS, Klein JO, eds. *Infectious disease of the fetus and newborn infant.* Philadelphia: Saunders, **1990**:196–224
17. Townsend JJ, Baringer RB, Wolinsky JS, et al. Progressive rubella panencephalitis: late onset after congenital rubella. *N Engl J Med* **1975**;292:990–993
18. Weil ML, Itabashi HH, Cremer NE, Oshiro LS, Lennette EH, Carnay L. Chronic progressive panencephalitis due to rubella virus simulating subacute sclerosing panencephalitis. *N Engl J Med* **1975**;292:994–998
19. Rorke LB, Spiro AJ. Cerebral lesions in congenital rubella syndrome. *J Pediatr* **1957**;70:243–255
20. Ishikawa A, Murayama T, Sakuma N, et al. Computed cranial tomography in congenital rubella syndrome. *Arch Neurol* **1982**;39:420–421
21. Marion RW, Wiznia AA, Hutcheon RG, et al. Fetal AIDS Syndrome Score: correlation between severity of dysmorphism and age at diagnosis of immunodeficiency. *Am J Dis Child* **1987**;141:429–431
22. Haney PJ, Yale-Loehr AJ, Nussbaum AR, Gellad FE. Imaging of infants and children with AIDS. *AJR* **1989**;152:1033–1041
23. Ratzan KR. Viral meningitis. *Med Clin North Am* **1985**; 69:399–413
24. Weiner LP, Fleming JO. Viral infections of the nervous system. *J Neurosurg* **1984**;61:207–224
25. Robb L, Butt W. Brain stem encephalitis due to herpes simplex virus. *Aust Paediatr J* **1989**;25:246–247
26. Enzmann DR, Ranson B, Norman D, Talberth E. Computed tomography of herpes simplex encephalitis. *Radiology* **1978**;129:419–425
27. Lester JW, Carter MP, Reynolds TL. Herpes encephalitis: MR monitoring of response to acyclovir therapy. *J Comput Assist Tomogr* **1988**;12:941–943
28. Donohue WL, Playfair FD, Whitaker L. Mumps encephalitis: pathology and pathogenesis. *J Pediatr* **1955**;47:395–412
29. Tarr RW, Edwards KM, Kessler RM, Kulkarni MV. MRI of mumps encephalitis: comparison with CT evaluation. *Pediatr Radiol* **1987**;17:59–62
30. Modi G, Campbell H, Brill P. Subacute sclerosing panencephalitis. *Neuroradiology* **1989**;31:433–434
31. Tsuchiga K, Yamanchi J, Furui S, Suda Y, Takenaka E. Mr imaging vs. CT in subacute sclerosing panencephalitis. *AJNR* **1988**;9:943–946
32. Lukes SA, Norman D. Computed tomography in acute disseminated encephalomyelitis. *Ann Neurol* **1983**;13:567–572
33. Sheldon JJ, Siddharthan R, Tobias J, Sherenata WA, Soila K, Viamonte M. MR imaging of multiple sclerosis: comparison with clinical and CT examinations in 74 patients. *AJR* **1985**;145:957–964
34. Atlas SW, Grossman RI, Goldberg HI, Hackney DB, Bilaniuk LT, Zimmerman RA. MR diagnosis of acute disseminated encephalomyelitis. *J Comput Assist Tomogr* **1986**;10:798–801
35. Dunn V, Bale JF, Zimmerman RA, Perdue Z, Bell WE. MRI in children with postinfectious disseminated encephalomyelitis. *Magn Reson Imaging* **1986**;4:25–32
36. Kuharik MA, Edwards MK, Farlow MR et al. Gd-enhanced MR imaging of acute and chronic experimental demyelinating lesions. *AJNR* **1988**;9:643–648
37. Classification for human immunodeficiency virus (HIV) infection in children under 13 years of age. *MMWR* **1987**;36:225–236
38. Belman AL, Diamond G, Dickson D, et al. Pediatric acquired immunodeficiency syndrome: neurologic syndromes. *Am J Dis Child* **1988**;142:29–35
39. Bradford BF, Abdenour GE Jr, Frank JL, Scott GB, Beerman R. Usual and unusual radiologic manifestations of acquired immunodeficiency syndroms (AIDS) and human immunodeficiency virus (HIV) infection in children. *Radiol Clin North Am* **1988**;26:341–353
40. Price DB, Jacobs J, Haller JO, et al. Pediatric AIDS: neuroradiologic and neurodevelopmental findings. *Pediatr Radiol* **1988**;18:445–448
41. Chamberlain MC, Nichols SL, Chase CH. Pediatric AIDS: Comparative cranial MRI and CT scans. *Pediatr Neurol* **1991**;7:357–362

Case Report

Posttraumatic Carotid Artery Dissection in Children: Evaluation with MR Angiography

Clifford I. Mann,[1] Rosalind B. Dietrich,[1] Mauricio T. Schrader,[1] Wallace W. Peck,[2] Debra S. Demos,[3] and William G. Bradley, Jr.[4]

Dissection of the cervical portion of the carotid artery is a rare event in children that usually occurs after blunt injury to the neck. Symptoms and signs of stroke may develop days to years after injury, leading to delays in therapy [1, 2]. Early reports have shown the usefulness of MR angiography in the evaluation of carotid artery disease in adults [3, 4]. As this technique is noninvasive and can be performed in conjunction with routine MR imaging, it is potentially useful in examining children suspected of having carotid artery dissection. We describe two cases that demonstrate the use of MR angiography in the examination of children with carotid artery dissection.

Case Reports

Case 1

A 10-year-old boy was well until 4 months before admission, when he fell and hit the left side of his neck against a pole while he was playing croquet. He had pain at the site of injury for several days and then was well until 6 weeks later, when he had sudden onset of right hemiparesis and aphasia. The signs and symptoms partially resolved during the next 48 hr and gradually improved over the next 2 months.

MR imaging 2 months after presentation showed infarction of the distribution of the left middle cerebral artery. The caliber of the left internal carotid artery appeared normal, and a signal void was present in this vessel. A follow-up study 1 month later showed an area of encephalomalacia and a decrease in caliber of the left internal carotid artery.

Right-sided weakness and aphasia recurred 2 1/2 months later. MR imaging showed progression in the encephalomalacia and an acute infarct involving the left basal ganglia. The caliber of the left internal and middle cerebral arteries was significantly decreased when compared with the right side. MR angiograms were obtained with a 1.0-T system (Siemens Magnetom 42SP, Iselin, NJ) with axial and coronal slabs through the circle of Willis and carotid arteries, respectively. A three-dimensional (3D) time-of-flight (TOF) fast imaging with steady-state free-precession gradient-recalled-echo (GRE) technique was used with 36–40/7–11/15–25° (TR/TE/flip angle), a 256 × 256 matrix, a 250-mm field of view, and 64 partitions. The partition thickness was 1 mm and the in-plane resolution was 0.98 mm. Presaturation pulses were applied in the oblique sagittal plane through the sagittal sinus for the circle of Willis study, and distal to the carotid artery bifurcation for the carotid artery study. On these studies, no flow was detected in the left internal carotid artery, and the diameter of the left middle cerebral artery was reduced (Figs. 1A and 1B).

Carotid Doppler sonography showed complete obstruction of the left common carotid artery, antegrade flow in the left internal carotid artery, and retrograde flow in the left external carotid artery (Fig. 1C). Transcranial Doppler imaging showed flow reversal in the left anterior cerebral artery. Conventional arch aortography and left carotid arteriography showed minimal antegrade flow in the left internal carotid artery with no flow in the left carotid artery beyond the proximal 3–4 cm (Figs. 1D and 1E).

The patient was treated with warfarin sodium and at the time of discharge had a mild residual right hemiparesis.

Received February 5, 1992; accepted after revision July 14, 1992.

[1]Department of Radiological Sciences, University of California, Irvine Medical Center, 101 City Dr., Orange, CA 92668-3298. Address reprint requests to R. B. Dietrich.

[2]Department of Radiology, St. Joseph Hospital and Children's Hospital of Orange, 1100 Stewart Dr., Orange, CA 92668-3298.

[3]Departments of Pediatrics and Neurology, University of California, Irvine Medical Center, Orange, CA 92668-3298.

[4]Memorial Magnetic Resonance Center, Memorial Medical Center of Long Beach, 2801 Atlantic Ave., Long Beach, CA 90806.

AJR **1993;160:134–136** 0361–803X/93/1601–0134

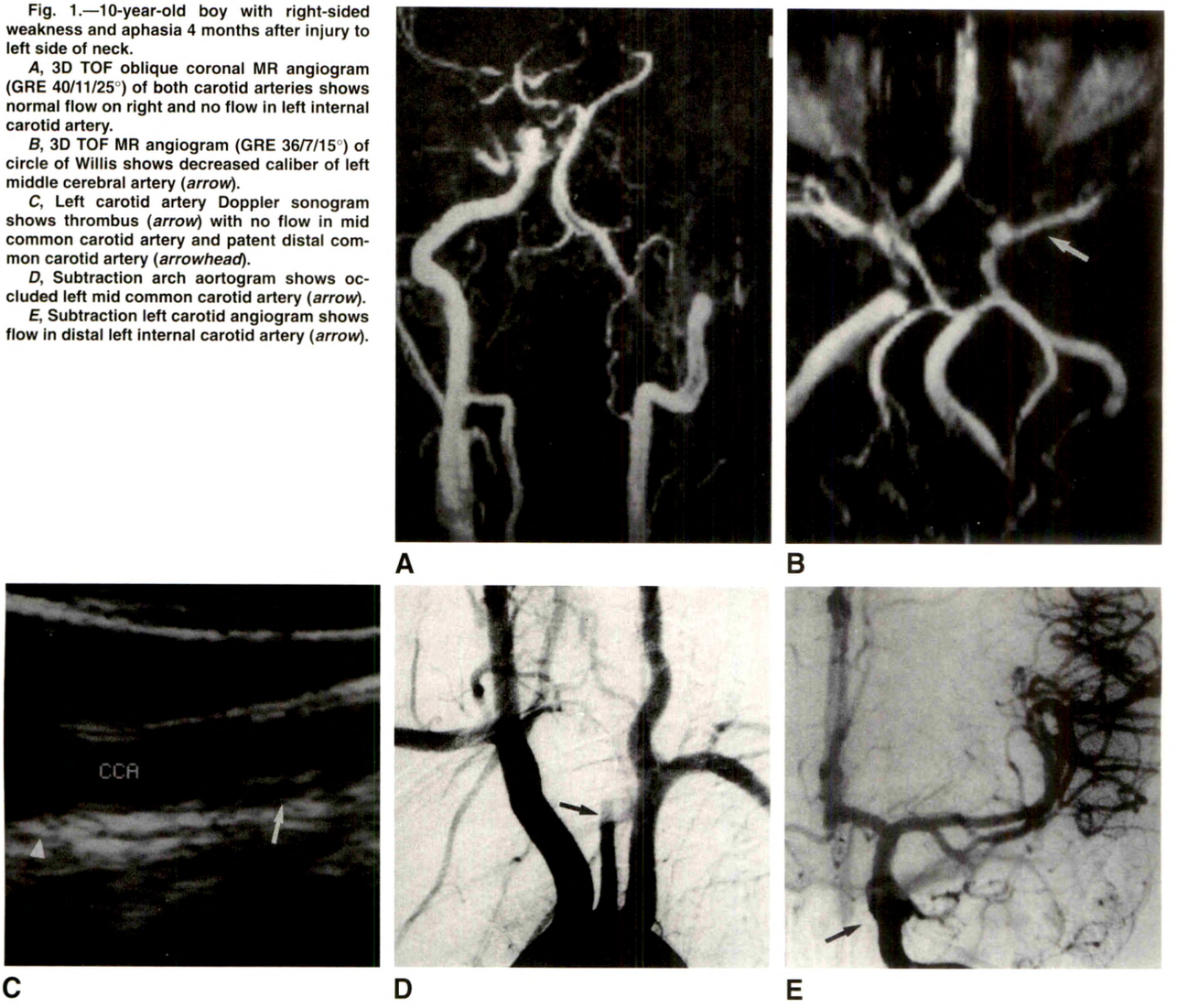

Fig. 1.—10-year-old boy with right-sided weakness and aphasia 4 months after injury to left side of neck.

***A*, 3D TOF oblique coronal MR angiogram (GRE 40/11/25°) of both carotid arteries shows normal flow on right and no flow in left internal carotid artery.**

***B*, 3D TOF MR angiogram (GRE 36/7/15°) of circle of Willis shows decreased caliber of left middle cerebral artery (*arrow*).**

***C*, Left carotid artery Doppler sonogram shows thrombus (*arrow*) with no flow in mid common carotid artery and patent distal common carotid artery (*arrowhead*).**

***D*, Subtraction arch aortogram shows occluded left mid common carotid artery (*arrow*).**

***E*, Subtraction left carotid angiogram shows flow in distal left internal carotid artery (*arrow*).**

Case 2

A 3300-g male infant was born at 42 weeks' gestation to a 24-year-old gravida 1 mother. Vaginal delivery was initially attempted, but because of poor maternal pushing efforts and the beginning of late fetal decelerations, vacuum delivery was then attempted. The head did not descend adequately, and an urgent cesarean section was subsequently performed. At birth, 3+ meconium was present and the Apgar scores were 1 and 9 at 1 and 5 min, respectively. Seizure activity was noted at 6 days of age and was controlled with medication. Physical examination revealed a right hemiparesis involving the face, arm, and leg. Subsequently, the right-sided hemiparesis resolved and the child was discharged from the hospital.

Carotid Doppler sonography 9 days after birth showed dramatic tapering of the left internal carotid artery immediately distal to the bifurcation. Flow was not detectable in this vessel 5 mm distal to the bifurcation (Fig. 2A).

MR imaging showed an infarct in the left middle cerebral artery distribution with absent signal void in the left internal carotid artery. MR angiograms were obtained with a 1.5-T system (Siemens 63SP) with axial and coronal slabs through the circle of Willis and carotid arteries, respectively. Imaging parameters were similar to those used in the first case. MR angiography of the neck showed occlusion of the left internal carotid artery just superior to the bifurcation of the carotid artery, with a positive string sign (Fig. 2B). Intracranial MR angiography showed the caliber of the left middle cerebral artery to be decreased when compared with the contralateral side.

Follow-up MR angiography of the circle of Willis and both carotid arteries approximately 10 months after birth showed recanalization of the left internal carotid artery, which was the same caliber as on the contralateral side (Fig. 2C). The left middle cerebral artery still appeared attenuated, and its appearance was not noticeably changed from the previous examination. Routine MR imaging performed at the same time showed the development of encephalomalacia in the region of the left middle cerebral artery infarction.

Discussion

Traumatic thrombosis of the internal carotid artery has been reported in children as a result of relatively minor injuries to the head or neck and may go unnoticed at the time of initial assessment [1, 2]. Signs include seizure or sensorimotor deficit [2]. Treatment may include anticoagulation or

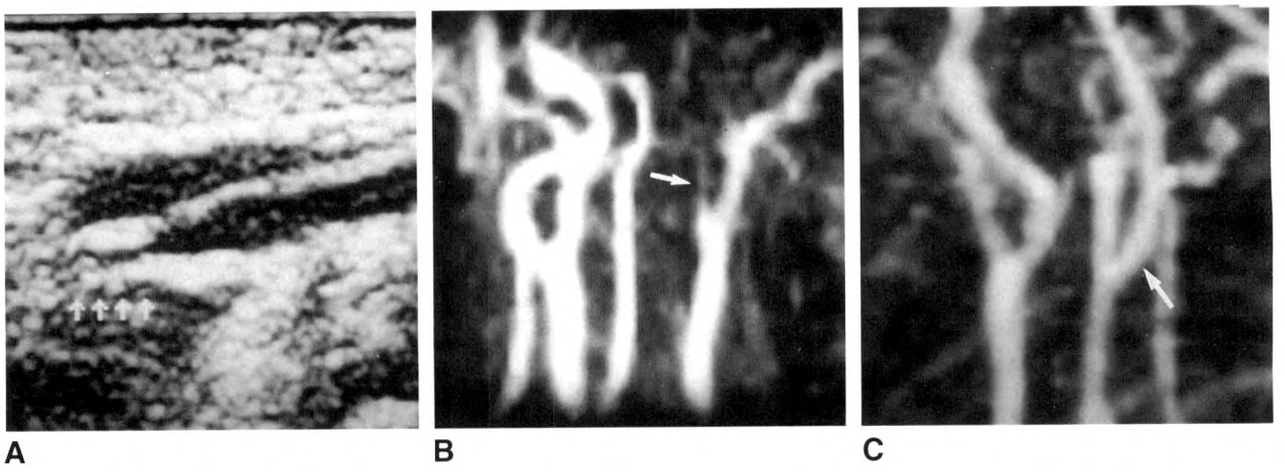

Fig. 2.—Neonate with infarct of left middle cerebral artery infarction.
***A*, Carotid sonogram 9 days after birth shows string sign in left internal carotid artery 1 cm from bifurcation (*arrows*). Doppler study showed dampening of signal in proximal left internal carotid artery.**
***B*, 3D TOF oblique coronal MR angiogram (GRE 40/7/15°) shows string sign (*arrow*) in proximal left internal carotid artery.**
***C*, Follow-up 3D TOF oblique coronal MR angiogram 10 months after birth shows recanalization of left internal carotid artery (*arrow*).**

thrombectomy if diagnosis is early and the site of obstruction is accessible [5]. Therefore, prompt diagnosis is important in such cases.

Both MR imaging and MR angiography have been shown to be useful in the evaluation of neurovascular disease in children, specifically in evaluation of moyamoya disease, sickle cell vasculitis [6], and in infants following extracorporeal membrane oxygenation therapy [7]. Advantages of MR angiography compared with conventional angiography include the ability to obtain noninvasive images in multiple projections, elimination of vessel overlap, the lack of contrast administration, and the ability to assess parenchymal abnormalities when used in conjunction with MR imaging.

Technically excellent studies were obtained in the two children described in this report. In one case shown here and in an additional case (not described), a string sign suggestive of carotid artery dissection was seen. Recanalization of the occluded carotid artery in the second child was shown with follow-up MR angiography and correlated with Doppler sonography. Conventional angiography was obtained in case 1, which demonstrated antegrade flow in the left internal carotid artery. The coronal TOF MR angiogram did not show this finding, which may be related to the insensitivity to in-plane flow that occurs in this type of MR angiography sequence.

Although observation of the string sign is useful in the diagnosis of carotid artery dissection, it is not entirely pathognomonic of this entity. A similar appearance may be seen in other disease processes, such as subacute partial thrombosis of the internal carotid artery, radiation vasculopathy, and congenital hypoplasia [8]. These conditions usually cannot be differentiated with MR imaging and carotid duplex sonography.

In conclusion, we found MR angiography extremely useful in the examination of children with suspected carotid artery dissection when initial MR imaging sequences show evidence of cerebral infarction. It also may be an extremely useful screening technique in patients with signs and symptoms suggestive of carotid artery dissection but in whom early CT or MR imaging studies show no evidence of infarction.

REFERENCES

1. Pozzati E, Giuliani G, Poppi M, et al. Blunt traumatic dissection with delayed symptoms. *Stroke* **1989**;20:412–416
2. Fisher RG. Strokes in children: their relationship to intrinsic pathology of the carotid artery. *Am Surg* **1982**;48:344–350
3. Masaryk TJ, Modic MT, Ruggieri PM, et al. Three-dimensional (volume) gradient-echo imaging of the carotid bifurcation: preliminary clinical experience. *Radiology* **1989**;171:801–806
4. Masaryk TJ, Laub GA, Modic MT, et al. Carotid-CNS MR flow imaging. *Magn Reson Med* **1990**;14:308–314
5. Watridge CB, Muhlbauer MS, Lowery RD. Traumatic carotid artery dissection: diagnosis and treatment. *J Neurosurg* **1989**;71:854–857
6. Wiznitzer M, Ruggieri PM, Masaryk TJ, et al. Diagnosis of cerebrovascular disease in sickle cell anemia by magnetic resonance imaging. *J Pediatr* **1990**;117:551–555
7. Lewin JS, Masaryk TJ, Modic MT, et al. Extracorporeal membrane oxygenation in infants: angiographic and parenchymal evaluation of the brain with MR imaging. *Radiology* **1989**;173:361–365
8. Fredericks RK, Thomas TD, Lefkowitz DS, et al. Implications of the angiographic string sign in carotid atherosclerosis. *Stroke* **1990**;21:476–479

Case Report

An Unusual First-Trimester Sonographic Finding Associated with Development of Hydatidiform Mole: The Hyperechoic Ovoid Mass

R. A. Bronson[1] and G. L. van de Vegte[2]

The characteristic vesicular sonographic appearance diagnostic of hydatidiform mole is generally not seen early in pregnancy, and first-trimester findings often cannot be distinguished from those of incomplete or missed abortion [1, 2]. This report describes the unusual finding of an ovoid hyperechoic mass within a well-defined gestational sac visualized on endovaginal sonograms at 6.5 weeks' gestation and associated with subsequent development of a molar pregnancy. It may represent the earliest reported sonographic appearance of a molar pregnancy.

Case Report

A 24-year-old nulliparous woman had had chronic intermittent pain in the right lower quadrant for 4 months and irregular menses (at 12 and 5 weeks before her visit). She was sexually active and had attempted to conceive during the past 9 months.

At the time of her first visit, physical examination showed minimal abdominal tenderness deep in the right lower quadrant of the abdomen. The right ovary was not tender on examination, and its size on a vaginal sonogram was 34 × 24 mm. Sonograms showed a hyperechoic unilocular cyst 15 mm in diameter at the proximal pole of the right ovary, which appeared to be consistent with a hemorrhagic corpus luteum or endometrioma. No evidence of intrauterine gestation was seen. Results of routine laboratory tests, including a complete blood cell count and SMA23, and levels of prolactin and thyroid-stimulating hormone were normal. The serum level of human chorionic gonadotropin (HCG) was 350 mIU/ml (first international reference preparation [IRP]) on the day of examination. Two weeks later, endovaginal sonography showed an intrauterine gestational sac, 17 × 12 mm, containing a uniformly hyperechoic ovoid mass 13 mm in greatest length (Fig. 1A). Neither a distinct fetal pole nor a yolk sac was seen. No cardiac activity was noted. Serum level of HCG at this time was 42,000 mIU/ml.

Ten days later, the patient had vaginal staining for 2 days, but without cramping. Physical examination showed that the size of the uterus was consistent with 8 weeks' gestation, which also was consistent with the last menstrual period. No adnexal masses or tenderness were present. Endovaginal sonograms showed an enlarged uterus, 57 × 47 mm in axial dimensions, containing a diffuse, central heterogeneous mass with several cystic regions (Fig. 1B). No definable fetal pole was detected. Serum level of HCG had risen to 140,000 mIU/ml. At this time, the patient complained of mild nausea and jitteriness.

Suction currettage was performed, and pathologic examination confirmed the diagnosis of a hydatidiform mole. Ten days later, the serum level of HCG had dropped to 6100 mIU/ml. The serum level subsequently plateaued at 6600 mIU/ml, and 1 week later was 6840 mIU/ml. At this time, the patient began taking methotrexate and leucovorin as an outpatient. Serum HCG measurements returned to undetectable levels and have remained so.

Discussion

Complete molar pregnancy has a classic second-trimester sonographic appearance of a central echogenic uterine mass with a characteristic vesicular pattern due to marked, generalized swelling of chorionic villi [3]. However, these

Received May 26, 1992; accepted after revision July 13, 1992.

[1]Department of Obstetrics/Gynecology, Health Sciences Center, State University of New York, Stony Brook, NY 11794. Address reprint requests to R. A. Bronson, Division of Reproductive Endocrinology, Health Sciences Center, T9-060, Stony Brook, NY 11794-8091.

[2]Department of Radiology, Health Sciences Center, State University of New York, Stony Brook, NY 11794.

AJR 1993;160:137–138 0361–803X/93/1601–0137

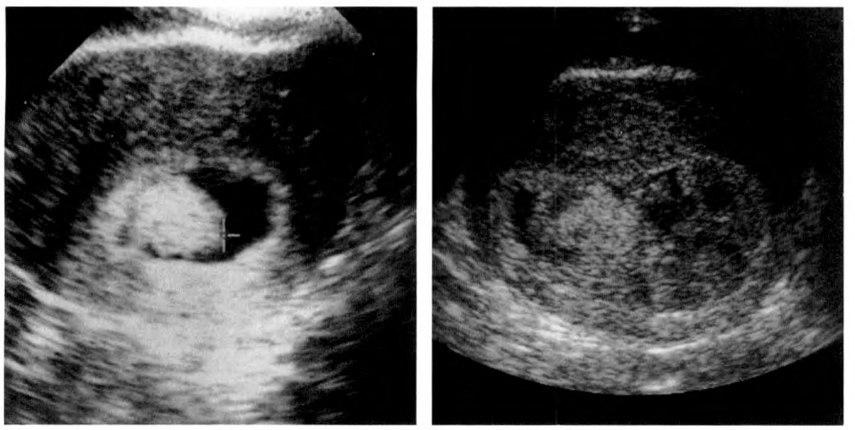

A **B**

Fig. 1.—24-year-old nulliparous woman with chronic intermittent pain in right lower quadrant of abdomen for 4 months and irregular menses.

***A*, Endovaginal sonogram shows a well-formed intrauterine gestational sac containing only a 13-mm echogenic ovoid mass (between *calipers*).**

***B*, Sonogram obtained 10 days after *A* shows no evidence of intrauterine gestational sac, but rather a central heterogeneous uterine mass with multiple cystic areas suggestive of molar gestation.**

typical findings may not be visible on transabdominal sonograms obtained early in the first trimester.

Szulman and Surti [4] have observed a linear relationship between gestational age of a molar pregnancy and the size of the hydropic villi on macroscopic examination. Hence, although vesicles are also present in first-trimester complete moles, they may be too small to be visualized on transabdominal sonograms. During the first trimester, then, molar pregnancies often lack the characteristic pattern of second-trimester trophoblastic disease and are often confused with missed or incomplete abortion.

During the first trimester, endovaginal sonography provides better imaging resolution than transabdominal scanning does, making it possible to diagnose an abnormal pregnancy earlier in gestation. A gestational sac can be observed on endovaginal sonograms at serum HCG levels as low as 1000–1500 mIU/ml (first IRP), vs the minimum HCG level of 6500 mIU/ml for visualization on transabdominal sonograms [5].

In the present case, an intrauterine gestation was confirmed by endovaginal sonography at 6.5 weeks' gestation. However, a recognizable fetal pole and yolk sac were not visualized, and the gestational sac contained only an ovoid, 13-mm, homogeneously echogenic mass. Further clinical monitoring in the first trimester showed that the uterus enlarged, containing a heterogeneous central mass with early vesicular features consistent with the appearance of a molar pregnancy.

In 1979, Anderson et al. [6] reported a similar unusual finding in a woman who was proved to have a hydatidiform mole. At 10 weeks' gestation, the uterus was clinically enlarged for dates, consistent with a pregnancy of 13–14 weeks, and contained an irregular gestational sac, with a uniformly echogenic mass adjacent to the sac wall. This mass was initially thought to be the remnants of a fetus, but no fetal tissue was found within the contents evacuated from the uterus.

The progression of findings in our case, as well as the previous report of Anderson et al. [6], leads us to suggest that the detection of a hyperechoic ovoid mass within an otherwise empty gestational sac during the first trimester should suggest the possibility of molar pregnancy and the need for follow-up studies.

REFERENCES

1. Woodward RM, Filly RA, Callen PW. First trimester molar pregnancy: nonspecific ultrasonographic appearance. *Obstet Gynecol* **1980**;55: 315–335
2. Wittmann BK, Fulton L, Cooperberg PL, Lyons EA, Miller C, Shaw D. Molar pregnancy: early diagnosis by ultrasound. *JCU J Clin Ultrasound* **1981**;9:153–156
3. Fleischer AC, James AE Jr, Krause DA, James JB. Sonographic patterns in trophoblastic disease. *Radiology* **1978**;126:215–220
4. Szulman AE, Surti U. The syndromes of hydatidiform mole. Morphologic evaluation of the complete and partial mole. *Am J Obstet Gynecol* **1978**;132:20–27
5. Kadar N, DeJore G, Romero R. Discriminatory HCG zone: its use in the sonographic evaluation for ectopic pregnancy. *Obstet Gynecol* **1981**; 58:156–161
6. Anderson JC, Faulker KC, Moir JE. Ultrasonography in an early hydatidiform mole. *Med J Aust* **1979**;1:407–408

Case Report

Wilms' Tumor in a Patient with Beckwith-Wiedemann Syndrome: Onset Detected with 3-Month Serial Sonography

Matthew W. Andrews[1] and Eugenio G. Amparo

Beckwith-Wiedemann syndrome is characterized by a group of clinical abnormalities, the most salient being macroglossia, gigantism, and exomphalos. Childhood malignant tumors are a recognized association of Beckwith-Wiedemann syndrome, and Wilms' tumor, in particular, is a frequent occurrence.

An 18-month-old child with Beckwith-Wiedemann syndrome had a Wilms' tumor first detected with abdominal sonography, which had been performed every 3 months since birth for surveillance. This case demonstrates the value of sonographic abdominal surveillance in children with Beckwith-Wiedemann syndrome. We know of no other published reports of development of a Wilms' tumor in an interval as short as 3 months. Because the long-term survival of children with Beckwith-Wiedemann syndrome depends on early detection and treatment of tumors [1], we believe that these children should have abdominal sonographic surveillance at intervals of 3 months or less.

Case Report

Beckwith-Wiedemann syndrome was clinically diagnosed at birth in a male child on the basis of macroglossia, omphalocele, and large birth weight and height. Abdominal sonography at 3 months showed bilateral renal enlargement to greater than the 95th percentile for age without focal abnormalities. Sonographic examination of this patient's abdomen was performed at 3-month intervals. At 18 months, sonography showed a solid mass with a greatest diameter of 3.6 cm in the left kidney (Fig. 1B). The mass had not been present on a sonogram obtained 3 months earlier (Fig. 1A). Subsequent CT evaluation (Fig. 1C) showed that the mass was confined to the kidney, and no metastases were found. Surgery confirmed the abdominal CT findings, and a left-sided total nephrectomy was performed. Examination of the right kidney at surgery showed no focal lesions. Histopathologic studies showed that the lesion in the left kidney was a Wilms' tumor.

Discussion

The long-term survival of patients with Wilms' tumor that is diagnosed early and treated appropriately is good [1]. Early detection of Wilms' tumor, to which patients with Beckwith-Wiedemann syndrome are predisposed, is imperative for a favorable prognosis.

Beckwith-Wiedemann syndrome is a rare syndrome characterized by macroglossia, omphalocele, and splanchnomegaly (kidneys, liver, and spleen). Other associated features, including neonatal hypoglycemia, large birth weight, increased height at birth, hemihypertrophy, craniofacial dysmorphism, microcephaly, other abdominal wall abnormalities (such as umbilical hernia and diastasis of rectus muscles), and midgut malrotation, may be present [2]. The syndrome is caused by an unknown growth disorder resulting in organ hypertrophy and hyperplasia with resultant gigantism. It may

This article originally appeared in the October 1992 issue of *AJR*. It is reprinted here because the printer transposed two figures in the original publication. Figure 1 in the article by Andrews and Amparo appeared in the article by Slovis, Meza, Rector, and Chang. Figure 1 in the article by Slovis et al. appeared in the article by Andrews and Amparo. Waverly Press apologizes for this error.

Received February 27, 1992; accepted after revision April 10, 1992.

[1]Both authors: Department of Radiology, University of California Davis Medical Center, 2516 Stockton Blvd., TICON II Bldg., Sacramento, CA 95817. Address reprint requests to E. G. Amparo.

AJR 1993;160:139–140 0361–803X/93/1601–0139

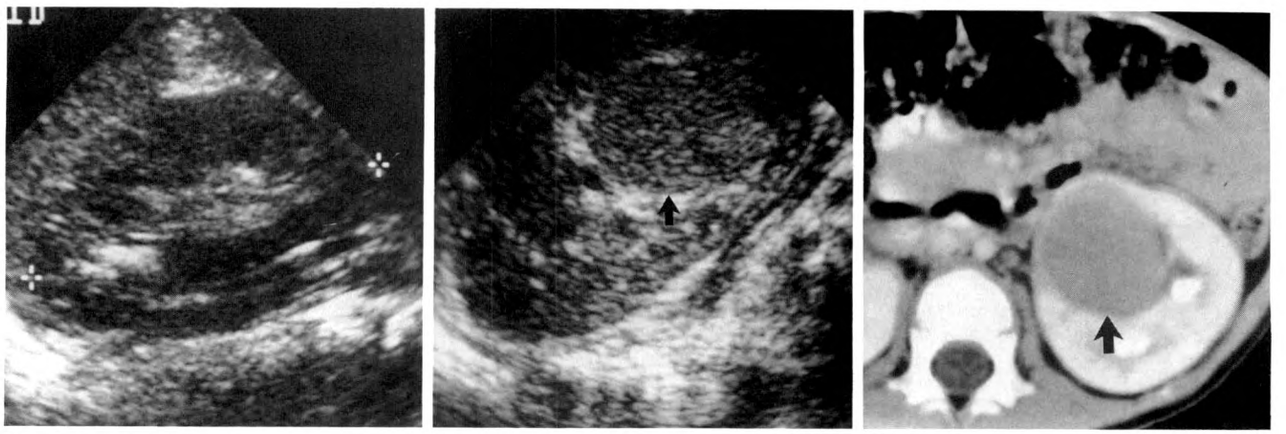

A B C

Fig. 1.—Child with Beckwith-Wiedemann syndrome.
***A*, Longitudinal sonogram of left kidney at age 15 months shows no lesions.**
***B*, Longitudinal sonogram of left kidney at age 18 months shows a 3.6 x 2.4 cm well-marginated, hyperechoic lesion (*arrow*) in middle of kidney.**
***C*, Contrast-enhanced CT scan through middle of left kidney at age 18 months shows a well-marginated mass (*arrow*) that is less dense than normal renal parenchyma.**

exist in complete or incomplete forms that involve single or multiple organs of the whole body or one side of it.

Children with Beckwith-Wiedemann syndrome are predisposed to tumor formation because of focal or diffuse growth abnormalities and the associated cellular anaplasia that can accompany hypertrophy and hyperplasia. The prevalence of malignant tumor formation in patients with Beckwith-Wiedemann syndrome has been reported at 6–10% [3]. Most tumors are intraabdominal, most often retroperitoneal. Wilms' tumors, adrenal cortical carcinomas, and hepatoblastomas are the most common malignant tumors, in that order [4]. Risk increases significantly when hemihypertrophy is present [3], and patients with some of the manifestations of Beckwith-Wiedemann syndrome appear to have the same potential for tumor development as those with all the signs and symptoms [5]. Other tumors reported include rhabdomyosarcoma, glioma, thoracic neural crest tumor, retroperitoneal ganglioneuroma, adrenal adenoma, cardiac hamartoma, cardiac myxoma, and carcinoid of the appendix [2, 5].

The age at which risk for neoplasia returns to close to normal has not been determined, but surveillance for tumor development has been suggested for patients with Beckwith-Wiedemann syndrome up to the age of 12 [3] and adolescence [6]. Most centers carry out surveillance sonography less often after the age of 6 years.

The appearance of Wilms' tumor during sonographic surveillance intervals of 9 and 5 months has been reported by Azouz et al. [3]. On the basis of their findings, they recommend sonography at intervals of 3 months. The appearance of a Wilms' tumor within a 3-month interval between sonograms in this case supports that protocol.

We believe that abdominal sonography should be performed at intervals of 3 months or less in patients with Beckwith-Wiedemann syndrome to detect early Wilms' tumors, thereby optimizing these patients' survival rates. This should form part of a tumor-screening protocol to detect early development of renal, hepatic, adrenal, and neural crest tumors.

REFERENCES

1. Snyder HM III, D'Angio GJ, Evans AE, Raney RB. Pediatric oncology. In: Walsh PC, Gittes RF, Perlmutter AD, Stamey TA, eds. *Campbell's urology*, 5th ed. Philadelphia: Saunders. **1986**:2244–2292
2. Sinnelli D, Silberman B, Baudon JJ, Sinnassamy P, Gruner M, Montagne JP. Beckwith-Wiedemann syndrome and neural crest tumors. *Pediatr Radiol* **1989**;19:242–245
3. Azouz EM, Larson EJ, Patel J, Gyepes MT. Beckwith-Wiedemann syndrome: development of nephroblastoma during the surveillance period. *Pediatr Radiol* **1990**;20:550–552
4. Tank ES, Kay R. Neoplasms associated with hemihypertrophy. Beckwith-Wiedemann syndrome and aniridia. *J Urol* **1980**;124:266–268
5. Sotelo-Avila C, Gonzalez-Crussi F, Fowler JW. Complete and incomplete forms of Beckwith-Wiedemann syndrome: their oncogenic potential. *J Pediatr* **1980**;96:47–50
6. Shah KJ. Beckwith-Wiedemann syndrome: role of ultrasound in its management. *Clin Radiol* **1983**;34:313–319

Case Report

Aneurysm of a Nonpatent Ductus Arteriosus in a Neonate: CT Findings

Thomas L. Slovis,[1] Manuel P. Meza,[1,2] Frederick E. Rector,[3] and Chung-Ho Chang[4,5]

The differential diagnosis of a middle mediastinal mass in a neonate or young infant includes a wide spectrum of entities: cystic hygroma, aberrant or abnormal vessels, ectopic thymus, duplication cyst, and enlarged lymph nodes. Abnormalities of the ductus arteriosus such as a large patent duck and aneurysms of the duct should be considered within the category of aberrant or abnormal vessels. Inasmuch as the ductal vessel may or may not be functional, enhancement on a CT scan is not mandatory for the diagnosis. We present a case of an aneurysm of a nonpatent ductus arteriosus in a neonate shown by CT.

Case Report

A full-term male neonate had mild respiratory distress at birth, without a history of perinatal asphyxia. A chest radiograph obtained 1 day after birth showed hyperexpansion of the lungs (Fig. 1A) and minimal opacities. A mass was noted in the aorticopulmonary window. The patient improved in the next 5 days and was sent home. A follow-up radiograph obtained 3 weeks later showed no change in the mass, and the infant was referred to Children's Hospital of Michigan for further workup. Dynamic contrast-enhanced CT scans showed nonenhancing mass extending lateral to the aorta and located between the top of the aortic arch and above the left pulmonary artery—in the aorticopulmonary window (Figs. 1B and 1C). The preoperative differential diagnosis included bronchogenic cyst, foregut duplication cyst, and a complex adenomatoid malformation.

Left-sided lateral thoracotomy was performed and showed that the mass was a large (2 x 1 x 1 cm) aneurysm of the ductus arteriosus. The content of the mass was firm and not pulsatile. Both ends of the ductus were ligated, and the aneurysm was resected. Clot filled the entire mass. The gross pathologic specimen revealed a saccular structure with clot. Histologic examination showed marked irregular fibrous thickening of the intima of the saccular structure and focal disruption and thinning of the underlying muscle layers. Focal destruction of the internal elastic lamina, accompanied by fibrosis, extended to the adjacent muscle layers. No obvious cellular inflammation was seen. The infant was discharged 2 days after surgery and has remained well for more than 1 year.

Discussion

In the fetus, the ductus arteriosus (connecting the pulmonary artery and aorta) is frequently the size of the aorta. During the first 10–15 hr after birth, pulmonary arterial pressure decreases and muscles in the ductal wall contract, resulting in a decrease in the size of the duct [1]. Anatomic closure occurs during the next 2–3 weeks, with nonthrombotic obliteration originating on the pulmonary side. The end product is the ligamentum arteriosus.

In neonates, the ductus arteriosus is not usually seen on chest films unless superimposition of the patent ductus arteriosus and the pulmonary artery (the ductus bump) occurs [2]. This may be seen as a mass on frontal radiographs

This article originally appeared in the October 1992 issue of *AJR*. It is reprinted here because the printer transposed two figures in the original publication. Figure 1 in the article by Andrews and Amparo appeared in the article by Slovis, Meza, Rector, and Chang. Figure 1 in the article by Slovis et al. appeared in the article by Andrews and Amparo. Waverly Press apologizes for this error.

Received March 23, 1992; accepted after revision May 7, 1992.

[1]Department of Radiology, Children's Hospital of Michigan, 3901 Beaubien Ave., Detroit, MI 48201. Address reprint requests to T. L. Slovis.
[2]Present address: Department of Radiology, Children's Hospital of Pittsburgh, 3705 5th Ave. at De Soto, One Children's Plaza, Pittsburgh, PA 15213.
[3]Present address: Department of Surgery, Children's Hospital of Michigan, 3901 Beaubien Ave., Detroit, MI 48201.
[4]Present address: Department of Pathology, Children's Hospital of Michigan, 3901 Beaubien Ave., Detroit, MI 48201.
[5]Present address: Department of Pathology, William Beaumont Hospital, 3601 W. 13 Mile Rd., Royal Oak, MI 48072.

AJR 1993;160:141–142 0361–803X/93/1601–0141

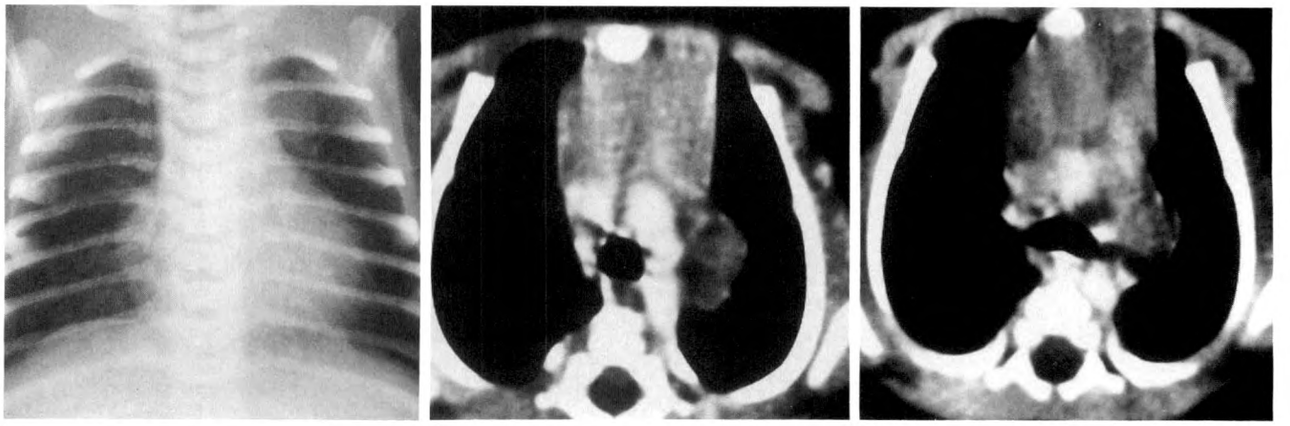

Fig. 1.—Nonpatent dissecting aneurysm of ductus arteriosus in a neonate.
***A*, Frontal radiograph obtained 1 day after birth shows mild hyperexpansion of lungs, increased markings, and a mass in aorticopulmonary window.**
***B* and *C*, Contrast-enhanced CT scans obtained 3 weeks after birth. Scan at level of aortic arch (*B*) shows a nonenhancing mass to left of aorta. Scan at level of pulmonary artery (*C*) shows nonenhancing mass is lateral to main pulmonary artery and anterior to left pulmonary artery.**

obtained in the first 72 hr after birth but not on radiographs obtained later, because the ductus arteriosus decreases in size and is no longer superimposed on the pulmonary artery.

The pathogenesis of aneurysm of the ductus arteriosus is uncertain, although some relationship to neonatal hypoxemia has been suggested [3]. The most logical theories are that (1) delay in closure of the aortic end of the ductus produces a diverticulum with continual exposure to systemic arterial pressures, causing myxoid degeneration and formation of the ductal aneurysm [1]; and (2) abnormal differentiation of the aortic wall, adjacent to the ductus arteriosus, promotes formation of an aneurysm [4]. A proposed anatomic classification of these aneurysms includes patent and nonpatent types of fusiform, tubular, and dissecting variants [5]. The prevalence of ductal aneurysm also is uncertain; in newborns, frequencies as high as eight aneurysms per 1000 autopsies have been reported [5]. More cases are now being discovered as, increasingly, diagnosis is based on findings on echocardiograms. In a significant number of cases the aneurysms resolve, with formation of a ligamentum arteriosum [5, 6]. Most infants with aneurysms of the ductus arteriosus are asymptomatic; however, fatal aneurysmal rupture, fatal dissection, thromboembolic phenomena with hypertension, and paralysis of the left side of the diaphragm and the left vocal cord have been reported [5, 7]. Many of the complications have occurred in adults.

Diagnosis of an aneurysm of the ductus arteriosus begins with the chest radiograph. The most important factor is the recognition of a mass, in a neonate or young infant, located in the aorticopulmonary window. The mass is convex to the left lung and is difficult to see on lateral radiographs. Echocardiography may show flow within the "cystic" mass if the aneurysm is patent. A CT scan will show the precise location of the mass, show if it is patent or nonpatent, and confirm its relationship to the vascular structures. It must be understood that a nonenhancing tubular mass in this location may be a nonpatent aneurysm of the ductus arteriosus. Although some have advocated observation of these masses in young infants, most often, as in our case, the mass is removed [5, 7].

The recognition of an aneurysm of the ductus arteriosus also should serve as a reminder that this condition is associated with coarctation of the aorta, aortic valvular disease, and Marfan syndrome [8].

REFERENCES

1. Kirks DR, McCook TA, Serwer GA, Oldham HN Jr. Aneurysm of the ductus arteriosus in the neonate. *AJR* **1980**;134:573–576
2. Berdon WE, Baker DH, James LS. The ductus bump: a transient physiologic mass in chest roentgenograms of newborn infants. *AJR* **1965**:95:91–98
3. Heikkinen ES, Simila S, Laitinen J, Larmi T. Infantile aneurysm of the ductus arteriosus. *Acta Paediatr Scand* **1974**;63:241–248
4. Bosman C, Leoncini B. On pathogenesis of a case of ductus arteriosus aneurysm. *Acta Cardiol* **1967**;22:279–288
5. Falcone MW, Perloff JK, Roberts W. Aneurysm of the nonpatent ductus arteriosus. *Am J Cardiol* **1972**;29:422–426
6. Malone PS, Cooper SG, Elliott M, Kiely EM, Spitz L. Aneurysm of the ductus arteriosus. *Arch Dis Child* **1989**;64:1386–1388
7. Morisot C, Dubos JP, Kacet N, Gremillet C, Remy-Jardin M, Lequien P. Neonatal hypertension and thrombosis of the ductus arteriosus. *Am J Perinatol* **1991**;8:77–79
8. Gillan JE, Costigan DC, Keeley FW, Rose V. Spontaneous dissecting aneurysm of the ductus arteriosus in an infant with Marfan syndrome. *J Pediatr* **1984**;105:952–955

Pseudotumor Cerebri: CT Findings and Correlation with Vision Loss

Wendell A. Gibby[1,2]
Mark S. Cohen[3]
Herbert I. Goldberg[1,4]
Robert C. Sergott[3]

OBJECTIVE. The purpose of this study was to determine if orbital and cerebral CT can be used to distinguish normal patients from those with pseudotumor cerebri, and to correlate CT findings with the severity of visual impairment.

SUBJECTS AND METHODS. Seventeen patients with a clinical diagnosis of pseudotumor cerebri were compared with 20 age- and sex-matched control subjects. Thin-section coronal and axial CT scans of the orbit and whole-brain axial CT scans were available for all subjects. The diameter of the optic nerve sheath, the degree of reversal of the optic nerve head, the presence and degree of empty sellae, and ventricular and sulcal sizes were evaluated without knowledge of whether or not the subject had pseudotumor cerebri. The same parameters were compared for two subgroups of patients with pseudotumor cerebri: those with mild vision loss and those with severe vision loss.

RESULTS. Patients with pseudotumor cerebri had significantly larger optic nerve sheaths than did control subjects (6.5 ± 0.83 mm vs 5.4 ± 0.69 mm). Radiologic evidence of papilledema with reversal of the optic nerve head was found in 12 of 17 patients compared with one of 20 control subjects. An empty sella was seen more frequently and to a greater degree in patients with pseudotumor cerebri than in control subjects (16 vs seven). Eight of nine patients with severe vision loss and four of eight patients with mild to moderate vision loss had reversal of the optic nerve head; the degree was greater in the group with severe vision loss. No difference in ventricular size or sulcal enlargement was seen between any of the groups. The opening CSF pressures of the two groups with vision loss were not significantly different (348 ± 80 mm H_2O vs 391 ± 98 mm H_2O).

CONCLUSION. In addition to the role of CT in excluding intracranial disease as a basis for the clinical syndrome of pseudotumor cerebri, thin-section CT of the orbits reveals a constellation of findings, including enlarged optic nerve sheaths, reversal of the optic nerve head, and empty sellae in patients with pseudotumor cerebri. Furthermore, severe vision loss in these patients correlates with more frequent and more severe reversal of the optic nerve head.

AJR **1993:160:143–146**

Pseudotumor cerebri or benign intracranial hypertension is a condition of unknown origin that most commonly occurs in obese middle-aged women [1–3]. The purpose of this study was to determine if orbital and cerebral CT findings can be used to distinguish patients with pseudotumor cerebri from control subjects who do not have this condition. We also sought to correlate CT findings with the eventual visual status of patients with pseudotumor cerebri.

Subjects and Methods

The study population consisted of 17 patients (16 women and one man) with clinical evidence of pseudotumor cerebri (papilledema, opening CSF pressure greater than 200 mm H_2O, normal CSF composition, and nonfocal neurologic examination). The average age of the patients with pseudotumor cerebri was 35 ± 12 years old (range, 19–63 years). *All had*

Received March 26, 1992; accepted after revision July 7, 1992.

Presented at the annual meeting of the American Society of Neuroradiology, Chicago, May 1988.

[1]Department of Radiology, University of Pennsylvania, 3400 Spruce St., Philadelphia, PA 19104.

[2]Present address: Department of Radiology, Utah Valley Regional Medical Center, 1034 N. 500 West, Provo, UT 84604. Address reprint requests to W. A. Gibby.

[3]Department of Neuro Ophthalmology, Wills Eye Hospital, North and Walnut St., Second Floor, Philadelphia, PA 19107.

[4]Department of Radiology, Wills Eye Hospital, Philadelphia, PA 19107.

0361–803X/93/1601–0143

thin-section axial and coronal CT scans (3- and 5-mm sections, respectively) through the orbits and routine axial images of the cranium (5-mm sections though the posterior fossa and 10-mm sections through the supratentorial compartment) that showed no diseased tissue. Twenty age- and sex-matched patients (19 females and one male) who were referred for evaluation of possible traumatic or inflammatory disease of the orbit served as control subjects. Their ages (37 ± 13 years; range 13–58 years) were not significantly different from those of the patients with pseudotumor cerebri. Measurements were made in the unaffected eyes of control subjects who had no clinical evidence of pseudotumor cerebri and no visual impairment in that eye. They had thin-section CT studies similar to those of the patients with pseudotumor cerebri.

The patients with pseudotumor cerebri were divided into two clinical groups: (1) those with minimal to moderate vision loss with sparing of central acuity and (2) those with severe vision loss that included a decreased visual field, a loss of central acuity, or both.

Optic nerve diameter, presence and degree of empty sellae, reversal of the optic nerve head, and ventricular and sulcal sizes were evaluated on CT scans of all subjects without knowledge of whether or not the patient had pseudotumor cerebri. The same CT parameters and the opening CSF pressures were compared between the two pseudotumor cerebri groups.

The optic nerve sheaths were measured approximately 1 cm behind the globe to avoid the variability noted with flaring of the distal portion of the optic nerve sheath and volume averaging as the nerve enters the globe. The sheaths were measured directly on both coronal and axial CT scans by using a small caliper with a magnifying glass and a millimeter ruler for standardization. For each patient, the coronal and axial CT measurements of the optic nerve sheath of the right or left eyes were the same and all measurements were averaged together, giving a single value for each patient in the data analysis. The optic nerve sizes were compared by using Student's t-test. Figure 1 shows where the measurements were taken in the axial and coronal planes, respectively, in a patient with pseudotumor cerebri and enlarged optic nerve sheaths.

The optic nerve head is usually concave posteriorly, but with increased CSF pressure transmitted down the optic nerve sheath, it can become edematous and bulge forward. We refer to this as reversal of the optic nerve head. Reversal of the optic nerve head was graded on a scale of 0–2. Grade 0 represents the normal convex outward appearance of the optic nerve head and sclera (Fig. 2), grade 1 represents minimal flattening of the optic nerve head (Fig. 3), and grade 2 represents prominent indentation of the optic nerve head (Fig. 4).

The presence and degree of empty sellae were graded from 0 to 3 on both coronal and axial images. Grade 0 represents the normal configuration of the sella turcica without CSF seen below the diaphragma sellae, grade 1 represents up to 50% filling of the sella with CSF (Fig. 5), grade 2 represents greater than 50% filling of the sella (Fig. 6), and grade 3 represents greater than 75% filling of the sella and bony enlargement (Fig. 7).

The sizes of the ventricles and sulci were graded subjectively on a 0–2 scale based on what was expected for the patient's age by an experienced neuroradiologic observer. Grade 0 was normal sulcal or ventricular size, grade 1 was minimal enlargement, and grade 2 was prominent enlargement of the CSF spaces.

All the CT scans were shuffled into a large stack and interpreted without the benefit of clinical history, although the diagnosis for several control subjects was obvious.

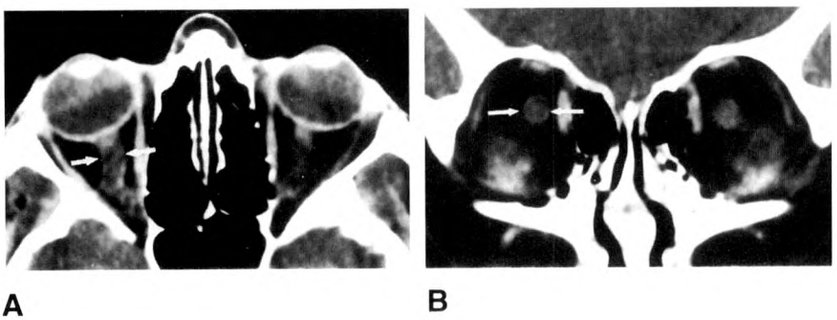

Fig. 1.—Enlarged optic nerve sheaths.
***A*, Axial 3-mm enhanced CT scan. Right optic nerve sheath (*arrows*) measures 7.0 mm.**
***B*, Coronal 5-mm CT scan approximately 1 cm behind globe. Enlarged optic nerve sheaths (*arrows*) measure 7.5 mm; CSF surrounds centrally positioned nerve.**

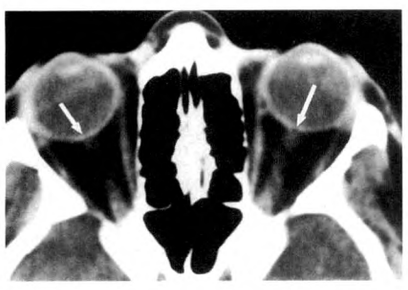

Fig. 2.—Normal optic nerve head. Axial CT scan shows normal (grade 0) appearance of sclera and optic nerve head with outward convexity at insertion of optic nerve head (*arrows*).

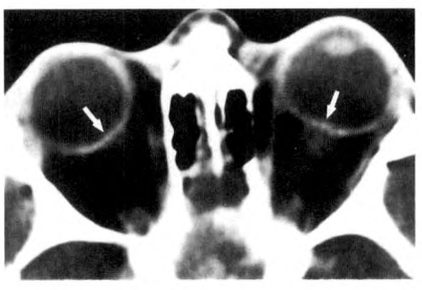

Fig. 3.—Grade 1 reversal of optic nerve head. Axial 3-mm enhanced CT scan shows optic nerve head reversal bilaterally (*arrows*), most evident on left side. Note flattening of normal outward convexity at insertion of optic nerve head. Optic nerve sheaths are enlarged bilaterally.

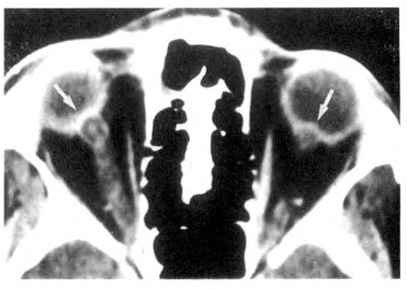

Fig. 4.—Grade 2 reversal of both optic nerve heads. Axial CT scan shows optic nerve heads (*arrows*) are indented well into vitreous by low-attenuation CSF immediately posterior to nerve head. This is the radiographic correlate of papilledema. Optic nerve sheaths are not dramatically enlarged.

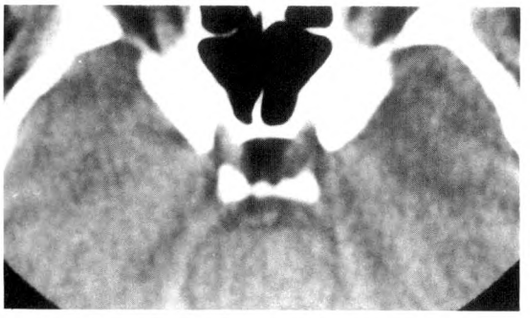

Fig. 5.—Grade 1 empty sella. Unenhanced axial CT scan through superior portion of sella turcica. CSF fills superior portion of sella, but filling was not seen inferiorly on adjacent sections. Coronal images (*not shown*) showed less than 50% filling of sella by CSF.

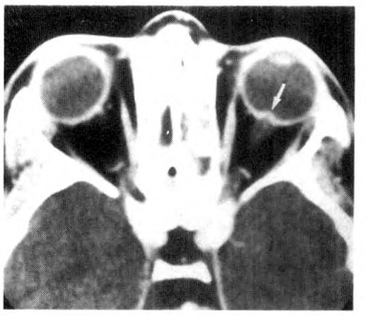

Fig. 6.—Grade 2 empty sella. Axial 3-mm enhanced CT scan through sella turcica. Sella is completely filled with CSF, which extended to sellar floor on lower sections. Small enhancing pituitary stalk is seen posteriorly. Grade 2 reversal of optic nerve head is seen on left side (*arrow*).

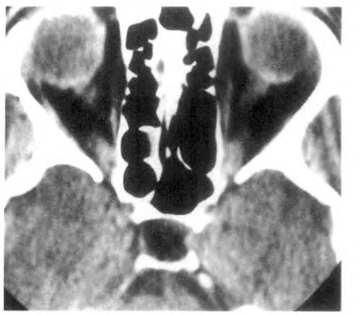

Fig. 7.—Grade 3 empty sella. Axial 3-mm unenhanced CT scan shows expanded sella turcica completely filled with CSF. CSF extended to sellar floor on adjacent sections.

Results

In the control subjects, optic nerve size was 5.4 ± 0.69 mm, whereas in the pseudotumor cerebri group it was 6.5 ± 0.83 mm. The t value was 4.42 and was highly significant ($p < .0003$).

Reversal of the optic nerve head was seen to some degree in one or both nerves in 12 of 17 patients with pseudotumor cerebri. Only one of 20 control subjects had a single grade 1 reversal of the optic nerve head. This patient also had a grade 3 empty sella. It was suspected that the patient might have clinically occult pseudotumor cerebri, although no symptoms suggestive of this were on the patient's chart and the patient was not available for further follow-up. χ^2 analysis revealed a significant difference between these two groups ($p < .001$).

Sixteen of 17 pseudotumor cerebri patients had some degree of empty sella: three grade 1, eight grade 2, and five grade 3; only seven of 20 control subjects had evidence of empty sella: three grade 1, two grade 2, and two grade 3. χ^2 analysis showed a significant difference between these populations ($p < .01$).

One control patient had grade 1 ventricular enlargement and one patient with pseudotumor cerebri had grade 2 ventricular enlargement. Some degree of sulcal enlargement was present in eight of 20 control subjects: five grade 1 and three grade 2. Only three pseudotumor patients had sulcal enlargement: three grade 1 and one grade 2. Using χ^2 analysis, we found no difference between the patients with pseudotumor cerebri and the control subjects in these categories. Smaller than normal ventricles or sulci were not observed in either group.

Correlation of the severity of vision loss with the various CT parameters revealed that eight of nine patients with severe vision loss had reversal of the optic nerve head: five grade 1 and three grade 2. Four of eight patients with mild to moderate vision loss had grade 1 reversal of the optic nerve head. The difference between these two groups approached significance ($\chi^2 = 4.8$, $.05 < p < .01$). Significantly, all the patients with grade 2 reversal of the optic nerve head were in the group with severe vision loss.

No significant difference in the degree of empty sellae, optic nerve size, ventricular size, or sulcal prominence in the pseudotumor cerebri population was found between the two categories of vision loss. Also, no significant difference was found between the opening CSF pressures in the two vision loss groups (none or moderate: 348 ± 80 mm H_2O; severe: 391 ± 98 mm H_2O; t = .98, NS).

Discussion

Although it is considered neurologically "benign," pseudotumor cerebri can cause some degree of vision loss in up to 50% of patients [4, 5]. In the series of Corbett et al. [4], 25% of cases progressed to severe vision loss or blindness. The pathogenesis of the vision loss may be related to the transmission of elevated pressure within the CSF down the optic nerve sheath to the optic nerve head, where this may cause ischemia of the nerve fibers entering through the sclera or disruption of axonal transport [6]. Why certain patients with this condition have vision loss while others do not may be related to differential sensitivity of the optic nerve head to chronic increased pressure. The prognosis of this disorder varies. In the patients who have permanent vision loss, it is certainly not a benign disorder. Of the potential clinical predictors of vision loss, systemic hypertension is the only condition that has been associated with a worse visual outcome [4]. In addition, vision loss may not occur for months to years after presentation.

Jinkins [6] first reported the reversal of the optic nerve head in a variety of conditions associated with increased intracranial pressure, including pseudotumor cerebri. The frequency of this finding in patients with pseudotumor cerebri is not known. In our series of patients with pseudotumor cerebri, all of whom had some loss of vision, approximately

70% of patients had this sign in one or both optic nerves, which was significantly different from the control subjects. Our data indicate that grade 2 reversal of the optic nerve head correlates with the greatest eventual loss of vision.

Another finding observed in patients with pseudotumor cerebri is that of enlarged optic nerve sheaths. In the series of Weisberg [7], two of 28 patients had enlarged optic nerves, although no measurements were provided and again no control values were available. In fact, we were unable to find control CT measurements for the optic nerve sheaths. In order to obtain reasonably accurate measurements of the optic nerve sheaths, thin sections must be obtained (3 mm or less in the axial plane and no greater than 5 mm in the coronal plane). Diameters of the optic nerve sheath were statistically significantly larger in the patients with pseudotumor cerebri than in the control subjects, but overlaps did exist.

The radiographic findings of pseudotumor cerebri have, at times, been conflicting and have not been well controlled. Dandy [8] described the ventricles as normal or even small during ventriculography or pneumoencephalography. Weisberg [7] described six of 28 patients as having a "small-sized ventricular system." Those examinations were performed on a second-generation CT scanner without controls and in a nonblinded fashion. The actual ventricular size is not mentioned, although the method used was based on planimetric measurement and compared with the control values in the series of Barron et al [9]. On the other hand, Boddie et al. [10] reported that 19 of 25 patients had ventricular volumes greater than normal. Huckman et al. [11] found no differences between the ventricular sizes of patients with pseudotumor cerebri and those of a control population. Our study compared age- and sex-matched control subjects in a blinded fashion and is in agreement with the findings of Huckman et al. [11]. Silbergleit et al. [12] studied six cases of pseudotumor cerebri and compared them with findings in six control subjects. Volumetric pixel analysis of the ventricular volume showed no difference between normal control subjects and patients with pseudotumor cerebri.

However, their analysis "revealed significantly larger subarachnoid space volumes" in patients with pseudotumor cerebri than in control subjects.

Increased brain water and increased resistance to CSF absorption have been proposed as factors involved in the pathogenesis of pseudotumor cerebri [13, 14]. In a study of MR imaging of pseudotumor cerebri, Moser et al. [15] found that two of 11 patients had focal areas of increased signal in their periventricular white matter. A white matter index related to CSF water intensity was measured and found to be slightly, although significantly, elevated in patients with pseudotumor cerebri compared with a control group. This was thought to represent a "diffuse low level of edema." However, Silbergleit et al. [12] reported MR imaging in six cases of pseudotumor cerebri, none of which exhibited white matter signal abnormality. Thus, the findings of white matter changes are of dubious significance.

Empty sellae have been associated with many conditions causing increased intracranial pressure. Empty sellae have been observed in 5% of 788 autopsies [16]. Previous reports have indicated that 5% of women with pseudotumor cerebri have empty sellae [17]. However, these data predate the era of CT scanning. The sensitivity of plain skull radiographs and pneumoencephalography is significantly less than that of CT for diagnosing this condition. In 20% of 225 routine autopsy cases, an intrasellar subarachnoid space was identified on radiographs [18]. Weisberg et al. [19] reported a 10% prevalence (5/50) of empty sellae on plain radiographs of the skull in patients with pseudotumor cerebri. In our patients with pseudotumor cerebri, 16 (94%) of 17 patients had at least a partially empty sella. In addition, the degree of empty sellae was significantly greater than in the control subjects. The high prevalence noted in our patients with pseudotumor cerebri is compatible with their chronic elevated intracranial pressure, which averaged 370 mm H_2O.

REFERENCES

1. Bucheit WA, Burton C, Haag B, Shaw D. Papilledema and idiopathic intracranial hypertension. *N Engl J Med* **1969**;280:938–942
2. Johnston I, Paterson A. Benign intracranial hypertension: I. Diagnosis and prognosis. *Brain* **1974**;97:289–300
3. Weisberg LA. The syndrome of increased intracranial pressure without localizing signs: a reappraisal. *Neurology* **1975**;25:85–88
4. Corbett JJ, Savino PJ, Thompson S, et al. Visual loss in pseudotumor cerebri: follow-up of 57 patients from 5 to 41 years and a profile of 14 patients with permanent severe visual loss. *Arch Neurol* **1982**;39:461–474
5. Krogsaa B, Sorensen PS, Seedorff HH, et al. Ophthalmologic prognosis in benign intracranial hypertension. *Acta Ophthalmol Suppl* (Copenh) **1985**;63[173]:62–64
6. Jinkins JR. "Papilledema": neuroradiologic evaluation of optic disk protrusion with dynamic orbital CT. *AJR* **1987**;149:793–802
7. Weisberg LA. Computed tomography in benign intracranial hypertension. *Neurology* **1985**;35:1075–1078
8. Dandy WE. Intracranial pressure without brain tumor, diagnosis, and treatment. *Ann Surg* **1937**;106:492–513
9. Barron SA, Jacobs L, Kinkel WR. Changes in size of normal lateral ventricles during aging determined by computerized tomography. *Neurology* **1976**;26:1011–1013
10. Boddie HG, Banna M, Bradley WG. "Benign" intracranial hypertension. *Brain* **1968**;97:313–326
11. Huckman MS, Fox JS, Ramsey RG, et al. Computed tomography in the diagnosis of pseudotumor cerebri. *Radiology* **1976**;119:593–597
12. Silbergleit R, Junck L, Gebarski SS, Hatfield MK. Idiopathic intracranial hypertension (pseudotumor cerebri): MR imaging. *Radiology* **1989**; 170:207–209
13. McComb JG. Recent research into the nature of cerebrospinal fluid formation and absorption. *J Neurosurg* **1983**;59:369–383
14. Raichle ME, Grubb RL Jr, Phelps ME, et al. Cerebral hemodynamics and metabolism in pseudotumor cerebri. *Ann Neurol* **1978**;4:104–111
15. Moser FG, Hilal SK, Abrams G, Bello JA, Schipper H, Silver A. MR imaging of pseudotumor cerebri. *AJNR* **1988**;9:39–45
16. Busch W. Die Morphologie der Sella Turcica und ihre Heziehungen zur Hypophyse. *Virchows Arch A Pathol Anat Histopathol* **1951**;320:437–458
17. Donaldson JO. Endocrinology of pseudotumor cerebri. *Neurol Clin* **1986**;4:919–927
18. Bergland RM, Ray BS, Torack RM. Anatomical variations in the pituitary gland and adjacent structures in 225 human autopsy cases. *J Neurosurg* **1968**;28:93–99
19. Weisberg LA, Housepian EM, Saur DP. Empty sella syndrome as complication of benign intracranial hypertension. *J Neurosurg* **1975**;43:177–180

Late CT Findings in Brain Trauma: Relationship to Cognitive and Behavioral Sequelae and to Vocational Outcome

I. Reider-Groswasser[1]
M. Cohen[2]
H. Costeff[2]
Z. Groswasser[2]

OBJECTIVE. The purpose of this study was to determine the degree of correlation between cerebral atrophy observed on CT scans after severe blunt brain trauma and later neuropsychological status, as well as to evaluate the relative prognostic values of a number of indexes of cerebral atrophy.

MATERIALS AND METHODS. The study group comprised 32 previously healthy men 18–65 years old who had severe blunt trauma of the brain (initial scores on Glasgow coma scale of 7 or less). Their cognitive and behavioral statuses were evaluated when the patients were discharged from the hospital, which occurred when the recovery process showed a plateau. Overall vocational status was evaluated 1 year after discharge. The clinical evaluation was performed by a multidisciplinary team. Multiple linear indexes derived from brain CT scans obtained about 3 months after injury in patients with blunt brain trauma were correlated with cognitive and behavioral sequelae of brain damage and with vocational placement, as evaluated by a rehabilitation team about 1 year after trauma.

RESULTS. A high correlation was found between the width of the third ventricle and outcome. The prognostic value of the width of the third ventricle was superior to that of any other index studied, and it correlated best with late cognitive status (Spearman $r = .57$, $p < .01$).

CONCLUSION. The width of the third ventricle is a useful prognostic index in cases of diffuse brain trauma. It indicates diencephalic atrophy, caused either by diffuse axonal injury or by hypoxia. It may indicate a role of diencephalic structures in higher cortical functions.

AJR 1993;160:147–152

Severe blunt brain trauma is known to be associated both with cerebral atrophy [1–4] and with neuropsychological deficits and functional disability [5–7]. The precise relationship between the atrophy and the neuropsychological deficits is yet unclear, and two questions addressing this relationship remain to be answered: (1) What is the degree of correlation between cerebral atrophy seen on CT scans and late neuropsychological status? and (2) Which indexes of cerebral atrophy are best correlated with neuropsychological outcome? The answers to these two questions may have both practical value in prognosticating neuropsychological outcome in blunt brain trauma and theoretical value in indicating the brain structures most closely associated with such outcome. Question number 2 is of particular interest, since it is not yet known whether linear indexes of atrophy correlate well with functional outcome, or if prognostication requires the use of labor-intensive planimetric or volumetric indexes.

We examined the CT scans obtained 3–4 months after injury in 32 patients with severe blunt brain trauma and calculated for each of them 14 supratentorial and infratentorial linear indexes of brain atrophy. These indexes have been correlated with late neuropsychological outcome, as determined by the evaluation of a multidisciplinary rehabilitation team.

Received March 23, 1992; accepted after revision July 8, 1992.

[1]Section of Neuroradiology, Tel-Aviv Sourasky Medical Center, Ichilov Hospital, Tel-Aviv, Israel.

[2]Loewenstein Rehabilitation Hospital, Ra'anana, Sackler Faculty of Medicine, Tel-Aviv University, Tel-Aviv, Israel. Address reprint requests to Z. Groswasser, Loewenstein Rehabilitation Hospital, P.O. Box 3, Ra'anana 43100, Israel.

0361–803X/93/1601–0147

Materials and Methods

Patients

The study group consisted of 32 male patients 18–65 years old who were hospitalized at our center for 1 year for rehabilitation following severe blunt brain trauma, and for whom CT scans were routinely obtained 3–4 months after injury. Twenty-seven patients were 45 years old or younger. None had a history of previous neurologic disorder, alcoholism, or drug abuse. All were employed or in full-time military service prior to injury. All suffered from blunt head injury for the first time. Their scores on the Glasgow coma scale, assessed 6 hr after injury, were all 7 or less.

Radiologic Methods

All CT scans reviewed were obtained 3–4 months after trauma on Elscint 905, 2002, and 2400 scanners. Slices were parallel to the orbitomeatal lines; slice thickness was 10 or 12 mm for supratentorial structures and the slices were contiguous. Among the supratentorial indexes were seven described by Gyldensted and Kosteljanetz [8]: left and right anterior horn widths (AHW)—the maximal width of each anterior horn measured along the line connecting the tips of the anterior horns and intersecting with a line derived from the continuation of the inner border of the septum pellucidum on each side; left and right septum-caudate distances (SCD)—the maximal distance between the caudate nucleus at its maximal convexity and the septum pellucidum; cella media distance (CMD)—the combined minimal width of the bodies of the lateral ventricles, including the septum pellucidum; third ventricle width (TVW)—maximal width of the third ventricle; and cella media index (CMI)—maximal external width of skull divided by the CMD (Fig. 1). Two cerebroventricular indexes, types 1 and 2 (CVI_1 and CVI_2), were described by Hahn and Rim [9]. CVI_1 is the ratio between the maximal bifrontal diameter measured along a line connecting the tips of the anterior horns, and the distance along the same line connecting the inner tables of the skull. CVI_2 is the ratio between the maximal bicaudate diameter measured along a line drawn from the midportions of the bodies of the caudate nuclei, and the distance between the inner tables of the skull measured along the same line.

Two other supratentorial indexes were the ventricular score (VS) and sulcal score (SS) described by Hughes and Gado [10]. The VS is the ratio of the sum of the TVW, plus the left SCD, plus the right SCD, plus the width of the anterior horns (including the septum pellucidum, just anterior to the foramen of Monro), plus the CMD, to the widest interparietal distance, measured along a line connecting the inner tables of the skull at the level of the bodies of the lateral ventricles. The SS is the sum of the widths of the four widest sulci seen in the upper three cuts.

The three infratentorial indexes were the cistern-brainstem ratio (CBR), the superior cerebellar cistern ratio (SCCR), and the fourth ventricle ratio (FVR), as described by Koller et al. [11]. The CBR is the ratio of the width of the prepontine cistern to the distance measured between the posterior clinoid process and the fourth ventricle; the SCCR is the ratio of the width of the superior cerebellar cistern to the distance between the inner tables of the skull along the same line; the FVR is the ratio of the lateral maximal width of the fourth ventricle to the distance between the outer tables of the skull measured along the same line (Fig. 1).

Mean values and standard deviations for indexes AHW, SCD, TVW, CMD, CMI, and SS were extracted and calculated for 34 healthy young adult men (age range, 18–45 years) from the original data of Gyldensted [12] (see Table 1). Mean values and standard deviations for healthy subjects were extracted from the data of Hahn and Rim [9] for CVI_1 and CVI_2, and from the data of Koller et al. [11] for CBR, SCCR, and FVR. These means and standard deviations were used to convert the indexes of our subjects to standard deviation scores for all of the indexes except VS. Because no data were available for the VS of normal subjects, the crude uncorrelated scores of this parameter were analyzed. Because the standard deviations for AHW, SCD, TVW, and CMI were based on the subjects in the study of Gyldensted [12], we calculated these values only for the 27 patients aged 45 and younger. Means and standard deviations for the remaining indexes, except VS, and the crude scores of VS were calculated for all 32 patients.

TABLE 1: Normal Values for Supratentorial Indexes Calculated for 34 Healthy Young Men

Indexes	Normal Values (Mean ± SD)
Left anterior horn width	17.11 ± 1.77
Right anterior horn width	17.00 ± 1.89
Left septum-caudate distance	7.35 ± 2.07
Right septum-caudate distance	7.35 ± 2.07
Cella media distance	28.44 ± 3.81
Cella media index	5.08 ± 0.78
Third ventricle width	3.59 ± 1.11
Sulcal score	2.74 ± 0.97

Note.—Values were calculated from the original data of Gyldensted [12].

Clinical Evaluation

Cognitive and behavioral statuses were evaluated when the patients were discharged from the hospital, which occurred when the recovery process showed a plateau between 3 and 18 months after injury. The discharge evaluation was performed by a multidisciplinary team that included physiatrists, psychologists, neuropsychologists, and psychiatrists. For both cognitive status and behavior, disturbances were grouped in four categories: none, mild, moderate, and severe. Mild cognitive disturbances were defined as deficits in attention concentration and memory alone. Moderate cognitive disturbances were defined as additional deficits in integrated functions such as drawing conclusions and forming social judgments. Severe cognitive disturbances were those of basic thought processes such as perceptive deficits and apraxia, in addition to the above-mentioned disorders. Mild behavioral disturbances were defined as dysphoria, irritability, passivity, and dependency without any other overt disturbances. Moderate behavioral disturbances included outbursts or frank depression in addition to the above. Severe behavioral disturbances were characterized by such phenomena as confabulations, delusions, and frankly maladaptive behavior.

The same team evaluated overall vocational status at outpatient follow-up examinations, which occurred 1 year after discharge. This status was also divided into four categories: skilled work, unskilled work on the open market, sheltered employment, and unemployability.

Statistical Analysis

The clinical outcome parameters that were cross correlated with the 14 radiologic indexes included cognition, behavior, vocational placement, speech clarity and fluency, semantic processing, independence in activities of daily living, and locomotion. All were evaluated and semiquantified by the multidisciplinary rehabilitation team responsible for follow-up of patients with blunt brain trauma. The parameters were graded in four hierarchical categories, of which category 1 was the best and 4 the worst. Only the first three parameters—cognition, behavior, and vocational placement—showed an

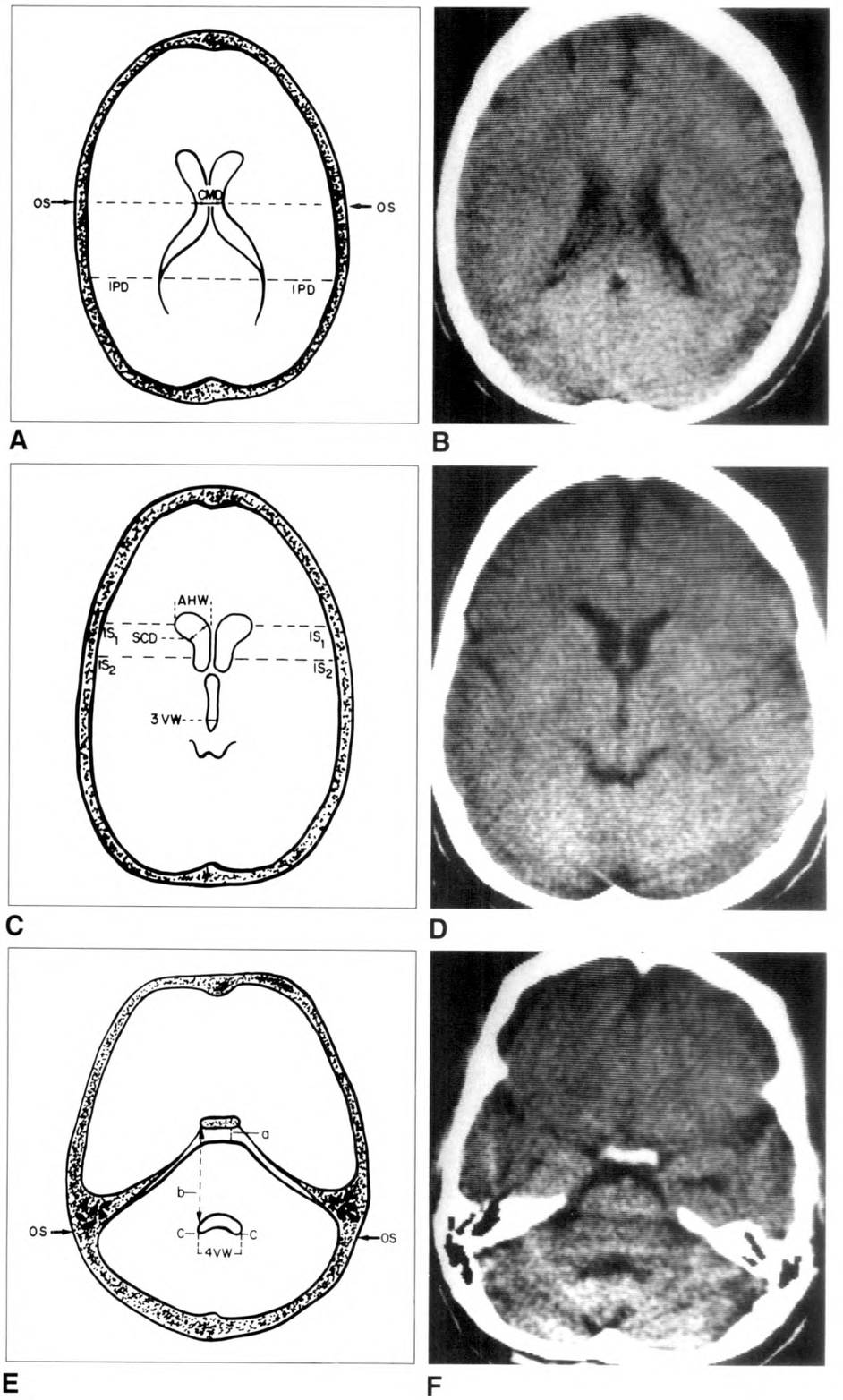

Fig. 1.—CT study of a 32-year-old patient 3 months after blunt trauma of brain.

***A* and *B*, Schematic drawing (*A*) and axial CT scan (*B*) at level of bodies of lateral ventricles. CMD = cella media distance, OS = maximal external width of skull, IPD = interparietal distance used as denominator for ventricular score. Cella media index = OS/CMD.**

***C* and *D*, Schematic drawing (*C*) and axial CT scan (*D*) at level of third ventricle. AHW = maximal width of anterior horn, SCD = septum-caudate distance, IS_1 = distance between inner skull tables at level of tips of anterior horns, IS_2 = distance between inner skull tables at level of mid frontal horns, 3VW = third ventricle width; IS_1 and IS_2 are denominators of cerebroventricular indexes, types 1 and 2, respectively. Note widening of interhemispheric fissure and cerebral sulci.**

***E* and *F*, Schematic drawing (*E*) and axial CT scan (*F*) at level of fourth ventricle. a = width of prepontine cistern, b = distance between posterior clinoid and floor of fourth ventricle, 4VW = width of fourth ventricle between points C, OS = outer skull along C-C line. Fourth ventricle ratio = 4VW/OS; cistern brainstem ratio = a/b).**

outcome distribution that was sufficiently widespread to permit meaningful correlation with the radiologic indexes (in the other four outcome parameters, the patients were bunched in category 1).

The main statistical analysis consisted of ranking the scores for each of the 14 radiologic indexes, ranking the grades of each of the three clinical outcome parameters, and calculating the Spearman rank correlation between each radiologic index and each clinical outcome parameter, correcting for tied ranks. Means and standard deviations of each radiologic index were calculated for each clinical outcome parameter (see Tables 2–4), but did not serve as a basis

for the analysis of statistical significance in view of the nonnormal distribution of the data.

For purposes of comparison, we used the same statistical technique to estimate the correlations between two nonradiologic prognostic factors—age and duration of coma—and the clinical outcome parameters.

Results

Cognitive status was the outcome parameter that correlated best with linear radiologic indexes. Table 2 shows a statistically significant correlation with five such indexes (right and left SCD, TVW, CVI_2, and VS), and a borderline correlation with a sixth (CVI_1). The range of values for the Spearman rank correlation coefficient was .32 to .57 for these six indexes.

Of the two remaining outcome parameters, vocational placement (Table 3) correlated slightly better with the radiologic parameters than did behavior (Table 4). Vocational outcome showed four significantly correlated radiologic parameters and one of borderline significance, with Spearman *r* values ranging from .37 to .48 for the five indexes, compared with three significant and two borderline radiologic parameters with a Spearman *r* range of .24–.45 for behavior.

The radiologic index that showed best overall correlation with the three clinical outcome parameters was TVW. Its coefficients of correlation were .57 with cognitive outcome and .45 with behavior, both significant at the .01 level, and .43 with vocational placement, significant at the .05 level. Among the other indexes, only the CVI_2 showed a significant correlation with all three outcome parameters, with Spearman *r* ranging from .44 (cognition) to .39 (behavior). The VS showed a good correlation ($r = .53$) with cognition, a fair one ($r = .42$) with vocational placement, and one of borderline significance ($r = .35$) with behavior. The left SCD showed significant correlation ($r = .46$) with cognition and borderline correlations ($r = .34$ and $r = .37$, respectively) with behavior and vocational placement. The right SCD showed significant correlations with cognition ($r = .46$) and with vocational outcome ($r = .48$), but not with behavior ($r = .24$). CVI_1 showed a borderline correlation ($r = .32$) with cognition but with nothing else. No other radiologic indexes showed any significant correlation with the degree of late clinical disability among the patients with blunt brain trauma, although some of the indexes (left AHW, CMD, and SS) did show a significant difference between the normal subjects of Gyldensted and Kosteljanetz [8] and our brain injury patients as a group.

Of the nonradiologic prognostic factors examined, age showed no significant correlation with clinical outcome; coma duration showed a significant correlation (Spearman $r = .45$) with vocational placement and one of only borderline significance (Spearman $r = .30$) with cognition.

Discussion

Structure-function relationship is one of the most puzzling questions in brain research, and brain trauma is no exception. CT scans can be normal even in severe head injury [5], and other techniques, like MR imaging, are necessary for showing late findings [13]. Structural changes after trauma are well recognized, but even well-trained clinicians in the field of brain trauma are sometimes puzzled by discrepancies between patients' radiologic findings and their clinical performance. Widening of the ventricular system after brain trauma is a common finding, but attempts have been made to correlate only a few of its parameters with clinical findings [1, 3].

Brain volume has been shown to be fairly stable in normal people less than 50 years old [14, 15]; Gyldensted [12] described differences in brain parameters between males and females. Therefore, only male patients from that study were used for our calculations, and the statistical analysis took into consideration the age of the patients.

The CT scans used for analysis were obtained at least 3 months after injury because it was assumed that most if not all acute-phase changes, such as brain edema and hemorrhage, would have resolved by that time. It is assumed that structural findings observed after that period are stable.

Coma duration is a well-known yardstick for assessing severity of brain trauma, and cognition and behavior are the domains mostly affected. Actual work placement was chosen as an integrative criterion for evaluating outcome as it provides a good indication of social reintegration and correlates with patients' subjective evaluation of quality of life [7, 16 18].

The outstanding finding of this study was a remarkably high correlation between outcome and the width of the third ventricle on CT. This correlation explains no less than a third of the cognitive variance, a fifth of the variance in behavioral status, and 18% of the variance in late vocational placement. The prognostic value of TVW 3–4 months after injury was far superior to that of another simple linear CT measurement studied here; it was also superior to the four compound measurements studied: the VS, SS, CVI_1, and CVI_2 indexes. Indeed, it predicted vocational placement as well as coma duration ($r = .30$), and it predicted cognitive outcome even more accurately ($r = .57$). Gomori et al. [14] have concluded that linear measurements are a simple and reliable method and that planimetric measurements have no significant advantage over linear measurements. Our findings also show the usefulness of the linear measurements.

It is not immediately obvious why TVW should correlate better than other ventricular measurements with functional outcome of diffuse brain injury, since one would expect functional outcome to be most closely related to frontal and temporal cortical injury. However, this may be understood if we take into account the findings of Teasdale et al. [19], who stated that "compression of the 3rd ventricle and basal cisterns correlated with an intracranial pressure >2 mmHg, with clinical signs of midbrain dysfunction and worse prognosis." The negative prognosis of compression of basal cisterns was described by other authors as well [20, 21]. The late results of such compression may well be thalamic atrophy; bearing in mind that most of the thalamic nuclei have well-developed reciprocal connections with the cortex, it is possible that damage to these crucial brain structures is related to neurobehavioral and vocational outcome in patients with blunt brain trauma. On the other hand, the diencephalic atrophy may also be due to the well-known diffuse axonal injury that is a common feature of closed head injury.

TABLE 2: Cognitive Disturbances Correlated with Significant CT Indexes After Traumatic Blunt Brain Injury

CT Index	Mean Value ± SD (No. of Cases)				Statistical Measures			
	No Disturbances	Mild Disturbances	Moderate Disturbances	Severe Disturbances	*r*	t	df	*p*
Septum-caudate distance								
Left	0.169 ± 0.46 (3)	-0.865 ± 1.31 (7)	1.512 ± 3.08 (11)	1.520 ± 1.67 (6)	.46	2.56	25	<.05
Right	-0.628 ± 0.46 (3)	-1.164 ± 1.16 (7)	0.986 ± 3.73 (11)	1.520 ± 2.64 (6)	.46	2.60	25	<.05
Third ventricle width	-0.261 ± 0 (3)	-1.118 ± 1.74 (7)	3.802 ± 4.66 (11)	5.192 ± 3.07 (6)	.57	3.51	25	<.01
Cerebroventricular index, type 1	0.523 ± 1.26 (3)	1.021 ± 1.26 (8)	2.788 ± 3.76 (12)	2.405 ± 2.09 (9)	.32	2.68	30	>.05–<.1
Cerebroventricular index, type 2	0.095 ± 0.55 (3)	-0.277 ± 1.28 (8)	0.839 ± 2.12 (12)	1.722 ± 1.47 (9)	.44	2.68	30	<.05
Ventricular score	43.67 ± 11.02	53.5 ± 12.15 (8)	68.25 ± 28.79 (12)	73.56 ± 18.12 (9)	.53	3.39	30	<.01

TABLE 3: Overall Vocational Outcome Correlated with Significant CT Indexes After Traumatic Blunt Brain Injury

CT Index	Mean Value ± SD (No. of Cases)				Statistical Measures			
	Skilled Work	Simple Work	Sheltered Work	Unemployable	*r*	t	df	*p*
Septum-caudate distance								
Left	0.834 ± 2.82 (2)	0.285 ± 2.79 (11)	2.994 ± 4.12 (12)	0.834 ± 1.69 (2)	.37	2.00	25	>.05–<.1
Right	0.435 ± 3.38 (2)	-0.224 ± 3.25 (11)	2.375 ± 3.80 (12)	0.435 ± 0 (2)	.48	2.75	25	<.05
Third ventricle width	1.229 ± 2.11 (2)	1.103 ± 3.44 (11)	5.259 ± 3.68 (12)	4.820 ± 1.05 (2)	.43	2.36	25	<.05
Cerebroventricular index, type 2	0.452 ± 1.61 (3)	-0.292 ± 0.97 (12)	1.405 ± 2.02 (12)	1.786 ± 1.80 (5)	.41	2.45	30	<.05
Ventricular score	62.33 ± 17.56 (3)	51.58 ± 18.25 (12)	73.33 ± 26.63 (12)	70.80 ± 16.92 (5)	.42	2.50	30	<.05

TABLE 4: Overall Behavioral Disturbances Correlated with Significant CT Indexes After Traumatic Blunt Brain Injury

CT Index	Mean Value ± SD (No. of Cases)				Statistical Measures			
	No Disturbances	Mild Disturbances	Moderate Disturbances	Severe Disturbances	*r*	t	df	*p*
Septum-caudate distance								
Left	0.435 ± 2.02 (6)	0.291 ± 2.92 (10)	4.224 ± 4.67 (7)	1.831 ± 2.47 (4)	.34	1.80	25	>.05–<.1
Right	0.169 ± 2.45 (6)	0.217 ± 3.38 (10)	2.581 ± 4.76 (7)	1.631 ± 2.48 (4)	.24	1.53	25	<.1
Third ventricle width	0.979 ± 2.73 (6)	2.897 ± 3.26 (10)	5.698 ± 4.78 (7)	3.458 ± 2.57 (4)	.45	2.85	25	>.01
Cerebroventricular index, type 2	-0.143 ± 1.01 (6)	0.214 ± 1.60 (12)	1.063 ± 2.09 (9)	1.500 ± 1.65 (5)	.39	2.33	30	<.05
Ventricular score	51.67 ± 16.32	61.58 ± 21.02 (12)	73.11 ± 31.45 (9)	66.60 ± 11.06 (5)	.35	2.01	30	>.05–<.1

On the basis of our findings, we recommend obtaining brain CT scans at about 3 months in patients with blunt brain trauma and of using linear measurements as predictors of neurobehavioral and vocational outcome. The width of the third ventricle is preferred to the other indexes studied here, including a complex index like the VS, because of the simplicity of its measurement. It is possible that measurements derived from MR may be of even greater prognostic value, in view of the greater sensitivity of MR to parenchymal changes following diffuse brain injury [13].

The prognostic information provided by such radiologic studies seems likely to be useful, but we believe that it cannot replace clinical follow-up in the treatment of brain-injured patients at this time.

REFERENCES

1. Timming R, Orrison W, Mikula JA. Computerized tomography and rehabilitation outcome after severe head trauma. *Arch Phys Med Rehabil* **1982**;63:154–159
2. Rao N, Jellineck HM, Harvey RF, et al. Computerized tomography head scans as predictors of rehabilitation outcome. *Arch Phys Med Rehabil* **1984**;65:18–20
3. Levin HS, Meyers CA, Grossman RG, Sarwar M. Ventricular enlargement after closed head injury. *Arch Neurol* **1981**;38:623–629
4. Teasdale E, Hadley DM. Radiodiagnosis in head injury. In: Vinken PJ, Bruyn GW, Klawans HL, et al., eds. *Handbook of clinical neurology*, vol. 57. *Head injury*. Amsterdam: Elsevier Science Publishers, **1990**:143–179
5. Lobato RD, Sarabia R, Rivas DJ, et al. Normal computerized tomography scans in severe head injury. *J Neurosurg* **1986**;65:784–789
6. Van Dongen KJ, Braakman R. Late computed tomography in survivors of severe head injury. *Neurosurgery* **1980**;7:14–22
7. Najenson T, Mendelson L, Schechter I, et al. Rehabilitation after severe head injury. *Scand J Rehabil Med* **1974**;6:5–14
8. Gyldensted C, Kosteljanetz M. Measurements of normal ventricular system with computer tomography of the brain: a preliminary study on 44 adults. *Neuroradiology* **1976**;11:204–213
9. Hahn FJY, Rim K. Frontal ventricular dimensions on normal computed tomography. *AJR* **1976**;126:593–596
10. Hughes CP, Gado M. Computed tomography and aging of the brain. *Radiology* **1981**;139:391–396
11. Koller C, Glatt SL, Perlik S, et al. Cerebellar atrophy demonstrated by computed tomography. *Neurology* (NY)**1981**;31:404–412

12. Gyldensted C. Measurements of the normal ventricular system and hemispheric sulci of 100 adults with computed tomography. *Neuroradiology* **1977**;14:183–192
13. Groswasser Z, Reider-Groswasser I, Soroker S, et al. Magnetic resonance imaging in head injury patients with normal late computed tomography. *Surg Neurol* **1987**;27:331–337
14. Gomori JM, Steiner E, Melamed E, et al. The assessment of brain changes in brain volume using combined linear measurements: a CT-scan study. *Neuroradiology* **1984**;26:21–24
15. Stafford JL, Alben MS, Naeser A, et al. Age-related differences in computed tomographic scan measurements. *Arch Neurol* **1988**;45:409–415
16. Najenson T, Groswasser Z, Mendelson L, et al. Rehabilitation outcome of brain damaged patients after severe head injury. *Int Rehabil Med* **1980**;2:17–22
17. Melamed S, Stern JM, Rahmani L, et al. Work congruence, behavioral pathology and rehabilitation status of severe craniocerebral injury patients. In: Lahav E, ed. *Psycho-social research in rehabilitation.* Israel: Ministry of Defence Publishing House, **1982**:59–74
18. Groswasser Z, Sazbon L. Outcome of 134 patients with posttraumatic unawareness. Part 2: Functional outcome of 72 patients recovering consciousness. *J Neurosurg* **1990**;72:81–84
19. Teasdale E, Cardoso E, Galbraith S, et al. CT scan in severe diffuse head injury: physiological and clinical correlations. *J Neurol Neurosurg Psychiatry* **1984**;47:600–603
20. Toutant SM, Klaubel MR, Marshall LF, et al. Absent or compressed basal cisterns on first CT scan: ominous predictors of outcome in severe head injury. *J Neurosurg* **1984**;61:691–694
21. Eisenberg HM, Gary HE, Aldrich EF, et al. Initial CT findings in 753 patients with severe head injury: a report from the Traumatic Coma Data Bank. *J Neurosurg* **1990**;73:688–698

MR Imaging of the Brain in Patients with AIDS: Value of Routine Use of IV Gadopentetate Dimeglumine

Maureen C. Jensen[1]
Michael Brant-Zawadzki

OBJECTIVE. A prospective study was conducted to explore the value of routine administration of IV gadopentetate dimeglumine for MR imaging of the brain in patients with AIDS.

SUBJECTS AND METHODS. Over a 19-month period, MR images of the brain in 51 consecutive AIDS patients were obtained routinely both with and without IV gadopentetate dimeglumine. Unenhanced and contrast-enhanced images from the resulting 63 studies were viewed together. Findings were classified into one or more of three categories: normal, mass or focal lesions, or white matter disease. The number of focal or mass lesions was recorded. Lesion conspicuity on the unenhanced and enhanced images was compared. Ventricular enlargement was also graded. Available medical records and laboratory data of the patients were reviewed.

RESULTS. Of the 63 MR studies reviewed, 39 (62%) were abnormal. In no case was a normal unenhanced MR study rendered abnormal after the administration of gadopentetate dimeglumine. Overall, T2-weighted images showed twice as many focal or mass lesions than contrast-enhanced T1-weighted images did. Most lesions detected on the T2-weighted images did not show enhancement with contrast material. White matter disease was the most common abnormality detected. The group of patients with white matter disease also had the highest occurrence of ventriculomegaly.

CONCLUSION. Our study does not support the routine use of gadopentetate dimeglumine for MR imaging of the brain in patients with AIDS. Our experience emphasizes the importance of a normal T2-weighted image.

AJR 1993;160:153–157

The World Health Organization estimates that 8–10 million adults and children worldwide are infected with HIV, and that by the year 2000, 40 million people may be seropositive for HIV. The Centers for Disease Control reports that at the end of 1991, AIDS was the second leading cause of death among men 25–44 years old in the United States [1]. Ten percent of patients with AIDS have neurologic signs and symptoms initially, and during the course of the disease, 39% have clinical evidence of CNS involvement [2]. Consequently, MR images of the brain are frequently obtained in these patients. The additional cost of routine administration of gadopentetate dimeglumine can be justified only if findings after administration of contrast material alter the diagnostic impression and affect clinical management. The additional diagnostic information provided by contrast-enhanced images is perhaps most convincing in patients thought to have metastatic disease [3–6]. This study addresses the role of gadopentetate dimeglumine in MR imaging of the brain in AIDS patients in a community where the prevalence of HIV infection is high.

Received April 20, 1992; accepted after revision July 17, 1992.

[1] Both authors: Department of Radiology, Hoag Memorial Hospital, 301 Newport Blvd., Newport Beach, CA 92663. Address reprint requests to M. Brant-Zawadzki.

0361–803X/93/1601–0153

Subjects and Methods

A prospective study was conducted over a 19-month period in which MR examinations of the brain in 51 consecutive AIDS patients were performed routinely with IV gadopentetate dimeglumine. A total of 63 gadopentetate dimeglumine–enhanced MR studies were performed. Although many patients had multiple scans, a scan was considered an additional study only if new clinical findings warranted initiating a new investigative workup. One

patient was a 44-year-old woman; 50 patients were 29- to 54-year-old men.

MR images were obtained with high-field (1.5-T) superconducting magnets (Signa; General Electric Co., Milwaukee, WI, and Magnetom; Siemens, Iselin, NJ). Unenhanced T1-weighted (600–800/16–20 [TR/TE], two excitations) and dual-echo T2-weighted (2500/22–90 [TR/TE], one excitation) spin-echo (SE) images were obtained first. Each patient then received 0.1 mmol of gadopentetate dimeglumine (Magnevist; Berlex Imaging, Wayne, NJ) per kilogram body weight, and T1-weighted images were obtained again. Technical parameters included a slice thickness of 5 mm with a 2-mm interslice gap, a 192 × 256 matrix, and a 22-cm field of view. For the unenhanced part of the study, sagittal (T1-weighted) and axial (dual-echo) planes were used. For contrast-enhanced images, the axial plane was used, with supplementary planes in selected instances.

Unenhanced and contrast-enhanced images were viewed together for the detection of lesions by two radiologists. Findings were classified into one or more of three categories: normal, mass or focal (well-defined margins) lesions, or white matter disease. Focal or mass lesions were scored as 1, 2, 3, 4, or ≥ 5. Lesion conspicuity on the unenhanced and enhanced images was compared. The ventricular enlargement was graded subjectively (0 = normal, 1 = mild, 2 = moderate, 3 = severe). Available medical records and laboratory data of the patients were reviewed.

Results

Of the 63 MR studies reviewed, 39 (62%) showed abnormal findings. Three scans were entered into both abnormal categories of focal/mass lesion and white matter disease. In no case did findings that were considered normal before the administration of gadopentetate dimeglumine become abnormal after administration of the contrast agent. Seventeen studies showed 51 focal or mass lesions on T2-weighted images. Corresponding contrast-enhanced T1-weighted images showed enhancement in 25 of these.

The focal or mass lesions were either isointense or of low signal on T1-weighted images; on T2-weighted images, all had high signal, with the exception of two lymphoma cases, which were of low signal intensity.

Of the 17 studies that showed focal abnormalities, biopsies were performed of six lesions. Histologic examination showed lymphoma in four cases and the presence of *Coccidioides* in one case. In the other case, the findings were nondiagnostic (necrotic and inflammatory cells, no yeast or fungus). A presumptive diagnosis of toxoplasmosis was made in five additional patients on the basis of MR findings and empiric response to treatment. The parameters used to determine treatment response included lesion regression on follow-up MR studies as well as clinical improvement. As specified in the Subjects and Methods section, routine follow-up studies were not considered as additional studies. One of the patients with toxoplasmosis initially responded to empiric therapy and then 6 months later had new neurologic signs and symptoms while still receiving antitoxoplasmosis therapy. A large recurrent mass lesion was detected in the left thalamus, where previously lesion regression had occurred (no corticosteroids had been administered). Histologic examination showed lymphoma. We believe this represents two pathologic processes occurring in the same anatomic location (Fig. 1). Analysis of CSF confirmed cryptococcal meningitis in two patients. In none of our patients, including our two cases of cryptococcal meningitis, was meningeal enhancement seen. In the remaining four patients, a neurologic diagnosis was not established either because the workup was deferred because of more acute medical problems or because the patient was not available for further follow-up.

Although no study was considered abnormal solely on the basis of findings seen on enhanced images, in two cases a single additional mass or focal lesion was detected on contrast-enhanced images only and not seen on T2-weighted images. In both of these cases, however, multiple lesions were seen on the T2-weighted images. The additional findings on the contrast-enhanced images did not affect the treatment of these patients.

In only one case could the diagnostic impression and treatment of the patient have been altered because of a finding that was seen on contrast-enhanced images only. This patient initially had more than five mass lesions. Subtle subependymal enhancement was detected on contrast-enhanced images. The patient subsequently underwent an empiric trial of antitoxoplasmoid therapy. Follow-up imaging 1 week after therapy was initiated showed lesion progression and more obvious subependymal enhancement (Fig. 2). Because of the constellation of findings on the serial studies, a biopsy was performed, which showed lymphoma.

White matter disease was the most common abnormality detected. Eleven studies demonstrated a diffuse white matter pallor with predominant involvement in the centrum semiovale (Fig. 3). Fifteen scans showed patchy areas of high signal in the deep white matter on T2-weighted images, most commonly in a periventricular distribution. None of these described areas of signal alteration in the white matter showed enhancement after the administration of contrast material. Of the 35 cases of ventriculomegaly, the group of patients with white matter disease had the highest occurrence. Sixty-nine percent (18/26) of the studies showing white matter disease also showed ventriculomegaly, compared with 45% (11/24) of those with normal scans and 41% (7/17) of those showing focal lesions. In addition, the patients with white matter disease had the highest grades of ventriculomegaly. As specified in the Subjects and Methods section, we graded ventricular size as normal or as mild, moderate, or severe enlargement. All but one of the patients who had moderate or severe hydrocephalus had white matter disease.

Discussion

Our referral base includes a community with one of the highest prevalences of AIDS cases per capita in California (Office of AIDS, Epidemiology and Research Section, Department of Health Services for California, personal communication). Because of this, it is assumed that our population is representative of AIDS patients who typically first present with nonspecific neurologic symptoms. Although our experience was limited to 51 patients (63 studies), a typical spectrum of CNS disease, ranging from neoplasms to opportunistic infectious processes, including direct infection by HIV-1, was seen. Our study reemphasizes the superior sensitivity of T2-weighted images for showing pathologic changes. Patients with no abnormal findings on unenhanced T2-weighted images also had no abnormal findings on contrast-enhanced T1-weighted images. In addition, twice as many mass or focal lesions were detected on T2-weighted images than on contrast-enhanced images.

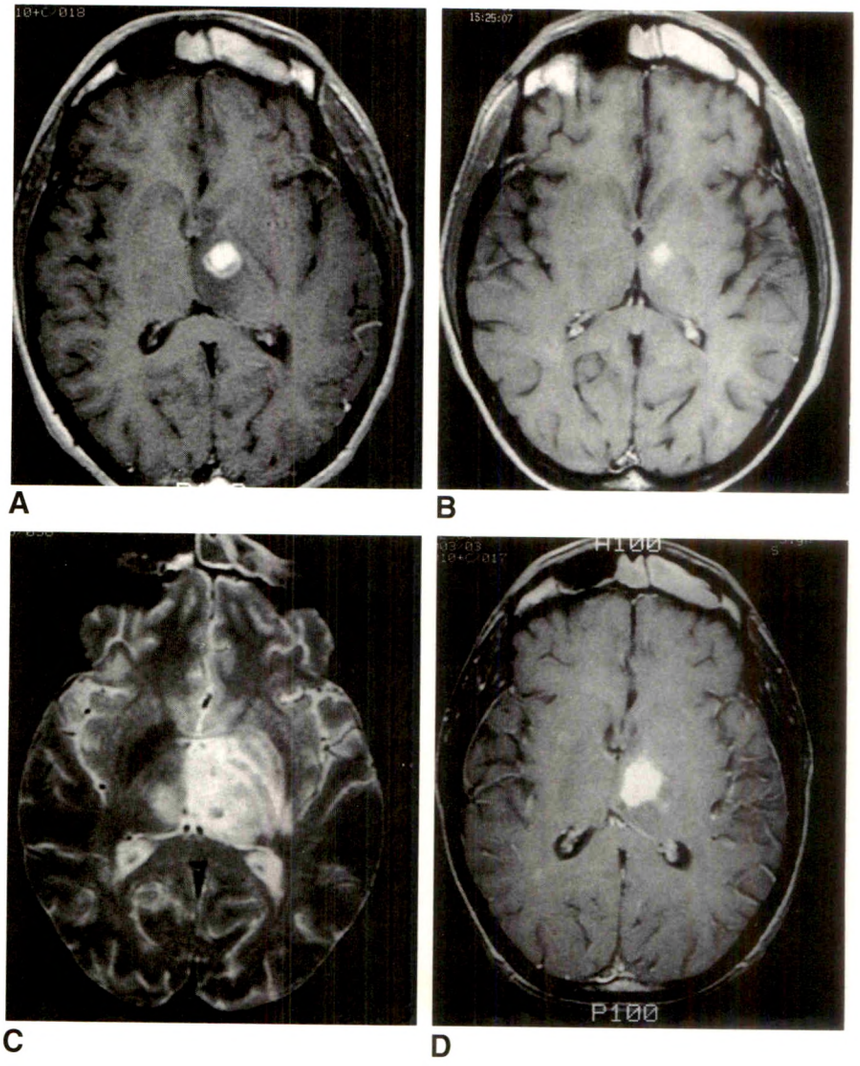

Fig. 1.—37-year-old man with AIDS who had headache and fever.

***A*, Axial T1-weighted (600/20) SE MR image with contrast material shows enhancing mass lesion in left thalamus. This lesion was well seen on T2-weighted MR image (*not shown*). Three smaller brain lesions were also seen on T2-weighted images, two of which showed enhancement after administration of contrast material.**

***B*, Axial contrast-enhanced T1-weighted (600/20) SE MR image obtained 2 weeks after institution of therapy for presumed toxoplasmosis shows lesion regression with a small residual focus of enhancement in left thalamus. Left thalamic lesion, as well as three smaller lesions, showed regression on T2-weighted image also (*not shown*).**

***C*, Axial unenhanced T2-weighted (2500/90) SE MR image obtained approximately 6 months after institution of antitoxoplasmoid therapy shows abnormal high signal in left thalamus extending into left internal capsule and globus pallidus. Additional lesion is seen in right thalamus.**

***D*, Axial T1-weighted (600/20) SE MR image with contrast material shows marked enhancement of left thalamic lesion. Lesion in right thalamus is not seen. Biopsy of lesion in left thalamus showed lymphoma.**

Toxoplasmosis and lymphoma are the two most common pathologic processes causing mass lesions of the CNS in patients with AIDS [6, 7]. Because of disparate clinical management, it is beneficial to be able to distinguish these two entities on MR images. However, many studies have shown that the patterns of contrast enhancement in these two processes are nonspecific and therefore cannot be relied on for their differentiation [2, 6–9]. Our patients also showed a variety of nonspecific enhancement patterns.

Ciricillo and Rosenblum [7] found that 71% of solitary mass lesions seen on MR images in AIDS patients were lymphomas. The detection of an additional lesion significantly alters the diagnostic impression, as toxoplasmosis then comes into stronger consideration. Our study suggests that a second lesion is more likely to be detected on T2-weighted MR images. Twice as many abnormalities in the category of focal or mass lesions were detected on unenhanced T2-weighted images than on contrast-enhanced T1-weighted images. In addition, T2-weighted images can be used to suggest lymphoma because of the relatively low signal intensity of the lesion [6].

However, in some situations, administration of contrast material might be helpful. The presence of subependymal enhancement is significant, as in our patient with multiple mass lesions. Thirty-eight percent of AIDS-related lymphomas are reported to show subependymal enhancement [6]. Because subependymal enhancement is rarely seen in toxoplasmosis, when present it suggests lymphoma [6].

Contrast-enhanced images can be useful for biopsy localization. Although gadopentetate dimeglumine is specific for areas of breakdown of the blood-brain barrier, not necessarily tumor sites, it can be useful for determining which area most likely will provide a satisfactory biopsy specimen. In AIDS patients with multiple lesions, it is particularly important to define the biopsy site, as disparate pathologic processes can coexist in this setting.

Absence of contrast enhancement can also help further characterize a lesion. A nonenhancing focal white matter lesion without mass effect suggests progressive multifocal leukoencephalopathy. Lack of enhancement in a mass lesion is reported to virtually exclude lymphoma [6]. Yet, one of our four biopsy-proved lymphomas did not show enhancement (Fig. 4).

In none of our patients, including those with proved cryptococcal meningitis, was meningeal enhancement seen. Earlier studies [10–13] reported that meningeal enhance-

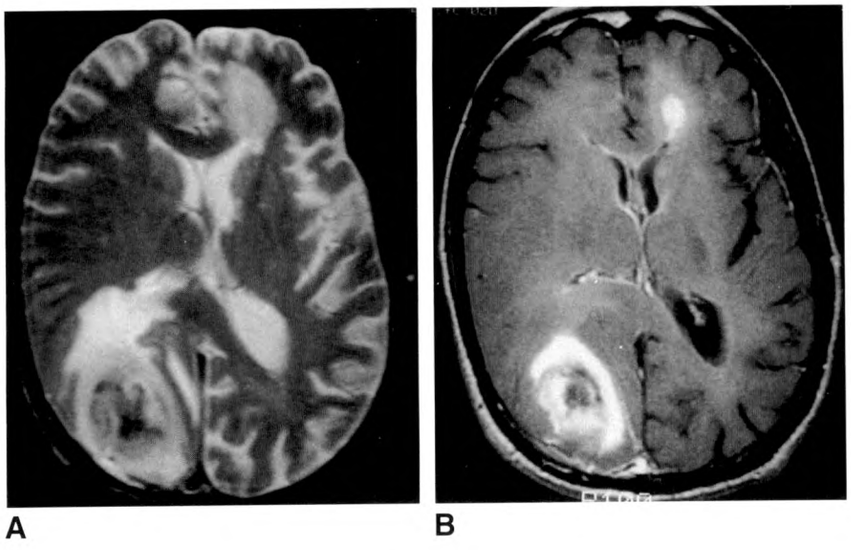

Fig. 2.—32-year-old man with AIDS who had sudden onset of confusion.

A, Axial unenhanced T2-weighted (2500/90) SE MR image shows a large mass lesion with central areas of low signal occupying right occipital lobe and a second lesion of increased signal in white matter of left frontal lobe.

B, Axial T1-weighted (600/20) SE MR image with contrast material shows heterogeneous enhancement of right occipital lesion and marked homogeneous enhancement of lesion in left frontal lobe. Subtle diffuse subependymal enhancement is also present. Biopsy of right occipital lesion showed lymphoma.

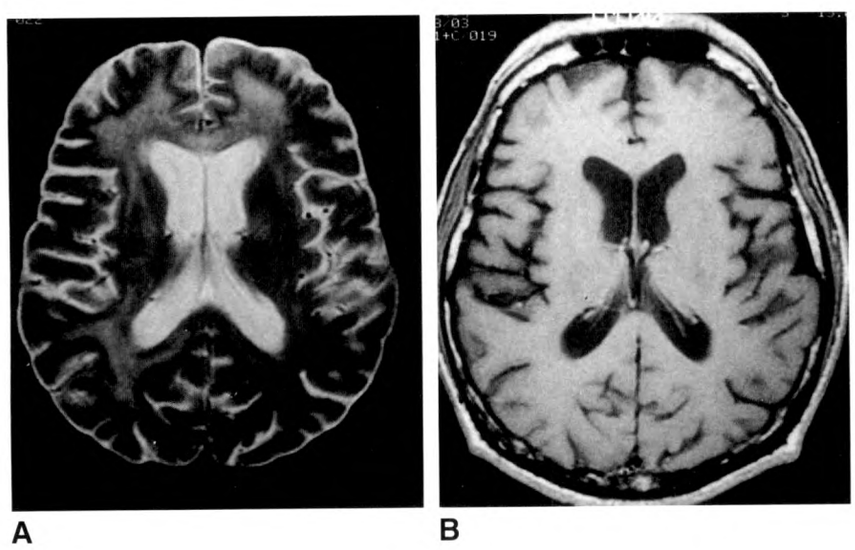

Fig. 3.—52-year-old man with AIDS who had a clinical diagnosis of AIDS dementia complex.

A, Axial unenhanced T2-weighted (2500/90) SE MR image shows diffuse high signal within periventricular white matter that extended into centrum semiovale.

B, Axial contrast-enhanced T1-weighted (600/20) SE MR image at corresponding level shows no abnormality other than moderate (grade 2) ventriculomegaly.

ment is rare in patients with AIDS because of the host's inability to mount a normal immune response. In this setting, the neurologic signs and symptoms are nonspecific, and MR imaging is generally performed to exclude other pathologic processes. The diagnosis of meningitis is based on the results of CSF analysis. Furthermore, our patients with cryptococcal meningitis had characteristic nonenhancing foci without mass effect in the region of the basal ganglia, best seen on T2-weighted images (Fig. 5). As previously reported [13, 14], these foci represent cystic collections of the cryptococcal organisms in the perivascular spaces of the perforating arteries. The contrast-enhanced images did not contribute to the diagnosis in these patients.

The AIDS dementia complex affects more than 30% of patients with AIDS [15]. Findings seen on MR images are nonspecific and consist of atrophy or diffuse white matter disease or both [16–19]. MR imaging is relatively insensitive in the detection of microglial nodules associated with direct HIV-1 infection [16, 17]. We have no histologic verification of intracranial HIV infection in our patients in whom these MR findings were described. None of these areas of signal alteration in the white matter showed enhancement after administration of contrast material.

In conclusion, our study does not support the routine use of gadopentetate dimeglumine for MR imaging of the brain in patients with AIDS. Our experience emphasizes the importance of a normal T2-weighted image. If the findings are abnormal on the T2-weighted image, then contrast material can help to further characterize a lesion, determine the best site for biopsy, or show subependymal spread. The limited diagnostic benefits obtained from gadopentetate dimeglumine–enhanced MR imaging of the brain in patients with AIDS do not appear to justify the routine use of the contrast material.

ACKNOWLEDGMENTS

We thank Marguerite T. Parisi for editorial assistance, Melody Anthony for data collaboration, and Janet Arnds for manuscript preparation.

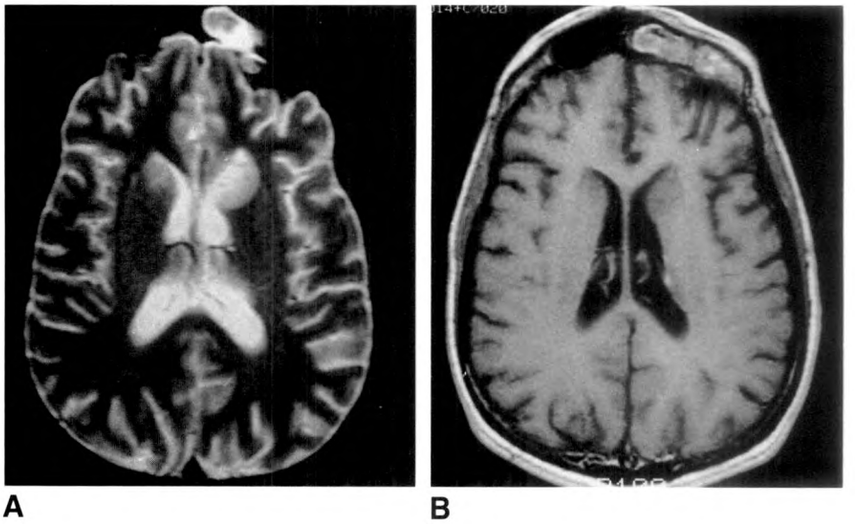

Fig. 4.—29-year-old man with AIDS who had alteration in mental status.

***A*, Axial unenhanced T2-weighted (2500/90) SE MR image shows high signal in heads of both caudate nuclei, left greater than right.**

***B*, Axial T1-weighted (600/20) SE MR image with contrast material shows no enhancement of lesions in caudate nuclei. Subtle enhancement is seen in a third lesion occupying body of left caudate nucleus; lesion was also detected on unenhanced T1-weighted MR image (*not shown*). Biopsy of lesion in head of left caudate nucleus showed lymphoma.**

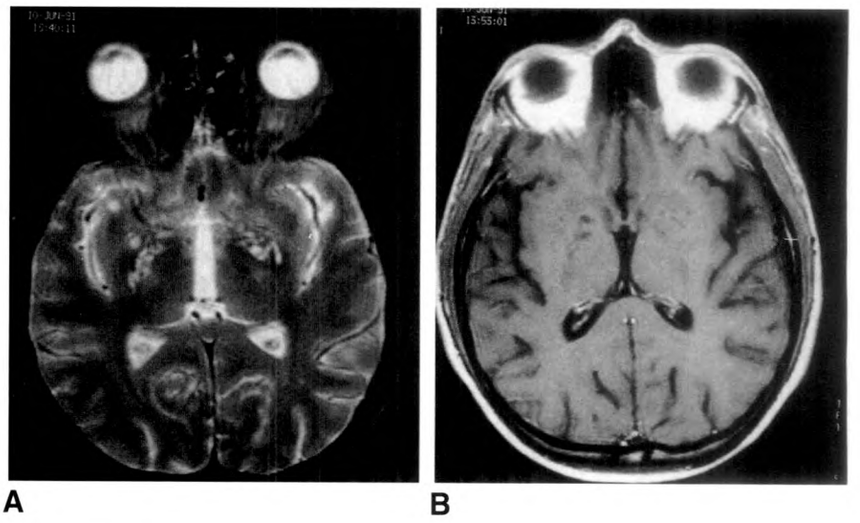

Fig. 5.—45-year-old man with AIDS who had cryptococcal meningitis.

***A*, Axial unenhanced T2-weighted (2500/90) SE MR image shows clustered hyperintense foci mainly within basal ganglia bilaterally, representing dilated Virchow-Robin spaces. A similar lesion is seen in anterior aspect of right insula.**

***B*, Axial T1-weighted (800/20) MR image with contrast material shows no evidence of lesion enhancement.**

REFERENCES

1. Centers for Disease Control. The HIV/AIDS epidemic: the first 10 years. *MMWR Morb Mortal Wkly Rep* **1991**;40:357–365
2. Levy RM, Rosenbloom S, Perrett LV. Neuroradiologic findings in AIDS: review of 200 cases. *AJNR* **1986**;7:833–839
3. Davis PC, Hudgins PA, Peterman SB, Hoffman JC Jr. Diagnosis of cerebral metastases: double-dose delayed CT vs contrast-enhanced MR imaging. *AJNR* **1991**;12:293–300
4. Hesselink JR, Healy ME, Press GA, Brahme FJ. Benefits of Gd-DTPA for MR imaging of intracranial abnormalities. *J Comput Assist Tomogr* **1988**;12:266–274
5. Russell EJ, Geremia GK, Johnson CE, et al. Multiple cerebral metastases: detectability with Gd-DTPA–enhanced MR imaging. *Radiology* **1987**;165:609–617
6. Dina TS. Primary central nervous system lymphoma versus toxoplasmosis in AIDS. *Radiology* **1991**;179:823–828
7. Ciricillo SF, Rosenblum ML. Use of CT and MR imaging to distinguish intracranial lesions and to define the need for biopsy in AIDS patients. *J Neurosurg* **1990**;73:720–724
8. Balakrishnan J, Becker PS, Kumar AJ, Zinreich SJ, McArthur JC, Bryan RN. Acquired immuno-deficiency syndrome: correlation of radiologic and pathologic findings in the brain. *RadioGraphics* **1990**;10:201–215
9. Rodesch G, Parizel PM, Farber CM, et al. Nervous system manifestations and neuroradiologic findings in acquired immunodeficiency syndrome (AIDS). *Neuroradiology* **1989**;31:33–39
10. Jarvik JG, Hesselink JR, Kennedy C, et al. Acquired immunodeficiency syndrome: magnetic resonance patterns of brain involvement with pathologic correlation. *Arch Neurol* **1988**;45:731–736
11. Ramsey RG, Geremia GK. CNS complications of AIDS: CT and MR findings. *AJR* **1988**;151:449–454
12. Sze G, Brant-Zawadzki M, Norman D, Newton TH. The neuroradiology of AIDS. *Semin Roentgenol* **1987**;22:42–53
13. Tien RD, Chu PK, Hesselink JR, Duberg A, Wiley C. Intracranial cryptococcosis in immunocompromised patients: CT and MR findings in 29 cases. *AJR* **1991**;156:1245–1251
14. Wehn SM, Heinz ER, Burger PC, Bach O. Dilated Virchow-Robin spaces in cryptococcal meningitis associated with AIDS: CT and MR findings. *J Comput Assist Tomogr* **1989**;13:756–762
15. Kirkwood RJ. *Essentials of neuroimaging.* New York: Churchill-Livingstone, **1990**:284–288
16. Grafe MR, Press GA, Berthoty DP, Hesselink JR, Wiley CA. Abnormalities of the brain in AIDS patients: correlation of postmortem MR findings with neuropathology. *AJNR* **1990**;11:905–911
17. Post MJ, Berger JR, Quencer RM. Asymptomatic and neurologically symptomatic HIV-seropositive individuals: prospective evaluation with cranial MR imaging. *Radiology* **1991**;178:131–139
18. Flowers CH, Mafee MF, Crowell R, et al. Encephalopathy in AIDS patients: evaluation with MR imaging. *AJNR* **1990**;11:1235–1245
19. Olsen WL, Longo FM, Mills CM, Norman D. White matter disease in AIDS: findings at MR imaging. *Radiology* **1988**;169:446–448

More Nominal Dysphasia in Medical Nomenclature

Peter M. Ronai[1]

In ancient Rome, a *nomenclator* (Latin: *nomen* = name; *calare* = to announce or proclaim) was a slave who accompanied his master, identifying—and announcing the names of—the people they met, especially during political campaigns [1]. This eventually led to our word *nomenclature*, meaning a classified system of names. In the preceding vignette [2], I gave a dozen examples of common errors in medical nomenclature. Another 11 examples follow.

Succinturiate lobe. The Roman military unit of 100 soldiers was commanded by a centurion (Latin: *centurio* = commander of 100 men). The officer, who substituted for the centurion when the latter was unavailable or indisposed, was the *succenturio* (Latin: *sub* = under; *centurio* = centurion). Succenturiate (not "succinturiate") therefore came to mean a substitute and then an accessory, as in the succenturiate lobe of the placenta. It is not related to *succinct* (Latin: *sub* = under; *cingere* = to gird or cinch), meaning "brief, concise."

Osteochondritis dessicans. This disorder of joints, in which fragmentation of articular cartilage and bone occurs, is correctly termed osteochondritis *dissecans* [3] from the Latin: *dissecare* = to cut into pieces. (Some authors prefer *osteochondrosis* dissecans [4], since this is not an inflammatory condition). Perhaps those authors who write "dessicans" believe that the condition results from a "drying out" of the cartilage. If so, they should write "desiccans" with one s and two c's (Latin: *desiccare* = to dry up completely). Nevertheless, the process of cartilaginous and osseous fragmentation requires the use of *dissecans.*

Decubitus film, as in "decubitus film of the abdomen," is almost always used incorrectly. *Decubitus* comes from the Latin: *decumbere* = to lie down; hence a decubitus film means simply a film taken with the patient lying down. What is usually meant is a "lateral decubitus film," taken with the patient lying on his or her side. Even this is not specific enough, since this film could be taken with horizontal, vertical, or angled beam. A horizontal beam, left lateral decubitus view of the abdomen leaves no room for confusion.

Saggital sections. The Latin for *arrow* is *sagitta* (with one g and two t's). The old anatomists considered the midline suture of the calvaria (for calvaria, see [2]) to be arrowlike, and named it the sagittal suture. Accordingly, the midline plane of the body became the sagittal plane. Strictly speaking, there is only one sagittal plane: the (median) plane that passes through the sagittal suture, dividing the body into two equal halves [5]. Sections in any plane parallel to the sagittal plane used to be called parasagittal sections [5] (Latin: *para* = beside), but most authorities now accept sagittal as including the planes parallel to the median plane.

Adnexae. The Latin word for *appendage* is *adnexus.* This is a fourth-declension noun whose plural is *adnexa*, not *adnexae* [6]. The adnexa uteri or appendages of the uterus are therefore the tubes and ovaries [5]. *Adnexa* is sometimes misused to refer to the regions of the pelvis where the tubes and ovaries reside, namely, the regions lateral to the uterus. The etymology does not support this meaning.

Viable, as in "viable fetus," has a very specific and medicolegally important meaning: a fetus that has developed sufficiently within the uterus to be able to live and continue normal development outside the uterus [7]. "Single, intrauterine viable fetus at 16 weeks' gestational age" clearly represents a misuse of the term *viable*, yet statements like this are frequently seen in sonography reports and even sometimes in the radiologic literature. *Living* should be used instead of *viable.*

Fetus also has a very specific meaning: it is restricted in humans to the developing offspring from the end of the second month of pregnancy until birth [7]. Before the end of the second month, the term embryo should be used [7]. "Single intrauterine fetus at 8 weeks' gestational age," "6-week gestational sac containing a fetal pole," and "fetal cardiac motion is usually evident by 6 weeks" all are examples of incorrect use of *fetus.* Embryo (or embryonic) should be used whenever the gestational age is 8 weeks or less.

Left mainstem bronchus. The correct nomenclature is *left main bronchus* [7]. *Left mainstem bronchus* is not in the mainstream of medical nomenclature, although recently one author thought that it should be, and called it the "left *mainstream* bronchus."

Nucular medicine, radioisotope, radionucleotide. The pronunciation "nucular" instead of "new-cle-ar" is not the only problem with nuclear nomenclature. Although common in the radiologic literature, the word *radioisotope*, as in "the radioisotope iodine-131," is reminiscent of the sound of one hand clapping. Isotopes (Greek: *isos* = equal; *topos* = place) are *two or more* nuclear species that have the same atomic number and therefore are in the same place in the periodic table. If they also happen to be radioactive, they are called *radio*isotopes. Iodine-125 and iodine-131 are radioisotopes—two radioactive nuclear species in the same place in the periodic table. Iodine-131, when considered in isolation, is a radionuclide (i.e., a nuclear species—or nuclide—that is radioactive). When iodine-131 is attached to a pharmaceutical product such as Hippuran (sodium *ortho*-iodohippurate), the combination is called a radiopharmaceutical. If it were attached to a nucleotide (purine or pyrimidine base-sugar-phosphate), the combination would be called a radionucleotide. It is amazing how many physicians say "radionucleotide" when they mean "radionuclide."

When authors exercise care in writing about their work and pay careful attention to correct nomenclature, readers will have confidence that equal care was used in carrying out the work described.

REFERENCES

1. *The new collegiate Latin and English dictionary.* New York: Bantam, **1966**:195
2. Ronai PM. Pitfalls in medical writing: nominal dysphasia. *AJR* **1992**;159:1198
3. Resnick D, Niwayama G. *Diagnosis of bone and joint disorders.* Philadelphia: Saunders, **1981**:2257
4. Greenfield G. *Radiology of bone diseases*, 4th ed. London: Lippincott, **1986**:203
5. *Butterworth's medical dictionary*, 2nd ed. London: Butterworth, **1978**:54, 1251, 1497
6. *Oxford Latin dictionary.* London: Oxford University Press, **1984**:51
7. *Stedman's medical dictionary*, 15th ed. Baltimore: Williams and Wilkins, **1990**:214, 501, 573, 1714

[1]Department of Imaging, Salem Hospital, P. O. Box 14001, Salem OR 97309.

Editor's note.—This is one of a series of vignettes, which will appear periodically in *AJR*, examining some of the common pitfalls of medical writing. The intent is to help authors communicate their observations and discoveries clearly and in accordance with accepted grammatical style.

AJR **1993;160:158** 0361–803X/93/1601–0158

Pictorial Essay

Neurofibromatosis: MR Imaging Findings Involving the Head and Spine

Hui Hua Shu,[1,2] Scott A. Mirowitz,[3] and Franz J. Wippold II[1]

MR imaging can be used to identify abnormalities of the head and spine in patients with neurofibromatosis. In this pictorial essay, we illustrate the craniospinal MR imaging findings in a large series of patients with neurofibromatosis.

The neurofibromatoses, currently recognized as two distinct genetic disorders, are the most common of the neurocutaneous syndromes. Although these disorders have multisystem organ involvement, craniospinal manifestations predominate. Criteria for the diagnosis of neurofibromatosis-1 (NF-1) and neurofibromatosis-2 (NF-2) have been proposed by the National Institutes of Health (NIH) Consensus Development Conference. NF-1 is the most common type, affecting 1/4000 persons. Fifty percent of cases of NF-1 result from spontaneous mutation; the remaining cases are transmitted by autosomal dominant inheritance. The gene for NF-1 has been localized to chromosome 17. Among its variable manifestations are café-au-lait macules, neurofibromas, plexiform neurofibromas, axillary or inguinal freckling, optic gliomas, Lisch nodules (iris hamartomas), and distinc-

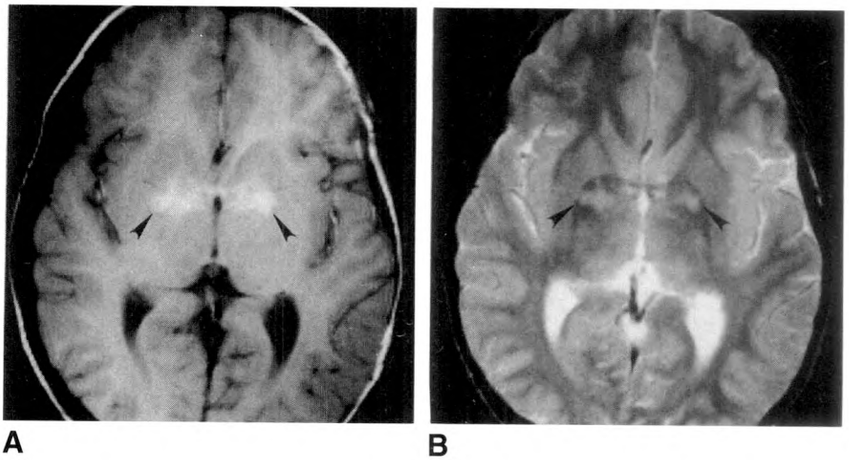

Fig. 1.—MR imaging findings in an 11-year-old boy with neurofibromatosis.
***A*, Axial T1-weighted (750/21) image shows bilaterally symmetric nodular regions of increased signal intensity in globi pallidi (*arrowheads*).**
***B*, Axial T2-weighted (3200/90) image shows focal nodular regions of increased signal intensity (*arrowheads*), which are somewhat more limited in extent than is apparent on T1-weighted image.**

Received February 27, 1992; accepted after revision June 15, 1992.
[1]Mallinckrodt Institute of Radiology, Washington University School of Medicine, 510 S. Kingshighway Blvd., St. Louis, MO 63110.
[2]Present address: Ernst Radiology Clinic, Inc., 3450 Bridgeland Dr., Suite C, Bridgetown, MO 63044.
[3]Department of Radiology, Jewish Hospital of St. Louis, Washington University School of Medicine, 216 S. Kingshighway Blvd., St. Louis, MO 63110. Address reprint requests to S. A. Mirowitz.

***AJR* 1993;160:159–164** 0361–803X/93/1601–0159

tive osseous lesions or dysplasias [1]. The second distinct disorder, NF-2, is less common and occurs in 1/50,000 persons. Its gene is located on chromosome 22 and it too is transmitted through autosomal dominant inheritance. Characteristic manifestations include eighth nerve tumors or schwannomas, other intracranial and intraspinal tumors such as neurinomas of other cranial nerves, and meningioma.

We reviewed 171 MR examinations done in a 5-year period in 85 patients with clinically documented neurofibromatosis. The patients were either symptomatic for the body part imaged or the examinations were performed as a follow-up for previously documented disease. Thirty-nine males and 46 females between 3 months and 73 years old (mean age, 20 years) were included. One hundred seven cranial MR examinations were performed in 70 patients, and 64 spinal studies were performed in 29 patients. The latter involved the cervical region in 25 patients, the thoracic region in 14, and the lumbar region in 25. Examinations were performed on Siemens Magnetom units operating at various field strengths (0.3–1.5 T). Standard T1-weighted, spin density–weighted, and T2-weighted spin-echo sequences were used. Gadopentetate dimeglumine (0.1 mmol/kg Magnevist; Berlex, Wayne, NJ) was administered IV during the course of 47 examinations (35 brain, 12 spine). Contrast material was used in all symptomatic patients and in follow-up examination of all patients who were more than 2 years old after July 1988. Serial examinations (two to six) were available in 32 patients (22 brain, 10 spine).

Cranial Examinations

Cranial MR examinations revealed abnormalities in 66 (94%) of the 70 patients. Multifocal lesions were present in most (48/66 patients; 73%). The most frequently seen abnormalities (30/70 patients; 43%) were focal areas of homogeneously increased signal intensity on T1- and/or T2-weighted images without associated mass effect, most often encountered in the basal ganglia. Contrast material was administered to 16 patients with such lesions; no abnormal contrast enhancement was observed. Signal intensity on T2-weighted images was increased in all 30 patients with these lesions, and in 10 of these patients, significant hyperintensity was present on T1-weighted images also (Figs. 1 and 2). Although the precise nature of these signal abnormalities is unknown, they are presumed to represent hamartomas containing cellular constituents such as glial tissue, Schwann cells, and melanocytes [2]. The last two tissues may be responsible for the observed T1 shortening, which was primarily seen with the basal ganglial lesions [3]. Although these lesions exhibited apparently benign features, with no evidence of progression on limited follow-up examinations in this series (serial examinations in seven patients: range,

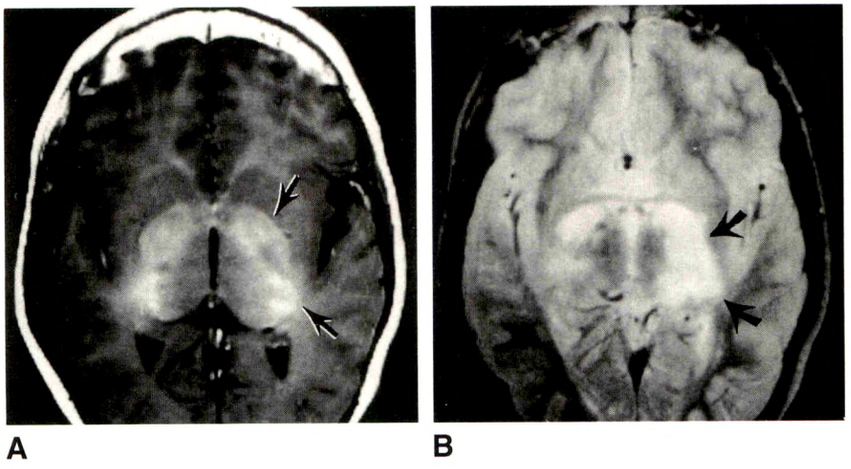

Fig. 2.—MR imaging findings in 8-year-old boy with neurofibromatosis.

***A* and *B*, Contrast-enhanced T1-weighted (750/20, *A*) and unenhanced T2-weighted (2500/90, *B*) images show diffusely increased signal intensity (*arrows*) in globi pallidi, posterior limbs of internal capsule, and posterolateral thalami. Distribution of signal abnormalities is different on T1- and T2-weighted images.**

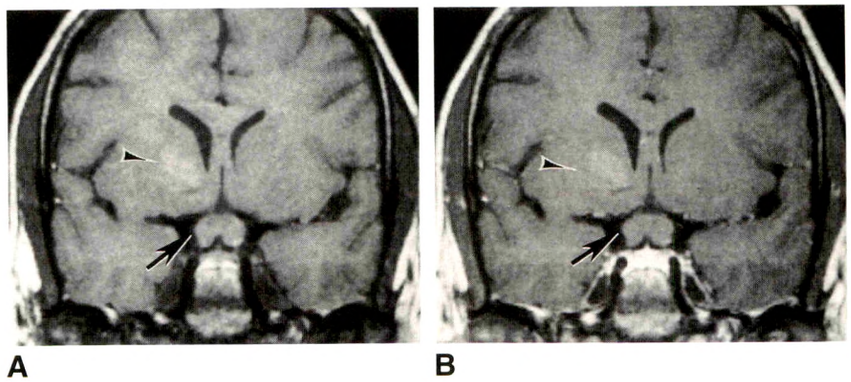

Fig. 3.—MR imaging findings in 15-year-old girl with optic glioma.

***A* and *B*, Coronal T1-weighted (750/21) images obtained before (*A*) and after (*B*) contrast enhancement show enlargement of optic chiasm and optic nerves without abnormal contrast enhancement (*arrows*), owing to presumed optic glioma. Signal intensity in right basal ganglia (*arrowheads*) is mildly increased.**

two–six examinations, mean, three), longitudinal examination of a larger number of patients is needed to exclude a low-grade malignant tumor or premalignant lesion.

The next most frequently seen abnormalities were gliomas of the optic system, which were present in 21 (30%) of 70 patients. MR imaging in these patients was prompted by visual symptoms or headaches. The optic chiasm was involved most often (19 patients), with optic nerve and optic tract involvement in 16 and six patients, respectively [4] (Figs. 3 and 4). Results of surgical biopsies were not available because these lesions were usually treated nonsurgically. These lesions had variable contrast enhancement. Other orbital lesions included neurofibromata, schwannomas (Figs. 5 and 6), and buphthalmos (Fig. 7) in two patients each. The orbital neurofibromata and schwannomas were proved surgically. Dural ectasia affecting the optic nerve was present in one patient. Complex masses were present in the hypothalamic/suprasellar region in four patients. One patient underwent open biopsy, the results of which revealed a glial neoplasm (Fig. 8).

Plexiform neurofibromata, most often infiltrated in or around the orbits or skull base, were present in nine patients (Fig. 9). This diagnosis was proved surgically in five patients. One patient had a largely extracranial neurofibrosarcoma. Additional cutaneous or bony lesions included subcutaneous neurofibromata in seven patients (Fig. 10), cranial bony dysplasia (three sphenoid, two parietal, one frontal) in six patients (Fig. 7), and basilar impression in one patient. Cerebral atrophy was present in eight patients; temporal lobe enlargement was evident in one patient, and generalized macrocephaly in another.

Four patients had hydrocephalus, which was attributable to a mass in the third ventricle in one patient. Increased signal intensity in the periventricular white matter was seen on T2-weighted images in seven patients. Prominent CSF spaces or arachnoid cysts were present in five patients (Fig.

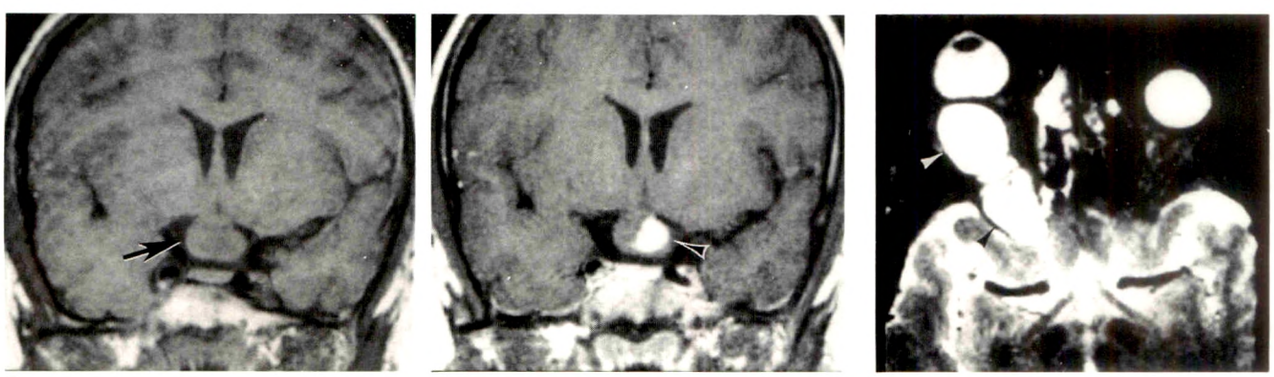

Fig. 4.—MR imaging findings in 7-year-old boy with glioma in optic chiasm.
***A* and *B*, Coronal T1-weighted (750/20) images obtained before (*A*) and after (*B*) contrast administration show a glioma (*arrow*) in optic chiasm. Intense contrast enhancement is present within central and left aspects of chiasmal mass (*arrowhead*).**

Fig. 5.—MR imaging findings in 47-year-old man with orbital neurofibroma. Axial T2-weighted (2800/90) image shows multilobular soft-tissue mass involving right optic nerve with markedly increased signal intensity and associated proptosis (*arrowheads*).

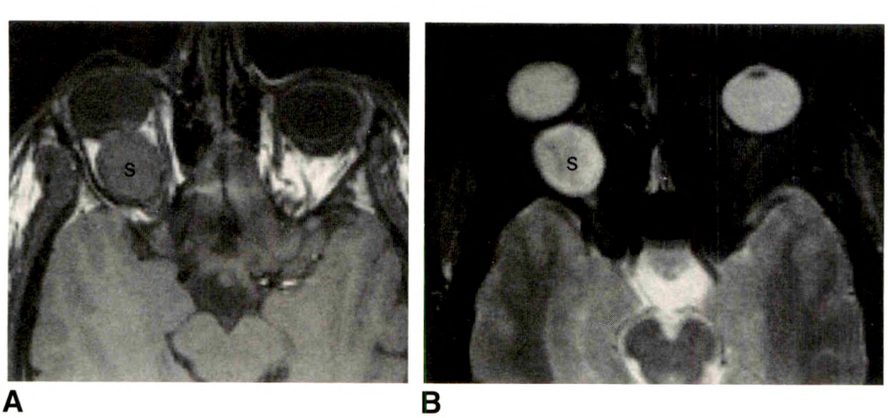

Fig. 6.—MR imaging findings in 18-year-old man with orbital schwannoma.
***A* and *B*, Axial T1-weighted (700/21, *A*) and T2-weighted (2500/90, *B*) images show a large orbital schwannoma (S) that displaces right optic nerve medially and superiorly and results in right-sided proptosis. Schwannoma was verified surgically.**

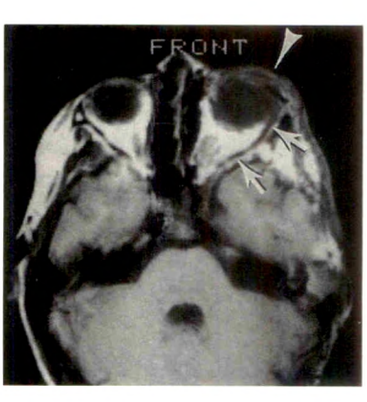

Fig. 7.—MR imaging findings in 11-year-old boy with buphthalmos. Axial T1-weighted (750/21) image shows left orbital buphthalmos (*arrowhead*) and dysplasia of left wing of sphenoid bone (*arrows*).

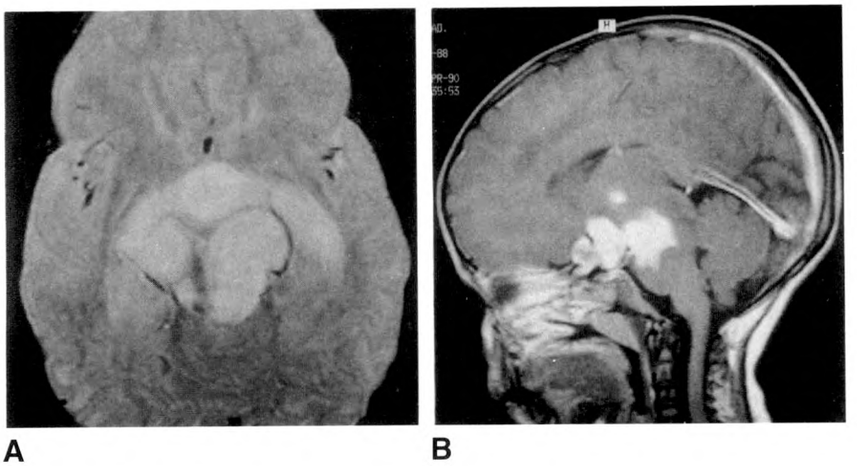

Fig. 8.—MR imaging findings in 2-year-old girl with family history of neurofibromatosis

A and B, Unenhanced axial T2-weighted (2400/90, *A*) and contrast enhanced sagittal T1-weighted (760/22, *B*) images show a primary glial neoplasm (surgically confirmed) that involves optic chiasm, optic tracts, optic pathways bilaterally, hypothalamus, cerebral peduncles, and upper pons.

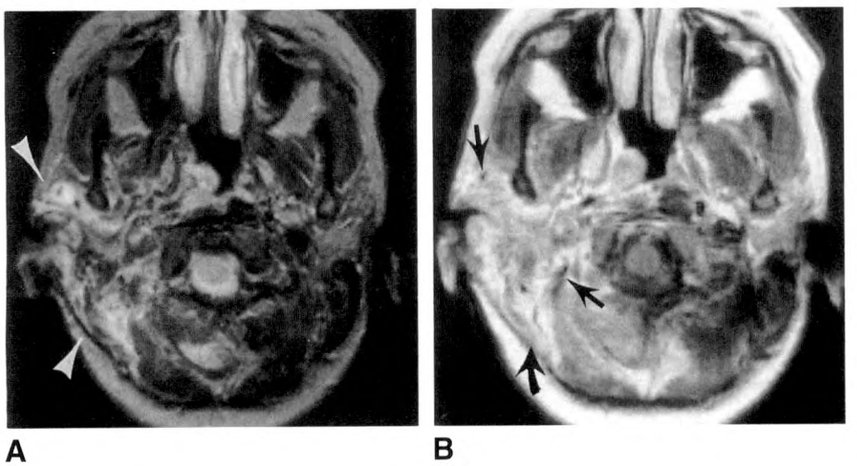

Fig. 9.—MR images of 23-year-old man with neurofibromatosis show a right-sided plexiform neurofibroma that infiltrates along base of right side of skull, involves portions of clivus and squamous portion of temporal bone, and encircles portions of C1 and C2 vertebral bodies.

A, On unenhanced axial T2-weighted (2200/90) image, mass shows heterogeneously increased signal (*arrowheads*).

B, Contrast-enhanced axial T1-weighted (750/20) image shows enhancement of mass (*arrows*). Tumor was less conspicuous on unenhanced T1-weighted images (*not shown*).

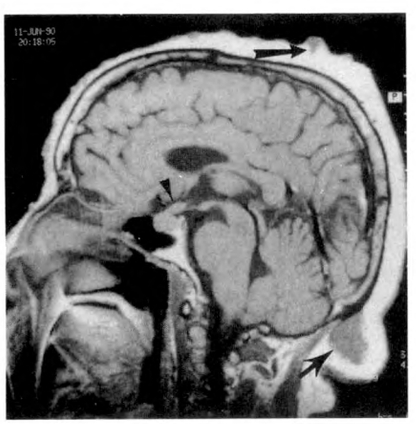

Fig. 10.—MR imaging findings in 70-year-old woman with neurofibromatosis. Sagittal T1-weighted (600/15) image shows multiple cutaneous and subcutaneous neurofibromata (*arrow*) located within scalp. Also optic chiasm is enlarged (*arrowhead*).

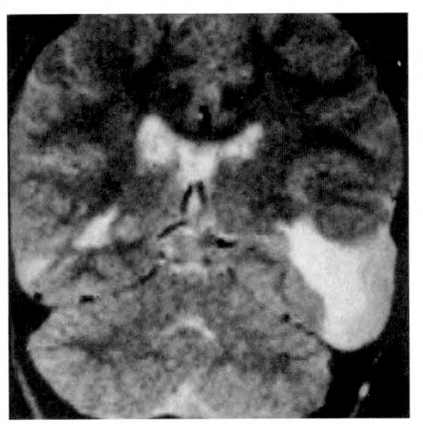

Fig. 11.—MR imaging findings in 8-year-old boy with neurofibromatosis. Coronal T2-weighted (2200/120) image shows a large arachnoid cyst lateral to left temporal lobe.

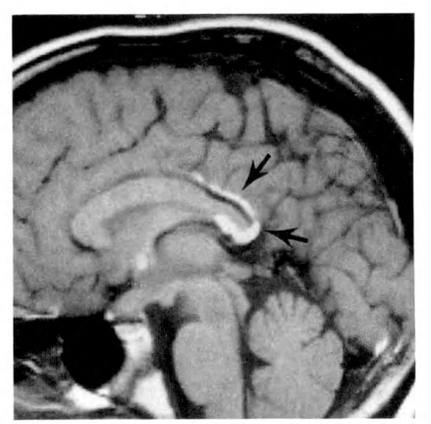

Fig. 12.—MR imaging findings in 15-year-old girl with neurofibromatosis. Sagittal T1-weighted (750/20) image shows hypoplasia of splenium of corpus callosum with an associated pericallosal lipoma (*arrows*).

11). Intracranial lipomas were present in two patients (Fig.12).

Lesions in the posterior fossa included bilateral acoustic schwannomas in three patients (Fig. 13), schwannomas involving cranial nerves V, IX, X, and XI in two patients (Fig. 14), dural ectasia affecting the internal auditory canals in two patients, cerebellar masses of undetermined origin in two patients (Fig. 15), epidermoid cyst in one patient, brainstem

gliomas in three patients, and meningioma in one patient (Fig. 14). The three patients with acoustic schwannomas were presumed to have NF-2, and the lesions were proved surgically. The remainder of the patients were presumed to have NF-1. The lesions of the eighth cranial nerve and the meningioma enhanced homogeneously, while enhancement in the cerebellar and brainstem lesions varied. The cerebellar masses had increased signal intensity on T2-weighted images and may have represented hamartomas or low-grade gliomatous lesions. No pathologic follow-up was available.

Spinal Examinations

MR examinations of the spine revealed abnormalities in 23 (79%) of 29 patients. Bony abnormalities included severe scoliosis in 10 patients (Fig. 16), kyphosis in two patients, and vertebral compression and basilar impression in one patient each. The scoliotic curve was acute and typically occurred in the thoracic region. Dural ectasia, with associated posterior vertebral scalloping, was present in seven patients (Fig. 17), and a lateral meningocele (Fig. 18) and a pseudomeningocele were present in one patient each.

Multiple neurofibromata involved the nerve roots in 10 patients (Fig. 19). These lesions enhanced after administration of contrast material and displayed the typical dumbbell shape on axial images (Figs. 19 and 20). Two patients had invasive neurofibrosarcomas. Plexiform neurofibromata involving the paraspinal regions and subcutaneous neurofibromata were seen in three and two patients, respectively.

An intraspinal lipoma and presumed astrocytoma were observed in one patient each, and nerve root clumping consistent with arachnoiditis was present in one patient.

Fig. 13.—MR imaging findings in 21-year-old deaf woman with neurofibromatosis-2. Large masses are present bilaterally in cerebellopontine angles and internal auditory canals.

***A* and *B*, Unenhanced (*A*) and contrast-enhanced (*B*) axial T1-weighted (750/20) images show that lesions, which represent surgically verified acoustic schwannomas, undergo homogeneous contrast enhancement and widen both internal auditory canals.**

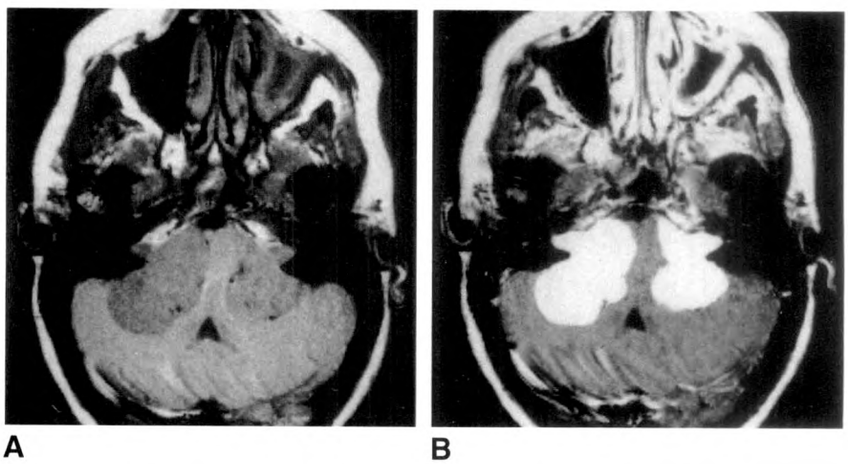

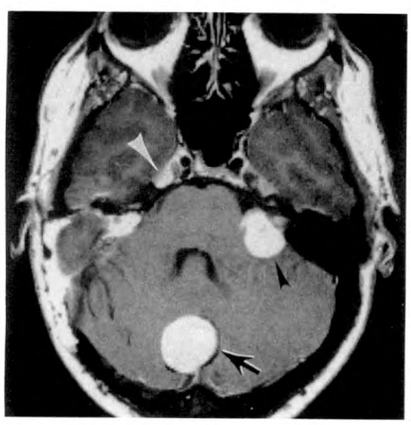

Fig. 14.—MR imaging findings in 19-year-old woman with neurofibromatosis-2. Contrast-enhanced axial T1-weighted (750/20) image shows homogeneously enhancing left-sided acoustic neuroma (*black arrowhead*) and midline posterior fossa meningioma (*arrow*). Patient had previously had a right-sided acoustic schwannoma resected, and recurrent tumor is now present. An enhancing trigeminal neuroma also is present in region of Meckel's cave on patient's right side (*white arrowhead*). All of these lesions were less conspicuous on unenhanced images (*not shown*).

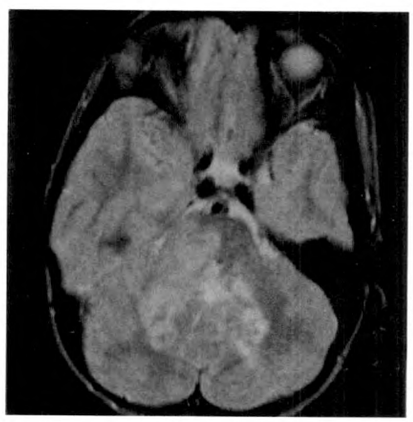

Fig. 15.— MR imaging findings in 2-year-old girl with neurofibromatosis. Axial T2-weighted (2400/900) image shows abnormally increased signal intensity in both cerebellar hemispheres extending into right aspect of pons. This represents either hamartoma or low-grade glioma. No significant change was noted when images were compared with images obtained 6 months earlier (*not shown*).

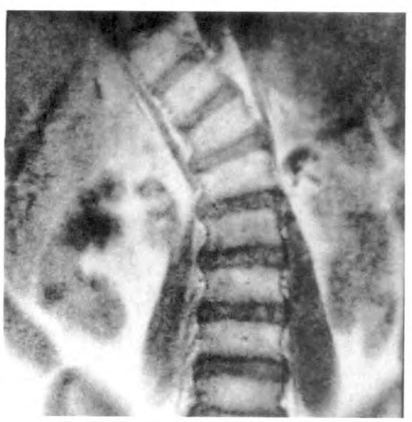

Fig. 16.—MR imaging findings in 9-year-old boy with neurofibromatosis and scoliosis. Acute levoscoliosis of thoracolumbar spine is shown on coronal T1-weighted (500/20) image.

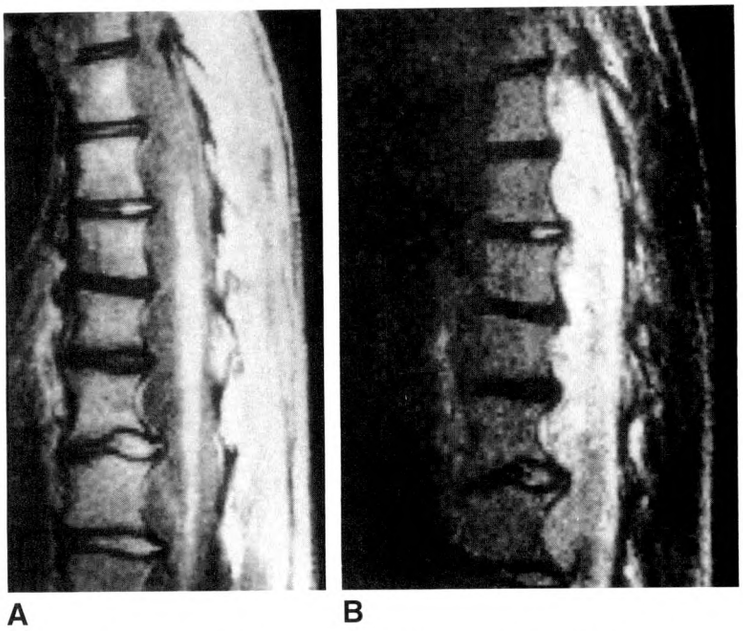

Fig. 17.—MR imaging findings in 16-year-old boy with dural ectasia.
A and *B*, Sagittal spin density–weighted (1700/35, *A*) and T2-weighted (1700/120, *B*) images show enlargement of CSF space and posterior vertebral scalloping throughout thoracic spine due to dural ectasia.

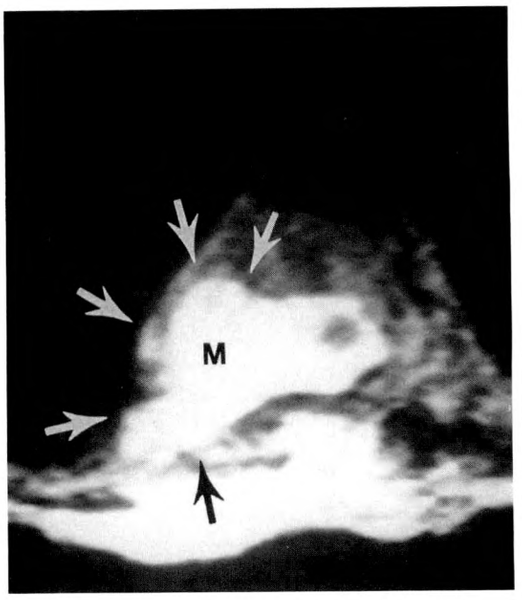

Fig. 18.—MR imaging findings in a 68-year-old woman with neurofibromatosis. Axial T2-weighted (2000/120) image shows scalloping of right pedicle (*arrows*) of thoracic vertebral body due to a lateral meningocele (M). This "mass" follows CSF signal intensity on T1-weighted and spin density–weighted images also.

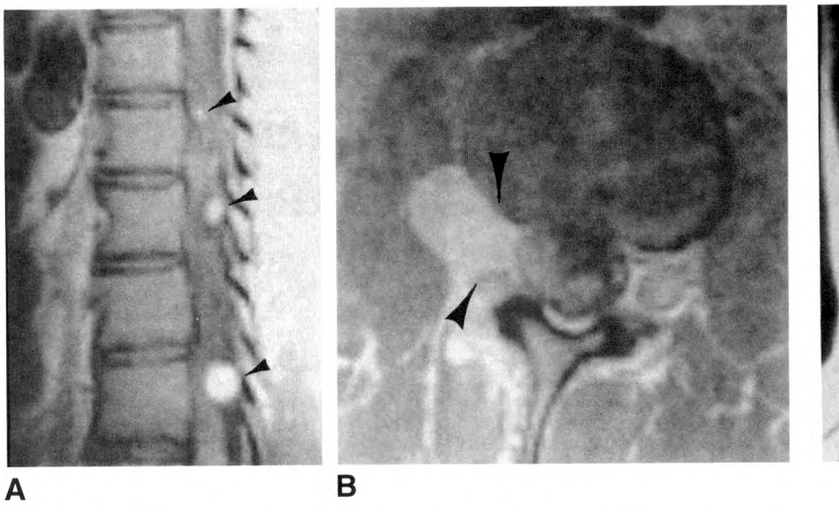

Fig. 19.—MR imaging findings in 19-year-old woman with neurofibromatosis-2.
A, Contrast-enhanced sagittal T1-weighted (820/15) image shows multiple enhancing intradural extramedullary masses adjacent to thoracic cord (*arrowheads*), representing neurofibromata.
B, Contrast-enhanced axial T1-weighted (720/15) image shows typical dumbbell-shaped enhancing mass extending through intervertebral neural foramina (*arrowheads*). These lesions were less conspicuous on corresponding unenhanced images (*not shown*).

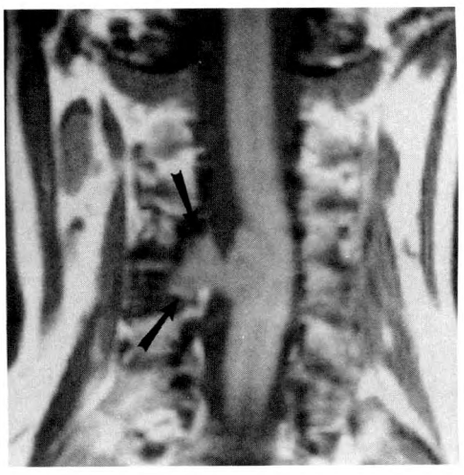

Fig. 20.—MR imaging findings in 40-year-old woman with neurofibromatosis. Coronal T1-weighted (500/20) image of cervical spine shows dumbbell-shaped nerve sheath tumor (*arrows*) with an intraspinal component displacing spinal cord and extending through intervertebral neural foramina.

REFERENCES

1. Riccardi VM. Von Recklinghausen neurofibromatosis. *N Engl J Med* **1981**;305:1617–1627
2. Hurst RW, Neuman SA, Cail WS. Multifocal intracranial MR abnormalities in neurofibromatosis. *AJNR* **1988**;9:293–296
3. Aoki S, Barkovich AJ, Nishimura K, et al. Neurofibromatosis types 1 and 2: cranial MR findings. *Radiology* **1989**;172:527–534
4. Brown EW, Riccardi VM, Mawad M, Handel S, Goldman A, Bryan RN. MR imaging of optic pathways in patients with neurofibromatosis. *AJNR* **1987**;8:1031–1036

Fluid Flow During Percutaneous Drainage Procedures: An In Vitro Study of the Effects of Fluid Viscosity, Catheter Size, and Adjunctive Urokinase

Jung K. Park[1]
Frederick C. Kraus[1,2]
John R. Haaga[1]

OBJECTIVE. An in vitro study was performed to determine the range of flow times of different bodily fluids through catheters of different diameters and to test the hypothesis that urokinase might decrease the viscosity of purulent material.

MATERIALS AND METHODS. A standard viscometer was used to measure the viscosities of water, blood, pseudocyst fluid, purulent material, and purulent material with admixed urokinase. For each fluid, Poiseuille's law was used to calculate the kinematic viscosity, from which theoretical drainage times through seven different sizes of catheters were calculated. These theoretical times were compared with the actual measured values to verify that flow was according to Poiseuille's law.

RESULTS. The calculated kinematic viscosities (in 10^{-6} stokes) were as follows: water, 0.695 ± 0.006; pseudocyst fluid, 2.185 ± 0.008; blood, 3.001 ± 0.049; abscess fluid without urokinase, 5.729 ± 0.064; and abscess fluid with urokinase, 4.416 ± 0.070. The viscosity of abscess fluid decreased by 23% with the addition of urokinase. Drainage time was considerably shorter with larger catheters.

CONCLUSION. Flow of various bodily fluids, including pus, is according to Poiseuille's law, confirming that for more viscous fluid, larger catheters provide more rapid drainage. Urokinase decreases viscosity of purulent material and increases flow for all sizes of catheters.

***AJR* 1993;160:165–169**

Although most reports on percutaneous drainage of abscesses have stated that larger catheters provide more effective drainage than smaller ones do, Gobien et al. [1] and Johnson et al. [2] found a poor correlation between catheter size and success rate. Furthermore, it has been reported that urokinase may decrease the viscosity of purulent material and thereby enhance percutaneous drainage [3]. We performed an in vitro study to determine the range of flow velocities of different bodily fluids through catheters of different sizes and to test the hypothesis that urokinase might decrease the viscosity of purulent material, thereby improving its flow and potentially reducing the time required for percutaneous drainage of an abscess.

Materials and Methods

According to traditional fluid mechanics, flow of bodily fluids should occur according to Poiseuille's law [4], which describes the rate of flow of a viscous fluid through a cylindrical structure. Poiseuille's law is expressed by the following equation:

$$Q = \frac{\pi}{128} \cdot \frac{D^4 \cdot g \cdot H(t)}{\gamma \cdot L},$$

where Q = flow, D = diameter of catheter, g = gravity, H(t) = difference in height of fluid columns at time t, γ = kinematic viscosity, and L = length of catheter. Simple calculus was

Received December 18, 1991; accepted after revision July 1, 1992.

[1]Department of Radiology, University Hospitals of Cleveland, 2074 Abington Rd., Cleveland, OH 44106. Address reprint requests to J. R. Haaga.

[2]Present address: Department of Radiology, University of Minnesota Hospitals, Harvard St. at East River Rd., Minneapolis, MN 55455.

0361–803X/93/1601–0165

applied to Poiseuille's law to express drainage time (T) as a function of these variables.

$$T = \frac{1}{\tau} \cdot \ln\left(1 - \frac{2}{A} \cdot \frac{V}{H(0)}\right),$$

where

$$\tau = -\frac{2}{A}\left(\frac{\pi}{128} \cdot \frac{D^4}{\gamma} \cdot \frac{g}{L}\right),$$

A = area of pipette, V = volume of fluid transmitted through the catheter, and H(0) = height difference at t = 0 of the two columns of fluid. All variables except catheter diameter (D) and kinematic viscosity (γ) were kept constant throughout the experiment.

Flow was measured with a standard Cannon-Manning semimicro viscometer (Cannon Co., State College, PA), a large 37.4°C water bath, and a series of catheters of different lengths fixed to standard 25-ml serologic pipettes (Falcon Co., Oxnard, CA; Figs. 1A and 1B). The outer diameters of the seven catheters used varied in size from 6-French to 18-French; the inner diameters were measured by using a Nikon Optiphot light microscope (Nikon Corp., Tokyo, Japan). A chronometer (Heuer-Leonidas, SA, Geneva, Switzerland) with an accuracy of 0.01 sec was used to measure the flow rates of the various fluids.

Five different fluids were used in the experiment: water, blood, pseudocyst fluid, purulent material without urokinase, and purulent material with urokinase. The blood was obtained by venipuncture, heparinized, and used the same day of the experiment. The pseudocyst fluid and purulent material had been collected from two different patients, and the samples were frozen at −70°C until the day of the experiment. For the urokinase treatment experiments, 5000 IU of urokinase (Abbokinase, 1.8 ml fluid volume), activated with 3.0 ml of serum, was added to 50 ml of abscess fluid.

For the measurement of kinematic viscosity, the viscometer was placed in the water bath, and measurements were made as follows: a standard volume (3 ml) of the appropriate fluid was placed into the viscometer reservoir while the opposite end of the viscometer was occluded to prevent flow. After the fluid was adjusted to the baseline, gravity flow was permitted. Drainage times were measured to the closest 0.01 sec by using the chronometer and visual observation. For each fluid, a mean drainage time from five trials was used in the drainage time equation to calculate the mean kinematic viscosity. The results were expressed in meters per second. The mean kinematic viscosity for each fluid was then used to create theoretical curves for flow for various catheter sizes. To determine whether flow was according to Poiseuille's law, we compared these theoretical values with actual measurements of flow obtained in subsequent experiments.

Actual fluid flows through the various catheters were measured as follows. The pipette catheter assembly was placed into the water bath, and the fluid level was adjusted to the baseline. Fluid was permitted to flow by gravity, without application of vacuum. The drainage time of 10 ml of fluid through each of the catheter devices was measured. The catheters were 30-cm lengths of seven different sizes between 6-French and 18-French. The same fluid was used for each experiment, going from the catheter with the largest caliber to the one with the smallest caliber. To minimize the effects of error associated with the manual chronometric measurements for each fluid and catheter, we measured flow 10 times for each combination. The mean was calculated after the highest and lowest values were discarded. Laminar flow was assumed for all measurements because the catheters were aligned so that no kinking or distortion of the lumen occurred.

Results

The kinematic viscosity (the ratio of the absolute viscosity to density of the material) in 10^{-6} stokes for each fluid was as follows: water, 0.695 ± 0.006; pseudocyst fluid, 2.185 ± 0.008; blood, 3.001 ± 0.049; abscess fluid without urokinase, 5.729 ± 0.064; abscess fluid with urokinase, 4.416 ± 0.070. The addition of urokinase decreased the viscosity of pus to 0.77 times the viscosity of pus without urokinase.

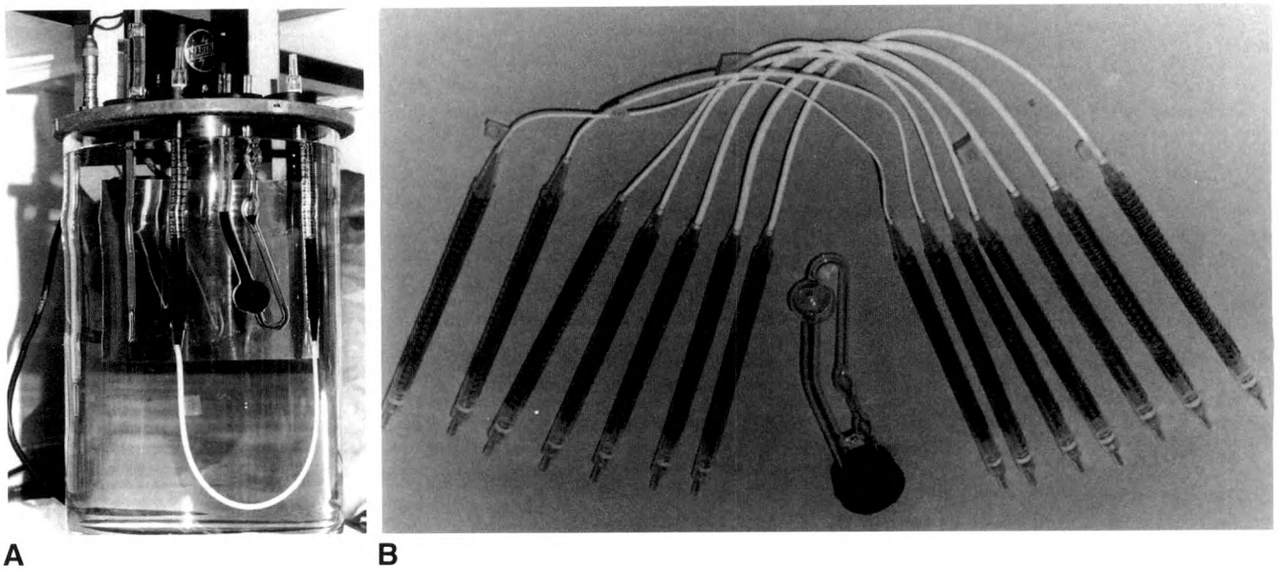

A B

Fig. 1.—*A* and *B*, Experimental apparatus for measuring drainage time of various liquids through different sizes of catheters includes large water bath in which a Cannon-Manning semimicro viscometer is suspended.

The actual and theoretical times required to drain 10 ml of various fluids through catheters with different diameters are shown in Figures 2A–2E.

The actual times for drainage of various fluids through catheters of different sizes are compared in Figure 3. The differences in viscosity had a significant effect on the time needed to drain 10 ml of the different fluids. Drainage time was also significantly improved with the larger diameter catheters as compared with the smaller diameter catheters. Flow was less dependent on fluid viscosity in the larger catheters. The addition of urokinase to the purulent material substantially reduced its drainage time for all catheter sizes.

Discussion

In the past decade, CT and sonographically guided percutaneous drainage of abscesses and fluid collections has become a widely used, safe, and effective technique. Various factors can hinder or delay successful drainage of intraabdominal abscesses, including the location and course of the abscess, the nature of the infecting organism, host resistance [5], choice of antibiotics, number and extent of cavities [6], multiloculations of phlegmon [7, 8], fistulous connections, and viscosity of the cavities' contents. Several procedure-related factors also can influence the effectiveness

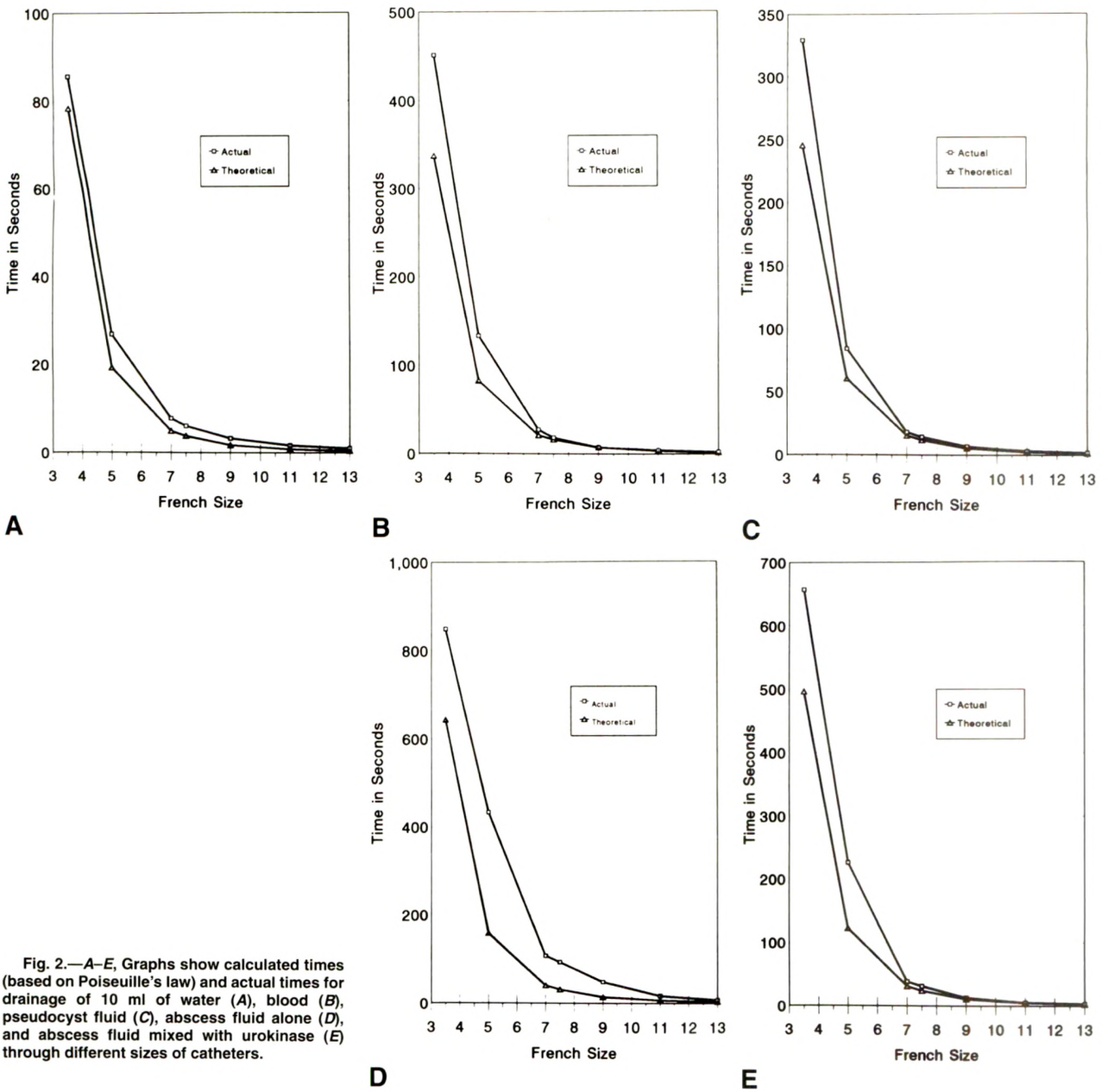

Fig. 2.—*A–E*, Graphs show calculated times (based on Poiseuille's law) and actual times for drainage of 10 ml of water (*A*), blood (*B*), pseudocyst fluid (*C*), abscess fluid alone (*D*), and abscess fluid mixed with urokinase (*E*) through different sizes of catheters.

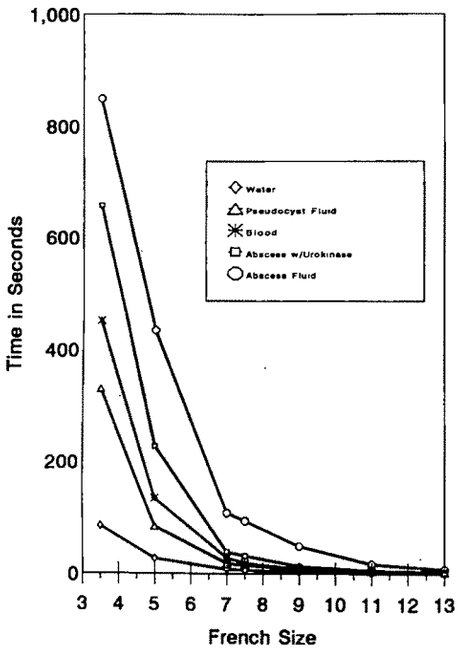

Fig. 3.—Composite graph shows measured flow rates of various fluids through different sizes of catheters. Note that rate of flow of purulent material is increased markedly by addition of urokinase.

of drainage, including type, number, and sites of catheters and type, frequency, and volume of irrigations given to ensure catheter patency.

In the early descriptions of percutaneous drainage of abscesses, the size of the abscess cavity, location of the abscess, safety of access route, and nature of the abscess determined the selection of size and type of catheter. Gerzof et al. [9] and Haaga and Weinstein [6] used 12- to 16-French trocars for large superficial abscesses without intervening structures and 7- to 8-French pigtail catheters for other fluid collections. Others [7, 8] suggested that large-bore, double-lumen sump catheters (12- to 14-French) be used for purulent collections larger than 100 ml, medium-bore nonsump catheters for nonviscous material (e.g., loculated ascites and seroma), and small-bore trocars for nonviscous collections smaller than 100 ml. Gobien et al. [1] found no statistically significant difference between the different-sized catheters in the frequency of successful drainage. They further suggested that attributing failures to catheter size alone may be an oversimplification for predicting failure in percutaneous drainage of an abscess. Jaques et al. [10] proposed that the abscess site alone (e.g., liver and subphrenic abscesses) was more predictive of successful percutaneous drainage. We have contended that the failure of these procedures could also be directly related to the viscosity of the fluid being evacuated from the abscess [6].

Our review of the literature suggests similar success for small- and large-diameter catheters. We tabulated the average number of days of drainage for small and large catheters (as defined by Mueller et al. [8]) from reported series. Unexpectedly, drainage times were less with the small-diameter catheters than with the large-diameter catheters (Table 1). The most plausible explanation for this paradox is that less-viscous collections were drained with small catheters. In the other cases, the viscosity of the material drained was great enough so that even the large-diameter catheters did not enhance drainage proportionately.

To our knowledge, only one report, by Tillett et al. [11], has described the value of fibrinolytic agents in reducing viscosity of purulent fluid collections. They compared the viscosity of a tuberculous pus sample alone with that of a sample mixed with urokinase and found that the viscosity changed from 150 times that of water to four times that of water (their method of measurement was not noted).

In our experiment, a variety of fluids were tested for their viscosity and flow through different sizes of catheters under standard conditions. We found that the flow of all these fluids, including pus, was according to Poiseuille's law. Using the measured drainage times, we were able to calculate the kinematic viscosities of various fluids, including water, blood, pseudocyst fluid, pus alone, and pus with urokinase. These values were then used to calculate a theoretical curve for fluid drainage through the various catheters, to which we compared our measured values (Figs. 2A–2E). The differences in viscosities produced expected differences in drainage times, although the actual measured times differed slightly from the theoretical times. From a practical point of view, this experiment shows the benefit of using larger catheters; flow rate is much higher for the larger catheters than for the smaller ones. Although the freezing and thawing could theoretically affect the viscosity of the pus by fracturing the cell membranes of the leukocytes, the relative measurements we made would still be valid because the same material was used for all measurements. The second important finding from our study is that urokinase produced a considerable reduction in the viscosity of purulent material and flow

TABLE 1: Effect of Catheter Diameter on Percutaneous Abscess Drainage

Catheter Category	Number	No.(%) Successfully Drained	Average Number of Days of Drainage (Range)
Small diameter (5–10 French)			
All reports	100	91 (91)	
Reports with days of drainage indicated	70	63 (90)	18.7 (2–90)
Large diameter (12–24 French)			
All reports	185	159 (86)	
Reports with days of drainage indicated	84	71 (85)	38.5 (3–110)
All diameters (5–24 French)			
All reports	623	530 (85)	
Reports with days of drainage indicated	317	282 (89)	19.9 (2–10)

Note.—The only reports tabulated are those [11–36] that specifically mentioned catheter sizes.

time through catheters of various sizes. The greatest benefit was noted with the smaller sizes of catheters. These results suggest that intracavitary urokinase might improve percutaneous drainage by reducing the viscosity of purulent material and, therefore, reducing flow time. An additional theoretical benefit might be the lysis of fibrinous adhesions and loculations, which also can delay or impair drainage.

In conclusion, our data indicate that various bodily fluids, including pus, flow according to Poiseuille's law, thereby confirming that, particularly for more viscous fluid, larger catheters provide significantly faster flow than smaller catheters do. Furthermore, our study shows that urokinase decreases the viscosity of purulent material and increases drainage flow rates for all sizes of catheters. This basic information suggests that use of intracavitary urokinase in conjunction with percutaneous abscess drainage might be useful if drainage after catheter placement is inadequate.

REFERENCES

1. Gobien RP, Stanley JH, Schabel SI, et al. The effect of drainage tube size on adequacy of percutaneous abscess drainage. *Cardiovasc Intervent Radiol* **1985**;8:100–102
2. Johnson WC, Gerzof SG, Robbins AH, Nabseth DC. Treatment of abdominal abscesses. *Ann Surg* **1981**;194:510–520
3. Haaga JR, Alfidi RJ, eds. *Computed tomography of the whole body*, 2nd ed. St. Louis: Mosby, **1988**
4. Whitaker S. *Introduction to fluid mechanics*. Englewood Cliffs, NJ: Prentice–Hall, **1968**:61
5. Dawson SL, Mueller PR, Ferrucci JT. Mucomyst for abscesses: a clinical comment. *Radiology* **1984**;151:342
6. Haaga JR, Weinstein AJ. CT-guided percutaneous aspiration and drainage of abscesses. *AJR* **1980**;135:1187–1194
7. vanSonnenberg E, Mueller PR, Ferrucci JT. Percutaneous drainage of 250 abdominal abscesses and fluid collections. Part I: results, failures and complications. *Radiology* **1984**;151:337–341
8. Mueller PR, vanSonnenberg E, Ferrucci JT. Percutaneous drainage of 250 abdominal abscesses and fluid collections. Part II: current procedural concepts. *Radiology* **1984**;151:343–347
9. Gerzof SG, Robbins AH, Birkett DH, Johnson WC, Pugatch RD, Vincent ME. Percutaneous catheter drainage of abdominal abscesses guided by ultrasound and computed tomography. *AJR* **1979**;133:1–8
10. Jaques P, Mauro M, Safrit H, Yankaskas B, Piggott B. CT features of intraabdominal abscesses: prediction of successful percutaneous drainage. *AJR* **1986**;146:1041–1045
11. Tillett WS, Sherry S, Read CT. The use of streptokinase-streptodornase in the treatment of chronic empyema. *J Thorac Surg* **1951**;21:325–341
12. Gronvall S, Gammelgaard J, Haubek A, Holm HH. Drainage of abdominal abscesses guided by sonography. *AJR* **1982**;138:527–529
13. Mueller PR, Simeone JF, Butch RJ, et al. Percutaneous drainage of subphrenic abscess: a review of 62 patients. *AJR* **1986**;147:1237–1240
14. Ball WS Jr, Bisset GS III, Towbin RB. Percutaneous drainage of chest abscesses in children. *Radiology* **1989**;171:431–434
15. Cronan JJ, Amis ES, Dorfman GS. Percutaneous drainage of renal abscesses. *AJR* **1984**;142:351–354
16. Neff CC, vanSonnenberg E, Casola G, et al. Diverticular abscesses: percutaneous drainage. *Radiology* **1987**;163:15–18
17. Bernardino ME, Berkman WA, Plemmons M, Sones PF, Price RB, Casarella WJ. Percutaneous drainage of multiseptated hepatic abscess. *J Comput Assist Tomogr* **1984**;8:38–41
18. Butch RJ, Mueller PR, Ferrucci JT, et al. Drainage of pelvic abscesses through the greater sciatic foramen. *Radiology* **1986**;158:487–491
19. Casola G, vanSonnenberg E, Neff CC, Saba RM, Withers C, Emarine CW. Abscesses in Crohn's disease: percutaneous drainage. *Radiology* **1987**;163:19–22
20. Ken JG, vanSonnenberg E, Casola G, Christensen R, Polansky AM. Perforated amebic liver abscesses: successful percutaneous treatment. *Radiology* **1989**;170:195–197
21. Kerlan RK, Jeffrey RB, Pogany AC, Ring EJ. Abdominal abscess with low-output fistula: successful percutaneous drainage. *Radiology* **1985**;155:73–75
22. Lambiase RE, Cronan JJ, Dorfman GS, Paolella LP, Haas RA. Postoperative abscesses with enteric communication: percutaneous treatment. *Radiology* **1989**;171:497–500
23. Letourneau JG, Hunter DW, Crass JR, Thompson WM, Sutherland DER. Percutaneous aspiration and drainage of abdominal fluid collections after pancreatic transplantation. *AJR* **1988**;150:805–809
24. MacErlean DP, Owens AP, Hourihane JB. Ultrasound guided percutaneous abdominal abscess drainage. *Br J Radiol* **1981**;54:394–397
25. Mueller PR, Dawson SL, Ferrucci JR, Nardi GL. Hepatic echinococcal cyst: successful percutaneous drainage. *Radiology* **1985**;155:627–628
26. Mueller PR, White EM, Glass-Royal M, et al. Infected abdominal tumors: percutaneous catheter drainage. *Radiology* **1989**;173:627–629
27. Mueller PR, Ferruci JT, Wittenberg J, Simeone JR, Butch RJ. Iliopsoas abscess: treatment by CT-guided percutaneous catheter drainage. *AJR* **1984**;142:359–362
28. Mueller PR, Ferrucci JT, Simeone JR, et al. Lesser sac abscesses and fluid collections: drainage by transhepatic approach. *Radiology* **1985**;155:615–618
29. Quinn SF, vanSonnenberg E, Casola G, Wittich GR, Neff CC. Interventional radiology in the spleen. *Radiology* **1986**;161:289–291
30. vanSonnenberg E, Nakamoto SK, Mueller PR, et al. CT- and ultrasound-guided catheter drainage of empyemas after chest tube failure. *Radiology* **1984**;151:349–353
31. vanWaes PFGM, Feldberg MAM, Mali WP, et al. Management of loculated abscesses that are difficult to drain: a new approach. *Radiology* **1983**;147:57–63
32. Kerlan RK, Pogany AC, Jeffrey RB, Goldberg HI, Ring EJ. Radiologic management of abdominal abscesses. *AJR* **1985**;144:145–149
33. Towbin RB, Strife JL. Percutaneous aspiration, drainage, and biopsies in children. *Radiology* **1985**;157:81–85
34. Safrit HD, Mauro MA, Jaques PF. Percutaneous abscess drainage in Crohn's disease. *AJR* **1987**;148:859–862
35. Meranze SG, LeVenn RF, Burke DR, Cope C, McLean GK. Transesophageal drainage of mediastinal abscesses. *Radiology* **1987**;165:395–398
36. Lerner RM, Spataro RF. Splenic abscess: percutaneous drainage. *Radiology* **1984**;153:643–645
37. vanSonnenberg E, Mueller PR, Schiffman HR, et al. Intrahepatic amebic abscesses: indications for and results of percutaneous catheter drainage. *Radiology* **1985**;156:631–635

The reader's attention is directed to the companion article that appears on pages 171-174.

Official Poster of the Radiology Centennial

The 1995 centennial celebration of the discovery of the X-ray will be a yearlong series of activities. Some, including special programs and exhibits scheduled for the annual meetings of sponsoring societies, are directed to the radiologic community; others are intended to inform the general public about the contributions of radiology to today's health care. Among the public-directed efforts will be books, television programs, news and feature articles, a school teaching package, and lecture materials. Exhibits and presentations will be available to radiology departments and private practices for use in their communities during the year.

Radiology Centennial, Inc., is an organization sponsored by 43 national radiologic societies, five boards and registries, three federal agencies, and 25 leading suppliers of radiologic equipment and material. Each sponsor is represented on the board of directors of Radiology Centennial, Inc., and on its dozen working committees.

The official poster of Radiology Centennial, Inc., was designed by artist Greg Harlin of Annapolis, MD, a noted magazine illustrator and designer. It is a montage depicting 100 years of change in diagnostic and therapeutic radiology and is intended to reflect the tremendous advances that have made radiology a vital part of the nation's health resources.

Art-quality prints of the 24 × 16 in. original are being presented to radiology groups and individuals who contribute $1000 or more to Radiology Centennial, Inc. Other donors receive centennial pins. The total budget for the organization has been set at $3 million, with half to come from radiologists and half from the companies that supply goods and services to them.

For further information about Radiology Centennial, Inc., contact RCI, 1891 Preston White Dr., Reston, VA 22091, or telephone (703) 648-8905.

***AJR* 1993;160:170** 0361–803X/93/1601–0170 © American Roentgen Ray Society

Safety of Intracavitary Urokinase with Percutaneous Abscess Drainage

John M. Lahorra[1]
John R. Haaga[1]
Thomas Stellato[2]
Timothy Flanigan[3]
Richard Graham[3]

OBJECTIVE. Percutaneous drainage of abscesses is an effective treatment, but the success rate is lower for abscesses that have septa and are multilocular. Several clinical and in vitro studies suggest urokinase may be useful in such cases. Our study was designed to determine the safety of urokinase administered into an abscess cavity during the course of percutaneous drainage.

SUBJECTS AND METHODS. Our study included 26 consecutive patients with 31 abscesses treated with percutaneous drainage. Exclusion criteria included age less than 18 or more than 95 years, CNS disorders (e.g., tumor, vascular problems), coagulation impairments, hepatic failure, pregnancy, and abscesses in the spleen, pancreas, or interloop area. Three doses were used: group 1 (nine patients), 1000 IU of urokinase per centimeter of abscess diameter; group 2 (11 patients), 2500 IU of urokinase per centimeter of abscess diameter; and group 3 (nine patients), 5000 IU of urokinase per centimeter of abscess diameter. These doses were administered every 8 hr for 3 days along with percutaneous drainage. Charts were reviewed to determine success and to detect adverse clinical events. Studies included sequential CT scans; serial serum determinations of hematocrit, prothrombin time, partial thromboplastin time, platelet count, fibrinogen levels, and levels of fibrin degradation products; and serial laboratory analysis of purulent material for fibrinogen and fibrin degradation products. Percutaneous drainage was considered successful if no surgical intervention was required.

RESULTS. Our results showed no significant change in hematologic studies and no bleeding complications. Analysis of purulent material indicated that urokinase remained active in the abscess milieu. Drainage was successful in seven of 11 patients in group 1, all nine patients in group 2, and 10 of 11 patients in group 3. All eight abscesses with septa were successfully drained.

CONCLUSION. Intracavitary urokinase can be given safely during percutaneous drainage of an abscess, with no associated bleeding complications or changes in coagulation parameters.

AJR 1993;160:171–174

Received December 18, 1992; accepted after revision June 16, 1992.

[1]Department of Radiology, University Hospitals of Cleveland, 2074 Abington Rd., Cleveland, OH 44106. Address reprint requests to J. R. Haaga.

[2]Department of General Surgery, University Hospitals of Cleveland, 2074 Abington Rd., Cleveland, OH 44106.

[3]Department of Internal Medicine, University Hospitals of Cleveland, 2074 Abington Rd., Cleveland, OH 44106.

0361–803X/93/1601–0171

Percutaneous abscess drainage is accepted as an effective alternative to surgical drainage, but some problems with the technique remain. Haaga et al. [1, 2], Gerzof et al. [3, 4], and Jacques et al. [5] have reported a success rate for the drainage of abscesses with loculi and septa and infected hematomas that is lower than the success rate for simple abscesses. Although two earlier reports described studies of the use and safety of streptokinase for treating pleural fluid collections, few data have been collected on the safety of urokinase used as an adjunct to percutaneous drainage in abscesses in other body locations. This phase I safety study, approved by the Food and Drug Administration, was designed to evaluate the safety of urokinase injected into abscess cavities as part of percutaneous drainage.

Subjects and Methods

Formal approval for this phase I safety study was obtained from the Institutional Review Board of University Hospitals of Cleveland and the Food and Drug Administration.

Between March 1989 and December 1990, 26 consecutive patients with 31 abscesses were treated with intracavitary urokinase. The average age of the patients was 51 years (range, 18–80 years). Half of the patients were men and half were women. The 31 abscesses were distributed anatomically as follows: 21 retroperitoneal, eight intraperitoneal, and two intrathoracic. Eleven of the abscesses were postoperative, five were sequelae of pancreatitis, nine were sequelae of pyelonephritis, two were sequelae of perforated ulcers, and four were of unknown cause.

The indications for inclusion in the urokinase study were quite broad; all patients treated by percutaneous drainage during the study period were included even if we saw evidence of septa, loculi, hematoma, thick purulent material, or fluid with high CT attenuation values. Criteria for exclusion included abscesses in the spleen, pancreas, or interloop area; CNS disorders, including brain abscess, tumor, arteriovenous malformation, aneurysm, or history of CNS bleeding; coagulation impairment, including partial thromboplastin time more than 4 sec beyond normal, platelet count less than 50,000, or low fibrinogen levels; fulminant hepatic failure; or pregnancy. Patients with pancreatic abscesses were excluded because use of a fibrinolytic agent might cause bleeding from vascular pseudoaneurysms, which are associated with inflammation of the pancreas and pseudocysts. Abscesses adjacent to or separate from the pancreas but resulting from pancreatitis were included. Patients with interloop abscesses were excluded because it was uncertain whether urokinase would prevent closure or enteric fistulas [6]. No patients were excluded because of septa, multiplicity of lesions, or increased viscosity of purulent material.

Urokinase treatment was started within 24 hr either after the catheter had been inserted and the pyogenic nature of the abscess confirmed or after it had been clinically determined that a fluid collection should be treated as an abscess. Urokinase, derived from human kidney cell culture (Abbokinase, Abbott Laboratories, North Chicago, IL), was supplied as a sterile, lyophilized preparation. It was reconstituted with sterile water for injection, to a final dilution of 5000 IU/ml. Percutaneous drainage catheters were placed as described earlier [1]. The dose of urokinase was selected according to the site of the abscess, and three different dosages were used. For each centimeter of maximal abscess diameter (determined from CT scans), group 1 (patients 1–11 with abscesses 1–10) received 1000 IU, group 2 (patients 12–20 with abscesses 11–20) received 2500 IU, and group 3 (patients 18–26 with abscesses 21–31) received 5000 IU of urokinase.

The urokinase solution was injected through the catheter into the abscess cavity. Although the urokinase concentration remained constant in the fluid, the volume of solution varied with the size of the cavity, that is, the smaller cavities received smaller amounts of fluid and the larger cavities received larger amounts of fluid. Therefore, for the purposes of this safety study, we considered the dilutional effects insignificant. The catheter was flushed with 5–10 ml of saline to clear the urokinase from the system. The catheter was clamped for 5–10 min and then opened to gravity drainage. The urokinase was administered every 8 hr for 3 days; for the duration of the drainage, the catheter was irrigated with 10 ml of saline every 8 hr.

Other than the administration of urokinase as described earlier, the abscesses were managed in a routine fashion according to previously described guidelines. CT scans were performed to assess the efficacy of treatment. Abscess drainage was considered successful if the abscess was cured by catheter drainage and no surgical treatment was required. Clinical safety was ascertained by daily clinical observation and a review of the charts at the end of the study.

Laboratory tests performed before and during therapy included serum determinations of hematocrit, WBC count, platelet count, prothrombin time, partial thromboplastin time, and levels of fibrinogen. Levels of fibrinogen and fibrin degradation products were measured in samples of abscess fluid also. Aliquots of purulent material were collected serially before and throughout the treatment period. Immediately after collection, the samples were frozen at –70°C. The samples were collected until the end of the study and then frozen and sent to an outside laboratory for evaluation. The results from serum samples obtained before and after administration of urokinase were compared. Student's t-test was used for statistical evaluation.

Results

All patients tolerated the drainage procedures and the instillation of urokinase well. No significant complications, including any form of hemorrhage, occurred. One patient complained of pain during the injection of urokinase, but the discomfort was not severe enough to warrant stopping treatment.

Treatment with urokinase caused no significant changes in hematocrit, prothrombin time, partial thromboplastin time, platelet count, or serum levels of fibrinogen or fibrin degradation products (Table 1).

TABLE 1: Mean Values of Results of Serum Analysis Before and During Urokinase Administration

Parameter	Time (hr)				
	0	24	48	72	96
Hematocrit (%)	32	31	32	32	31
Platelets ($\times 10^9$/l)	526	522	537	538	556
Prothrombin time (sec)	13.7	13.7	13.8	13.6	13.5
Partial thromboplastin time (sec)	27	28	27	27	28
Fibrinogen (mg/dl)	515	521	510	512	506
Fibrin degradation products (mg/ml)	26[a]	45[a]	22	28	25

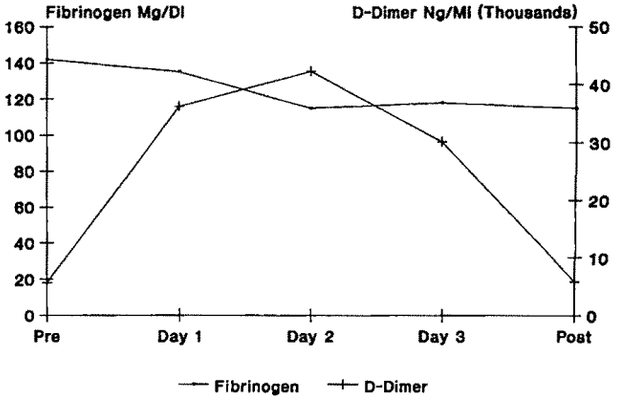

Fig. 1.—Graph shows mean levels of fibrinogen and D-dimer (fibrin split product) in abscess fluid during treatment with intracavitary urokinase and percutaneous abscess drainage. Initial rise in D-dimer indicates activity of urokinase in abscess cavity. Change in fibrinogen was not statistically significant, whereas change in D-dimer was ($p < .05$, $t = 2.38$, Student's t-test). Dl = deciliters, Ml = milliliters, Mg = milligrams, Ng = nanograms.

In abscess fluid, the level of fibrinogen decreased initially while levels of fibrin degradation products increased sharply and then returned to pretreatment levels after the cessation of therapy (Fig. 1).

Abscess characteristics and results of therapy are included in Table 2. These abscesses included eight septate abscesses (determined by CT or sonography), three infected hematomas, one fungal abscess, and one recurrent abscess (Fig. 2). The overall success rate for urokinase regimen one (n = 11) was 63%, for regimen two (n = 9) was 100%, and for regimen three (n = 11) was 90%.

TABLE 2: Abscess Characteristics and Results of Therapy

Characteristics of Abscess	Number Treated	No.(%) of Successes
Simple	23	18 (78)
Complex	8	8 (100)
Small (≤5 cm)	17	15 (88)
Large (>5 cm)	14	11 (79)
Retroperitoneal	21	18 (86)
Intraperitoneal	8	7 (88)
Thoracic	2	1 (50)
Culture positive for		
Bacteria	27	23 (85)
Fungus	2	1 (50)
Culture negative	2	2 (100)

Discussion

The rationale for using fibrinolytic agents to improve the results with percutaneous abscess drainage is apparent if the role of fibrin in the pathogenesis and evolution of an abscess, anecdotal cases reported in the literature, and the results of our in vitro study [7] are considered. Before definitive study of urokinase efficacy can be initiated, the safety of this treatment must be established.

Fibrin has long been regarded as one of the primary host defense mechanisms in intraabdominal infections [8]. Leukocytes, which aggregate near a site of infection, release permeability factors such as histamine. These factors, in turn, lead to the exudation of fibrinogen and other proteins from surrounding blood vessels. Fibrinogen is converted to fibrin by tissue thromboplastin and helps to localize the spread of infection [9].

Under physiologic conditions, fibrin is lysed by plasmin, a protease derived from the enzyme precursor plasminogen. Studies have shown that fibrinolytic activity depends on plasminogen activators, such as urokinase, streptokinase, and tissue plasminogen activator [9].

The role of fibrin in abscess formation and the potential benefit of fibrinolytic agents is suggested by the results of several animal abscess models. Prinz et al. [10] showed that heparin administration prevented the formation of ab-

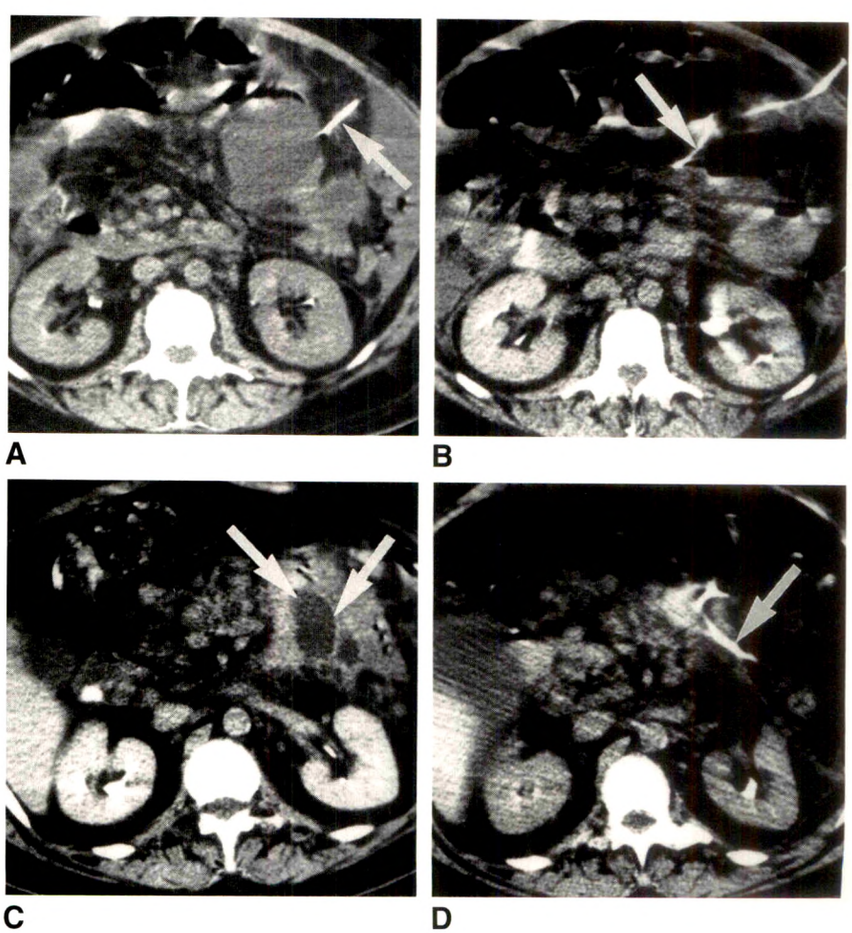

Fig. 2.—38-year-old man with chronic lymphocytic leukemia who had had splenectomy 6 months earlier.

***A*, CT scan shows an abscess in left side of abdomen with needle (*arrow*) directed toward abscess.**

***B*, CT scan obtained after percutaneous drainage of abscess without use of urokinase shows drained cavity with catheter (*arrow*) in place. Abscess recurred 1 month later and was surgically drained.**

***C*, CT scan obtained several weeks later shows recurrence of abscess (*arrows*) in left side of abdomen.**

***D*, CT scan obtained after percutaneous drainage was repeated with adjunctive urokinase shows resolution of fluid collection with catheter (*arrow*) in cavity. Abscess did not recur.**

scesses. Rotstein and Kao (presented at the International Surgical Infectious Disease Congress, Hamburg, 1986) used the same model to show that tissue plasminogen activator also prevented the formation of abscesses in the rat model.

In addition to animal data, several clinical reports indicated that urokinase may improve the drainage of abscesses. Tillet et al. [11] treated chronic empyema with streptokinase-streptodornase. More recent reports [12, 13] support the use of fibrinolytics as an adjunct to the treatment of infected empyemas and hematomas. Berglin et al. [14] described the effectiveness and safety of streptokinase for treatment of empyema. They noted that streptokinase did not produce any complications or any adverse systemic effects. They found that serum coagulation factors were within normal limits except for a slight elevation of the fibrin split products, which quickly returned to normal after 24 hr. Moulton et al. [15] reported on the use of urokinase as an intrapleural agent in a similar group of patients. They found that intrapleural instillation of urokinase was safe and did not produce complications, adverse effects, or alterations of the serum coagulation factors. They did not, however, specify the types of coagulation factors measured. They stated that they thought that the urokinase treatment was effective, but they could not be certain because they did not have a controlled study. Vogelzang et al. [13] reported on the use of urokinase and streptokinase for the treatment of two infected hematomas. They claimed these fibrinolytic agents were effective and that there were no complications, but they did not specifically comment about the measurement of coagulation factors. Our study provides important data regarding the use of urokinase in abdominal abscesses not evaluated in other studies.

The safety of intracavitary use of urokinase for routine abdominal and pelvic abscesses was confirmed by our study. No complications, side effects, or hemorrhage occurred in any of the patients, and no significant changes were observed in serum samples for any of the coagulation factors measured. The only change was an increase in the serum level of fibrin degradation products 24 hr after initiation of urokinase therapy; the importance of this finding is questionable because the change was not statistically significant.

Analysis of the abscess fluids was especially enlightening. The concentrations of fibrinogen within the purulent material during the treatment period decreased. The amount of fibrin degradation products increased during the first 2 days of treatment and then returned to pretreatment levels (Fig. 1). One plausible explanation for these findings is that an abscess treated with intracavitary urokinase has an increased turnover of fibrin. Ongoing infection probably stimulates the conversion of fibrinogen to fibrin. Urokinase converts plasminogen to plasmin, which degrades fibrin and causes an increase in the fibrin split products. Although we had originally intended to determine the level of plasmin in the abscess to confirm the enzymatic activity of urokinase in this setting, we were unable to locate any clinical or commercial laboratory that does assays for plasmin. Because of the increased levels of fibrin split product and the reduced levels of fibrinogen in the abscess fluid shown in our study, we believe that one can conclude that urokinase and plasminogen maintain their activity even in an abscess.

In conclusion, this study suggests that intracavitary urokinase can be given safely without significant side effects or alterations in serum levels of coagulation factors. The results of the assays of abscess fluid suggest that fibrin is present in significant amounts within abscesses, and that urokinase increased the amount of fibrin split products; thus, the enzymatic and chemical milieu of abscess fluid does not negate the enzymatic activity of urokinase or plasmin. Because our study lacks a control group, a carefully controlled prospective study is warranted to determine the efficacy of intracavitary urokinase for improving the outcome of percutaneous abscess drainage. We are cautiously enthusiastic about the potential value of urokinase treatment as an adjunct to percutaneous drainage of abscesses.

REFERENCES

1. Haaga JR, George C, Weinstein AJ, Cooperman AM. New interventional techniques in the diagnosis and management of inflammatory disease within the abdomen. *Radiol Clin North Am* **1979**;17:485–513
2. Haaga JR. CT interventional procedures. In: Haaga JR, Alfidi RJ, eds. *Computed tomography of the whole body.* St. Louis: Mosby **1988**:1200–1320
3. Gerzof SG, Robbins AH, Birkett DH, Johnson WC, Pugatch RD, Vincent ME. Percutaneous catheter drainage of abdominal abscesses guided by ultrasound and computed tomography. *AJR* **1979**;133:1–8
4. Gerzof SG, Johnson WC, Robbins AH, Nabseth DC. Expanded criteria for percutaneous abscess drainage. *Arch Surg* **1985**;120:227–232
5. Jacques P, Mauro M, Safrit H, Yankaskas B, Piggott B. CT features of intraabdominal abscesses. *AJR* **1986**;146:1041–1045
6. Olak J, Christou NV, Stein LA, et al. Operative versus percutaneous drainage of intraabdominal abscesses: comparison of morbidity and mortality. *Arch Surg* **1986**;121:141–146
7. Park JK, Kraus FC, Haaga JR. Fluid flow during percutaneous drainage procedures: an in vitro study of the effects of fluid viscosity, catheter size, and adjunctive urokinase. *AJR* **1993**;160:165–169
8. Ellis H, Harrison W, Hugh TB. The healing of peritoneum under normal and pathologic conditions. *Br J Surg* **1965**;52:471–476
9. Dunn DL, Simmons RL. Fibrin in peritonitis: III. The mechanism of bacterial trapping in polymerizing fibrin. *Surgery* **1982**;92:513–519
10. Prinz RA, Shuber Z, Fareed J, Bird T, Sandberg L. Effect of heparin and heparin fractions on experimental abscess formation. *Arch Surg* **1986**;121:1173–1176
11. Tillet WS, Sherry S, Read CT. The use of streptokinase-streptodornase in the treatment of chronic empyema. *J Thorac Surg* **1951**;21:325–341
12. Bergh NP, Ekroth R, Larsson S, Nagy P. Intrapleural streptokinase in the treatment of haemothorax and empyema. *Scand J Thorac Cardiovasc Surg* **1977**;11:265–268
13. Vogelzang RL, Tobin RS, Burstein S, Anschuetz SL, Marzano M, Kozlowski M. Transcatheter intracavitary fibrinolysis of infected extravascular hematomas. *AJR* **1987**;148:378–380
14. Berglin E, Ekroth R, Teger-Nilsson C, William-Olsson G. Intrapleural instillation of streptokinase: effects on systemic fibrinolysis. *Thorac Cardiovasc Surg* **1981**;29:124–126
15. Moulton JS, Moore PT, Mencini RA. Treatment of loculated pleural effusions with transcatheter intracavitary urokinase. *AJR* **1989**;153:941–945

Value of Having a Cytopathologist Present During Percutaneous Fine-Needle Aspiration Biopsy of Lung: Report of 55 Cancer Patients and Metaanalysis of the Literature

John H. M. Austin[1]
Michael B. Cohen[2]

OBJECTIVE. Percutaneous fine-needle aspiration biopsy is an accepted procedure for diagnosing intrathoracic malignant disease. The value of having a cytopathologist present during the procedure was studied with respect to the number of needle passes, the accuracy of the procedure, and complications. A metaanalysis was performed on the combined results of the present and previous series.

SUBJECTS AND METHODS. We analyzed data from 55 adult patients who underwent percutaneous CT-guided fine-needle (22-gauge) aspiration biopsy of the lung for a lesion that either the biopsy or another subsequent invasive procedure showed to be nonlymphomatous and malignant. A cytopathologist was present for the first 25 procedures and not present for the next 30 procedures. When present, the cytopathologist stained the aspirated material with toluidine blue and gave an immediate opinion on the diagnostic adequacy of the specimen based on microscopic evaluation. If appropriate, the radiologist obtained additional biopsy specimens. When a cytopathologist was not present, the radiologist assessed the adequacy of the specimen by gross examination. A metaanalysis was performed of 211 cases from the present study and two previous series with respect to the effect of the presence of a cytopathologist on the diagnostic accuracy of the procedure.

RESULTS. Biopsy specimens showed cancer in 25 (100%) of 25 patients when obtained while the cytopathologist was present, and in 24 (80%) of 30 patients when obtained while the cytopathologist was absent ($p < .05$, Fisher exact test). No significant differences in the number of needle passes performed or in the frequency of pneumothorax when aerated lung was traversed were noted between the two groups. Although two previous studies showed nonsignificant trends toward increased accuracy of thoracic fine-needle aspiration when a cytopathologist participated in the procedure, metaanalysis revealed significantly increased accuracy when a cytopathologist was present ($p < .02$, Mantel-Haenszel χ^2-test).

CONCLUSION. An accurate diagnosis from fine-needle aspiration biopsy of intrathoracic cancer was more likely when a cytopathologist was present than when not present during the procedure.

AJR 1993;160:175–177

Fine-needle aspiration biopsy is well established as a method for assessing malignant intrathoracic disease [1–5], but the value of having a cytopathologist present when the procedure is performed remains controversial [3–6].

Because immediate cytologic assessment of a specimen can lead to a decision to perform another biopsy without delay, we studied the value of having a cytopathologist present during the biopsy with regard to the number of needle passes, accuracy, and complications. Using data from the present series and two previous comparable studies [3, 5], we also performed a metaanalysis (statistical analysis combining the results of more than one series [7]) of the association between the accuracy of the results of fine-needle aspiration biopsy of lung lesions and the presence or absence of a cytopathologist during the procedure.

Received April 28, 1992; accepted after revision July 24, 1992.

[1]Department of Radiology, Columbia-Presbyterian Medical Center, 622 W. 168th St., New York, NY 10032. Address reprint requests to J. H. M. Austin.

[2]Department of Pathology, Columbia-Presbyterian Medical Center, New York, NY 10032. Present address: Department of Pathology, University of Iowa Hospitals and Clinics, Iowa City, IA 52242.

0361–803X/93/1601–0175

Subjects and Methods

From July 1987 through June 1991, we performed percutaneous CT-guided fine-needle aspiration biopsy of focal lung lesions in 100 adult patients referred by an internist or surgeon for evaluation of a nodule or mass. Twenty-two (22%) patients with no biopsy evidence of cancer and a subsequent clinical course indicative of nonmalignant disease were excluded from further analysis. In eight patients, the biopsy procedure was not successful in obtaining tissue from the lesion; these patients were excluded from further analysis. In another eight patients, a cutting (Vim-Silverman) needle provided a core of tissue for histopathologic analysis; these patients also were excluded from further analysis. Seven of the patients were later shown to have a lymphoma; because lymphoma is a difficult cytologic diagnosis, these patients were excluded from further analysis. The remaining 55 patients constitute the cohort studied; in each of these patients, the diagnosis of cancer was proved either by the fine-needle aspiration biopsy (n = 49) or by another subsequent invasive procedure (n = 6). An unrevealing bronchoscopic examination had been performed prior to referral in 26 (47%) of the 55 patients.

Each biopsy was performed by a resident or fellow and supervised by a senior attending radiologist experienced in thoracic needle biopsy procedures. The skills and experience of the operators were comparable throughout the period of study. The technique included CT documentation of placement of the needle in the lesion, usually near a margin, and aspiration into an empty 10-ml syringe while the needle was moved rapidly in and out over a distance of approximately 2–5 mm. The study did not include biopsies performed of mediastinal, pleural, or chest wall lesions.

An experienced attending cytopathologist was present for the first consecutive 25 biopsy procedures (covering the first 22 months of the study, 45% of 55 subjects) and not present for the remaining 30 procedures (covering the next 26 months of study, 55% of the 55 subjects). The age (mean ± SD) of the patients was 66 ± 13 years (range, 38–88) for the combined groups (55 patients), 65 ± 12 for the first 25 procedures and 67 ± 13 for the remaining 30 procedures. Twenty-eight (51%) of the patients were men and 27 (49%) were women (13 men and 12 women for the first 25 procedures, 15 men and 15 women for the remaining 30 procedures).

Diagnoses for the first 25 patients (cytopathologist present) were non–small-cell carcinoma (n = 17), adenocarcinoma (n = 2), squamous carcinoma (n = 2), metastatic renal cell carcinoma (n = 2), malignant fibrous histiocytoma (n = 1), and large-cell carcinoma (n = 1). Mean diameter of these 25 lesions was 4.6 ± 2.9 cm. Diagnoses for the next 30 patients (cytopathologist not present) were non–small-cell carcinoma (n = 17), adenocarcinoma (n = 9), squamous carcinoma (n = 3), and metastatic hepatoma (n = 1). The mean diameter of these 30 lesions was 3.6 ± 1.6 cm (no significant difference from previous group, unpaired t-test).

When present, the cytopathologist brought a light microscope on a mobile cart to the CT suite, stained the aspirated material with toluidine blue [8], and gave an opinion within about a minute on the diagnostic adequacy (quantity and quality of material sufficient for diagnosis) of the specimen. If appropriate, additional specimens were obtained until the pathologist accepted the material as adequate. When the pathologist was not present, the radiologists assessed the adequacy (fragments of tissue evident visually) of each specimen by gross examination, placed the specimen in normal saline solution, and promptly delivered the material in person to the cytology laboratory for analysis.

The presence of pneumothorax as a complication of fine-needle aspiration biopsy was assessed by evaluation of CT images, obtained both during and immediately after the biopsy. We also recorded whether the needle traversed aerated lung to enter the target lesion or passed through the chest wall directly into the lesion. The number of needle passes was also noted for each patient. When pneumothorax developed, the course of its management also was noted. The development of pneumothorax (in six [11%] of the 55 patients) did not affect decisions concerning possible rebiopsy for any of these patients.

We used the χ^2-test of Mantel and Haenszel [9] to perform a metaanalysis combining data from two previously published series [3, 5] and the data of our series. This test is a variant of χ^2 analysis that assesses comparable two-by-two tables from multiple series, yielding an overall probability value. A p value less than .05 was considered statistically significant.

Results

Material from 25 (100%) of the first 25 patients (cytopathologist present during biopsy) showed cytologic evidence of cancer. Material from 24 (80%) of the remaining 30 patients (cytopathologist not present during biopsy) showed cytologic evidence of cancer. These results were significantly different (p = .027, Fisher exact test, two-tailed). Overall, the accuracy of the total series was 89% (49 of 55 patients). However, each of the six examinations (11%) in which the biopsy findings were false-negative was in the cohort of 30 procedures in which a cytopathologist was not present during biopsy. No false-positive diagnoses of cancer were made.

The number of needle passes for the first 25 patients (cytopathologist present) was a median of one and a mean of 1.7 ± 0.9 (one pass, 13 cases; two passes, seven cases; three passes, four cases; four passes, one case). The number of needle passes for the remaining 30 patients (cytopathologist not present) was a median of one and a mean of 1.3 ± 0.5 (one pass: n = 20, two passes, n = 10). Although five (20%) of the first 25 patients and none of the remaining 30 patients underwent three or four needle passes, the number of needle passes was not statistically significantly different between the two groups (Wilcoxon rank sum test, p = .12). In the cohort of six patients with false-negative needle biopsies, five of the patients had a single needle pass and one of the patients had two needle passes.

In four (16%) of the first 25 patients (cytopathologist present), pneumothorax developed. Pneumothorax developed in two (7%) of the remaining 30 patients (cytopathologist not present). The difference between the rates of pneumothorax in each of these two groups was statistically significant (p = .04, Fisher exact test, two-tailed). However, pneumothorax developed only in patients in whom the needle passed through aerated lung [10]. If only these patients are considered (nine in the first 25 and 18 in the second 30), the rate of pneumothorax was not significantly different between the two groups. Pneumothorax developed in four (44%) of the nine patients from the first group and in two (11%) of the 18 patients from the second group (p = .14, Fisher exact test, two-tailed). The nine patients from the first group had a median of two and a mean of 2.1 ± 1.1 needle passes; the 18 patients in the second group had a median of one and a mean of 1.2 ± 0.4 needle passes (p = .029, unpaired t-test). None of the six patients in whom a pneumothorax developed required a chest tube.

Metaanalysis of the data from our series combined with comparable data of two previous series (Table 1) yielded a Mantel-Haenszel χ^2 value of 6.22 (p = .013). This result

indicates that the pooled data of these three series show that having a cytopathologist present during fine-needle aspiration biopsy was associated with a statistically significant increase in diagnostic accuracy compared with those procedures performed when a cytopathologist was not present.

Discussion

The major finding in this study was that having a cytopathologist present during thoracic fine-needle aspiration biopsy was associated with significantly greater accuracy in diagnosis ($p < .05$) than not having a cytopathologist present. Moreover, this result applies not only to the data of our series but also to the combination of series we used for metaanalysis. In particular, the only two previous reports that, to our knowledge, have addressed this question [3, 5] each showed trends toward the same result, but the data were not statistically significant (Table 1). However, metaanalysis of the data of all three series actually lowered the probability value for accuracy of diagnosis ($p = .013$) compared with that of our series alone ($p = .027$). The combined data of all three series make up a study of a total of 211 biopsy procedures.

Some authors [1, 6] recommend routinely using more than one needle pass for fine-needle aspiration biopsy, although not all do so [2]. By design, our study does not answer this question, but the limited data (five false-negative results associated with one needle pass each, one false-negative result associated with two passes) lend modest support to the practice. On the other hand, having a cytopathologist present during a biopsy has been advocated as a way to decrease the total number of needle passes and therefore the rate of pneumothorax [4]. In our study, when a cytopathologist was not present, no further passes were obtained whenever gross inspection of aspirated material suggested that the material contained fragments of tissue. With this approach, the rate of pneumothorax was low (7%) but the rate of false-negative results was higher (20%) than when a cytopathologist was present (0%). Our data suggest that only with a cytopathologist present can determination of adequacy of the specimen be assured.

Our data also confirm prior observations that the risk of pneumothorax rises as the number of needle passes increases [4, 5, 10], provided that the needle tract traverses aerated lung [10].

The overall rate of pneumothorax in the present study (11% of 55 patients) is lower than the rates of 21–34% reported in major series [1, 2, 4, 5, 11]. In part, this finding is biased because our study included 28 patients with pulmonary lesions adjacent to the chest wall. Careful positioning of the needle under CT guidance directed the needle into the lesion in each of these 28 patients without traversal of aerated lung. Pneumothorax developed in none of these subjects [10]. In the remaining 27 subjects (needle traversing aerated lung), the overall likelihood of pneumothorax was 22% (i.e., in the expected range for this complication).

Having a cytopathologist present during biopsy offers possibilities for immediate decisions concerning triage of specimens for ancillary studies [2, 6, 8]. For example, immunochemical studies [12], electron microscopy, and culture for microorganisms require specific methods for proper preparation of tissue for analysis. When a pathologist is available to evaluate freshly obtained biopsy material, circumstances are appropriate for optimal decisions concerning disposition of the material obtained, as well as decisions concerning the desirability of obtaining more material.

TABLE 1: Accuracy of Results of Thoracic Fine-Needle Aspiration Biopsy Performed with and Without a Cytopathologist Present in 211 Cases

Series	Biopsy Results with Cytopathologist Present		Biopsy Results with Cytopathologist not Present		
	Accurate	Inaccurate	Accurate	Inaccurate	*p* Value
Pak et al. [3]	36	1	13	2	.20[a]
Miller et al. [5]	48	4	44	8	.35[a]
Present series	25	0	24	6	.027[b]

Note.—Data represent number of patients undergoing biopsy. *p* Value = probability value for comparison of accuracy of results for biopsies performed with and without a cytopathologist present during the procedure.

[a] χ^2-test.

[b] Fisher exact test, two-tailed.

ACKNOWLEDGMENTS

We thank Nancy B. Austin and Livia Turgeon for statistical assistance.

REFERENCES

1. Westcott JL. Direct percutaneous needle aspiration of localized pulmonary lesions: results in 422 patients. *Radiology* **1980**;137:31–35
2. Johnson RD, Gobien RP, Valicenti JF Jr. Current status of radiologically directed pulmonary thin needle aspiration biopsy: an analysis of 200 consecutive biopsies and review of the literature. *Ann Clin Lab Sci* **1983**;13:225–239
3. Pak HY, Yokota S, Teplitz RL, Shaw SL, Werner JL. Rapid staining techniques employed in fine needle aspirations of the lung. *Acta Cytol* **1981**;25:178–184
4. Johnsrude IS, Silverman JF, Weaver MD, McConnell RW. Rapid cytology to decrease pneumothorax incidence after percutaneous biopsy. *AJR* **1985**;144:793–794
5. Miller DA, Carrasco CH, Katz RL, Cramer FM, Wallace S, Charnsangavej C. Fine needle aspiration biopsy: the role of immediate cytologic assessment. *AJR* **1986**:147:155–158
6. Silverman JF, Finley JL, O'Brien KF, et al. Diagnostic accuracy and role of immediate interpretation of fine needle aspiration biopsy specimens from various sites. *Acta Cytol* **1989**;33:791–796
7. Sacks HS, Berrier J, Reitman D, Ancona-Berk VA, Chalmers TC. Meta-analysis of randomized controlled trials. *N Engl J Med* **1987**;316:450–455
8. Ducatman BS, Hogan CL, Wang HH. A triage system for processing fine needle aspiration cytology specimens. *Acta Cytol* **1989**;33:797–799
9. Fleiss JL. *Statistical methods for rates and proportions*, 2nd ed. New York: Wiley, **1981**:113–119
10. Haramati LB, Austin JHM. Complications after CT-guided needle biopsy through aerated versus nonaerated lung. *Radiology* **1991**;181:778
11. Sinner WN. Complication of percutaneous transthoracic needle aspiration biopsy. *Acta Radiol* **1976**;17:813–828
12. Yam LT. Immunocytochemistry of fine needle aspirates: a tactical approach. *Acta Cytol* **1990**;34:789–796

Books Received

Receipt of books is acknowledged as a courtesy to the sender. Books considered of sufficient interest are reviewed as space permits. If the book has been reviewed in the *AJR*, the date of its review is given in parentheses.

MRI of the Brain I. Non-Neoplastic Disease. Edited by William G. Bradley, Jr., and Michael Brant-Zawadzki. (One of 10 volumes in The Raven MRI File. Series editors: Robert B. Lufkin, William G. Bradley, Jr., and Michael Brant-Zawadzki.) New York: Raven, 254 pp., 1991. $60 (10/92)

Diagnostic Ultrasound. Physics, Biology, and Instrumentation. By Stuart C. Bushong and Benjamin R. Archer. St. Louis: Mosby–Year Book, 177 pp., 1991. $34.95 (10/92)

Ultrasonography of Infants and Children. By Rita Littlewood Teele and Jane Chrestman Share. Philadelphia: Saunders, 534 pp., 1991. $95 (10/92)

Diagnostic Imaging of the Premature Infant. Edited by Rodrigo Dominguez. New York: Churchill Livingstone, 288 pp., 1992. $89.95 (10/92)

Diagnostic Radiology. An Anglo-American Textbook of Imaging, 2nd ed., vols. 1–3. Edited by Ronald G. Grainger and David J. Allison. New York: Churchill Livingstone, 2443 pp., 1992. $450 (10/92)

Radioisotopic Methods for Biological and Medical Research. By Herman W. Knoche. New York: Oxford University Press, 432 pp., 1991. $42.50 (11/92)

Introduction to Abdominal Ultrasonography. By Y. Higashi, A. Mizushima, and H. Matsumoto. New York: Springer-Verlag, 215 pp., 1991. $59 (11/92)

Imaging of the Temporal Bone, 2nd ed. By Joel D. Swartz and H. Ric Harnsberger. New York: Thieme, 353 pp., 1992. $99 (11/92)

Basic Doppler Physics. By Hans-Jorgen Smith and James A. Zagzebski. Madison, WI: Medical Physics Publishing, 121 pp., 1991. $39 (11/92)

Nuclear Medicine Procedure Manual, 2nd ed. Edited by Wm. C. Klingensmith III, Dennis Eshima, and John Goddard. Englewood, CO: Wick Publishing, 123 pp., 1992. Print format, $155; disk format, $135; both formats, $245 (11/92)

Outline of Medical Imaging, vols. 1 and 2. By Louis Kreel and Anna Thornton. Stoneham, MA: Butterworth-Heinemann, 1302 pp., 1992. $395 (11/92)

Gamuts in Ultrasound. By Michael R. Williamson and Susan L. Williamson. Philadelphia: Saunders, 240 pp., 1992. $25 (11/92)

A Radiologic Approach to Diseases of the Chest. By Irwin M. Freundlich and David G. Bragg. Baltimore: Williams & Wilkins, 560 pp., 1992. $95 (11/92)

Peripheral Vascular Sonography. A Practical Guide. By Joseph F. Polak. Baltimore: Williams & Wilkins, 364 pp., 1992. $75 (11/92)

Diagnostic Imaging of the Lung. Edited by Charles E. Putman. (No. 46 in the series Lung Biology in Health and Disease.) New York: Marcel Dekker, 769 pp., 1990. $165 (12/92)

MRI Physics for Radiologists. A Visual Approach, 2nd ed. By Alfred L. Horowitz. New York: Springer-Verlag, 187 pp., 1992. $25 (12/92)

Practical Pediatric Imaging. Diagnostic Radiology of Infants and Children, 2nd ed. Edited by Donald R. Kirks. Boston: Little, Brown, 1099 pp., 1991. $150 (12/92)

Nonpalpable Breast Cancer. Diagnosis and Management. By George Hermann, Ira S. Schwartz, and Paul I. Tartter. New York: Igaku-Shoin, 132 pp., 1992. $59.50 (12/92)

Musculoskeletal Oncology. A Multidisciplinary Approach. Edited by Michael M. Lewis. Philadelphia: Saunders, 529 pp., 1992. $95 (12/92)

Double Contrast Gastrointestinal Radiology, 2nd ed. By Igor Laufer and Marc S. Levine. Philadelphia: Saunders, 735 pp., 1992. $125 (12/92)

Current Opinion in Radiology. Neuroradiology and Radiology of the Head and Neck: 1992. Guest editors: A. James Barkovich, Thomas J. Vogl, and William P. Dillon. Philadelphia: Current Science, February 1992;4(1):1–173. $30; by subscription, 6 issues annually for $145 (12/92)

"The President Has Been Shot." Confusion, Disability, and the 25th Amendment in the Aftermath of the Attempted Assassination of Ronald Reagan. By Herbert L. Abrams. New York: Norton, 363 pp., 1992. $22.95 (12/92)

Measurement of Dose Equivalents from External Photon and Electron Radiations. (Report No. 47.) Edited by ICRU. Bethesda: ICRU, 40 pp., 1992. $40

Photon, Electron, Proton and Neutron Interaction Data for Body Tissues. Edited by ICRU. Bethesda: ICRU, 207 pp., 1992. $40

Radiopharmaceuticals. Chemistry and Pharmacology. Edited by Adrian D. Nunn. New York: Marcel Dekker, 460 pp., 1992. $165

World Health Statistics. By the World Health Organization. Geneva: WHO, 164 pp., 1992.

Pictorial Essay

Devices for Transcatheter Closure of Intracardiac Defects

Valerie S. Mandell,[1] Katherine Nimkin,[1,2] Fredric A. Hoffer,[1] and Nancy D. Bridges[3,4]

Transcatheter closure of intracardiac defects is an investigational procedure that is in use at a number of centers in North America and Europe. A radiologist should be able to recognize these devices on a chest radiograph, understand their actual physical appearance, and be able to recognize their expected location. This essay summarizes the indications for, technical aspects of, and radiologic appearance of these devices.

Devices and Techniques

In 1987, Rashkind et al. [1] described a "double umbrella" occlusion device (Rashkind PDA Occluder System, USCI–C. R. Bard, Billerica, MA) that can be inserted transvenously through an 8-French sheath to close a patent ductus arteriosus. The Rashkind device consists of two polyurethane disks mounted on opposing three- or four-arm spine assemblies resembling two umbrellas (Fig. 1). This device is available in 12- and 17-mm disk sizes. In 1989, Lock et al. [2] described a modified double-umbrella device that could be introduced through an 11-French sheath (Bard Clamshell Septal Umbrella, USCI–C. R. Bard). This device has been used successfully to close congenital atrial and ventricular septal defects, as well as a variety of other intracardiac communications [2, 3]. The Lock clamshell device, available in five sizes from 17 to 40 mm, has an extra hinge in each arm that folds its Dacron square patch back on itself for better apposition to a septal surface (Fig. 1). The double hinge resembles a closed shell.

The size and location of the cardiac defect is assessed first by echocardiography. At catheterization, contrast medium is injected initially to show the communication that must be closed. After the defect has been crossed by guidewire and catheter, usually by a transvenous approach, sizing is accomplished by pulling an inflated balloon of increasing diameter across the defect until a snug fit is achieved. The delivery sheath is introduced, and the device, mounted on its delivery shaft, is inserted into the sheath. The sheath is withdrawn to expose the distal arms first, allowing them to expand. If positioning is satisfactory, the sheath is further withdrawn, opening the proximal arms on the other side of the defect, and the device is released.

After placement of the device, contrast material is injected again to assess the adequacy of the closure and the final position of the device. A portable chest radiograph is obtained to check that the position is stable. Radiographs are obtained at various intervals during long-term follow-up.

Specific Clinical Applications

Patent ductus arteriosus was the first cardiac defect closed by transcatheter technique. In a continuing investigational protocol, approximately 700 of these defects have been closed at various centers in North America, with an additional 2000 in Europe. In our hospital, most have been closed by using the Rashkind device (Figs. 2 and 3), although larger defects have been closed successfully by using the clamshell device.

The new clamshell device is designed to cover a septal defect with a closely adherent Dacron shield that eventually

Received April 16, 1992; accepted after revision July 14, 1992.
[1]Department of Radiology, Children's Hospital and Harvard Medical School, 300 Longwood Ave., Boston, MA 02115. Address reprint requests to V. S. Mandell.
[2]Present address: Department of Radiology, University of Massachusetts Medical Center, Worcester, MA 01606.
[3]Department of Cardiology, Children's Hospital and Harvard Medical School, Boston, MA 02115.
[4]Present address: Cardiology Division, St. Louis Children's Hospital, St. Louis, MO 63110.

AJR 1993;160:179–184 0361–803X/93/1601–0179

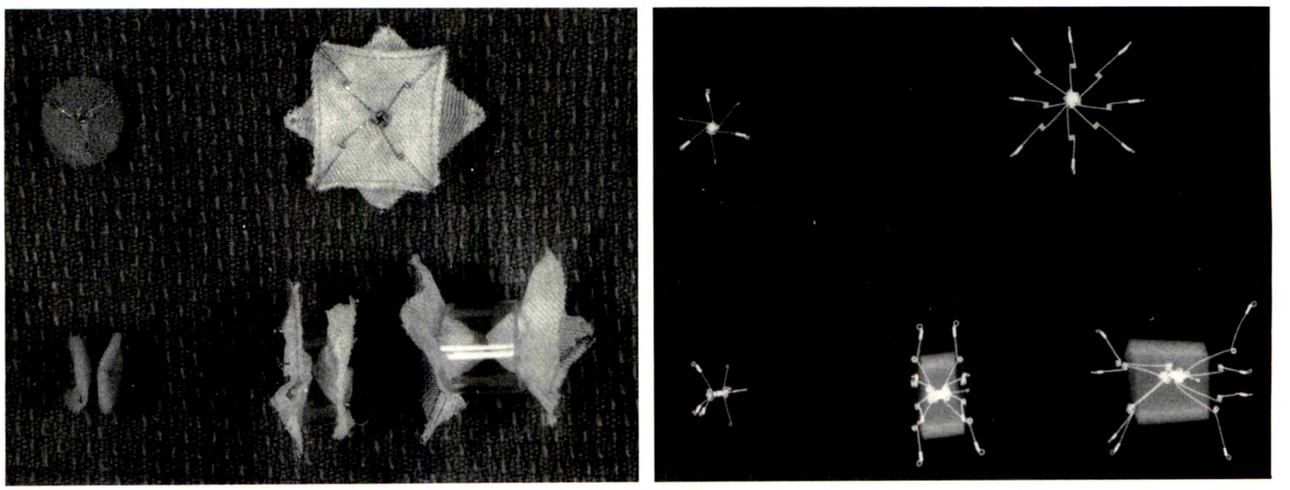

A B

Fig. 1.—*A* and *B*, Photograph (*A*) and radiograph (*B*) of devices for transcatheter closure of intracardiac defects. Frontal (*top left*) and lateral (*bottom left*) views of 12-mm Rashkind ductus closure device (17-mm device has four arms and is not pictured). Frontal view (*top right*) of 28-mm Lock clamshell device shows offset Dacron squares and hinged arms. Side views show device as it would appear in atrial septum (*bottom middle*) and in ventricular septum (*bottom right*).

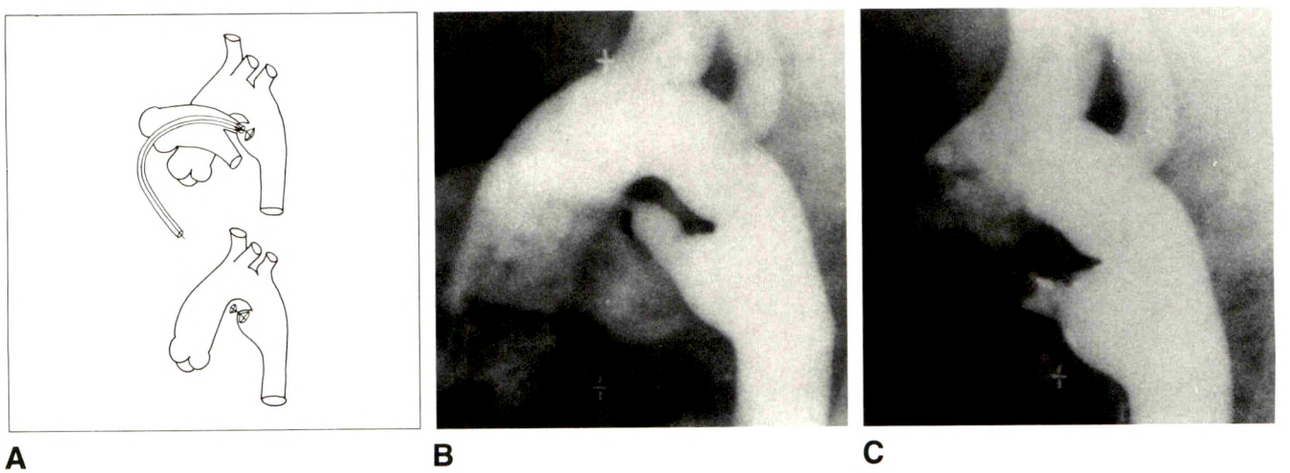

A B C

Fig. 2.—Transcatheter technique for closure of patent ductus arteriosus.
A, Diagram of procedures. Device is released from transvenous sheath by exposing aortic arms first (*top*). Bottom diagram shows position of open device after release.
B and *C*, Lateral aortograms show long ductus arteriosus with prominent aortic diverticulum before (*B*) and after (*C*) closure of ductus arteriosus with 12-mm device. Note occlusion of ductus arteriosus after closure.

becomes completely endothelialized. At our hospital and at other centers in North America, approximately 300 patients have had a clamshell device placed to close an atrial septal defect. The delivery and placement techniques are similar to those used for the patent ductus arteriosus (Fig. 4).

For certain postoperative residual ventricular septal defects and for defects in the muscular septum, which might require left ventriculotomy for repair, transcatheter closure is a useful alternative to surgery (Fig. 5). In patients with complex anatomy, this technique has been combined with subsequent staged surgical repair [4]. Placement of multiple devices has made "septal reconstruction" possible in selected cases (Fig. 6).

Modified Fontan repair is used to separate the venous and arterial circulations in children who cannot have a two-ventricle repair. The clamshell device is used for postoperative closure of a surgically created (temporary) fenestra in the atrial baffle [5]. Figure 7 shows the appearance of a "fenestrated Fontan" on angiograms and radiographs before and after transcatheter closure of the fenestra.

Transcatheter devices, either the Rashkind umbrella or the Lock clamshell, have been used to close a variety of

Fig. 3.—Transcatheter closure of patent ductus arteriosus.

A and *B*, Frontal (*A*) and lateral (*B*) chest radiographs show position of 17-mm device (*arrows*) used for transcatheter closure of patent ductus arteriosus.

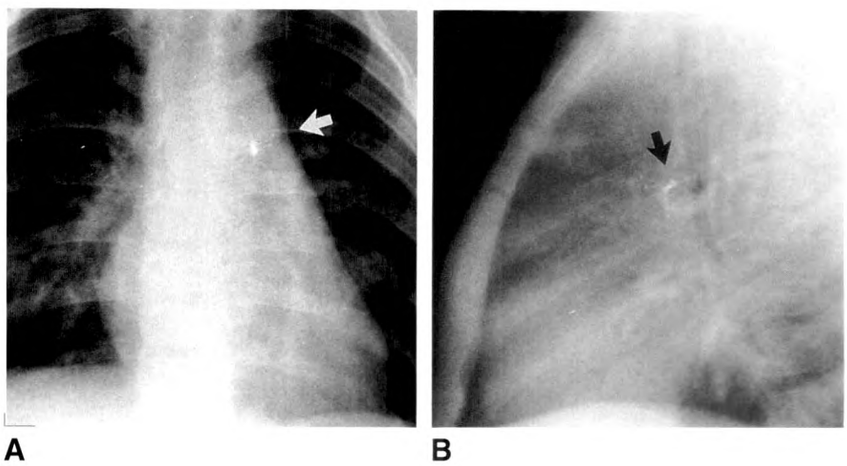

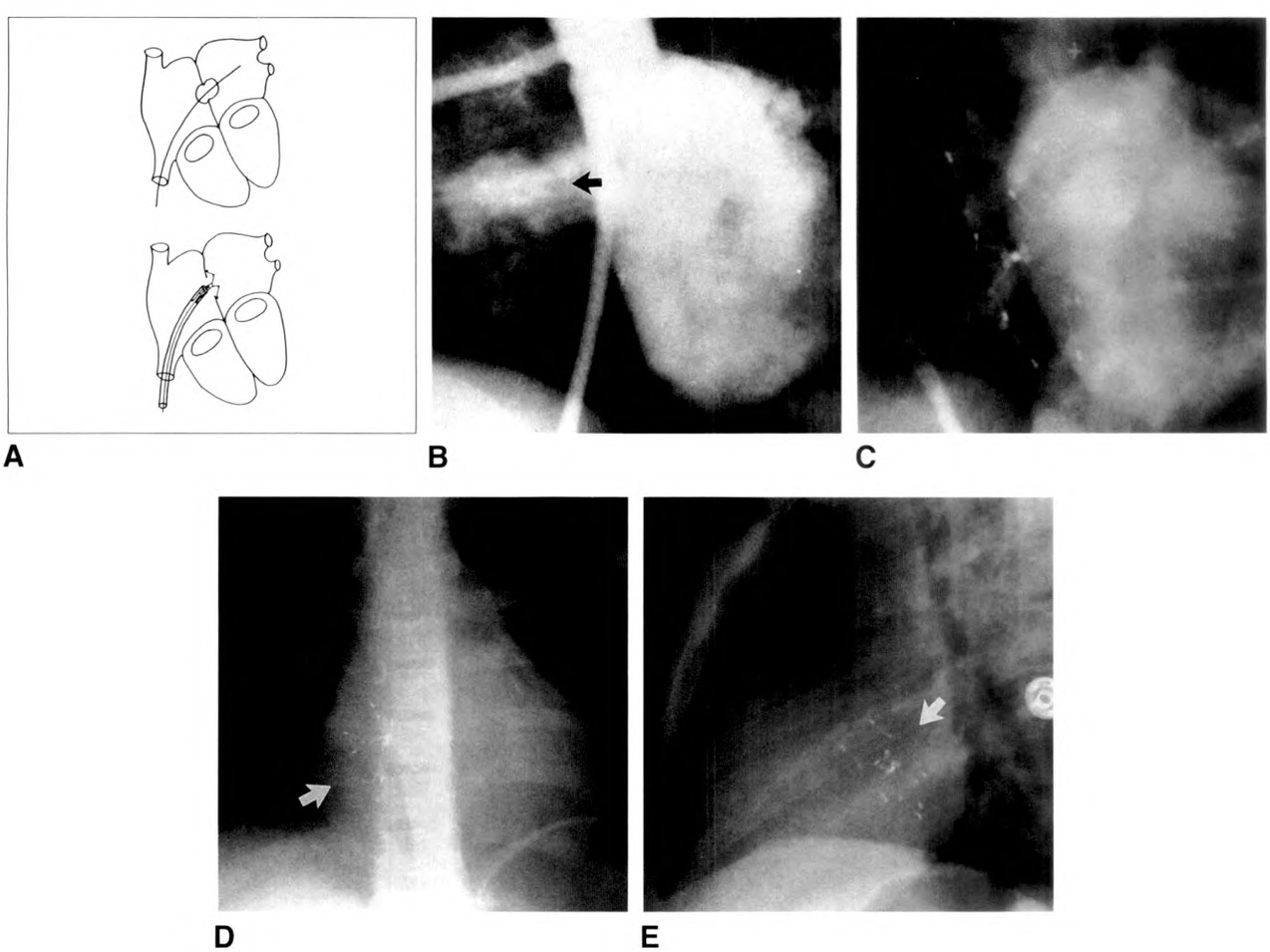

Fig. 4.—Transcatheter technique for closure of atrial septal defect.

A, Diagram of procedure. Balloon catheter is used in choosing device size (*top*). Device is delivered via transvenous sheath. Arms are first released on left atrial side (*bottom*). Further withdrawal of sheath releases right atrial arms in position across septum.

B, Cineangiogram shows left atrial injection in a left anterior oblique view with cranial angulation. Note left-to-right atrial shunt (*arrow*).

C, Cineangiogram of levophase of right atrial injections shows complete closure of atrial defect by clamshell device.

D and *E*, Frontal (*D*) and lateral (*E*) chest radiographs show position of device (*arrows*) in atrial septum.

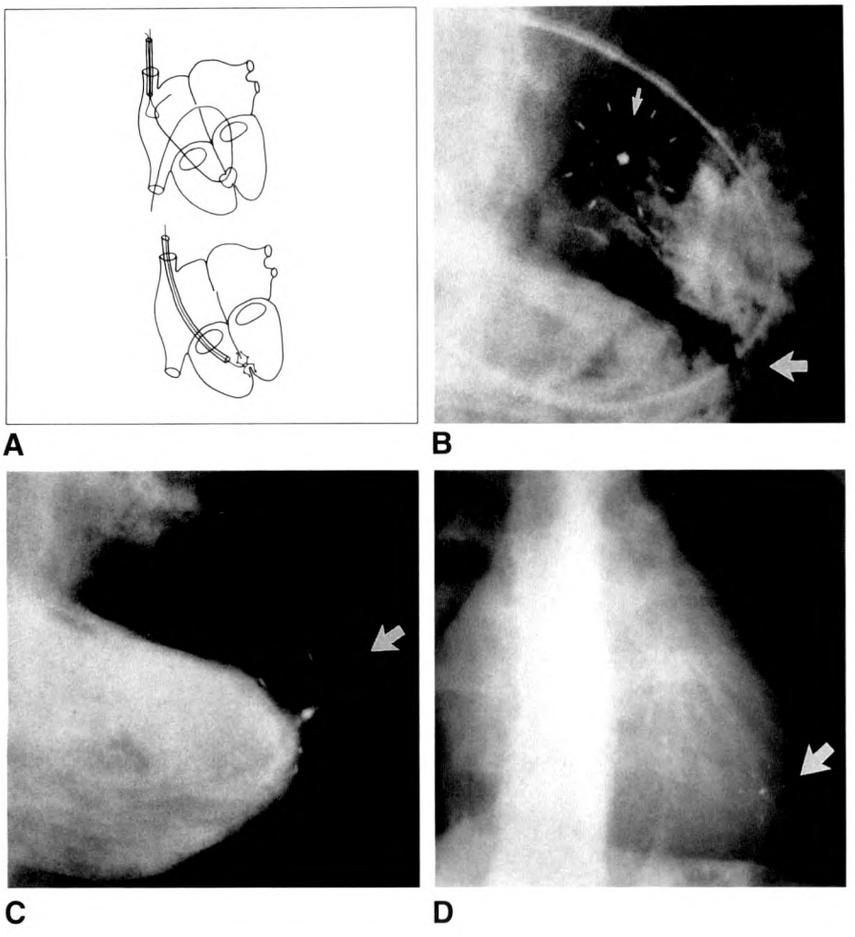

Fig. 5.—Transcatheter technique for closure of muscular ventricular septal defect.

A, Diagram of procedure. Defect is approached by a transvenous route, across atrial septum and through mitral valve, and is probed from smooth left ventricular side. Then defect is crossed and balloon-sized, (see text). Guidewire is snared from a superior vena caval approach (*top*). Sheath is introduced from superior vena cava, and clamshell device is delivered and released in position across ventricular defect (*bottom*).

B, Cineangiogram in oblique projection shows an apical ventricular septal defect (*large arrow*) in a patient with corrected transposition. (Undelivered clamshell closure device [*small arrow*], still in its package, is on patient's chest as a reference for size.)

C, Left ventriculogram shows closure of apical ventricular septal defect. Note extended position of arms of device (*arrow*) due to thickness of ventricular septum.

D, Chest radiograph shows apical position of device (*arrow*) in ventricular septum.

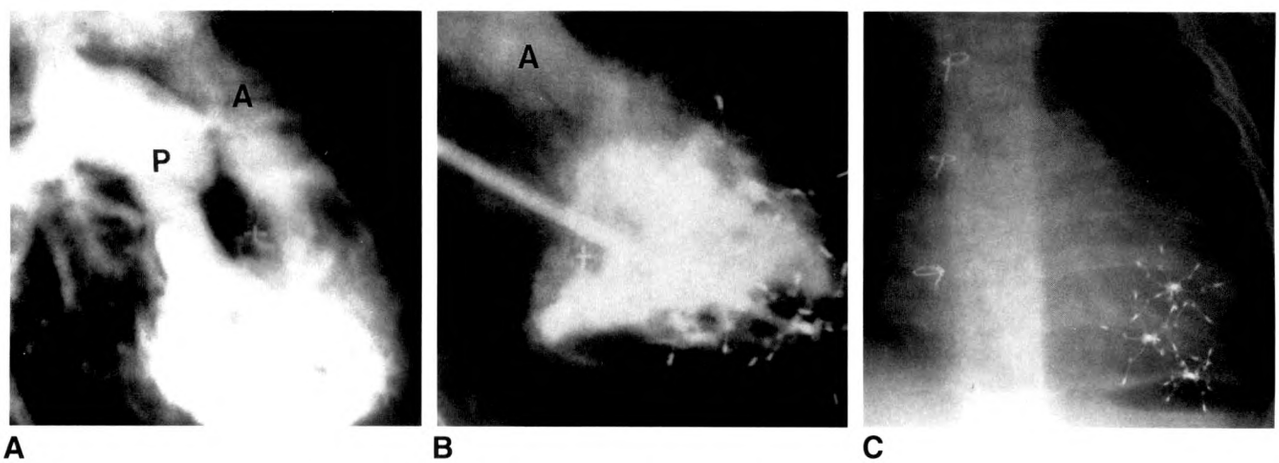

Fig. 6.—Infant with transposition of great arteries and multiple defects in muscular ventricular septum.

A, Cine left ventriculogram in right anterior oblique projection shows transposition and defects before placement of closure device.

B, Cine right ventriculogram in right anterior oblique projection obtained after three clamshell devices were placed in three separate procedures. Muscular septum was effectively reconstructed before subsequently successful arterial switch procedure.

C, Frontal chest radiograph shows locations of devices.

A = aorta, P = pulmonary artery.

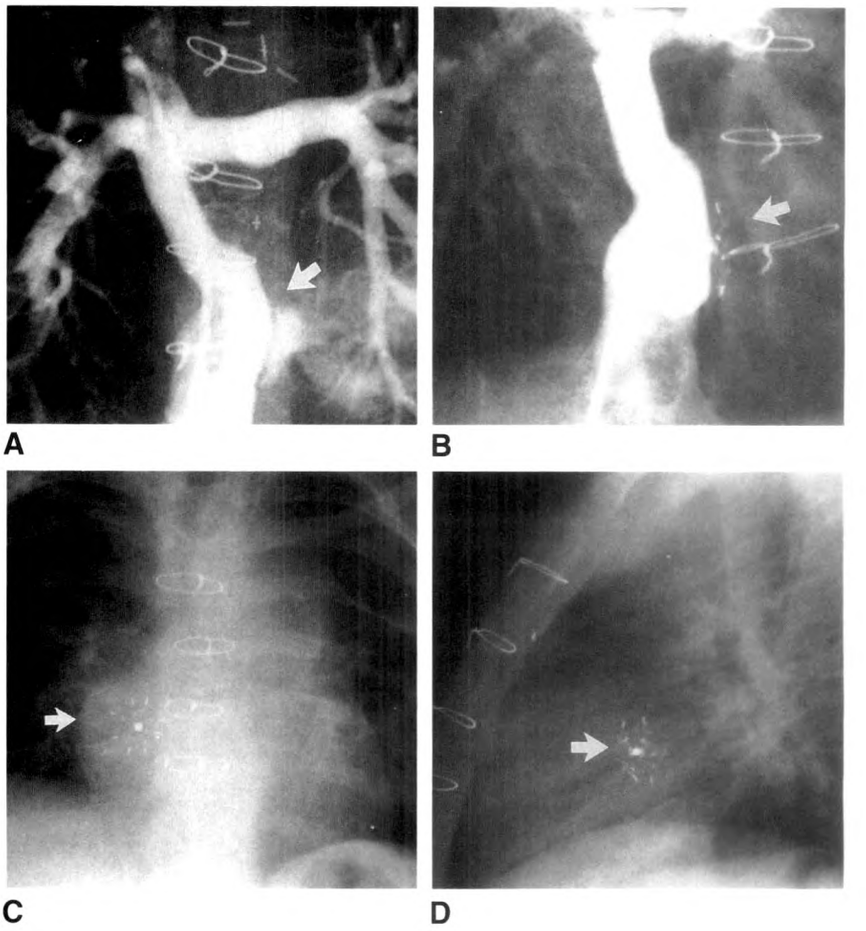

Fig. 7.—Fenestrated Fontan baffles.
A, Cineangiogram in frontal projection shows injection into a modified Fontan baffle. Surgeon has left a small fenestra (*arrow*), which allows right-to-left shunting in early postoperative period.
B, Cineangiogram in right anterior oblique projection shows closure of baffle fenestra with a 17-mm clamshell device (*arrow*).
C and *D*, Frontal (*C*) and lateral (*D*) chest radiographs show location of device (*arrows*).

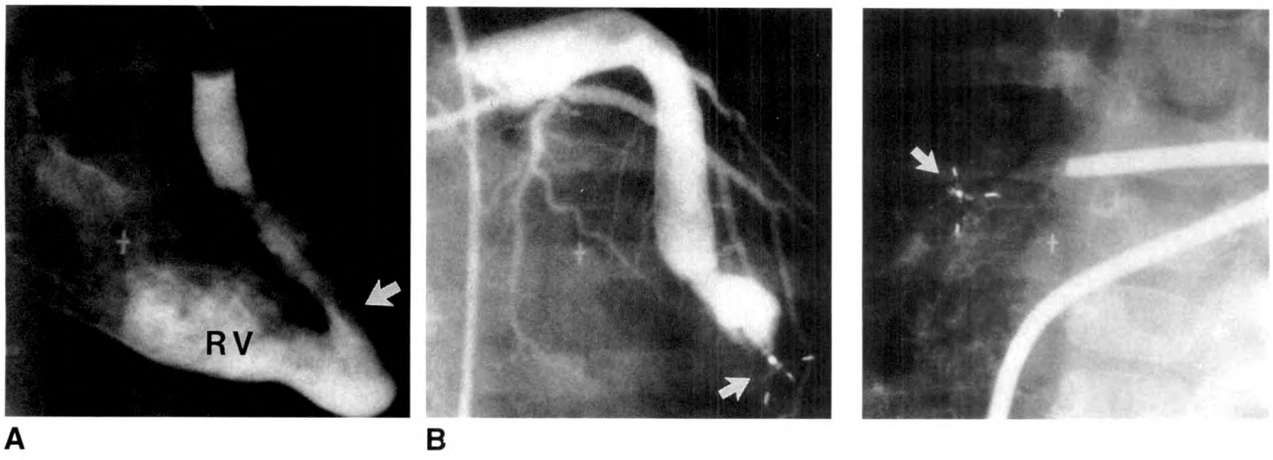

Fig. 8.—Closure of fistula in coronary artery.
A, Angiogram obtained after retrograde injection of contrast material through balloon catheter into left coronary artery shows fistula (*arrow*) between coronary artery and right ventricle (RV).
B, Coronary angiogram shows Rashkind device (*arrow*) occluding fistulous connection and enhancing filling of normal branches of left coronary artery.

Fig. 9.—Cineradiograph shows location of dislodged Rashkind device (*arrow*) immediately after placement into a large, patent ductus arteriosus. Device was snared by using a stone basket and retrieved percutaneously from femoral vein. Larger clamshell device was successfully placed.

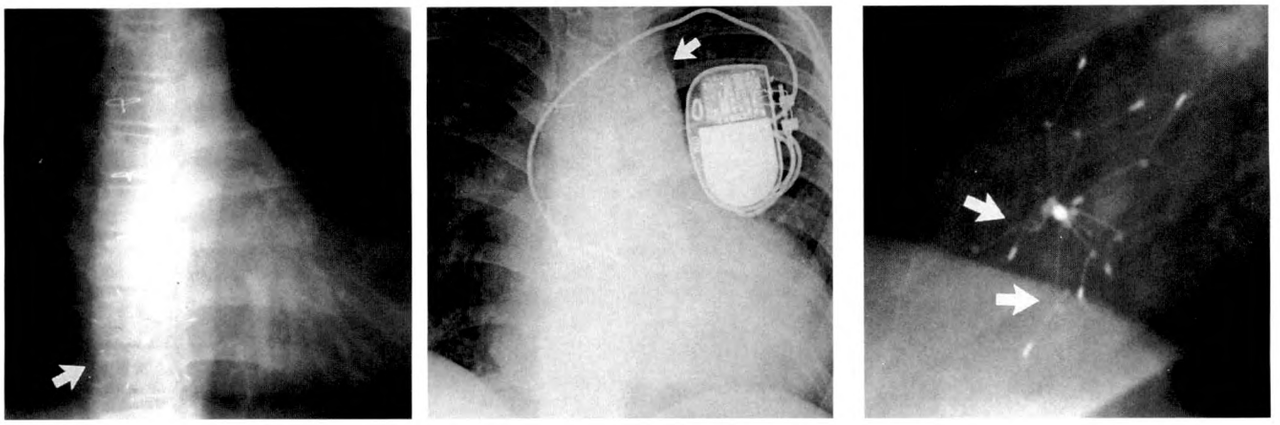

A B

Fig. 10.—Patient with a Mustard atrial baffle for transposition.
***A*, Frontal chest radiograph shows device (*arrow*) closing residual atrial defect.**
***B*, Portable chest radiograph obtained day after transvenous placement of pacemaker shows that device had been dislodged, presumably due to wire manipulation, into right-sided pulmonary venous atrium and then via right ventricle into aortic arch, where it lodged (*arrow*). Device was retrieved by using a stone basket and was removed from femoral artery via cutdown.**

Fig. 11.—Magnified view of lateral chest radiograph shows clamshell device in correct location after closure of atrial septal defect. Note two overlapping arms (*arrows*), indicating fracture at two hinge points.

other abnormal intracardiac communications, including persistent communication between the superior vena cava and the right atrium after Glenn operation, aortic paravalvular leak, and coronary artery fistula (Fig. 8).

Complications

Embolization of the device at the time of placement, usually due to underestimation of the defect's size, can occur (Fig. 9). The device can be retrieved by using techniques for transcatheter removal of a foreign body; rarely, cutdown is required for removal of the device at the skin site. In a few instances, embolization has occurred after the patient has left the catheterization laboratory and has been recognized when radiographs obtained after placement show a change in the device's location (Fig. 10). We know of no instance in which the device has migrated after the patient's discharge from the hospital.

Follow-up radiographs after clamshell placement to close atrial and ventricular septal defects have shown that late fracture of one or more arms, especially with the larger clamshell devices (Fig. 11), is not rare. To date, no clinical sequelae related to the fractures have been identified, presumably because the fractures have occurred after substantial endothelialization. Use of the device for elective closure of atrial septal defects is being deferred while the design is being modified; however, the present device is still being implanted in Fontan baffles, muscular ventricular septal defects, and postoperative residual defects.

REFERENCES

1. Rashkind WJ, Mullins CE, Hellenbrand WE, Tait MA. Nonsurgical closure of patent ductus arteriosus: clinical application of the Rashkind PDA Occluder System. *Circulation* **1987**;75:583–592
2. Lock JE, Rome JJ, Davis R, et al. Transcatheter closure of atrial septal defects. *Circulation* **1989**;79:1091–1099
3. Lock JE, Block PC, McKay RG, Baim DS, Keane JF. Transcatheter closure of ventricular septal defects. *Circulation* **1988**;78:361–368
4. Bridges ND, Perry SB, Keane JF, et al. Preoperative transcatheter closure of congenital muscular ventricular septal defects. *N Engl J Med* **1991**; 324:1312–1317
5. Bridges ND, Lock JE, Castaneda AR. Baffle fenestration with subsequent transcatheter closure: modification of the Fontan operation for patients at increased risk. *Circulation* **1990**;82:1681–1689

Computers in Radiology

An Automated Radiology Reporting System That Uses HyperCard

David A. Bluemke[1] and John Eng

SCRIBE is an automated radiology reporting system that uses the HyperCard environment on Macintosh computers. Radiologic findings and anatomic terms are presented in graphic form, and the appropriate terms are selected by using a trackball or touch-sensitive video screen. Additional lists of more specific terms and differential diagnoses can be requested by the user for abnormal findings. The system is suited to the reporting of plain films and is being used in the emergency room of a large academic radiology department. Advantages of the system include low cost, operational familiarity to Macintosh users, and elimination of transcription costs. Finished reports are immediately available in both printed and electronic forms.

In traditional radiology film reporting, the radiologist uses dictation equipment to record a report, which is then typed by a transcriptionist. Reports are later returned to the radiologist for correction and signature, either in printed or electronic form. Preprogrammed reports and codes, known as "macros" [1], can decrease transcription time and cost, but a typist is still involved. Several approaches to automating radiology film reporting have been described [2]. These systems attempt to eliminate the transcriptionist in one of two ways: (1) direct radiologist interaction with a computer system or (2) indirect interaction through the use of coded forms or bar codes that can be read by a computer [3].

An automated system for plain film reporting, the Siemens SIREP system, has been used successfully at The Johns Hopkins Hospital since the early 1970s [4]. With SIREP, the radiologist constructs a report by choosing appropriate words and phrases from lists of standard terms presented graphically on a touch-activated screen. For experienced users and noncomplex reports, reporting speeds may be up to 80–95% of dictation speed [4]. Although the system is still in use at Johns Hopkins, the high cost of each workstation resulted in limited distribution of the unit.

In this report, we describe an automated reporting system that operates on a Macintosh computer. Advantages of this system include low cost with installation on widely available microcomputers, high system reliability, and easy customization of the user display. In addition, we compare a touch-sensitive screen with a trackball as user input devices.

Materials and Methods

System Design

The Apple Macintosh microcomputer (Apple Computer, Inc., Cupertino, CA) was chosen as the platform for software development because of its graphics-oriented user interface. System hardware consists of either the Macintosh IIsi or IIci model with 5.0 megabytes of random access memory (RAM), an internal 80-megabyte hard disk drive, and a 19-in. monitor with interface card (model 1960 color Trinitron display and 8XLi display board, RasterOps Corp., Santa Clara, CA). Input devices include a trackball (Kensington Microware, Ltd., San Mateo, CA) and a MouseTouch touch-sensitive screen (Information Strategies, Inc., Richardson, TX).

The software program, named SCRIBE, was written in the HyperCard scripting language (HyperCard version 2.1, Claris Corp., Santa Clara, CA). To increase program execution speed, several functions were written in Pascal (THINK Pascal, Symantec Corp., Cupertino,

Received June 1, 1992; accepted after revision July 23, 1992.

[1] Both authors: The Russell H. Morgan Department of Radiology and Radiologic Science, The Johns Hopkins Hospital, 600 N. Wolfe St., Baltimore, MD 21287. Address reprint requests to D. A. Bluemke.

AJR **1993;160:185–187** 0361–803X/93/1601–0185

CA) as HyperCard extensions (XCMDs). Pascal also was used to write routines that interact with our hospital-wide radiology information system to request information on patients and upload completed reports. SCRIBE contains routines supporting a standard Health Level Seven (HL7) interface as well as standard serial communications with mainframe computers. The SCRIBE HyperCard stack is 1.5 megabytes in size and contains approximately 4000 lines of program code.

The minimum system requirements for operating the program include a Macintosh computer with at least 4.0 megabytes of available RAM, a 1024 × 768 pixel monochrome display monitor, a trackball or mouse, HyperCard 2.1 software, a hard disk drive, and a printer. The cost of a basic system (Macintosh IIsi, monochrome monitor, trackball, dot-matrix printer) is approximately $3500. A touch screen is optional and costs approximately $1000.

The SCRIBE software was written to emulate the appearance and operation of the SIREP [2, 4] reporting system. The SCRIBE system contains 55 different displays, or "frames." Of the 55 frames, 27 consist of "main" display frames, and the remaining frames contain less common terms and more specific differential diagnoses related to radiologic findings on the main frames.

The central portion of the display, outlined by a heavy black box, consists of a 12 × 12 array of terms and phrases that describe radiologic findings for a specific type of plain film, as shown for the ankle in Figure 1. Terms in the central display area are further divided into two types: abnormal findings (e.g., "fracture") and anatomic descriptors (e.g., "medial malleolus"). Anatomic terms are frequently displayed with a graphic representation. General words and phrases potentially useful for all types of examinations are positioned around the periphery of the display. The user can activate buttons in the top two rows of the screen to move between different main frames. The response time is the time between the user activating a screen "button" and the computer completing the action. For selecting radiologic terms, the response time is approximately 0.45 sec on the Macintosh IIci unit in 1-bit mode. The response time to move between different main frames is approximately 0.72 sec.

Operation

System operation begins with the radiologist selecting his or her name from a list of authorized users in the department. At our hospital, the radiologist then enters a four-digit accession number for the radiologic examination. An information "header" corresponding to the accession number is downloaded to the SCRIBE software from the radiology information system. Header information typically consists of the patient's name, history number, age, race, and sex, and a code for the type of radiologic examination. On the basis of the

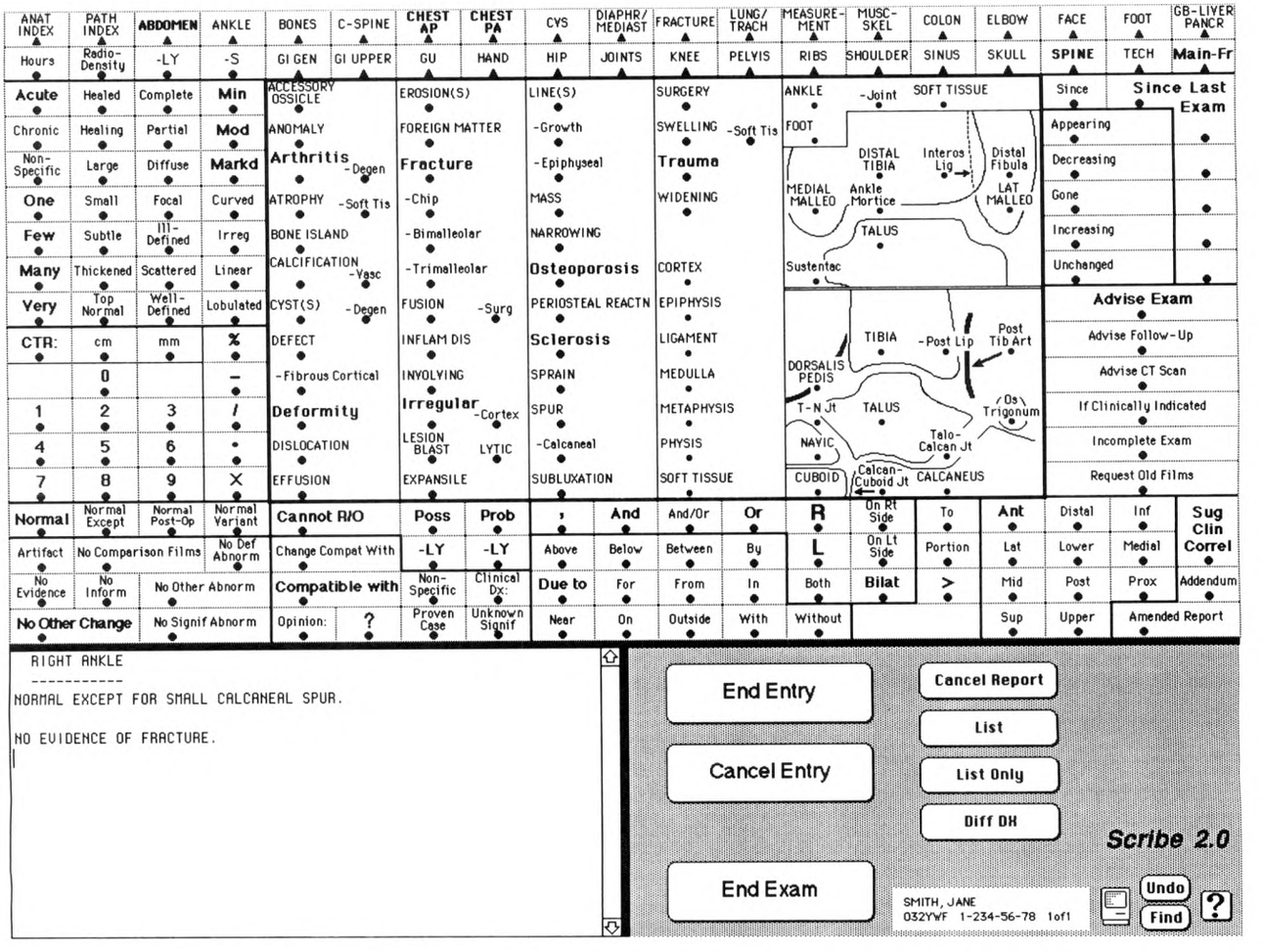

Fig. 1.—Main display frame for the ankle. Terminology specific to ankle is contained within central heavy black-outlined box. General descriptive terminology is grouped around periphery of display. Report is displayed in lower left corner.

type of examination, the SCRIBE program selects a main frame containing appropriate terminology.

The radiologist touches the display screen or operates the trackball to select the appropriate terms. As each item on the display is selected, feedback is provided to the user by flashing the active screen position and sounding a "beep." A keyboard with cursor control is provided for editing and for typing terms that are not listed on the display. When the "End Exam" button is activated, the report is saved to the Macintosh hard disk. A copy of the report is printed and uploaded to the radiology information system. Reports can be designated as preliminary when they are generated by residents and can be recalled from the hard disk at a later time if editing is needed.

Results

Report generation times with the SCRIBE system were evaluated with a touch screen and a trackball as pointing devices for selecting screen items. Seven radiologists were given five printed reports and asked to enter them by using both pointing devices. The average length of a report was eight lines, containing five words per line. Reporting times for different users ranged from 76 to 115 sec per report. The mean reporting time was 94 sec for the touch screen and 99 sec for the trackball, but the difference was not statistically significant. The average time required for dictation was approximately 40 sec, not including the transcriptionist's time or the radiologist's verification time.

The SCRIBE system was installed in the emergency department of our hospital as a backup system to other methods of reporting. Radiology residents were requested to use the system at their discretion. During a 4-month test period, approximately 1600 reports were generated with the use of SCRIBE out of approximately 8000 total emergency department radiology reports. Users who were familiar with the SIREP system required only four or five reports on the SCRIBE system before becoming familiar with its operation. In general, we estimate that users new to either system require 5–10 hr of use to learn the SCRIBE system.

Discussion

The SCRIBE reporting system is an alternative to dictating radiology reports. A major benefit of the system is that printed reports are available immediately after each film is interpreted. Accuracy in report generation is improved because proofreading is integral to the creation of the report. Preliminary results show good acceptance of the SCRIBE system by our radiologists. Except for improved report editing capabilities with the SCRIBE system, users found the human interface of the Macintosh-based system to be very similar to that of the SIREP system. A high degree of user acceptance has been the result of involvement of radiologists in software design, seeking to minimize changes in existing reporting patterns.

One important drawback to the SCRIBE system is that it requires more of the radiologist's time than dictation would. Because this problem is most pronounced with the reporting of complex cases, automated reporting in our department is not used for films of patients in the intensive care unit or for complicated orthopedic descriptions. Another disadvantage of the SCRIBE system is that the radiologist must look away from the film, often repeatedly, while generating the report. If time were instead spent looking at the film, it is possible that fewer findings would be missed. The implementation of voice-recognition technology [5] could help to solve this problem, and we believe that the concise format of SCRIBE reporting would be an excellent base to which this capability could be added. However, current voice-recognition systems also require a significant amount of time looking away from the film to verify the correctness of the voice recognition. The accuracy of voice-recognition technology is also limited by noisy environments, such as a busy emergency department.

The SCRIBE system is particularly suited to the academic radiology environment. Preliminary reports generated by residents are immediately accessible to clinical colleagues and can be reviewed later by attending radiologists alongside the films. Although some radiologists and referring clinicians may find the concise, telegraphic wording of SCRIBE reports too restrictive, the system does promote a uniform reporting style among different users. This is a practical benefit in departments such as ours, where 30 to 40 attending radiologists, fellows, and residents interpret plain films.

ACKNOWLEDGMENT

We thank William Brody and William Scott, Jr., for support and helpful discussions throughout this work.

REFERENCES

1. Schwartz LH, Brill PW, Winchester P. A PC-based semiautomated reporting system. *AJR* **1991**;157:1117–1118
2. Jost GR. Radiology reporting. *Radiol Clin North Am* **1986**;24:19–26
3. Mani RL. RAPORT radiology system: results of clinical trials. *AJR* **1976**;127:811–816
4. Wheeler PS, Simborg DW, Gitlin JN. The Johns Hopkins radiology reporting system. *Radiology* **1976**;119:315–319
5. Robbins AH, Horowitz DM, Srinivasan MK, et al. Speech-controlled generation of radiology reports. *Radiology* **1987**;164:569–573

Book Review

The Year Book of Ultrasound 1991. Edited by Christopher R. B. Merritt, Barbara A. Carroll, Carol A. Mittelstaedt, and David A. Nyberg. St. Louis: Mosby–Year Book, 311 pp., 1991. $57.95

The 1991 edition of *The Year Book of Ultrasound* is a new addition to the Mosby–Year Book series of literature reviews. It follows the standard format for such collections and shares with similar review the limitations of publication delay and variable quality of summaries and commentaries written by several different authors. All the articles included were published in 1990. Approximately 60% of the reviewed papers were originally published in *Radiology, AJR*, or *Journal of Ultrasound in Medicine*, although papers from several less widely circulated journals in the diagnostic radiology literature and from major journals in the fields of obstetrics and gynecology and surgery are also included. The book is divided into nine sections: obstetric and gynecologic, abdominal, genitourinary, vascular, pediatric, thyroid and parathyroid, and musculoskeletal sonography; miscellaneous topics; and physics and instrumentation. The obstetrics and gynecology section was written by David Nyberg; the abdominal, genitourinary, neck, and musculoskeletal sections, by Carol Mittelstaedt; the vascular and miscellaneous sections, by Barbara Carroll; and the pediatrics and physics sections, by C. R. B. Merritt.

Throughout the book, the number of reproduced illustrations is generous, and their quality is good to excellent. The reviews are generally clear, concise, and reasonably complete. The variations in quality lie chiefly in the value of the editorial comments that follow each review. In the obstetric and gynecologic and vascular sections, these comments provide helpful critical evaluation of the significance of each paper's contribution to the existing body of sonographic knowledge and include appropriate references directing interested readers to relevant background or alternative information. In the abdominal, genitourinary, pediatric, and miscellaneous sections, the editor's comments rarely exceed a few sentences advising the reader to be aware of the described clinical application; these sections are sparsely if at all referenced.

It seems probable that most readers who have an active interest in new developments in sonography will already have access to the major journals reviewed in this collection. I doubt that the abbreviated versions of papers from *Radiology, AJR,* and *Journal of Ultrasound in Medicine* will be of sufficiently compelling interest to move many readers to a complete study of this book, particularly as the summarized articles have been in print now for 2 years. The text cannot be considered timely. I doubt that many readers would consider the purchase price of $57.95 or the time invested in studying and evaluating the majority of reviews in this book well spent.

Barbara E. Demas
Kaiser Foundation Hospital
Redwood City, CA 94063

Perspective

Early History of Diagnostic Ultrasound: The Role of American Radiologists

Barry B. Goldberg,[1] Raymond Gramiak,[2] and Atis K. Freimanis[3]

First Step into the Unknown

In the late 1940s, after World War II, a few scattered enthusiasts recognized the potential of ultrasonic energy to provide information that could be useful in medical diagnosis. The efforts of these innovators resulted in new concepts and in unique early images that motivated both the manufacturers of instruments and the clinical pioneers to begin to establish meaningful clinical applications for this new phenomenon. The early successes of these individuals created a momentum that encouraged additional users and provided a firm foothold and broadened horizons for this emerging technology. This article examines the highlights of this era as it unfolds up to the late 1960s with emphasis on the contributions of American radiologists.

The earliest pioneers in the United States included three physicians, John Wild, a surgeon, George Ludwig, an internist, and Douglas Howry, a radiologist [1–6]. Of this group, Douglas Howry had the greatest influence on the other pioneers in radiology. In the late 1940s he left a formal residency program at Denver Veterans Administration Hospital to devote more time to ultrasound research. Working in his basement with engineers William Roderick Bliss and George Posakony, Howry pursued his goal of using ultrasound to produce accurate anatomic pictures of soft-tissue structures.

In 1949 Howry and coworkers used surplus radio and Air Force radar parts to build a pulse-echo ultrasonic scanner capable of making two-dimensional images. In 1950, using a 35-mm camera, Howry recorded the first cross-sectional images with ultrasound. However, since only a simple scanning motion was used, without compound sector scanning, the completeness of the anatomic image was not as great because interfaces not perpendicular to the beam could not be recorded. Subsequent instruments were able to correct this initial limitation.

Developing a Clinically Usable Scanner

In 1951 Joseph Holmes, a nephrologist at Denver Veterans Administration Hospital, where Howry was a resident, became associated with Howry and obtained the institutional support needed for the project to proceed. As a result, space was obtained along with a grant. In 1951 Howry and his engineers Bliss and Posakony developed a two-dimensional compound ultrasound scanner. They incorporated an immersion tank by using a cattle-watering container with an ultrasonic transducer mounted on a wooden rail [7]. The transducer, immersed in the tank with the object under study, moved horizontally along the rail [7] (Fig. 1). This method allowed the use of a large transducer (better sensitivity) that could be held away from the patient. The greater distance between the transducer and the patient allowed for better focusing of the ultrasound beam. As a result, the images

Received March 27, 1992; accepted after revision July 28, 1992.

In preparation for the 1995 centennial celebration of the discovery of the X-ray, the *AJR* will periodically publish historical articles that describe events leading up to and occurring around the time of the discovery.

[1]Department of Radiology, Division of Diagnostic Ultrasound, Thomas Jefferson University Hospital, 7th Floor Main Bldg., 132 S. 10th St., Philadelphia, PA 19107. Address reprint requests to B. B. Goldberg.

[2]University of Rochester, Emeritus, 650 Seneca Parkway, Rochester, NY 14613.

[3]Department of Radiology, College of Medicine, Michigan State University, East Lansing, MI 48824.

***AJR* 1993;160:189–194** 0361–803X/93/1601–0189

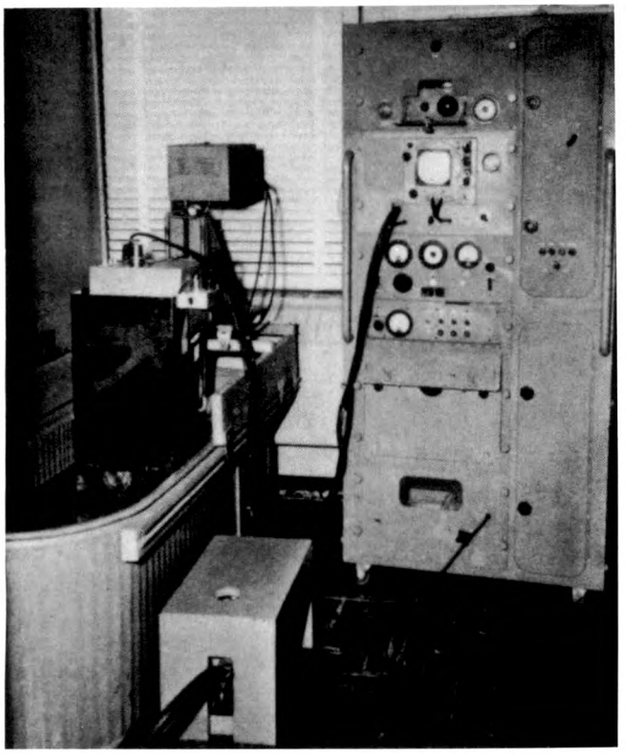

Fig. 1.—Colorado group's earliest successful immersion tank system: the cattle-tank scanner. Transducer, which cannot be seen on this image owing to its submersion in the water bath, was mounted on a wooden rail that ran along outside of tank, which was a watering tank for livestock readily available in the Denver area. Note that, as mounted, the transducer could not completely circle the patient being imaged. (Reprinted with permission from *Medical Diagnostic Ultrasound: A Retrospective on Its 40th Anniversary.*)

obtained with the water-bath method were better than those acquired with the early contact scanners. The first paper on this new development was published in 1952 [5].

A later version, introduced in 1954, included a transducer mounted on a rotating ring gear from a B-29 gun turret, which in turn was mounted around the rim of a large metal cup that served as the immersion tank [7]. This permitted complete horizontal circling of the periphery of the tank while a second motor produced a sectoring motion as the transducer was moved around the tank, producing a compound scanning image of the immersed subject [7] (Fig. 2). Because ill patients could not reasonably be immersed for the long periods that were required for scanning [7], this led to the development, in the late 1950s, of a scanner in which the transducer carriage rotated on a semicircular water-filled pan that was strapped to the patient's body in order to eliminate the need for total immersion [7, 8] (Fig. 3).

Clinical Pioneers

Howry and coworkers recognized the inherent problems with these water-bath coupling systems. In the early 1960s, with collaboration from engineers William Wright and

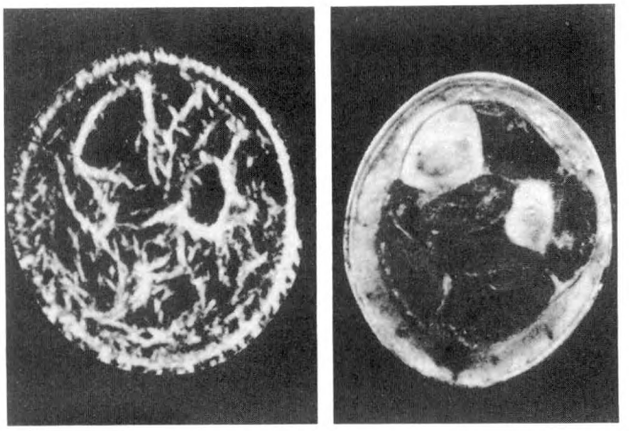

Fig. 2.—Ultrasonic image of human leg produced by compound scanning with the cattle-tank scanner. Leg was placed inside tank, transducer moved in a horizontal path around leg, and a motor provided a second back-and-forth motion of the transducer. (Reprinted with permission from *Medical Diagnostic Ultrasound: A Retrospective on Its 40th Anniversary.)*

Fig. 3.—Howry team's "pan scanner," developed about 1957–1958. Patient sat in a modified dental chair and was strapped against plastic window of a semicircular pan filled with a saline solution. Transducer rotated through the solution in a semicircular arc around the patient. A great many clinical scans were performed with this scanner, which was more appropriate for use on patients than earlier total immersion scanners were. (Reprinted with permission from *Medical Diagnostic Ultrasound: A Retrospective on Its 40th Anniversary.)*

Edward Meyer, the group developed a direct contact scanner. The transducer, mounted within a scanning head, could be positioned by the operator [7].

In 1961, engineers Wright and Meyer left this project to form Physionics Engineering, Inc., and, by 1962, they had produced the prototype of the first hand-held scanner articulated with an arm commercially available in the United States. Physionics marketed this scanner in 1964 as a three-jointed scanning arm incorporating positioning potentiometers at each joint [7].

Howry left Denver in 1962 to join the department of radiology at Massachusetts General Hospital, where he worked until his death in 1969 [9]. Joseph Holmes continued to direct the ultrasound research at the University of Colorado Medical Center until his death in 1982, and influenced a number of radiologists during the 1960s and early 1970s [7]. From this group, in 1966, a medical student, Michael Johnson, worked with Holmes on several projects, including the use of ultrasound in the long-term evaluation of polycystic kidneys and various aspects of echocardiography [10]. Johnson later became a radiologist, then director of ultrasound at the University of Colorado, and is now chairman of the radiology department there.

Looking into the Brain

Another physician influenced by the Howry group was Donald King, a young radiologist at Columbia Presbyterian Medical Center. He was later to combine his efforts with those of Juan Taveras and Ray Brinker in the purchase of ultrasound equipment for that institution. In the spring of 1962, he paid a visit to the University of Colorado. His interest in ultrasound had been stimulated by reading an article in a popular magazine that included an illustration that Howry and Holmes had made of the organs in the body. At that time, Juan Taveras, the director of radiology of the Neurologic Institute also at the Columbia-Presbyterian Medical Center, had an interest in echoencephalography and asked Ray Brinker, who had just completed his radiology residency, to "read up" on what was known about ultrasound. As a result, they combined efforts to obtain a commercial metal flaw detector from Branson Instruments in Stanford, CT, which was used for evaluating the midline of the brain [11]. Branson Instruments later supplied the ultrasound equipment sold by Smith Kline Instruments, which eventually bought Branson. Thereafter, another echoencephalographic instrument made by Physionics was purchased by Brinker, King, and Taveras and, subsequently, in 1964 the first contact two-dimensional ultrasound imager was ordered in an attempt to obtain cross-sectional imaging of the brain [12]. In 1965, Brinker followed Taveras to the Mallinckrodt Institute in St. Louis. There, Brinker developed a water-immersion ultrasound scanner that was unsuccessful because of the difficulty of transmitting the ultrasound beam through the skull [13, 14]. He also carried out early research in Doppler ultrasound [15, 16]. Brinker is currently chairman of the department of radiology at the Medical College of Ohio at Toledo. King, as director of ultrasound at Columbia-Presbyterian, has devoted most of his time to echocardiography.

Abdominal Applications

Another group that influenced a number of radiologists was led by J. Stauffer Lehman, former chairman of radiology at Hahnemann Medical School in Philadelphia. He was a pioneer in clinical applications of ultrasound, specifically, in the diagnosis of abdominal and pelvic abnormalities. The program developed as a result of a chance meeting in 1964 between Luther Brady, chairman of radiation therapy at Hahnemann, and Murray Smyth, also a radiologist, who was involved in promoting the clinical uses of ultrasound equipment produced by Smith Kline Industries. He had approached several other medical schools and facilities in Philadelphia but found no interest. At that time, Smith Kline was producing the Ekoline A- and M-mode series for echoencephalography and echocardiography and was considering adding B-mode two-dimensional ultrasound instruments to its product line. At Brady's suggestion, Smith Kline Instruments provided the B-mode equipment and Lehman provided the staff to perform the clinical tests [7] (Fig. 4).

George Evans, a young radiologist who had trained at Hahnemann, was asked to organize the ultrasound laboratory and supervise the clinical testing [7]. It was his job to investigate the diagnostic applications of bi-stable ultrasound water-bath techniques and abdominal scanning. Insights into the personalities of Lehman and Evans are provided by a letter written by George Evans: "My personal aggressive enthusiasm toward ultrasound was tempered by the conservative yet perceptive approach of Dr. Lehman. His painstaking diligence and his profound circumscription infected all who worked with him. His insistence for accuracy and reproducibility of results were ubiquitous. These characteristics were so ingrained in his approach to research that we did not make unfounded conclusions as regards to the diagnostic capabilities of ultrasound."

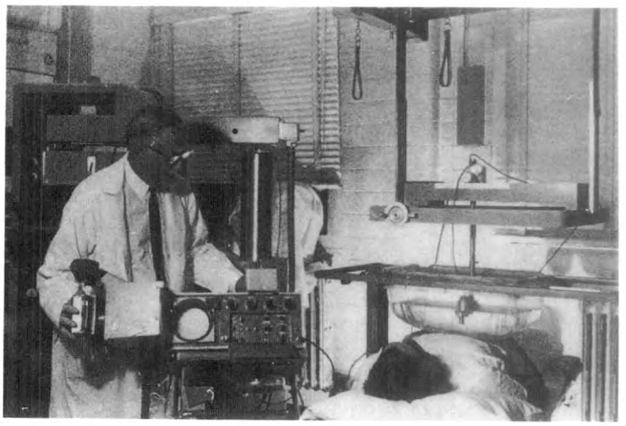

Fig. 4—J. Stauffer Lehman scanning a patient with a compound scanner built by Smith Kline Instruments and General Precision Instruments. Transducer moved in a water bath lowered over patient's abdomen. (Reprinted with permission from *Medical Diagnostic Ultrasound: A Retrospective on Its 40th Anniversary.*)

Broadening Horizons

Marvin Ziskin, currently a professor of radiology at Temple University, became aware of ultrasound as a student in biomedical engineering at Drexel University in 1964, when Murray Smyth presented a seminar. In 1965, Ziskin became a research associate in the diagnostic ultrasound laboratory at Hahnemann under the direction of Lehman, who died in 1974, and Evans, who is currently in private radiologic practice in Detroit. This group did some of the earliest large-scale clinical research with ultrasound imaging [17, 18]. In addition to investigating abdominal applications, they also carried out research in echoencephalography, echocardiography, and Doppler ultrasound [19–21]. Evans' first paper was presented in December 1964 at the Greater Philadelphia Chapter of the Federation for Clinical Research. The ultrasound images from the Hahnemann laboratory were published in *Life* magazine in January and September 1965. This group presented the first exhibit on ultrasound at the annual meeting of the American Roentgen Ray Society in September 1965 and again at the Radiological Society of North America (RSNA) in November 1965.

Lehman, Evans, and Ziskin worked with practically every type of ultrasound instrument manufacturer in the country at that time and it is said that Lehman was instrumental in persuading Picker to become involved in ultrasound. Picker later bought Physionics and became the dominant force in two-dimensional ultrasound imaging in the 1960s and early 1970s. The company helped disseminate the use of ultrasound throughout the radiologic community.

In 1968 Barry Goldberg joined the staff at Hahnemann, where he worked closely with Lehman in expanding the clinical usefulness of ultrasound [22]. Goldberg developed an interest in ultrasound during his radiology residency in Philadelphia at the Albert Einstein Medical Center in 1964. J. Gershon-Cohen, former chairman of radiology at the Center and a pioneer in X-ray mammography, had just bought one of Smith Kline Instruments' first Ekoline A-mode ultrasound machines. A few weeks after Goldberg started his residency he asked Dr. Gershon-Cohen about the machine in the hallway. Gershon-Cohen replied, "Well, that's something new, ultrasound, see what you can do with it." Goldberg became enthusiastic about the technique as he and his colleagues taught themselves to use the equipment. Working with several members of the radiology staff, he published articles on a variety of subjects, including echoencephalography, echocardiography, and abdominal and pelvic diseases, as well as producing images of the fetus [23–28]. With John Kirkpatrick, then chairman of radiology at St. Christopher's Hospital in Philadelphia, Goldberg was one of the first to investigate the use of ultrasound in pediatric radiology. Goldberg and H. H. Holm, a urologist from Denmark, were the first to develop ultrasound-guided aspiration biopsy techniques. In 1965, Goldberg delivered one of the first ultrasound papers given by a radiologist at a meeting of the RSNA. He pioneered the development of formal educational programs for physicians and technologists. He is now director of ultrasound at Thomas Jefferson University Hospital.

George Leopold began his radiology residency in 1965 at Presbyterian Hospital in Pittsburgh. Elliott Lasser, then chairman of radiology, obtained a Smith Kline Instruments' ultrasound A-mode unit after the 1966 annual meeting of the RSNA and assigned several residents to evaluate its capabilities. Leopold was the only resident to maintain an interest, working first with echoencephalography and then echocardiography. His introduction to B-mode imaging was a Picker machine lent by the company to the hospital for evaluation. Shortly after a visit to Lehman's laboratory, Leopold followed Lasser to the University of California at San Diego and dedicated himself to the clinical applications of diagnostic ultrasound [7]. When Leopold arrived in San Diego in 1968, he called a local Picker salesman and told him that he wanted to order an ultrasound machine. The salesman said, "Fine, Doctor, what is it? If we have such an instrument, we'd be happy to sell it to you." This was to be the first such machine on the West Coast. Leopold's early research was on abdominal ultrasound [29, 30]. He is now chairman of the department of radiology at the University of California, San Diego. Like Goldberg, Leopold stressed education, providing both formal and informal training programs. They, along with other early clinical pioneers, educated a whole generation of radiologists and technologists in the usefulness of diagnostic ultrasound.

Ultrasound Becomes Popular

Another center of clinical research and training was developed under Atis Freimanis, a radiologist at Ohio State University, who in the mid-1960s also visited Lehman's laboratory to observe clinical work with the Smith Kline Instruments' water-bath prototype [7]. Originally interested in its application in studying the nervous system, Freimanis became impressed with the general diagnostic capabilities of ultrasound [7]. At Ohio State he worked with Michael Asher, at that time a medical student interested in developing some collaborative research projects [7]. He and Freimanis conducted early research on the imaging of enlarged retroperitoneal lymph nodes, and they designed their own scanning system and techniques [31]. Shortly thereafter, another radiologist, Roy Filly, then a medical student, joined them in some of their early ultrasound research on pancreatic abnormalities. Asher is now in private practice and Filly is now the director of ultrasound at the University of California, San Francisco. This is yet another example of how the early pioneers in clinical ultrasound provided the stimulus for the next generation of radiologists, who, in subsequent decades, took ultrasound to its current high levels of use. Freimanis eventually became chairman of radiology at the Medical College of Ohio at Toledo and then at Ohio State; he now continues in academic practice at Michigan State University.

In the 1960s, a number of radiologists directed their initial efforts toward research with echoencephalography. Many of these individuals did not further pursue ultrasound, probably because of the difficulty in obtaining adequate images of the brain due to the poor penetration of the ultrasound beam as it passed through the adult skull. It was not until the 1970s, when researchers began to use the fontanelle in pediatric patients for placement of the transducer, that adequate information from two-dimensional imaging became available. In

1967, for instance, at Downstate Medical Center of the State University of New York, Lewis Grossman, a neuroradiologist and amateur physicist, directed an active laboratory at the Neurologic Institute with the assistance of Georgina Wodrowska, who was one of the earliest ultrasound technologists. Unfortunately, Grossman died in 1969. Michael Tenner, also a neuroradiologist and now chairman of radiology at New York Medical College, was asked to head the service. He helped to extend the use of echoencephalography beyond simple midline detection by identifying various components of intracranial anatomy. In 1963, Marc Lapayowker, a radiologist at Temple University in Philadelphia, and John Kirkpatrick used an Ekoline instrument to perform echoencephalography examinations, including examinations of children [32, 33]. With Renata Soulen, another radiologist, they attempted to duplicate the early work of Harvey Feigenbaum, a cardiologist, in the ultrasound evaluation of pericardial effusion [34, 35]. Lapayowker was the first chairman of the American College of Radiology Commission on Ultrasound and is currently chairman of radiology at Abington Hospital near Philadelphia.

Fred Winsberg, a radiologist and currently director of ultrasound at Mount Sinai Hospital, was first introduced to ultrasound in 1967 while working at Lincoln Hospital in New York. As he stated, "Although I had been promised a renovated X-ray department, construction was delayed by the usual governmental red tape and the only items I was able to purchase were those not requiring construction. Thus, I acquired a Hoffrel ultrasound machine designed for echoencephalography with M-mode capability." This machine was designed by Russ Uphoff, an engineer who had left Branson to form his own company. Winsberg soon became disenchanted with cerebral midlines, but fascinated with echocardiography. He presented his first work in differentiating the left from the right ventricle in 1968 at the annual meeting of the American Institute of Ultrasound in Medicine. In the spring of 1970, he traveled to Germany to see the first and only real-time ultrasound instrument at that time, a Vidoson sold by Siemens. He was the first to use this machine in North America at McGill University in Montreal, Canada, where he performed ultrasound on a full-time basis. Winsberg worked with another radiologist at McGill, the late Catherine Cole-Beuglet. Using the Vidoson, which featured a rotating transducer placed at the focal point of a parabolic mirror producing real-time images [36], they were able to visualize the aorta and show pulsations, establishing the value of real-time ultrasound.

Raymond Gramiak, a radiologist at the University of Rochester, began his involvement with ultrasound in 1966 when the radiology department unexpectedly discovered a budget surplus. Purchase of an ultrasound machine was suggested by Elliott Lipchik, cardiovascular radiologist, because it appeared new and exciting. A Physionics unit was selected because it featured a storage oscilloscope for monitoring image build-up during M-mode sweeping or B-mode scanning. Gramiak showed the greatest interest in mastering use of the new machine and soon obtained meaningful M-mode images of the mitral valve, virtually the only regularly recognized cardiac structure at that time. By varying beam directions away from the mitral landmark and into the area expected to contain the aortic valve, an echo-pattern complex that seemed to represent the aortic valve could be detected. By good fortune and, at about the same point in his development as an echocardiographer, Gramiak examined a patient in the cardiac catheterization laboratory during cardiac output studies with indocyanine green. Each intracardiac injection of the agent resulted in an intense contrast effect, which he instantly recognized as an excellent method to correlate cardiac anatomy with the nonanatomic display of M-mode sonography. It became apparent that the aortic valve echo complex could be anatomically validated by injection of contrast material [37]. This work was soon followed by a more comprehensive study in which the anatomy of the cardiac chamber, patterns of the mitral, tricuspid, and aortic valves, and a variety of clinical conditions were shown by using ultrasound and injections of contrast material [38].

A number of others, both radiologists and nonradiologists, have made important contributions. Nonradiologists include Ross Brown, who was director of ultrasound in the department of radiology at the University of Oklahoma in the 1960s and early 1970s, and Kenneth Taylor from England, who has been the director of the division of ultrasound in the department of radiology at Yale since the early 1970s. In addition, in the early 1970s, Roger Sanders, another Englishman and a radiologist, former director of ultrasound at Johns Hopkins University, made important contributions, and Donn Brascho, now medical director at Baptist Cancer Hospital, was the first radiologist to use ultrasound as an aid in planning radiation treatment.

Epilogue

The decade of the 1960s was a dynamic, challenging, and somewhat difficult period for radiologists involved in diagnostic ultrasound. At the onset of this period, ultrasound evolved from a medical curiosity to a recognized clinical procedure, capable of providing unique diagnostic information. However, instrumentation was crude and huge voids in interpreting images confronted the dedicated practitioner. In radiology, the established hierarchy was skeptical, particularly because tissue representation in the ultrasound image was different from that on conventional radiologic images, so physicians with considerable skill and experience in interpreting X-ray images could not readily interpret sonograms. The relatively poor resolution and the difficulty in imaging tissue such as lung, bowel, and bone also proved barriers to acceptance even though different tissue properties were evident on sonograms as compared with radiographs. As a result, radiologists striving to make their mark in ultrasound often received less than optimal departmental support. Despite this atmosphere of resistance and lack of instrumentation, radiologists persevered and made progress in the development of diagnostic ultrasound.

ACKNOWLEDGMENTS

All artwork was provided by the AIUM Archives, which acquired all prints by donation from the pioneers, or the pioneers' associates

or descendants. The archives, including prints, equipment, videotapes, and printed material, were accumulated under the direction of Joseph Holmes, the first AIUM Archives Committee chairman, and Barry B. Goldberg, the current chairman. A historian, Barbara Kimmelman, helped in its organization.

REFERENCES

1. Ludwig GD. The velocity of sound through tissues and the acoustic impedance of tissues. *J Acoust Soc Am* **1950**;22:862–866
2. Ludwig GD, Bolt RH, Heuter TF, Ballantine HT Jr. Factors influencing the use of ultrasound as a diagnostic aid. *Trans Am Neurol Assoc* **1950**;75:225–228
3. Wild JJ. The use of ultrasonic pulses for the measurement of biologic tissues and the detection of tissue density changes. *Surgery* **1950**;27:183–188
4. Wild JJ, Reid JM. Further pilot echographic studies on the histologic structure of tumors of the living intact human breast. *Am J Pathol* **1952**;28:839–854
5. Howry DH, Bliss NR. Ultrasonic visualization of soft tissue structures of the body. *J Lab Clin Med* **1952**;40:579–592
6. Howry DH, Holmes JH, Cushman JJ, Posakony GJ. Ultrasonic visualization of living organs and tissues, with observations on some disease processes. *Geriatrics* **1955**;10:123–128
7. Kimmelman B. *Medical Diagnostic Ultrasound: a retrospective on its 40th anniversary.* Washington, DC: American Institute of Ultrasound in Medicine, **1988**
8. Holmes J, Howry D, Posakony G, Cushman CR. The ultrasonic visualization of soft tissue structures in the human body. *Trans Am Clin Climatol Assoc* **1955**;66:208–225
9. Howry DH. A brief atlas of diagnostic ultrasonic radiologic results. *Radiol Clin North Am* **1965**;3:433–452
10. Johnson ML, Paton BC, Holmes JH. Ultrasonic evaluation of prosthetic valve motion. *Circulation* **1970**;11[Suppl II]:3-II-9
11. Brinker R, King D, Taveras J. Echoencephalography. *AJR* **1965**;93:781–790
12. Brinker R, Taveras J. Ultrasound cross-sectional pictures of the head. *Acta Radiol* **1966**;5:745–753
13. Brinker R, Holman B. Compound sector echoencephalography: anatomical correlations in the dog. *Invest Radiol* **1967**;2:160–164
14. Brinker R. Simultaneous presentation echoencephalography. *Radiology* **1967**;88:360–361
15. Staple T, Brinker R. The ultrasound flowmeter as an adjunct to femoral arteriography. *Radiology* **1968**;90:341–342
16. Brinker R, Landiss D, Croley T. Detection of carotid artery bifurcation stenosis by Doppler ultrasound. *J Neurosurg* **1968**;29:143–148
17. Lehman JS. Ultrasound in the diagnosis of hepatobiliary disease. *Radiol Clin North Am* **1966**;4:605–623
18. Lehman JS, Evans GC, Brady LD. Ultrasound exploration of the spleen. In: Grossman CC, Holmes JH, Joyner C, Purnell EW. eds. *Diagnostic ultrasound.* New York: Plenum, **1966**:264–295
19. Evans GC, Lehman JS, Segal BS, Likoff W, Ziskin MC, Kingsley B. Echoaortography. *Am J Cardiol* **1967**,19:91–96
20. Ziskin MC, Lehman JS, Evans GC. An investigation of a cause of false-positive results in the ultrasonic diagnosis of pericardial effusion (abstr). *Proceedings of the annual meeting of the American Institute of Ultrasonics in Medicine.* New Orleans, **1968**
21. Ziskin MC. Detection of carotid artery bifurcation stenosis by Doppler ultrasound: a review. *Invest Radiol* **1969**;4:112
22. Goldberg BB, Lehman JS. Some observations on the practical uses of A-mode ultrasound. *AJR* **1969**;107:198–205
23. Goldberg BB, Isard HJ, Gershon-Cohen J, Ostrum BJ. Ultrasound fetal cephalometry. *Radiology* **1966**;87:328–332
24. Goldberg BB, Ostrum BJ, Isard HJ. Ultrasonic aortography. *JAMA* **1966**;198:353–358
25. Ostrum BJ, Goldberg BB, Isard HJ. A-mode ultrasound differentiation of soft tissue masses. *Radiology* **1967**;88:745–749
26. Goldberg BB, Ostrum BJ, Isard HJ. Ultrasonic determinations of pericardial effusion. *JAMA* **1967**;202:927–930
27. Goldberg BB, Ostrum BJ, Isard HJ. Nephrosonography: ultrasound differentiation of renal masses. *Radiology* **1968**;90:1113–1118
28. Goldberg BB, Sklaroff DM, Isard HJ. Echoencephalography in the management of patients receiving radiation therapy. *Radiology* **1968**;91:363–366
29. Leopold GR. Renal transplant size measured by reflected ultrasound. *Radiology* **1970**;95:687–689
30. Leopold GR. Ultrasonic abdominal aortography. *Radiology* **1970**;96:9–14
31. Asher MW, Freimanis A. Echographic diagnosis of retroperitoneal lymph node enlargement. *AJR* **1969**;105:438–445
32. Lapayowker MS, Christen GE. Echoencephalography in general hospital practice. *AJR* **1965**;93:803–810
33. Lapayowker MS, Kirkpatrick JA, Murtagh F. Echoencephalography in the evaluation of hydrocephalus. *Radiology* **1966**;86:1052–1055
34. Soulen RL, Lapayowker MS, Gimenez JL. Echocardiography in the diagnosis of pericardial effusions. *Radiology* **1966**;86:1047–1051
35. Soulen RL, Lapayowker MS, Cortes FM. Distribution of pericardial fluid: dynamic and static influences. *AJR* **1968**;103:583–585
36. Krause W, Soldner R. Ultrasonic imaging technique (B scan) with high image rate for medical diagnosis. *Electromedica* **1967**:4:1–5
37. Gramiak R, Shah PM. Echocardiography of the aortic root. *Invest Radiol* **1968**;3:356–366
38. Gramiak R, Shah PM, Kramer DH. Ultrasound cardiography: contrast studies in anatomy and function. *Radiology* **1969**;92:939–948

Meeting News

The Impact of New Imaging Technology on Worldwide Health Care, Research, and Teaching: Fifth International Symposium, August 1992

Elizabeth Whalen[1]

This unique meeting was the fifth international symposium organized by the University of California, San Francisco, to bring together leaders in health care from all over the world to discuss the impact of new technology on radiology worldwide. Held August 27–29, 1992, at the Fairmont Hotel in San Francisco, the program was attended by 180 participants from 26 countries. From within the United States, 14 states and Washington, DC, were represented. Speakers included researchers, industry representatives, and experts in the economics or technology of the 1990s. Included in the presentations were discussions on the following topics: the impact of the economy on advances in the practice of medicine and radiology in various countries, the role of government in medical practice and progress, the relationship of industry to the practice of radiology in developed nations and emerging nations, the changes in radiologic practice that have occurred in response to changing technologies, the role of electronic image transmission, the worldwide distribution of radiologic resources and its effect on education and clinical care, and the future developments in research that will be incorporated into clinical practice. In addition, eminent speakers presented lectures on the prospects for science in the United States, the present status and future outlook for the world economy, the intelligent application of technology in developing nations, research activities of a university-administered national research laboratory in a time of change, and the role of Project HOPE in improving worldwide health care. New horizons in neuroradiology and in cardiac imaging were the topics of two panel discussions.

Because of *AJR* space limitations, we can report only a fraction of the information and ideas that were presented at the meeting. However, the following pages contain summaries of 13 of the 79 talks given, and we hope this summary will at least provide readers with an accurate impression of the multicultural, multinational nature of the meeting, and offer details on some of the material presented.

Goals of the Symposium

The symposium was chaired by Ronald L. Arenson, Charles A. Gooding, and Alexander R. Margulis, all of the University of California, San Francisco. After Dr. Arenson welcomed the participants, Dr. Margulis (who had started organizing these meetings in 1974) made a brief statement about the goals of the 1992 meeting. He began by recalling that "one great achievement" of the four previous meetings (1974, 1978, 1982, and 1986) was that the participants at each meeting always discussed how bad the situation was for radiologists and then, at the next meeting, wished that things were "as good as they used to be." Since 1986, dramatic technologic changes have occurred, including MR imaging and MR fast-scanning techniques, spiral CT with

[1] Contributing editor, *American Journal of Roentgenology*, Ste. 103, 2223 Avenida de la Playa, La Jolla, CA 92037, and medical writer, Advanced Tissue Sciences, Inc., La Jolla, CA 92037.

Editor's note.—"Meeting News" articles report the highlights of important national radiology meetings. The articles will not undergo the peer review usually required of *AJR* publications, nor will they offer a critique of the information provided. The sole purpose of the series is to provide Journal readers with succinct, substantive, and accurate reviews of topics of current interest, written in a readable fashion and published promptly after the meeting.

AJR 1993;160:195–201 0361–803X/93/1601–0195

three-dimensional acquisition, color Doppler sonography, videoscopic surgical techniques, and amazing interventional techniques such as transjugular portacaval shunts. Among the most important concerns in 1992 is the rising cost of health care since 1986. The cost of Medicare physician services, other Medicare costs, and health care spending have all increased faster than the gross national product has. The public and lawmakers look particularly at physician-service costs: from close to $800 billion in health spending, almost 20 cents of every dollar goes to physicians. Radiologists can look for an increase in turf wars as legislatures nationwide begin to address the problem of accelerating physician costs. Also, the amount of money available for research projects has been steadily decreasing since 1986. Although "new technology" often receives blame for increasing health costs, national expenditures for diagnostic imaging in the United States in 1990 and 1991 represented only about 0.54% of the total national expenditures for health care. The largest share of the imaging dollars "pie" still goes to conventional radiology equipment, but MR imaging costs are advancing faster than costs for any other imaging technology; costs for CT are remaining fairly steady.

Dr. Margulis recalled the conclusions from the 1986 New Technology Symposium: (1) radiologists need to prove the cost-effectiveness of new imaging techniques; (2) the least costly but sophisticated imaging instruments need to be developed; and (3) radiologists in all the industrialized countries have the responsibility to support the training of radiologists and sharing of knowledge throughout the world. The situation in 1992 supports those conclusions; proof of cost-effectiveness has become increasingly important as the spotlight shines on medical spending, equipment that ranges widely in price and sophistication (from a Model T to a Ferrari) is available for basic radiologic examinations, and radiologists are sharing expertise, time, and equipment through such organizations as Project HOPE and the World Health Organization.

Prospects for Science in the United States

Kenneth I. Shine, President of the Institute of Medicine (National Academy of Sciences, Washington, DC), sees exciting opportunities for radiology in today's world. Along with advances in molecular biology and organ transplantation, the techniques of rapid diagnosis (including brain mapping with positron-emission tomography) offer new hope for many patients. Dr. Shine stressed five important issues to consider in order to have a balanced view of the future of health care research. First, the globalization of science has become a reality through advances in communications and international meetings such as this one; however, a concern about patents and secrets endangers scientific communication. As Dr. Shine said, "If free trade is important, free science is essential," and he pointedly used Roentgen as an excellent example of a scientist who did not worry about patents and thus saw his discoveries used and developed. Although of course researchers and their institutions will always be concerned with patenting new technologies, secrecy cannot be the primary motivation in medicine, in which new knowledge may save lives. Second, the disintegration of the Soviet Union has resulted in a significant downsizing of the U.S. armed forces, the Department of Defense (DOD), and the Department of Energy (DOE). Both the DOD and DOE had been notable supporters of high-quality medical research: for example, DOE-supported research has lead to advances in nuclear imaging, and the DOD has contributed funds to studies of trauma. The decrease in funding of these departments means a decrease in research moneys from their budgets. Third, American research universities have been a driving force of much of the progress in recent years. However, the continued success of these universities is now threatened by the huge financial pressures from ever-tightening state and federal budgets that have severely reduced the ability of the universities to assume research costs. Fourth, an overwhelming consensus in the United States today dictates that health care costs must be controlled. Unless medical technology can show value for money that is comparable to the value for money spent on education, infrastructure, and inner city improvement, government spending for medical research will be reduced.

Dr. Shine sees industry as having an increasingly important role in funding research, but he warns that attention must be paid to retaining the independence of the university and its researchers. Continuing, high-quality research will depend on a new relationship between the university scientist and industry, but conflicts of interest must be avoided. Fifth, accountability of physicians for their work has taken on new importance in recent years. Radiologists should welcome the opportunity to take responsibility—to show that the value of the service provided is appropriate and to prove the cost-effectiveness of new technology in terms of early diagnosis. If radiologists do not evaluate the cost-effectiveness of their own services, outsiders will do so in the name of cutting health care costs, and the results of such evaluations will become increasingly painful. Accountability also requires that both industry and academia assess the role of minorities and women in health care research and adjust those roles appropriately. The key to the best use of today's amazing technology is not to decry the paucity of funds but rather to thoughtfully and responsibly manage available health care resources while accepting full accountability for the value of services provided.

The Impact of the Economy on the Practice of Radiology Worldwide

Imaging Technology in the European Community—Are Borders Disappearing?

Henri Nahum (Hôpital Beaujon, Clichy, France) discussed the emergence of the European Community—or, as he described them, 12 countries trying to live together. Varying in area from 2500 km^2 (Luxembourg) to 547,000 km^2 (France) and in population from 400,000 (Luxembourg) to 61 million (Germany), the nations of the European Community include Belgium, Denmark, France, Germany, Greece, Ireland, Italy, Luxembourg, the Netherlands, Poland, Spain, and the United Kingdom. In all these countries, purchase of large equipment such as MR imagers or CT scanners

requires some government authorization. The number of radiologic machines differs greatly among the countries; for example, Ireland has only two CT scanners per million people, whereas Belgium boasts 12.1 CT scanners per million. Furthermore, quality control of medical care varies among the countries, partly by virtue of the number of physicians available: Ireland has only 1300 physicians per one million people, but Italy has more than twice that number (2900 physicians per one million people). Radiologists in some countries are usually full-time employees of hospitals, and in others, they are usually in private practice; in some countries, radiologists are allowed to work part-time for a hospital and part-time in private practice, but in others, hospital radiologists are not allowed to do any private-practice work.

The range of education required for the practice of radiology is very wide among European nations, as is the range of income earned. However, in almost all these countries, the governments determine how many radiologists will be trained and will practice within their borders; the number and training of radiology technicians are also often dictated by the government. Throughout Europe, most radiologic examinations are performed by radiologists themselves (in the Netherlands, a full 98% of examinations are performed by radiologists rather than technicians). However, in general, great variation exists in the health care systems, reimbursement procedures, and costs of examinations. Dr. Nahum concluded that, despite movements toward economic cooperation, the borders have not disappeared between the 12 countries of the European Community—especially in terms of health care systems and medical economics. However, when we consider the scope of the changes that have occurred within the last decade, who can say what agreements and sharing of technology may happen by the year 2000?

Radiology in Sweden—Today and Tomorrow

In an overview of the rapidly changing scene in radiology in Sweden, Peter Aspelin (Hudinge Hospital, Karolinska Institute, Stockholm, Sweden) discussed the national statistics, the educational system for training radiologists, the reimbursement procedures, and the current controversies. Of the radiologists in Sweden, 98% are in government practice (99% of these are in hospitals) and only 2% are in private practice. Not including private practice, the number of radiologic examinations has been relatively stable at about 4,300,000 per year during recent years. However, the number of radiologists has increased from 650 in 1985 to 835 in 1991. The chest radiograph is still the most common examination, performed at a rate of 125 per 1000 inhabitants (rates for stomach, colon, and gallbladder radiographic studies are 4.1, 11.0, and 2.3 per 1000 inhabitants, respectively). Other examinations that are performed relatively frequently include mammography, sonography, and CT at rates of 42, 37, and 17 studies per 1000 people, respectively.

The year 1992 marked a change in the way radiologists are trained in Sweden. Before 1992, requirements included 4.5 years of studying radiology and 0.5 years of training in nonradiologic clinical medicine. Now, radiologists must study radiology for a full 5 years to fulfill the training requirement; however, there is no obligatory examination they must pass (there is a voluntary examination), and revisions have been made in the training they receive in the hospitals.

Reimbursement policies in Sweden also changed in 1992. Before, the health care economy was organized on a totally socialist basis. Now, about half of the reimbursement is still socialist-based, but the other half is on a "buy-sell" system, which means that the government gives money to general practitioners, who use it to buy hospital care and radiologic services for their patients. Included in the important effects of this change are the following: it is easier to obtain new equipment, patient waiting lists are shorter, and quality assurance is being developed in radiology departments as they compete for the available money.

The controversies that Swedish radiologists face today include turf battles that may be familiar to some U.S. radiologists. Cardiologists are vying with radiologists to perform coronary angiography and percutaneous transluminal coronary angioplasty, while clinicians are showing interest in performing their own sonographic and nuclear medicine examinations. Overall, however, Dr. Aspelin believes that the future looks bright as radiologists will benefit from the new buy-sell system of reimbursement.

German Unification—Economic Consequences for the Practice of Radiology

Peter E. Peters (University of Münster, Münster, Germany) spoke about the changes in the practice and economics of radiology in the newly unified Germany. Although the new Germany is the size of Montana, it is home to a population 100 times that of Montana; reunification resulted in some statistical decreases in health care availability (e.g., the proportion of CT scanners to population changed from 12 per one million to only nine per one million). In 1990, the year of unification, Germany had 1.7 MR imagers per one million people (compared with 8.5 per million and 6.5 per million for the United States and Japan, respectively). Since 1990, however, the number of CT scanners in Germany has increased sixfold, and the number of MR imagers has increased 20-fold. For this 2-year period, the cost of improvements to diagnostic radiology alone was $800 million, which was paid mostly by the government with some aid from private donations.

The purely government-run, centralized health care system of the old East Germany is slowly being converted to the very different West German system of providing health care, in which radiologists are often paid by insurance companies, sometimes paid by patients, and only occasionally paid by the government. Moreover, the government-supported large research academies of the old East Germany are being replaced by institutions that must work in a highly competitive environment for research dollars.

Dr. Peters also discussed the necessity to close gaps between the old East and West Germany. He stressed the need for training in cross-sectional imaging, training in management and in research, and elimination of the differences in salaries (to stop the "brain drain" that is now occurring from east to west).

Selected Problems of Education of Radiologists in Eastern Europe

Bogdan Pruszynski (Central Medical Academy, Warsaw, Poland) discussed three aspects of radiology education in Poland: the actual system of training in diagnostic radiology, the difficulties in realizing the goals of the program, and the proposed changes in that educational system. With a population of 39 million people, Poland has 12 medical universities; of 35,000 medical students, 2400 graduate each year.

Undergraduate training of radiologists in Poland consists of 30 hours of studying nuclear medicine in the fourth year of work, 65 hours of studying diagnostic radiology during the fifth year, and 15 hours of radiotherapy in the sixth year. Of these hours, 30% are spent in seminars, and most of the rest of the hours are devoted to working sessions. Seven years of postgraduate training are required of Polish radiologists: a 1-year clinical course in radiology, followed by two 3-year courses in specialty training (each of which is followed by an examination in the specialty).

Three problems interfere with the radiology student completing the required studies. First, little objective motivation exists for professional advancement. Second, access to well-equipped radiologic facilities is difficult. Third, there is a significant shortage of new textbooks and recent professional literature.

In attempts to resolve these problems, the number of students admitted to the program is being reduced to allow more individualized training. Also, curriculum developers are working toward improving the integration of undergraduate radiology training into the basic medical curriculum, and decreasing the number of "specialization periods" from two (of 3 years each) to one (of 5 years). The medical schools are also trying to alter their training programs to make them more practical and more up-to-date, with standards comparable to Western standards.

Dr. Pruszynski concluded by saying that the past training programs in Eastern Europe have not been very effective, but the expected changes in the organization of health services should lead to improvement of both undergraduate and graduate programs. He stressed that assistance from developed countries will be necessary to upgrade the medical training, and therefore the standard of care, in Eastern European countries.

Radiology in Czechoslovakia in a Time of Change

A country that is continuing to go through great political and economic changes, Czechoslovakia is also striving to improve its old state-run health care system, and Jan Spindrich (Charles University Prague, Prague, Czechoslovakia) spoke briefly about the ways that system is being improved. In 1992, the population of Czechoslovakia was about 16 million, including about 10.6 million in the Czech Republic and 5.4 million in the Slovak Republic. The Czechoslovakian health care system between 1948 and 1989 had depended on a rigid budget of state funding. Although medical care was free, political criteria prevailed in the making of medical decisions. Physicians' salaries were extremely low; the average radiologist earned about $2200 a year. Generally poor medical care resulted from an inefficient system based on a strictly hierarchical organization and dependent on a shadow economy. By the late 1980s in Czechoslovakia, an economic crisis and rising costs of medical equipment led to a growing retardation of medical care.

Under the new liberal system, some improvement is being seen: the role of the state in health care is limited, adequate health care is guaranteed for all, private medical practice and free choice of physician are allowed, obligatory health insurance leads to multiresource funding of health services, and medical professional societies are becoming active. The medical community hopes to improve training programs, too. Now, the basic medical study takes 6 years; to qualify to practice as a radiologist, 8 more years are required (3 years for first-degree specialty and 5 years for second-degree specialty). The proposed changes would allow a student to receive a diploma in diagnostic radiology after the basic medical studies and a 5-year residency; for a higher diploma, 3 more years of study in a specialty (e.g., neuroradiology, pediatric radiology, angio-interventional radiology) would be required.

The improvement in medical care in Czechoslovakia can be seen by the great increase in the availability of diagnostic imaging equipment since 1989. In that year, there were only 180 sonographic units in the country; in 1992, there are 800. The number of angiographic imagers has increased from 18 to 28; CT scanners, from 15 to 65; and MR imagers, from two to four. Dr. Spindrich expects more improvements in the Czech system, both for radiologists and for their patients, in the coming years.

Technology and Practice of Radiology in Central America

Francisco Arredondo (Francisco Marroquin University, Guatemala City, Guatemala) explained that Central America consists of a group of seven independent countries, with a total area of about 500,000 km^2 and a total population of 32 million. At this time, the population is 60% rural, but that characteristic is rapidly changing; by the year 2000, 55–60% of the population will probably be living in urban areas.

In much of Central America, the governments cannot provide adequate health care because of obsolete legislation and poor management skills. Moreover, much of the available hospital equipment is not in working condition. Except for Panama and Costa Rica, hospitals do not even have imaging equipment; although private clinics do have some imaging equipment, 80% of these are in urban areas (overall, there is one sonographic imager per 80,000 people, one CT scanner per 1.2 million people, one MR imager per 15 million people, and one radiologist for every 92,000 people). Most patients pay for their own medical care, and the cost for radiologic procedures is at least one third lower than the cost in the United States (e.g., a brain CT costs $70, including technician and physician fees; a sonogram costs $16). Naturally, this means that the salaries of radiologists are much lower than in the United States; they average about $18,000 a year. Despite the low cost of procedures, the equipment available is rarely used at full capacity because the citizens cannot afford even the small amount that they must pay. Very little interventional radiology is performed,

and all interventional radiology is done in collaboration with surgeons or gastroenterologists.

Most doctors who practice in Central America are trained in the United States, Mexico, or Europe. In Central American countries, some training programs exist but they are limited by insufficient funding, too few full-time staff members, and lack of up-to-date textbooks and medical journals. However, Dr. Arredondo sees hope for the future of health care in Central America in that many of the young radiologists with whom he works are highly motivated both academically and professionally.

Helping Developing Countries Improve Their Health Care Systems

The Radiology Outreach Foundation

According to Charles A. Gooding (University of California, San Francisco), a radiologist visiting medical facilities in a "developing" nation may find four babies in one incubator, a radiographic unit that looks like it was built before 1895, and malnutrition and infectious diseases prevailing throughout the population. In an attempt to share knowledge and expertise, the Radiology Outreach Foundation, formed about 3 1/2 years ago and supported by major radiologic societies (including the ARRS), has distributed 14,650 textbooks to 73 institutions in 41 countries, including China and nations in Eastern Europe, Africa, Central America, South America, and the Indian subcontinent. In addition, 2353 educational videotapes have been donated to eight universities in eight countries, and visiting professors have lent their expertise to medical institutions in Kenya, Guatemala, Brazil, and Nepal.

Specific to the field of radiology, the Radiology Outreach Foundation has sent radiographic cassettes, sonographic units, angiographic catheters, radiographic film and processing chemicals, and videotape recorders—a total of more than $1 million worth of equipment and supplies. One of the most recent projects is a mobile CT scanner that can provide CT services to populations that are widely separated geographically.

The Radiology Outreach Foundation collaborates with other organizations, such as the International Medical Scholars Program, Project HOPE (particularly in the Shanghai Children's Hospital and the current Swaziland program), and the Pan American Development Foundation. However, the continuing existence of the Foundation depends on donations from private donors and on radiologists who are willing to serve as visiting professors in developing countries. Dr. Gooding ended his talk with a request for the attendees to "join" the Foundation; whether they feel they can donate textbooks or equipment, contribute financial gifts, volunteer to be visiting professors, or just send good wishes, Dr. Gooding sees the support of the radiologic community as essential to this effort to bring high-quality medical care to people all over the world.

The Intelligent Application of Technology in Developing Nations

"Where will the funds come from?" and "Who should help—or interfere—with the health care in developing countries?" were two questions posed by Thomas W. Langfitt, President, The Pew Charitable Trusts (Philadelphia, PA) in the introduction to his talk. Although he could not provide the answers to those questions, he did describe eloquently some of the problems being faced in trying to use scarce resources to benefit the most people. The disease burden and allocation of health care resources undergo major changes each year, and what makes sense one year may be a poor use of resources the next. For example, AIDS is a continuing and overwhelming problem in many African countries; Uganda is the most severely affected by the epidemic—in June 1992, a rough estimate placed the number of AIDS cases in Uganda at 34,000 (the actual number could be three to five times higher). For problems such as this, researchers and physicians must try to use resources in the most rational manner—will AIDS eventually decimate the population of Uganda or will its incidence level off, as it appears to be doing in the United States?

Almost every developing country has a health care system built on a "universal model," starting with basic community care, then up to the District Hospital for more sophisticated care, and then up to the Regional Hospital for the best care available. This type of system is effective, unless the components of the system are understaffed, underfunded, and underused (as is true in many developing nations). So, the fundamental structure of a good health care system is in place in many countries, and another positive sign is the development of a core of health care middle-management in the emerging countries. Poverty is the defining factor of developing countries; the real gross national product (GNP) in sub-Saharan Africa has decreased by 15% in recent years, and resources that are present are often badly distributed (as in Thailand, where 15 of the nation's 25 neurosurgeons are in Bangkok, leaving 10 to care for the rest of the nation, comprising 40 million people).

Before long, many countries left to their own resources will "hit the wall" of improving the standards of national health care. Dr. Langfitt said that one particularly great need in developing countries is diagnostic radiology. The simple recipe of appropriate training of personnel plus sufficient diagnostic equipment will help these countries improve their success at treating the most important medical problems at the least cost. Radiologists who will work in Nepal, for example, should not undergo exactly the same training as those who work in Thailand or in the United States; the leading causes of death—which should be the highest health priorities—differ greatly among the three countries. In Nepal, with a GNP of $300 per capita and an average life expectancy of less than 50 years, the leading causes of death are acute respiratory ailments, digestive diseases (diarrhea), tuberculosis, trauma, and measles. In contrast, the GNP of Thailand is $180 per capita but average life expectancy is in the mid 60s; the major fatal illnesses are trauma, cardiovascular disease, digestive disorders (diarrhea), lung disease, and cancer. And, in the United States, where the GNP is $2800 per capita and the average life expectancy is more than 70 years, the most frequent causes of death are cardiovascular disease, cancer, trauma, lung disease, and liver cirrhosis. Therefore, it is most important for those who want to help develop diagnostic radiology resources in emerging

countries to provide equipment and training that are appropriate for that environment. Cost-effectiveness, in this era of dwindling charitable revenues, is again the key word as charities such as The Pew Charitable Trusts decide on the ways to spend the donations entrusted to them.

Technology and Hospital Budgets in an Era of Retrenchment

The President of the University Hospital in Denver, CO, Dennis Brimhall, provided a different perspective on technology, health care, and economics. Today's hospitals in the United States are beset with conflicting pressures; although reimbursements are decreasing, the greater expectations of consumers require the latest in technology, higher quality care, new clinical programs (e.g., organ transplantation), and more accurate diagnosis. As more sophisticated procedures are developed, hospitals must decide whether to spend the money not only on the new equipment but also on the specialized practitioners needed. An additional pressure comes from competition, which drives hospitals to offer special programs in order to differentiate themselves from other hospitals. While the costs of health care are rising at a rate that is higher than the inflation rate, reimbursement grows at a rate that is slower than or equal to the inflation rate. Moreover, much reimbursement is fixed (either by reason for admission or by set daily charges for hospital stays) and does not take into account either conventional diagnostic procedures or investigative procedures.

The squeeze on hospital administrators is, therefore, caused by patients who expect new technology, competition with other hospitals, and the powerful research engine that has developed in the United States (i.e., if technology is available, it must be used). To decrease the pressure, more collaboration and cooperation are needed, the limitations of hospital resources must be recognized and accepted, and national health care reform must be started (with physicians taking the lead in reform rather than fighting it). Brimhall did say that technology is one area that will be less affected by budget crunches because it tends to pay for itself in the long run. In the short run, however, physicians and hospital administrators must work together to provide high-quality health care with increasingly limited resources.

Research Activities of a University-Administered National Research Laboratory in a Time of Change

Roger W. Werne (Lawrence Livermore National Laboratory, Livermoré, CA) described how scientists at Lawrence Livermore are "using bomb technology to further medical diagnostics." The health-related studies at the laboratory went through an interesting history of development, starting with studies of the effects of nuclear radiation on the human body, through studies of other environmental insults, to human genome research. Chromosome investigations have led to the discovery of the gene that causes a form of muscular dystrophy. Perhaps of more interest to the vision-oriented radiologist is the DYNA3D software, which can model dynamic structural performance under load (such as the effect of the impact of an automobile accident on the brain and body). Engineers in industry are using DYNA3D to develop anthropomorphic dummies to model all human organs, including the musculoskeletal system.

Although the biotechnology program at Lawrence Livermore Laboratory is relatively "small" ($35 to $40 million per year), it is making advances that may directly affect radiology in the future, advances that all derive from the Laboratory's expertise in low signal-to-noise problems. Specifically, work is being done on enhanced digital mammography, microtomography, and signal processing of vibration from heart valves. The goal of laboratory studies on digital mammography is to use laboratory technology and knowledge to identify and highlight microcalcifications in high-resolution digitized mammography. Using a calcification finder based on artificial intelligence techniques, mammographers can find calcified areas on a digital representation of a mediolateral mammogram with the soft tissue removed by the computer program. Then the breast tissue is added back to localize the calcification, and the result is high-resolution (70 μm) of a portion of the digitized image. An X-ray tomographic microscope can characterize fine structural features in bones and provide information in three dimensions. For this technology, the data-processing and data-storage requirements are still formidable, but Dr. Werne expects that these problems will be solved in the next 3 years. For example, Dr. Werne showed resolutions of 10 μm that have been achieved in a rat femur with microtomography; in the future, radiologists will be able to look at cross-sections at any location in the human body—at present, they are collaborating with researchers at the University of California, San Francisco, to look at uses of microtomographic images of teeth. Finally, the problem of accurate signal processing and classification of heart valve defects is closely connected with basic signal-to-noise problems. The goal of this specific research is to identify single-strut fractures in artificial heart valves by using known techniques for accurate acoustic signal processing, identification, and classification. They have already learned that the key piece of information is discoverable at the point that the valve opens (not when it is closing), and they are developing an artificial intelligence algorithm that can identify a broken strut. The scientists at this laboratory must be considered valuable assets as imaging technology moves ever faster toward the year 2000. At this site, where bombs were once so efficiently produced, researchers are now developing ways to improve the speed and quality of diagnostic imaging.

Conclusion and Summary

At the end of the final session, one of the co-chairs, Ronald L. Arenson (University of California, San Francisco) summarized the main points made at the conference. He mentioned that the talks had shown both the differences and

similarities among the world's nations and that computers have become vital tools for radiologic practice and research. Dr. Arenson discussed four major themes that the symposium had brought into focus: the importance of cost-effectiveness analyses; the need to provide radiologic equipment to developing countries; the significance of worldwide training programs in radiology; and the search for continuing support for research.

The government, industry, and academia all have great interest in cost-effectiveness. Radiologists in the future will be required even more than in the past to justify expenditures on equipment and to explain the benefits of sophisticated examinations. As leaders in radiology, the participants were encouraged to take the "offensive" in showing how new, admittedly expensive, technology can save lives and money in the long run–especially in terms of early diagnosis. Dr. Arenson suggested a conference was needed to address the single issue of cost-effectiveness of radiologic medicine and to start a "think tank" that could develop approaches to the problems of rationally calculating cost-effectiveness.

Research is needed to provide an inexpensive field radiology unit for use in developing countries. The fields of industry and research have made tremendous progress in providing sophisticated equipment appropriate for hospitals in industrialized nations, but doctors in developing countries need mobile units, which are especially useful when one radiologist must serve tens of thousands of people. Dr. Arenson suggested exploring the use of computed radiography, so that no film or processing supplies are necessary, and providing through that unit a link over telephone lines to hospitals with radiologic expertise for special cases.

Worldwide training of radiologists must move toward the goals of both standardizing educational requirements and providing education that is relevant for each country's situation (e.g., life expectancy, GNP per capita, leading causes of death). Also, training must be provided for technologists and other health care workers—particularly in regions in which there are too few radiologists. Such training could be done in conjunction with the field unit described in the preceding paragraph, so that examinations could be performed by technologists in the field and then the images could be interpreted via computer hook-up by radiology experts in large hospitals that may be far away from the patient.

With the decline in both government and clinical funds, new sources need to be found so that research into diagnostic and therapeutic radiology can continue. Radiology's industrial partners may be able to help support more research, as long as the researchers remain independent of industry. A formalized relationship between academia and industry for support of important research would benefit both. Furthermore, findings that are significant for the health of patients can be verified more quickly if research centers share data to a greater extent and cooperate with one another to get the combined data published.

Forthcoming Articles

CARDIOPULMONARY RADIOLOGY

Thoracic metastases from carcinoma of the nasopharynx: high frequency of hilar and mediastinal lymphadenopathy. *Daly BD, Leung SF, Cheung H, Metreweli C*

Increased density of the azygos lobe on frontal chest radiographs simulating disease: CT findings in seven patients. *Caceres J, Mata JM, Alegret X, Palmer J, Franquet T*

Pictorial essay. Ground-glass opacity of the lung parenchyma: a guide to analysis with high-resolution CT. *Engeler CE, Tashjian JH, Trenkner SW, Walsh JW*

Pictorial essay. Bronchiectasis: CT evaluation. *McGuinness G, Naidich DP, Leitman B, McCauley DI*

BREAST RADIOLOGY

Tubular carcinoma of the breast: mammographic appearance. *Leibman AJ, Lewis M, Kruse B*

Mammographic findings in men with breast cancer. *Dershaw DD, Borgen PI, Deutch BM, Liberman L*

Quality assurance in mammography: status of residency education. *Bassett LW, Lubisich JP, Bresch JP, Jessop NW, Hendrick RE*

GASTROINTESTINAL RADIOLOGY

Periportal low density on CT in patients with blunt trauma: association with elevated venous pressure. *Shanmuganathan K, Mirvis SE, Amorosa M*

False-positive diagnoses based on CT portography: correlation with pathologic findings. *Soyer P, Lacheheb D, Levesque M*

Hepatic artery thrombosis in pediatric liver transplant recipients: false-positive findings on arteriography. *Rollins NK, Timmons C, Superina RA, Andrews WS*

Value of 3DFT-FISP MR imaging to determine the effect of transcatheter arterial chemoembolization on hepatocellular carcinoma: pathologic correlation in 10 cases. *Murakami T, Nakamura H, Tsuda K, et al.*

Response of early-stage hepatocellular carcinoma and borderline lesions to therapeutic arterial embolization. *Takayasu K, Wakao F, Moriyama N, et al.*

Technical note. Three-dimensional localization of hepatic neoplasms with computer-generated scissurae re-created from axial CT and MR images. *Waggenspack GA, Tabb DR, Tiruchelvam V, Ziegler L, Waltersdorff K*

Evaluation of the pharyngeal airway in patients with sleep apnea: value of ultrafast MR imaging. *Suto Y, Matsuo T, Kato T, et al.*

Colonic submucosal tumors: a new classification based on radiologic characteristics. *Kawamoto K, Motooka M, Hirata N, et al.*

GENITOURINARY RADIOLOGY

CT diagnosis of primary aldosteronism: sensitivity in 29 patients. *Dunnick NR, Leight GS, Roubidoux MA, Leder RA, Paulson E, Kurylo L*

Safety and efficacy of kidney transplant biopsy: Tru-Cut needle vs sonographically guided Biopty gun. *Mahoney MC, Racadio JM, Merhar GL, First MR*

Pictorial essay. Pelvic fistulas: findings on MR imaging. *Outwater E, Schiebler ML,*

MUSCULOSKELETAL RADIOLOGY

Acute fracture of the femoral neck: assessment of femoral head perfusion with gadopentetate dimeglumine–enhanced MR imaging. *Lang P, Mauz M, Schörner W, et al.*

Meniscal tears of the knee: preliminary comparison of three-dimensional MR reconstruction with two-dimensional MR imaging and arthroscopy. *Disler DG, Kattapuram SV, Chew FS, Rosenthal DI, Patel D*

PEDIATRIC RADIOLOGY

Hepatic injury from blunt trauma in children: follow-up evaluation with CT. *Bulas DI, Eichelberger MR, Sivit CJ, Wright CJ, Gotschall CS*

Obstructive vs nonobstructive dilatation of the renal collecting system in children: distinction with duplex sonography. *Kessler RM, Quevedo H, Lankau CA, et al.*

Renal calcification in patients with autosomal recessive polycystic renal disease: prevalence and cause. *Lucaya J, Enriquez G, Nieto J, Callis L, Pena PG, Dominguez C*

Case report. Bilateral persisting mesonephric duct. *Pereira JK, Chait PG, Daneman A*

Case report. Extragonadal yolk sac tumor: sonographic and CT findings. *Lev MH, Blickman JG*

Case report. Characteristic MR findings in a neonate with incontinentia pigmenti. *Chatkupt S, Gozo AO, Wolansky LJ, Sun S*

VASCULAR RADIOLOGY

Distinction between partial anomalous pulmonary venous drainage of the left upper lobe and duplication of the superior vena cava based on CT findings. *Dillon EH, Camputaro C*

Coronary artery fistula after cardiac transplantation: atypical location. *Barlan MM, Polak JF, Bjork L*

Case report. Compression repair of a postcatheterization pseudoaneurysm of the brachial artery under sonographic guidance. *Skibo L, Polak JF*

Case report. Migration of the Simon nitinol vena cava filter to the chest. *LaPlante JS, Contractor FM, Kiproff PM, Khoury MB*

NEURORADIOLOGY

Parietal lobe abnormalities detected by MR in patients with infantile autism. *Courchesne E, Press GA, Yeung-Courchesne R*

Pictorial essay. Acoustic schwannoma: MR findings in 84 tumors. *Mulkens TH, Parizel PM, Degryse HR, et al.*

CONTRAST MATERIAL

Perfluorooctylbromide as a contrast agent for CT and sonography: preliminary clinical results. *Behan M, Connell DO, Mattrey RF, Carney DN*

RADIATION EXPOSURE

Technical note. Audible radiation monitors: reducing the radiation exposure of fluoroscopy personnel. *Hough DM, Brady A, Stevenson GW*

CLINICAL PROBLEM SOLVING

Clinical problem solving. *Pauker SG, Kopelman RI*

An incidental finding: a radiologist's perspective. *Royal HD, Siegel BA, Murphy WA*

RADIOLOGY JOURNALISM

Perspective. Manuscript peer review: general concepts and the *AJR* process. *Chew FS*

Perspective. The *AJR* of the future: electronic publication and distribution. *Fishman EK, Ney DR, Brody WR*

Letters

Extravasation Injury with Nonionic Contrast Material

We read with interest the recent letter from Pond and Dorr [1] describing cutaneous ulceration after extravasation of iohexol delivered by an automatic power injector. The authors point out that skin and soft-tissue necrosis are well recognized complications of extravasation of high-osmolality contrast materials [2]. Experimental evidence and clinical reports suggest that injury caused by extravasation of low-osmolality agents is uncommon and rarely requires medical or surgical intervention [3, 4].

Recently, we treated a 67-year-old woman who had chest CT for evaluation of a suspected left-sided perihilar mass. Contrast enhancement was thought to be indicated, and a 22-gauge plastic cannula was inserted into the volar surface of the left distal forearm by a certified technologist trained in venous cannulation. Iohexol (350 mg I/ml) was administered by means of a power injector. Administration of the initial 50-ml bolus was monitored visually, and an additional 130 ml was injected at the rate of 1 ml/sec. The patient made no complaint during the course of the CT examination, but after the scanning, the technologist noticed visual evidence of extravasation of contrast material into the forearm. The supervising radiologist was notified immediately. The involved limb was elevated, and cold compresses were applied to the site [3]. The patient was closely monitored for the next 2 hr, and serial measurements showed increases in the girth of the forearm compared with the uninvolved arm. The patient subsequently began to have decreased sensorimotor function and a feeling of severe tightness within the forearm. Approximately 3 hr after the extravasation occurred, capillary refill became poor, and the patient's radial and ulnar pulses were difficult to palpate. A plastic surgeon was consulted. The consultant thought that the patient was experiencing an acute compartmental syndrome related to the extravasation, and emergent fasciotomy was performed. The patient's postoperative course was unremarkable, and her forearm healed with no persistent deficit.

Although nonionic contrast agents have had a remarkably safe track record with regard to extravasation, close monitoring of patients who receive these agents is still necessary. Caution should be exercised in the management of all cases of extravasation of contrast medium, especially with the moderate to large volumes of medium that may be extravasated when power injectors are used.

Mark Memolo
Ray Dyer
Ronald J. Zagoria
Bowman Gray School of Medicine
North Carolina Baptist Hospital
Winston-Salem, NC 27157-1088

REFERENCES

1. Pond GD, Dorr RT. Skin ulceration from extravasation of low-osmolality contrast medium: a complication of automation(letter). *AJR* **1992**; 158:915–916
2. Spigos DG, Thane TT, Capek V. Skin necrosis following extravasation during peripheral phlebography. *Radiology* **1977**;123:605–606
3. Elam EA, Dorr RT, Lagel KE, Pond GD. Cutaneous ulceration due to contrast extravasation. *Invest Radiol* **1991**;26:13–16
4. Sistrom CL, Gay SB, Peffley L. Extravasation of iopamidol and iohexol during contrast-enhanced CT: report of 28 cases. *Radiology* **1991**; 180:707–710

Reply

The case reported by Memolo et al. is apparently the first in which extravasation of low-osmolality contrast material required surgical intervention. Inadvertent subfascial placement of a needle is, in our opinion, the most likely explanation for this case. We reached this conclusion for the following reasons: (1) Subfascial extravasation of the initial 50-ml bolus of contrast material would not be easily seen, and nonionic agents do not ordinarily cause pain when extravasated. (2) A total of 180 ml of any fluid injected deep to the antebrachial fascia would produce considerable pressure and hypothetically would compromise vascular supply. (3) Although iohexol is "low osmolality," it is still hypertonic (844 mOsm/kg H_2O); its osmolality is almost three times that of plasma. It would further increase pressure within the compartment by creating an osmotic gradient in a confined space. The progressive signs and symptoms and the ultimate development of an acute compartmental syndrome 3 hr after extravasation fit well with the hypothesis that the agent was injected subfascially. (4) Although contrast material might have moved from a subcutaneous location to a subfascial one, our colleagues in the anatomy department tell us this is unlikely. Furthermore, we have never observed contrast material in the subfascia on plain films obtained after extravasation, and we suspect that such a finding is rare. (5) To our knowledge, compartmental syndromes associated with extravasation of contrast material (even high-osmolality, ionic agents) have not been reported.

Whatever the mechanism for the complication reported, this case illustrates yet another risk of peripheral power injection of contrast material. We are currently developing a device that may detect large volumes of extravasated materials before they become critical. Unfortunately, manufacturers have shown little interest, probably because the prevalence of injury such as that described by Memolo et al. is quite low. Our experience, however, suggests that extravasation occurs in approximately 1% of all peripheral power injections of contrast material. None of these produced any sequelae, mostly

because low-osmolality agents were used in all our cases. We are concerned, however, that a trend toward the use of less expensive but higher osmolality contrast agents may result in a higher number of complications in the future.

Gerald D. Pond
Robert Dorr
University of Arizona, Health Sciences Center
Tucson, AZ 85724

High-Resolution Sonography of the Diaphragmatic Pleura

In a review article on pleural imaging [1], McLoud and Flower describe two sonographic findings that can be used to differentiate exudative from transudative pleural effusions: (1) the presence of thin, mobile, linear structures, which tend to occur in protein-rich exudates and have a honeycomb appearance when extensive; and (2) the presence of a uniform mass of tiny echogenic structures that move in a swirling fashion with respiration. The authors repeatedly stress that sonographic detection of pleural thickening is generally difficult. However, if easily detectable, pleural thickening would be another sonographic finding that could be used to differentiate an exudate from a transudate.

For 2 months, we used high-resolution sonography with 7.5-MHz sector transducers (Sonoline AC, Siemens, Inc.) to evaluate diaphragmatic pleural thickening in two groups of patients. The first group consisted of seven patients with an exudative effusion (two empyemas and five tuberculous pleural effusions). The second consisted of 10 patients with a transudative effusion (five effusions associated with congestive cardiac failure and five associated with uremia). The nature of the effusion was confirmed in all patients by using either diagnostic aspiration or pleural biopsy. Scanning was performed in the coronal plane along the axillary lines; the scanning plane was directed toward the surface of the diaphragmatic pleura.

High-resolution sonograms showed a distinctly thick and irregular diaphragmatic pleural surface in six patients in the first group (Fig. 1). Swirling internal echoes and mobile fibrinous tags were visualized in four of these six. In the remaining two, the changes in the diaphragmatic pleura provided the only clue to the nature of the effusion. None of the patients in the second group had any abnormality involving the diaphragmatic pleura. Sonographic demonstration of diaphragmatic pleural thickening cannot supplant diagnostic thoracentesis for ascertaining the true nature of pleural effusion. However, detection of diaphragmatic pleural thickening on sonograms suggests that the effusion is an exudate, and thus diagnostic aspiration is necessary, even though the clinical situation is more suggestive of a transudate.

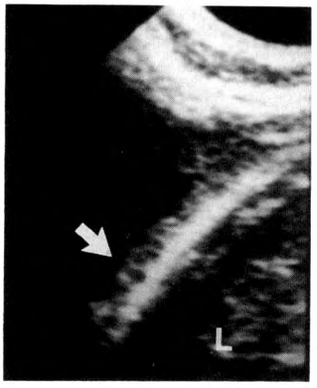

Fig.1 High-resolution sonogram shows thick and irregular diaphragmatic pleura (*arrow*). L = liver.

Hiten M. Malde
Deepa Chadha
K. E. M. Hospital
Bombay, India

REFERENCE

1. McLoud TC, Flower CDR. Imaging the pleura: sonography, CT, and MR imaging. *AJR* **1991**;156:1145–1153

Reply

We thank Drs. Malde and Chadha for their interesting observations. The abnormality they describe is an irregular echogenic line immediately cephalad to the diaphragm. This may he due to thickening of the pleura, to debris, or to a combination of the two. It is noteworthy that they did not detect the same changes over the chest wall aspects of the pleural fluid collections.

Regardless of the presence or absence of these changes (or indeed the presence or absence of internal echoes as described by us [1]), we recommend needle aspiration in all cases of unexplained pleural effusions.

Theresa C. McLoud
Harvard Medical School
Massachusetts General Hospital
Boston, MA 02114
Christopher D. R. Flower
Addenbrooke's Hospital
Cambridge, England CB2 2QQ

REFERENCE

1. McLoud TC, Flower, CDR. Imaging the pleura: sonography, CT and MR imaging. *AJR* **1991**;156:1145–1153

Benign Fibrous Mesothelioma of the Pleura: MR Findings

I read with interest the recent article by Lee et al. [1] on CT-pathologic correlation of benign fibrous mesothelioma. We recently obtained MR images of a patient with such a tumor who had mild exertional dyspnea. CT scans showed a large pleura-based mass abutting the middle and posterior mediastinum and paravertebral area that enhanced mildly after administration of contrast medium. MR images were obtained to further delineate possible vascular encasement and invasion of the neural foramina suggested by the CT findings.

The mass had intermediate signal intensity similar to that of muscle on both T1- and T2-weighted images (Fig. 1A). Contrast enhancement with gadopentetate dimeglumine produced a minimal increase in signal intensity (Fig. 1B). Vascular structures were seen as either tubular areas with signal void (arterioles) or serpiginous

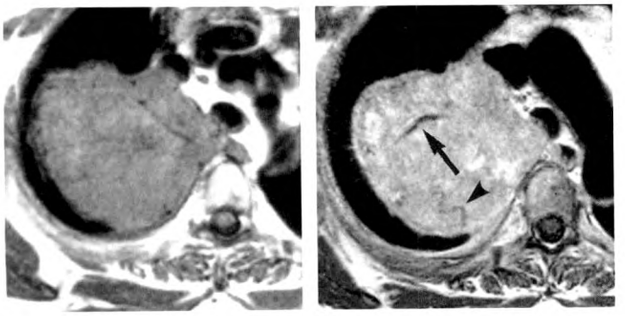

Fig. 1.—*A* and *B*, T1-weighted (750/28) MR images in a patient with benign fibrous mesothelioma. Unenhanced image (A) shows large inhomogeneous pleura-based mass abutting mediastinum and paravertebral area. Contrast-enhanced image (*B*) shows an arteriole (*arrow*) and venous sinusoid (*arrowhead*) within mass

areas with low signal intensity (venous sinusoids). No evidence of vascular encasement or involvement of the neural foramina was found.

Joseph C. George
St. Luke's Medical Center
Milwaukee, WI 53215

REFERENCE

1. Lee KS, Im J-G, Choe KO, Kim CJ, Lee BH. CT findings in benign fibrous mesothelioma of the pleura: pathologic correlation in nine patients. *AJR* **1992**;158:983–986

Reply

We thank Dr. George for his letter on MR findings of benign fibrous mesothelioma of the pleura. Recently, we also obtained MR images in two patients with this type of tumor. In both cases, the tumors had intermediate-intensity signal similar to that of muscle on T1-weighted images (Fig. 1A) and high-intensity signal on T2-weighted images (Fig. 2B). In one case, the tumor contained areas of cystic degeneration and prominent vascular structures. Contrast-enhanced images, which were obtained in one case, showed high-intensity signal in the main lesion (Fig. 1C).

The MR findings reported by Dr. George, including vascular structures in the tumor and no evidence of vascular encasement or involvement of the neural foramina, are comparable to our CT and pathologic findings of high tumor vascularity [1]. In Dr. George's case, the tumor had the same signal intensity (intermediate) on T1- and T2-weighted MR images, whereas in our cases, the tumors had intermediate signal intensity on T1-weighted images and high signal intensity on T2-weighted images. We speculate that the different findings on T2-weighted images are due to differences in the main component of the tumor (the amount of collagen and fibrocytes and/or fibroblasts). Cystic degeneration of the tumor may result in a high-intensity signal on T2-weighted images. The enhancement we observed with gadopentetate dimeglumine was greater than that observed by Dr. George. We still think that the enhancement of the tumor is due to its high tumor vascularity.

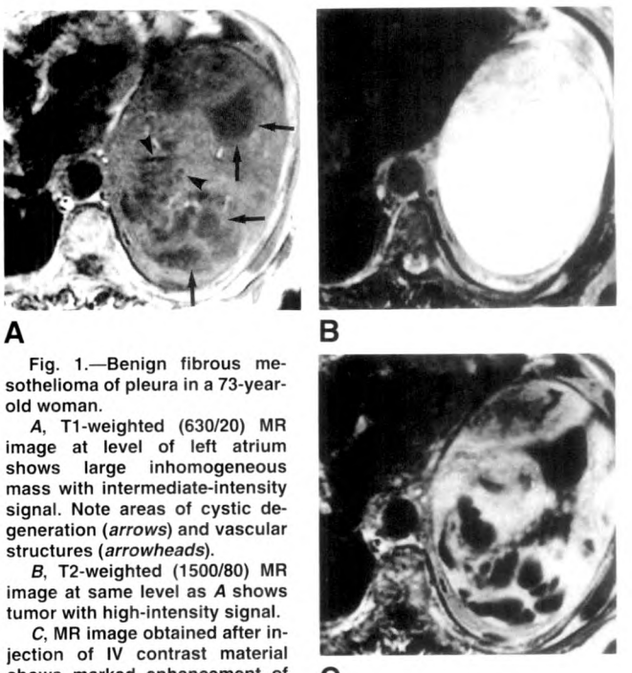

Fig. 1.—Benign fibrous mesothelioma of pleura in a 73-year-old woman.

***A*, T1-weighted (630/20) MR image at level of left atrium shows large inhomogeneous mass with intermediate-intensity signal. Note areas of cystic degeneration (*arrows*) and vascular structures (*arrowheads*).**

***B*, T2-weighted (1500/80) MR image at same level as *A* shows tumor with high-intensity signal.**

***C*, MR image obtained after injection of IV contrast material shows marked enhancement of tumor.**

(Courtesy of Koun Sik Song, Asan Medical Center, Seoul, Korea.)

Kyung Soo Lee
Soonchunhyang University Hospital
Chunan, 330-100, Korea
Jung-Gi Im
Seoul National University Hospital
Seoul, 110-460, Korea

REFERENCE

1. Lee KS, Im J-G, Choe KO, Kim CJ, Lee BH. CT findings in benign fibrous mesothelioma of the pleura: pathologic correlation in nine patients. *AJR* **1992**;158:983–986

Bronchiolitis Obliterans Organizing Pneumonia with Migratory Infiltrates: A Late Complication of Radiation Therapy

The article by Epstein et al. [1] suggested that bronchiolitis obliterans organizing pneumonia should be added to the gamut of causes of migratory pulmonary air-space opacities. We describe a case corroborating this impression in which the pneumonia clearly was a late complication of radiation therapy.

A 63-year-old woman had a 5-year history of recurrent fever and apparent pneumonia, with slight right-sided pleuritic chest pain and a dry cough accompanying each episode. Right-sided infiltrates had been observed in several locations. She had had a radical right mastectomy and postoperative irradiation therapy 18 years before this admission. Chest radiographs showed poorly defined infiltrates peripherally in the right mid and lower zones of the lungs. CT scans showed poorly defined peripheral air-space shadowing confined to

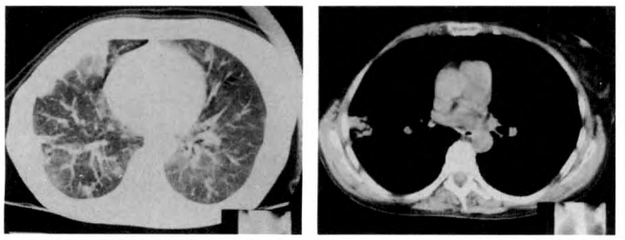

A B

Fig. 1.—*A* and *B*, CT scans of chest show peripheral opacities within area irradiated 18 years earlier. Note absence of right breast (*B*).

the portion of lung that had been irradiated after the mastectomy (Fig. 1). During several weeks of observation, the infiltrates clearly migrated within the relevant portion of lung. The patient's leucocyte count was normal. Open lung biopsy showed features of bronchiolitis obliterans organizing pneumonia. Administration of systemic corticosteroid resulted in rapid, sustained, and complete clinical and radiologic resolution of the opacities. Bronchiolitis obliterans organizing pneumonia has been observed as a late consequence of radiation [2] as opposed to the more commonly seen parenchymal fibrosis. The latter is well established and stable by 12 months after the completion of radiation therapy. Our case broadens the range of documented late pulmonary effects associated with irradiation [3]. It also confirms the possibility of migratory manifestation of bronchiolitis obliterans organizing pneumonia.

Milton E. Tobias
Marshall Plit
Brenthurst Clinic
Johannesburg 2000, South Africa

REFERENCES

1. Epstein DM, Bennett MR. Bronchiolitis obliterans organizing pneumonia with migratory pulmonary infiltrates. *AJR* **1992**;158:515–517
2. Fraser RG, Paré JAP, Paré PD, Fraser RS, Genereux GP. *Diagnosis of diseases of the chest*, 3rd ed. Philadelphia: Saunders, **1991**:2551–2564
3. Fujita J, Bungo M, Nakamura H, et al. Atypical distribution of bacterial pneumonia after radiation therapy (letter). *AJR* **1990**;155:1135

Reply

We appreciate the interest Drs. Tobias and Plit have shown in our article [1]. Their observation of bronchiolitis obliterans organizing pneumonia as a late complication of radiation therapy has merit.

The bronchiolar epithelium and type II pneumocytes are quite sensitive to the effects of radiation and show signs of injury early in the course of radiation therapy. Subsequently, disorganized repair may lead to pulmonary fibrosis or, more rarely, bronchiolitis obliterans organizing pneumonia. Usually, any injury associated with irradiation becomes apparent within 6 months of therapy, but lung remodeling may continue for up to 2 years [2].

Although in most cases, radiation injury is confined to the area of the radiation port, infiltrates outside the area of the port and in the contralateral lung have been reported [3]. Whether these unusual manifestations of radiation injury are actually bronchiolitis obliterans organizing pneumonia is still speculative, as biopsies of the areas are rarely done.

The report of Drs. Tobias and Plit reinforces our premise that bronchiolitis obliterans organizing pneumonia manifested as migratory infiltrates is an underdiagnosed entity, likely seen in a variety of disease states.

Michael R. Bennett
David M. Epstein
The Western Pennsylvania Hospital
Pittsburgh, PA 15224

REFERENCES

1. Epstein DM, Bennett MR. Bronchiolitis obliterans organizing pneumonia with migratory pulmonary infiltrates. *AJR* **1992**;158:515–517
2. Fraser RG, Paré JAP, Paré PD, Fraser RS, Genereux GP. *Diagnosis of diseases of the chest*, 3rd ed. Philadelphia: Saunders, **1991**:2551–2564
3. Rosiello RA, Marrill WW. Radiation-induced lung injury. *Clin Chest Med* **1991**;11:65–71

Conversion of Gastrostomy Tube to Gastrojejunostomy Tube by Using a Peel-Away Sheath

Percutaneous placement of gastrostomy and gastrojejunostomy tubes has become a common interventional radiologic procedure. We frequently have been asked to convert gastrostomy tubes to gastrojejunostomy tubes in patients who need long-term tube feedings, but who have episodes of aspiration because of gastroesophageal reflux. We have found that use of a peel-away sheath greatly decreases the time needed to convert a gastrostomy tube to a gastrojejunostomy tube.

Gastrostomy tubes are usually placed lateral to the rectus sheath to decrease the chance of bleeding from branches of the superior epigastric artery. This usually places the tip of the gastrostomy tube in the fundus of the stomach directed away from the pylorus. In addition, patients who have gastrostomy tubes tend to be thin, and the antrum of the stomach is decompressed. Consequently, attempts to cross the midline toward the pylorus are hindered. Typically, guidewires and catheters simply buckle into the fundus. We have found that a 16-French peel-away sheath provides enough support to overcome these problems.

Generally, we remove the preexisting gastrostomy tube over a straight-tipped 0.035-in. (0.089-cm) hydrophilically coated guidewire (Medi-tech, Watertown, MA). A 16-French peel-away sheath is then advanced over the wire and directed toward the pylorus. The stiffness of the sheath enables us to torque it toward the antrum and advance the tip to the pylorus. A 5-French multipurpose catheter (Cook, Bloomington, IN) is placed over the wire and through the sheath, and the catheter and guidewire are used to cross through the pylorus and advance through the duodenum to the ligament of Treitz. The peel-away sheath prevents buckling of the catheter and guidewire into the fundus and helps direct them to the pylorus. Once the ligament of Treitz is reached, the catheter is removed, and an 18-French gastrojejunostomy tube (Medical Innovations Corporation, Milpitas, CA) is advanced over the wire and through the sheath (Fig. 1). The sheath again prevents buckling of the tube into the fundus of the stomach. When the tube is positioned correctly, the guidewire and sheath are removed, and the gastrojejunostomy tube is secured.

This method saves considerable time. In most instances, the conversion can be accomplished in 10 min or less. The peel-away sheath helps direct the catheter and guidewire toward the pylorus, prevents buckling into the fundus, and eliminates resistance to advancement of the gastrojejunostomy tube at the anterior abdominal wall [1]. My colleagues and I have used this procedure in four patients so far and have found it quite practical.

Scott R. Kerns
University of Florida
Gainesville, FL 32610-0374

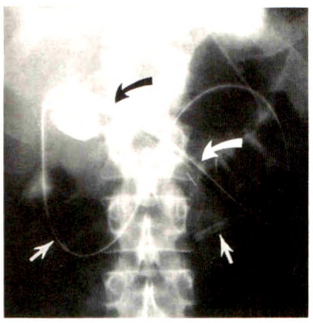

Fig. 1.—Radiograph shows gastrojejunostomy tube (*straight arrows*) advanced through sheath (*curved arrows*) past ligament of Treitz.

REFERENCE

1. Alzate GD, Coons HG, Elliot J, Carey PH. Percutaneous gastrostomy for jejunal feeding: a new technique. *AJR* **1986**;147:822–825

Bacillary Angiomatosis in a Patient with HIV Infection

We read with interest the article by Radin and Kanel [1] on peliosis hepatis in HIV infection and the follow-up letter to the editor by Dr. Radin [2]. We recently treated an AIDS patient with bacillary angiomatosis who had similar CT findings.

A 34-year-old man with AIDS was hospitalized because of fever, upper abdominal pain, and weight loss. Physical examination showed hepatosplenomegaly and several erythematous skin nodules. Contrast-enhanced abdominal CT showed an enlarged liver containing diffuse tiny hypodense nodules; adenopathy in the portal, mesenteric, and paraaortic regions; and a moderate-sized right-sided pleural effusion (Fig. 1). Contrast-enhanced abdominal CT scans obtained 6 weeks earlier were normal.

Biopsy of a skin nodule showed clumps of bacteria, and tests with Warthin-Starry stain were positive for bacillary angiomatosis. A liver biopsy was not performed. The patient was treated with erythromycin, and, as shown by physical examination, the size of the liver decreased rapidly. The patient was discharged 2 weeks after admission. Three months later, he had increasing venous distension of the lower extremities. Contrast-enhanced abdominal CT scan obtained at that time was normal.

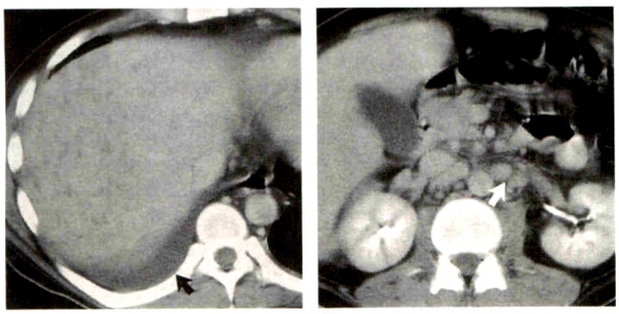

A B

Fig. 1.—Bacillary angiomatosis in a patient with HIV infection.
***A*, CT scan shows numerous tiny hypodense nodules in liver and a right-sided pleural effusion (*arrow*).**
***B*, CT scan at level inferior to that in *A* shows paraaortic adenopathy (*arrow*).**

Bacillary angiomatosis is caused by a bacillus similar to the one associated with cat-scratch disease. It occurs with increased frequency in immunocompromised patients, including those with AIDS, and may involve the skin, liver, spleen, lymph nodes, bone marrow, and pleura [3, 4]. Histologic examination of the liver and spleen shows a proliferation of endothelial cells forming vascular spaces, similar to the findings reported in peliosis hepatis.

Recent publications [5, 6] suggest that peliosis hepatis in patients with HIV infection is caused by the same organism that causes bacillary angiomatosis. The rapid development and resolution of the abdominal CT findings in our patient strongly suggest visceral involvement by bacillary angiomatosis. The similarity of these CT findings to those reported by Dr. Radin is consistent with the theory that peliosis hepatis and bacillary angiomatosis in patients with HIV infection result from either the same or closely related organisms.

Philip Goodman
Suppiah Balachandran
University of Texas Medical Branch
Galveston, TX 77555-0709

REFERENCES

1. Radin DR, Kanel GC. Peliosis hepatis in a patient with human immunodeficiency virus infection. *AJR* **1991**;156:91–92
2. Radin DR. Spontaneous resolution of peliosis of the liver and spleen in a patient with HIV infection (letter). *AJR* **1992**;158:1409
3. Kemper CA, Lombard CM, Deresinski SC, Tompkins LS. Visceral bacillary epithelioid angiomatosis: possible manifestations of disseminated cat scratch disease in the immunocompromised host: a report of two cases. *Am J Med* **1990**;89:216–222
4. Schlossberg D, Morad Y, Krouse TB, Wear DJ, English CK. Culture-proved disseminated cat-scratch disease in acquired immunodeficiency syndrome. *Arch Intern Med* **1989**;149:1437–1439
5. Perkocha LA, Geaghan SM, Yen TSB, et al. Clinical and pathological features of bacillary peliosis hepatis in association with human immunodeficiency virus infection. *N Engl J Med* **1990**;323:1581–1586
6. Relman DA, Falkow S, LeBoit PE, et al. The organism causing bacillary angiomatosis, peliosis hepatis, and fever and bacteremia in immunocompromised patients. *N Engl J Med* **1991**;324:1514

Reply

As noted by Goodman and Balachandran, evidence is available that peliosis hepatis in patients with HIV infection may be caused by the same organism that causes cutaneous bacillary angiomatosis. In liver tissue from eight HIV-infected patients with peliosis hepatis, Perkocha et al. [1] detected bacilli that were morphologically identical to the bacilli found in the skin lesions of bacillary angiomatosis. The authors suggested that "bacillary peliosis hepatis" and bacillary angiomatosis may represent different responses of endothelial cells in the liver and skin, respectively, to an angiogenic factor elaborated by the bacilli.

Three aspects of our case [2, 3] are noteworthy. No evidence of cutaneous bacillary angiomatosis was found, as was the case in six of eight patients described by Perkocha et al. [1]. Tests with Gomori methenamine silver and Warthin-Starry stains did not show organisms in the liver biopsy specimen from our patient. Although bacillary peliosis has been treated successfully with antibiotics [1], our patient showed evidence of spontaneous resolution of peliosis.

Autopsy (at Los Angeles County–University of Southern California Medical Center) of a 28-year-old man with AIDS who died of *Pneumocystis carinii* pneumonia showed extensive hepatic and mild splenic involvement by peliosis. No skin lesions were found. Tests with Gomori methenamine silver and Warthin-Starry stains did not show bacilli. At Children's Hospital of Los Angeles, a 9-year-old boy with previous diagnoses of Down's syndrome, leukemia, and HIV infection was admitted for evaluation of fever and hepatospleno-

megaly (Hansch L, personal communication). He had no cutaneous lesions. After abdominal CT scans showed multiple tiny hypoattenuating lesions in the liver and spleen, splenectomy and wedge biopsy of the liver were performed. Pathologic examination showed peliosis of the liver and spleen. Tests with Warthin-Starry stain did not show any organism, but interpretation of the results was difficult because of high background staining. Whether no bacilli were found in these two cases and in our original case because no organisms were present or because technical problems occurred is not known.

In summary, current evidence suggests that peliosis of the liver and spleen in patients with HIV infection is due to a specific bacterial infection, commonly causes fever and hepatosplenomegaly, and responds to treatment with antibiotics. Cutaneous lesions of bacillary angiomatosis may or may not be present. Pathologic examination of the liver and spleen may or may not show the offending bacillus in association with the peliotic lesions. CT scans may show enlargement of the liver and spleen, with or without hypoattenuating nodules, and lymphadenopathy. In the absence of cutaneous bacillary angiomatosis, clinical and radiologic findings are nonspecific and suggest a more common mycobacterial or fungal infection in a patient with HIV infection. If no acid-fast bacillus or fungus is detected in the blood, then biopsy may be necessary. If cutaneous bacillary angiomatosis is present, then specific antibiotic treatment and clinical and radiologic follow-up to evaluate the response to therapy may be sufficient.

D. Randall Radin
Los Angeles County–University of Southern California, Medical Center
Los Angeles, CA 90033
Gary C. Kanel
Rancho Los Amigos Medical Center
Downey, CA 90242

REFERENCES

1. Perkocha LA, Geaghan SM, Yen TSB, et al. Clinical and pathological features of bacillary peliosis hepatis in association with human immunodeficiency virus infection. *N Engl J Med* **1990**;323:1581–1586
2. Radin DR, Kanel GC. Peliosis hepatis in a patient with human immunodeficiency virus infection. *AJR* **1991**;156:91–92
3. Radin DR. Spontaneous resolution of peliosis of the liver and spleen in a patient with HIV infection (letter). *AJR* **1992**;158:1409

Dilated Small Bowel Simulating a Submucosal Gastric Mass

Use of single- or double-contrast barium examination to detect submucosal gastric mass lesions is routine. The differential diagnosis includes benign masses (leiomyoma, hamartoma, lipoma, neurofibroma, hematoma, eosinophilic granuloma, ectopic pancreas), primary malignant tumors (lymphoma, leiomyosarcoma, tumors arising from adjacent organs), and metastatic lesions (melanoma, carcinomas of the breast and lung). Solid organs (liver, spleen, pancreas) and colon can compress the stomach and simulate an extraluminal or submucosal lesion. The perceptive radiologist should also consider extrinsic compression produced by the small bowel, a finding not mentioned in current textbooks or teaching materials for gastrointestinal radiology [1–3].

The case illustrated here shows that the small bowel, when dilated because of partial or complete obstruction, can act as an extrinsic mass and can produce a compressive vector at an unexpected angle (Fig. 1). The classic radiologic signs of an intramural (submucosal) mass are a smooth, well-defined mucosal border with an acute angle. The classic radiologic signs of an extrinsic mass are a smooth, well-defined mucosal border with an obtuse angle.

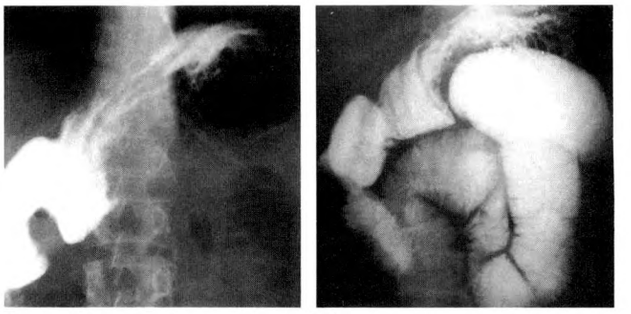

A B

Fig. 1.—*A* and *B*, Barium examination shows large mass effect on greater curvature of stomach (*A*) is caused by dilated jejunum (*B*), which was associated with distal ileal obstruction caused by adhesions.

In the case illustrated, the oblique vector displacing the gastric wall at an acute angle suggested a mass lesion of gastric origin. Furthermore, the superimposition of intraluminal contrast material and gastric folds may be confusing, leading to possible consideration of primary gastric abnormalities.

Richard M. Steinman
Juri V. Kaude
University of Florida, College of Medicine
Gainesville, FL 32610-0374

REFERENCES

1. Eisenberg RL. *Gastrointestinal radiology.* Philadelphia: Lippincott, **1983**:296–308
2. Felson B, Reeder MM. *Gamuts in radiology,* 2nd ed. Cincinnati: Audiovisual Radiology of Cincinnati, **1987**:636–714
3. Eisenberg RL. *Clinical imaging: an atlas of differential diagnosis,* 2nd ed. Gaithersburg, MD: Aspen, **1992**:276–280

Use of Transperineal Sonography to Locate an Obstructing Urethral Calculus

Transperineal sonography is useful in females for showing the level and thickness of tissue in vaginal atresia [1]; evaluating the cervix in late pregnancy for cervical incompetence, placenta previa, and indications of possible preterm labor [2]; and detecting diverticula of the urethra [3]. To our knowledge, no one has reported using this technique to detect an obstructing urethral stone.

A 21-year-old woman who had had a kidney transplant because of renal failure associated with chronic glomerulonephritis came to our clinic because of a 2-day history of gross hematuria and difficulty in voiding. The bladder was evacuated via a catheter, and the patient was dismissed from the clinic. Shortly after removal of the catheter, she had recurrent urinary retention and severe pelvic pain. Subsequent attempts to insert a catheter into the bladder were unsuccessful. Abdominal sonograms showed a distended bladder and no hydronephrosis of the transplanted kidney (Fig. 1A).

Transperineal sonograms obtained with a 5-MHz transducer showed a 2-cm stone in the urethra (Fig. 1B). At cystoscopy, a large calculus in the urethra was pushed back into the bladder and crushed, and the fragments were removed. Suture material was the nidus of the calculus.

Transperineal sonography is a noninvasive well-tolerated procedure that enables detailed evaluation of the cervix, vagina, and urethra in females. The study takes about 5–10 min and does not require that the patient have a full bladder. With the patient supine and the thighs abducted, the transducer is placed on the perineum

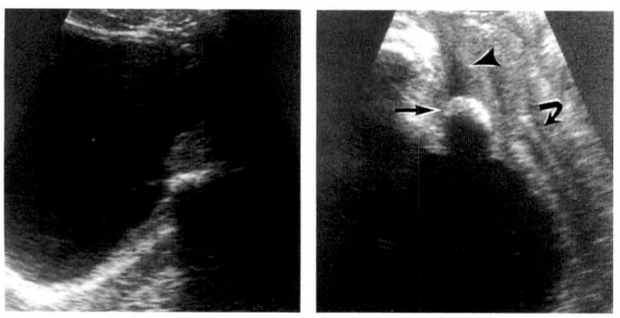

A B

Fig. 1.—Obstructing urethral calculus in a 21-year-old woman with a transplanted kidney.

***A*, Abdominal sonogram shows distended urinary bladder. No stones were seen within bladder lumen.**

***B*, Sagittal transperineal sonogram shows a large calculus (*straight arrow*) within urethra distal to bladder base. Hypoechoic channel (*arrowhead*) is more distal, nondistended urethra. Echogenic stripe (*curved arrow*) is vaginal mucosa.**

between the labia majora. The sagittal orientation optimizes visualization of the urethra as a hypoechoic stripe. Sonographers should be familiar with the performance of this procedure and should use it whenever detailed examination of the urethra in a female is necessary.

Sarah Lewellyn
Patricia L. Abbitt
University of Florida College of Medicine
Gainesville, FL 32610-0374

REFERENCES

1. Scanlan KA, Pozniak MA, Fagerholm M, Shapiro S. Value of transperineal sonography in the assessment of vaginal atresia. *AJR* **1990**;154:545–548
2. Hertzberg BS, Bowie JD, Weber TM, Carroll BA, Kliewer MA, Jordan SG. Sonography of the cervix during the third trimester of pregnancy: value of the transperineal approach. *AJR* **1991**;157:73–76
3. Keefe B, Warshauer DM, Tucker MS, Mittelstaedt CA. Diverticula of the female urethra: diagnosis by endovaginal and transperineal sonography. *AJR* **1991**;156:1195–1197

Blood-Fluid Level Within a Renal Cyst

Nyberg et al. [1] have emphasized that echogenic intraperitoneal fluid correlates with hemoperitoneum in patients with a ruptured ectopic pregnancy. We have found this correlation between echogenic fluid and hemorrhage applicable in detecting hemorrhage within renal cysts in patients with adult polycystic kidney disease.

A 34-year-old man had hematuria after blunt abdominal trauma. The patient had a family history suggestive of polycystic renal disease, and physical examination showed bilateral, nodular renal lumps. Abdominal sonograms obtained with a 3.5-MHz sector transducer (Sonoline AC, Siemens Medical System) showed bilateral, renal cysts of various sizes, characteristic of adult polycystic kidney disease. A few hepatic cysts were also visualized. The fluid within some of these cysts showed marked echogenicity, suggestive of internal hemorrhage. In some of the cysts, a distinct blood-fluid level was visualized, and its position changed when the patient changed position (Fig. 1). A high-frequency transducer (7.5-MHz sector transducer) was superior to the 3.5-MHz transducer for showing the echogenic nature of the internal hemorrhage in some of the superficial cysts. Sonographically guided aspiration of the fluid within the largest cyst was performed. Analysis of the fluid confirmed the presence of internal hemorrhage and the absence of infection.

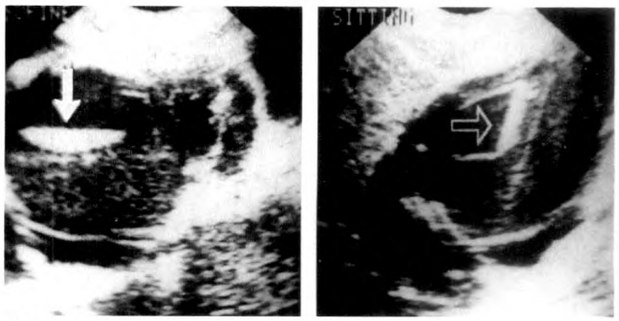

A B

Fig.1.—Renal cyst in a 34-year-old man with adult polycystic kidney disease.

***A* and *B*, Sonograms obtained with patient supine (*A*) and sitting (*B*) show blood-fluid level (*arrows*) within a renal cyst complicated by internal hemorrhage.**

Abdominal sonograms show the cysts of adult polycystic kidney disease as anechoic, thin-walled, circular lesions without any internal echoes or debris, the presence of which would suggest either infection or internal hemorrhage [2]. In the past, studies [2] showed that findings on abdominal sonograms could not be used to differentiate infection from internal hemorrhage. Consequently, differentiation of these two complications required abdominal CT [3] or guided fluid aspiration. We think that the sonographic finding of markedly echogenic fluid within a renal cyst is highly characteristic of internal hemorrhage and obviates any further investigations. High-frequency (7.5-MHz) transducers are superior to 3.5-MHz transducers for highlighting this echogenicity in superficial lesions.

Hiten M. Malde
Deepa Chadha
K. E. M. Hospital
Bombay, India

REFERENCES

1. Nyberg DA, Hughes MP, Mack LA, Wang KY. Extrauterine findings of ectopic pregnancy at transvaginal US: importance of echogenic fluid. *Radiology* **1991**;178:823–826
2. Goldman SM, Hortman DS. Autosomal dominant polycystic kidney disease. In: Pollack HM, ed. *Clinical urography.* Philadelphia: Saunders, **1990**:1092–1112
3. Levine E, Grantham JJ. High-density renal cysts in autosomal dominant polycystic kidney disease demonstrated by CT. *Radiology* **1985**;154: 477–482

Adrenal Pheochromocytoma

I read with considerable enjoyment the radiologic-pathologic conference on adrenal pheochromocytoma presented by Disler and Chew [1]. I must take issue with one sentence of their otherwise quite eloquent and well-illustrated case report. They state that "calcification in the rim and central necrosis are common but not diagnostically specific." Although I agree with the nonspecificity of these findings and the frequency of the central necrosis in pheochromocytoma, I think that the prevalence of calcification is actually quite low. Although calcification has been reported [2], and peripheral calcification has been described as a distinctive finding of pheochromocytoma [3], several series have reported that calcification occurs infrequently in this entity. In a study of 100 patients in which 86 had adrenal pheochromocytomas, only one of the 86 tumors was calcified [4]. In a study Bob Stanley and I did [5], only two (6%) of 33 calcified adrenal masses were pheochromocytoma. In my personal

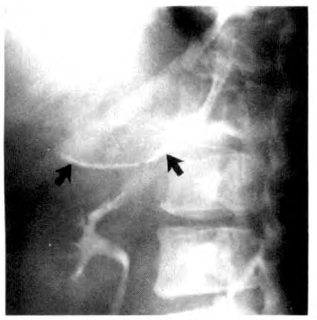

Fig. 1.—Radiograph of surgically proved adrenal cyst shows calcification (*arrows*) in inferior margin only.

experience with 28 cases of pheochromocytoma, these two are the only calcified ones I have seen, for an overall prevalence of 7%. Thus, pheochromocytomas not only calcify infrequently but also account for a low percentage of the total of calcified adrenal masses. Clearly, some pheochromocytomas have peripheral calcification, and most of these also have central necrosis.

However, peripheral curvilinear calcification is a frequent finding in so-called adrenal cysts (most of which are actually pseudocysts). Although a rare entity, adrenal cysts accounted for 18% of calcified adrenal masses in the series reported by Stanley and me [5]. Seven (78%) of the nine adrenal cysts I have seen were calcified.

Intriguingly, in four of them (57% of those calcified), the calcification was limited to, or greatest in, the inferior margin (Fig. 1). This pattern of calcification is in contrast to that seen in the case reported by Disler and Chew, in which the calcification appears to be predominately in the superior aspect of the mass. The same superior predominate pattern was seen in one of the cases of Grainger et al. [3].

In summary, although curvilinear calcification does occur in pheochromocytoma, it is more often seen in a calcified adrenal cyst. The diagnosis of pheochromocytoma, however, should be obvious because of clinical and biochemical evidence of abnormally high levels of catecholamine, which would not be found in a case of adrenal cyst. I do not think that the superior vs inferior predominance of calcification has been discussed before. I wonder if Drs. Disler and Chew have any comments on this topic.

Philip J. Kenney
University of Alabama at Birmingham, School of Medicine
Birmingham, AL 35233

REFERENCES

1. Disler DG, Chew FS. Adrenal pheochromocytoma. *AJR* **1992**;158:1056
2. Meyers MA, King MC. Unusual radiologic features of pheochromocytoma. *Clin Radiol* **1969**;20:52–56
3. Grainger RG, Lloyd GAS, Williams JL. Egg-shell calcifications: a sign of phaeochromocytoma. *Clin Radiol* **1967**;18:282–286
4. Melicow MM. One hundred cases of pheochromocytoma (107 tumors) at the Columbia-Presbyterian Medical Center, 1926–1976: a clinicopathological analysis. *Cancer* **1988**;40:1987–2004
5. Kenney PJ, Stanley RJ. Calcified adrenal masses. *Urol Radiol* **1987**;9:9–15

Reply

We stand corrected by Dr. Kenney on the prevalence of radiographically demonstrable rim calcification in adrenal pheochromocytoma. Concerning the distribution of calcification in the superior vs the inferior portion of the rim of a cystic region of an adrenal mass, we are unaware of any pathophysiologic basis for a difference between pheochromocytoma and cyst, and have not ourselves made the observation that Dr. Kenney has.

David G. Disler
Felix S. Chew
Massachusetts General Hospital
Harvard Medical School
Boston, MA 02114

Subtle Clue to Duplication of Inferior Vena Cava

Prophylactic or therapeutic placement of an inferior vena caval filter may not prevent a pulmonary embolus if the inferior vena cava is duplicated [1–4]. The following is described as an example.

A 62-year-old man had an 11-year history of seizures. For approximately 1 year, he had voluntarily discontinued medication for control of the seizures. A seizure and fall precipitated his admission to another hospital, where CT of the head showed a small subdural hematoma. Seven days after admission for observation, the patient complained of pain in the right calf. The lower extremity was swollen, and a venogram showed extensive thrombosis of the right superficial femoral vein. Evidence of intracranial hemorrhage precluded anticoagulation therapy. Percutaneous placement of an inferior vena caval filter via the right common femoral vein was unsuccessful, as access to the vein could not be achieved. Approach via the right internal jugular vein was successful, and inferior venacavography was performed before placement of the filter. Despite satisfactory placement of the filter at the appropriate level, it was noted during the procedure that the patient might have had a pulmonary embolus. A precipitous fall in oxygen saturation, evidence on chest radiograph of oligemia in the right upper lung, and findings on a ventilation-perfusion scan suggestive of pulmonary embolism were followed by progressive cyanosis and hypotension. The patient was transferred to our institution for possible pulmonary embolectomy.

A review of the original inferior venacavogram showed that the uppermost segment of the inferior vena cava had a considerably larger diameter than did the longer lower segment (Fig. 1A). It appeared that the upper segment was formed by the confluence of two vessels of equal diameter, and that this confluence was not typical of the nearly right-angled juncture of a normal left renal vein with the inferior vena cava (Fig. 1B). In anticipation of possible pulmonary embolectomy, pulmonary arteriography was performed via catheterization of the left common femoral vein. The catheter passed superiorly to the left of the midline in the lower abdomen and then obliquely to the right of the midline in the upper abdomen. Pulmonary arteriograms showed an embolus in the right upper lobe of the lung. The catheter was withdrawn to the lower abdomen, and venacavograms showed the duplicated infrarenal inferior vena cava (Fig. 1C). The left renal vein joined the left inferior vena cava at a right angle. The left inferior vena cava then coursed in its characteristic oblique fashion upward and to the right, where it joined the right vena cava containing the filter that had been placed initially. A second filter was placed percutaneously in the left inferior vena cava via the established left femoral vein access. Figure 1D shows the locations of the two filters in the duplicated inferior vena cava. The clinical course of the patient stabilized and improved during the described procedures. Pulmonary embolectomy was deferred, and after a rapid recovery, the patient was discharged from the hospital.

William J. Smolinski
Allen J. Weinstein
Lehigh Valley Hospital
Allentown, PA 18105

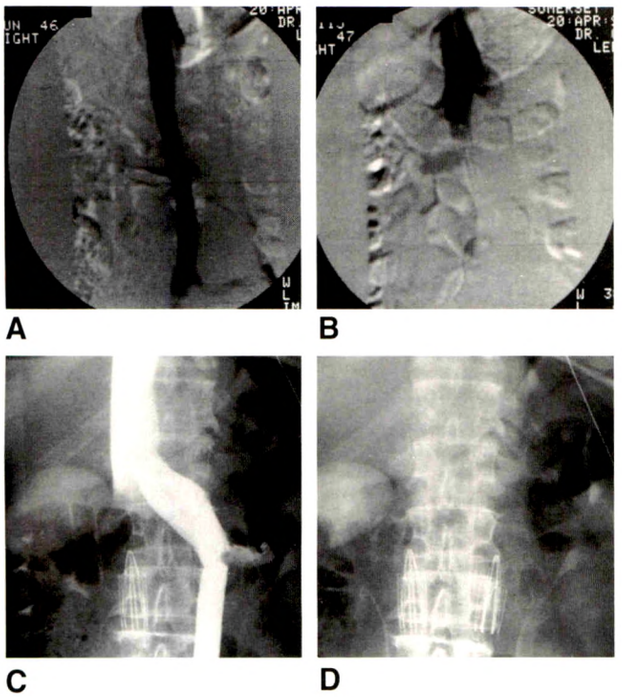

Fig. 1.—Duplication of inferior vena cava.
***A* and *B*, Venacavograms show right infrarenal inferior vena cava (*A*) and proximal segments of right and left inferior vena cavae (*B*) in continuity with upper main segment of vessel.**
***C*, Left femoral venacavogram shows filter in right inferior vena cava and left inferior vena cava without a filter.**
***D*, Venacavogram shows filters at identical levels in right and left inferior vena cavae.**

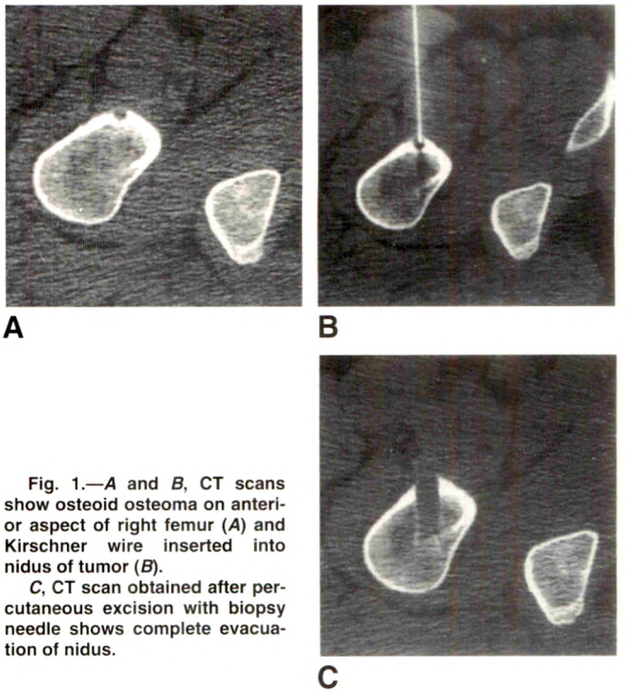

Fig. 1.—*A* and *B*, CT scans show osteoid osteoma on anterior aspect of right femur (*A*) and Kirschner wire inserted into nidus of tumor (*B*).
***C*, CT scan obtained after percutaneous excision with biopsy needle shows complete evacuation of nidus.**

REFERENCES

1. Greenfield LJ, Michna BA. Twelve-year experience with the Greenfield vena cava filter. *Surgery* **1988**;104:706-712
2. Towne JB. Discussion. In: Greenfield LJ, Michna BA. Twelve-year experience with the Greenfield vena cava filter. *Surgery* **1988**;104:706-712
3. Rohrer MJ, Cutler BS. Placement of two Greenfield filters in a duplicated vena cava. *Surgery* **1988**;104:572-574
4. Ferris EJ, Carver DK, McCowan TC. Inferior vena cava filters: technical aspects and follow up. In: Mueller PR, ed. *Syllabus: a categorical course in diagnostic radiology.* Oak Brook, IL: Radiological Society of North America, **1991**:169-178

CT-Guided Excision of Osteoid Osteoma

Incomplete surgical excision of the nidus of an osteoid osteoma is the most commonly cited reason for recurrent signs and symptoms and surgical failures [1]. The common intracortical location and exuberant periosteal reaction hinder intraoperative localization. Several preoperative and intraoperative techniques for localization of the nidus have been described, including use of drill holes, technetium-99m, bone scanning, and fluorescence with tetracycline [2, 3]. All these methods are cumbersome and ineffective. In many cases, placement of hardware is needed after large areas of cortical bone are removed [1, 2–4].

Recently, preoperative CT localization and marking of the nidus followed by en bloc resection were reported [1, 5]. We describe a simple method in which a Kirschner wire and a CORB biopsy needle (Zimmer Manufacturing Co., Warsaw, IN) are used to remove the nidus. The procedure is performed in the CT scan unit. Local anesthesia is used, and the patient is discharged shortly after the procedure is completed.

After the lesion is localized by using CT (Fig. 1A), a Kirschner wire is inserted and drilled through the cortex into the nidus (Fig. 1B). A CORB biopsy needle is inserted over the wire into the bone through a small incision, and the specimen is evacuated. CT scans obtained after excision show the completeness of the evacuation (Fig. 1C).

Dan Atar
Soroka Medical Center
P.O. Box 151
Beer-Sheva, Israel 84101
Wallace B. Lehman
Alfred D. Grant
Hospital for Joint Diseases
New York, NY 10003

REFERENCES

1. Norman A. Persistence or recurrence of pain: a sign of surgical failure in osteoid osteoma. *Clin Orthop* **1978**;130:263–266
2. Ghelman BG, Thompson SM, Arnold WD. Intraoperative radioactive localization of an osteoid osteoma. *J Bone Joint Surg [Am]* **1981**;63-A:826–827
3. Ayala AG, Murray JA, Erling MA, Raymond AK. Osteoid osteoma: intraoperative tetracycline fluorescence demonstration of the nidus. *J Bone Joint Surg [Am]* **1986**;68-A:747–751
4. Marcove RC, Huvos AG, Healy JH. Osteoid osteoma: diagnosis, localization and treatment. *Clin Orthop* **1991**;267:197–201
5. Voto SJ, Cook AJ, Weiner DS, Ewing JW, Arrington E. Treatment of osteoid osteoma by computed tomography guided excision in pediatric patient. *J Pediatr Orthop* **1990**;10:510–513

In Utero Clue to Congenital Lethal Osteogenesis Imperfecta

Sonographic criteria for the diagnosis of congenital lethal osteogenesis imperfecta in utero are shortened, deformed limbs; small concave chest with rib deformities; and cranial deformity, with an unusual clarity ("supervisualization") of intracranial structures. Use of high-resolution, state-of-the-art sonographic equipment highlights this supervisualization of intracranial anatomy, which may be the initial clue leading to the diagnosis of osteogenesis imperfecta.

A 29-year-old pregnant woman (38 weeks' gestation) was referred to our tertiary-care medical center for consultative obstetric sonography for evaluation of fetal intracranial abnormalities. The patient indicated that she had had eight previous sonographic examinations during this pregnancy, all performed elsewhere, but no films of the findings had been obtained. Scanning of the fetus at this time showed marked clarity of normal intracranial structures (Fig. 1A), suggesting a possible diagnosis of osteogenesis imperfecta. Careful assessment of the limbs showed severe fracture deformities of the long bones, characteristic of osteogenesis imperfecta. The patient had an elective cesarean delivery, and the infant died shortly after birth. Radiographs of the neonate confirmed the diagnosis of congenital lethal osteogenesis imperfecta (Fig. 1B).

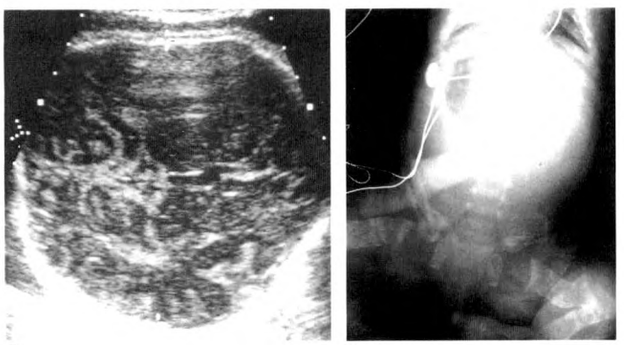

Fig. 1.—Congenital lethal osteogenesis imperfecta.
***A*, Sonogram of head of fetus at level of third ventricle shows deformity of cranial contour and unusual clarity of third ventricle, gyri, and sulci.**
***B*, Postnatal radiograph shows gross bony deformities and healing fractures, diagnostic of congenital, lethal osteogenesis imperfecta.**

Sonographic criteria for the diagnosis of osteogenesis imperfecta in utero have been well described [1]. Supervisualization of normal intracranial structures, which is due to poor calvarial ossification, may be recognized instantaneously when the head of the fetus is scanned. When supervisualization is observed, careful assessment of the fetal limbs should be performed. The only differential diagnosis for these cranial findings is hypophosphatasia.

Matthew Andrews
Eugenio G. Amparo
University of California, Davis Medical Center
Sacramento, CA 95817

REFERENCE

1. Constantine G, McCormack J, McHugo J, Fowlie A. Prenatal diagnosis of severe osteogenesis imperfecta. *Prenat Diagn* **1991**;11:103–111

Segmental Septa in Takayasu Arteritis of the Carotid Artery

We present an unusual case of Takayasu arteritis in which segmental septa were found in the dilated common carotid arteries. A 25-year-old woman was admitted because of fever, pain and pulsatile masses in both sides of the neck, elevated erythrocyte sedimentation rate, and a positive test for C-reactive protein. Sonography, CT, and MR imaging of the neck showed marked dilatation and weblike septa in both common carotid arteries. Aortography showed aortic regurgitation (grade 3), stenosis of the proximal left subclavian and common carotid arteries, and marked dilatation with weblike septa of both common carotid arteries (Fig. 1A). These findings were consistent with a diagnosis of Takayasu arteritis. Selective cineangiography of the left common carotid artery, with sequential rotation from anteroposterior to left anterior oblique projections, showed the segmental septa were circumferential (Figs. 1B–1D).

A combination of stenotic and dilated lesions occurred in this case. The primary pathologic findings in Takayasu arteritis are destruction of elastic fibers in the media, cellular infiltration of the adventitia and media, and fibrosis and hyperplasia of the intima without cellular infiltration [1]. When destruction of the aortic wall is extensive and production of supporting fibrous tissue is deficient, the weakened aortic wall expands. According to Ueda et al. [2], stenotic or occlusive changes occur when fibrosis and hyperplasia of the intima are more marked than the changes in the media and adventitia, and dilatation or aneurysm develops when the destruction of the medial elastic fibers occurs in association with changes in

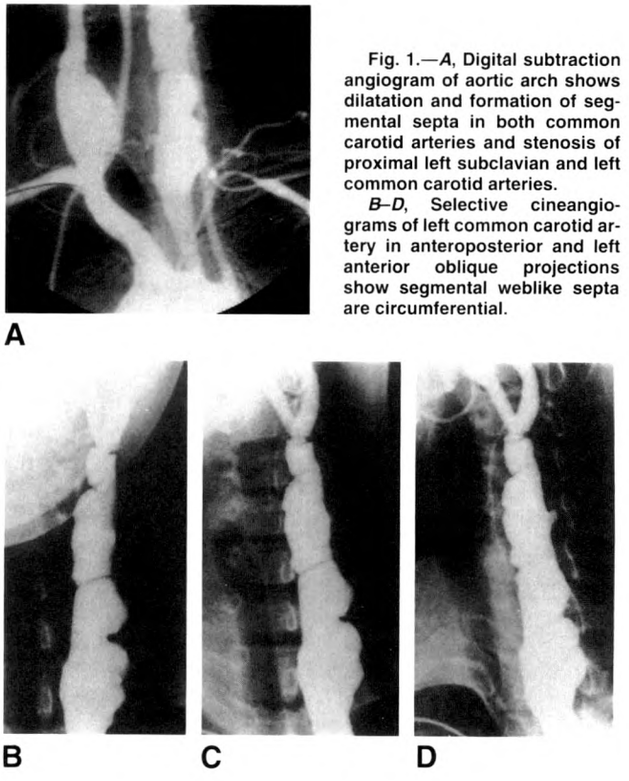

Fig. 1.—*A*, Digital subtraction angiogram of aortic arch shows dilatation and formation of segmental septa in both common carotid arteries and stenosis of proximal left subclavian and left common carotid arteries.
***B–D*, Selective cineangiograms of left common carotid artery in anteroposterior and left anterior oblique projections show segmental weblike septa are circumferential.**

the adventitia. Therefore, it is speculated that only those arterial segments with prominent inflammation show dilatation. Local hemodynamic effects or congenital arterial abnormalities may allow development of aneurysms. The degree of destruction of the arterial wall depends on the sites and stages of the inflammation.

Naofumi Matsunaga
Kuniaki Hayashi
Minoru Morikawa
and colleagues

Nagasaki University School of Medicine
Nagasaki 852, Japan

REFERENCES

1. Nasu T, Mamiya N. Pathogenesis of trunco-arteritis productiva obliterans: so-called pulseless disease or aortic arch syndrome. *Jpn Circ J* **1966**;30:68–71
2. Ueda H, Ohno K, Ito I, Takeda T, Saito Y, Ueno A. Two cases of aortitis syndrome with aneurysmal formation. *Jpn Heart J* **1968**;9:88–96

Letters are published at the discretion of the Editor and are subject to editing.

Letters to the Editor must not be more that two *double-spaced*, typewritten pages. One or two figures may be included. Abbreviations should not be used. Limit the number of authors to four, or we will list only the first three and add "and colleagues" to the end of the list. See Author Guidelines.

Material being submitted or published elsewhere should not be duplicated in letters, and authors of letters must disclose financial associations or other possible conflicts of interest.

Letters concerning a paper published in the *AJR* will be sent to the authors of the paper for a reply to be published in the same issue. Opinions expressed in the Letters to the Editor section do not necessarily reflect the opinions of the Editor.

American Roentgen Ray Society: Officers, Committees, and Membership Information

Officers

President: A. Everette James, Jr.

President-elect: Andrew K. Poznanski

1st Vice-president: George R. Leopold

2nd Vice-president: Ralph J. Alfidi

Secretary: Joseph T. Ferrucci, Jr.

Treasurer: Beverly P. Wood

Executive Council: R. J. Alfidi, R. N. Berk, M. P. Capp, W. J. Casarella, D. O. Davis, N. R. Dunnick, J. T. Ferrucci, Jr., A. E. James, Jr., J. A. Kirkpatrick, Jr., A. M. Landry, Jr., G. R. Leopold, J. E. Madewell, T. C. McLoud, A. A. Moss, A. K. Poznanski, R. J. Stanley, J. H. Thrall, N. O. Whitley, B. P. Wood, K. H. Vydareny, chair

Committees

Editorial Policy: R. N. Berk, E. Buonocore, M. M. Figley, P. C. Freeny, N. Thorne Griscom, R. G. Levitt, C. R. B. Merritt, K. Valji, W. J. Casarella, chair

Education and Research: G. M. Glazer, R. R. Hattery, C. B. Higgins, R. J. Stanley, W. M. Thompson, N. O. Whitley, chair

Finance and Budget: D. J. Anderson, R. K. Gedgaudas-McClees, J. E. Madewell, A. A. Moss, J. H. Thrall, chair

Nominating: M. P. Capp, C. A. Rohrmann, Jr., J. E. Madewell, chair

Publication: E. Buonocore, P. C. Freeny, N. Thorne Griscom, R. G. Levitt, C. R. B. Merritt, W. J. Casarella, chair

Membership: D. O. Davis, J. E. Madewell, T. C. McLoud, A. A. Moss, chair

Representatives to Other Organizations

American Board of Radiology: W. J. Casarella, J. A. Kirkpatrick, Jr., L. F. Rogers

American College of Radiology: R. A. Gagliardi, J. E. Madewell, B. L. McClennan, N. H. Messinger, R. J. Stanley

American Medical Association: R. A. Gagliardi, delegate; R. G. Evens, alternate; T. G. Goergen, CPT Advisory Committee

American National Standards Institute: M. E. Haskin

National Council on Radiation Protection and Measurements: F. D. Miraldi, E. L. Saenger

Armed Forces Institute of Pathology: J. E. Madewell

Meeting Arrangements

Annual Meetings: April 25–30, 1993, Marriott San Francisco, San Francisco, CA; April 24–29, 1994, New Orleans Hilton, New Orleans, LA

Annual Meeting Committee: J. K. Crowe, N. R. Dunnick, R. R. Lukin, N. H. Messinger, R. J. Stanley, R. D. Steele, Jr., A. M. Landry, Jr., chair

Instructional Courses: B. L. McClennan, associate chair, R. J. Stanley, chair

Scientific Program: P. H. Arger, W. R. Brody, G. D. Fullerton, R. M. Gore, D. C. Kushner, D. L. Resnick, W. M. Thompson, J. H. Thrall, C. J. Zylak, A. K. Poznanski, chair

Scientific Exhibits: F. S. Chew, J. M. Destouet, J. R. Haaga, D. S. Hartman, L. A. Mack, R. G. Ramsey, A. E. Schlesinger, T. J. Welch, N. R. Dunnick, chair

ARRS Membership

Application forms may be obtained from the ARRS offices in Reston, VA. Qualified applicants will be admitted quarterly. Send completed forms to American Roentgen Ray Society, 1891 Preston White Dr., Reston, VA 22091. Active members are graduates of an approved medical or osteopathic school or hold an advanced degree in an allied science. They must practice radiology or work in an associated science in the United States or Canada and be certified by the American Board of Radiology, American Osteopathic Board of Radiology, or Royal College of Physicians of Canada or otherwise adequately document training and credentials. International members are foreign radiologists or scientists who are active in radiology or an allied science. Members-in-training are residents or fellows in radiology or postgraduate students in an allied science.

Business Office

Paul R. Fullagar, Executive Director, American Roentgen Ray Society, 1891 Preston White Dr., Reston, VA 22091; (703) 648-8992; 1-800-438-2777.

Review of Current Literature

Initials and addresses of corresponding authors are provided in parentheses for each article so that the reader can obtain reprints directly. Abstracts are printed verbatim from each journal.

The New England Journal of Medicine

Identification of the uncultured bacillus of Whipple's disease. Relman DA, Schmidt TM, MacDermott RP, Falkow S (DAR, Palo Alto Dept. of Veterans Affairs Medical Center, 154T, 3801 Miranda Ave., Palo Alto, CA 94304). *N Engl J Med* 327(5):293–301, July 30, 1992

Background. Whipple's disease is a systemic disorder known for 85 years to be associated with an uncultured, and therefore unidentified, bacillus.

Methods. We used a molecular genetic approach to identify this organism. The bacterial 16S ribosomal RNA (rRNA) sequence was amplified directly from tissues of five unrelated patients with Whipple's disease by means of the polymerase chain reaction, first with broad-range primers and then with specific primers. We determined and analyzed the nucleotide sequence of the amplification products.

Results. A unique 1321-base bacterial 16S rRNA sequence was amplified from duodenal tissue of one patient. This sequence indicated the presence of a previously uncharacterized organism. We then detected this sequence in tissues from all 5 patients with Whipple's disease, but in none of those from 10 patients without the disorder. According to phylogenetic analysis, this bacterium is a gram-positive actinomycete that is not closely related to any known genus.

Conclusions. We have identified the uncultured bacillus associated with Whipple's disease. The phylogenetic relations of this bacterium, its distinct morphologic characteristics, and the unusual features of the disease are sufficient grounds for naming this bacillus *Tropheryma whippelii* gen. nov. sp. nov. Our findings also provide a basis for a specific diagnostic test for this organism.

Reactivation of unstable angina after the discontinuation of heparin. Théroux P, Waters D, Lam J, Juneau M, McCans J (PT, Montreal Heart Institute, 5000 Belanger St., Montreal, Quebec, H1T 1C8, Canada). *N Engl J Med* 327(3):141–145, July 16, 1992

Background. Heparin is an effective, widely used treatment for unstable angina. Among patients enrolled in a double-blind, randomized, placebo-controlled trial comparing intravenous heparin, aspirin, both treatments, and neither during the acute phase of unstable angina, we encountered patients in whom unstable angina was reactivated after heparin was discontinued.

Methods. The study population included 403 of the original 479 patients in the trial who had completed six days of blinded therapy without refractory angina of myocardial infarction. After the discontinuation of therapy, clinical events, including reactivation of unstable angina and myocardial infarction occurring within 96 hours after hospitalization, were closely monitored.

Results. Early reactivation occurred in 14 of the 107 patients who received heparin alone, as compared with only 5 patients in each of the other three study groups ($P<0.01$). These reactivations required urgent intervention (thrombolysis, angioplasty, or coronary-bypass surgery) in 11 patients treated with heparin alone, but in only 2 patients in the other groups combined ($P<0.01$). Four of the six patients who had a myocardial infarction during a reactivation of their disease were in the heparin group. Reactivations in this group occurred in a cluster a mean (±SD) of 9.5±5 hours after the discontinuation of the study drug but were randomly distributed over the initial 96 hours in the other three groups.

Conclusions. Although heparin is beneficial in treating unstable angina, the disease process may be activated within hours of the discontinuation of this drug. Concomitant therapy with aspirin may prevent this withdrawal phenomenon.

Gastric-outlet obstruction induced by prostaglandin therapy in neonates. Peled N, Dagan O, Babyn P, et al. (G. Koren, Division of Clinical Pharmacology, Hospital for Sick Children, 555 University Ave., Toronto, Ontario, M5G 1X8 Canada). *N Engl J Med* 327(8):505–510, Aug. 20, 1992

Background. An infusion of prostaglandin E_1 is widely used to maintain patency of the ductus arteriosus in neonates with congenital heart disease. After gastric-outlet obstruction was recognized in several infants who received prostaglandin E_1, we studied the association between the drug and this complication.

Methods. We evaluated all neonates who received prostaglandin E_1 in our hospital between October 1, 1989, and September 30, 1991, for clinical, radiologic, or pathological evidence of acute gastric-outlet obstruction.

Results. Of the 74 neonates evaluated, 65 had no signs of gastric obstruction and were considered normal; 5 had clinical and radiologic or pathological evidence of gastric obstruction consistent with the presence of antral mucosal hyperplasia. The remaining four neonates had clinical signs of gastric obstruction, but no radiologic or pathological examinations were performed.

The 5 neonates with antral hyperplasia had received prostaglandin E_1 for longer periods (mean [±SD] duration, 569±341 hours) than the 65 normal neonates (54±58 hours, $P<0.01$) or the 4 neonates with clinical signs of gastric obstruction (119±60 hours, $P<0.05$). The cumulative dose of prostaglandin E_1 was higher in the neonates with antral hyperplasia (2982±1392 μg per kilogram of body weight) than in the normal neonates (279±270 μg per kilogram, $P<0.001$) or the neonates with signs of gastric obstruction (528±306 μg per kilogram, $P<0.01$). In two neonates with antral hyperplasia, the cessation of therapy lessened the gastric-outlet obstruction.

Conclusions. The administration of prostaglandin E_1 to neonates can cause gastric-outlet obstruction due to antral hyperplasia. Neonates who receive prostaglandin E_1 at recommended doses for more than 120 hours should be closely monitored for evidence of antral hyperplasia.

Nitric oxide synthase activity in infantile hypertrophic pyloric stenosis. Vanderwinden J-M, Mailleux P, Schiffmann SN, Vanderhaeghen J-J, De Laet M-H (JMV, Laboratory of Neuropathology and Neuropeptide Research, Université Libre de Bruxelles, Campus Erasme, CP 601, 808 route de Lennik, 1070 Brussels, Belgium). *N Engl J Med* 327(8):511–515, Aug. 20, 1992

Background. Hypertrophic pyloric stenosis is a common infantile disorder characterized by enlarged pyloric musculature and gastric-outlet obstruction. Its physiopathologic mechanism is not known, but a defect in pyloric relaxation (pylorospasm) has been postulated. Nitric oxide is a mediator of relaxation in the mammalian digestive tract, raising the possibility that pylorospasm could be caused by a defect in nitric oxide production. Since neuronal nitric oxide synthase and NADPH diaphorase are identical, we used the NADPH diaphorase histochemical reaction to study the distribution of nitric oxide synthase in pyloric tissue from patients with infantile hypertrophic pyloric stenosis.

Methods. We studied pyloric tissue from nine infants with infantile hypertrophic pyloric stenosis and seven control infants and children. Cryostat sections were processed for NADPH diaphorase histochemical analysis. A polyclonal tau antiserum was used to identify the enteric nervous system by immunohistochemical methods.

Results. NADPH diaphorase activity was restricted to the enteric nervous system and blood vessels. In the pyloric tissues from the control patients, intense diaphorase activity was present in the nerve fibers of the circular musculature, in the neurons and nerve bundles of the myenteric plexus, and in some nerve fibers of the longitudinal musculature. In the pyloric tissues from patients with infantile hypertrophic pyloric stenosis, the enteric nerve fibers in the hypertrophied circular musculature were enlarged and distorted and did not contain diaphorase activity, whereas the activity in the myenteric plexus and the longitudinal musculature was preserved.

Conclusions. We suggest that a lack of nitric oxide synthase in pyloric tissue is responsible for pylorospasm in infantile hypertrophic pyloric stenosis.

Chest

Measurement of lung density by means of quantitative CT scanning: a study of correlations with pulmonary function tests. Heremans A, Verschakelen JA, Van fraeyenhoven L, Demedts M (JAV, Dept. of Radiology, University Hospital Leuven, Leuven, Belgium B-3000). *Chest* 102(3):805–811, Sept. 1992

In recent years, much attention has been given to the role of CT in detecting and quantitating pulmonary emphysema. We measured CT lung density in 45 patients undergoing a diagnostic work-up and compared this with pulmonary function tests. The CT lung densities measured with the sector method and with the whole lung method were very highly correlated with each other ($r=0.96$, $p<0.001$), and measurements at TLC systematically gave a lower density than those at FRC ($p<0.0001$). Also, CT density measurements at TLC and even more so at FRC correlated well with pulmonary function indices of airway obstruction and of hyperinflation, but not with indices that are considered more specific for emphysema (single breath DCO, static lung compliance). We conclude that CT lung density gives a good reflection of the degree of hyperinflation, *ie*, enlargement of distal airways, but is not sensitive to detect whether or not this is associated with emphysema.

Circulation

Thrombus regression in deep venous thrombosis: quantification of spontaneous thrombolysis with duplex scanning. van Ramshorst B, van Bemmelen PS, Hoeneveld H, Faber JAJ, Eikelboom BC (BVR, Dept. of Surgery, St. Antonius Hospital, P. O. Box 2500, 3430 EM Nieuwegein, Holland). *Circulation* 86:414–419, 1992

Background. Thrombus regression in heparin-treated, acute deep venous thrombosis of the lower extremity is poorly documented in the literature; different rates of thrombus resolution and recanalization are reported.

Methods and Results. In a prospective follow-up study, duplex scanning was used to evaluate the thrombus regression in patients with documented acute femoropopliteal thrombosis. Eighty vein segments in 20 legs of 18 patients were subjected to repeat duplex scans at 1, 3, 6, 12, and 26 weeks after diagnosis; 49 segments showed thrombus at diagnosis. The popliteal vein showed the highest thrombus load at diagnosis, followed in descending order by the superficial femoral, profunda femoris, and common femoral vein segments ($p<0.001$). Thrombus regression was significant ($p<0.001$) in all segments and proceeded at an exponential rate that was equal in the different vein segments of the upper leg. Both thrombus resolution and recanalization appeared to be a function of the initial thrombus load and could not be related to individual vein segments. Recanalization was seen in 23 of 31 initially occluded segments and occurred within the first 6 weeks after diagnosis in 20 of 23 segments. Extension of thrombus despite anticoagulant therapy was observed in 15 vein segments and was not related to the initial thrombosis score ($p=0.1$) or individual vein segments ($p=0.23$). Thrombus extension in seven patients with prethrombotic conditions was not different ($p=0.9$) from the other patients.

Conclusions. Duplex scanning is an important noninvasive tool to quantify thrombus regression in acute deep venous thrombosis in detail without unnecessary discomfort to the patient.

Gastroenterology

Oropharyngeal swallowing in normal adults of different ages. Robbins J, Hamilton JW, Lof GL, Kempster GB (JR, Dept. of Neurology, University of Wisconsin, Madison, WI). *Gastroenterology* 103:823–829, 1992

In an effort to evaluate the effect of normal aging on oropharyngeal events of swallowing, 80 normal volunteers, stratified by gender into four age groups, were studied. Liquid and semisolid swallows were performed and recorded simultaneously using videofluoroscopy and manometry. Several parameters, including total duration of oropharyngeal swallowing, were significantly longer in the oldest age group than in any other age group. A delay in initiation of maximal hyolaryngeal excursion primarily accounted for the longer durations with increased age. Significant durational changes also were found as a function of bolus consistency and presence or absence of the manometry tube. Females had a longer duration of upper esophageal sphincter (UES) opening. The amplitude of pharyngeal pressures, duration of peak pharyngeal pressures, and rate of propagation of the contractions were not significantly different for age, gender, or consistency of bolus. No significant differences were found between age groups or between genders in UES pressure. Normal aging affects some parameters of swallowing, while others are preserved.

A wave of inhibition precedes primary peristaltic contractions in the human esophagus. Sifrim D, Janssens J, Vantrappen G (DS, Centre for Gastrointestinal Research, Dept. of Medical Research, University of Louvain, Louvain, Belgium). *Gastroenterology* 103:876–882, 1992

Animal studies have shown that primary esophageal peristalsis is preceded by a wave of inhibition spreading rapidly down the esophagus and lasting longer in more distal segments. In humans, its presence in the esophageal body cannot be demonstrated manometrically because of the absence of tone. To study deglutitive inhibition in humans, an artificial high-pressure zone was created by inflating an intraesophageal balloon to a critical level. The pressure changes at the interface between the balloon and the esophageal wall at various levels along the esophagus were measured. In this artificial high-pressure zone, deglutition induced a relaxation beginning simultaneously at various levels of the esophagus but lasting progressively longer in progressively more distal segments. Latency from onset of deglutition to onset of relaxation at 13 cm and 8 cm above the lower esophageal sphincter and at the lower esophageal sphincter was 0.06 ± 0.19 seconds, 0.10 ± 0.31 seconds, and $0.89 \pm$

0.53 seconds, respectively; latency to contraction was 4.45 ± 0.54 seconds, 6.04 ± 0.79 seconds, and 9.14 ± 1.04 seconds, respectively. This is the first direct evidence that deglutition produces in the human esophagus a wave of inhibition that precedes the primary peristaltic contraction.

Clinical Orthopaedics and Related Research

Staging and treatment of primary and persistent (recurrent) osteoid osteoma: evaluation of intraoperative nuclear scanning, tetracycline fluorescence, and tomography. Lee DH, Malawer MM (DHL, Division of Orthopedic Surgery, University of Alabama at Birmingham, 1813 Sixth Ave., S., 507 MEB, Birmingham, AL 35233). *Clin Orthop* 281:229–238, Aug. 1992

The purposes of this study were (1) to evaluate the various methods of preoperative staging of osteoid osteomas, (2) to compare the different methods of intraoperative localization and excision of the tumor, and (3) to develop a clinical strategy for the treatment of persistent (recurrent) lesions. From 1978 until 1986, 14 consecutive patients had excision of osteoid osteomas. All patients' operative reports, roentgenograms, bone scans, computed tomographic scans and histologic studies were reviewed. With an average follow-up period of 94.5 months, 13 of 14 patients were cured with one operative procedure. One patient required two procedures. No patient developed a recurrence. Eleven of 14 niduses were confirmed on hematoxylin and eosin sections. Computed tomographic scan was the most useful preoperative study in localizing the nidus. It helped determine the surgical approach and the portion of bone to be resected. Intraoperative nuclear scanning (IONS) is a reliable technique in confirming complete removal of the nidus, with no increase in operative time. Intraoperative scanning did not appreciably affect the amount of bone resected. Recurrent tumors can be reliably resected, with a high cure rate, by careful preoperative staging and with use of IONS.

The Journal of Pediatrics

Renovascular disease in childhood. Deal JE, Snell MF, Barratt TM, Dillon MJ (JED, Dept. of Paediatric Nephrology, Guy's Hospital, St. Thomas' St., London SE1 9RT, United Kingdom). *J Pediatr* 121:378–384, 1992

Fifty-four children referred for investigation of hypertension has renovascular disease. In eight patients it was associated with neurofibromatosis, in three with idiopathic hypercalcemia of infancy, and in five cases it followed an arteritic illness. Fibromuscular dysplasia was the underlying abnormality in the majority of cases (46%). Twenty-six patients (48%) were first seen with accelerated hypertension; 38 children (70%) had bilateral renal arterial disease, and in 41 (76%), disease of the small intrarenal vessels was found. Renal vein renin ratios indicated unilateral disease in 31 cases; the results correlated with arteriography findings in 32 (62%) of 51 patients. Eleven children also had the middle aortic syndrome, and 9 of 16 patients, investigated by cerebral arteriography because of cranial bruits or focal neurologic signs, had cerebral vascular abnormalities. Twenty patients were treated surgically—10 by reconstructive procedures, 11 by nephrectomy or heminephrectomy, and 6 by transluminal angioplasty. Of these, 9 (45%) are normotensive with no treatment, 10 have a decreased requirement for antihypertensive drugs, and 1 had no improvement. Thirty-four patients were treated medically because of the extent of their disease; two patients have died of hypertensive complications. We conclude that renal vascular disease in children is often widespread, may be associated with intracerebral vascular disease, frequently affects both kidneys, including both intrarenal and extrarenal vessels, and is therefore not always amenable to surgical intervention and cure.

Tibia vara: a complication of adolescent obesity. Henderson RC (RCH, Dept. of Pediatrics, University of North Carolina, 237 Burnett-Womack Bldg. 229H, Campus Box 7055, Chapel Hill, NC 27599). *J Pediatr* 121:482–486, 1992

Tibia vara is characterized by inhibited growth of the medial portion of the proximal tibial growth plate, leading to progressive bow-leg deformity. Twenty-nine adolescent patients with this condition were reviewed: all were black, 27 (93%) were male, and 19 (66%) had only one side affected. Progressive deformity rather than knee discomfort was the most common presenting complaint. The deformity reportedly developed rapidly during the adolescent growth spurt. The body weights of these patients exceeded the 95th percentile for age and gender by an average of 43 kg. The absence of significant symptoms and a body habitus that obscured the deformity often resulted in delayed diagnosis. Physicians involved in the care of obese black male adolescents should carefully examine them for tibia vara, which has a reported prevalence of 2% to 3% in this population. Treatment options are severely restricted if the condition is not diagnosed early.

Surgery, Gynecology and Obstetrics

Surgical treatment for cholelithiasis. Herzog U, Messmer P, Sutter M, Tondelli P (UH, Dept. of Surgery, St. Claraspital, CH-4016, Basel, Switzerland). *Surg Gynecol Obstet* 175:238–292, 1992

In a retrospective study, the results of 1,631 consecutive operations for cholelithiasis were analyzed. With an overall mortality rate of 0.18 percent and a reoperation rate of 1.3 percent, conventional cholecystectomy proved to be a safe method. Mortality proved to be age dependent, with a zero mortality rate for patients less than 60 years of age. Choledochotomy has a 13-fold greater mortality rate than simple cholecystectomy (0.92 versus 0.07 percent). For acute cholecystitis, we observed an unusual zero mortality rate, whereas the mortality rate in chronic cholecystitis was 0.2 percent. All three patients who died had an accompanying cirrhosis of the liver. Morbidity, defined as reoperation during the same period of hospitalization, was mainly the result of retained stones after choledochotomy; endoscopic papillotomy was the treatment of choice. Cholecystectomy remains the "gold standard" in the treatment of cholelithiasis.

Journal of Ultrasound in Medicine

Longitudinal evaluation of uterine myoma growth during pregnancy: a sonographic study. Rosati P, Exacoustòs C, Mancuso S (PR, Dept. of Obstetrics and Gynecology, Università Cattolica del Sacro Cuore, L. Go A Gemelli 8, Rome 00168, Italy). *J Ultrasound Med* 11:511–515, Oct. 1992

Thirty-six pregnant women with a single uterine myoma were examined by ultrasonography at 2 to 4 week intervals. The initial diagnosis was made in 12 patients before pregnancy and in the other 24 patients between 9 and 12 weeks of gestation. Thirty-four women had a scan 4 weeks after delivery. A reduction in size was observed in puerperium, which may indicate a return to its initial volume. Myoma growth was analyzed in different periods of gestation. An increase in volume during pregnancy was observed in 31.6% of cases. A statistically significant change in volume was noted between the first and the third trimesters ($P < 0.001$). The greatest increase in volume of myomas occurred before the 10th week of gestation. The relationship between myoma volume and myoma growth in the different gestational periods considered was not statistically significant. On the other hand, when myoma volume was related to complications during pregnancy or at delivery, a statistically significant difference was observed. Myomas with volumes greater than 200 cm^3 show a higher rate of complications than those with volumes equal to or less than 100 cm^3.

Journal of Computer Assisted Tomography

Abdominal CT scans in patients with blunt trauma: low yield in the absence of clinical findings. Fried AM, Humphries R, Schofield CN (AMF, Dept. of Diagnostic Radiology, Albert B. Chandler Medical Center, 800 Rose St., HX317, Lexington, KY 40536-0084). *J Comput Assist Tomogr* 16(5):717–721, Sept./Oct. 1992

This study undertook to determine the yield of abdominal CT scans ordered only because the patient's sensorium was decreased or general anesthesia was planned. The abdominal CT scans and hospital charts of 191 consecutive patients examined following blunt trauma were reviewed with respect to clinical indications prompting the study. In 143, some clinical or laboratory justification was in evidence. In this group, 55 patients (38.5%) were found to have trauma-related pathology at CT scan. In 48 patients, no clinical or laboratory suggestion of abdominal pathology was evident. Instead, the primary indications for ordering the CT scan were decreased sensorium (28 cases), the planning of general anesthesia for orthopedic procedures (8 cases), and a variety of non-abdominal-trauma-related reasons. In this group, only a single positive finding was identified (small pneumothorax), and in no case was the clinical course altered by findings at abdominal CT scan. Performance of abdominal CT scans without clinical or laboratory evidence of trauma, merely because of decreased patient sensorium or prophylactically prior to general anesthesia for non-abdomen-related surgery, is an extremely low yield study and should be discouraged. In the current study, no significant abdominal pathology would have been overlooked by omission of such scans. Similar findings have been reported in children. To our knowledge, this is the first such report in a largely adult population.

News

AFIP Neuropathology Review Course

The Armed Forces Institute of Pathology (AFIP) and the American Registry of Pathology are cosponsoring the 14th annual AFIP Neuropathology Review Course, Jan. 17–22, at the Hyatt Regency, New Orleans. Basic neuropathology and recent developments in the pathophysiology of neurologic disorders will be discussed. Fee: Dept. of Defense employees, full-time employees of the Dept. of Veterans Affairs, and commissioned officers of the Public Health Service, $225; all others, $530. Information: Education Division, Armed Forces Institute of Pathology, Washington, DC 20306-6000; telephone: (301) 427-5231; fax: (301) 427-5001.

Conference on Breast Cancer in Younger Women

The Clinical Investigations Branch, Cancer Therapy Evaluation Program, National Cancer Institute, is sponsoring a conference on Breast Cancer in Younger Women, Jan. 28–29, at the National Institutes of Health, Bethesda. The purpose of the conference is to foster an understanding of breast cancer in younger women. Persons from a variety of disciplines will gather to determine strategies for future research. Deadline for registration: Jan. 15. Fee: $50. Information: Carmen L. Warren or Peggy Sweitzer, TASCON, Inc., 7101 Wisconsin Ave., Ste. 1125, Bethesda, MD 20814; telephone: (301) 907-3844; fax: (301) 907-9655.

AFIP Neuroradiology Review Course

The Armed Forces Institute of Pathology (AFIP), the American Registry of Pathology, and the American College of Radiology are sponsoring the 8th annual AFIP Neuroradiology Review Course, Feb. 27–28, at the Hyatt Regency Bethesda, Bethesda, MD. The course will review basic concepts in neuroradiology, with an emphasis on pathologic correlation and pathophysiology. Course directors: James G. Smirniotopoulos and Frances M. Murphy. Category 1 credit: approximately 12 hr. Information: Education Division, Armed Forces Institute of Pathology, Washington, DC 20306-6000; telephone:(301) 427-5231; fax: (301) 427-5001.

First Pittsburgh Symposium in Diagnostic Imaging

The Western Pennsylvania Hospital is sponsoring the First Pittsburgh Symposium in Diagnostic Imaging, March 11–13, at the Westin William Penn Hotel, Pittsburgh. The symposium will address the latest developments in abdominal CT, musculoskeletal MR imaging, gastrointestinal radiology, chest radiology, and neuroradiology. Program directors: Kathleen M. Harris, Ellen B. Mendelson, Ingrid E. Naugle, and William R. Poller. Faculty: C. A. Helms, E. Kanal, E. K. Kazam, R. E. Latchaw, I. Laufer, and S. S. Sagel. Category 1 credit: 22.5 hr. Fee (through Feb. 13/after Feb. 13): physicians, $495/$525 for entire course, $175/$200 for one day; fellows, residents (letter required), and technologists, $300/$350 for entire course, $125/$150 for one day. Information: MaryAnn Cooper, Dept. of Continuing Medical Education, West Penn Hospital, 4800 Friendship Ave., Pittsburgh, PA 15224; telephone: (412) 578-5337; fax: (412) 578-5479.

Focus on Hemodialysis Access

The Dept. of Radiology, University of California, San Diego, School of Medicine, is sponsoring Focus on Hemodialysis Access: Creation, Maintenance, and Salvage, March 13, at the Le Meridien Hotel, Coronado, CA. The course, which is designed for nephrologists, vascular surgeons, and interventional radiologists, will explore dialysis from a vertical interdisciplinary approach. Topics will include thrombolysis, angioplasty, atherectomy, and stenting of dialysis (and other) conduits. Category 1 credit: 6.5 hr. Fee: $75. Information: Conference Management Associates, P. O. Box 2586, La Jolla, CA 92038; (619) 454-3212.

Society of Thoracic Radiology Annual Meeting

The Society of Thoracic Radiology will hold its annual meeting March 14–19 at the Westin Resort Hotel, Hilton Head Island, SC. Program director: Robert Pugatch. Category 1 credit: 27 hr (pending). Fee: $595. Information: Dawne Ryals and Associates, P. O. Box 1925, Roswell, GA 30077-1925; telephone: (404) 641-9773; fax: (404) 552-9859.

Challenges in Sonographic Imaging: 1993

The Dept. of Radiology, University of California, San Diego, School of Medicine, is sponsoring Challenges in Sonographic Imaging: 1993, March 25–28, at the Westin Resort Hotel, Hilton Head Island, SC. Program directors: George R. Leopold and Sandra Hagen-Ansert. Category 1 credit: 21 hr. Fee: physicians, $475; residents, fellows, and technologists, $350. Information: Dawne Ryals and Associates, P. O. Box 1925, Roswell, GA 30077-1925; telephone: (404) 641-9773; fax: (404) 552-9859.

Society of Breast Imaging Annual Meeting

The Society of Breast Imaging will hold its 1st annual meeting April 14–18 at the Ritz-Carlton Resort Hotel, Amelia Island, FL. Program directors: Lawrence Bassett and Valerie P. Jackson. Category

1 credit: 25 hr. Fee: society members and fellows, $575; nonmember physicians, $650; residents and fellows in training, $350. Information: Dawne Ryals and Associates, P. O. Box 1925, Roswell, GA 30077-1925; telephone: (404) 641-9773; fax: (404) 552-9859.

Residents' Radiology Review Course

The Dept. of Radiology, University of California, San Diego, School of Medicine, is sponsoring the 13th annual Residents' Radiology Review Course, April 18–23, at the Hotel Del Coronado, San Diego, CA. The course will review all pertinent and essential facts in all major fields of diagnostic radiology. Program directors: Anne Roberts and Giovanna Casola. Category 1 credit: 41 hr. Fee: physicians, $600; residents, $450. Information: Dawne Ryals and Associates, P. O. Box 1925, Roswell, GA 30077-1925; telephone: (404) 641-9773; fax: (404) 552-9859.

Principles and Practice of Clinical MRI

The Dept. of Radiology, Division of Magnetic Resonance Imaging, The Johns Hopkins University School of Medicine, is sponsoring Principles and Practice of Clinical MRI, April 22–25, at the Stouffer Harborplace Hotel, Baltimore. Information: Program Coordinator, The Johns Hopkins Medical Institutions, Office of Continuing Education, Turner Bldg., 720 Rutland Ave., Baltimore, MD 21205; (410) 955-2959.

University of Florida Radiology Review Course

The University of Florida is sponsoring the 5th annual Radiology Review Course, May 1–6, at the Hyatt Orlando, Orlando, FL. The course is designed for senior residents and practicing radiologists who desire a comprehensive review of diagnostic radiology. Program director: Pablo R. Ros. Category 1 credit: 36.5 hr. Fee: physicians, $475; residents, fellows, and military personnel, $375. Information: Dawne Ryals and Associates, P. O. Box 1925, Roswell, GA 30077-1925; telephone: (404) 641-9773; fax: (404) 552-9859.

Cleveland Radiological Society Officers

The officers of the Cleveland Radiological Society for the year 1992–1993 are Craig Irish, president; Gary Lammert, president-elect; Bradford Richmond, secretary-treasurer; Alan Cohen, Charles Lanzieri, and Ronald Lorig, program directors; and David Einstein, James Lieberman, and Wendy Shaw, members-at-large.

The American Board of Radiology Examinations

Written examinations for the American Board of Radiology (ABR) are scheduled for Sept. 23–24. Oral examinations will be held at the Executive West Hotel in Louisville, KY, June 7–10. The ABR will accept applications for admission to the examinations after July 1, but not later than Sept. 30, in the year *preceding* the year in which the examination is to be taken. For application forms and further information: Office of the Executive Director, The American Board of Radiology, 2301 W. Big Beaver Rd., Ste. 625, Troy, MI 48084.

Meeting and Course Review

For the reader's convenience, a summary of upcoming meetings and courses is provided. Detailed listings are given in the *AJR* issue given in parentheses.

Visiting Fellowships in Interventional Radiology, times arranged, Baltimore (Sept 1992)
Preceptorships in Ultrasound, times arranged, Baltimore (Sept 1992)
Postgraduate Imaging Seminar, Dec. 28, 1992–Jan. 1, 1993, Maui, HI (Sept 1992)
Holiday Imaging Update, Dec. 28, 1992–Jan. 1, 1993, Aspen, CO (Sept 1992)
The Complete MRI Course, Jan. 4–8, Maui, HI (Sept 1992)
Musculoskeletal MR Course, Jan 4–8, Naples, FL (Oct 1992)
Society of Uroradiology Annual Meeting, Jan. 9–15, Naples, FL (Oct 1992)
Advanced Seminars in Diagnostic Imaging, Jan. 13–15, Feb. 24–27, and April 15–17, Laguna Niguel, CA (Nov 1992)
Robert D. Moseley, Jr. Award, deadline for submissions, Jan. 15 (Oct 1992)
Midwinter Radiological Conference, Jan. 15–17, Los Angeles (Dec 1992)
Interventional Radiology Update, Jan. 16–17, Laguna Niguel, CA (Oct 1992)
Society of Gastrointestinal Radiologists Annual Meeting, Jan. 17–22, Scottsdale, AZ (Sept 1992)
Neuroradiology Update, Jan. 18–20, Laguna Niguel, CA (Oct 1992)
Breast Imaging Update, Jan. 21–24, Laguna Niguel, CA (Oct 1992)
Seminars in MRI, Jan. 23–30, Vail, CO (Nov 1992)
Breast Imaging Course, Jan. 25–28, Naples, FL (Oct 1992)
International Symposium on MR Imaging, Jan. 27–31, Garmisch-Partenkirchen (Bavaria), Germany (Oct 1992)
Big Sky Radiology Conference, Jan. 31–Feb. 4, Big Sky, MT (Nov 1992)
Computed Body Tomography 1993—The Cutting Edge, Feb. 4–7, Orlando, FL (Oct 1992)
U. B. C. Practical Radiology at Whistler, Feb. 6–12, Whistler/Blackcomb Mountain, B.C. (Oct 1992)
Current Topics in Diagnostic Imaging, Feb. 8–12, Cerromar Beach, Puerto Rico (Nov 1992)
Duke Radiology Winter Postgraduate Course, Feb. 8–12, Aspen, CO (Dec 1992)
Diagnostic Imaging Update, Feb. 15–19, Palm Beach, FL (Oct 1992)
Sun Valley Imaging Meeting, Feb. 20–27, Sun Valley, ID (Oct 1992)
Intermountain Imaging Conference, Feb. 20–27, Snowmass, CO (Nov 1992)
MRI Update 1993, Feb. 22–26, La Quinta, CA (Oct 1992)
Diagnostic Imaging Update, Feb. 22–26, Maui, HI (Oct 1992)
Magnetic Resonance Imaging, Feb. 22–26, Naples, FL (Oct 1992)
Positron Emission Tomography, Feb. 28–March 2, Dana Point, CA (Oct 1992)
Society of Computed Body Tomography and Magnetic Resonance Annual Course, March 1–5, Lake Buena Vista, FL (Nov 1992)
Musculoskeletal Imaging for Orthopedic Surgeons and General Radiologists, March 1–5, St. Thomas, U.S. Virgin Islands (Nov 1992)
International Course on Epidemiology of Nutrition and Cancer, March 1–12, Lyon, France (Dec 1992)
San Diego Postgraduate Magnetic Resonance Imaging Course, March 8–12, San Diego (Nov 1992)
PET and SPECT Imaging of Living Brain Chemistry, March 10–12, Baltimore (Nov 1992)
Interactive Surgery and Imaging of Paranasal Sinuses, Skull Base, Brain, and Spine, March 14–17, Snowmass Village, CO (Dec 1992)

MRI Workshop in Hawaii, March 21–16, Maui, HI (Nov 1992)
Orthopedic Radiology, March 22–24, Boston (Dec 1992)
International Diagnostic Course in Davos, March 27–April 2, Davos, Switzerland (Oct 1992)
Ultrasound 1993, March 28–31, Boston (Dec 1992)
General Radiology Review Course, March 28–April 2, Marina Del Rey, CA (Dec 1992)
National Council on Radiation Protection and Measurements Annual Meeting, April 7–8, Arlington, VA (Dec 1992)
Clinical Nuclear Medicine 1993, April 13–16, Boston (Dec 1992)
CIRSE and SCVIR Annual Meeting, June 20–25, Budapest, Hungary (Oct 1992)
World Association of Sarcoidosis and Other Granulomatous Disorders Meeting, Sept. 8–11, Los Angeles (Nov 1992)
International Society of Lymphology Congress, Sept. 20–26, Washington, DC (Dec 1992)

AJR carries announcements of courses, symposia, and meetings of interest to its readers if received a minimum of 5 months before the event. There is no charge; receipt of items by the *AJR* Editorial Office is not acknowledged. Submit items for publication typed double-spaced. Provide title, date, location, brief description, sponsor, course directors, fees, category 1 credit, and address and telephone number for additional information. Faculty from the host institution will not be listed. Guest faculty names will appear **only** if initials are provided. Mail news items to *AJR* Editorial Office, 2223 Avenida de la Playa, Suite 103, La Jolla, CA 92037-3218.

1993 ARRS Residents in Radiology Awards

President's Award

- The winner of the President's Award will be presented a certificate and receive an honorarium of ***$2,000.***

Executive Council Awards

- The two winners of the Executive Council Award will each receive a certificate and an honorarium of ***$1,000.***

RULES AND REGULATIONS

- Papers must be submitted on the clinical application of the discipline of radiology and radiological science.
- The event is open to residents in radiology and radiological sciences. If not the sole author, it is expected that the resident will have performed the majority of the work and be the senior author.
- Manuscripts should not exceed 5,000 words and 10 illustrations.
- Winners will be announced by March 16, 1993.
- Papers will be presented at the American Roentgen Ray Society 93rd Annual Scientific Meeting at the San Francisco Marriott, San Francisco, CA, April 25-30,1993, and be submitted for publication to the *American Journal of Roentgenology.*
- Manuscripts will be returned to candidates not receiving awards.

DEADLINE

- Four copies of the paper and four packages of the illustrations should be submitted no later than **February 12, 1993,** to:

Nancy O. Whitley, M.D.
Chairman, Committee on Education & Research
American Roentgen Ray Society
1891 Preston White Drive
Reston, Virginia 22091

American Roentgen Ray Society 93rd Annual Meeting, San Francisco, CA

Mark Your Calendar Now!

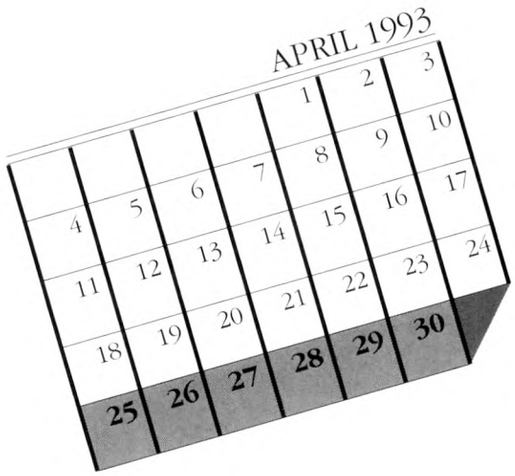

The American Roentgen Ray Society will return to San Francisco in 1993, and plans are already underway for what promises to be an educationally fulfilling and socially enjoyable week in the city by the bay. Look for the San Francisco logo in the next several issues of the *AJR* for updated meeting information.

Categorical Course

The topic of the 1993 Categorical Course is Ultrasound. A summary of topics and faculty for this course will appear in the February 1993 issue of the *AJR*.

Refresher Courses

Plans are underway to present at least 60 instructional courses on various topics of interest to the radiology community. A summary of these courses will be included in the February *AJR*. Early registration is strongly suggested, as these courses fill up quickly.

Residents' Award Papers

The society offers three cash awards for the best scientific papers prepared by residents in radiology. The President's Award has a cash prize of $2,000, and there are two Executive Council Awards with a cash prize of $1,000 each. The winners of these three awards are invited to present their papers during the opening ceremonies at the annual meeting. Papers must be submitted by February 12, 1993, for consideration in this competition. For additional information on these awards, contact the ARRS administrative offices at 1-800-438-2777.

Local Arrangements

The San Francisco area offers many opportunities for sightseeing, shopping and entertainment. Check the February *AJR* for detailed information on local tours developed especially for ARRS meeting attendees.

Registration and Hotel Reservations

All meeting activities will take place in the beautiful new San Francisco Marriott, centrally located on Market Street. The society has negotiated special room rates for meeting attendees, and the February *AJR* will contain meeting registration and hotel reservation forms. As in previous years, early registration is strongly suggested.

Travel

The society will make arrangements with United Airlines and a major car rental firm for preferred rates for meeting attendees. Taking advantage of these special rates benefits both you and the society - you save money on your reservations, and the society receives discounts to send staff and supplies to the meeting. Plan now to check the February issue of the *AJR* for details.

Classified Advertisements

Positions Available

GADSDEN RADIOLOGY ASSOCIATES is a 3-member radiology group seeking a fourth board-certified/eligible radiologist. Gadsden Radiology covers Baptist Memorial Hospital, a 250-bed hospital performing more that 55,000 radiologic exams/yr. All radiologic modalities are available, including state-of-the-art CT, SPECT, nuclear medicine, special procedures, and MRI. Gadsden Radiology Associates also covers their private office, imaging center, and a breast center. Teleradiography is used for call. Gadsden, AL, is a safe, clean city centrally located on the Coosa River approximately 1 hr from Birmingham, 90 Min. from Chattanooga, and 2 hrs from Atlanta, GA. Salary and vacation are excellent. Health insurance and malpractice is paid. Interested candidates contact Homer A. Spencer, M.D., 401 Bay Street, Gadsden, AL 35999; (205) 543-3200, or fax (205) 546-7908. 7–1ap

CENTRAL WISCONSIN—Established radiology group in independent practice is seeking 2 additional radiologists for growing practice in central Wisconsin. All imaging modalities. Competitive first yr salary with full partner status available second yr. Full benefits. Excellent schools, recreation, and quality of life. Contact David E. Enerson, M.D., 900 Illinois Ave., Stevens Point, WI 54481; (715) 346-5140 or Andrew M. Lucas, M.D., 410 Dewey St., Wisconsin Rapids, WI 54495-8080; (715) 423-6060. 12xa

MAINE—BC/BE diagnostic radiologist with MRI and/or interventional skills. Join well-established multidimensional group. Associate leading to partnership. Competitive financial package. Family oriented small city. Business and cultural center. Major university. One hr to coast. Easy access to ski areas. Send CV to New England Health Search, 63 Forest Ave., Orono, ME 04473; (207) 866-5680. 12xa

PARTNERSHIP POSITION IN PALM SPRINGS, CA—Well-established, 9-member group has openings for 2 board-certified radiologists. A physician with a strong background in MRI is sought as director of the section of MRI. The other position requires a physician with mammography experience to direct imaging in the breast health section of a new comprehensive cancer center. The group covers a 350-bed hospital and 2 offices in a desirable, rapidly expanding area of southern California. MRI facilities include 1.5-T Picker Vista HPQ with MRA package, ViStar imaging computer, and 1.5-T GE Signa. Other equipment includes 3 CT, a Cemax image processor, 2 Acuson color-flow Doppler ultrasound, 4 nuclear cameras including 2 SPECT, and all other diagnostic modalities. Ground has just been broken on a new 25,000 sq. ft. radiology wing, which will be furnished with state-of-the-art equipment. New trauma center, cancer center, and rehab hospital being built. Excellent compensation and benefits package leading to full partnership. Beaches and large-city amenities of Los Angeles only 2 hrs away. Yr-round sunny weather. Ample free time to enjoy southern California and the unparalleled recreational opportunities offered by the resort community of Palm Springs. Direct inquiries to Curtis E. Manning, M.D., Desert Hospital, Dept. of Radiology, 1150 N. Indian Canyon Dr., Palm Springs, CA 92262. 12xa

SUPERB PARTNERSHIP POSITION IN LAS VEGAS—Rapidly expanding 7-member group practice covering 2 full-service imaging centers and a small hospital has an immediate opening. We are looking for an additional board-certified radiologist with an uncommon dedication to excellence in patient care. Our outpatient facilities include 2 MR, 2 CT, angio with a 4-bed recovery area, 5 ultrasound, 5 mammography, 3 SPECT, plus R&F. This is an excellent opportunity for a partnership position with a well-respected group in a growing community. Please send CV to Dr. Mark Winkler, SDMI, 2950 S. Maryland Pkwy., Las Vegas, NV 89109. 3–2ap

SAN ANTONIO, TEXAS—Large group covering multiple hospitals and outpatient facilities seeks radiologists with angiography skills. Send CV to Search Committee, M&S X-Ray Associates, P.O. Box 15920, San Antonio, TX 78212-9510. 7–12ap

SOUTH CENTRAL FLORIDA—Immediate opening for board-certified (or eligible with intention to certify), Florida licensed general diagnostic radiologist. Four radiologists are now covering 3 hospitals totaling 250 beds as well as private diagnostic office with mammography. Onsite MRI at 1 hospital and mobile unit at another. Expertise in all modalities including interventional and angiography. Competitive package including early partnership. Send CV to Lawrence S. Ross, M.D., Radiology Consultants, P.A., 114 Medical Center, Sebring, FL 33870. 12xa

CENTRAL NEW JERSEY, IMMEDIATE OPENING—Full-time and part-time radiologists with fellowship training or equivalent experience in vascular/interventional and/or in MR imaging to join 6-member group. Must be willing to do other aspects of diagnostic radiology, mammography, ultrasound, CT, and nuclear medicine. Practice includes a 340-bed community hospital, a private radiology office, and an MRI facility. Area is within a 10-mi. radius of Princeton and is near New York City and Philadelphia. Competitive salary, excellent benefits, and partnership opportunity. Send CV or call Margaret M. Beck, Business Manager, 2127 Hamilton Ave., Trenton, NJ 08619; (609) 587-9410. 12xa

ISRAEL, DIAGNOSTIC RADIOLOGY—Opportunities for 3– to 4–wk or longer working vacations in a number of Israeli medical centers, on a volunteer basis. Positions varied, arrangements flexible. For information contact Jonathan H. Fish, M.D., 1844 San Miguel Dr., #302, Walnut Creek, CA 94596; (510) 947-0560. 11–1xa

NUCLEAR MEDICINE—RADIOLOGIST—CALIFORNIA—Immediate opening for diagnostic radiologist with nuclear medicine boards or special competency in growing private practice in the San Fernando Valley 20 minutes north of UCLA. Candidate to supervise growth of nuclear medicine dept. in addition to general diagnostic radiology work. Full partnership tract with excellent salary. Practice includes hospital and imaging centers. Group consists of young enthusiastic radiologists all with fellowship training. Equipment includes Sopha Spect nuclear, GE 1.5-T MRI with angio, 2 Acuson ultrasound, Siemens Angiostar specials, and 2 Picker 1200 CT scanners. Send CV to T. Sprague M.D., Holy Cross Medical Center, 15031 Rinaldi St., Mission Hills, CA 91345;.fax (818) 898-4451. 9–2ap

DIAGNOSTIC RADIOLOGIST with skills in CT, MR, interventional, ultrasound, and nuclear medicine needed to join group of 8 board-certified radiologists. Growing practice in eastern Washington at a 228-bed hospital, a new multimodality imaging center and 1 private office. Potential for long-term practice is excellent. Top-notch school system, including 3 first-rate universities. Excellent hunting, fishing, boating and skiing. Contact Eric W. Koelsch, N. 5901 Lidgerwood, Ste. 18B, Spokane, WA 99207; (509) 487-1264. 8-1ap

VASCULAR/INTERVENTIONAL RADIOLOGIST—The University of Arizona Dept. of Radiology is recruiting a fellowship-trained vascular/interventional radiologist to join the faculty at the assistant associate professor level. Facilities at the University Hospital (300-bed) and Tucson Veteran's Hospital (300-bed) are state-of-the-art. Income is based on AAMC guidelines, but is negotiable. Contact Gerald D. Pond, M.D., Head, Section of Vascular and Interventional Radiology, University of Arizona Health Sciences Center, Tucson, AZ 85724; (602) 626-6794. Women and minorities are encouraged to apply. The University of Arizona is an EEO/AA employer. Applications will be accepted until position is filled. 12xa

ULTRASOUND/CT/MRI—Opportunity for board-certified radiologist specializing in ultrasound, body CT, and body MRI to pursue academic career at the New York Hospital-Cornell Medical Center. Dept. provides state-of-the-art equipment, including Acuson and ATL ultrasound, GE 9800 CT, and GE Signa 1.5-T MR. Wide variety of ultrasound examinations include abdominal, OB/GYN, color Doppler, small parts, neonatal head, transvaginal, and transrectal. Prefer candidate with prior fellowship in sectional imaging or ultrasound. Responsibilities include clinical practice, teaching, and research. Position available 7-1-93. Please send CV to Elias Kazam, M.D., Dept. of Radiology, New York Hospital-Cornell Medical Center, 525 E. 68th St., New York, NY 10021. 10–1a

INTERVENTIONAL NEURORADIOLOGIST, COASTAL VIRGINIA—A 32-physician private radiology group which practices in 6 hospitals and several offices is seeking an interventional neuroradiologist who is eligible for senior membership in the American Society of Neuroradiology. The individual's clinical responsibilities would be primarily limited to a 644-bed tertiary-care center with level 1 trauma status. Diagnostic equipment includes 2 state-of-the-art Signa 1.5-T GE MR scanners (4.79 software and angio package), a DFP 60A bi-plane bi-digital 1024 matrix Toshiba DSA system (with digital stereo capabilities), and a Siemens DRH as well as a GE 9800 CT scanner. Some time would be spent at a 250-bed hospital with a Hitachi MRP-5000 0.2-T MR unit and a GE 9800.CT scanner with Hi-Light advantage software. Two (2) year fellowship trained neuroradiologists are already on staff. The practice is affiliated with a medical school and residency program which allows the pursuit of academic interests. The practice is located in a coastal resort area with a temperate climate and all water sports available. Interested persons should send a CV or contact Carl V. Bundschuh, M.D., Director of Neuroradiology and MRI, Medical Center Radiologists, Inc., 6161 Kempsville Circle, Ste. 330, Norfolk, VA 23502; (804) 466-0089. 12xa

MAMMOGRAPHER—Large private multi-hospital group in a coastal city of Virginia seeks a radiologist with special interests in all aspects of mammography. The practice includes a tertiary-care hospital which is affiliated with both a medical school and a radiology residency training program, thereby offering the benefits of both private practice and academics. The position would include directorship of future mammography clinics. Additional aptitude in other aspects of diagnostic radiology with specialized and/or fellowship training preferred. Interested applicants please send CV or inquiries to Medical Center Radiologists, Halifax Building, Ste. 330, 6161 Kempsville Circle, Norfolk, VA 23502; (804) 466-0089. 12xa

NW ROCKY MOUNTAINS—Highly respected 8-person group with strong subspecialty interests seeks highly qualified radiologist. Fellowship or academic experience preferred. Body imaging/MRI or nuclear medicine with boards or ABR special competency strongly desired. Position includes all aspects of radiology. Practice is located in Boise, ID , which has many recreational and cultural amenities. Reply to Paul Traughber, M.D., or J. Tim Hall, M.D., Dept. of Radiology, St. Alphonsus Regional Medical Center, 1055 No. Curtis Rd., Boise, ID 83706; (208) 378-2161. 8–1ap

DIAGNOSTIC RADIOLOGIST, NEW MILFORD, CT—A third radiologist is sought for a busy, private practice located in one of the most beautiful areas of Connecticut. We provide the full range of diagnostic services for a modern, well-equipped, community hospital. Choice environment; excellent compensation. Send inquiries and CV to Jules White, M.D., New Milford Hospital, 21 Elm St., New Milford, CT 06776; (203) 355-2611, ext. 235. 10–1a

EXCITING RADIOLOGIST OPPORTUNITIES NATIONWIDE!—Now is the time to make your move! ABSOLUTELY NO COST TO YOU. We specialize in RADIOLOGY only, so we understand your needs. Positions from Sunbelt to Northern-most regions. Both salaried and private practice opportunities with top money offered. Utilizing the Snelling Search Computer Network. We know of the positions first and give you the inside tracks! Fax your CV to (214) 258-1092, or mail to Snelling Search Medical Group. 1303 Walnut Hill Lane, Ste. 103, Irving, TX 75038. For information on specific positions call toll free (800) 259-5973. Ask for Roman. 12xa

FACULTY POSITION IN ABDOMINAL IMAGING—Opportunity for board-certified radiologist specializing in abdominal imaging with emphasis on gastrointestinal studies, sonography, and abdominal CT and MR to pursue an academic career at the New York Hospital-Cornell Medical Center. The dept. provides state-of-the-art equipment, including fluoroscopy Acuson and ATL ultrasound, GE 9800 CT, and GE Signa 1.5-T MR. Wide variety of abdominal examinations are done. Prefer candidate with prior fellowship in sectional imaging CT, MR, or ultrasound. Responsibilities include clinical practice, teaching, and research. Position is available July 1, 1992. Send CV to Claudia Henschke, Ph.D., M.D., Director, Starr 9 Division (GI, GU, Chest), Dept. of Radiology, The New York Hospital-Cornell Medical Center 525 E. 68th St., New York, NY 10021. 11–1a

THE LOUISIANA STATE UNIVERSITY MEDICAL CENTER is actively seeking candidates for ultrasound/CT/MRI, bone, chest, nuclear medicine, GI, GU, neuroradiology, angiography/interventional, emergency room, pediatrics and mammography. We are expanding our dept. significantly and are looking for enthusiastic individuals who want to develop a more expansive clinical practice, teaching program and research activities. A perfect opportunity to shape your own section. Applicants must be BE/BC and qualify for licensure in Louisiana. Salaries are competitive nationwide. The university is developing areas of special interest, including a multidisciplinary center for study of neurosciences and plans are underway to purchase all new state-of-the-art equipment. Enjoy the cultural and jazz music of New Orleans. The beaches of Northern Florida are only 3 1/2 hrs away. LSUMC is an AA/EOE. Send CV and 3 references to Jane Clayton, M.D., Acting Chairman, Dept. of Radiology, LSUMC, 1542 Tulane Ave., New Orleans, LA 70112; (504) 568-4647, fax (504) 568-8955. 10–1a

DIAGNOSTIC RADIOLOGIST, HOUSTON, TX—18-member private practice group seeks BC individual with musculoskeletal or body imaging fellowship. State-of-the-art practice in 1,500-bed teaching hospital with 4 MRI, 5 CT, 7 ultrasound units. Contact P.C. Smith M.D., The Methodist Hospital, 6550 Fannin (ms d-281), Houston, TX 77030. 11–4xa

NEURORADIOLOGIST—A 25-person radiologic group in central New Jersey seeks a fourth neuroradiologist well-versed in all neuroimaging modalities and procedures. Senior member status eligibility in the ASNR is required. Practice includes 2,450-bed hospital, 3 offices, 3 MRI scanners, 5 CT scanners, a radiology residency, and medical student teaching. Send CV to Richard Feinstein, M.D., c/o Kathy McGrath, Radiology Group of New Brunswick, 230 Old Bridge Turnpike, South River, NJ 08882. 10–3a

IMMEDIATE OPENING for full-time or part-time board-certified/eligible radiologist(s) to join an established 4-man radiology group in the Pacific Northwest. All modalities including MRI. Attractive salary/benefits; partnership opportunity. Community offers quality lifestyle and yr-round recreational opportunities. Send CV to Lynn Ball, Tri-City Radiology, 969 Stevens Dr., Ste. 1-B, Richland, WA 99352. 11–1a

CARDIOVASCULAR AND INTERVENTIONAL RADIOLOGIST—The State University of New York Health Science Center at Brooklyn seeks a board-certified/eligible radiologist with fellowship training in interventional radiology for a faculty position. The institution is a 1,700-bed facility, including the Kings County and the State University Hospitals. The medical center performs approximately 2,000 diagnostic and interventional procedures including angioplasty, embolization, caval filters, gastrointestinal, genitourinary, and pulmonary interventions. When ongoing renovations are complete, there will be 5 new vascular digital rooms. Research time and facilities are available. Rank and salary are commensurate with qualifications. CV should be addressed to Salvatore J.A. Sclafani, M.D., Kings County Hospital Center, Dept. of Radiology, 451 Clarkson Ave., Brooklyn, NY 11203; (718) 245-4447. An EO/AA. 11–1ap

GENERAL RADIOLOGY—Board-certified radiologist with mammographic experience for outpatient facility at the New York Hospital-Cornell University Medical College. The dept. provides 2 state-of-the-art (GE-CGR) mammographic units, an Acuson ultrasound, modern fluoroscopic and radiographic multi-room facility and access to GE Signa 1.5-T MR. Responsibilities include clinical practice, resident and medical student teaching and academic programs. Facility is accredited by ACR in mammography. Qualification for ACR mammographic certification required. Please send CV to Michael D. F. Deck, M.D., Acting Chairman, Dept. of Radiology, The New York Hospital-Cornell University Medical Center, 525 E. 68th St., New York, NY 10021 AA/EEO 11–1a

NEURORADIOLOGY, ASST/ASSOC. PROFESSOR—Board-certified neuro-radiologist interested in academic practice with strong clinical and medical student and resident teaching orientation at the New York Hospital-Cornell University Medical College. The dept. provides state-of-the-art equipment with basic research opportunities available through Cornell University Medical College and close affiliation with Memorial Sloan Kettering Cancer Hospital and Rockefeller University. Senior membership of the American Society of Neuroradiology required. Please send CV to Robert Zimmerman, M.D., Dept. of Radiology, New York Hospital-Cornell University Medical Center, 525 E. 68th St., New York, NY 10021; (212) 746-2574, fax (212) 746-8597. AA/EEO. 11–1a

PACIFIC NORTHWEST—Opportunity for BC/BE general diagnostic radiologists to join group of 5 board-certified radiologists. Experience in all modalities desired. Practice includes 2 hospitals and private office in Southern Oregon. Competitive starting salary with early full partnership. Excellent lifestyle with abundant recreational activities from Pacific Coast to Oregon Cascades. Practice in a family-oriented community with natural beauty. Send CV to Larry Strickland, Administrator, Roseburg Radiologists, P.C., P.O. Box 1547, Roseburg, OR 97470; (503) 673-4303.

DIAGNOSTIC RADIOLOGIST, NORTHEAST MICHIGAN—Excellent practice opportunity available for a diagnostic radiologist to commence in the autumn of 1992. Alpena Radiology, P.C., seeks a BC/BE radiologist to complete our 3-man group. We offer excellent income, early partnership and idyllic lifestyle. We require a friendly, hard-working individual who will be a team player. The ability to work well with us and our excellent medical staff is a must. Alpena General Hospital is a modern 175-bed facility located on the shores of Lake Huron. The hospital provides all radiology equipment including: new R&F equipment (G.E.), Siemens CT, SPECT nuclear imaging, color flow Doppler, DSA, ACR accredited mammography. Siemens mobile MRI will commence shortly. The hospital administration is very supportive. The Alpena area is a sportsman's paradise. Sailing, boating, golf, fishing, hunting, skiing, etc. are all minutes away. Our moderate winters and Mediterranean summers are ideal. For more information please contact Steven Zweig, M.D. or James Weeks, M.D., Dept. of Radiology, Alpena General Hospital, 1501 W. Chisholm St., Alpena, MI 49707; (517) 356-7250. 11–1a

TRAUMA RADIOLOGIST—The State University of New York Health Science Center at Brooklyn seeks to add a board-certified/eligible radiologist to join the Division of Traumatology at Kings County Hospital Center, a 1,300-bed tertiary facility/Level I Trauma Center with an international reputation in trauma services. The radiologist is an integral member of the trauma service of the dept. of surgery. Opportunities to join ongoing clinical investigations of the use of radiography, CT, angiography/interventional radiology, and ultrasound in the trauma patient are available. Academic rank and salary are commensurate with experience. CV should be addressed to Salvatore J. A. Sclafani, M.D., Dept. of Radiology, Kings County Hospital Center, 451 Clarkson Ave., Brooklyn, NY 11203. An EO/AA employer. 11–1ap

STATE COLLEGE, PA—Two positions available in private billing, hospital-based group. Mammoradiologist, BC/BE preferable with fellowship to run ACR accredited breast center. Will replace retiring mammoradiologist currently performing 6,400 exams/yr. Liberal salary and benefits. No call or weekends. General diagnostic radiologist BC/BE, competent in all modalities. Salary and benefit package well above average. Modern, well-equipped hospital including new G.E. 1.5-T Signa Advantage MRI. We offer excellent quality of life in a beautiful central PA college town, home of Penn State U. Send CV to R.A. Rockower, M.D., Dept. of Radiology, Centre Community Hospital, 1800 E. Park Ave., State College, PA 16803; (814) 234-6137. 11–1ap

DIAGNOSTIC RADIOLOGIST—Mallinckrodt Institute of Radiology, Washington University, seeks an additional board-certified radiologist with academic interest to join 2 radiologists at a satellite hospital of Barnes Hospital in St. Louis. This satellite radiology facility in St. Louis County performs all aspects of diagnostic radiology, including CT, MRI, ultrasound, and nuclear medicine. Equipment is brand new and state-of-the-art. Candidates must be competent in all aspects of diagnostic radiology and must be able to do cross-sectional interventional procedures. Academic rank and salary are dependent on qualifications and previous experience. The Institute is conducting research in teleradiology and outcomes research at the satellite facility. Washington University is an equal opportunity employer, applications from women and minority group members are encouraged. Send CV to R. Gilbert Jost, M.D., Chief of Diagnosis, Mallinckrodt Institute of Radiology, 510 S. Kingshighway Blvd., St. Louis, MO 63110. 11–1ap

DIAGNOSTIC RADIOLOGIST—Large private multi-hospital group in a coastal resort area of Virginia is seeking a BC/BE general diagnostic radiologist with proficiency in mammography, ultrasound, CT and general diagnostic radiology. MRI proficiency would also be helpful. The practice includes 5 large hospitals, 2 private offices and several outpatient imaging sites. The practice is also affiliated with a medical school and supports a residency program with 14 residents, thereby offering the benefits of both private practice and the pursuit of academic interests. Fellowship training preferred. Interested applicants should send their CV to Medical Center Radiologists, Inc., Halifax Bldg., Ste. 330, 6161 Kempsville Circle, Norfolk, VA 23502; (804) 466-0089 for further information. 12xa

RADIOLOGIST NEEDED—Thomaston, GA approximately 60 miles south of Atlanta, GA. Because of future retirement of a senior partner we are looking for a board-certified or eligible partner around June or July 1993. Interested in someone with special interest in imaging (CT & MRI) but at the same time comfortable with angiography and general radiology. Excellent salary and fringe benefits. Contact Ken Morgan, M.D., (706) 647-9745 or 647-1431; Fax (706) 647-9370. 11–2a

WATERFRONT, SOUTHERN MICHIGAN—X-ray Associates of Port Huron, MI, is seeking a seventh BC/BE diagnostic radiologist. Our 3 hospital-based practice features nuclear medicine, CT, ultrasound, Doppler, accredited mammography, and general radiography at all sites. Two sites also feature modern cardiovascular suites. A tri-hospital MRI center is featured at the largest site. Interventional skills are desirable but not mandatory. A hardworking, congenial, adaptable individual is an ideal candidate for our team-oriented radiology practice. Salary commensurate with experience, usual benefits, partnership in 2 yrs. Our Canadian-border community of 40,000 has seen rapid commercial growth in spite of the nation-wide recession. We have a small town atmosphere, good local school system, all water related outdoor activities, and most small city amenities. Please send CV to Clare A. Scheurer, M.D., 1002 Tenth Ave., Port Huron, MI 48060. For more information call (313) 987-1237, evenings. 11–4a

FLORIDA, STAFF RADIOLOGIST—Opportunity for board-certified/eligible diagnostic radiologist with experience in reading plain films, fluoroscopy, ultrasound, CT, nuclear medicine, and some angiography in radiology service at this GM&S Dept. of Veterans Affairs (VA) Medical Center. Affiliation in surgery with the University of Florida. Excellent employment benefits including 30 days paid vacation and 15 paid days sick leave per yr; liberal life and health insurance benefits; malpractice insurance; and retirement program. Moving expenses paid. Lake City, FL is located in northern Florida with a mild climate yr round. Extensive outdoor recreational activities. Reasonable cost of living, no state income tax, fine schools, local community college, and nearby universities which provide opportunities for continuing education and cultural diversion. Licensure in any state acceptable. Contact or send CV to Richard Parker, M.D., Chief of Radiology, VA Medical Center, Lake City, FL 32055-5898; (904) 755-3016 ext. 2543. An equal opportunity employer. 11–5a

CHEST RADIOLOGIST—Large private multi-hospital group in a coastal resort area of Virginia is seeking a BC/BE general diagnostic radiologist with expertise in pulmonary radiology. The practice includes 5 large hospitals, 2 private offices and several outpatient imaging sites. The practice is also affiliated with a medical school and supports a residency program with 14 residents, thereby offering the benefits of both private practice and the pursuit of academic interests. Fellowship training preferred. Interested applicants should please send their CV to Medical Center Radiologists, Inc., Halifax Bldg., Ste.330, 6161 Kempsville Circle, Norfolk, VA 23502; (804) 466-0089 for further information. 12xa

MRI/NEURORADIOLOGY/FLORIDA—Private MRI center seeks board-certified radiologist with MRI experience to oversee and direct diagnostic center. Excellent salary, complete benefit package and excellent recreational activities in growing Ft. Lauderdale community. Reply to Michael Abrahams, M.D., 6971 W. Sunrise Blvd., Plantation, FL 33317; (305) 792-1110. 11–1a

LOUISIANA—Diagnostic radiologist needed in busy practice including all modalities including vascular and MRI. Excellent benefits, salary, and early partnership. Partner retiring. University community of 100,000 with abundant outdoor recreation. CV to Dan Davidson, M.D., 3000 W. Deborah Dr., Monroe, LA 71201; (318) 388-7810. 11–1a

MRI/CT/ULTRASOUND—The State University of New York/Health Science Center at Brooklyn seeks a board-certified/eligible physician to join the faculty in cross-sectional imaging. The medical center is a 1,700-bed facility including Kings County Hospital and the State University Hospital. The medical center performs over 250,000 diagnostic procedures/yr. Currently 4 state-of-the-art CT scanners with a fifth to be installed shortly. A GE Signa was recently installed and a second is planned. Seventeen ultrasound units are in clinical use. Research time and facilities are available. The 2 hospitals are connected with a PACS System via a microwave link. Rank and salary are commensurate with qualifications. CV should be addressed to Joshua A. Becker, M.D., Professor and Chairman, Dept. of Radiology, SUNY/Health Science Center at Brooklyn, 450 Clarkson Ave., Brooklyn, NY 11203. Equal opportunity employer 11–1ap

MAMMOGRAPHY/RESEARCH, UNIVERSITY OF PENNSYLVANIA—Half-time position in mammography or full-time position combining clinical mammography and a partially grant-funded research program in image perception and transmission with Dr. Harold Kundel. High volume, rapidly expanding clinical section with ongoing problem solving mammography, breast ultrasound and needle localizations. Opportunities for additional collaborative projects with radiation oncology, MRI and surgery. Resident and student teaching responsibilities as well as participation in outpatient bone and chest radiology. Position available immediately. Applicant must be ABR certified and able to obtain license in Pennsylvania. University of Pennsylvania is an affirmative action, equal opportunity employer and specifically encourages applications from women and minorities. Send letter and CV to Rosalind H. Troupin, M.D., Dept. of Radiology, Hospital of the University of Pennsylvania, 3400 Spruce St., Philadelphia, PA 19104. 12–2a

SEATTLE-AREA/TWO POSITIONS—Ten-person group seeks radiologist with fellowship training in ultrasound and body imaging for 200-bed hospital and outpatient imaging center. Established practice in Bellevue area. Applicant must be board-certified and licensed in Washington state. Competitive salaries and excellent benefits offered. Address inquiries and current CV to Eastside Radiology, Dr. Allen, P.O. Box 806, Bellevue, WA 98009. Dedicated mammography for outpatient practice requires fellowship-trained or equivalent experience, board-certified and licensed in Washington state. Send inquiries to above address, Dr. Philip Lowe.12–1a

RADIOLOGIST TO HEAD WOMEN'S CLINIC, WITH SPECIAL EXPERTISE IN MAMMOGRAPHY AND ULTRASOUND—A regional women's clinic for mammography, breast ultrasound, and mammographically controlled needle aspirations and biopsies will open soon at John L. McClellan Veteran's Medical Center in Little Rock, AR. A radiologist to head this section is urgently needed. That individual will be assigned to certain general radiology duties part-time until a similar clinic opens at the University of Arkansas for Medical Sciences, at which time supervision of both women's centers will presumably be a full-time position. Applications should be submitted to University of Arkansas for Medical Sciences, Ernest J. Ferris, M.D., Professor and Chairman, Dept. of Radiology, Slot 556, 4301 W. Markham St., Little Rock, AR 72205; (501) 686-5740. 12–2a

VASCULAR AND INTERVENTIONAL RADIOLOGIST—The University of Arkansas for Medical Sciences is seeking a faculty member for our vascular and interventional radiology section. Candidates should be board-certified and fellowship-trained, and interested in a combined clinical, teaching and research environment. Clinical duties include coverage of a university hospital, a large veteran's hospital and a children's hospital. Active vascular and non-vascular research programs are in place. Salary and fringe benefits are competitive. Applications should include a current CV. For further information, please contact either David R. McFarland, M.D., Chief, Section of Vascular and Interventional Radiology, Steven K. Teplick, M.D., Professor and Vice Chairman, or Ernest J. Ferris, M.D., Professor and Chairman, Dept. of Radiology/556, University of Arkansas for Medical Sciences, 4301 W. Markham, Little Rock, AR 72205; (501) 686-6910. 12–2a

MAINE—BC/BE diagnostic radiologist with interventional skills. Join well-established multidimensional group. Associate leading to partnership. Competitive financial package. Family-oriented small city. Business and cultural center. Major university. One hr to coast. Easy access to ski areas. Send CV to New England Health Search, 63 Forest Ave., Orono, ME 04473; (207) 866-5680. 12–2ap

MUSCULOSKELETAL RADIOLOGIST, CHARLOTTE, NC—A 13-member, subspecialized group serving a 660-bed, private community hospital, outpatient diagnostic center desires a fellowship-trained or staff level musculoskeletal radiologist. GE 9800 CT and Signa 1.5-T equipment. Family-oriented community with warm 4-season climate, centrally located between coast and mountains. Send CV to P. O. Box 221211, Charlotte, NC 28222. 12–2a

GENERAL RADIOLOGIST WITH ANGIO/INTERVENTIONAL SKILLS—The Dept. of Radiology at Graduate Hospital is looking for a general radiologist with a subspecialty interest in vascular/interventional radiology. Other special interests or experience welcome. The successful applicant will join a 13-person radiology group in a tertiary-care hospital in Center City, Philadelphia, affiliated with the University of Pennsylvania. A new, state-of-the-art angiography suite has just been installed. Inquiries and CVs should be addressed to Jerome G. Jacobstein, M.D., Chairman, Dept. of Radiology, Graduate Hospital, One Graduate Plaza, Philadelphia, PA 19146; (215) 893-2041. 12–2a

MRI RADIOLOGIST WANTED for private MRI facility in beautiful, safe area in New York, close to beaches, 50 min. from New York City. Experience in MRI interpretation required. New graduates with MRI fellowship/background welcome. Send CV to *AJR* Box reply # 12 (see address this section) 12–1a

PRACTICE OPPORTUNITY IN FAST GROWING LAS VEGAS, NV—Expanding 9-member radiology group is seeking 2 additional BE/BC radiologists for July 1993. We currently serve 2 hospitals and 1 outpatient center with 2 additional outpatient centers scheduled to open within the yr. Outstanding salary and benefits package leading to full partnership in 2 yrs. Send CV or contact Marc Pomerantz M.D., Head of Search Committee, 1925 Spode Ave., Henderson, NV 89014; (702) 458-3191. 12–5ap

RESIDENTS—Due to a recently approved expansion of the program, the University of Michigan is seeking to recruit radiology residents for July 1993 at the second yr level. This fully accredited program provides training in all imaging modalities at the University of Michigan Hospitals and affiliated Veterans Administration Medical Center. Applicants must be eligible for Michigan licensure. Please forward your CV and letter of interest to N. Reed Dunnick, M.D., Professor and Chair, Dept. of Radiology, University of Michigan Hospitals, 1500 E. Medical Center Dr., Ann Arbor, MI 48109-0030. A nondiscriminatory, affirmative action employer. 12–1a

RADIOLOGIST—Eight-person group seeks general radiologist with fellowship training and special interest in MRI for 92-bed hospital and several imaging centers. Practice in the rapidly growing north San Diego and Temecula Valley areas. Send CV to North Coast Imaging Radiology Medical Group, Inc., 1582 W. San Marcos Blvd., Ste. 104, San Marcos, CA 92069; (619) 744-6442.

RADIOLOGIST—Full-time BC/BE, VA Medical Center, 165-bed GM & S. Excellent GE equipment, duplex Doppler, ultrasound, diagnostic and fluoroscopic, CT interpretation, state university city and hills and lakes in NW Arkansas, with cultural and recreational attractions. Competitive salary (approximately $125,000), excellent benefits/retirement . No malpractice insurance needed. Basic 40 hr work week. Call Chief of Staff, (501) 444-5050. 12–2a

DIAGNOSTIC RADIOLOGIST—Recent fellowship or faculty status preferred. Early partnership. We are a private practice group of 10 board-certified radiologists practicing general radiology with specialty interests accommodating all diagnostic and interventional modalities, including MRI. Our 350-bed hospital is a primary teaching affiliate of the University of Massachusetts Medical School with yr-round medical students and house-staff in several depts. The Berkshire Mountains are a desirable summer, winter and foliage resort community, less than 3 hrs drive to Boston, New York City, Vermont skiing and ocean. Quality of our practice, hospital and affiliates offices, and style of life are superior. Please respond with CV to Stuart J. Masters, M.D., Chairman, Dept. of Radiology, Berkshire Medical Center, 725 North St., Pittsfield, MA 01201. 12–2cp

CONNECTICUT, GENERAL DIAGNOSTIC RADIOLOGIST—Opening in July 1993 for BC/BE radiologist. Additional fellowship training may be a consideration in selection but is not a requirement. Nine-radiologist practice includes a 430-bed university affiliated, community hospital and a 60-physician multispecialty clinic. Approximately 110,000 exams/per yr including MRI, CT, nuclear medicine, ultrasound and an active angiographic and interventional service. Excellent salary and benefits leading to full partnership. For more information, send CV to David A. Lund, M.D., Dept. of Radiology, New Britain General Hospital, 100 Grand St., New Britain, CT 06050. 12–3a

INTERVENTIONAL RADIOLOGIST—Large radiology group with a 2-hospital-based practice and multiple private offices seeks a board-certified interventional radiologist interested in a full-time position. Training in CT, ultrasound, MRI and/or nuclear medicine is also preferred. Your interventional/angiography responsibilities would amount to approximately 30% of your time. Excellent southern New Jersey location. Competitive salary and benefit package. Send CV to RABC, P.O. Box 729, Mt. Holly, NJ 08060. 12–3a

BC/BE RADIOLOGIST to join VA Medical Center in Martinsburg, WV, a 316-bed hospital, 150-bed nursing home and 520-bed domiciliary located 75 miles from Washington, DC, or Baltimore, MD, in the Shenandoah Valley. Comprehensive benefit package. EOE. Contact J. Henderson, Office of COS, VAMC, Martinsburg, WV 25401; (304) 263-0811 ext. 4015. 12–2a

RADIOLOGIST—East Hudson Radiologists, P.C., located in the greater region of upstate New York, is recruiting radiologists with fellowship(s) in cross-sectional, interventional, and/or neuroradiology. Our practice provides services to 6 hospitals, 4 practice-owned imaging centers, and numerous private offices and health related facilities. Candidates must be board-certified/eligible and meet American College of Radiology standards, as well as all facility credentialing. Please send CV to Shirish Parikh, M.D., President/CEO, East Hudson Radiologists, P.C., 451 Hoosick St., Troy, NY 12180.

INTERVENTIONAL RADIOLOGIST, SOUTH JERSEY—Radiologist with fellowship training or equivalent experience in interventional radiology to join 5-member group with active hospital-based practice. State-of-the-art angiography equipment on-site. The hospital is affiliated with the University Medicine and Dentistry of New Jersey School of Osteopathic Medicine in Stratford, NJ. Position includes patient care and resident teaching. Excellent location 1/2 hr from Philadelphia and 1 hr from the Jersey Shore. Great lifestyle. Competitive salary and benefits. Send CV or call Beth K. Reichman, Corporate Director, Physician Relations, Kennedy Memorial Hospitals-UMC, 500 Marlboro Ave., Cherry Hill, NJ 08003; (609) 661-5149.12–1a

PEDIATRIC RADIOLOGIST—Fellowship-trained pediatric radiologist to join an 11-member group servicing a 493-bed community hospital with a large outpatient service. Two CT scanners, 2 MRI scanners, and digital fluoroscopy. Currently performing 300 pediatric exams/month with expanding service. Please send CV to Sumner Holtz, M.D., 232 So. Woods Mill Rd., St. Louis, MO 63017. 1–6a

DIAGNOSTIC IMAGING AND ANGIO/INTERVENTIONAL—Two positions available. The 10-member diagnostic radiology section of Guthrie Clinic and Robert Packer Hospital desire associates with fellowship training and/or expertise in the above areas. The Guthrie Clinic provides tertiary-care in the southern tier of New York and the northern tier of Pennsylvania in the beautiful endless mountains. Outstanding practice opportunities with state-of-the-art equipment in an environment free of urban hassle. Please send letter of inquiry with CV or call Ralph D. Zehr, M.D., Acting Chairman, Dept. of Radiology, Guthrie Clinic Ltd., Sayre, PA 18840; (717) 882-4032, (800) 724-1295.

OPEN RANK—Opportunity for board-certified interventional radiologist in accredited radiological program committed to quality clinical care and teaching. The University of Miami School of Medicine is recruiting a full-time vascular and interventional radiologist. The section currently consists of 44 staff members and 3 fellows and performs all angiographic and interventional procedures except for cardiac and neuroradiology, approximately 3,000 exams/yr. The University of Miami is an affirmative action equal opportunity employer. Send CV to Jose M. Yrizarry, M.D., Chief, Vascular/Interventional Radiology, University of Miami School of Medicine, Dept. of Radiology (R109), P.O. Box 016960, Miami, FL 33101; (305) 585-6894. 1–6a

MARTHA'S VINEYARD, MA—Seeks BC radiologist 5 one-half days/week September–May, full-time in summer. Teleradiology back-up which will handle 99% of call responsibilities. Ideal lifestyle for interested candidate. Plain radiographs, fluro, myelography, ultrasound, and NM. Biopsies, no angio. Call Teleradiology Associates at (919) 419-1000. 1–2a

VASCULAR/INTERVENTIONAL STAFF POSITION, 1993—The Dept. of Radiology at Boston's Beth Israel Hospital is seeking an additional BC/BE radiologist with fellowship or equivalent experience in vascular and interventional radiology to join 3 established interventionalists performing a comprehensive array of both vascular and nonvascular procedures. Beth Israel Hospital is a 500-bed major teaching affiliate of Harvard Medical School and is an affirmative action/equal opportunity employer. The CVIR section performs approximately 1,400 procedures/yr. Additional opportunities for participation in CT, ultrasound, MRI, and research. Please send inquiries with CV to Sven Paulin, M.D., Radiologist-in-Chief, Beth Israel Hospital, 330 Brookline Ave., Boston, MA 02215; (617) 735-2506. 1a

COLORADO—Practice of MR, CT, ultrasound, mammo, angio, and general radiology in small mountain valley city. Radiologist seeks BC/BE associate for 1993. Send letter and CV to *AJR* Box 1 (address this section).

RADIOLOGIST—Second radiologist needed for a 54-physician multispecialty clinic located in the western Rockies. Experience or formal training in mammography a must. General radiologic procedures excluding CT and MRI. Offered salary and benefits generous. Four season recreational opportunities abound. City is home of University of Montana. Send CV to Administrator, Western Montana Clinic, P.C., P.O. Box 7609, Missoula, MT 59807. 1–2a

CT/ULTRASOUND/MR RADIOLOGIST—Position available at a 400-bed, 2-division community hospital in northeast Philadelphia. Twelve full-time radiologists presently on staff. Will need fellowship-trained body imager because of expansion of our ultrasound division. Send CV to Dr. Marc Silver, Frankford Hospital, Torresdale Division, Knights and Red Lion Rd., Philadelphia, PA 19114; (215) 934-4020.

MR RESEARCH SCIENTIST FULL-TIME FACULTY POSITION, Dept. of Radiology, Children's Hospital, Boston, MA. Academic rank assistant professor to professor, Dept. of Radiology, Harvard Medical School, available January 1, 1993. Salary and fringe benefits are highly competitive; salary is based on academic rank and experience. Candidates must have a Ph.D. or its equivalent; must have a minimum of 1 yr of experience in clinical and research magnetic resonance spectroscopy (MRS). Duties include development of pediatric MRS research program as well as teaching. A 1.5-T clinical MR system and 4.7-T MR research system are available. The candidate must have a demonstrated interest and qualifications in basic and/or clinical pediatric MRS research. Children's Hospital and Harvard Medical School are affirmative action/equal opportunity employers. Address inquiry and CV to Donald R. Kirks, M.D., Radiologist-in-Chief, Dept. of Radiology, Children's Hospital, 300 Longwood Ave., Boston, MA 02115; (617) 735-6291. 1a

ULTRASOUND—The new Diagnostic Imaging Center at Roswell Park Cancer Institute is seeking a board-certified diagnostic radiologist with special interests in ultrasound. The newly renovated and equipped ultrasound section will include color Doppler ultrasound, intraoperative ultrasound, endoscopic ultrasound, and prostatic ultrasound with nationally recognized multidisciplinary clinics. Opportunity for multimodality clinical diagnostic imaging, research and academic activity is outstanding. Salaries are competitive. Construction of new diagnostic imaging center and hospital begins in 1993. A faculty appointment will be at the School of Medicine and Biomedical Sciences, SUNY at Buffalo. Please send CV to Paul C. Stomper, M.D., Diagnostic Radiology, Roswell Park Cancer Institute, Elm and Carlton Streets, Buffalo, NY 14263. An equal opportunity employer M/F/D/V. 1a

DIAGNOSTIC IMAGING AND BREAST IMAGING—The new Diagnostic Imaging Center at Roswell Park Cancer Institute is seeking board-certified radiologists specializing in CT/MRI, breast imaging, and general oncologic radiology. The dept. will have been totally renovated with all new equipment by Spring 1993, including the new magnetic resonance imaging center, the new multidisciplinary breast imaging center, and new CT, ultrasound, and flouroscopy suites. Construction of a new diagnostic imaging center and hospital is underway in 1993. Opportunity for multimodality clinical diagnostic imaging, research, and academic activity is outstanding. Salaries are competitive. A faculty appointment will be at the School of Medicine and Biomedical Sciences, SUNY at Buffalo, according to the level of professional qualifications. Please send CV to Paul C. Stomper, M.D., Diagnostic Radiology, Roswell Park Cancer Institute, Elm and Carlton Streets, Buffalo, NY 14263. An equal opportunity employer M/F/D/V. 1a

ABDOMINAL IMAGING RADIOLOGIST—Temple University Hospital and School of Medicine are seeking a board-certified radiologist with fellowship training in abdominal imaging to serve in the section of abdominal imaging. This is a faculty position at the rank of assistant/associate professor. The candidate should have strong clinical skills in CT, MRI, ultrasound, gastrointestinal radiology, and urography. The position involves major teaching responsibilities for both residents and medical students. Candidates with established research support would be preferred. Send cover letter/CV to Francis J. Shea, M.D., Professor and Deputy Chairperson, SmithKline Beecham, Dept. of Diagnostic Imaging, Temple University Hospital, 3401 N. Broad St., Philadelphia, PA 19140. Temple University Hospital is an affirmative action/equal opportunity employer. 1a

NEBRASKA—Two positions now available for well-trained BE/BC individuals to join a group of 5 BC diagnostic radiologists. Additional training or experience in nuclear medicine or MRI will be an advantage to applicants. Enjoy the best of a family-oriented community of 25,000 with clean air, affordable housing, and friendly hard-working people while practicing at a busy, very modern 267-bed hospital. New 1.5-T MRI currently being installed. Nearby recreation with wildlife, lakes, natural beauty and just 4 hrs from Steamboat Springs, CO, or Black hills of SD. Competitive salary, excellent vacation and call. Call our office today for more information on this excellent opportunity, (308) 630-1374, or nationwide toll-free 1 (800) 967-2144. 1a

WEST HAVEN VA MEDICAL CENTER/YALE UNIVERSITY SCHOOL OF MEDICINE—BC/BE radiologist. Academic radiologist position available 7-1-93 at the assistant/associate professor level. Position entails interpretation of general diagnostic films (excluding mammography), CT, and fluoroscopic procedures. Additional subspecialty skills or training in ultrasound (including vascular) or angiography (general, neuro, or interventional) would be beneficial. Affiliation with Yale School of Medicine provides opportunity for participating in ongoing research, developing new projects, teaching, and additional potential of part-time clinical duties at Yale New Haven Hospital. Supervision and training of residents is an important aspect of the program. The candidate should be qualified to hold a faculty position with Yale University School of Medicine and be a US citizen or permanent resident of the United States. Please send CV to Caroline Taylor, M.D., Chief, Radiology, VA Medical Center, West Haven, CT 06516; fax (203) 737-4035. The West Haven VA Medical Center and Yale University are equal opportunity/affirmative action employers. Applications from women and minority group members are encouraged. Application deadline is April 1, 1993. 1–3a

BOSTON UNIVERSITY SCHOOL OF MEDICINE, DEPT. OF RADIOLOGY—University Hospital, Boston City Hospital, has radiology fellowships offering 1-yr programs in neuroradiology, cardiovascular/interventional, nuclear medicine, pediatric radiology, abdominal radiology, ACGME accreditation application pending. For further information or application contact Joseph T. Ferrucci, M.D., Chairman, Dept. of Radiology, University Hospital, 88 E. Newton St., Boston, MA 02118. 1–2a

DIAGNOSTIC RADIOLOGIST with general radiology, MRI and CT experience for 2 established free-standing state-of-the-art facilities in Brooklyn, New York. Excellent salary and fringe benefits package in very pleasant working environments. Please call (718) 624-2222 or fax resume to (718) 858-7839. 1a

IMMEDIATE OPENING—The Dept. of Radiology at the University of Massachusetts Medical Center has a full-time position available in the musculoskeletal division at a rank and salary commensurate with experience. The medical center is a 370-bed university hospital and medical school located approximately 40 miles west of Boston. The dept. consists of 25 staff, 15 residents, and 24 fellows and does approximately 140,000 exams/yr. The dept is well-equipped with 2 GE 9800 HiLite CT scanners as well as 2 GE 1.5-T MRI scanners and a 2.0-T small-bore unit for animal research in a stand-alone facility. The hospital is a level I trauma center maintaining a full-time trauma service and an active emergency room with an associated emergency medicine residency of approximately 36 residents. The hospital is serviced by a Life Flight helicopter. A strong interest in teaching and collaborative clinical research is desired. For further information contact Edward H. Smith, M.D. Professor and Chairman, Dept. of Radiology, University of Massachusetts Medical Center, 55 Lake Ave. North, Worcester, MA 01655; (508) 856-3253. UMMC is an equal opportunity/affirmative action employer. 1ap

IMMEDIATE OPENING FOR BOARD-CERTIFIED RADIOLOGIST—Beautiful coastal Bar Harbor, ME, has an immediate opening for a radiologist in our friendly, community hospital. We are immediately adjacent to Acadia National Park. We have: Picker I.Q., CT scanner, Kodak laser printer and MED-RAD automatic injector (new in 92), Diasonics Spectra color Doppler unit (new in 92), ACOMA mammography unit (new in 91), 2 radiographic/fluoroscopic units (1 new in 91), Siemens basicamera nuclear medicine unit. Please direct all inquiries to James A. Mroch, President, Mount Desert Island Hospital, P.O. Box #8, Bar Harbor, ME 04609; (207) 288-5080, ext 330, fax (207) 795-2444. 1a

EXCELLENT OPPORTUNITY FOR BE/BC DIAGNOSTIC RADIOLOGIST with training in all modalities to join active 7-member group in Midwestern university town with medical school affiliation. Abundance of cultural opportunities and outdoor recreation. Excellent salary with early partnership. Please send inquiries and CV to Dean Hountras, M.D., 1000 S. Columbia Rd., Grand Forks, ND 58206-6003; (701) 780-6596. 1–3ap

MUSCULOSKELETAL RADIOLOGIST—Twenty-eight-member group in major southeast city seeks a musculoskeletal radiologist with sports medicine interest. General radiology skills necessary. This well-established practice has expanded and now requires a second musculoskeletal radiologist to staff recently completed 200-bed hospital and internationally recognized Sports Medicine Institute. Equipment is state-of-the-art 1.5-T GE MRI, GE 9800 Hilite CT, GE digital angiography and flouroscopy suites, and SPECT imaging. Interested candidates should send CV to *AJR* Box 11 (address this section) 1–4ap

DIVISION OF PEDIATRIC RADIOLOGY, OREGON HEALTH SCIENCES UNIVERSITY, PORTLAND, OR, invites applications for a faculty position. Completion of approved fellowship in pediatric radiology; ABR certification required. CV to Frederick S. Keller, M.D., Diagnostic Radiology, L340, Oregon Health Sciences University, Portland, OR 97201-3098; (503) 494-4498. Equal opportunity, affirmative action employer. 1a

APPLICATIONS ACCEPTED for faculty position of Director of Body Imaging, Dept. of Diagnostic Radiology, Oregon Health Sciences University, Portland, OR. Five yrs experience and ABR certification required. CV to Frederick S. Keller, M.D., Diagnostic Radiology, L340, Oregon Health Sciences University, Portland, OR 97201-3098. (503) 494-4498. Affirmative action, equal opportunity employer. 1a

OPTIMAL LIFESTYLE AND WORK ENVIRONMENT IN THE NORTHWEST—Three-man group seeks BC/BE radiologist interested in pleasant, stimulating work environment and generous vacation schedule. General radiology practice including MR, angio, interventional with up-to-date equipment and quality technical staff. Good income 1 yr to partnership. Family-oriented community in south-central Idaho with extensive, nearby outdoor activities. Dry climate with 4 seasons, 80 miles to Sun Valley, ID. If interested, please send CV and references to Dr. Evan Thomas, Southern Idaho Radiology, P.O. Box AB, Twin Falls, ID 83303.

DIAGNOSTIC RADIOLOGIST—Excellent opportunity to join pair at 100-bed hospital in northwestern Ohio town of Fremont, close to Toledo and major tourist attractions. Skills needed in general radiology including CT, ultrasound, and planar nuclear medicine. Additional experience in MRI, interventional radiology, and SPECT desirable but can be learned on the job. BC status also desirable, but BE radiologist would be trained to pass boards. Offer excellent salary and generous vacation and CME-related time off, as well as maternity or paternity leave. Also provide immediate retirement and other benefits plus full partnership within 2 yrs. Please contact Adrian Boyle at (800) 374-4425, or mail your CV to Physician Sourcing & Search, 2300 Peachford Rd., Ste 1100, Atlanta, GA 30338; fax (404) 455-6074. 1–2a

Fellowships and Residencies

FELLOWSHIP IN VASCULAR AND INTERVENTIONAL RADIOLOGY—The University of Arizona is sponsoring a 1-yr fellowship in vascular and interventional radiology beginning July 1, 1994. In-depth clinical experience and training in all aspects of interventional radiology will be offered. Facilities at the university hospital (300-bed) and Tucson Veterans Hospital (300-bed) are state-of-the-art. Interested applicants should submit a current CV and 3 letters of recommendation (including one from their program director) to Gerald D. Pond, M.D., Head, Section of Vascular and Interventional Radiology, University of Arizona Health Sciences Center, Tucson, AZ 85724. For further information please contact Ruth Kneup at (602) 626-6794. 12xc

FELLOWSHIPS AT THOMAS JEFFERSON UNIVERSITY HOSPITAL—The Dept. of Radiology at Thomas Jefferson University Hospital in Philadelphia offers the following fellowship programs each yr: (1) Ultrasound/CT/MRI—Jefferson's ultrasound division is one of the largest in the world and performs all currently available exams, including obstetric, vascular, lithotripsy, invasive, and endoluminal. We also operate 4 GE 1.5-T MRI units and 3 CT scanners. Contact Barry Goldberg, M.D. regarding this program. (2) Cardiovascular/interventional—This division is housed in a new suite containing Philips angio units with DSA and performs the full range of vascular and non-vascular interventional procedures. Contact Geoffrey Gardiner, Jr., M.D. (3) Neuro/ENT radiology—very active clinical services supply a wealth of material to this division, which is housed in a neurosciences imaging center containing all imaging modalities. Contact Carlos Gonzales, M.D. (4) Breast imaging—Jefferson's new breast-imaging center performs approximately 85 studies/day including ultrasound and needle localizations. Contact Stephen Feig, M.D. (5) Chest—includes biopsies and CT. Contact Robert Steiner, M.D. (6) MRI—a dedicated body MRI program including excellent research opportunities in addition to a large clinical case load. Contact Donald Mitchell, M.D. (7) Ultrasound—a dedicated ultrasound program. Contact Barry Goldberg, M.D. (8) Musculoskeletal—includes MRI of the musculoskeletal system. Contact David Karasick, M.D. All program directors listed above can be contacted at the Dept. of Radiology, Thomas Jefferson University Hospital, Philadelphia, PA 19107. Jefferson is an equal opportunity/affirmative action employer. 12xc

ONCORADIOLOGY/MAMMOGRAPHY FELLOWSHIP—The Dept. of Radiology at the Dana-Farber Cancer Institute and Brigham and Women's Hospital, which are Harvard Medical School affiliates, offers a 1-yr fellowship position beginning July 1, 1993. All imaging modalities involved in the diagnosis, staging, and follow-up of patients with malignant disease are integrated into this program. An additional feature is a concentrated experience in the performance of interventional breast diagnostic procedures. Please contact Jack E. Meyer, M.D., Director of Diagnostic Radiology, Brigham and Women's Hospital and Dana-Farber Cancer Institute, 75 Francis St., Boston, MA 02115; (617) 732-6269. Brigham and Women's Hospital/Dana Farber Cancer Institute/Harvard Medical School is an affirmative action/equal opportunity educator and employer. 5–4c

INTEGRATED CHEST RADIOLOGY FELLOWSHIP AT JOHNS HOPKINS UNIVERSITY HOSPITAL—The Dept. of Radiology, Division of Thoracic Imaging, Johns Hopkins University, is offering a 1- or 2-yr academically-oriented fellowship in chest radiology. The fellowship offers an integrated experience in cross-sectional imaging including over 4,000 chest CT exams/yr and 1,000 thoracic MRI examinations. Strong research interests in high-resolution computed tomography, magnetic resonance imaging, and interventional thoracic radiology offer the potential candidate an exciting environment to work in. The fellowship is available starting July 1, 1993, or July 1, 1994. Contact Janet E. Kuhlman, M.D., Director of Chest Radiology, Dept. of Radiology, Johns Hopkins Hospital, Baltimore, MD 21287; (410) 955-4419. 10–1cp

ACCREDITED FELLOWSHIPS IN PEDIATRIC RADIOLOGY AND PEDIATRIC NEURORADIOLOGY—Dept. of Radiology, Children's Hospital Medical Center, Cincinnati, OH, offers 1- or 2-yr accredited (Residency Review Committee for Radiology of ACGME) fellowships in pediatric radiology beginning July 1, 1994. A 1-yr pediatric neuroradiology fellowship program is also offered and may be taken separately or combined with 1 yr of adult neuroradiology fellowship at the University of Cincinnati Medical Center. Children's Hospital Medical Center (CHMC) is a 355-bed institution. The dept. performs over 105,000 radiological exams/yr in the largest children's hospital and ambulatory practice in the U.S. The dept. has 14 full-time faculty pediatric radiologists, 1 full-time research faculty, 7 fellows, and many resident trainees. Six pediatric radiology and 1 pediatric neuroradiology fellowship positions are available annually. Training includes all aspects of pediatric imaging neonatal radiology; neuroimaging; musculoskeletal radiology; cardiovascular and thoracic imaging; abdominal imaging; oncologic imaging; ultrasonography; nuclear medicine; computed tomography; MRI; and vascular/interventional procedures. The dept. has an active clinical service with state-of-the-art equipment as follows: digital fluoroscopy; Acuson and ATL ultrasound units with Doppler and color flow Doppler capabilities; planar SPECT gamma cameras; GE 9800 Quick CT scanner; 1.5-T GE MRI with spectroscopy, and cardiac catheterization/angiographic suite with digital vascular imaging. The fellowship provides a broad clinical experience in pediatric radiology as well as numerous opportunities to participate in both clinical and basic research. Candidates must be board-certified or board-qualified in diagnostic radiology and must obtain an Ohio medical license. Salary and fringe benefits are highly competitive. Applications are due prior to February 1993 with interviews scheduled during the fall and winter of 1992–93. There are numerous career opportunities in pediatric radiology and pediatric neuroradiology in both academic and private practice settings. To receive more information about the fellowships at CHMC or careers in pediatric radiology, please contact Director, Dept. of Radiology, Children's Hospital Medical Center, Cincinnati, OH 45229-2899; (513) 559-8058. Children's Hospital Medical Center and the University of Cincinnati College of Medicine are affirmative action/equal opportunity employers. 7–1cp

MRI FELLOWSHIPS—Fellowship positions in MRI are available from July 1994 and July 1995 at the Johns Hopkins Dept. of Radiology and Radiological Science. Flexible fellowship programs with clinical or research emphasis are available. The MRI division is equipped with 3 1.5-T GE scanners and 2 1.5-T Siemens scanners, both with cardiac imaging and spectroscopic capabilities. Over 9,000 exams are performed yearly. Over 2,000 of these exams are body MRI studies. In addition, a 4.7-T and an 8.5-T instrument with spectroscopic and imaging capabilities are available for research. The main interests of the section are in oncologic, cardiovascular, and musculoskeletal imaging. Rotating fellowships with CT and/or ultrasound or a straight MR fellowship are offered. For additional information and application, contact Elias A. Zerhouni, M.D., Director, Thoracic Imaging & MRI, Johns Hopkins Hospital, Baltimore, MD 21287; (410) 955-4062. 11–1cp

FELLOWSHIP IN ULTRASOUND AND BODY CT/MRI—One-yr fellowships in ultrasound and body CT/MRI beginning July 1, 1993, and July 1, 1994, are being offered by the New York Hospital-Cornell Medical Center. The dept. provides state-of-the-art equipment, including Acuson and ATL ultrasound, GE 9800 CT, and Ge Signa 1.5-T MR. Wide variety of ultrasound examinations include abdominal, OB/GYN, color Doppler, small parts, neonatal head, transvaginal, and transrectal. Applicants should be ABR eligible or certified. Send CV to Elias Kazam, M.D., Dept. of Radiology, New York Hospital-Cornell Medical Center, 525 E. 68th St., New York, NY 10021. 10–1c

FELLOWSHIP IN VASCULAR/INTERVENTIONAL RADIOLOGY—The Yale University Dept. of Radiology has an unexpected opening for a third fellowship position starting July 1993. The section has an active clinical service performing a wide range of vascular and interventional procedures including: diagnostic angiography, angioplasty, stenting, atherectomy, infusion therapy, embolotherapy, IVC filter placement, and percutaneous renal, biliary, and abscess management. Additionally, there is an inpatient admitting service and clinic. The fellowship is for 1 yr. Please send CV and 3 letters of recommendation to Jeffrey Pollak, M.D., Section Chief, Dept. of Diagnostic Radiology, Yale University School of Medicine, 333 Cedar St., P.O. Box 3333, New Haven, CT 06501, (203) 785-4746, (203) 785-3024 fax. Yale University is an equal opportunity/affirmative action employer. Applications from women and minority group members are encouraged.

CARDIAC IMAGING FELLOWSHIP (CLEVELAND CLINIC FOUNDATION)—The section of cardio-vascular imaging (division of radiology) announces to interested and qualified BC/BE radiologists a 2-yr cardiac imaging fellowship position (July 1, 1994 – June 30, 1996). This fellowship emphasizes integrated diagnostic imaging of acquired and congenital diseases of the heart and thoracic vasculature using non-invasive radiologic techniques (plain-film xray, CT, MRI, Nuclear Cardiology including PET) through a balance of practical clinical and research experiences. Research activities are complemented by lectures and technical assistance from the division's biostatistician. Didactic training both in cardiac catherterization/cine cardioangiographic interpretation and in performance/intepretation of echocardiography is coordinated with the dept. of cardiology for clinical and research cross-correlation. Direct all correspondences to Richard D. White, M.D. Head, Section of Cardio-Vascular Imaging, Division of Radiology L-10, Cleveland Clinic Foundation, 9500 Euclid Ave. Cleveland, OH, 44195; (216) 444-2740. 10–1c

UNEXPECTED IMMEDIATE OPENING, FELLOWSHIP IN IMAGING/ANGIO-INTERVENTIONAL—There is an unexpected opening for a 1-yr fellowship program available immediately at the Lehigh Valley Hospital in Allentown, PA. The fellowship program offers training in CT (head and body), ultrasound, MR, angiography, and interventional radiography. LVH is a 514-bed acute-care, university-affiliated hospital. For further information contact Robert Kricun, M.D., Dept. of Radiology, Lehigh Valley Hospital, P.O. Box 689, Allentown, PA 18105-1556; (215) 402-8088.

FELLOWSHIP POSITIONS—The Dept. of Radiology, University of Utah School of Medicine. The University of Utah Dept. of Diagnostic Radiology is offering 2 1-yr fellowships to begin July 1993 in the following areas: (1) musculoskeletal radiology, (2) chest/breast imaging. Active services with outstanding clinical colleagues and up-to-date facilities. Academic time is built into the fellowships and research time is available on the magnets. Applicants must be board-eligible and have obtained a Utah medical license prior to commencing training. Please send CV specifying your area of interest to B. J. Manaster, M.D., Ph.D, Associate Professor of Radiology, Dept. of Radiology, 50 North Medical Dr., Salt Lake City, UT 84132. The University of Utah is an equal opportunity/affirmative action employer and encourages applications from members of minority groups and women. 12–3c

FELLOWSHIP POSITIONS—The Dept. of Radiology of the Brigham and Women's Hospital-Harvard Medical School has 1- or 2-yr fellowship positions in the following areas: (1) cardiovascular and interventional, (2) neuroradiology, (3) CT/ultrasound/MR/interventional, (4) oncoradiology, (5) chest, (6) bone, (7) nuclear medicine, and (8) computer science. For more information, please send CV specifying your area of interest to B. Leonard Holman, M.D., Chairman, Dept. of Radiology, Brigham and Women's Hospital, 75 Francis St., Boston, MA 02115. Harvard Medical School and Brigham and Women's Hospital are equal opportunity, affirmative action employers. 5–4c

FELLOWSHIP IN ULTRASOUND, BODY CT AND MRI—July 1, 1994. 1-yr program featuring ultrasound, body CT, body MRI and noninvasive vascular diagnosis. For information and application contact William Zwiebel, M.D., Dept. of Radiology, University of Utah Hospital, Salt Lake City, UT 84132; (801) 581-7553. 4–2c

FELLOWSHIP IN PEDIATRIC IMAGING, DUKE UNIVERSITY MEDICAL CENTER—The Dept. of Radiology at Duke University Medical Center offers a 1- or 2-yr fellowship in pediatric imaging. This fellowship is designed to prepare the trainee for a career in pediatric radiology in a university, community or children's hospital setting. The fellow will work closely with pediatric radiologists and academic subspecialists in radiology. Clinical exposure includes pediatric imaging in neuroradiology, musculoskeletal radiology, cardiac radiology, chest radiology, GI radiology, GU radiology, and oncologic radiology. Imaging modalities include conventional and digital radiography, ultrasonography, nuclear medicine, computed tomography, magnetic resonance imaging, angiography, and interventional techniques. The fellow will participate in ongoing clinical research projects. Elective time during the second fellowship yr would permit the fellow to participate in basic and clinical research and to gain additional subspecialty experience. For further information, contact Carl E. Ravin, M.D., Professor and Chairman, Dept. of Radiology, Duke University Medical Center, Box 3808, Durham, NC 27710, Herman Grossman, M.D., Professor of Radiology and Pediatrics, Chief, Pediatric Imaging, Dept. of Radiology, Duke University Med. Center, Box 3834, Durham, NC 27710. Duke University is an affirmative action equal opportunity employer. 12–2c

FELLOWSHIP IN BODY MRI, CT, AND ULTRASOUND—The Dept. of Radiology at Hahnemann University Hospital, Philadelphia, PA, offers a 1-yr fellowship in body imaging. Three positions are available for July 1994 to June 1995. The fellowship will provide state-of-the-art training on ultrasound/CT/MRI. Equipment includes: Acuson and ATL ultrasound with color Doppler, 2 GE 9800 and a Signa 1.5-T MRI. Applicants must have completed an approved residency in diagnostic radiology and be board-eligible/certified. For inquiries, please contact Thomas Niedbala, M.D., Dept. of Diagnostic Radiology, Hahnemann University Hospital, Broad and Vine Streets, Philadelphia, PA 19102; (215) 762-8742. An equal opportunity employer. 12–2cp

PENN STATE UNIVERSITY, FELLOWSHIP IN CARDIOVASCULAR/INTERVENTIONAL RADIOLOGY—The Pennsylvania State University Dept. of Radiology offers 1- or 2- yr fellowships in cardiovascular/interventional radiology. Fellows will receive training in all aspects of diagnostic and interventional angiography (including neuro and pulmonary angiography), percutaneous and percutaneous/peroral GI interventions, GU interventions, venography, IVC filter placement, embolizations, foreign body retrievals, biopsy, drainage, and stenting procedures. Appointment at the instructor level is required, necessitating a Pennsylvania medical license, university hospital medical staff privileges, and ABR eligibility (at time of application) and certification (during first program yr). Independent original research is expected and is well supported. The animal research facility is excellent. A dedicated MR research facility with angiographic and spectroscopic capability exists. Both facilities are fully staffed by research associates and faculty and are equipped with state-of-the-art equipment. Eligibility: The fellowship is open to individuals who have completed an accredited residency program in radiology, can obtain a Pennsylvania medical license, and have fulfilled ABR requirements for board-certification/eligibility. Stipend: A generous and competitive salary and benefits package are offered. Academic, biophotographic, and secretarial support are also provided. Applications: Applicants should respond with a letter of interest and current CV. Please direct inquiries and requests for application forms to John F. Cardella, M.D., Assoc. Professor and Chief, Cardiovascular/Interventional Radiology Section, Penn State University/Hershey Medical Center, Box 850, Hershey, PA 17033. Penn State University is an affirmative action, equal opportunity employer; women and minorities are encouraged to apply. 11–1c

FELLOWSHIP IN VASCULAR/INTERVENTIONAL RADIOLOGY—The University of Maryland Medical Center has an opening for a fellow in the section of vascular and interventional radiology beginning July 1, 1993. The medical center is an 800-bed acute-care hospital and tertiary referral center with an active and varied vascular/interventional practice. In addition, a new 324-bed VA hospital, adjacent to and connected to the medical center, will be opening in November. The fellow will participate in all aspects of diagnostic vascular radiology as well as the full range of vascular and nonvascular interventional procedures. Interested persons should contact Dr. Philip A. Templeton, Acting Chairman, Dept. of Diagnostic Radiology, 22 S. Greene St., Baltimore, MD 21201. 1c

MR FELLOWSHIPS, IMMEDIATE OPENINGS—The Dept. of Radiology, University of Rochester Medical Center, MR fellowship offers a broad range of experience in both body and neuro MR. Associated imaging experience is available with CT. Research opportunities are available. Two 1.5-T G.E. Signa magnets with the latest software are in use and a third is being planned. Three CT units are in use. Eligible applicants must be board-certified or eligible for certification in diagnostic radiology and should be eligible for licensing in the state of New York. Contact Deborah Rubens, M.D., Dept. of Radiology, Box 648, University of Rochester Medical Center, Rochester, NY 14642; (716) 275-8365. EO/AA/M-F. 10–12c

ACCREDITED FELLOWSHIPS IN PEDIATRIC RADIOLOGY AND PEDIATRIC NEURORADIOLOGY—The Dept. of Radiology, Children's Hospital and Harvard Medical School, Boston, MA, offers 1- or 2-yr accredited (Residency Review Committee for Radiology of ACGME) fellowships in pediatric radiology beginning July 1, 1994. A 1-yr pediatric neuroradiology fellowship program is also offered. Children's Hospital is a 350-bed institution. The dept. performs over 102,000 radiological exams/annually in one of the largest children's hospitals in North America. The dept. has 16 faculty pediatric radiologists, 2 research faculty, 1 physicist, 9 pediatric radiology fellows, 2 neuroradiology fellows, and many resident trainees. Six pediatric radiology and 1 pediatric neuroradiology fellowship positions are available annually. Training includes all aspects of pediatric imaging: neonatal radiology; neuroimaging; musculoskeletal radiology; cardiovascular and thoracic imaging; abdominal imaging; oncologic imaging; ultrasonography; nuclear medicine; computed tomography; MRI; and vascular/interventional procedures. The dept. has an extremely active clinical service with state-of-the-art equipment as follows: digital fluoroscopy; computed radiography; Acuson ultrasound units with Doppler and color-flow Doppler capabilities; planar and SPECT gamma cameras; GE 9800 Highlight Advantage CT scanner; 1.5-T GE MRI with spectroscopy and MR angiography; angiocardiography suites with digital vascular imaging; and vascular/interventional suite with digital vascular imaging. The dept. provides extensive academic support; the Stem Memorial Radiology Library and departmental librarian are valuable resources. The fellowship provides a broad clinical experience in pediatric radiology as well as numerous opportunities to participate in both clinical and basic research. There are opportunities for collaborative research efforts at Children's Hospital, other Harvard teaching hospitals, and Harvard Medical School. Candidates must be board-certified or board-qualified in diagnostic radiology and must obtain a Massachusetts Medical License. Salary and fringe benefits are highly competitive. Applications are due no later than February 1993 with interviews scheduled during the fall and winter of 1992-93; there are numerous career opportunities in pediatric radiology and pediatric neuroradiology in both academic and private practice settings. To receive more information about the fellowships at Children's Hospital or careers in pediatric radiology, please contact Donald R. Kirks, M.D., Chairman, Dept. of Radiology, Radiologist-in-Chief, Children's Hospital, 300 Longwood Ave., Boston, MA 02115; (617) 735-6291. Children's Hospital and Harvard Medical School are affirmative action/equal opportunity employers. 12–3c

INTERVENTIONAL MAMMOGRAPHY AND BREAST IMAGING FELLOWSHIP—The University of Arizona is offering a flexible 1-yr fellowship in interventional mammography and breast imaging beginning July 1993. The section performs more than 14,000 mammograms per/yr and over 500 breast interventional procedures, including percutaneous stereotaxic breast needle biopsy, preoperative localizations, and galactography. Equipment includes 7 state-of-the-art mammographic units and 5 stereotaxic devices. The fellowship will include 20% academic/protected research time and up to 4 months could be spent in other areas of body imaging (CT, ultrasound, or MRI). We have an active research program including clinical, basic science and technology assessment/outcome analysis research-related breast imaging. Other benefits include: relocation allowance, office space with computer, and funds to attend national meetings. No "night call" responsibilities. Salary $38,500. Must be BC/BE. Will need Arizona license upon arrival. For further information please contact, Laurie L. Fajardo, M.D., Director, Mammography and Breast Imaging, University of Arizona, 1501 N. Campbell Ave., Tucson, AZ 85724. Application deadline, January 31, 1993. The University of Arizona is an equal opportunity/affirmative action employer. 10–1a

VASCULAR AND INTERVENTIONAL RADIOLOGY FELLOWSHIP—The University of Arkansas for Medical Sciences is offering a 1-yr fellowship in vascular and interventional radiology starting July 1, 1994. Training includes all aspects of angiography and vascular and nonvascular interventions. Ample clinical material is available at a university hospital, a large veteran's hospital and a children's hospital. Active vascular and non-vascular research programs are in place. Stipend and fringe benefits are competitive. Candidates must be board-certified or eligible in diagnostic radiology. Applications should include a current CV and 3 letters of reference. For further information, please contact either David R. McFarland, M.D., Chief, Section of Vascular and Interventional Radiology, Steven K. Teplick, M.D., Professor and Vice Chairman, or Ernest J. Ferris, M.D., Professor and Chairman, Dept. of Radiology/556, University of Arkansas for Medical Sciences, 4301 W. Markham, Little Rock, AR 72205; (501) 686-6910. 12–2c

BODY IMAGING FELLOWSHIP (ULTRASOUND, BODY CT, AND MRI), TO BEGIN JULY 1993.— The Dept. of Radiology at Albert Einstein Medical Center Hospital in Philadelphia, PA, offers a 1-yr body imaging fellowship. Albert Einstein Medical Center is a 650-bed, advanced tertiary-care teaching hospital. The fellowship emphasizes diagnostic ultrasound with rotations in body magnetic resonance imaging and computed body tomography. The program is flexible and negotiable. Examinations in all areas of sonography are performed and include obstetrics and gynecology, vascular/Doppler, abdominal, prostate, pediatrics, breast and small parts. There is state-of-the-art equipment in all areas of the dept. Fellows participate in procedures guided by ultrasound and computed tomography and have ample opportunity to participate in conference presentations and research projects, many of which culminate in publication. Inquiries should be addressed to Henrietta Kotlus Rosenberg, M.D., Chairman, Dept. of Radiology, Albert Einstein Medical Center, 5501 Old York Rd., Philadelphia, PA 19141. 12–2c

MAGNETIC RESONANCE IMAGING (COMBINED NEURO, MUSCULOSKELETAL AND BODY) FELLOWSHIP, THOMAS JEFFERSON UNIVERSITY HOSPITAL—The Dept. of Radiology at Thomas Jefferson University Hospital has created 2 new openings for 1-yr fellows beginning July 1, 1993. Responsibilities will be split between active neuroradiology and body/musculoskeletal MRI sections. Equipment includes 4 1.5-T GE Signa systems with state-of-the-art and advanced prototype hardware and software. Ample opportunities for clinical responsibility are provided. Interested candidates should contact Donald G. Mitchell, M.D., Director of MRI, Dept. of Radiology, 1096 Main Building, Thomas Jefferson University Hospital, Philadelphia, PA 19107; (215) 955-4809. Jefferson is an equal opportunity/affirmative action employer.

INTERVENTIONAL RADIOLOGY FELLOWSHIP—The University of Tennessee, Memphis, in conjunction with UT Medical Group, Inc., is actively recruiting for a fellow in vascular and interventional radiology. The fellowship program offers a 1-yr post-residency position beginning July 1, 1993, and July 1, 1994. Graduates will be eligible for certification of additional qualifications (CAQ) in interventional radiology as it is anticipated that the program will receive formal accreditation by the ACGME in the spring of 1993. The interventional radiology section provides interventional radiology services for 1,600 adult and pediatric beds in an urban medical center which includes the Regional Medical Center at Memphis and its Level I trauma center, the tertiary UT/Bowld Hospital and its active renal, liver, and pancreas transplant service, the Memphis VA Medical Center, the LeBonheur Children's Hospital and the St. Jude Cancer Research Institute. Over 2,000 vascular and interventional procedures are performed each yr including a comprehensive range of all endovascular procedures such as angioplasty, embolization, vena cava filter placements, and peripheral thrombolysis and nonvascular diagnostic and interventional procedures including percutaneous and intraoperative nephrostomies, biliary interventions, and simple and complex abscess drainages. A graduate of the program will be prepared to enter either private or academic medicine. Three full-time fellowship-trained members of the SCVIR work in this busy but pleasant atmosphere using state-of-the-art equipment. The fellow assists in the teaching of residents, participates in ongoing research and conferences, and has the opportunity to conduct research. Applicants must be board-certified or eligible in diagnostic radiology and eligible for licensure by the state of Tennessee. The University of Tennessee, Memphis, is an equal employment opportunity/Title IX/Section 504/ADA affirmative action employer. Send letter of inquiry to Morris L. Gavant, M.D., Interventional Radiology Program Director, University of Tennessee, Memphis, Dept. of Radiology, 800 Madison Ave., Memphis, TN 38163; (901) 577-8248. 1c

CALIFORNIA, FELLOWSHIP offers training in angio/interventional and cross-sectional imaging (MRI, CT, ultrasound). Saint Mary Medical Center is a 500+-bed, acute-care trauma center affiliated with UCLA. Please send CV to Robert T. Reinke, M.D., Dept. of Radiology, St. Mary Medical Center, 1050 Linden Ave., Long Beach, CA 90813; (310) 491-9900 for further information. 1xa

VASCULAR-INTERVENTIONAL RADIOLOGY FELLOWSHIP, 1993—The Dept. of Radiology at Boston's Beth Israel Hospital has a fellowship opening in vascular and interventional radiology for July 1993. Beth Israel Hospital is a 500-bed major teaching affiliate of Harvard Medical School and is an affirmative action/equal opportunity employer. The CVIR section performs approximately 1,400 procedures/yr, covering a wide gamut of both vascular and nonvascular interventions. Additional opportunities for limited participation in CT, ultrasound, MRI, and research. Candidates should be ABR certified/eligible. Please send inquiries with CV to Sven Paulin, M.D., Radiologist-in-Chief, Beth Israel Hospital, 330 Brookline Ave., Boston, MA 02215; (617) 735-2506. 1c

MUSCULOSKELETAL RADIOLOGY FELLOWSHIP, 1993—The Dept. of Radiology at the University of Virginia offers a 1-yr comprehensive musculoskeletal radiology fellowship beginning July 1, 1993. The UVA Health Sciences Center is a 670-bed tertiary-care medical center with a large variety and high-volume of musculoskeletal exams and a large residency training program. Close relationship with orthopedics, rheumatology, and radiation physicists. Fellowship includes all aspects of musculoskeletal imaging: conventional radiography, arthrography, CT, MR, and biopsies. Training includes clinical work, research, and teaching responsibilities. Direct inquiries to Phoebe A. Kaplan, M.D., Dept. of Radiology, University of Virginia Health Sciences Center, Box 170, Charlottesville, VA 22908; (804) 982-0211, fax (804) 982-1618. The University of Virginia is an equal opportunity/affirmative action employer. 1–2c

BODY IMAGING FELLOWSHIP (MRI, CT, ULTRASOUND)—One-yr fellowship position commencing July 1, 1994, at St. Luke's-Roosevelt Hospital Center in New York City. We offer extensive clinical experience and opportunities for research utilizing state-of-the-art equipment (GE 1.5-T Signa Advantage MRI, GE 9800 Hilight/Advantage and Picker PQ2000 slip ring CT, Acuson and ATL ultrasound including color Doppler). The hospital is a 1,315-bed voluntary university hospital of Columbia University College of Physicians and Surgeons. Applicants should be ABR eligible or certified. Applications requires CV, 3 letters of recommendation. Send inquiries to Benjamin Bashist, M.D., St. Luke's-Roosevelt Hospital Center, Dept. of Radiology, 428 West 59th St., New York, NY 10019. An equal opportunity employer M/F.1c

FELLOWSHIP IN VASCULAR AND INTERVENTIONAL RADIOLOGY—Loma Linda University Medical Center, Southern California, has made available an additional fellowship position beginning July 1, 1993. Over 2,000 vascular and nonvascular special procedures are performed annually. The 1-yr fellowship appointment is intensive while well supervised allowing for graded responsibility in the performance of and interpretation of examinations including diagnostic angiography, angioplasty, vascular and nonvascular stenting, TIPS, drainage procedures, and percutaneous biopsies. For additional information contact Frank C. Taylor, M.D., Interventional Radiology, Loma Linda University Medical Center, P.O. Box 2000, Rm., 2605E, Loma Linda, CA 92354; (714) 824-4370, fax (714) 824-4157. 1c

ONE-YR FELLOWSHIP IN ANGIOGRAPHY/INTERVENTIONAL RADIOLOGY—The Dept. of Radiology, The George Washington University Medical Center, Washington, D.C., is accepting applications for a 1-yr fellowship in angiography/interventional radiology beginning July 1, 1994. The section consists of 2 adjoining state-of-the-art angio suites sharing a large common control room. The section is responsible for all non-neuro and non-cardiac diagnostic angiography as well as all nonvascular image guided interventions, utilizing ultrasound, CT, or fluoro. The section is clinically-oriented and actively involved in direct patient care. A full range of diagnostic and therapeutic procedures are performed. Cross-training in vascular ultrasound and vascular MRI is possible. Approximately 800 cases/yr. Applicants must be graduates of an approved US medical school or its equivalent, must have completed an approved residency in diagnostic radiology, be eligible for ABR certification, and be eligible for medical licensure in the District of Columbia. Please send inquiries with CV to Edward M. Druy, M.D., Dept. of Radiology, The George Washington University Medical Center, 901 23rd St., N.W., Washington, D.C., 20037. The George Washington University is an EEO/affirmative action employer.

FELLOWSHIP IN MAGNETIC RESONANCE IMAGING at Central Massachusetts Magnetic Imaging Center, July 1994 through June 1995. CMMIC is a consortium of 3 area teaching hospitals (The Medical Center of Central Massachusetts, St. Vincent Hospital, and the University of Massachusetts Medical Center) with clinical, research, and teaching responsibilities. CMMIC currently utilizes 2 state-of-the-art clinical 1.5-T GE Signa systems as well as a 2.0-T GE Fremont CSI research system. The fellowship includes thorough training in MRI physics, imaging principles, clinical applications, and image interpretation. Duties include: interpretation of neuro, musculoskeletal, abdominal, pediatric, and cardiac studies and participation in CMMIC's teaching and research activities. Requirements include satisfactory completion of a 4-yr accredited radiology training program and board-eligible or certified. Please send inquiries to James F. Lingley, M.D., Medical Director, CMMIC, Inc., 367 Plantation St., Worcester, MA 01605 1–2c

BODY IMAGING FELLOWSHIP (BODY CT, ULTRASOUND, BODY MRI) TO BEGIN JULY 1994—The Dept. of Radiology of the University of Vermont offers a 1-yr fellowship in body imaging. Included is training in body CT utilizing 2 GE Fast Scan helical systems, ultrasound (abdominal, vascular, and high risk obstetrics) with 5 color flow Acuson units, and body MRI with a completely equipped GE Signa (MRA, Fast SE, and phased array). The Medical Center Hospital of Vermont is a regional referral center for trauma, tertiary obstetrics, and oncology; there are strong programs in surgery, transplant, and orthopedics. Clinical research opportunities are available and well-supported. The University of Vermont is located in Burlington, a family-oriented community of 50,000 on Lake Champlain and in the Green Mountains; unsurpassed recreation is nearby. Low crime, no traffic, great schools, abundant cultural life. Please send CV to William P. Shuman, M.D., Director, CT/MR/Ultrasound, Dept. of Radiology, Medical Center Hospital of Vermont, Burlington, VT 05401. 1–4c

THE UNIVERSITY OF WISCONSIN RADIOLOGY has an opening for an angiography/interventional fellow for 1-yr commencing July 1, 1994. Four fellowship-trained faculty, 1 fellow and 2 residents staff the section which does over 2,500 procedures/yr. Experience in magnetic resonance angiography is available. Letters of inquiry and CV should be sent to Andrew B. Crummy, M.D., Professor, Dept. of Radiology, 600 Highland Ave., Madison, WI 53792-3252. 1c

FELLOW, PEDIATRIC RADIOLOGY, OTTAWA, CANADA—The Dept. of Radiology of the Children's Hospital of Eastern Ontario is seeking a fellow in general pediatric radiology for a 1- or 2-yr term. Address inquiries to Dr. Mary Ann Matzinger, Chief, Dept. of Radiology, 401 Smyth, Ottawa, ONT K1H 8L1.

Remember the last time you saw lesions this clearly?

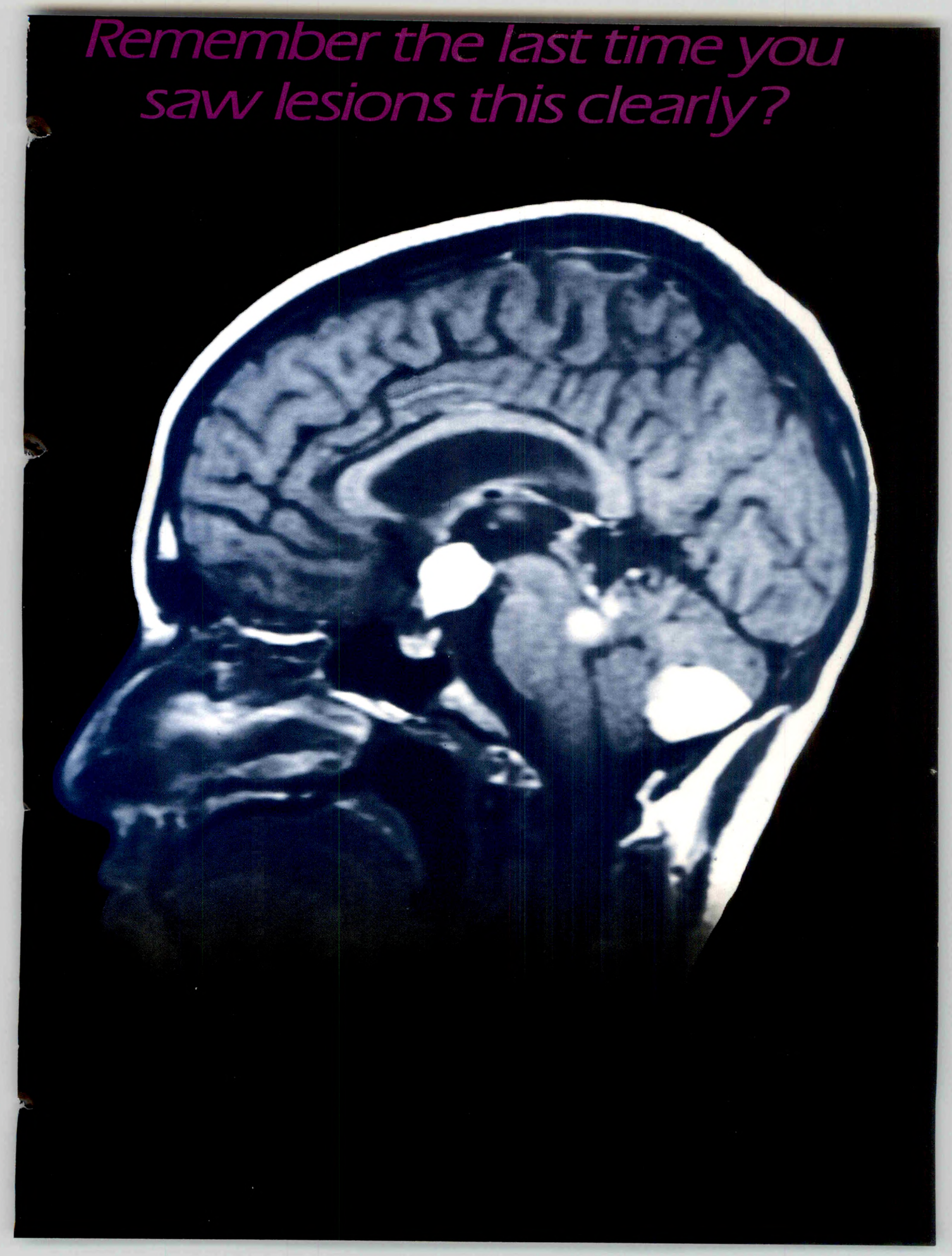

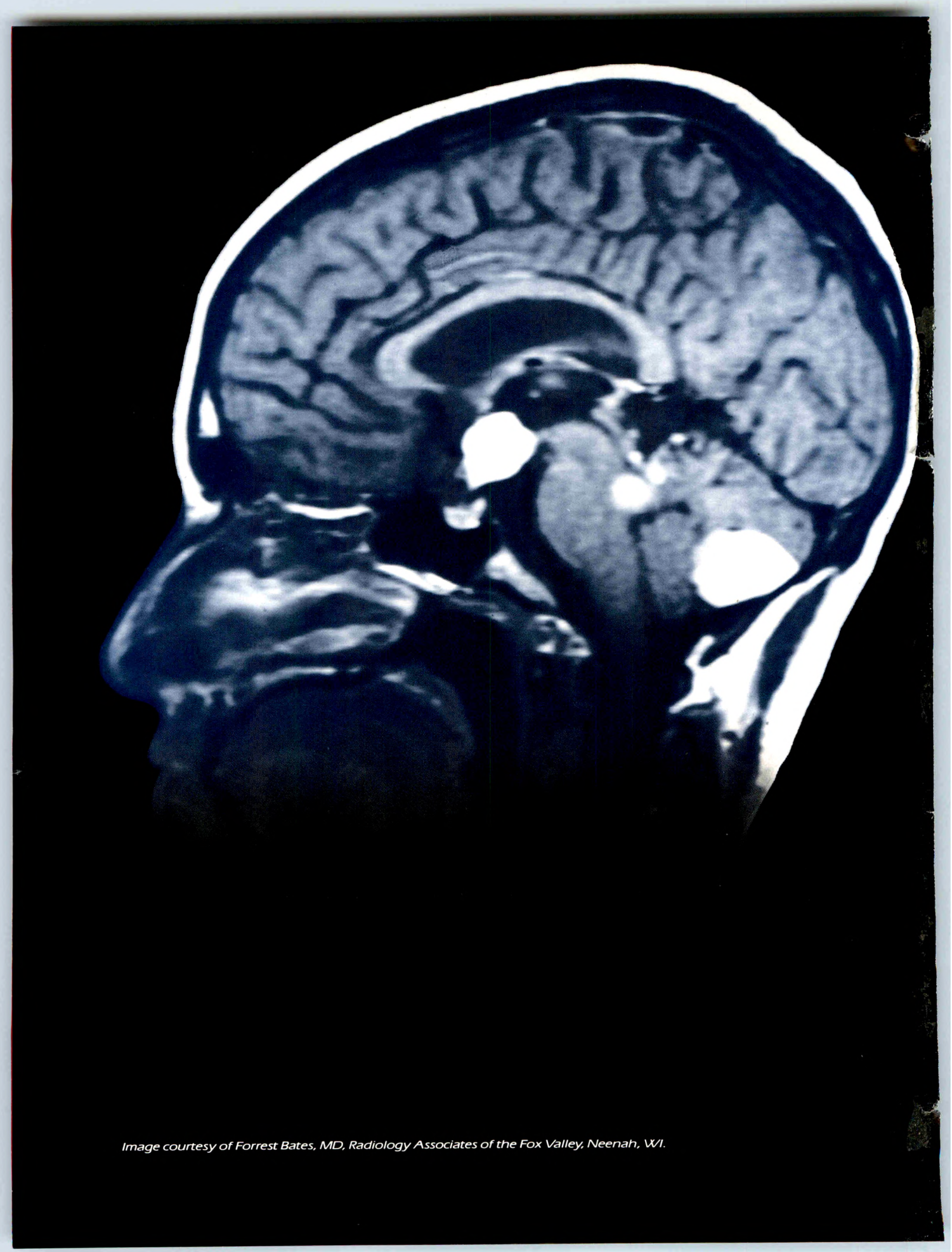

Image courtesy of Forrest Bates, MD, Radiology Associates of the Fox Valley, Neenah, WI.

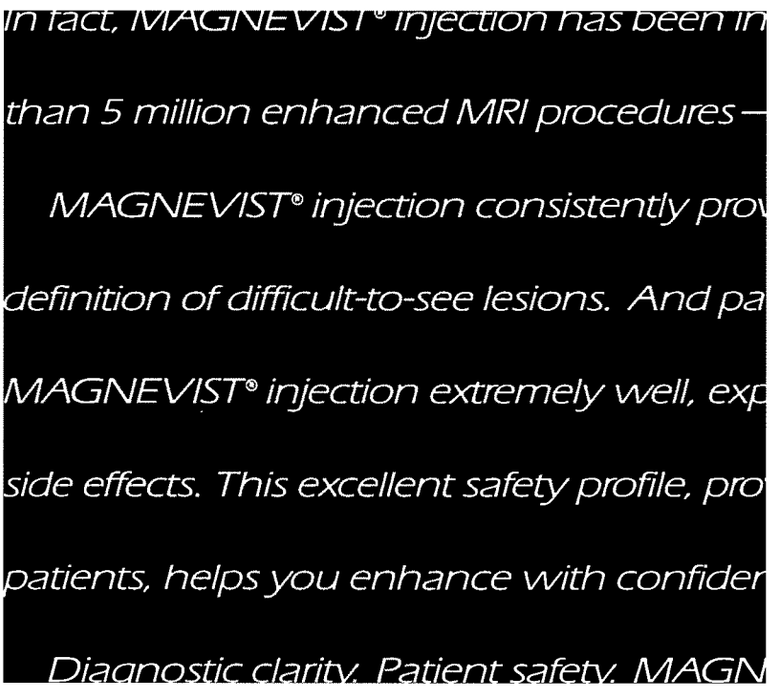
In fact, MAGNEVIST® injection has been in
than 5 million enhanced MRI procedures—
MAGNEVIST® injection consistently prov
definition of difficult-to-see lesions. And pa
MAGNEVIST® injection extremely well, exp
side effects. This excellent safety profile, pro
patients, helps you enhance with confider
Diagnostic clarity. Patient safety. MAGN

Well tolerated[1] The most common adverse reactions reported were headache (8.7%) and injection-site coldness/localized coldness (4.8%). The majority of headaches were transient and of mild to moderate severity. An asymptomatic transient rise in serum iron was experienced by 15% to 30% of patients. Hypotension and anaphylactoid reactions have occurred in less than 1% of patients. The safety of MAGNEVIST® Injection in patients with hemolytic disorders has not been studied.

1. Data on file, Berlex Laboratories.

BRIEF SUMMARY

INDICATIONS AND USAGE

MAGNEVIST® Injection is indicated for use with magnetic resonance imaging (MRI) in adults and children (2 years of age and older) to provide contrast enhancement in those intracranial lesions with abnormal vascularity or those thought to cause an abnormality in the blood-brain barrier. MAGNEVIST® Injection has been shown to facilitate visualization of intracranial lesions including but not limited to tumors.

MAGNEVIST® Injection is also indicated for use with MRI in adults and children (2 years of age and older) to provide contrast enhancement and facilitate visualization of lesions in the spine and associated tissues. There is, however, only limited clinical experience in children for this indication.

CONTRAINDICATIONS

None known.

WARNINGS

The accepted safety considerations and procedures that are required for magnetic resonance imaging are applicable when MAGNEVIST® Injection is used for contrast enhancement. In addition, deoxygenated sickle erythrocytes have been shown in *in vitro* studies to align perpendicular to a magnetic field which may result in vaso-occlusive complications *in vivo*. The enhancement of magnetic moment by gadopentetate dimeglumine may possibly potentiate sickle erythrocyte alignment. MAGNEVIST® Injection in patients with sickle cell anemia and other hemoglobinopathies has not been studied.

Patients with other hemolytic anemias have not been adequately evaluated following administration of MAGNEVIST® Injection to exclude the possibility of increased hemolysis.

Hypotension may occur in some patients after injection of MAGNEVIST® Injection. In clinical trials two cases were reported and in addition, there was one case of a vasovagal reaction and two cases of pallor with dizziness, sweating and nausea in one and substernal pain and flushing in the other. These were reported within 25 to 85 minutes after injection except for the vasovagal reaction which was described as mild by the patient and occurred after 6-1/2 hours. In a study in normal volunteers one subject experienced syncope after arising from a sitting position two hours after administration of the drug. Although the relationship of gadopentetate dimeglumine to these events is uncertain, patients should be observed for several hours after drug administration.

Magnevist®
(gadopentetate dimeglumine 469.01 mg/mL)
INJECTION

PRECAUTIONS - General

Diagnostic procedures that involve the use of contrast agents should be carried out under direction of a physician with the prerequisite training and a thorough knowledge of the procedure to be performed.

In a patient with a history of grand mal seizures, MAGNEVIST® Injection was reported to induce such a seizure.

Since gadopentetate dimeglumine is cleared from the body by glomerular filtration, caution should be exercised in patients with severely impaired renal function.

The possibility of a reaction, including serious, life-threatening, fatal, anaphylactoid or cardiovascular reactions or other idiosyncratic reactions should always be considered (see ADVERSE REACTIONS) especially in those patients with a known clinical hypersensitivity or a history of asthma or other allergic respiratory disorders.

Animal studies suggest that gadopentetate dimeglumine may alter red cell membrane morphology resulting in a slight degree of extravascular (splenic) hemolysis. In clinical trials 15-30% of the patients experienced an asymptomatic transient rise in serum iron. Serum bilirubin levels were slightly elevated in approximately 3.4% of patients. Levels generally returned to baseline within 24 to 48 hours. Hematocrit and red blood cell count were unaffected and liver enzymes were not elevated in these patients. While the effects of gadopentetate dimeglumine on serum iron and bilirubin have not been associated with clinical manifestations, the effect of the drug in patients with hepatic disease is not known and caution is therefore advised.

When MAGNEVIST® Injection is to be injected using plastic disposable syringes, the contrast medium should be drawn into the syringe and used immediately.

If nondisposable equipment is used, scrupulous care should be taken to prevent residual contamination with traces of cleansing agents.

Repeat Procedures: If in the clinical judgment of the physician sequential or repeat examinations are required, a suitable interval of time between administrations should be observed to allow for normal clearance of the drug from the body.

Information for Patients:

Patients receiving MAGNEVIST® Injection should be instructed to:

1. Inform your physician if you are pregnant or breast feeding.
2. Inform your physician if you have anemia or any diseases that affect red blood cells.
3. Inform your physician if you have asthma or other allergic respiratory disorders.

LABORATORY TEST FINDINGS

Transitory changes in serum iron and bilirubin levels have been reported in patients with normal and abnormal liver function (See PRECAUTIONS - General).

CARCINOGENESIS, MUTAGENESIS, AND IMPAIRMENT OF FERTILITY

No animal studies have been performed to evaluate the carcinogenic potential of gadopentetate dimeglumine.

Gadopentetate dimeglumine did not evoke any evidence of mutagenic potential in the Ames test (histidine-dependent *Salmonella typhimurium*) nor in a reverse mutation assay using tryptophan-dependent *Escherichia coli*. Gadopentetate dimeglumine did not induce a positive response in the (C3H 10T1/2) mouse embryo fibroblast cellular transformation assay, nor did it induce unscheduled DNA repair synthesis in primary cultures of rat hepatocytes at concentrations up to 5000 μg/mL. However, the drug did show some evidence of mutagenic potential *in vivo* in the mouse dominant lethal assay at doses of 6 mmol/kg, but did not show any such potential in the mouse and dog micronucleus tests at intravenous doses of 9 mmol/kg and 2.5 mmol/kg, respectively.

The results of a reproductive study in rats showed that gadopentetate dimeglumine when administered in daily doses of 0.1-2.5 mmol/kg, did not cause a significant change in the pregnancy rate in comparison to a control group. However, suppression of body weight gain and food consumption and a decrease in the mean weights of testis and epididymis occurred in male rats at the 2.5 mmol/kg dose. In female rats a decrease in the number of corpora lutea at the 0.1 mmol/kg dose and the suppression of body weight gain and food consumption at the 2.5 mmol/kg dose were observed.

In a separate experiment, 16 daily intravenous injections were administered to male rats. At a dose of 5 mmol/kg of gadopentetate dimeglumine, spermatogenic cell atrophy was observed. This atrophy was not reversed within a 16-day observation period following the discontinuation of the drug. This effect was not observed at a dose of 2.5 mmol/kg.

PREGNANCY CATEGORY C

Gadopentetate dimeglumine has been shown to retard development slightly in rats when given in doses 2.5 times the human dose, and in rabbits when given in doses of 7.5 and 12.5 times the human dose. The drug did not exhibit this effect in rabbits when given in doses 2.5 times the human dose. No congenital anomalies were noted in either species.

There are no adequate and well-controlled studies in pregnant women. MAGNEVIST® Injection should be used during pregnancy only if the potential benefit justifies the potential risk to the fetus.

NURSING MOTHERS

C^{14} labelled gadopentetate dimeglumine was administered intravenously to lactating rats at a dose of 0.5 mmol/kg. Less than 0.2% of the total dose was transferred to the neonate via the milk during the 24-hour evaluation period. It is not known to what extent MAGNEVIST® Injection is excreted in human milk. Because many drugs are excreted in human milk, caution should be exercised when the drug is administered to a nursing mother and consideration should be given to temporarily discontinuing nursing.

PEDIATRIC USE

Safety and efficacy in children under the age of 2 years have not been established. (See Indications and Usage and Dosage and Administration sections).

ADVERSE REACTIONS

The most commonly noted adverse experience is headache with an incidence of 8.7%. The majority of headaches are transient and of mild to moderate severity. In 42.3% of the cases it was felt that the headaches were not related to MAGNEVIST® Injection. Injection site coldness/localized coldness is the second most common adverse experience at 4.8%. Nausea occurs in 3.2% of the patients.

Localized pain, vomiting, paresthesia, dizziness and localized warmth occur in less than 2% of the patients.

The following additional adverse events occur in less than 1% of the patients:

Body as a Whole: Injection site symptoms, namely, pain, warmth, burning; localized burning sensation, substernal chest pain, fever, weakness, generalized coldness, localized edema, tiredness, chest tightness, regional lymphangitis and anaphylactoid reactions (characterized by cardiovascular, respiratory and cutaneous symptoms) rarely resulting in death.

Cardiovascular: Hypotension, vasodilation, pallor, non-specific ECG changes, angina pectoris, phlebitis.

Digestive: Gastrointestinal distress, stomach pain, teeth pain, increased salivation.

Nervous System: Agitation, thirst, convulsions (including grand mal).

Respiratory System: Throat irritation, rhinorrhea, sneezing, dyspnea, wheezing, laryngismus, cough.

Skin: Rash, sweating, pruritus, urticaria (hives).

Special Senses: Tinnitus, conjunctivitis, visual field defect, taste abnormality, dry mouth, lacrimation disorder (tearing), eye irritation.

Laboratory: Transient elevation of serum transaminases.

The following other adverse events were reported. A causal relationship has neither been established nor refuted.

Body as a Whole: Back pain, pain, generalized warmth.

Cardiovascular: Hypertension, tachycardia, migraine, syncope, death related to myocardial infarction or other undetermined causes.

Digestive: Constipation, diarrhea.

Nervous System: Anxiety, anorexia, nystagmus, drowsiness, diplopia, stupor.

Skin: Facial edema, erythema multiforme, epidermal necrolysis.

Special Senses: Eye pain, ear pain.

Data from foreign studies did not reveal any additional adverse experiences.

OVERDOSAGE

The LD_{50} of intravenously administered gadopentetate dimeglumine injection in mice is 5-12.5 mmol/kg and in rats it is 10-15 mmol/kg. The LD_{50} of intravenously administered MAGNEVIST® Injection in dogs is greater than 6 mmol/kg.

Clinical consequences of overdose with MAGNEVIST® Injection have not been reported.

DOSAGE AND ADMINISTRATION

The recommended dosage of MAGNEVIST® Injection is 0.2 mL/kg (0.1 mmol/kg), administered intravenously, at a rate not to exceed 10 mL per minute. More rapid injection rates may be associated with nausea. The maximum total dose is 20 mL. Any unused portion must be discarded.

DOSAGE CHART

Body Weight (kg)	Dose in mL	Approx Duration of Injection in Seconds
10	2.0	20
20	4.0	30
30	6.0	40
40	8.0	50
50	10.0	60
60	12.0	70
70	14.0	80
80	16.0	95
90	18.0	110
100	20.0	120

To ensure complete injection of the contrast medium, the injection should be followed by a 5-mL normal saline flush. The imaging procedure should be completed within 1 hour of injection of MAGNEVIST® Injection.

Parenteral products should be inspected visually for particulate matter and discoloration prior to administration, whenever solution and container permit.

For full prescribing information, see package insert.

Caution: Federal Law Prohibits Dispensing Without Prescription.

Berlex Laboratories
Wayne, New Jersey 07470
60626-1 Revised 8/91

BERLEX IMAGING®

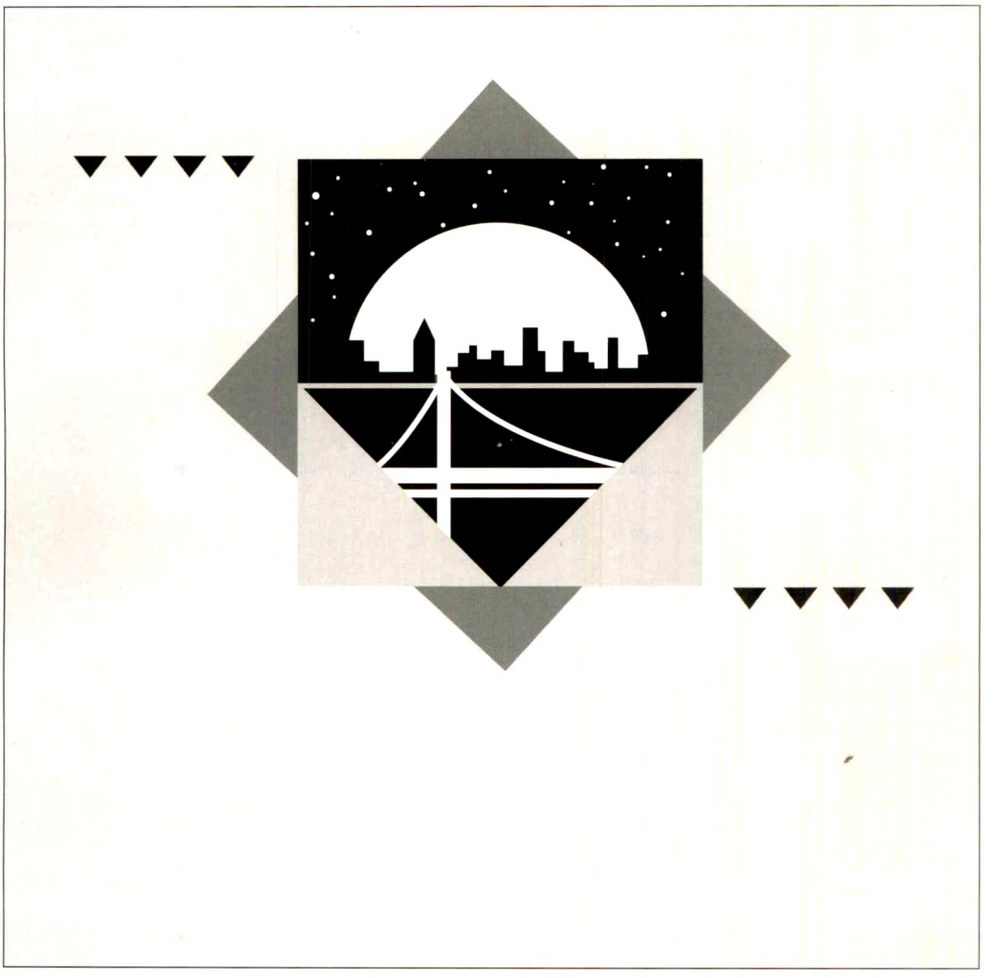

San Francisco

American Roentgen Ray Society

93rd Annual Meeting

April 25–30, 1993

San Francisco Marriott • San Francisco, CA

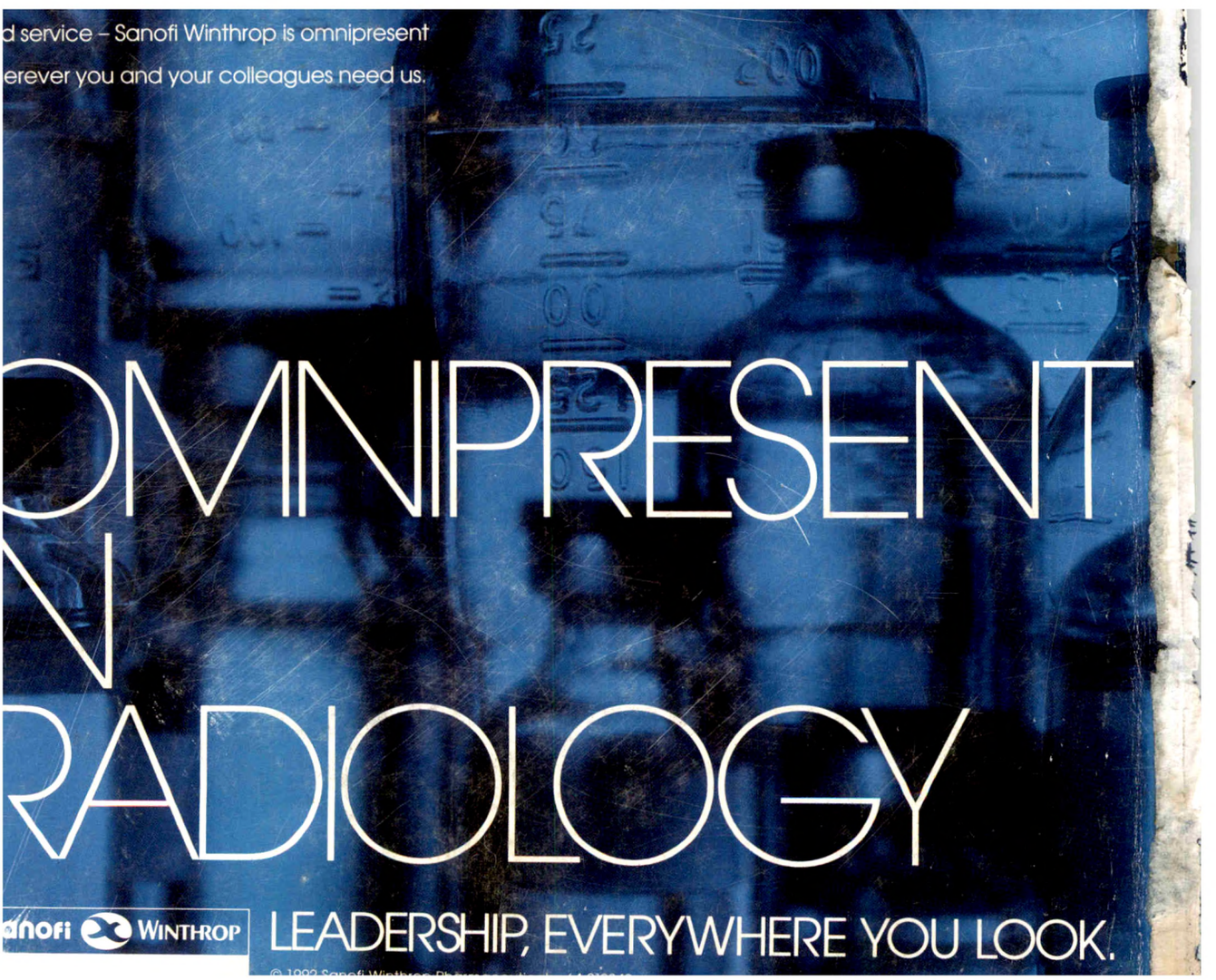
d service – Sanofi Winthrop is omnipresent
erever you and your colleagues need us.
OMNIPRESENT
N
RADIOLOGY
anofi WINTHROP
LEADERSHIP, EVERYWHERE YOU LOOK.

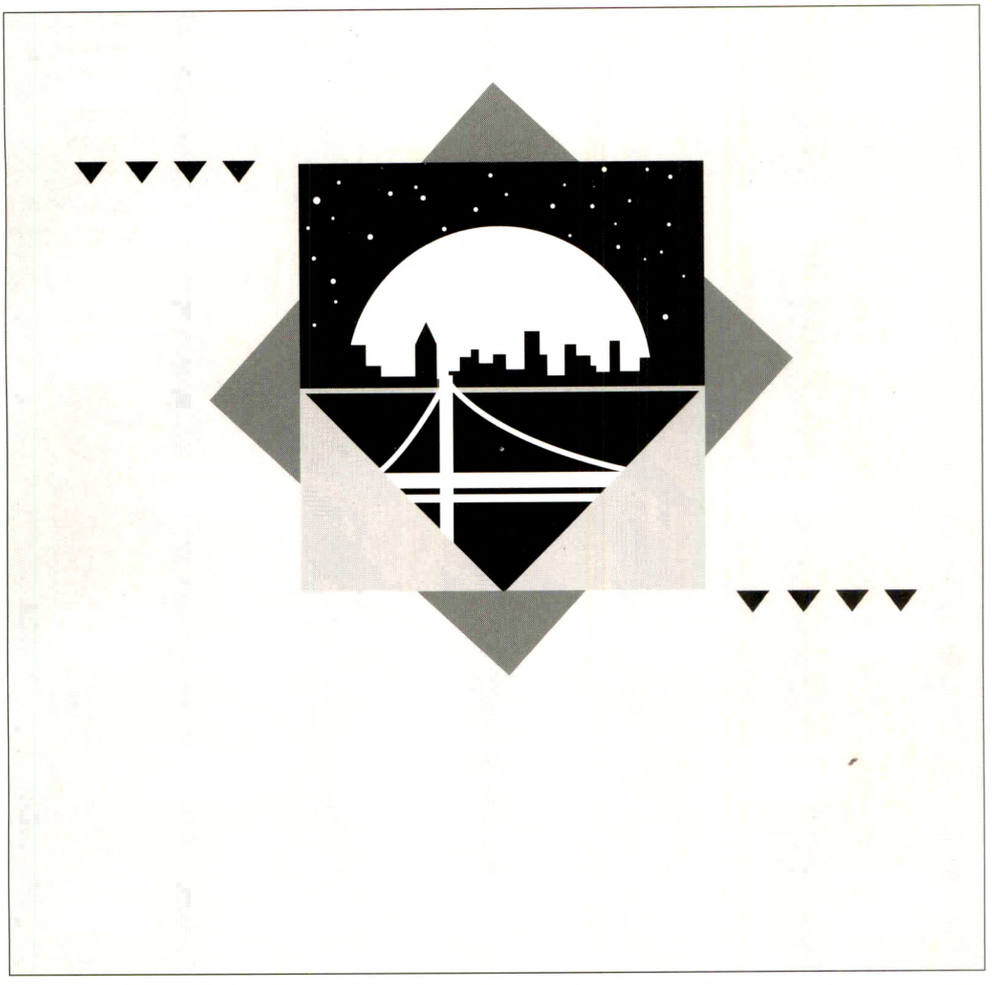

San Francisco

American Roentgen Ray Society

93rd Annual Meeting

April 25–30, 1993

San Francisco Marriott • San Francisco, CA

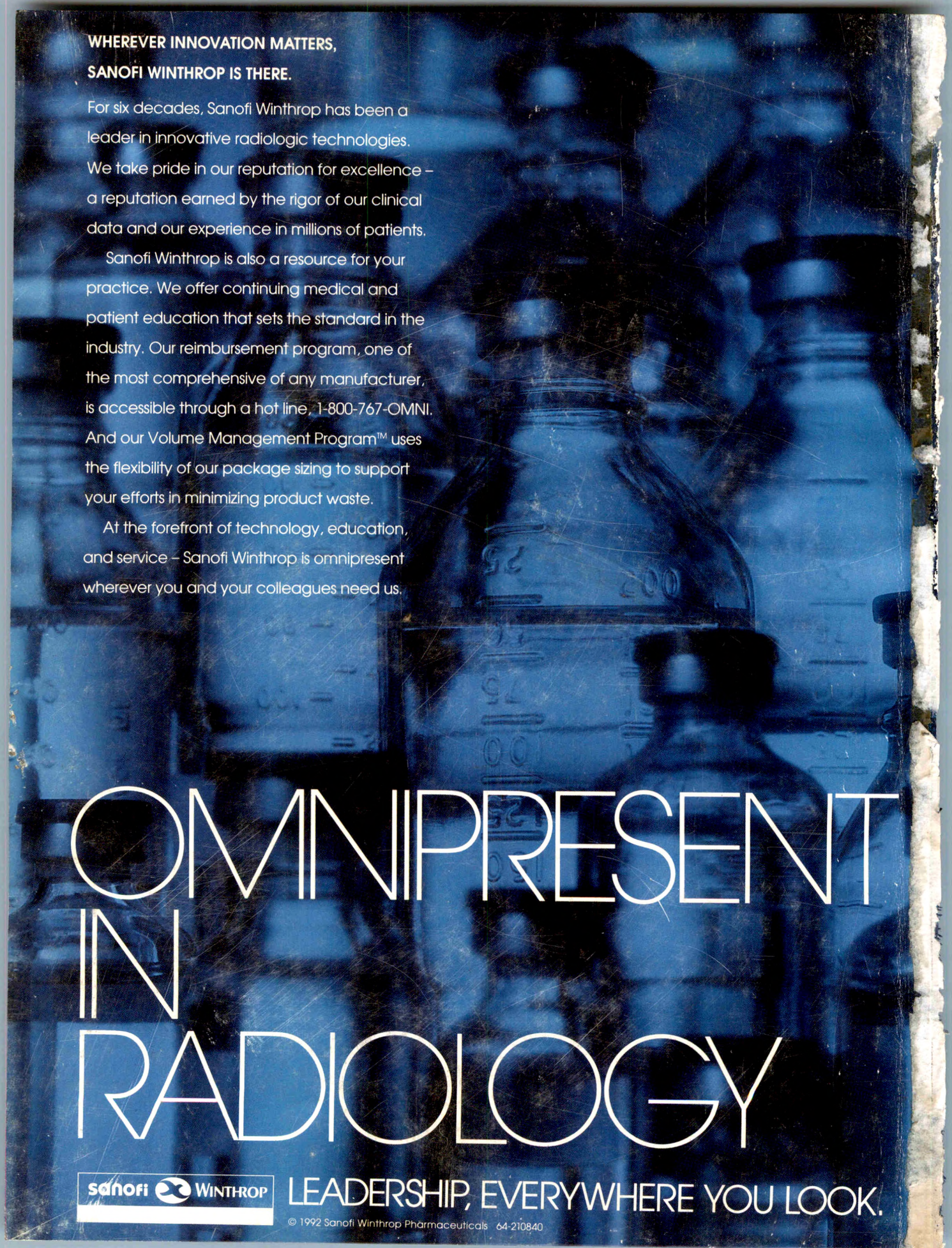
WHEREVER INNOVATION MATTERS,
SANOFI WINTHROP IS THERE.
For six decades, Sanofi Winthrop has been a leader in innovative radiologic technologies. We take pride in our reputation for excellence – a reputation earned by the rigor of our clinical data and our experience in millions of patients.
Sanofi Winthrop is also a resource for your practice. We offer continuing medical and patient education that sets the standard in the industry. Our reimbursement program, one of the most comprehensive of any manufacturer, is accessible through a hot line, 1-800-767-OMNI. And our Volume Management Program™ uses the flexibility of our package sizing to support your efforts in minimizing product waste.
At the forefront of technology, education, and service – Sanofi Winthrop is omnipresent wherever you and your colleagues need us.
OMNIPRESENT IN RADIOLOGY
sanofi WINTHROP
LEADERSHIP, EVERYWHERE YOU LOOK.
© 1992 Sanofi Winthrop Pharmaceuticals 64-210840